

In compliance with the
Canadian Privacy Legislation
some supporting forms
may have been removed from
this dissertation.

While these forms may be included
in the document page count,
their removal does not represent
any loss of content from the dissertation.

University of Alberta

**Geology, Diagenesis and Paleofluid flow in the Devonian Southesk-Cairn Carbonate
Complex in west-central Alberta, Canada**

By



Beate Elisabeth Buschkuehle

**A thesis submitted to the Faculty of Graduate Studies and Research in partial
fulfillment of the requirements for the Degree of Doctor of Philosophy.**

Department of Earth And Atmospheric Sciences

**Edmonton, Alberta
Fall 2003**



National Library
of Canada

Bibliothèque nationale
du Canada

Acquisitions and
Bibliographic Services

Acquisisitons et
services bibliographiques

395 Wellington Street
Ottawa ON K1A 0N4
Canada

395, rue Wellington
Ottawa ON K1A 0N4
Canada

Your file *Votre référence*
ISBN: 0-612-87945-3
Our file *Notre référence*
ISBN: 0-612-87945-3

The author has granted a non-exclusive licence allowing the National Library of Canada to reproduce, loan, distribute or sell copies of this thesis in microform, paper or electronic formats.

L'auteur a accordé une licence non exclusive permettant à la Bibliothèque nationale du Canada de reproduire, prêter, distribuer ou vendre des copies de cette thèse sous la forme de microfiche/film, de reproduction sur papier ou sur format électronique.

The author retains ownership of the copyright in this thesis. Neither the thesis nor substantial extracts from it may be printed or otherwise reproduced without the author's permission.

L'auteur conserve la propriété du droit d'auteur qui protège cette thèse. Ni la thèse ni des extraits substantiels de celle-ci ne doivent être imprimés ou autrement reproduits sans son autorisation.

Canada

UNIVERSITY OF ALBERTA

Library Release Form

Name of Author: **Beate Elisabeth Buschkuehle**

Title of Thesis: **Geology, Diagenesis and Paleofluid flow in the Devonian Southesk-Cairn Carbonate Complex in west-central Alberta, Canada**

Degree: **Doctor of Philosophy**

Year this Degree Granted: **2003**

Permission is hereby granted to the University of Alberta Library to reproduce single copies of this thesis and to lend or sell such copies for private, scholarly, or scientific research purposes only.

The author reserves all other publication and other rights in association with the copyright in the thesis and except as herein before provided, neither the thesis nor any substantial portion thereof may be printed or otherwise reproduced in any material form whatever without the author's prior written permission.

Date: Sept 25 / 2003

**“One is continually faced by
great opportunities brilliantly
disguised as insoluble problems.”**

Anonymous

UNIVERSITY OF ALBERTA

Faculty of Graduate Studies and Research

The undersigned certify that they have read, and recommend to the Faculty of Graduate Studies and Research for acceptance, a thesis entitled **Geology, Diagenesis and Paleofluid flow in the Devonian Southesk-Cairn Carbonate Complex in west-central Alberta, Canada**

by Beate Elisabeth Buschkuehle in partial fulfillment of the requirements for the Degree of **Doctor of Philosophy**

Dr. Hans G. Machel

Dr. Brian Jones

Dr. Karlis Muehlenbachs

Dr. Martyn Unsworth

Dr. Jay M. Gregg

Date: _____

Sept 23/03

For My Father
Clemens Buschkühle

ABSTRACT

One of the largest geological features in the deep part of the Alberta Basin in western Canada is the Middle to Upper Devonian Southesk-Cairn carbonate complex (SCCC). The SCCC lies at depths of about 5000 m adjacent to the disturbed belt of the Rocky Mountains and is rising to depths of 2000 m in a northeasterly direction over a distance of 150 km.

The complex consists of four stacked carbonate platforms with associated reefs, which are intervened by marls and evaporites. The carbonates adjacent to the deformation front build a contiguous aquifer because the intervening aquitards are missing. Also, a carbonate-rich unit exists in the Wild River Basin, which has been named „Berland Carbonate“.

The SCCC contains several gas pools, which have up to about 30% H₂S. This study focused on the diagenesis and concurrent pore fluid flow in the SCCC. The complex diagenetic sequence could be grouped into 5 stages: (1) synsedimentary to shallow burial, (2) intermediate burial, (3) deep burial, (4) maximum burial, and (5) present depth. Each of these stages influenced the quality of the reservoir rocks.

Stage 4 is of special interest because the strontium isotopes of late diagenetic calcite cements suggest the influence of basin-external fluids. The ⁸⁷Sr/⁸⁶Sr-isotope ratios of these calcite cements are high directly adjacent to the disturbed belt and they decrease with increasing distance towards the foreland basin. This radiogenic strontium signal can be traced for about 100 km into the foreland basin. Circumstantial evidence suggests that the radiogenic strontium was carried by fluids that were expelled during the Laramide orogeny from the Rocky Mountain Main Ranges and/or the underlying basement.

Geochemical data indicate that the pore fluids evolved from Devonian seawater that was subsequently changed by evaporation, gypsum dehydration, influx of metamorphic waters, and thermochemical sulfate reduction.

Fluid inclusion data and stable isotope data indicate distinct temperature ranges for early diagenetic, medium diagenetic, and late diagenetic mineral phases. The temperatures may have been as high as 220 °C at the maximum burial during the Late Cretaceous / Early Tertiary.

Fluid inclusion salinities and chemistry data from drill stem tests indicate a low-salinity brine in the deepest part of the area, which is migrating updip, displacing a more saline brine. This migration pattern suggests a flow direction from the SW to the NE, from the peak of the Laramide orogeny to the present.

Acknowledgments

This thesis was financially supported by funds from a Natural Science and Engineering Research Council (NSERC) strategic grant to Hans G. Machel (University of Alberta) that has been supplemented by funds from Chevron Canada Resources Ltd., Amoco Canada Petroleum Company Ltd., Crestar, Imperial Oil, Petrocanada, Husky Oil and Shell Canada Ltd.. The author, furthermore, gratefully acknowledges two Grant-in-Aid Scholarships from the American Association of Petroleum Geologists (AAPG), a scholarship from the Society of Professional Well Log Analysts Foundation (SPWLA), and a grant from the Canadian Association of Petroleum Producers (CAPP).

I am grateful to Hans Machel and Pat Cavell for valuable discussions and editorial suggestions throughout many stages of the completion of this thesis. I am also thankful to Brian Jones and Karlis Muehlenbachs for their support and guidance. Discussions with Eric Mountjoy, Jack Wendte, Marc Mallamo, Steve Switzer, Nigel Watts, Les Eliuk, Ben Rostron, Stefan Bachu, Eva Drivet, Darryl Green, Ian Hunter, Bev Harris and many others provided helpful insights and ideas. Matt Grobe, Catherine Skilliter, Marianne McKenzie, Jeff Lonnee, Mikel Erkiaga, Judit Nadal, Alex MacNeil and Karsten Michael made live in and around 3-16 enjoyable and fun.

My warmest appreciation go to Anita and Eric Mountjoy who supported me through the years with their love, encouragement, hospitality, and much, much more. I thank my mother and father for their love. A loving thanks to Karsten, who always believed in me.

TABLE OF CONTENTS

CHAPTER 1: INTRODUCTION.....	1
1.1 Rationale.....	1
1.2 Study Area.....	6
1.3 Exploration History.....	7
1.4 Objectives.....	8
1.5 Methods and Database.....	10
1.6 Contribution to Original Scientific Knowledge.....	11
CHAPTER 2: GEOLOGY.....	13
2.1 Geologic Framework.....	13
2.2 Previous Studies.....	22
CHAPTER 3: STRATIGRAPHY AND FACIES ANALYSIS.....	25
3.1 Stratigraphic Nomenclature.....	25
3.2 Methodology for Stratigraphy and Facies Interpretation.....	36
3.3 Lithostratigraphy.....	41
3.4 Facies Development.....	49
3.5 Sequence Stratigraphy.....	57
3.6 Hydrostratigraphy.....	61
CHAPTER 4: DIAGENESIS.....	65
4.1 Stage 1: Near-Surface Diagenesis.....	68
4.1.1: Micritization or micrite envelopes.....	70
4.1.2: Anhydrite and laminated dolomite.....	70
4.1.3: Pyrite I.....	72
4.1.4: Calcite I.....	72
4.1.5: Calcite II.....	73
4.1.6: Fascicular optic fibrous calcite (FOFC).....	76
4.2 Stage 2: Shallow Burial Diagenesis.....	78
4.2.1: Calcite III.....	78
4.2.2: Matrix replacement dolomite.....	79
4.2.3: Dissolution.....	84
4.2.4: Pressure solution features.....	87
4.2.5: Dolomites associated with stylolites.....	91
4.2.6: Pyrite II.....	91
4.2.7: Fracture I.....	92
4.2.8: Calcite cements in small fractures.....	92

4.3 Stage 3: Intermediate Burial Diagenesis.....	94
4.3.1: Secondary anhydrite.....	94
4.3.2: Fracture II.....	95
4.3.3: Hydrocarbons and solid bitumen.....	95
4.4 Stage 4: Deep Burial.....	98
4.4.1: Fracture III.....	100
4.4.2: Saddle dolomites.....	100
4.4.3: Calcite cement L (late diagenetic).....	102
4.4.4: Elemental sulfur.....	105
4.4.5: Pyrite III/ sphalerite.....	106
4.4.6: Microfractures.....	106
4.4.7: Hydrogen sulfide (H ₂ S).....	107
4.5 Stage 5: Post-Orogenic Uplift.....	108
4.5.1: Tertiary anhydrite.....	109
4.6 Porosity Evolution.....	109
CHAPTER 5: GEOCHEMICAL DATA AND FLUID INCLUSIONS.....	114
5.1 Introduction.....	114
5.1.1: $\delta^{18}\text{O}/\delta^{13}\text{C}/\delta^{34}\text{S}$ of solids.....	114
5.1.2: $\delta^{18}\text{O}/\delta\text{D}$ of fluids.....	119
5.1.3: $^{87}\text{Sr}/^{86}\text{Sr}$ isotopes.....	121
5.1.4: Fluid inclusions.....	122
5.2 Analytical Methods.....	127
5.3 Analytical Results.....	129
5.3.1: Stable isotopes.....	129
5.3.2: Strontium isotopes.....	132
5.3.3: Fluid inclusion data.....	136
5.3.4: Geochemistry of present-day formation brines.....	142
5.4 Discussion.....	145
5.4.1: Late Devonian marine isotope baseline.....	145
5.4.2: Interpretation of stable isotope data of the solids.....	148
5.4.3: Interpretation of strontium isotope data of solids.....	153
5.4.4: Interpretation of the geochemistry of present-day formation brines.....	160
5.4.5: Interpretation of fluid inclusion data.....	165
5.4.6: Interpretation of the sulfur isotopes of fluids and solids.....	171

CHAPTER 6: SUMMARY AND CONCLUSIONS.....	174
6.1 Restatement of Objectives and Review.....	174
6.2 Dolomitization.....	175
6.3 Tectonic Expulsion of Formation Fluids.....	179
6.4 Fluid Evolution, Flow Mechanisms and Paragenetic Sequence of the SCCC.....	180
6.5 Fluid Flow in the Alberta Basin.....	189
6.6 Future Work.....	190
CHAPTER 7: REFERENCES.....	192
APPENDIX I: List of the 52 logged core locations, cored formations, core lengths, and general lithology.....	217
APPENDIX II: Schematic lithologs of 48 cores from the Southesk-Cairn carbonate complex.....	221
APPENDIX III: List of samples, including depths and general description.....	292
APPENDIX IV: List of wells and formation tops that have been used for stratigraphic and structural interpretations.....	299
APPENDIX V: Carbon and Oxygen Isotope Data.....	304
APPENDIX VI: Strontium Isotope Data.....	307
APPENDIX VII: Fluid Inclusion Data.....	311
APPENDIX VIII: Publications.....	320

LIST OF TABLES

CHAPTER 3

Table 3.1: Stratigraphic correlation chart of the Upper Devonian.....	29
Table 3.2: Textural classification of carbonates.....	50

CHAPTER 4

Table 4.1: Present day guide values for porosity and permeability of the four Devonian carbonate units.....	113
--	-----

CHAPTER 5

Table 5.1: Summary of stable isotope variations in different waters.....	119
Table 5.2: Summary table of isotope data for brine samples from the SCCC.....	143

LIST OF FIGURES

CHAPTER 1

Figure 1.1: Location map of study area in west-central Alberta.....	2
Figure 1.2: (a) Block diagram of an orogen during active thrusting and indicated brine migration pattern.....	4
(b) Schematic evolution of thrust sheets in a tectonic convergence zone....	4

CHAPTER 2

Figure 2.1: Morphogeological belts of the Canadian Cordillera.....	14
Figure 2.2: Location of the Western Canada Sedimentary Basin relative to the Canadian Cordillera.....	15
Figure 2.3: Cross-section A-B across the Canadian Cordillera into the western part of the Alberta basin.....	16
Figure 2.4: Major structural elements that influenced the deposition of Woodbend (D3) and Winterburn (D2) Group carbonates.....	18
Figure 2.5: Late Devonian paleogeographic reconstruction of the Laurussia/Euamerica continent.....	21

CHAPTER 3

Figure 3.1: Distribution of major Woodbend reef complexes and shale basins.....	26
Figure 3.2: Schematic regional cross section illustrating the cyclicity of Devonian sequences.....	31
Figure 3.3: Schematic regional cross-section showing the Woodbend-Winterburn and Beaverhill Lake Stratigraphy.....	32
Figure 3.4: Schematic regional cross-section showing the subdivision of the Woodbend-Winterburn strata.....	34
Figure 3.5: Overview over the logged core well locations.....	37
Figure 3.6: Typical log signals and lithology distribution for the northeastern part of the study area.....	38
Figure 3.7: Typical log signals and lithology for Woodbend, Winterburn and Wabamun Group carbonates.....	39
Figure 3.8: Typical log signals for the shales and argillaceous limestone succession in the Woodbend-Winterburn strata.....	40
Figure 3.9: Devonian stratigraphy along a NW-SE cross-section (A to A').....	43
Figure 3.10: Stratigraphic NW-SE cross-section (B to B') through the shallow part of the study area.....	44
Figure 3.11: Stratigraphic NW-SE cross-section (C to C') through the deep part of the study area.....	45
Figure 3.12: Devonian stratigraphy in a SW-NE structural cross-section across the Wild River Basin.....	46
Figure 3.13: Facies model for Middle and Upper Devonian carbonates.....	51
Figure 3.14: Facies model for the carbonates in the SCCC.....	52
Figure 3.15: Major eustatic sea level changes and stratigraphy of the Woodbend and Winterburn Groups.....	58
Figure 3.16: Sequence stratigraphy.....	59

Figure 3.17: Lithology and hydrostratigraphy of the Cambrian-Devonian Succession.....	62
---	----

CHAPTER 4

Figure 4.1: Diagenetic paragenesis of the Southesk-Cairn Complex.....	66
Figure 4.2: Burial curve for the carbonates of the Southesk-Cairn Complex.....	67
Figure 4.3: Diagenetic settings.....	68
Figure 4.4: Early marine diagenetic products on a microscopic scale.....	69
Figure 4.5: Micritic envelopes within a crinoid ossicle.....	71
Figure 4.6: Early marine cements in limestone core.....	74
Figure 4.7: Micritic envelopes, peloids, and early marine cements.....	75
Figure 4.8a: Extinction patterns and vibration directions in fibrous cements.....	77
Figure 4.8b: Fibrous calcite in three different microscopic views.....	77
Figure 4.9: Dolomitization pattern and distribution throughout logged core in the SCCC.....	80
Figure 4.10: Dolomite classification.....	81
Figure 4.11: Different Dolomitization degrees in the SCCC.....	82
Figure 4.12: Dissolution enhanced vuggy and intercrystalline porosity.....	85
Figure 4.13: Pressure solution features with increasing degree of pressure.....	88
Figure 4.14: Pressure solution features on a microscopic scale.....	89
Figure 4.15: Summary of intermediate diagenetic features on microscopic scale.....	93
Figure 4.16: Microfractures.....	96
Figure 4.17: Stability fields of various hydrocarbons as well as the onset temperatures for deasphalting of natural gas.....	98
Figure 4.18: Late burial diagenetic products on a microscopic scale.....	99
Figure 4.19: Pictures of various saddle dolomite cements.....	101
Figure 4.20: Late calcite cements in fractures and vugs.....	103
Figure 4.21: Distribution of various diagenetic products throughout the study area.....	104
Figure 4.22: Examples of secondary and tertiary anhydrite.....	110
Figure 4.23: Change in porosity of mechanically compacted mud and sand sediments with depths.....	111

CHAPTER 5

Figure 5.1: Summary of the effects of various processes on the isotopic composition of carbonates.....	115
Figure 5.2: Carbon isotopic compositions of common carbon-bearing compounds.....	116
Figure 5.3: Diagenetic CO ₂ within different diagenetic zones.....	117
Figure 5.4: Theoretical distribution of δ ³⁴ S values for sulfides.....	118
Figure 5.5: Trajectories and fields for the isotopic composition of various waters.....	120
Figure 5.6: Variations of the ⁸⁷ Sr/ ⁸⁶ Sr ratio of marine carbonates during Phanerozoic times.....	122
Figure 5.7: Diagram illustrating the occurrence of primary fluid inclusions in carbonate crystals.....	123
Figure 5.8: Salinity calculation from fluid inclusion data.....	125
Figure 5.9: Pressure-Temperature plots for H ₂ O-NaCl systems.....	126

Figure 5.10: Stable isotope data of early calcites, matrix dolomites, late diagenetic saddle dolomite, and late calcite cements.....	130
Figure 5.11: Sulfur isotope variations.....	131
Figure 5.12: Strontium isotope data.....	133
Figure 5.13: Strontium isotope ratios over Oxygen isotope ratios.....	134
Figure 5.14: Strontium isotope ratios over Carbon isotope ratios.....	135
Figure 5.15: Summary plot of fluid inclusion measurements.....	137
Figure 5.16: Overview over single sample fluid inclusion data.....	138
Figure 5.17: Sample locations, present day temperatures and geochemistry of brines..	142
Figure 5.18: Isotopic composition of brines.....	138
Figure 5.19: Phanerozoic Carbon and Oxygen isotope trend.....	144
Figure 5.20: Sr isotope variations during the Devonian.....	147
Figure 5.21: Sulfur isotope variations in Devonian evaporites.....	148
Figure 5.22: Plot of equilibrium relationships between fluid and solids in a calcite system.....	149
Figure 5.23: Plot of equilibrium relationships between fluid and solids in a dolomite system.....	151
Figure 5.24: Strontium isotope ratios in relation to distance from disturbed belt.....	155
Figure 5.25: Strontium isotope distribution of late calcite cements in the study area...	156
Figure 5.26: Pressure corrected fluid inclusion data throughout the study area.....	159
Figure 5.27: Salinity distribution of present-day brines.....	161
Figure 5.28: Pressure elevation plot for the study area.....	167
Figure 5.29: Fluid inclusion homogenization temperatures.....	168
Figure 5.30: Equilibrium relationships between analytical and equilibrium calcite, present day temperature, present day brines and fluid inclusion data.....	170
Figure 5.31: Schematic evolution of sulfur isotope ratios.....	173
 CHAPTER 6	
Figure 6.1: Dolomitization models and predicted dolomite distribution patterns.....	176
Figure 6.2: Diagenetic paragenesis of the Southesk-Cairn Complex.....	181
Figure 6.3: Conceptual evolution of flow patterns in the deep Alberta Basin.....	182/183
Figure 6.4: Present day salinity distribution and inferred flow directions.....	188

CHAPTER 1: INTRODUCTION

1.1 Rationale

The Upper Devonian Southesk-Cairn Carbonate Complex (SCCC) is located in west-central Alberta and contains some of the deepest hydrocarbon pools in the Alberta Basin (Fig. 1.1). The potential for sour gas is higher than elsewhere in the Basin, because the average maximum burial temperature exceeded 120^oC. It is estimated that recoverable resources not yet located may be 35% of the known reserves (EUB, 2000). A better understanding of the sedimentology, controls on diagenesis and fluid dynamics will improve exploration success, avoid blowouts of sour gas wells, and reduce the overall costs for the petroleum industry.

There are several possible fluid mechanisms in discussion for a tectonically overprinted area like the SCCC. Oliver (1986) introduced a paleo-fluid flow model, the so-called "squeegee model", that is still controversial (Fig. 1.2). The model was based on a synthesis of several papers including the ideas by Rickard et al. (1979), who proposed that tectonic loading of thrust sheets produced a regional-scale fluid flow in the Scandinavian Caledonides and was responsible for Pb-Zn mineralization in that area. Oliver (1986) generalized this idea and suggested that fluids become expelled from continental margin sediments, and then travel into the foreland basins and the adjacent continental interiors due to the burial of continental margins beneath thrust sheets in zones of convergence and formation of a fold-and-thrust belt. Oliver (1986) further suggested that these expelled fluids force hydrocarbon migration, are involved in metal

transportation, faulting, magma generation, metamorphism, and in the development of paleomagnetism.

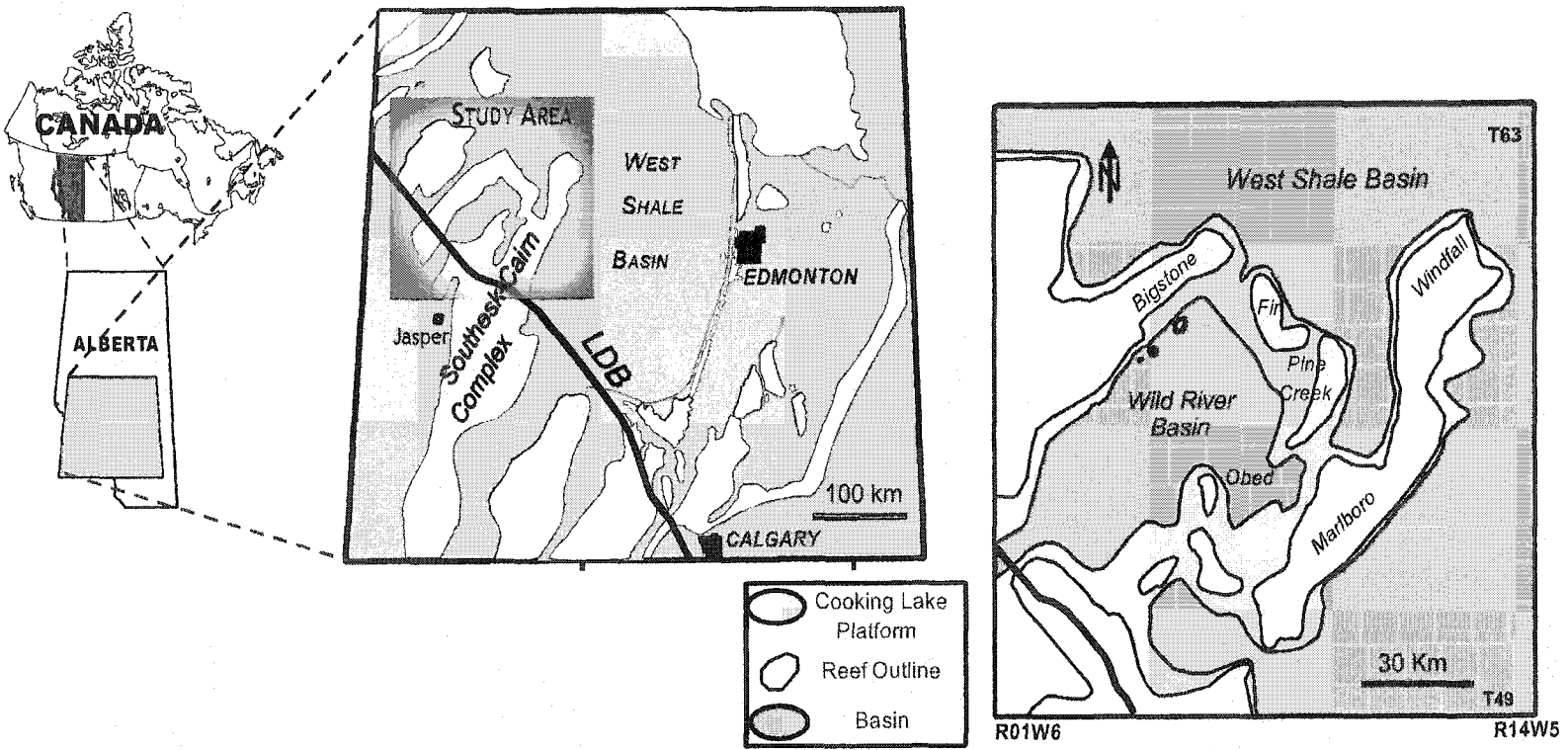


Figure 1.1: Location map of study area in west-central Alberta, showing the distribution of platform and reef carbonates of the Late Devonian Woodbend Group (D-3) in the Alberta Basin (modified from Mossop and Shetsen, 1994). The part northeast of the limit of the disturbed belt (LDB) is in the subsurface and has been defined by seismic, whereas southwest of the LDB the rocks are cropping out in the Rocky Mountains. The enlarged study area shows the distribution of the Cooking Lake Platform and associated reefs in the Southesk-Cairn complex. The carbonates are surrounded by marls and shales of the West Shale Basin and enclose the Wild River Basin.

There are several possible fluid mechanisms in discussion for a tectonically overprinted area like the SCCC. Oliver (1986) introduced a paleo-fluid flow model, the so-called "squeegee model", that is still controversial (Fig. 1.2). The model was based on a synthesis of several papers including the ideas by Rickard et al. (1979), who proposed that tectonic loading of thrust sheets produced a regional-scale fluid flow in the Scandinavian Caledonides and was responsible for Pb-Zn mineralization in that area. Oliver (1986) generalized this idea and suggested that fluids become expelled from continental margin sediments, and then travel into the foreland basins and the adjacent continental interiors due to the burial of continental margins beneath thrust sheets in zones of convergence and formation of a fold-and-thrust belt. Oliver (1986) further suggested that these expelled fluids force hydrocarbon migration, are involved in metal transportation, faulting, magma generation, metamorphism, and in the development of paleomagnetism.

Squeegee-type or tectonically induced flow has several implications for the diagenetic evolution in the study area. The first one is the composition of the pore-fluids, which could contain water molecules of metamorphic mineral reactions. Secondly, tectonic loading and heat flow would have influenced the fluid potential gradient. If fluids with a metamorphic signal became injected into the thrust sheets and the foreland basin, they would have driven forward the connate brines that were previously stored in the rock units and/or would have mixed with them. The cements that precipitated from these fluids should be clearly different from earlier diagenetic mineral phases that formed before the Laramide orogeny.

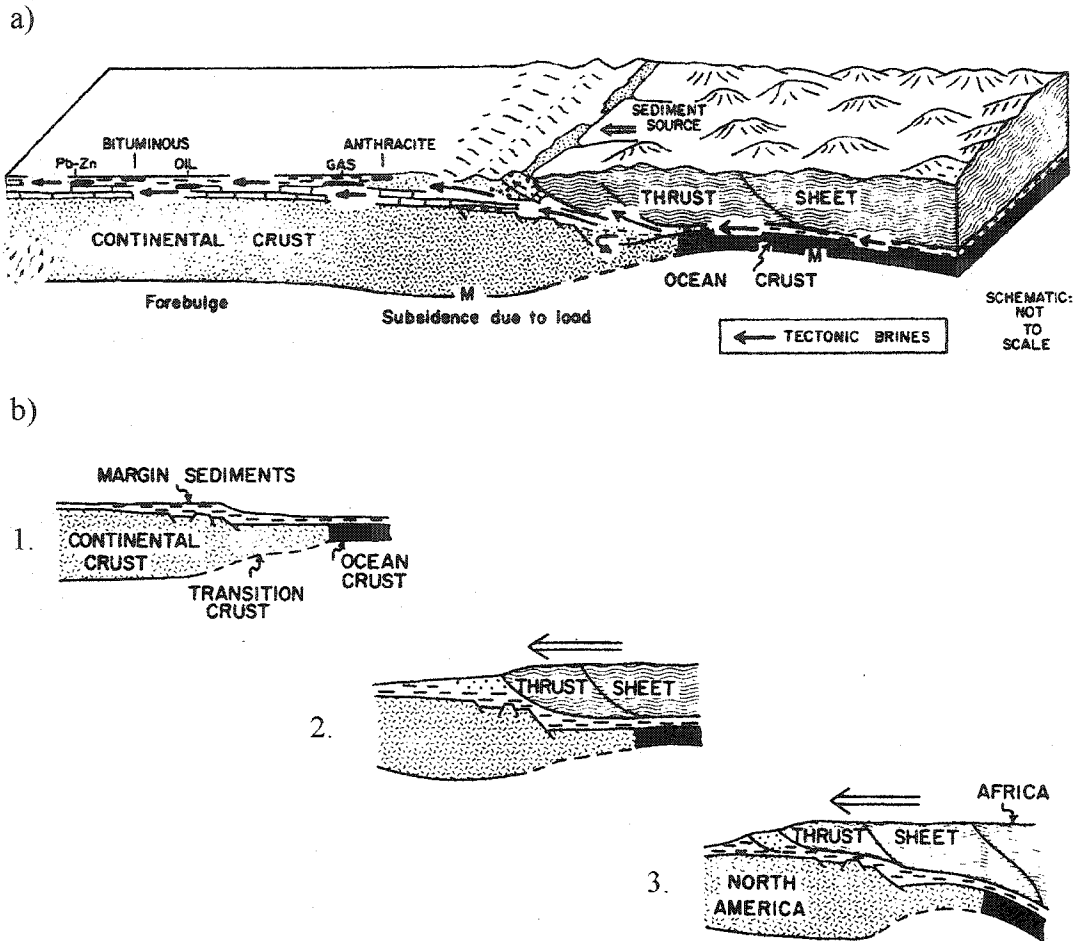


Figure 1.2: a) Block diagram of an orogen during active thrusting. The heavy arrows schematically illustrate flow of tectonic brines expelled from buried sediments. b) Schematic evolution of thrust sheets in a tectonic convergence zone. (from Oliver, 1986).

Oliver's (1986) model is partly based on a few case studies, however it is highly hypothetical and needs further investigations. The remaining questions are about the fluxes, the flow directions, and the timing of fluid flow. In this study special emphasis is placed on the spatial distribution and geochemical composition of deep burial, late diagenetic, sparry calcite and dolomite cements, as well as Cambrian clastics and

Precambrian metasediments that make up the underlying basement and much of the adjacent Rocky Mountain Main Ranges. The late cements are inferred to have formed during fluid flow caused by tectonic loading and are used to answer some of the remaining questions of Oliver's (1986) flow-model.

Tectonically-driven fluid flow was first considered for this part of the WCSB by Machel et al. (1996) and Machel & Cavell (1999). They found that at Obed, located within the SCCC (Fig. 1.2), anomalously high Sr-isotope values in late-diagenetic calcite cements probably resulted from Squeegee-type fluid flow during the Laramide orogeny. In addition, Mountjoy et al. (1999) found evidence for vertical flow through faults from the underlying rocks in the northeastern part of the study area. This study will try to not only prove the squeegee type flow model, but also differentiate between horizontal and vertical flow mechanisms. Another important objective is to find evidence for one of the numerous suggested dolomitization models for the Devonian of Alberta.

This study focuses on the causes for the present porosity and permeability distribution, and secondly the directions and approximate fluxes of paleo fluid flow. The understanding of paleo hydrology in the SCCC, which is located close to a zone of deformation (active mountain building front of the Rocky Mountains, Fig. 1.1), is of particular importance for both science and the petroleum industry. The scientific aspect of such a study includes information about pore fluid changes and the mineral products that form from the fluids, as well as their timing of formation. The petroleum industry will benefit in finding more reserves and better exploitation of the known reserves.

1.2 Study Area

The area of interest is located in the subsurface of west-central Alberta approximately 200 km west of the city of Edmonton (Fig. 1.1) in the Alberta Basin. The Alberta Basin is the west-central part of the Western Canada Sedimentary Basin (WCSB) that continues eastward into the Williston Basin of Saskatchewan. The Phanerozoic rock record consists of a southwestward thickening wedge that reaches a thickness of over 6 km close to the limit of the disturbed belt (LDB) of the Rocky Mountains (Wright et al. 1994). Towards the NE the wedge is subcropping onto the Canadian Shield, where it is terminated by erosion or non-deposition (Mossop & Shetsen, 1994). The study area extends from Township 63 Range 14 W6 in the NW to Township 49 Range 14 W5 in the SE (Fig. 1.1). The Devonian strata lie unconformably on top of Cambrian clastics and are conformably overlain by Mississippian carbonates.

The Upper Devonian Southesk-Cairn carbonate complex is one of the largest geological features in the study area and is of economic significance, as it contains several hydrocarbon pools. The SCCC is located at depths of 4000 to 5000 m close to the Rocky Mountains in the SW part of the area, and rises northeastward to depths of about 2000 m. The SCCC consists of two main "branches", the northern Bigstone arm and the southern Windfall/Marlboro arm, which are linked in the northeast by the Fir and Pine Creek reefs and platform trend (Fig. 1.1). The complex is bordered in the southwest by the limit of the disturbed belt (LDB) and encloses the Wild River Basin.

1.3 Exploration History

The Southesk-Cairn carbonate complex has been an exploration target since the 1950ies. Although some 30 pools are being exploited at present, the remaining established reserves are about $1579.3 \times 10^3 \text{m}^3$ crude oil and $26,045 \times 10^6 \text{m}^3$ natural gas, as well as 702×10^3 tonnes of sulfur (calculated using data from EUB, 2000).

The most important hydrocarbon fields in the study area are Bigstone, Harley, Berland River, Fir, Pine Creek, Windfall, Marlboro, Obed, Dalehurst, Hinton and Robb (Fig. 1.1). The discovery years range from 1955 to 1998, not including confidential data. All of these fields contain light to medium crude oil in the Mesozoic strata, whereas the main production in the Paleozoic is natural gas. Exceptions are the Kaybob and the Kaybob-South field (64-19W5 and 60-19W5, respectively) which produce light to medium crude oil out of the Upper Devonian Nisku Formation and Middle Devonian Beaverhill Lake Group, as well as from the Granite Wash Formation. The Granite Wash A pool was discovered in 1955, followed by the Beaverhill Lake A in 1957, the Beaverhill Lake B and D pools in 1961, the Nisku C pool in 1978, and Nisku D pool in 1995. The average formation depth below Kelly bushing (KB) for the Nisku is 2,500 m, whereas the Middle Devonian pools are located ~ 3,000 m below KB. The remaining established reserves of light to medium crude oil are $937.2 \times 10^3 \text{m}^3$ for these two pools (EUB, 1998). The Pine creek oil pool was discovered in 1959 and produced crude oil out of the D-3 C pool, with an average depths below KB of 3304 m. Initial oil in place was estimated to be $113.0 \times 10^3 \text{m}^3$. To date $31.5 \times 10^3 \text{m}^3$ have been produced, corresponding with the initial

established reserves. Another oil producing field in the area is Windfall in the northeast of the study area. This field is the shallowest of the investigated locations (2500 to 2950 m below KB). Production of oil in Windfall is out of the Upper Devonian Nisku (D-2) and Leduc Formation (D-3) stratigraphic horizons. The first pool was discovered in 1955 and the latest in 1990. Remaining established reserves of oil for the Windfall area are $6.426 \times 10^6 \text{m}^3$.

The main production out of the Devonian in the subsurface part of the Southesk-Cairn complex is natural gas, with a total established reserves of $26534 \times 10^6 \text{m}^3$. In 1998 due to a re-evaluation of initial volume in place, a major change in gas reserves occurred in the Beaverhill Lake C pool at Kaybob and Marlboro with $927 \times 10^6 \text{m}^3$ and $910 \times 10^6 \text{m}^3$ less gas, respectively. In the same year an additional volume of $968 \times 10^6 \text{m}^3$ gas was discovered at Lambert. In addition the Kaybob South and the Pine Creek fields are important sulphur producers, with a total of 702×10^3 tonnes of remaining established reserves.

1.4 Objectives

An earlier study (Patey, 1995; Machel et al., 1996) of the Obed field within the Southesk-Cairn Carbonate Complex (current study area) presented evidence for a complex diagenetic history spanning syndepositional events to late diagenetic cements that may have been related to the Laramide orogeny. This thesis addresses on much larger regional scale the diagenetic history of the Southesk-Cairn Carbonate Complex (SCCC), the

relationship of various diagenetic events to paleo fluid flow(s), and their effects on reservoir development.

The major objective of this study is to determine the causes for dolomitization of the matrix rocks and different cementation generations, as well as causes for the present porosity and permeability distribution, which is related to the aforementioned processes. A second objective is to determine the directions and approximate fluxes of paleo fluid flow and their implications for petroleum exploration.

In Chapter 1, the study area and the problems related to fluid flow and fluid processes in areas adjacent to a mountain thrust and fold belts are described. Chapter 2 gives an overview of the geologic framework, the basin definition, history and paleogeography of the SCCC area adjacent to the Rocky Mountain Fold and Thrust Belt. In Chapter 3 the dual stratigraphic nomenclature is defined, because the study area deals with subsurface rocks and outcrop data, for which different stratigraphic terms are in use. In addition, the new, informal unit "Berland Shale" was introduced. Furthermore, the lithological features of the four Devonian Groups (Beaverhill Lake, Woodbend, Winterburn and Wabamun) are described, as well as the facies development and the related dolomitization patterns. Chapter 4 contains the description of the diagenetic products and processes, which are interpreted to having been formed in five major stages of burial and pore-water evolution. In Chapter 5 the isotopic data and fluid inclusion homogenization temperatures are presented, analyzed and integrated into the analysis of the burial history. This final chapter integrates observations and interpretations from the previous ones into a synopsis of the dolomitization processes, tectonic expulsion, paragenetic sequence,

burial history, and the evolution of pore fluids in the west-central part of the deep Alberta Basin.

1.5 Methods and Database

A total of 52 cores were logged and sampled from the area of the SCCC and Wild River basin to investigate the local stratigraphy and facies distribution (see Appendix I for core list). Most of the cores were retrieved from the platform and reefs, whereas four are from the Wild River basin. The primary criterion for the core selection was to obtain a good aerial coverage for the SCCC and its regional extent. About 300 samples (see Appendix II for sample list) were taken from the core material and 150 polished thin-sections were studied with conventional and cathodoluminescence petrographic techniques, using a Zeiss Jenapol Polarizing Microscope and a CL microscope with a cold cathode Premier American Technologies ELM-3R Luminoscope. Operating conditions for CL petrography were a beam voltage of 15 to 10 kv and a beam current of 0.5 mA in a 35 to 50 mTorr vacuum under air pressure. The thin-sections were stained with Alizarin Red-S and potassium ferricyanide, according to the method of Dickson (1966). The samples were impregnated with blue epoxy to make the porosity more visible

Electric wire line logs of about 250 wells were used to construct cross-sections, isopach maps and structural maps to establish the geometry of the SCCC (see Appendix III for formation tops).

Powder samples for geochemical analyses were obtained using a low speed dental drill assembly. Each of the main diagenetic phases, e.g., matrix dolomite, saddle dolomite,

late calcite cement and anhydrite, were extracted separately and a total of 150 powder samples was produced. Seven formation brines were retrieved from wellheads and analyzed for δD and $\delta^{18}O$ and strontium isotope ratios. Sulfur isotopes of brines, anhydrite, elemental sulfur and bitumen were measured

All data have been corrected with respect to their standards.

The fluid inclusion samples for this study have been chosen to areally cover most of the SCCC. However, the sample number was limited to 10 (185 fluid inclusion measurements) and the data is summarized in Appendix VII. Because of the limited sample number, fluid inclusion studies from Green (1999) in the northern part of the complex and Smith (2001) in the central Obed area have been incorporated into the interpretation. All fluid inclusions are simple two-phase liquid gas (L-G) inclusions.

All analytical methods are described in more detail in the respective chapters 3 and 5.

1.6 Contribution to original scientific knowledge

This thesis is the first study that focuses on the entire subsurface part of the Southesk-Cairn Carbonate complex. Therefore, many aspects of this thesis constitute contributions to original knowledge. The following aspects are considered particularly noteworthy:

(1) The first comparison of subsurface stratigraphic terms versus surface terms for this part of the basin adjacent to the fold and thrust belt.

- (2) The first official recognition of the “Berland Carbonate” unit and its occurrence within the strata of the Wild River Basin.
- (3) The first regional study to document that strontium isotope data of late-diagenetic calcite cements show a regional variation.
- (4) The first study in this part of the WCSB to identify maximum burial temperature of 200°C using pressure-corrected homogenization temperatures.
- (5) The first study that measured fluid inclusion salinities, which indicate a dilution of brines close to the fold and thrust belt.
- (6) The first isotopic analyses of subsurface brines for this part of the Alberta Basin indicating significant differences between brines in the deep basin and the shallow parts of the Alberta Basin.
- (7) Combining aspects (1) to (6) above, this study is the first to provide physical (rock, fluids, and geochemical data) evidence for squeegee-type fluid flow in the deepest part of the foreland basin in front of an orogenic belt worldwide.

CHAPTER 2: GEOLOGY

2.1 Geologic Framework

- Basin Definition and History

The Western Canada Sedimentary Basin is a large, elongated feature that spans the provinces of British Columbia, Alberta, Saskatchewan and Manitoba (with a minor excursion into the northern U.S.A.) (Figs. 2.1, 2.2). The Western Canada Sedimentary Basin is divided into the Alberta Basin and the Williston Basin, the border of which roughly coincides with the so-called Bow Island Arch, which is a Precambrian structural high that crosses the Alberta-Saskatchewan border in the south (Figs. 2.1, 2.2).

The structural development of the Western Canada Sedimentary Basin is well known throughout the Phanerozoic and is closely related to the tectonic evolution of the Canadian Cordillera (Price, 1994) (Figs. 2.2, 2.3). The development of the basin took place in two fundamentally different tectono-sedimentary realms: the long-lived passive margin, and the foreland basin. The Devonian strata were deposited on the passive margin of the ancestral North American continent. Four orogenies affected the region, i.e., Antler (Devonian - Carboniferous), Sonoma (Late Permian?), Columbian (Jurassic - Early Cretaceous), and Laramide (Mid-Late Cretaceous - Tertiary). Two of these orogenies, the Antler and the Laramide, significantly shaped the size, depth, accommodation space, subsidence, and uplift of the Western Canada Sedimentary Basin.

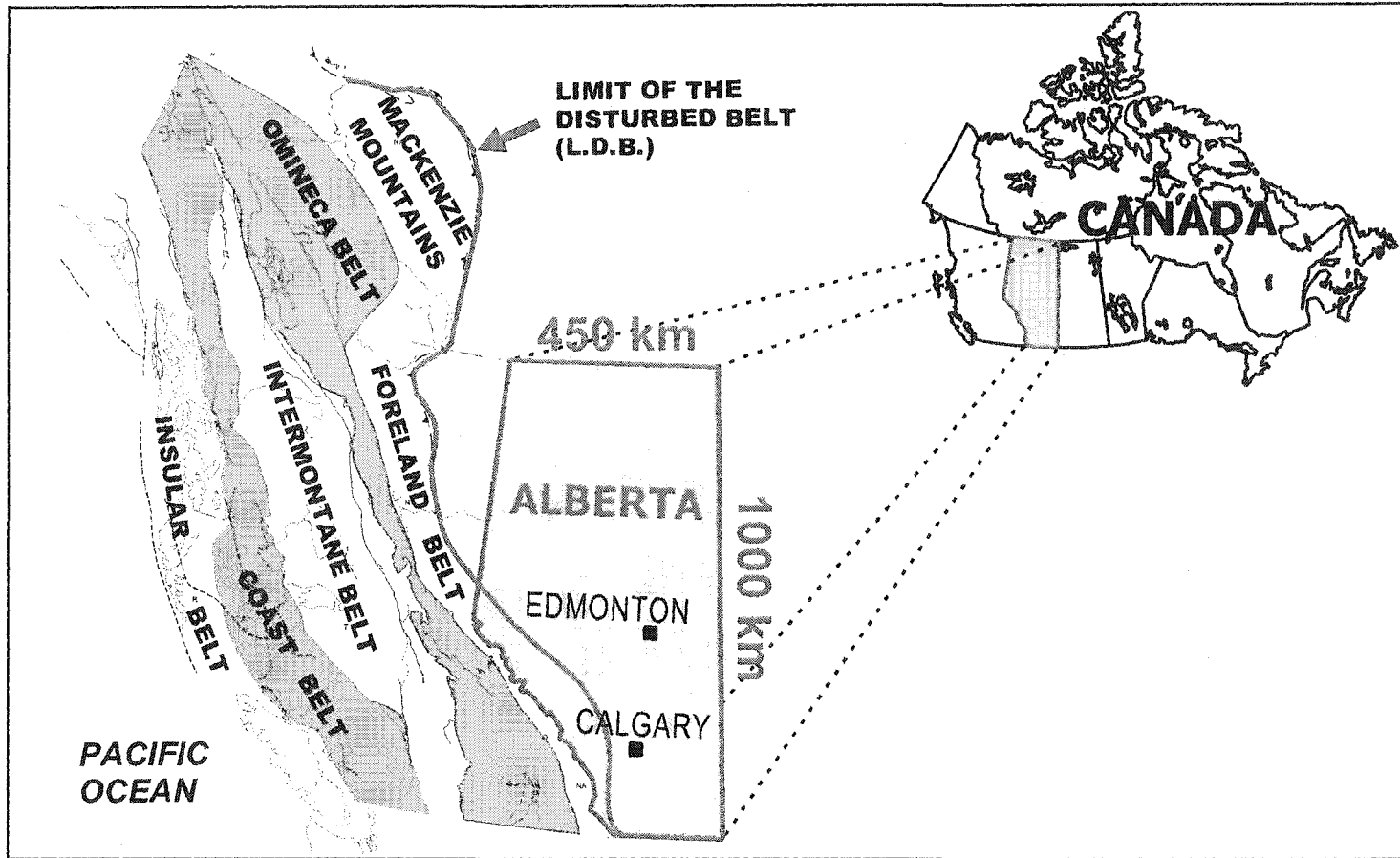


Figure 2.1: Morphogeological belts of the Canadian Cordillera that formed due to the accretion of several terranes and subsequently built the Rocky Mountains. Also shown are the location, outline, and size of the province of Alberta. The limit of the Disturbed Belt is the outer limit of Laramide tectonic deformation, with tectonically undisturbed strata to the east. Map is modified from Price (1994).

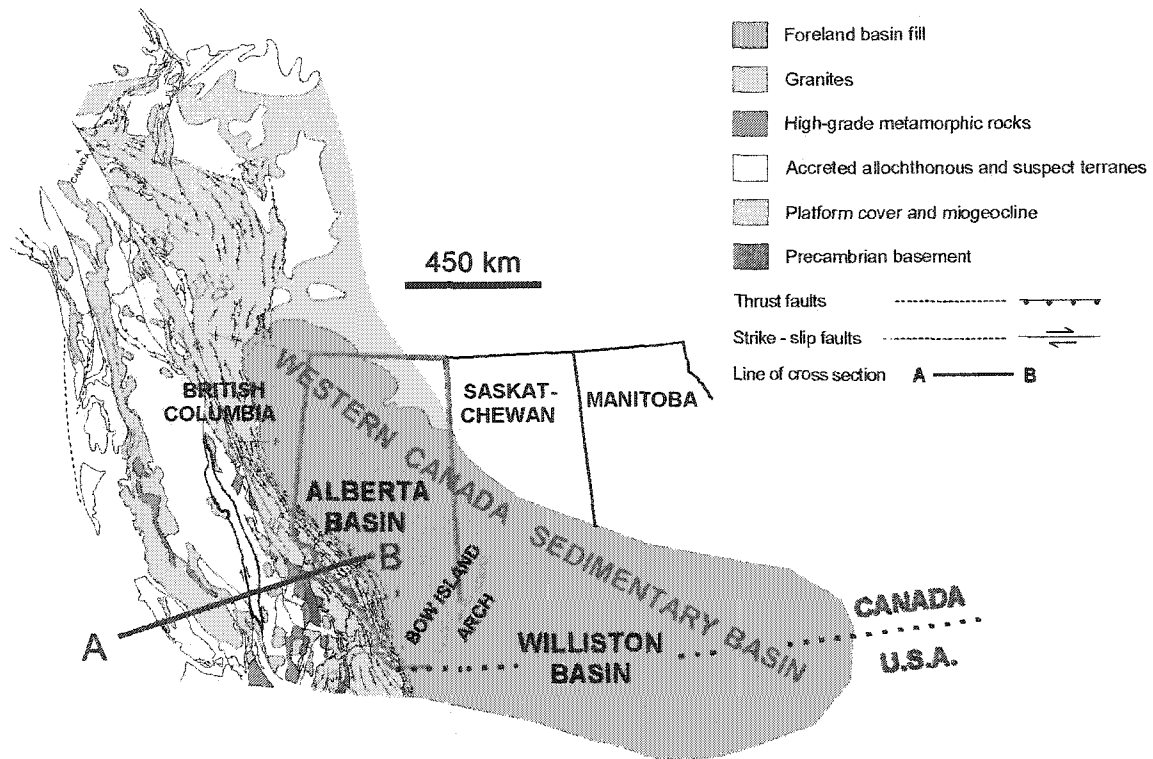


Figure 2.2: Location of the Western Canada Sedimentary Basin (WCSB) relative to the Canadian Cordillera. The WCSB stretches across the Northwest Territories, British Columbia, Alberta, Saskatchewan, Manitoba, and into the northern United States. It is divided into the Alberta Basin and the Williston Basin. The former forms the foreland basin of the Rocky Mountains. Line of Cross section A-B refers to Figure 2.3. Map is modified from Price (1994).

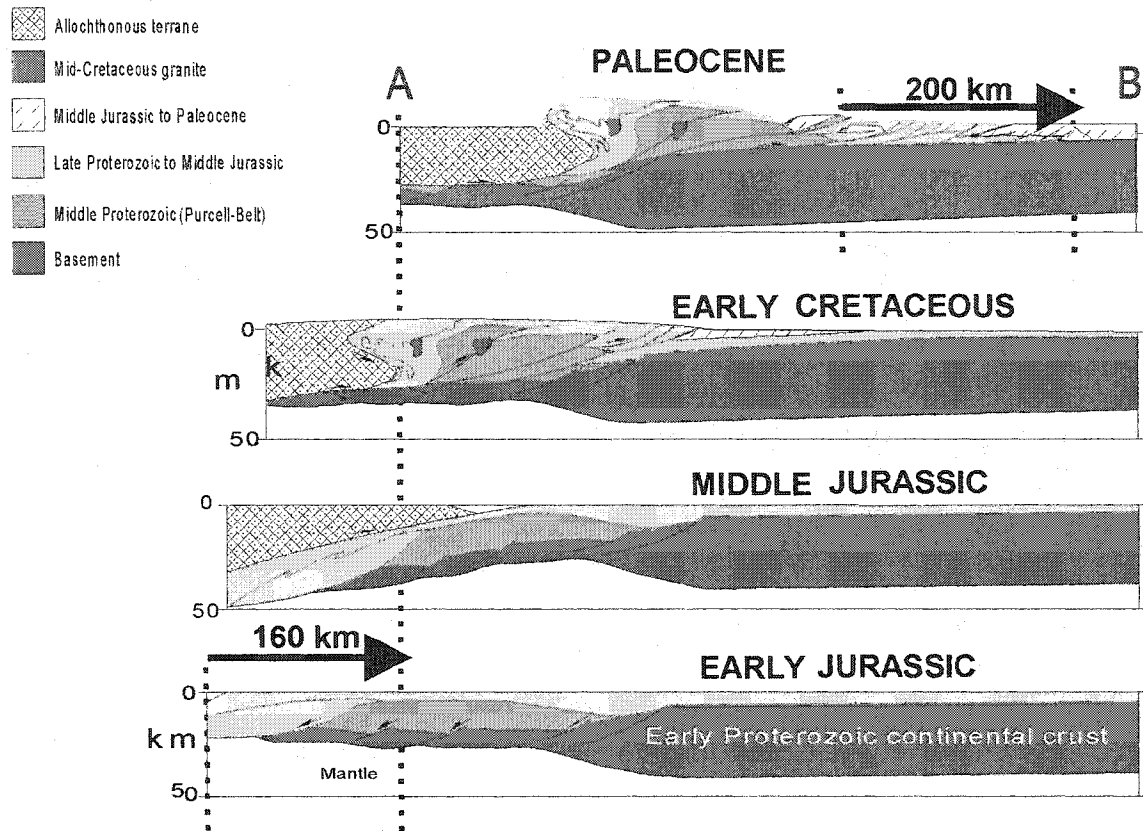


Figure 2.3: Cross section A-B across the Canadian Cordillera into the western part of the Alberta Basin (see Fig. 2.2 for line of cross section). The four sections show diagrammatically the deformation and approximate extent of tectonic shortening between the early Jurassic and the Paleocene. W-E compression shortened the Cordillera by approximately 160 km in the west and by about 200 km in the Rocky Mountains in the east. Modified from Price (1994).

Today, the Alberta Basin constitutes the foreland basin of the Rocky Mountains. Due to the asymmetry of the Alberta Basin, the Devonian strata form a basin-wide, structural homocline that dips gently from outcrops in northeastern Alberta to nearly 7 km in southwestern Alberta next to the Rocky Mountain fold and thrust belt (geographically known as the Foreland Belt – see Fig. 2.1).

Paleomagnetic, gravimetric, and seismic surveys have identified a number of structural highs (Fig. 2.4) and two fault systems that strike about NW-SE and SSE-NNW in the Precambrian basement (Switzer et al., 1994; Edwards et al., 1995). These structural features controlled deposition of the Devonian sedimentary strata to some degree. For example, deposition of the elongate Rimbey-Meadowbrook reef trend probably was controlled by a lineament in the Precambrian basement, the Rimbey Arc. Furthermore, at least some of the many basement faults that are located in this area appear to have been active during the Paleozoic and Mesozoic, influencing fluid flow and petroleum migration, as discussed further below.

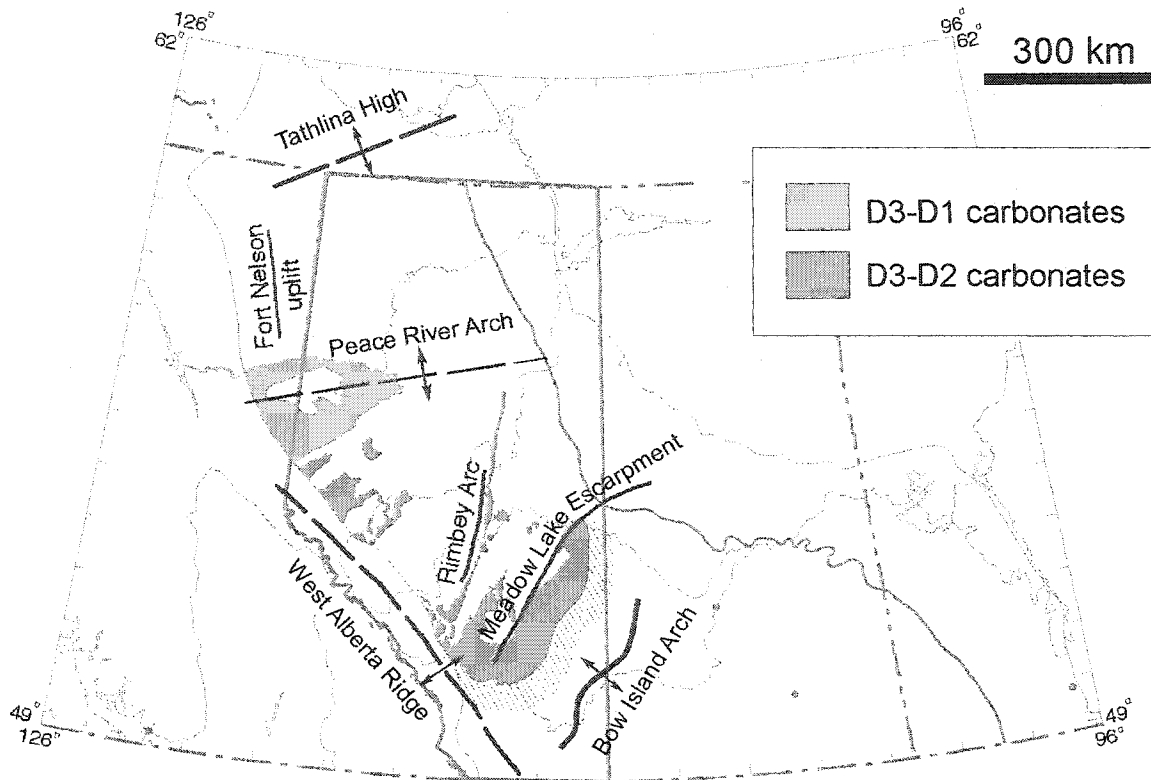


Figure 2.4: Major structural elements that influenced the deposition of Woodbend (D3) and Winterburn (D2) Group carbonates (modified from Switzer et al., 1994).

Another important example for the influence of basement structure on the Devonian petroleum system is the crystalline Peace River Arch that separates the Alberta Basin into northern and southern parts (Figs. 2.1, 2.4), each having different tectonic, depositional, geothermal, and hydrogeologic histories. The Peace River Arch forms a SW-NE oriented flexure in the Precambrian that was an emergent landmass throughout much of the Paleozoic until it collapsed in the Mississippian to Permian (e.g., Ross, 1990). The arch led to the deposition of an Upper Devonian fringing reef complex (Figs. 1.2) and a number of other distinct sedimentologic and diagenetic-hydrothermal phenomena (e.g., Dix, 1993). Detached from the orogenies that affected the entire region, the Peace River

Arch area had its own tectonic and geothermal dynamics (Stephenson et al., 1989; Ross, 1990).

North of the Peace River Arch, regional easterly flow of formation fluids probably formed MVT mineralization at Pine Point (Qing and Mountjoy, 1992, 1994). There is no evidence for a corresponding regional flow system south of the Peach River Arch, and no comparable Pb-Zn sulfide mineralization. Furthermore, the general burial and geothermal histories appear to have differed significantly north and south of the Peace River Arch. North of the arch in the Liard sub-basin area, a regional event of high heat flow reaching maximum temperatures between the end of the Paleozoic and the Jurassic caused oil maturation and migration in the Late Devonian to Carboniferous (Morrow et al., 1993). In that area, there is circumstantial evidence for late Paleozoic large-scale hydrothermal fluid convection via faults up and through the Devonian carbonates when they were at very shallow burial depths (Morrow et al., 1993; Morrow and Aulstead, 1995). There probably were six distinct fluid events in the northernmost part of the Western Canada Sedimentary Basin (Morris and Nesbitt, 1998), i.e., in the southern MacKenzie Mountains (see Fig. 2.1). These events, however, cannot be correlated to time-equivalent events south of the Peace River Arch, even though there are some similarities. Rather, geothermal gradients in the southern part of the WCSB appear to have been near normal from the late Paleozoic to the Laramide orogeny, and then again after the orogeny. This orogeny led to oil and gas maturation and migration in the Late Cretaceous to early Tertiary (Hacquebard, 1977; Stoakes and Creaney, 1984; Dawson and Kalkreuth, 1994). Also, there is no tangible evidence for large-scale late Paleozoic or Mesozoic convection

of hydrothermal fluids in the southern part of the Western Canada Sedimentary Basin, even though Morrow (1999) recently advocated thermal convection on the basis of circumstantial evidence.

- Paleogeography

Alberta was located along the western margin of the Laurussia continent during the Devonian. The Laurussia continent was formed during the latest Silurian when the North America-Greenland craton and the European craton collided (Ziegler, 1988). The suture/boundary is called the Caledonian Fold Belt. According to Witzke & Heckel (1988), Alberta was located between 8° and 16° south of the equator between the arid belt and the equatorial belt (Fig. 2.5). Hence the climate was very hot, and a shallow epicontinental sea covered Western Canada. These circumstances led to the formation of the enormous Middle Devonian Elk Point evaporites.

During the late Middle Devonian, the epicontinental seas expanded and a transcontinental seaway breached through North America connecting the Elk Point (Williston) basin with Iowa. Alberta was still located within the carbonate belt and drifted a bit north closer to the equator. As a result, thick shallow water reefal carbonates grew during the Middle Devonian, like the Winnipegosis/ Keg River Formation and the Swan Hills Formation. Evaporites still formed, thus, the Elk Point salts extended into North Dakota and the Middle Devonian Prairie – Muskeg evaporites formed in central and east Alberta. During the Late Devonian, Laurussia moved even farther north, placing Alberta closer to the equator. The extensive occurrences of evaporites, indicating a dry tropical climate, and a

northeast to southwest water circulation are consistent with an easterly trade wind belt parallel to the paleo-equator (Wendte et al., 1992).

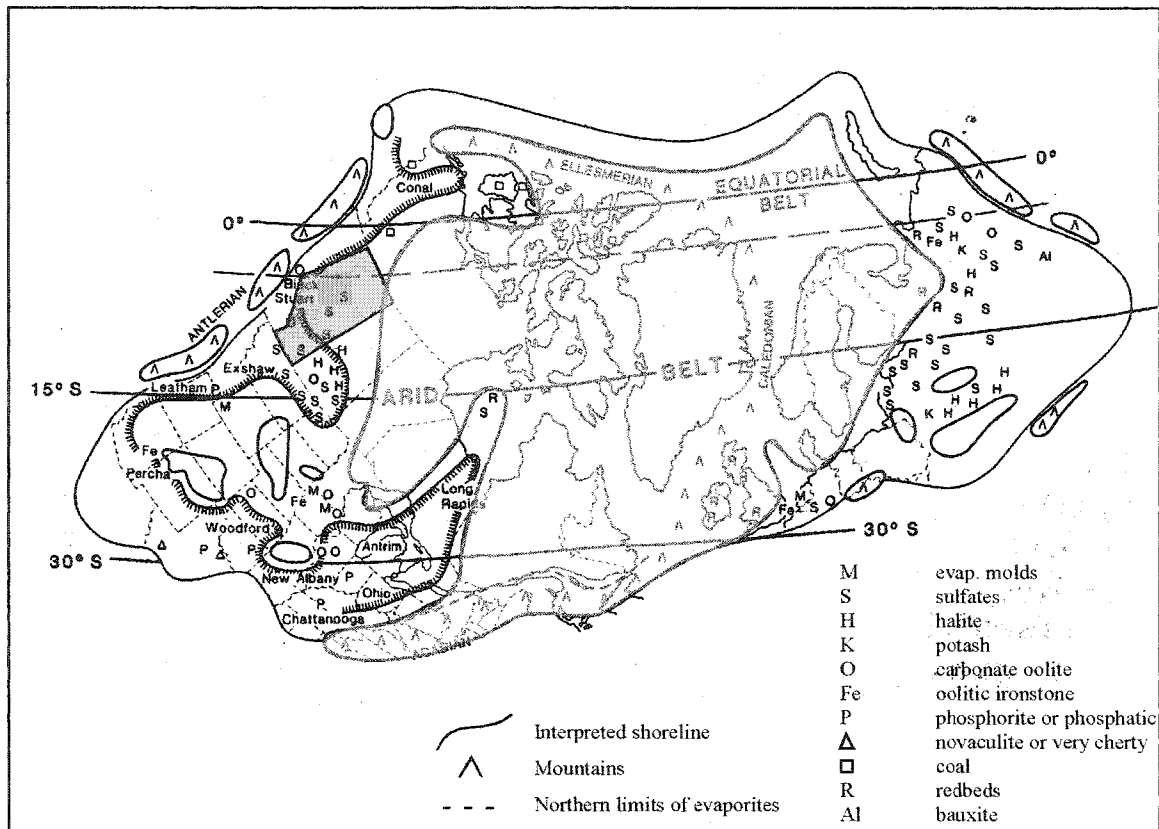


Figure 2.5: Late Devonian paleogeographic reconstruction of the Laurussia/Euamerica continent with Alberta being gray-shaded. Alberta was covered by a shallow epicontinental sea with a hot and tropic climate similar to the modern shallow water carbonate belts between low latitudes of 30° from either side of the equator. Modified after Witzcke and Heckel, 1988.

Thick shallow water carbonates of the Beaverhill Lake Group were deposited, as well as reefal carbonates of the Woodbend and Winterburn Groups, and again shallow water carbonates during the Wabamun Group. The evaporite borders shifted south-eastward

from central Alberta to Saskatchewan, Montana and North Dakota (Witzke & Heckel (1988). This is consistent with the northern movement of Laurussia. The main clastic sediment input during the Woodbend and Winterburn Groups was from the north and the northeast i.e., the ancestral Canadian Shield.

2.2 Previous Studies

The Devonian System forms the most productive oil and gas reservoirs in Canada (Moore, 1989), with major production from reefs of Givetian (Swan Hills Fm.) and Frasnian (Leduc Fm. And Nisku Fm.) age. The deposition of the Devonian strata was cyclical and developed in four stratigraphic levels, commonly referred to as D1, D2, D3 and D4. The sediments range in age from Givetian (Beaverhill Lake Group)[375 m.y.] to Frasnian (Woodbend and Winterburn Group) and Famennian (Wabamun Group) [363 m.y.].

The Devonian strata that crop out in the Rocky Mountains along several thrust sheets are well described by Belyea (1954), DeWit & McLaren (1950), Price (1964), Mountjoy, (1960, 1965, 1967, 1978, 1979, 1987); MacKenzie (1965), Workum & Hedinger (1987), Andrews (1987), and many others. Belyea and McLaren (1964) were the first to correlate the outcrop strata to the Devonian subsurface strata. The subsurface part of the Devonian in the Alberta Basin can be subdivided into the Leduc fringing reef around the Peace River arch, the deep basin (study area), the Rimbey-Meadowbrook reef trend, the Bashaw

reef complex, the Killam Barrier reef and the Grosmont platform. The Devonian of the Peace River Arch has been studied by Dix (1993) and McKenzie (1999). An overview of the Rimbey-Meadowbrook reef trend was first provided by Andrichuk (1958) and more detailed studies of facies, diagenesis and geochemistry followed in subsequent years (McNamara & Wardlaw 1991; Drivet 1993; Weissenberger 1994; Marquez 1994; Amthor et al. 1993, 1994). According to these studies the dolomitization of the Rimbey-Meadowbrook reef trend occurred during shallow to intermediate burial in the late Devonian/ early Mississippian from modified late Devonian seawater. Hearn (1995) studied the Bashaw reef complex. The facies, diagenesis and paleohydrology of the Grosmont Platform was studied by Cutler (1983), Huebscher (1996) and Machel (2000). Kaufman (1989) and Saller et al. (2002) focused on the Swan Hills Formation in the Rosevear field, which is located in the deep part of the basin just east of this study area, and described the diagenesis and geochemistry of the area. Green (1999) worked on the Southesk-Cairn complex, focusing on the Kaybob and Kaybob South as well as the Pine Creek and Fir fields. Patey (1995) and Green (1999) both observed highly radiogenic strontium compositions in late-diagenetic carbonate cements and interpreted them as expulsion-controlled and fault-controlled products, respectively. The Swan Hills Simonette reefal build-up was investigated by Duggan (1997) and Rock (1999). The latter compared the Leduc formation at Simonette and Ante Creek. Both authors inferred the involvement of faults in the formation of late dolomite and calcite cements.

The present study focuses on parts of the Southesk-Cairn Carbonate Complex that have not yet been examined in detail and provides further information on the stratigraphy, flow

patterns, fluid compositions, directions and timing, as well as fluid amounts that were involved over the history of the basin. It also incorporates data and conclusions from the above-mentioned investigations.

CHAPTER 3: STRATIGRAPHY

The general regional stratigraphic development, as documented in Switzer et al. (1994) and sources cited therein, forms the basic stratigraphic framework for this study. The overall division of the Upper Devonian stratigraphy into D1 to D4 (Wabamun, Winterburn, Woodbend, and Beaverhill Lake Groups) and their regional distribution are reasonably well understood. Furthermore, it is well established that the Upper Devonian reflects four major cycles of eustatic sea level changes that are divided by higher order cycles in many parts of the basin. However, in the area of the Southesk-Cairn Carbonate Complex the stratigraphic evolution and cyclicity is relatively poorly documented. The objective of this chapter is to provide additional new information in terms of stratigraphic description and facies analysis.

3.1 Stratigraphic Nomenclature

Most of the current stratigraphic nomenclature and correlation between outcrop and subsurface strata of the Upper Devonian in the study area dates back to the first surface/subsurface correlations, done in the early 1950's (Belyea, 1954). The nomenclature used in this thesis is presented in the following section.

The Fairholme Group strata are exposed in the Fairholme Reef Complex, the Cline channel, the Southesk-Cairn Reef Complex and in isolated reef complexes such as the Miette, Ancient Wall, and Berland (Fig. 3.1).

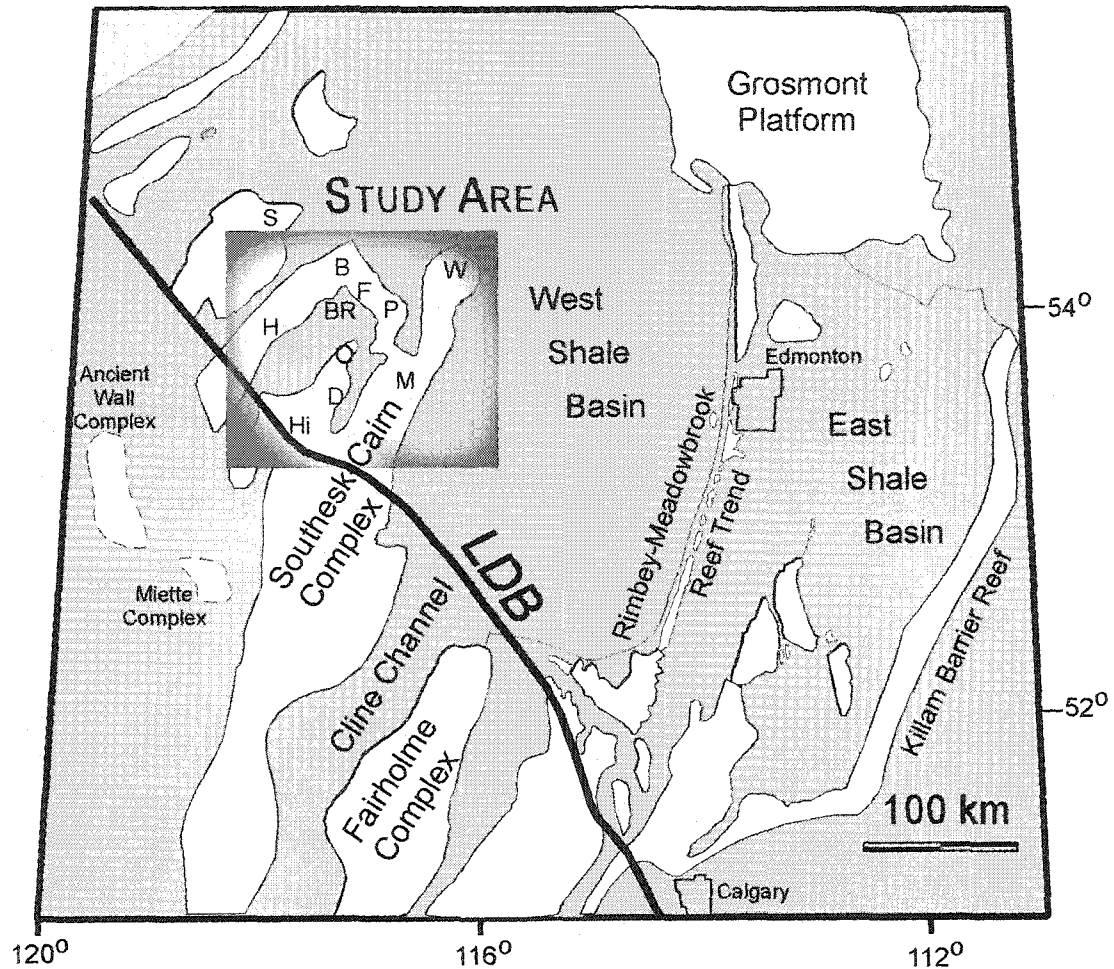


Figure 3.1: Distribution of major Woodbend reef complexes and shale basins (palinspastically restored; after Switzer et al., 1994). Also shown are the major gas fields that produce from the Devonian in the Southesk-Cairn Complex: B = Bigstone, BR=Berland River, F = Fir, P = Pine Creek, W = Windfall, M = Marlboro, H = Harley, O = Obed, D = Dalehurst, Hi = Hinton. LDB = Limit of Deformed Belt.

In general, these carbonates crop out in the Rocky Mountains in several thrust sheets and extend from the Main Ranges across the Front Ranges into the Foothills (Figs. 1.2, 3.1). The Bigstone, Windfall, Wild River, Obed, Fir, Pine Creek, Harley and Dalehurst fields produce from the Woodbend / Winterburn Groups, which are the subsurface equivalents of the Fairholme Group. The subsurface carbonates form a northeasterly trend similar to

the trend of the SCCC-outcrop. The reason for this trend, which is repeated elsewhere in the basin, is not well known. It may have been controlled by regional syndepositional tectonic flexures related to zones of weakness in the underlying Precambrian Shield (Mountjoy, 1980; Mountjoy & Geldsetzer, 1981).

The outcrops have been studied by numerous geologists, e.g., Raymond (1930), Allan et al. (1932), deWit and McLaren (1950), McLaren (1956), Mountjoy (1960, 1965), and McLaren and Mountjoy (1962). McLaren (1953, 1956) described the regional Devonian succession and introduced the Alexo and Mount Hawk Formations. He also defined the Southesk and Cairn Formations within the Fairholme Group (Tab. 3.1). Belyea & McLaren (1956, 1964) correlated outcrop sections with the subsurface. Belyea & McLaren (1957) subdivided the Southesk Formation into the Arcs, Grotto, and Peechee Members. At the same time, Taylor (1957) suggested correlations of the Leduc and Nisku Formations (Winterburn Group and Woodbend Group, respectively) from the subsurface to the mountain sections. He did not recognize the boundary between the Southesk and Cairn Formations, and introduced the term Maligne Formation for the upper member of the Flume Formation, named earlier by Raymond (1930). Mountjoy (1960, 1965, and 1981) described and mapped the stratigraphic relationships and geology of the Miette reef complex and surrounding areas and revised the type section of the Mount Hawk Formation at Roche Miette, recognizing the interfingering with the Southesk Formation. Investigation of the Ancient Wall reef complex provided additional information and different stratigraphic relationships between the Southesk and Cairn Formations and the basinal Perdrix and Mount Hawk Formations. In subsequent years, Workum (1978) and

Workum & Hedinger (1987) described and discussed the stratigraphy of the Southesk Formation at Cripple Creek, which is part of the Fairholme Reef Complex. Andrews (1987) provided a regional study of Devonian Leduc outcrop reef-edge models and compared them to subsurface seismic anomalies in the Woodbend Group. Weissenberger and McIlreath (1989) described and outlined parts of the Southesk Cairn Reef Complex.

Front Ranges / Foothills		Wild River Basin		West-central Alberta						
EXSHAW		EXSHAW								
FAMENNIAN	PALLISER		WABAMUN		WABAMUN		Wabamun Group	D1		
	SASSENACH		GRAMINIA		GRAMINIA					
FRASNIAN	FAIRHOLME GROUP	SOUTHESK	RONDE	SIMLA	ALEXO	BLUERIDGE	BLUERIDGE	WINTERBURN GROUP	D2	
				CALMAR		CALMAR	CALMAR			
			ARCS	MOUNT HAWK		NISKU	WOLF LAKE			CYNTHIA
	GROTTO			BERLAND	IRETON	LEDUC				
	PEECHEE	PERDRIX	LEDUC	IRETON	DUVERWAY	LEDUC				
	CAIRN				COOKING LAKE					
		MALIGNE	COOKING LAKE		MAJEAU LAKE					
		FLUME	SWAN HILLS		WATERWAYS					
			SLAVE POINT		SLAVE POINT					
					FORT VERMILLION					
GIVETIAN							Beaverhill Lake Group	D4		
							WOODBEND GROUP	D3		

Table 3.1: Stratigraphic correlation of the Upper Devonian between outcrop in the Foothills and Front Ranges of the Rocky Mountains and the subsurface in the Wild River Basin and the west-central part of the Alberta Basin (see text for references).

The stratigraphy of the subsurface equivalents of these strata in the Alberta Basin has also been studied by numerous authors (Belyea, 1964; Switzer et al., 1994 and references cited therein). One of the best-studied areas is the Rimbey-Meadowbrook reef trend (Fig. 3.1), which is located about 200 km ESE of the SCCC (Waring and Layer, 1950; Andrichuk, 1958; Klovan, 1964; McGillivray and Mountjoy, 1975; Walls, 1983; Marquez, 1994, Wendte, 1994; Mountjoy et al., 1999). The stratigraphy of the subsurface part of the SCCC is less well known. Wendte (1992, 1998) and Switzer et al. (1994) have provided the most detailed overviews. The stratigraphy of the SCCC consists of four carbonate platforms and associated strata that have been subdivided into four stratigraphic groups (Tab. 3.1; Fig. 3.2).

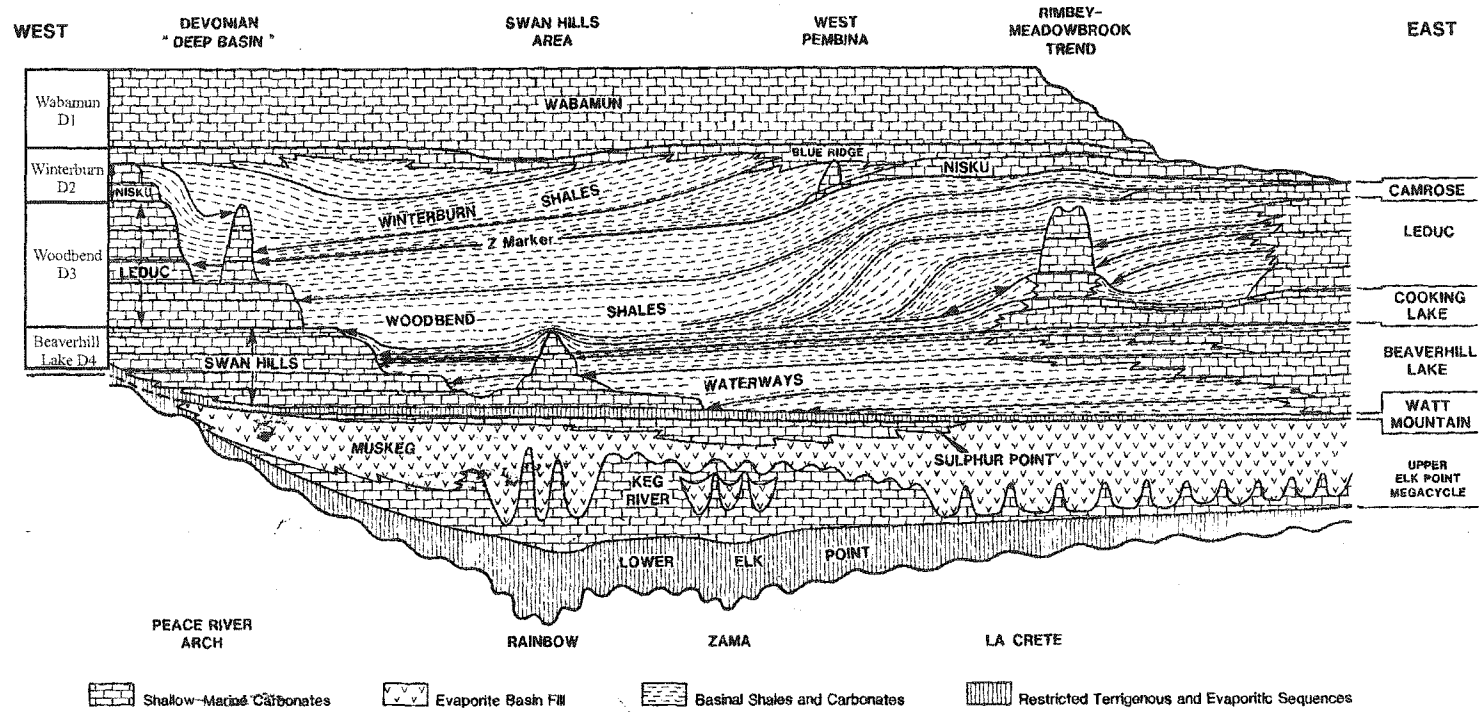


Figure 3.2: Schematic regional cross section (west to east) illustrating cyclicity of Devonian sequences and the distribution of Devonian sequences and the general distribution of their major facies in the Alberta Basin (modified from Wendte, 1992).

The middle to Upper Devonian Beaverhill Lake Group (D4) is the oldest of the four stacked carbonate platforms. It includes the Fort Vermilion, Waterways, Slave Point and Swan Hills Formations (Tab. 3.1; Figs. 3.3). The upper part of the Swan Hills Formation is equivalent to the outcrop Flume and/or Maligne Formation (Weihmann, 1980).

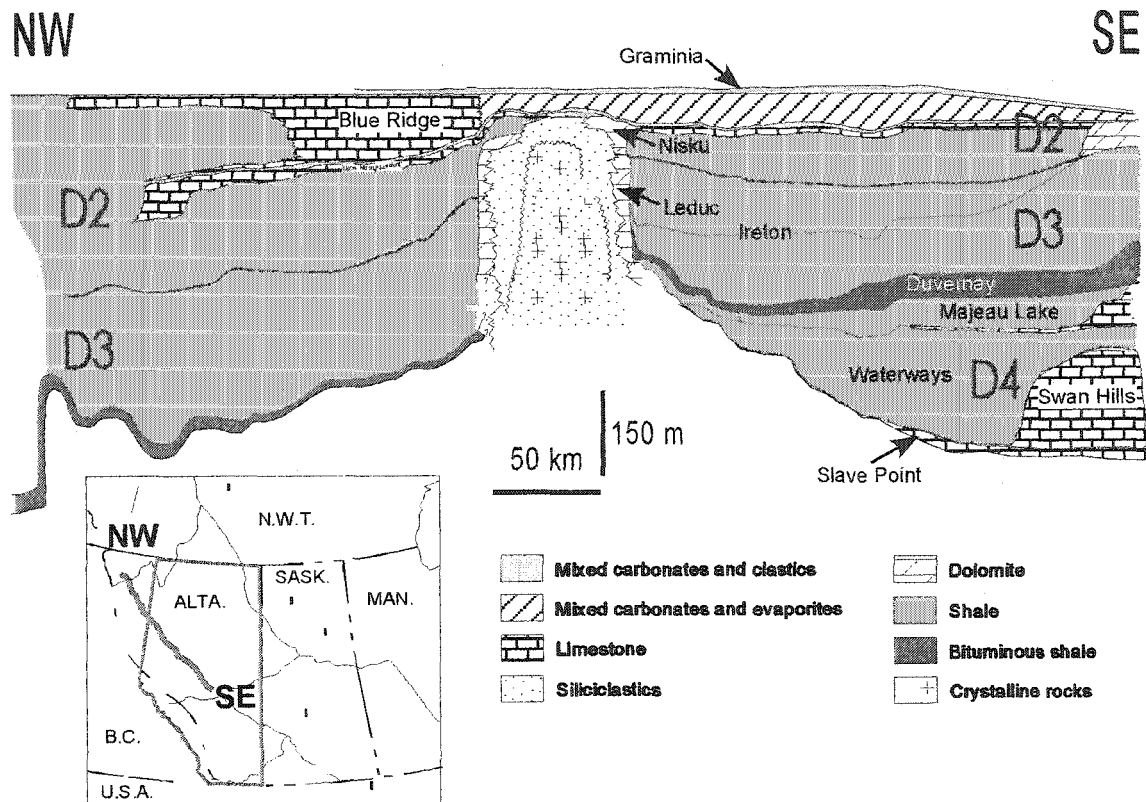


Fig.3.3: Schematic regional cross section showing the Woodbend-Winterburn and Beaverhill Lake stratigraphy around the Peace River Arch (modified from Oldale and Munday, 1994; Switzer et. al, 1994).

The Upper Devonian Woodbend Group (D3) is subdivided into the basinal/off-reef Duvernay Formation and Ireton Formation, and the platform/reefal Cooking Lake and Leduc formations (Figs. 3.3 and 3.4). The surface equivalent of the Cooking Lake Formation is considered to be the Maligne Formation, or part of the lower Cairn Formation. The Leduc Formation is equivalent to the reefal Cairn Formation and to the overlying Peechee Member, the basal member of the Southesk Formation. The Duvernay is approximately equivalent to the Perdrix Formation and the Ireton to the main part of the Mount Hawk Formation. The Upper Devonian Winterburn Group (D2) is divided into the Nisku, the Calmar, the Blueridge and the Graminia formations (Chevron, 1979; Machel, 1984; Anderson, 1985; Machel & Anderson, 1989; Watts, 1987). The Nisku in the West Pembina area has been further divided into Lobstick, Bigoray, Zeta Lake, Cynthia and Wolf Lake Members (Tab. 3.1; Fig. 3.4). This division is not easily correlated with the strata of the Wild River Basin. For the Upper Ireton and the Nisku members, an equivalent new informal unit "Berland-carbonate" is proposed in this study. The surface equivalents for the subsurface Winterburn Group are the Grotto, Arcs and Ronde-Simla members of the Southesk Formation. The Wabamun Group (D1) is the fourth carbonate unit and is equivalent to the Palliser Formation in the Rocky Mountains.

The subsurface terminology will be used for most parts of this study, considering that most of the study area is located in the subsurface. The term Southesk-Cairn Carbonate Complex is used both in the subsurface and the surface.

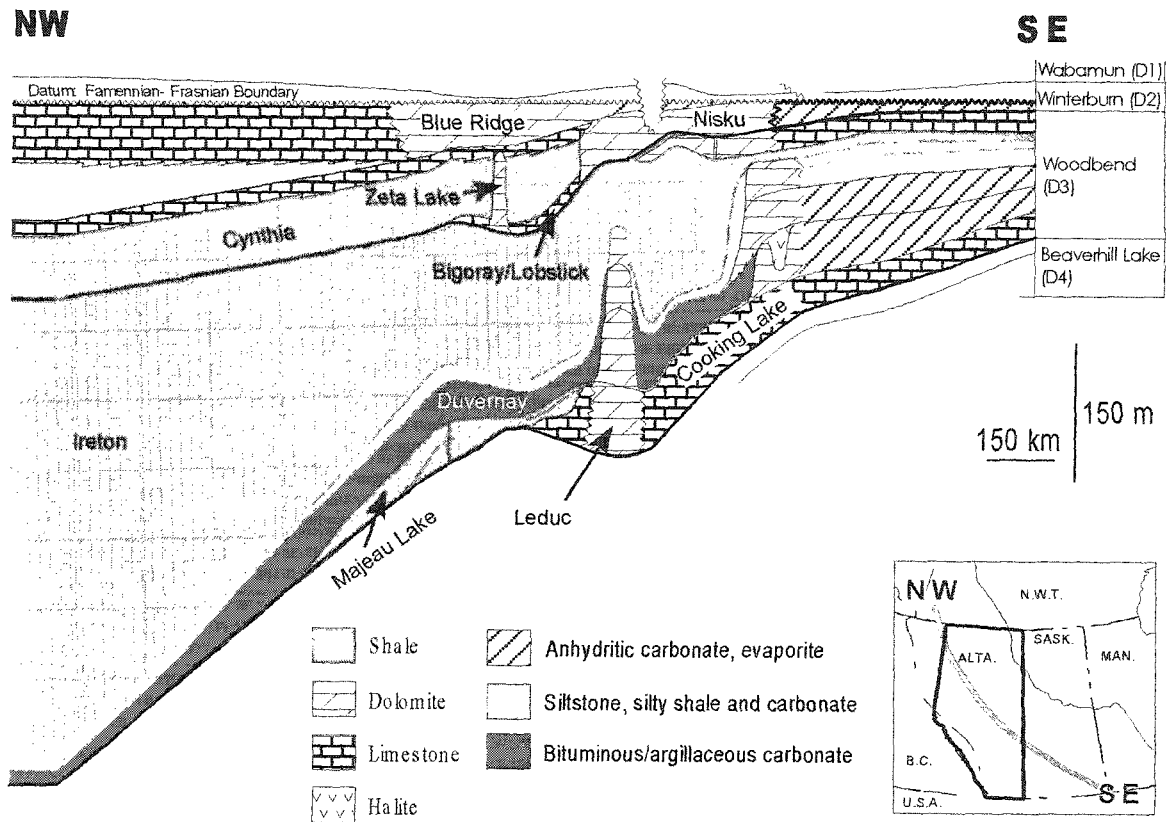


Fig.3.4: Schematic regional cross section showing the subdivision of Woodbend Winterburn strata (modified from Switzer et al., 1994).

The basin-fill in most parts of the Wild River basin is not easily correlated to the typical basin fill of the West Shale Basin in the Woodbend/Winterburn groups. In the West Shale Basin the infill usually consists of two thick shale packages for the Woodbend Group, i.e., the Duvernay and the Ireton shales, respectively. The Winterburn Group consists of interlayered shales, limestones and dolostones. In the Wild River Basin the time equivalent to the Upper Ireton and the Lower Winterburn is more carbonate-rich and has a higher porosity in most parts. This carbonate unit is here informally called the Berland

Carbonate. Note, however, that this unit is informally called the Berland Shale in the Calgary oil patch (McLean, pers. comm. 1999). The question that arises is whether this is a new member or merely a different sedimentation pattern that is governed by the proximity of surrounding reef complexes in the relatively small Wild River sub-basin.

Whalen et al. (2000) compared the Late Devonian Miette and Ancient Wall platforms (Fig. 3.1), which are equivalent to the Leduc (D3) platforms in the subsurface part of the SCCC. They described variations in platform margin geometry that are controlled by sea level and sediment supply. Slope and basinal sediments interfinger with progradational margins and onlap aggradational bypass margins of the build-ups. Redeposited carbonates were shed from the build-ups and adjacent upper slope as various types of gravity flow deposits. It is therefore concluded that the Berland carbonate is time-equivalent to the basinal Ireton and Duvernay shales. However, due to different internal architecture of the platform interior in the SCCC, the sediments are more carbonate rich and most likely were upper slope deposits shed from the surrounding reefs mainly from west to east. The basin-fill sediments of the West Shale Basin are fine-grained clastic sediments from a far-removed source and were deposited from east to west (Stoakes, 1980).

3.2 Methodology for Stratigraphy and Facies Interpretation

A total of 52 cores (Figure 3.5) were logged and sampled from the area of the SCCC and Wild River basin to investigate the local stratigraphy and facies distribution (see Appendix I for core list). Most of the cores were retrieved from the platform and reefs, whereas four are from the Wild River basin. The primary criterion for the core selection was to obtain a good aerial coverage for the SCCC and its regional extent. About 300 samples (see Appendix II for sample list) were taken from the core material and 150 polished thin-sections were studied with conventional and cathodoluminescence petrographic techniques, using a Zeiss Jenapol Polarizing Microscope and a CL microscope with a cold cathode Premier American Technologies ELM-3R Luminoscope. Operating conditions for CL petrography were a beam voltage of 15 to 10 kv and a beam current of 0.5 mA in a 35 to 50 mTorr vacuum under air pressure. The thin-sections were stained with Alizarin Red-S and potassium ferricyanide, according to the method of Dickson (1966). The samples were impregnated with blue epoxy to make the porosity more visible

Electric wireline logs provide information about formation tops, thickness of formations, lithology, porosity and type of formation fluid. About 250 well logs were used to construct cross-sections, isopach maps and structural maps to establish the geometry of the SCCC (see Appendix III for formation tops). Figures 3.6 to 3.8 show typical log responses for the various lithologies in the Upper Devonian strata that were used for the lithostratigraphic correlations in this study. Note that the cores only allow a small insight into one well whereas the logs cover the entire depths of a particular well.

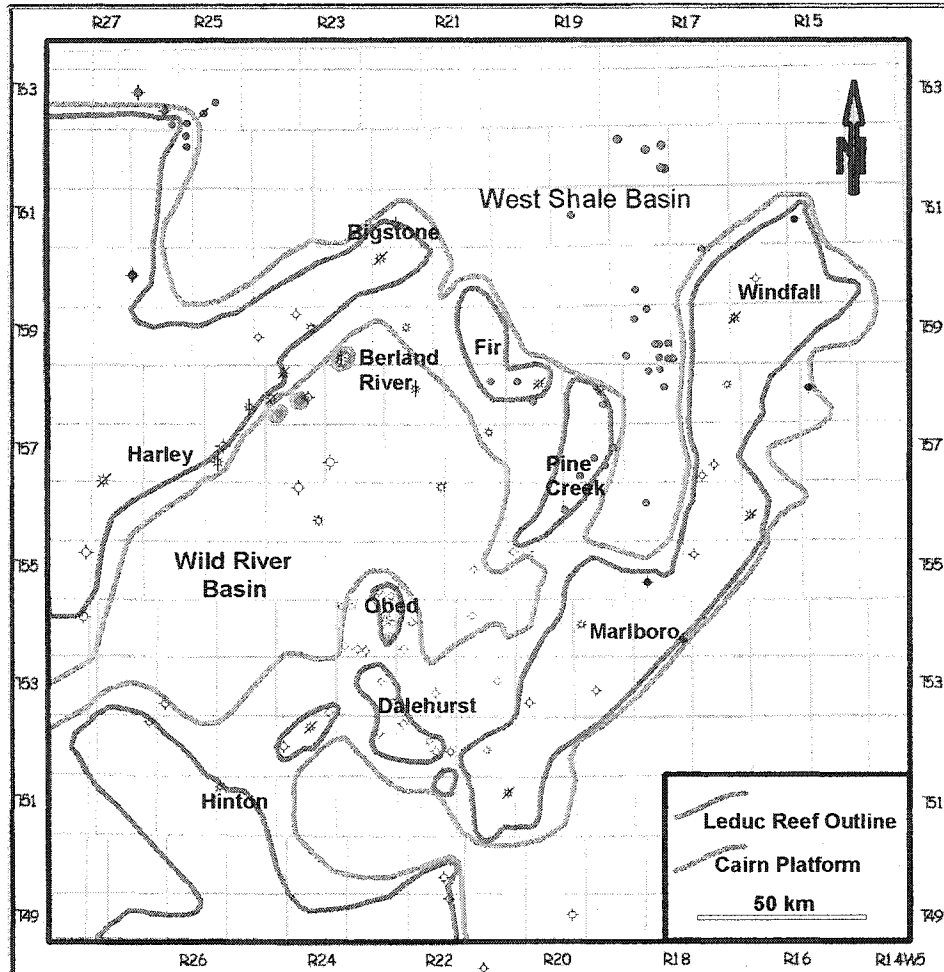


Fig. 3.5: Overview over the analyzed core material incorporated into this study.

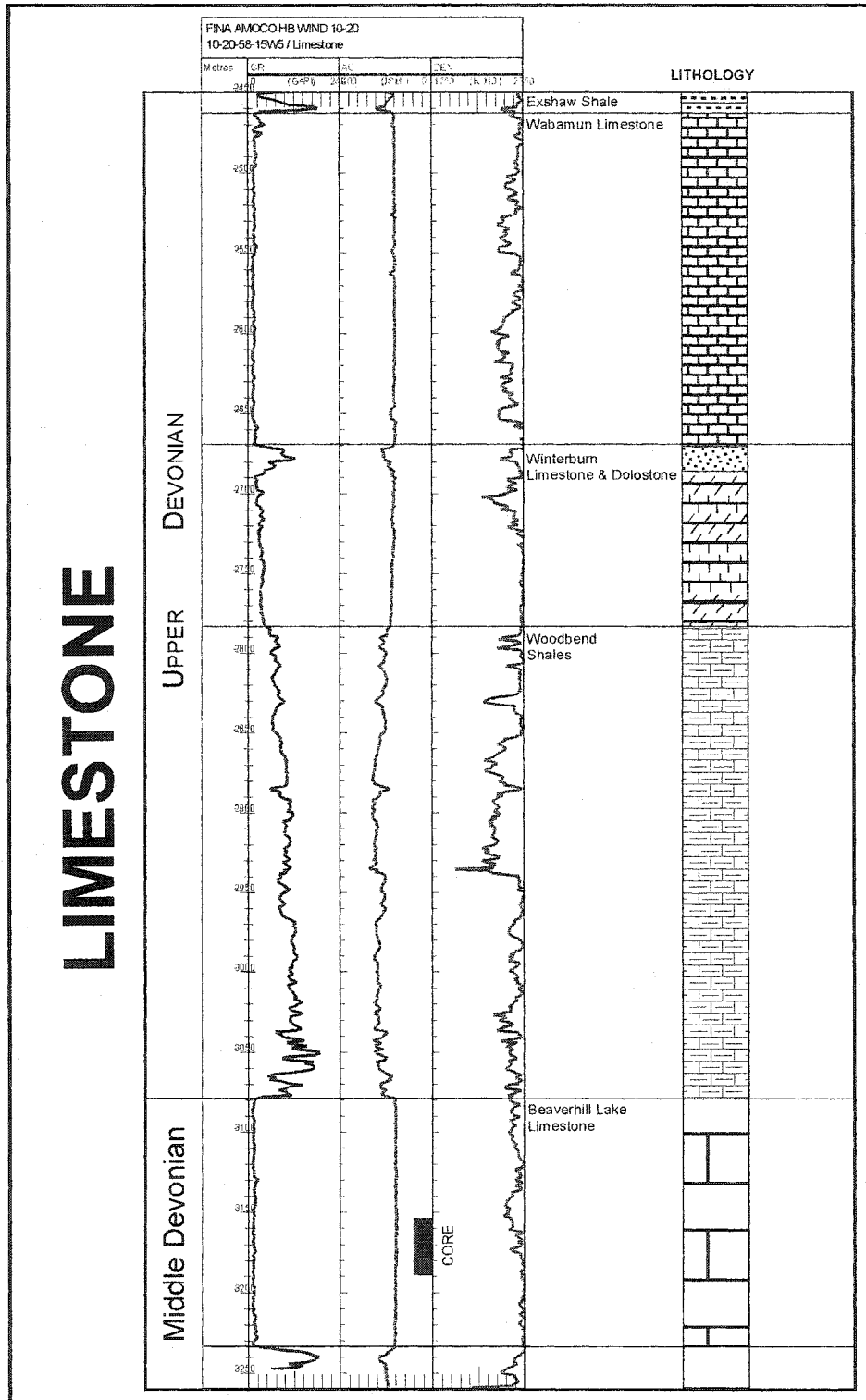


Figure 3.6: Typical log signals and lithology distribution that are characteristic for the Devonian strata in the northeastern part of the study area.

Alberta Deep Basin Core Example For Upper Devonian

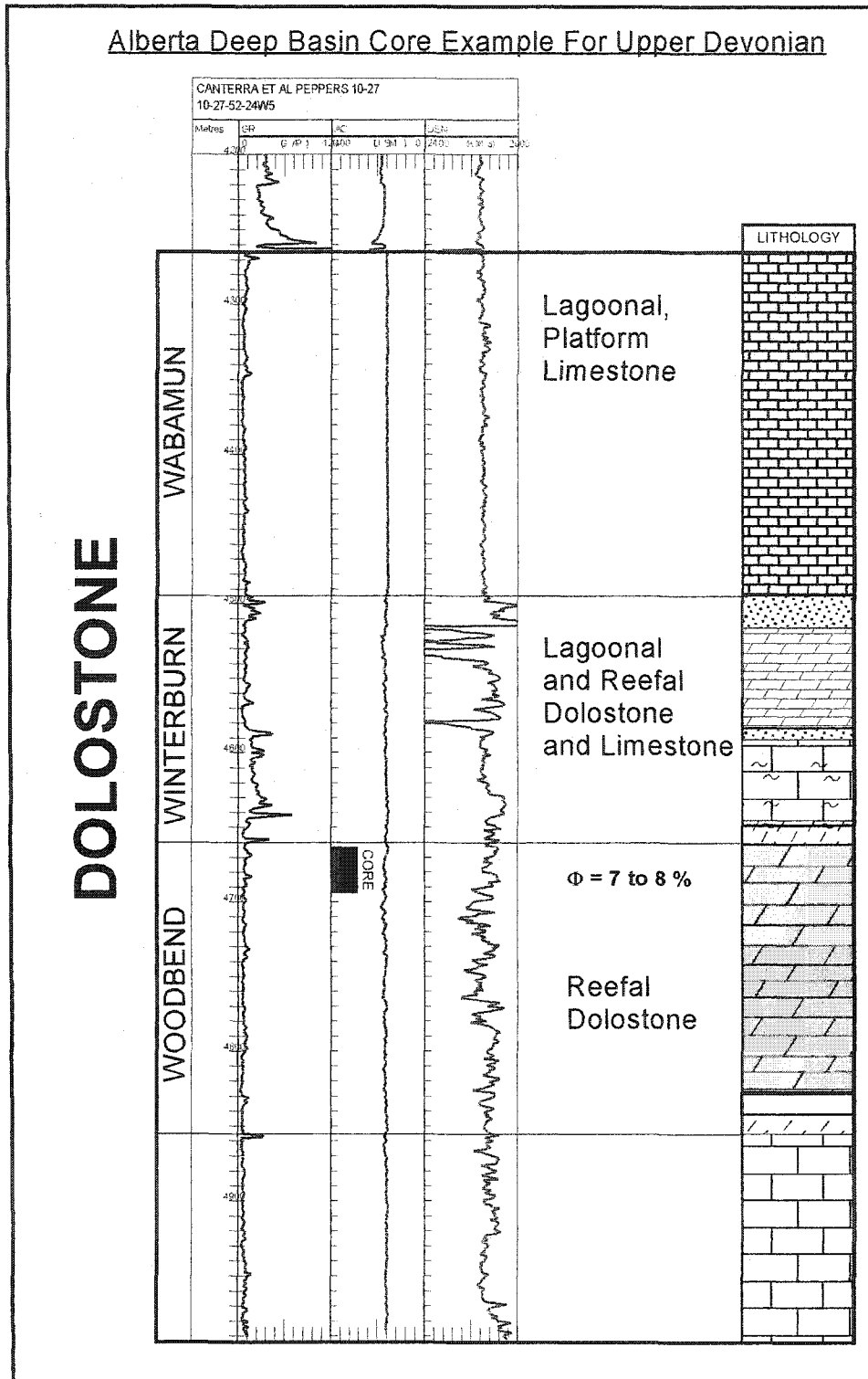


Figure 3.7: Typical log signals and lithology for a Leduc dolostone and Winterburn and Wabamun limestones and dolostones.

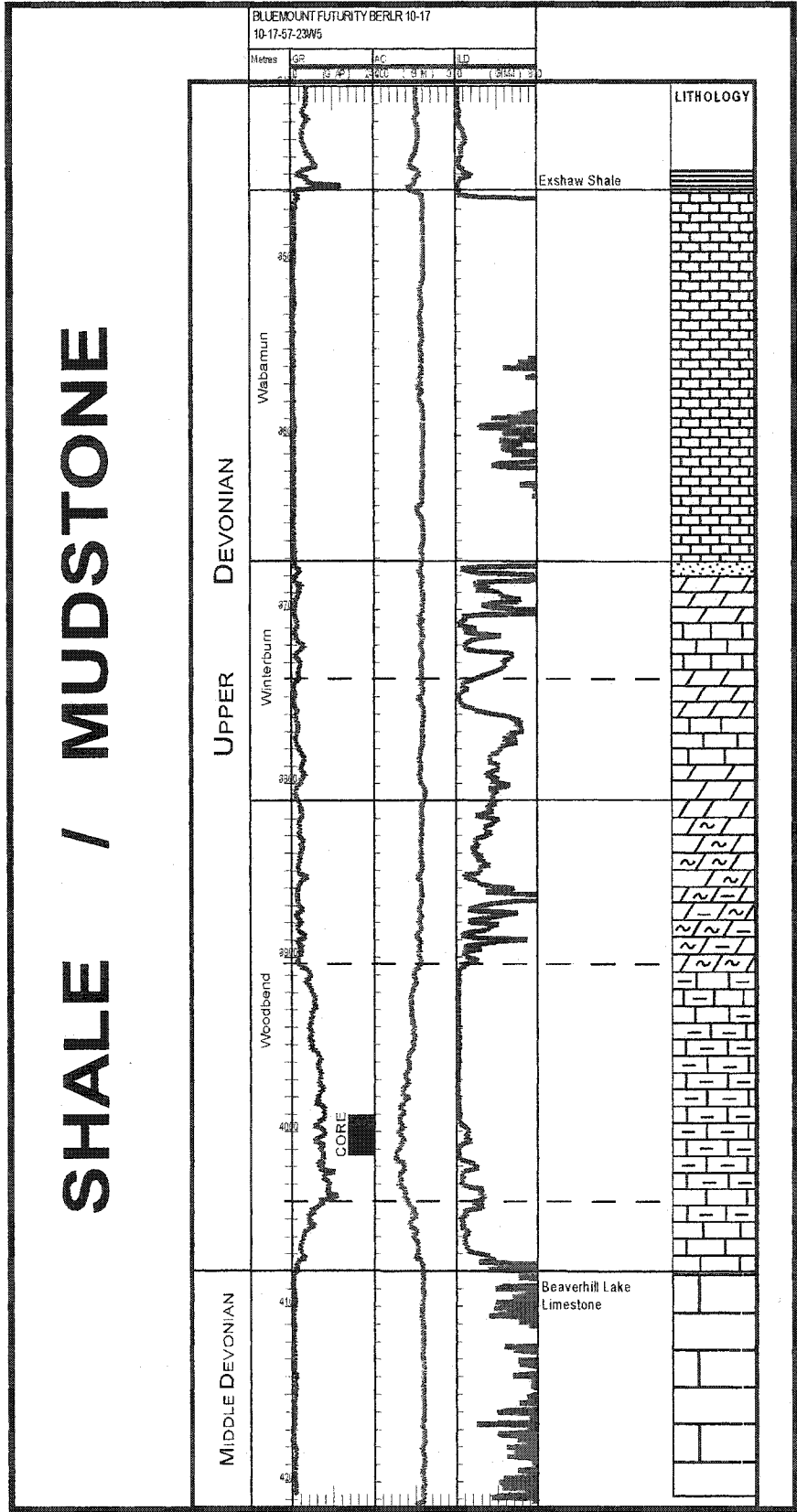


Figure 3.8: Typical log signals for the shale and argillaceous limestone succession in the Woodbend-Winterburn strata.

3.3 Lithostratigraphy

Beaverhill Lake Group (D4):

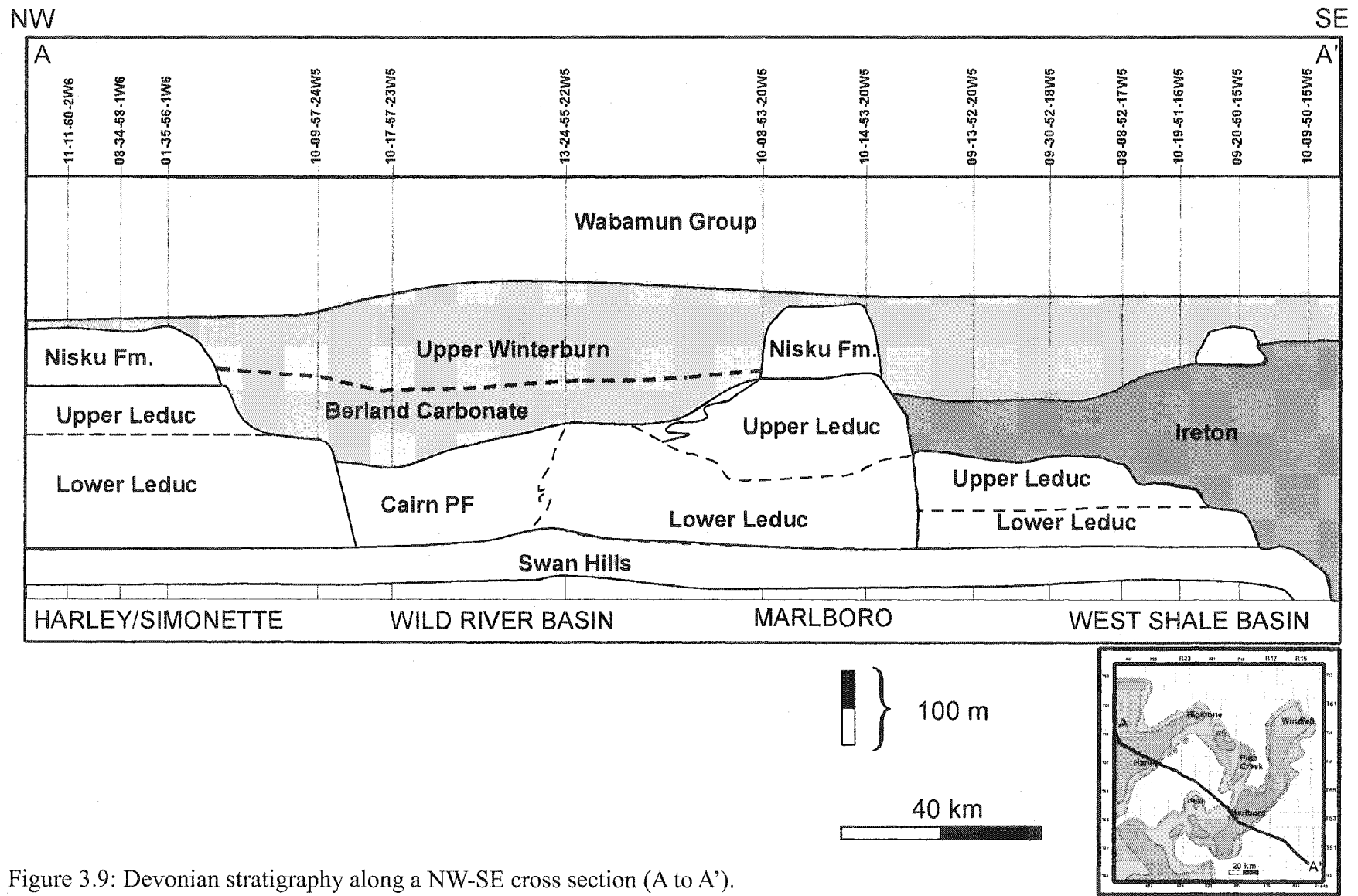
The Beaverhill Lake Group is divided into the Fort Vermilion, the Waterways, the Slave Point, and the Swan Hills formations in west-central Alberta. The Beaverhill Lake Group is generally between 150 and 220 m thick, however, it thins to zero around the Peace River Arch (Fig. 3.3).

The thinly bedded anhydrites of the Fort Vermilion Formation only occur north and east of the study area and in the central plains of Alberta with a thickness of ~40 m. However, they thin to the southwest to about 8 m in the Swan Hills area and are missing completely farther south in the Wild River area. The Waterways Formation is the basinal facies equivalent of the Beaverhill Lake Group and is about 200 m thick in northeastern Alberta, thinning towards the south and west to 6 m in the Swan Hills area. This formation consists of black shales, shaly limestones, and fossiliferous limestones that contain layers of ostracods and small to large brachiopods. They surround and overlay the platform and reef carbonates of the Slave Point and Swan Hills Formations, respectively. The Slave Point Formation forms the platform carbonate in the Beaverhill Lake Group and is made of massive dark gray to black limestones (Windfall area) that contain large stromatoporoids and irregular white calcite filled vugs in some locations. The Swan Hills Formation forms the reefs of the Beaverhill Lake Group that are between 15 and 150 m thick. The reefs are dolomitized along the platform margins and contain large amounts of various types of stromatoporoids. Some pelletoidal limestones with minor amount of bioclastic material indicate deposition under stressed conditions (Fluegel, 1982).

Woodbend Group (D3):

The Woodbend Group is the main target of investigation for this project, partly because core control within this group is best. The base of the Woodbend Group is formed by the Duvernay Formation (Figs. 3.3 and 3.4), which usually consists of interbedded dark brown, organic-rich shales, dark brown calcareous shales and dense argillaceous limestones (Imperial Oil, 1950). The thickness varies considerably from 60 m in the West Shale Basin to only a few meters in the Wild River area.

The Duvernay Formation shale is overlain by the Ireton Formation shale, which, in the West Shale Basin, is a dark grey to greenish shale or shaly limestone that contains thin layers of shell fragments of ostracods and small brachiopods. The Ireton Formation shale ranges in thickness from zero to 250 meters in the West Shale Basin (Fig. 3.9 and 3.10). Skilliter (1999) investigated both the Ireton and the Duvernay Formation shales more closely. The Ireton shale is especially thin on top of Leduc reefs as well as close to the limit of the disturbed belt (Figs. 3.10 and 3.11). In the Wild River area the upper part of the Ireton Formation is more calcareous than elsewhere and probably time-equivalent with the Lower Nisku Formation, thus it is here informally introduced as the “Berland Carbonate” (Tab. 3.1). The Berland Carbonate is thick in the west and thins to the east (Fig. 3.9), therefore, it probably was shed from the west into the Wild River basin. It consists of argillaceous limestones that appear to be more permeable than the Ireton Formation shales.



43 Figure 3.9: Devonian stratigraphy along a NW-SE cross section (A to A').

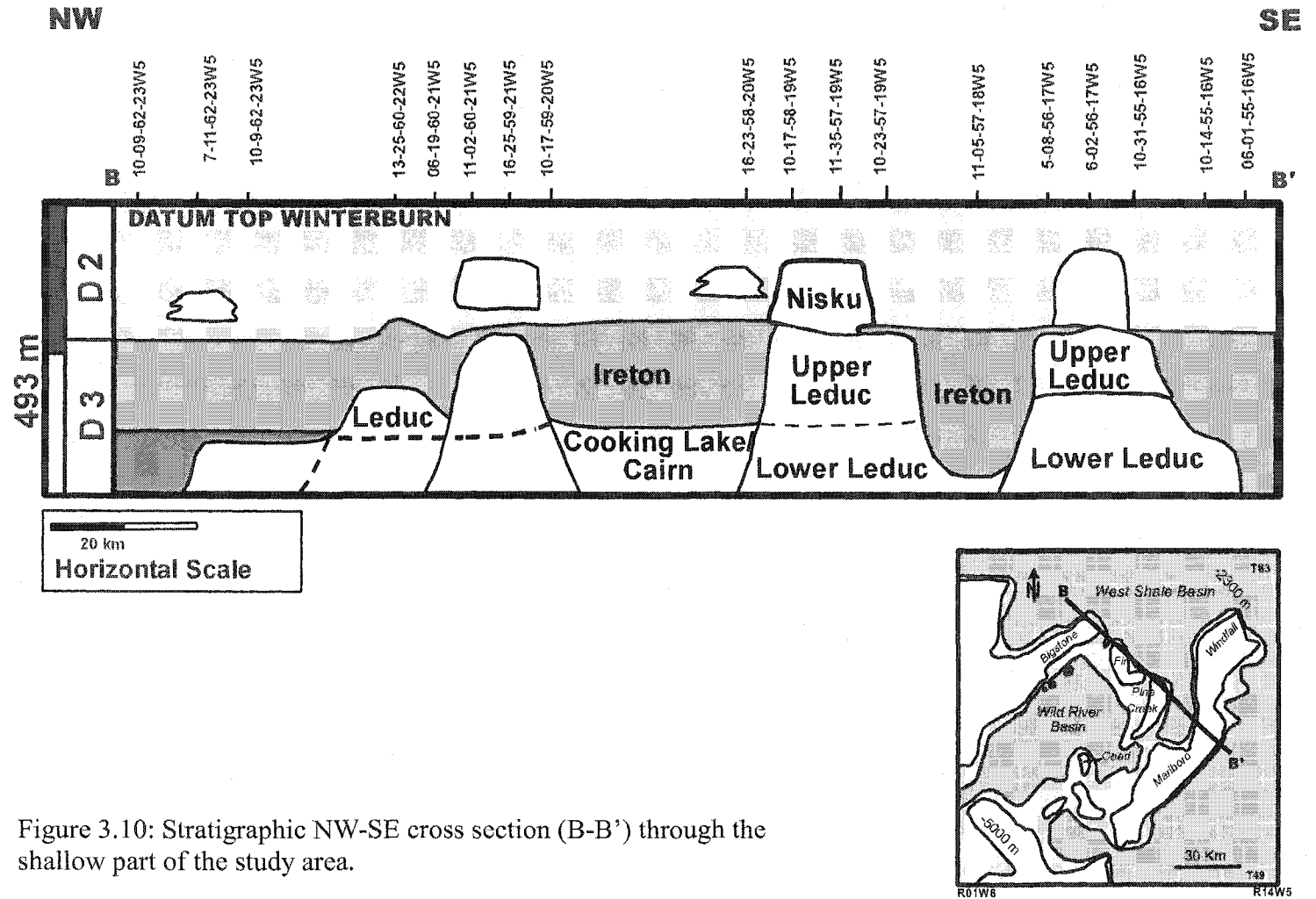


Figure 3.10: Stratigraphic NW-SE cross section (B-B') through the shallow part of the study area.

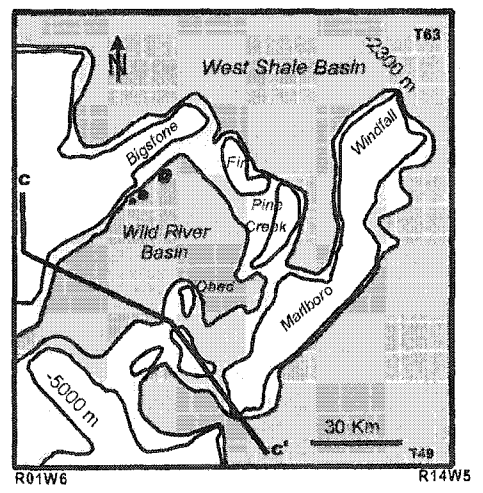
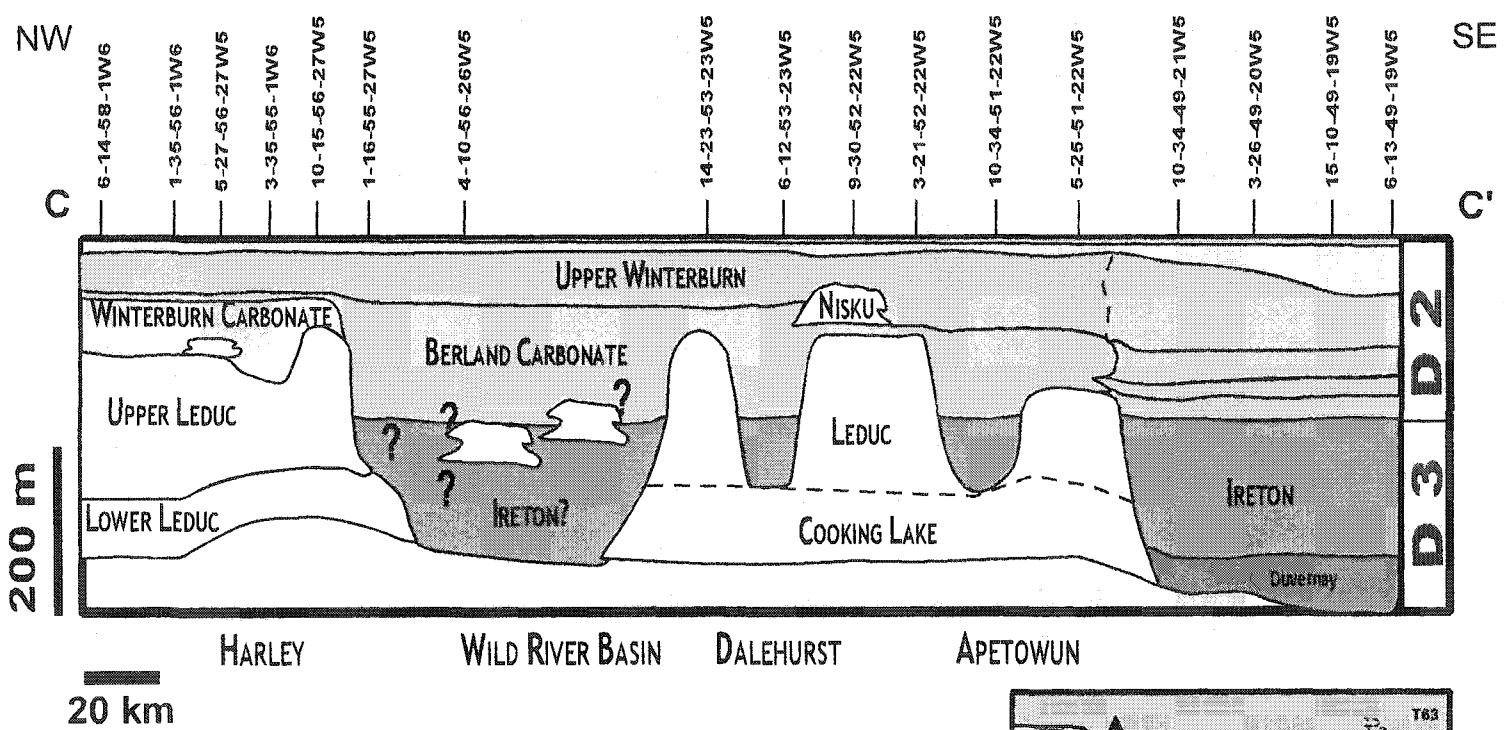


Figure 3.11: Stratigraphic NW-SE cross section (C-C') through the deep part of the study area.

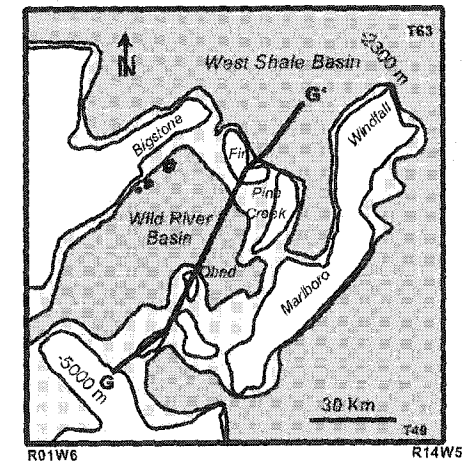
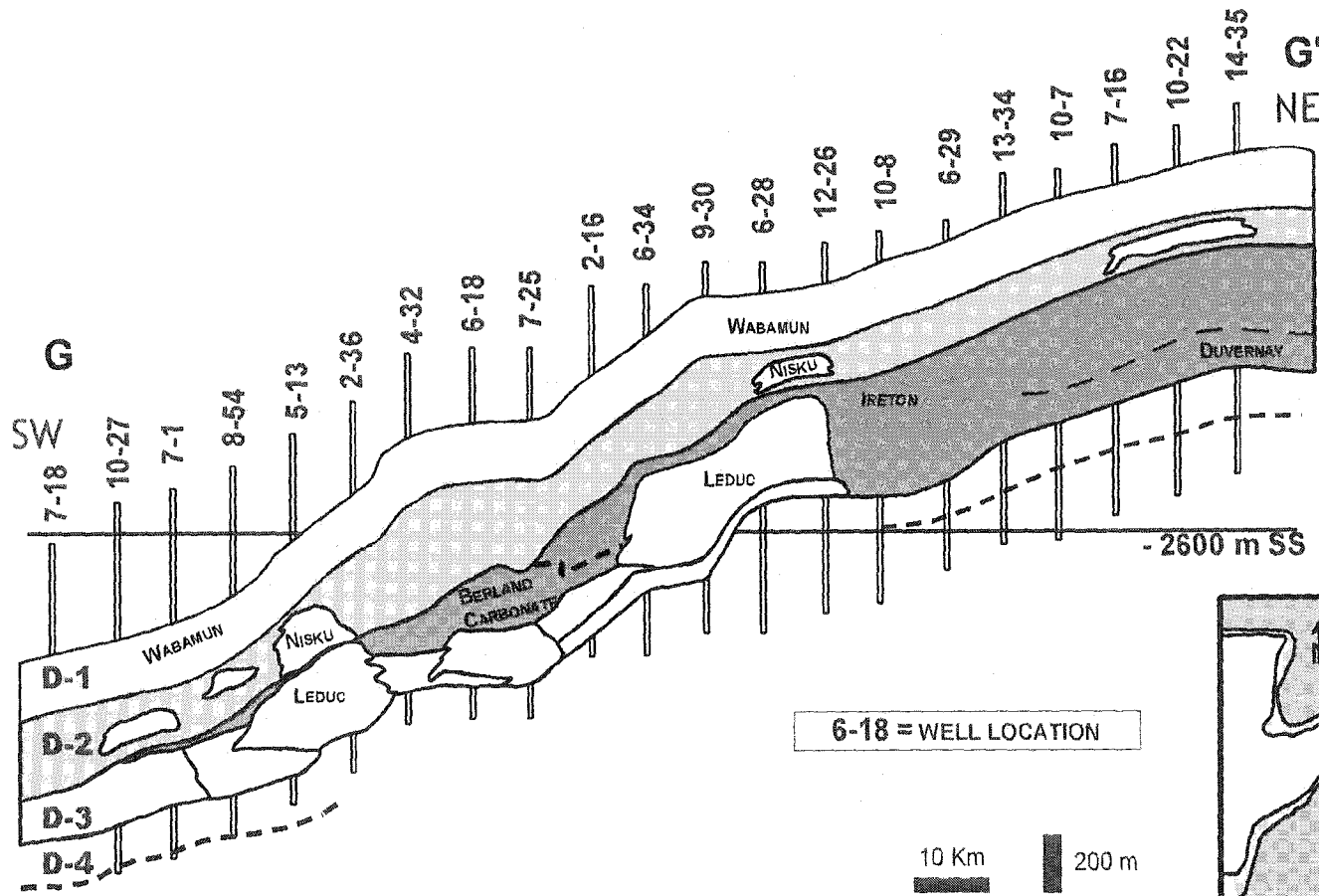


Figure 3.12: Devonian stratigraphy in a SW-NE cross section across the Wild River Basin. The carbonates of the four Devonian Groups form one continuous aquifer in the deep part of the basin (SE), but are subdivided by thick shales in the NE towards the West Shale Basin.

The Cooking Lake Formation forms the platform carbonates in the Woodbend Group and is equivalent to the Lower Leduc. It normally consists of light gray limestone, but is dolomitized locally. The Cooking Lake Formation reaches a thickness between 60m and 90m, and, in places, has Leduc reefs developed on it (Fig. 3.11). The lithologies of the Cooking Lake carbonates include nodular mudstones, grainstones, brown gray stromatoporoid rudstones, and floatstones. The overlying Leduc reefs are the main stratigraphic interval studied, because they contain the most prolific hydrocarbon reservoirs. The Leduc lithology varies in many ways according to the facies variation in a shallow water reef system (see also Whalen, et al., 2000). Most of these reefs are pervasively dolomitized, and the original facies patterns are largely destroyed. The reefs reach a thickness of up to 250 m.

Winterburn Group (D2):

The Winterburn Group consists of the Nisku, Blue Ridge, Calmar and Graminia formations (Tab. 3.1; Figs. 3.3 and 3.4). In the West Pembina area the Nisku Formation can be further subdivided into Lobstick, Bigoray, Zeta Lake, Dismal Creek, Cynthia and Wolf Lake Members (Tab. 3.1) (Chevron, 1979; Machel, 1984). In west-central Alberta the Winterburn Group is up to 350 m thick, and a division into Lower Winterburn and Upper Winterburn (Fig. 3-11; Table 3-1) is recommended, because the prominent shale break of the Cynthia Member is not always traceable. In the Wild River area another argillaceous carbonate unit seems to be time-equivalent with the Upper Ireton and Lower Winterburn, and was earlier introduced as the “Berland Carbonate” (Figs. 3.9 and 3.11;

see previous sections). In some parts of the study area the Lower Winterburn is an argillaceous to carbonate-rich unit with two predominant shale breaks. The Upper Winterburn has a higher carbonate content, however, irregular shale log peaks are common. Pure carbonate units, mostly dolomites of varying thickness, occur in the Lower as well as Upper Winterburn and are interpreted as Nisku reefs. The Calmar siltstone, the Blue Ridge carbonate, and the Graminia siltstone commonly overlie the Nisku Formation. The Blueridge carbonate consists of laminated dolomites and anhydrites, which formed during a sea level lowstand in the area.

Wabamun Group (D1):

The Wabamun Group overlies the three other Devonian packages and represents a major eustatic sea level rise that resulted in the deposition of a thick (250 m) succession of shallow-water ramp carbonates (Stoakes, 1992). The underlying Winterburn succession had filled in almost all of the preexisting topography in the WCSB, so that the Wabamun sediments are preserved as a rather monotonous package of low-angle mud-dominated ramps. The filling of the basin took place from the northwest resulting in the deposition of basinal shales followed by thick limestone sequences in northern Alberta. The Wabamun becomes increasingly dolomitic and eventually anhydritic in southeastern Alberta and southwest Saskatchewan.

In the SCCC study area, the Wabamun is represented mainly by a thick limestone succession with a few exceptions, e.g., Pine Creek (Green 1998), where it is dolomitized.

The four platforms form one contiguous carbonate package (Figs. 3.9 and 3.12) in the southwestern part of the study area where the above-described shaly formations are not developed.

3.4 Facies Development

The Middle- to Upper Devonian facies distribution in the WCSB has received considerable attention (e.g., Andrews, 1987; Anderson & Machel, 1989; Eliuk, 1989; Hedinger & Workum, 1989; Machel & Hunter, 1994). One enigma that remains in debate about the Devonian reefs is the dolomitization pattern. The spatial and temporal relationships between the sedimentary facies and the distribution of dolomite is of particular importance, as it might provide clues about preferential pathways for dolomitizing fluids.

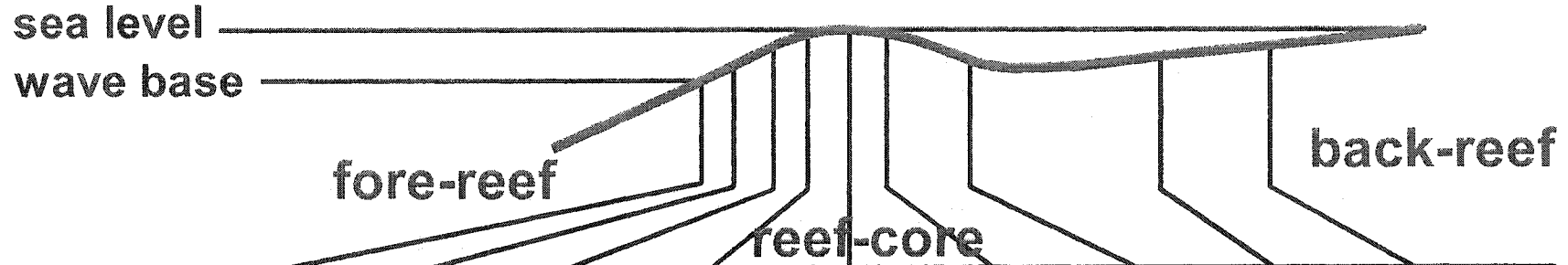
In the following discussion, the carbonate classification of Dunham (1962) (Table 3.2) and the facies model of Machel & Hunter (1994) (Fig. 3.13) are used to describe the facies types characteristic for the strata of the study area. Machel & Hunter (1994) have used a series of facies models that have been integrated into this thesis (see also references in Machel & Hunter). The facies zones have been adequately illustrated in Klovan (1964), Krebs (1972), and Weller (1991) and references cited therein. This section provides a detailed description of the depositional environments ending with a facies interpretation for the SCCC (Fig. 3.14). Included are specific primary fabrics and porosity patterns that provided sufficient pathways for the dolomitizing fluids.

The depositional environments for the SCCC carbonates are divided into a platform, reef and basinal setting, which include six platform/ reefal facies types and one basinal facies type.

ORIGINAL COMPONENTS NOT ORGANICALLY BOUND DURING DEPOSITION				ORIGINAL COMPONENTS ORGANICALLY BOUND DURING DEPOSITION				
of the allochems, less than 10% > 2 mm			of the allochems, more than 10% > 2 mm		BOUNDSTONE			
CONTAINS CARBONATE MUD (particles less than 0.03 mm Ø)		MUD ABSENT	matrix supported	grain supported				
MUD SUPPORTED		GRAIN SUPPORTED						
< 10% GRAINS	> 10% GRAINS							
MUD STONE	WACKE STONE	PACK STONE	GRAIN STONE	FLOAT STONE	RUD STONE	BAFFLE STONE	BIND STONE	FRAME STONE

Table 3.2: Textural classification of carbonates. Based on Dunham (1962), Embry & Klovan (1971) and James (1984).

MIDDLE-LATE DEVONIAN REEF FACIES MODEL



	I f	II f	III f	IV f	IVV	V	IV b	III b	II b	I b	
A	WATER ENERGY	quiet water below wave base	intermittently agitated water	slightly agitated water	moderately agitated water	strongly agitated water	moderately agitated water	slightly agitated water	intermittently agitated water	intermittently agitated water	
		negligible turbulence	episodic turbulence	moderate turbulence	strong turbulence	strong turbulence	strong turbulence	moderate turbulence	episodic turbulence	episodic turbulence	
	ROUNDING	mostly original fossil shapes	poor to good	moderate to good	good to moderate	very good to moderate	good to moderate	moderate to good	poor to good	mostly original fossil shapes	
SORTING	angular fragments if broken	matrix: good fossils: poor to good	matrix: moderate fossils: moderate to good	good to moderate	matrix: moderate fossils: poor	good to moderate	matrix: moderate fossils: moderate to good	matrix: good fossils: poor to good	angular fragments if broken		
B	TEXTURE	packstones grainstones mudstones	packstones grainstones rare floatstones	floatstones grainstones rare rudstones	rudstones bafflestones	rudstones bindstones rare grainstones	bindstones framestones rudstones	rudstones bafflestones	floatstones grainstones rare rudstones	packstones grainstones	mudstones wackestones
C	AMOUNT OF MICRITE	primary micrite increasing SS				fibrous calcite, sparite, micrite		→ primary micrite increasing			
D	POROSITY TYPES	intraparticle	intraparticle interparticle	interparticle shelter voids intraparticle	shelter voids growth framework interparticle	shelter voids interparticle	shelter voids growth framework interparticle	shelter voids growth framework interparticle	shelter voids intraparticle interparticle	intraparticle fenestral	intraparticle fenestral
	SIZE OF PORES		small	medium to small	medium to small	large to medium	medium to small	large to medium	medium to small	small	
	AMOUNT OF POROSITY	below 10%	up to 10% but mostly below 5%	up to 15%	up to 10%	up to 25%	up to 10%	up to 40%	up to 10%	up to 20%	up to 30%
E	FOSSIL ASSEMBLAGE	calcspheres foraminifers	small crinoids	large crinoids	tabulate corals <i>Stachyodes</i> brachiopods crinoids <i>Girvanella Renalcis</i>	crinoids tabular stromatoporoids	bulbous & massive stromatoporoids micrite envelopes syntaxial rim cements	<i>Stachyodes Girvanella Renalcis</i>	<i>Amphipora Parathurammina</i> ostracods	algae (fenestral pores)	algae (fenestral laminites)
F	INDICATOR FOSSILS	crinoids / goniattites / brachiopods				crinoids <i>Solenopora</i> <i>Keega</i>		<i>Amphipora</i> <i>calcspheres</i> / <i>Parathurammina</i> <i>Vermiporella</i> encrusting <i>Sphaerocodium</i>			

Figure 3.13: Facies model from Machel and Hunter (1994).

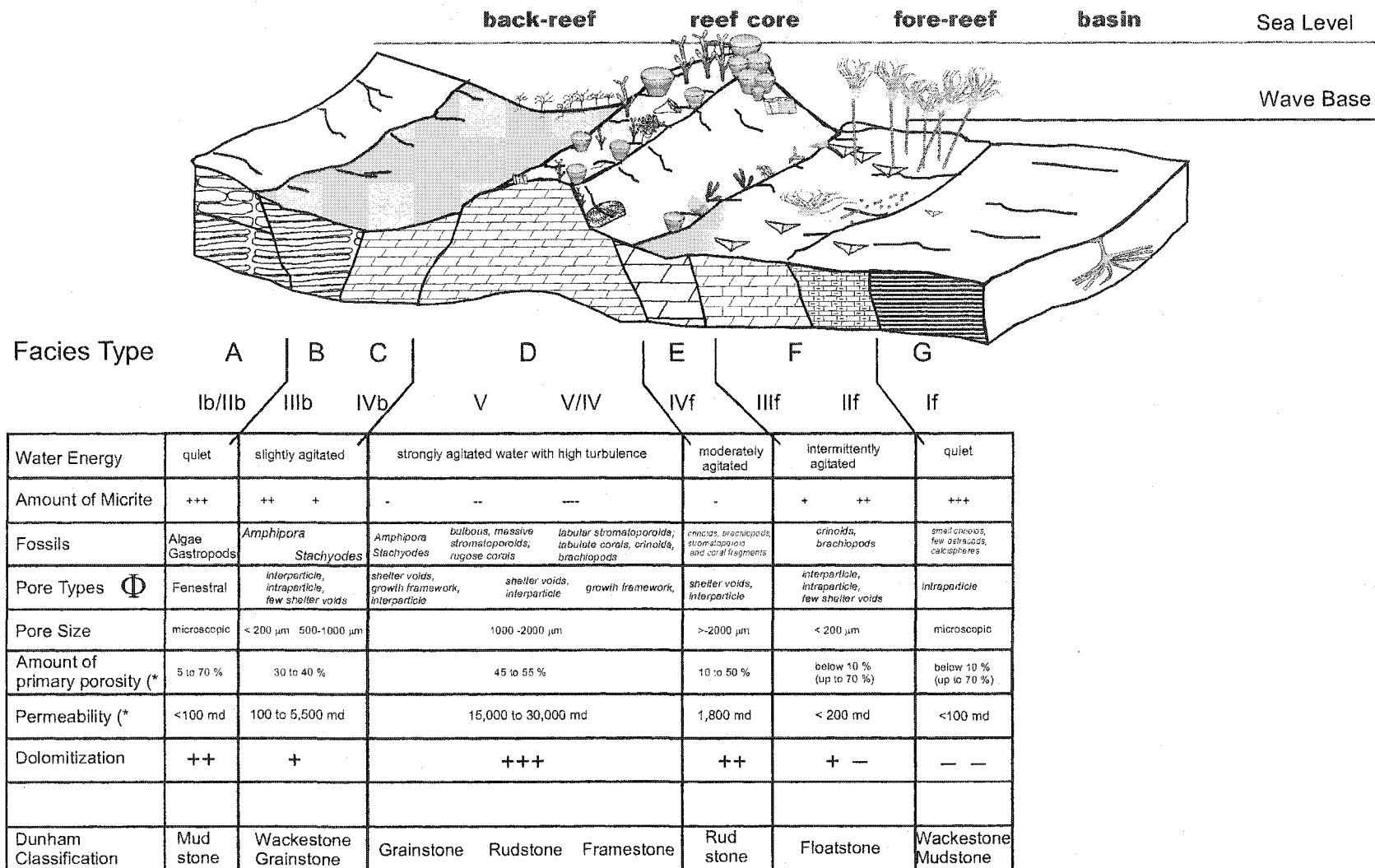


Figure 3.14: Facies model for the carbonates in the Southesk Cairn Complex (* porosity & permeability estimated after Lucia (1999) and references cited therein).

Facies type A: “Laminated dolo-mudstone with anhydrite”

A medium to light gray, fine grained (< 4 µm) mudstone with laminae of dolomite and anhydrite is representative of an intertidal to lagoonal setting. This facies type contains fenestral pores that are elongated parallel to bedding, a few gastropods, as well as small chain-like accumulations of framboidal pyrite (<25 µm). The interlayering of anhydrite and dolomite represents frequent changes in seawater salinity due to episodic periods of flooding and evaporation. The laminae probably were formed by algae activity in a saline environment, with only a few organisms that fed on the algal mats. This facies type corresponds to facies zones **Ib** and **IIb** of Machel and Hunter (1994), which refer to a quiet back-reef environment with intermittently agitated water that is occasionally interrupted by storms. The primary porosity in these rocks is usually less than 3 % and permeabilities are also low. According to Machel and Hunter (1994) the porosity increases to 30 %, where fenestral pores are well developed.

Facies type B: “Sparsely fossiliferous wackestone to packstone”

Medium gray to light gray wackestones to sparsely fossiliferous packstones. The rocks consist of fine-crystalline micrite and dolomitic micrite with a few *Amphipora* sp. and minor amounts of other fossils. This facies type represents the shoreward part of a shallow lagoon and the scarcity of fossils reflects a shallow area with open water circulation, with possibly slightly higher salinities than normal, and/or terrigenous input (Fluegel, 1972). The primary porosity is low (<3%) due to the generally high mud content, but was enlarged after fossils became dissolved and moldic pores were formed. The

Amphipora- bearing wackestone/packstone facies corresponds with the zones **IIIb** and **IIIb** of Machel and Hunter (1994) and gradually changes into the next facies, type C.

Facies type C “Fossiliferous floatstones to grainstone”:

This light gray to medium gray floatstone to grainstone facies usually contains abundant *Amphipora* and a variety of laminated/tabular stromatoporoids, smaller bivalve fragments, coral fragments, as well as peloids and other coated grains. The fabric is either grain-supported and/or mud-supported, however, the primary porosity is in both cases high and can reach up to 30 %. This facies type is characteristic of back reef areas. Facies type C corresponds to Machel & Hunter’s (1994) zones **IIIb** and **IVb**, with moderate to strong water turbulence. The main pore types are shelter voids, intraparticle and interparticle pores.

Facies type D: “massive stromatoporoid frame- to boundstone”

The massive stromatoporoid frame- to boundstone facies constitutes the parts of the reef crest facies. The light gray rocks consist almost completely of massive stromatoporoids, and their colonies can reach up to several m in size. Among the abundant smaller frame work builders are *Stachyodes* sp., tabular and bulbous stromatoporoids, as well as thamnoporoid corals. The main porosity types are shelter voids, growth framework, and interparticle pores. The porosity is on average between 6 to 7 % but reaches up to 15%

with good to very good permeabilities up to 170 md (calculated from core analyses). In rare cases where this facies is preserved as limestones, they have low and insignificant porosity and permeability, and contain some very well preserved early marine diagenetic products (see Chapter 4). Facies type D corresponds to Machel and Hunter's (1994) zone V and V/IV, which they describe as the reef core with a rigid framework that formed in strongly agitated and turbulent waters.

Facies type E: "fossiliferous rudstone"

The fossiliferous rudstone facies represent a high-energy, proximal fore reef environment. The medium-gray to light gray rocks contain large amounts of fossils, including thick bulbous stromatoporoids, rugose and tabulate coral fragments, crinoids, and brachiopods. The porosity is formed by shelter voids, growth framework, and interparticle pores. The overall porosity in this facies type reached up to 24 –30 %, but part of this porosity is secondary and due to intensive dissolution of fossil fragments. These rocks form the best reservoir rocks in the study area, with permeabilities up to 200 md (core analyses). Facies type E corresponds to zones IV/V and IVf of Machel and Hunter (1994).

Facies type F: “floatstones”

Fine- to medium grained, mud-rich floatstones of facies F contain a few fragments of stromatoporoids and corals, whereby crinoids and brachiopods are the most abundant fossil assemblage. The water was slightly agitated with episodic turbulence, which led to the accumulation of crinoid grainstones in depressions and/or channels. The primary porosity in this facies type is mainly interparticle and shelter voids, commonly below 5 % with accordingly low permeabilities (core analyses). Facies type F represents zones **IIIF** and **IIF** of Machel and Hunter (1994).

Facies type G: “mudstones”

Dark-gray, fine-grained mudstones represent the basinal facies in the study area. Argillaceous limestones and marls are predominant with small amounts of ostracods and calcispheres. The water was usually quiet and below fair weather wave base. The porosity and permeability is low due to a high content of mud in the sediments and low amount of bioclastic material. However, this was different in areas where the rocks contain relatively high amounts of carbonate and/or where they thin above reefs. In these cases they appear to have enough porosity and permeability to qualify as leaky aquitards, e.g. Bigstone, Windfall and Obed (Fig. 3-11). Facies type G is equivalent to Machel and Hunter's (1994) zone **IF**, which represents a basinal setting in front of the reef / platform slope.

3.5 Sequence Stratigraphy

Sequence stratigraphy has been applied only in recent years to the Frasnian carbonates of the WCSB (Switzer et al., 1994; Wendte et al., 1992; 1994; 1998; van Buchem et al., 2000). However, no sequence stratigraphic analysis has been done in the study area of the SCCC. Nevertheless, data from some neighboring can be used, within limits, for comparison.

The following account of sequence stratigraphy in the Woodbend/Winterburn Group (Fairholme Group) strata is based on a comparison of the Miette and Redwater buildups by van Buchem et al. (2000). This example was chosen because the Miette buildup crops out in the Rocky Mountains close to Jasper, and the Redwater buildup is a subsurface equivalent just northeast of Edmonton, and thus very similar to the strata in the Wild River area. The sequence stratigraphy of this area is presented in Figure 3.15, and the corresponding conodont biostratigraphy is shown in Fig. 3.16.

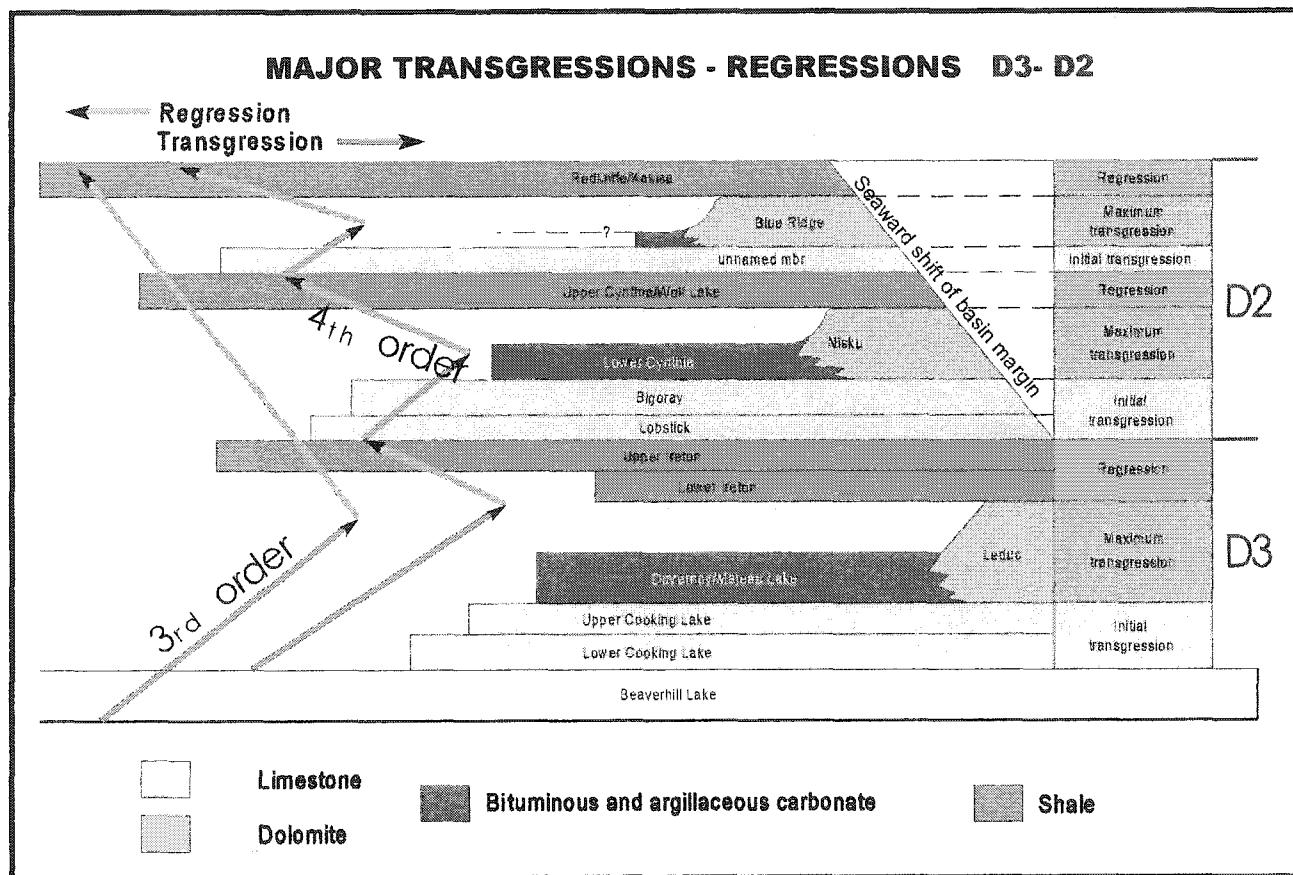


Figure 3.15: Major eustatic sea level changes and stratigraphy of the Woodbend (D3) and the Winterburn (D2) Groups in the Western Canada Sedimentary Basin. The D3-D2 represent third-order cycle, superimposed upon which are several fourth order cycles. Diagram is modified from Switzer et al. (1994).

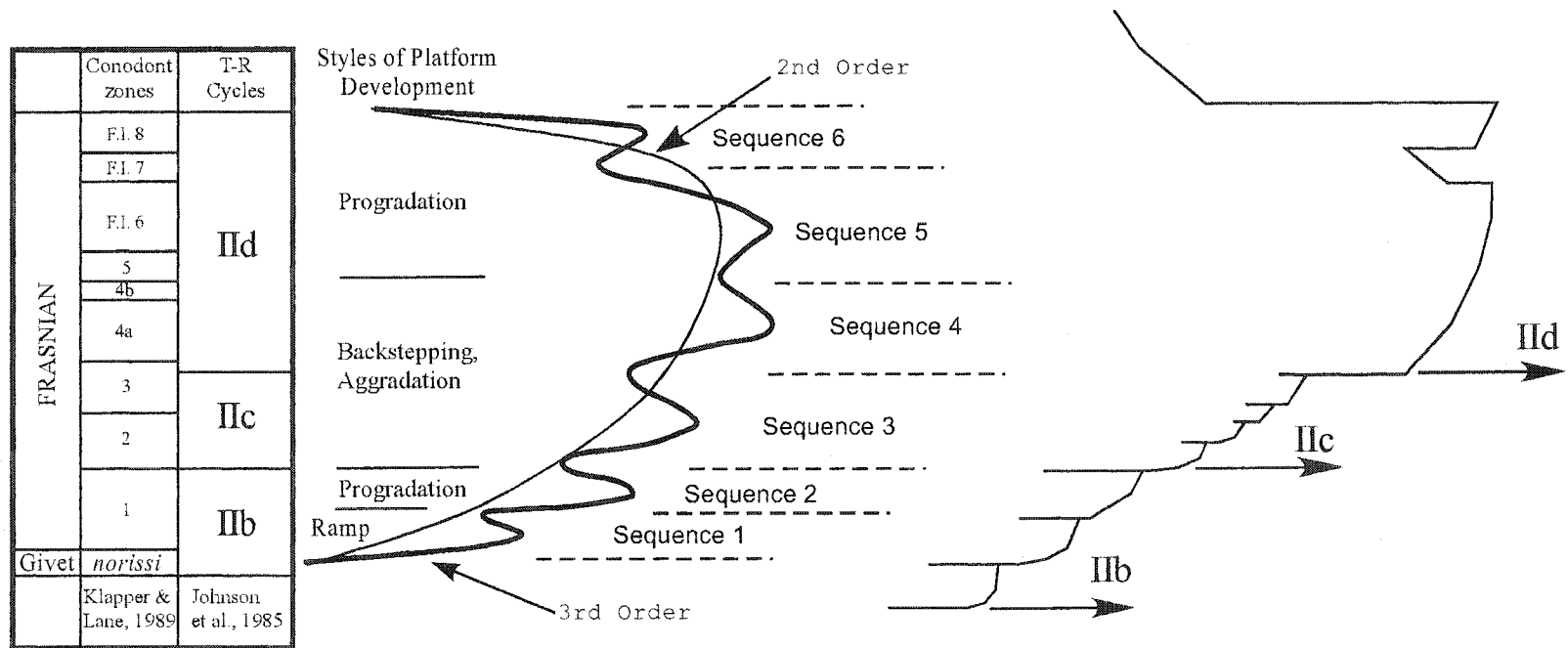


Figure 3.16: Sequence stratigraphy, patterns of platform development, and interpreted Upper Frasnian second- and third-order sea level curves based on the study by van Buchem et al., 2000. Conodont zonations (Klapper and Lane, 1989) and the sea level curve of Johnson et al. (1985) are also illustrated. Modified after van Buchem et al. (2000).

The Miette buildup has a total thickness of approximately 450 m and represents a 2nd order, transgressive-regressive depositional sequence. An initially flat platform, or low gradient homoclinal ramp (Flume Formation) developed into isolated, rimmed, carbonate platforms (Cairn and Peechee members), with onlapping, organic-rich basinal deposits (Perdrix Formation). Subsequent flooding deposited basinal shales (lower Mt. Hawk Formation) on top of the platform. Clays of the Upper Mt. Hawk Formation filled the basin, allowing the platforms (Arcs and Ronde Members) to prograde basinward. In general, the distribution of carbonate, clays, silts, and organic matter vary both in a vertical and lateral sense during the 2nd order sequence as shown in the geochemical logs. Furthermore, van Buchem et al. (2000) identified six medium-scale depositional sequences (3rd order) within the overall transgressive-regressive cycle. Thicknesses in each sequence vary on the platform between 60 and 100 m, and in the basin between 25 and 170 m.

Van Buchem et al. (2000) distinguish three orders of sequences in the Redwater buildup: a) the long-term 2nd order sequence, which covers the entire Woodbend/Winterburn succession; b) the 3rd order sequences, which correspond to packages at the decameter to hectometer scale; and c) 4th order sequences, which correspond to packages at the meter to decameter scale, and are referred to as cycles. The 2nd order transgressive-regressive depositional sequence has a total thickness of approximately 425 m. Carbonate reefs/build-ups developed on top of the flat, shallow- water platform of the Cooking Lake Formation during an overall sea level rise. These reef build-ups are surrounded by basinal black shales of the Duvernay Formation. During the last phase of the 2nd order

transgression, large amounts of clay accumulated in the basin (Ireton Formation), reducing the carbonate production during maximum flooding. Subsequently, the next generation of carbonate platforms prograded out during an overall regression (Nisku Formation and Blue Ridge Member/Calmar Formation).

Within the overall transgressive-regressive cycle six medium-scale depositional sequences (3rd order) were defined (Fig. 3.16). The thickness of each sequence varies in the platform between 165 and 40 m, and in the basin between 155 and 30 m.

3.6 Hydrostratigraphy

The hydrostratigraphy of the Devonian succession (i.e., subdivision into aquifers and aquitards) may be inferred from the general lithology of the stratigraphic formations in combination with hydrostratigraphic delineations from previous, hydrogeological investigations in the literature (e.g., Hitchon, 1969a,b; Hitchon, 1984; Hitchon et al., 1990; Bachu, 1995; Michael et al., 2000) (Fig. 3.17). In a general sense, the hydrogeological terms “aquifer” and “aquitard” are equivalent to the terms “reservoir rock” or “carrier bed”, and “source rock” or “seal”, respectively, which are used in petroleum geology.

The crystalline Precambrian basement forms the lower boundary for the entire stratigraphic succession, and is considered to act as a basin-wide aquiclude (Toth, 1978; Hitchon et al., 1990; Bachu, 1995). Middle Cambrian sandstones form the thin Basal

Sandstone aquifer (Bachu et al., 1986). This aquifer is confined at the top by the Middle - Upper Cambrian aquitard, consisting of interbedded shales, siltstones and carbonates. The Cambrian is absent in the northwestern corner of the study area due to non-deposition or erosion, and here Devonian sediments directly overlie the crystalline basement.

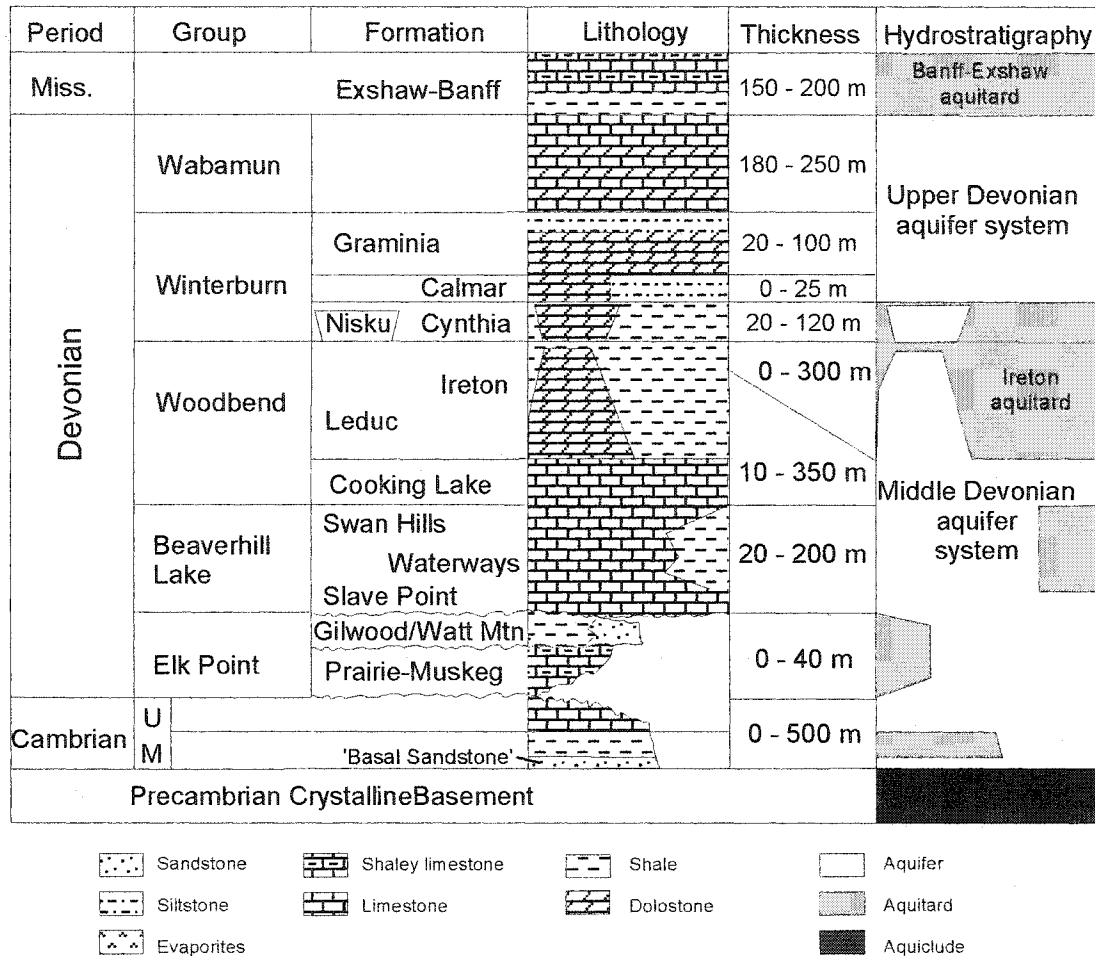


Figure 3.17: General lithology and hydrostratigraphy of the Cambrian-Devonian succession in the study area (from Michael 2002).

Mixed near-shore clastics of the Elk Point Group, derived from the Peace River Arch and Western Alberta Ridge landmasses, and a thin succession of carbonates at the top of the

underlying Cambrian, form the so-called Elk Point aquifer. The carbonates of the Beaverhill Lake and Woodbend Groups form a major aquifer system with enhanced hydraulic permeability in the dolomitized reef structures and along the reef margins of the Swan Hills and Cooking Lake platforms. On a regional scale the Elk Point and Woodbend-Beaverhill Lake aquifers represent one contiguous aquifer system within the study area. Along some platform edges, however, the thin intervening Watt Mountain and Waterways shales form local aquitards at the top of the Elk Point and within the Woodbend-Beaverhill Lake aquifers, respectively.

The Woodbend Ireton shales constitute the major aquitard in the study area, separating the Woodbend-Beaverhill Lake carbonate aquifers from the overlying Upper Devonian aquifer system, consisting of the Winterburn and Wabamun Groups. The Ireton aquitard thins considerably over many of the Woodbend Leduc reefs in the Southesk-Cairn Complex, and cross-formational flow at such locations has been identified in other parts of the Alberta Basin (Bachu & Underschultz, 1993; Hearn, 1996; Rostron & Toth, 1997; Anfort et al., 2001). The isolated reefs and restricted platform carbonates to argillaceous basin-fill sediments in the lower part of the Winterburn Group form a somewhat discontinuous aquifer due to the laterally heterogeneous permeability distribution. In contrast, the silty dolostones and siltstones of the Graminia Formation in the upper part of the Winterburn Group form a thin aquitard at the top of the Winterburn Group. Overlying the Graminia Formation are massive, partly dolomitized limestones of the Wabamun Group (Saller & Yaremko, 1994), which act as an aquitard only in the non-dolomitized areas, particularly in the southern half of the study area.

All shaly aquitards within the Devonian succession, from the Watt Mountain to Graminia, thin out southwestward near the deformation front. Here the entire Devonian succession forms one contiguous, stacked aquifer system (Skilliter, 1999; Buschkuehle & Machel, 2001; 2002). The Carboniferous shales of the Exshaw and Lower Banff formations form a thick, continuous aquitard at the top of the entire Devonian hydrostratigraphic succession.

CHAPTER 4: DIAGENESIS

The Devonian carbonates of the SCCC underwent a complex diagenetic history. The paragenetic sequence of the complex (Fig. 4.1) shows both similarities and distinct differences compared to other Devonian carbonates in the Alberta Basin, which is due to their deep burial (Kaufman et al., 1990; Amthor et al., 1993; Marquez & Mountjoy, 1996; Machel, 2000). The carbonate rocks contain 22 distinct diagenetic products, which reflect diagenetic realms ranging from the syndepositional environments to deep burial (max. ~7 km). Among the diagenetic products are four major types of dolomite (dolomite Type 1 to 4). Some of the diagenetic products are confined to specific locations, but most of them occur throughout the carbonate complex. The 22 products reflect five main stages of pore water evolution (Fig. 4.2). These stages can be fitted to the four diagenetic settings/stages or environments as distinguished by Machel (1999) (Fig. 4.3) into: 1) near-surface environments, 2) shallow burial (between 300 and 1000m), 3) intermediate burial (2000 to 3000 m) and 4) deep burial (below 2000-3000m). In addition, a fifth diagenetic stage corresponds to the present day depths and processes in the reservoirs.

Diagenesis greatly influenced the porosity and permeability of the reservoir rocks, and modified the reservoir quality. This chapter includes a detailed description of the diagenetic products and an interpretation of their respective diagenetic realms. It also will provide insight into the porosity and permeability modification during diagenesis.

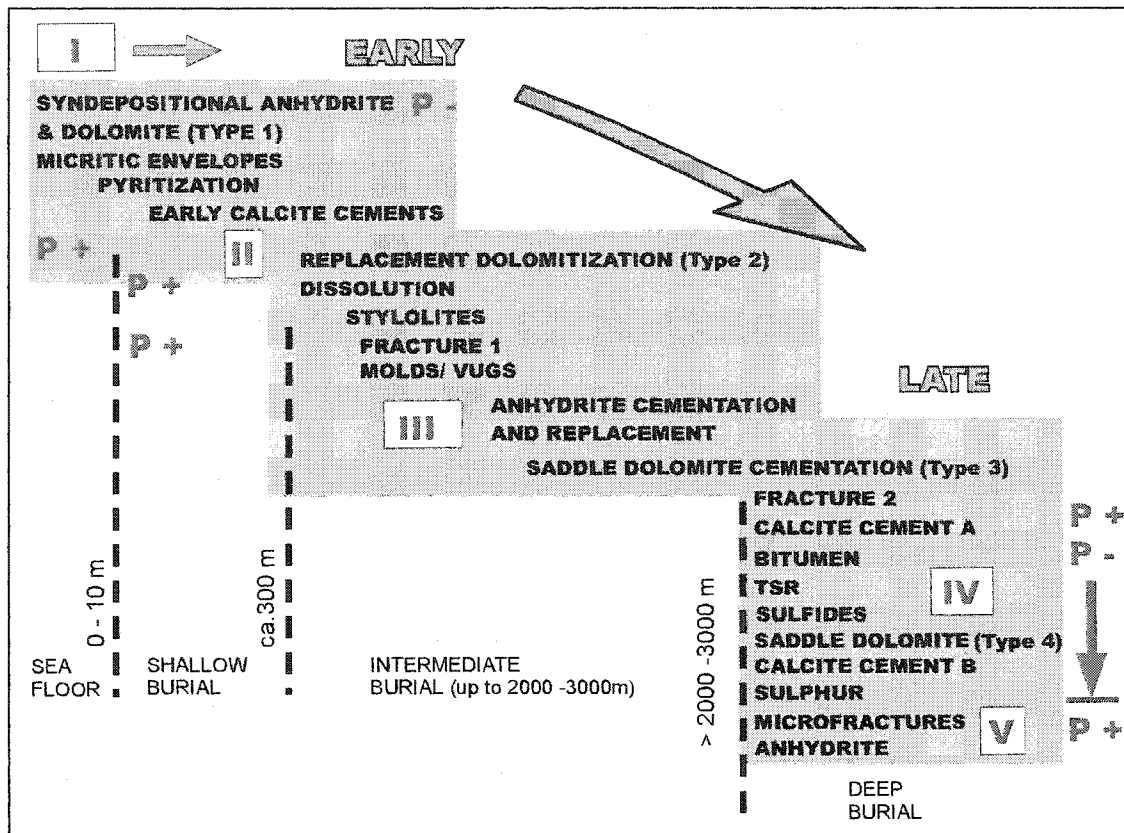


Figure 4.1: Diagenetic paragenesis of the Southesk-Cairn Complex from petrographic examination of core, hand samples and thin sections. Roman numerals indicate fluid events/ diagenetic stage and P+ indicates increase in porosity, whereas P- indicates decrease in porosity.

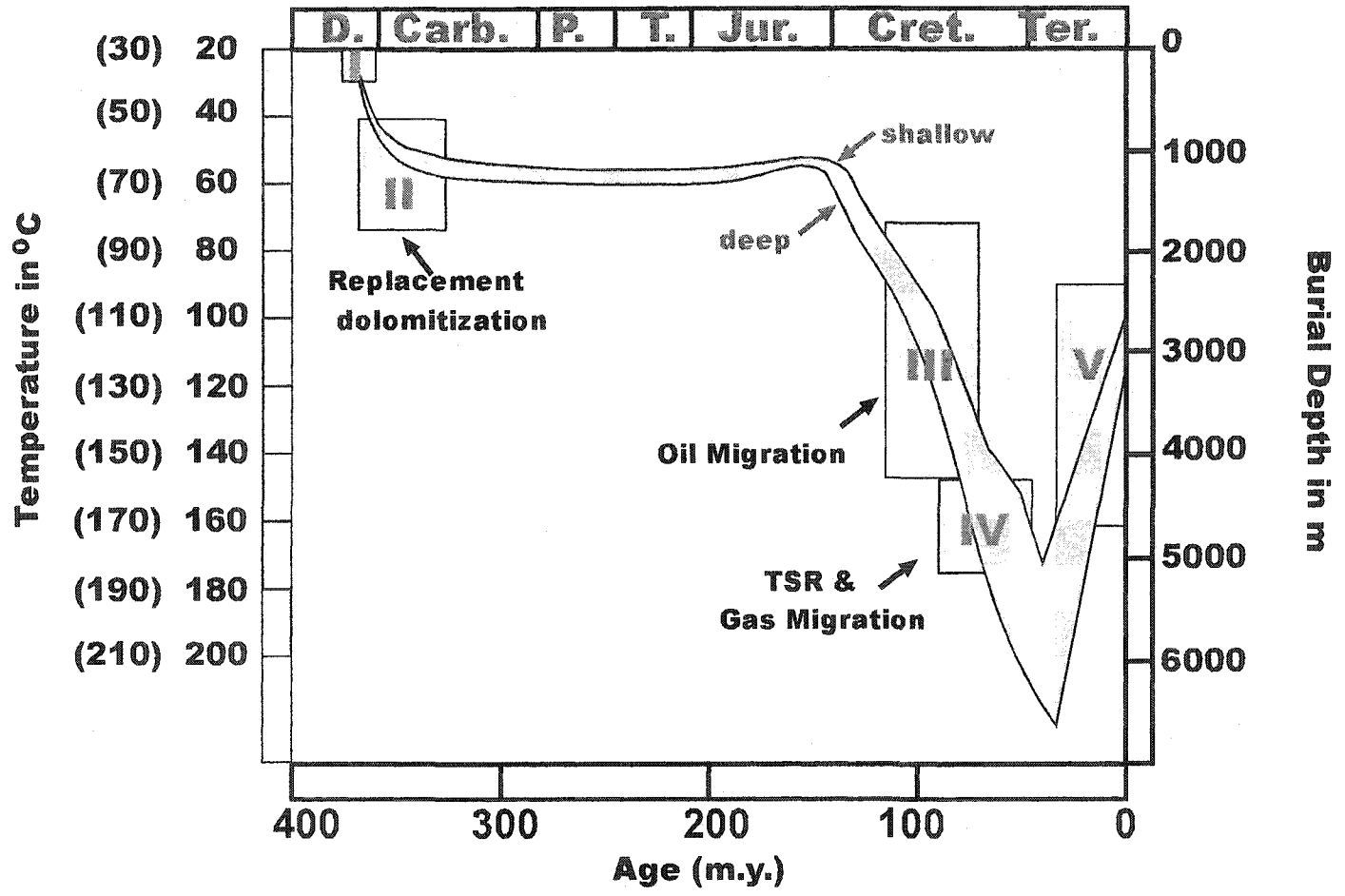


Figure 4.2: Burial curve for the carbonates of the Southesk-Cairn Complex as determined from the paragenetic sequence, bottom hole temperatures and fluid inclusion data (curves are also inferred from Green, 1999). Temperatures were determined assuming a geothermal gradient of 20°C and, in brackets, 30°C. The five fluid stages that affected the Southesk-Cairn Complex are indicated in bold roman numerals. TSR = Thermochemical sulfate reduction.

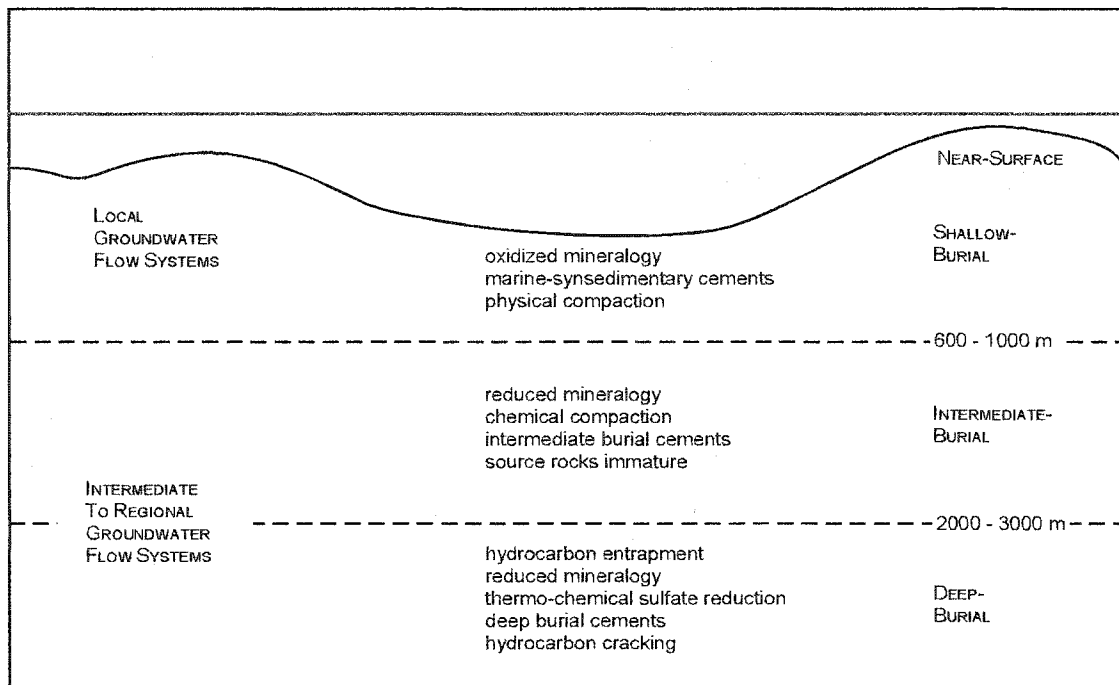


Figure 4.3: Diagenetic settings as defined by Machel (1999).

4.1 Stage 1: Near-Surface Diagenesis

Near-surface diagenesis occurred during sedimentation and initial stages of shallow burial and is summarized in Figure 4.4. The products of this stage consist of micrite envelopes, early marine calcite cements, primary anhydrite and associated dolomite (Dolomite-Type 1) as well as early diagenetic pyrite. Early diagenesis led to a general decrease in porosity. The early diagenetic products are best preserved in the rare limestones of the study area. Later dolomitization (Type 2) that affected most of the carbonates was fabric destructive and obscured most of these features (see stage 2 diagenesis).

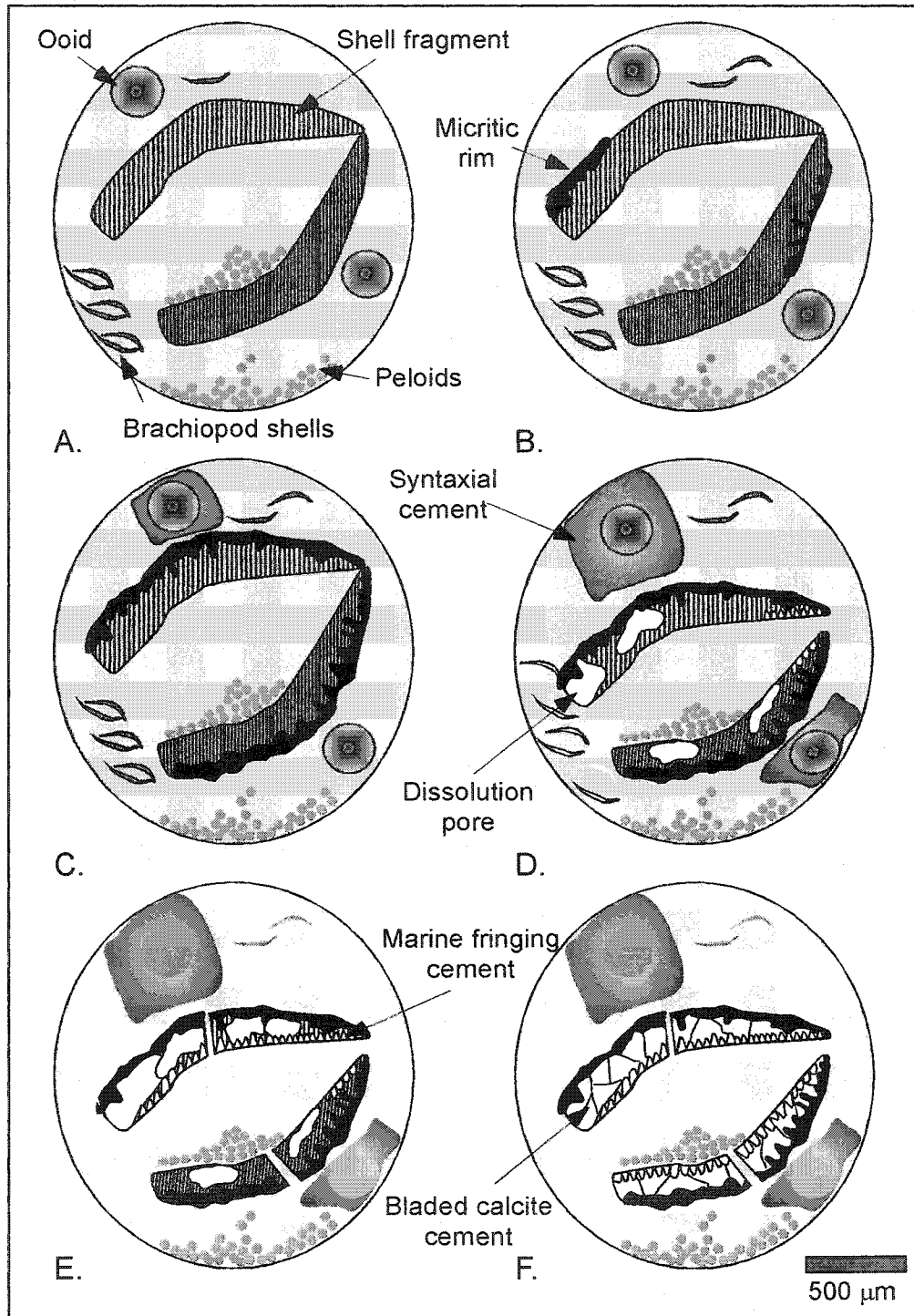


Figure 4.4: Early marine diagenetic products on a microscopic scale: A represents the syndimentary setting in a shallow marine environment with unaltered shells, ooids and peloids. B depicts the first stages of micritization, whereas C shows further micritization, and syntaxial cements on ooids. The first stages of dissolution and minor compaction (squished peloids) occur during D, and E and F show early marine fringing and bladed calcite cements within and around bioclasts.

4.1.1 Micritization or micrite envelopes

A dark gray micrite seam usually 30 to 200 μm wide surrounds some bioclasts and lithoclasts. The outside margin is always sharp and smooth. The inner boundary is commonly irregular and often continues in a columnar pattern into the clast (Fig. 4.5). Some micritization occurs in the meteoric environment (James & Choquette, 1990), however this is unlikely in this case, because there are no other indications for meteoric diagenesis, such as meniscus or gravity cements. The more likely cause for the micrite envelopes are boring microorganisms like algae, fungi or bacteria (Bathurst, 1975). These organisms build a filament where nanno-crystals may form, or they physically destroy the substrate leaving small holes behind that later became filled with (bacterial?) micrite. Pervasive micritization may lead to the rounding and total destruction of carbonate grains and textures.

4.1.2 Anhydrite and laminated dolomite (Type 1 Dolomite)

Primary anhydrite nodules and angular pieces of anhydrite occur in finely laminated gray dolostones, interlayered with white anhydrite. The mineral assemblage is rather fine grained and represents in cases cyclicity, with the finely laminated dolostones at the bottom and an increased anhydrite content towards the top, overlain abruptly by clean dolomite. Overall, these types of cyclical deposits are low in abundance in the study area. They mainly occur in the Wabamun Group and in the Blueridge Formation of the Winterburn Group.

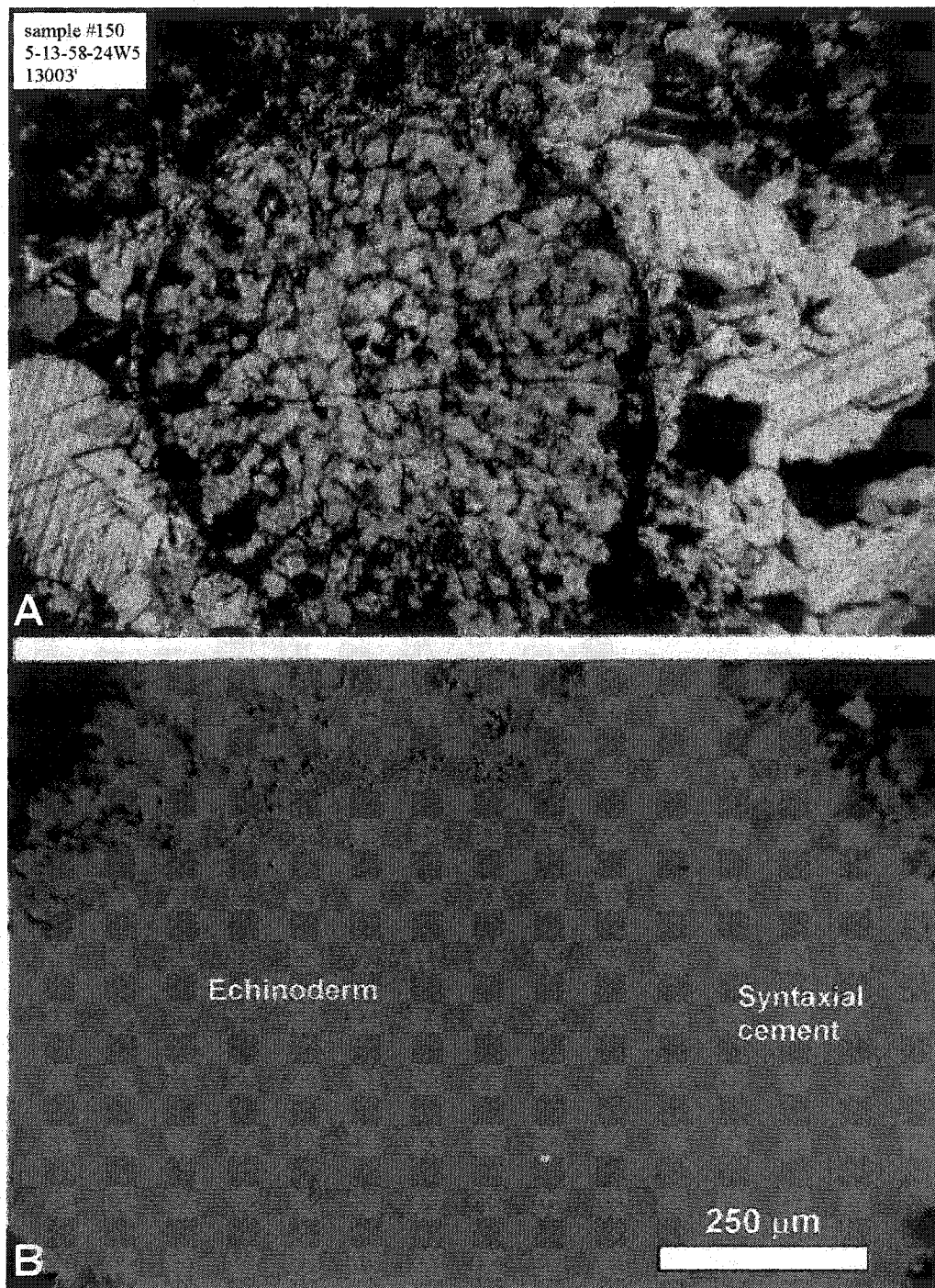


Figure 4.5: Micritic envelopes around and within a crinoid ossicle under (A) plane polarized light and (B) cathodoluminescence. Also noteworthy is the bright luminescence of the cement in contrast to the duller luminescence of the crinoid.

The cyclical interlayering of dolomite and anhydrite is commonly interpreted as being the result of deposition in a shallow lagoon, and represents alternating supratidal (anhydrite) and intertidal (dolomite) settings (Bebout & Maiklem, 1973). This interpretation is based mainly on similarities with the modern progradational sabkha deposits of the Trucial coast (e.g., Butler, 1969; 1970). As temperatures and salinities increase saturation with respect to gypsum and anhydrite is reached and /or exceeded (Butler, 1973). These evaporites may indicate the proximity of a shoreline, or they may reflect a lagoonal setting and/or very local changes in sea level fluctuations related to paleo-topography.

4.1.3 Pyrite I

Pyrite occurs as cubic crystals in mm size or as framboidal (raspberry-like) aggregates with single crystals in μm size in laminated dolostones/mudstones and/or is found within shells of mollusks. This pyrite is being interpreted as an early diagenetic, probably marine product. Berner (1970; 1984) and Rickard (1970) described early diagenetic pyrites in marine mudstones and fossil shells as the product of reducing microenvironments, where sulfate-reducing bacteria in anaerobic settings produce H_2S and pyrite through oxidation of disseminated organic material.

4.1.4 Calcite I

Calcite cement I is finely crystalline (50-to 100 μm), equant and clear. It fringes bioclasts, is isopachous and is often nucleating on micritic envelopes (Fig. 4.6).

Fringing equant calcite spar cements are interpreted as shallow marine products because of their grain size and shape, their occurrence in primary interparticle pores, as well as their close relationship to micrite envelopes (Tucker, 1990). They are distinguished from meteoric products by their absence of meniscus or stalactitic fabrics and/or the absence of iron, which is common in the meteoric-phreatic zone. Phreatic waters are often reducing, thus iron is in a ferrous (Fe^{2+}) state and can be incorporated into the calcite lattice (James & Choquette, 1990).

4.1.5 Calcite II

Calcite II cements were precipitated on the surface of Calcite I as seams of elongated fibrous calcite, with the crystals about 200 μm long and 10 to 20 μm wide and are shown in Figure 4.7. Calcite II as well as Calcite I are cut by stylolites, which clearly places their origin before the pressure solution. Longman (1980) interpreted these cements as early, marine phreatic products, which were originally Mg-calcite. Schroeder (1972) described modern fibrous cements, which do have primary high-Mg-calcite mineralogy and formed in an early diagenetic marine environment.

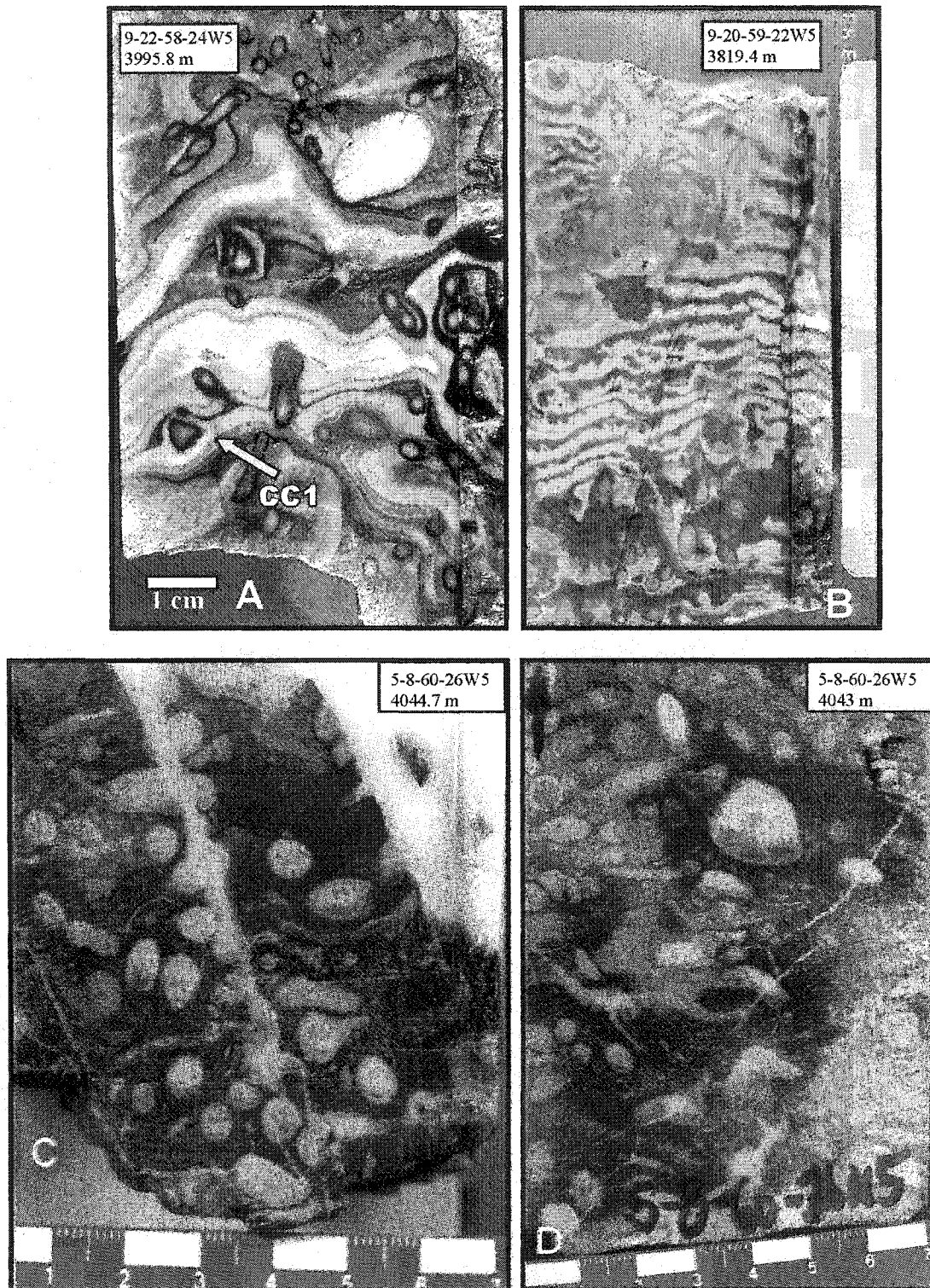


Figure 4.6: A shows early marine cements in a limestone core of a laminar stromatoporoid facies, ;B depicts syndepositional fenestral fabrics, C shows shell filling calcite cements, that are disrupted by an early fracture phase, whereas D shows shell internal early cements and geopetals. The scale bar on the bottom is in cm.

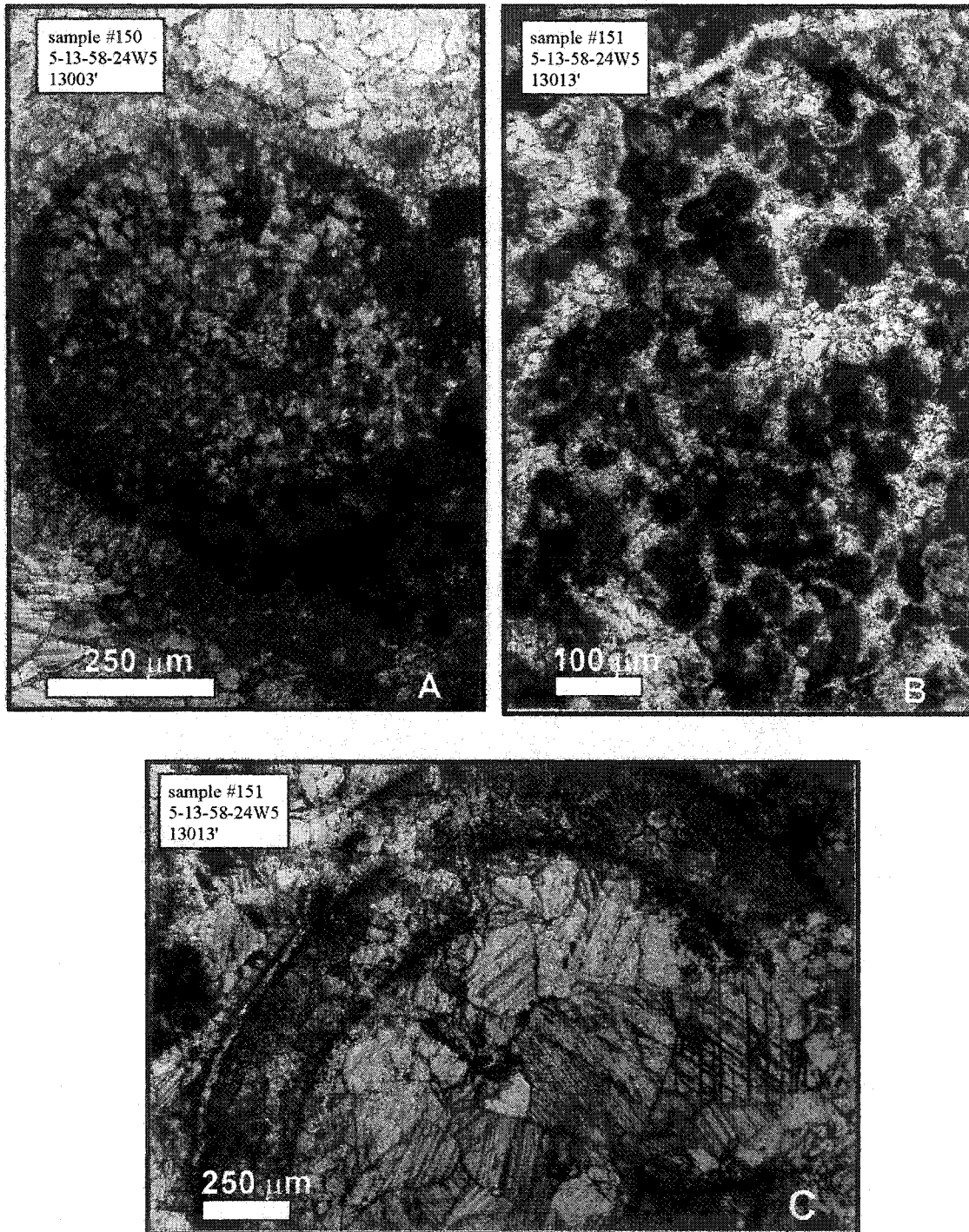


Figure 4.7: Micritic envelopes (A)/(C) and peloids (B) surrounded by early marine isopachous cements and subsequent precipitated calcite spar. Burial compaction led to the breakage of grains (C).

4.1.6 Fascicular optic fibrous calcite (FOFC)

Fascicular-optic fibrous calcite cement is shown in Figures 4.8a and 4.8b and is characterized by a significant length elongation, a sweeping extinction opposite to the microscope turning stage and curved twin planes, concave away from the substrate. The crystal size is between a few μm and 200 μm . Fascicular-optic fibrous calcite cement belongs to the group of radial-fibrous and radiaxial fibrous calcite cements (Fig. 4.8a), which have been described as cavity fills of Paleozoic reefs and are composed of crystals with a cloudy/ turbid appearance and/or undulose extinction (Kendall & Tucker, 1973; Walls, et al; 1979). Although the radiaxial fibrous cements and fascicular-optic fibrous calcite cement commonly occur together, the latter is much rarer. All three varieties of these cements have commonly been interpreted as marine products, although their occurrence in modern equivalents is sparse to absent. These complicated fabrics were first interpreted to be a replacement of a precursor acicular cement (Kendall & Tucker, 1973). However, Kendall (1985) revised the former interpretation and concluded on the basis of well-preserved crystal forms, that the cements are truly primary cements (commonly magnesium calcite), which grew as composite crystals in the marine phreatic realm. Accordingly, the composite character is due to split-crystal growth, which is caused by crystal poisoning or by growth from highly supersaturated solutions.

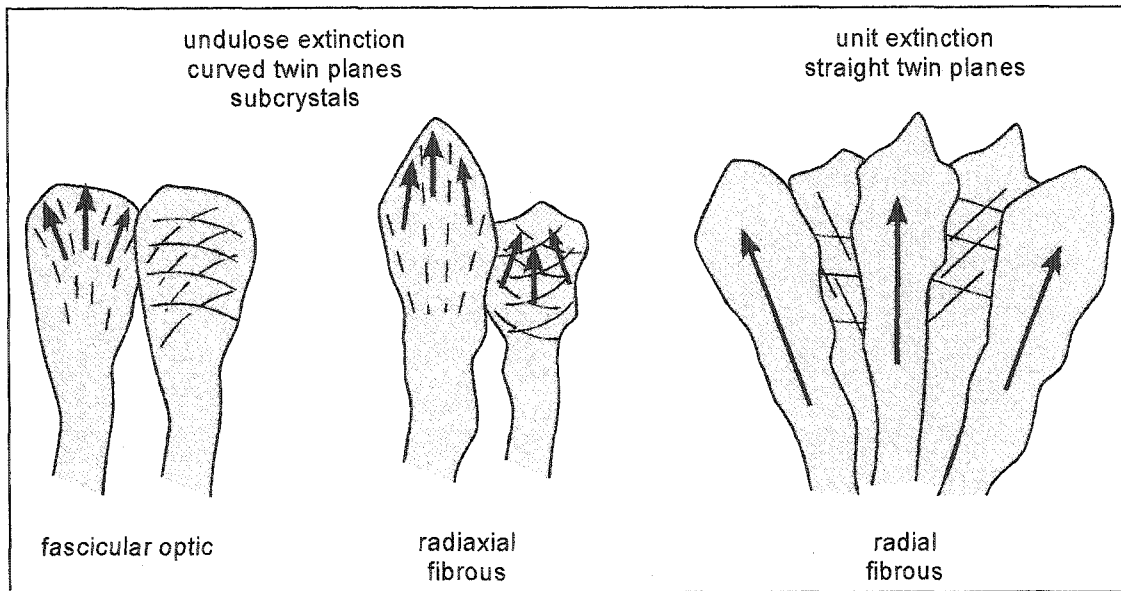


Figure 4.8a: Fibrous calcite: the fabrics of radiaxial fibrous, fascicular-optic fibrous calcite and radial-fibrous calcite. The arrows show the fast vibration directions in each case, and the dashed lines in RFC and FOFC represent subcrystal boundaries. After Kendall (1985).

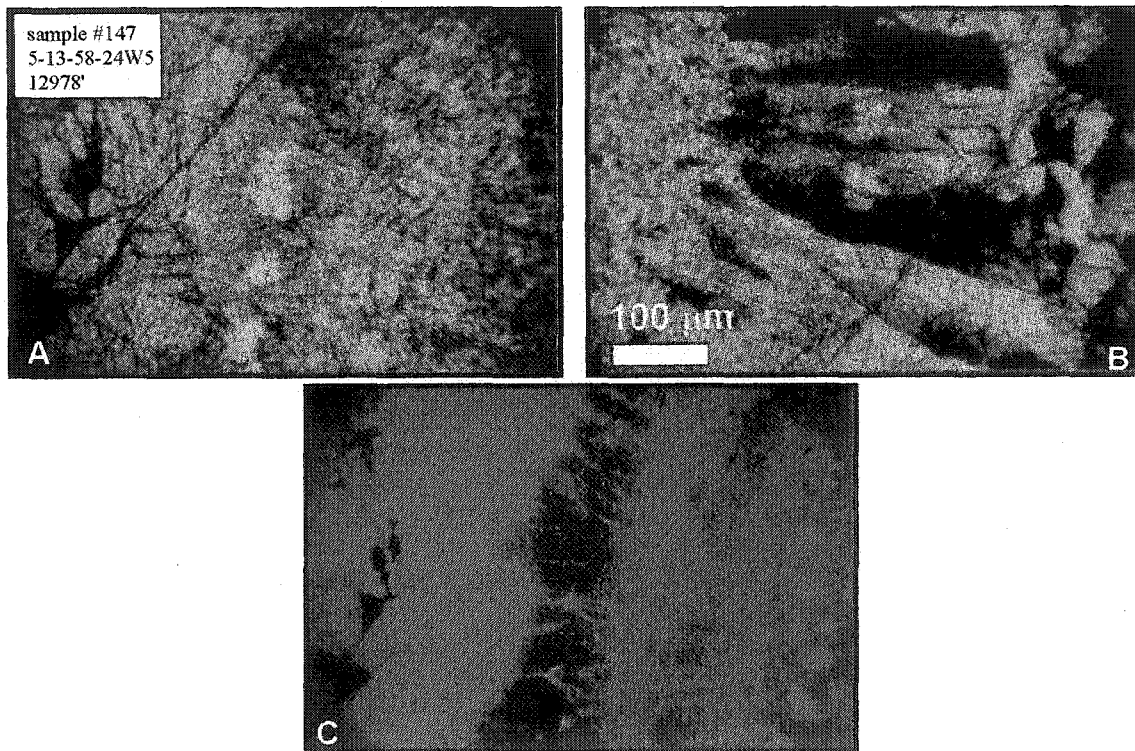


Figure 4.8b: Fibrous calcite shown under three different microscopic views: A) cement under normal polarized light where the features are hard to recognize. B) cement under crossed polars showing its cloudy-wavy extinction. C) CL-photograph showing different growth zones due to chemistry changes during precipitation.

4.2 Stage 2: Shallow Burial Diagenesis

This stage took place in a shallow burial setting up to a 1000 m and the main diagenetic products/events are calcite cement III, stylolites, matrix dolomite, pyrite II and fracture event 1.

4.2.1 Calcite III

These syntaxial calcite cements grew in optical continuity with echinoderm fragments. Their shape often is irregular and they reach sizes up to 500 μm . Calcite III cement is inclusion poor and shows concentric zonations under cathodoluminescence.

Calcite III probably formed shortly before matrix dolomitization, because it is preserved as dolomite following the matrix replacement dolomitization. Calcite III formed before pressure solution, because it is cut by stylolites.

Cements texturally similar or identical to Calcite III have been interpreted to be of meteoric origin (tucker, 1985; Longman, (1980). However, Walkden & Berry (1984) proved that these syntaxial cements can also form in a burial environment by showing that they are highly zoned, clear and less inclusion rich than their meteoric-vadose counterparts (Tucker, 1990, Chapter 7). Calcite cement III is therefore interpreted to being formed during shallow burial because there are no indications for meteoric water in put in the SCCC.

4.2.2 Matrix replacement dolomite (Type 2 Dolomite)

Matrix replacement dolomites occur throughout the study area (Fig. 4.9) and throughout the WCSB. They are the main dolomite stage and form about 86% of the carbonates in the WCSB. They consist of anhedral, mosaic or sucrosic crystal assemblages with grain sizes between 20 and 100 μm . They often show a dirty brownish color and are inclusion rich, although the inclusions are very tiny and very difficult to study and sample. Using the classification by Greg and Sibley (1984) (Fig. 4.10) the matrix dolomite can be described as an idiotopic-S dolomite, subhedral to anhedral dolomite crystal, straight, with common compromise boundaries and many of the crystals have preserved crystal-face junctions, the crystal size is on average between 4 and 25 μm (Fig. 4.11d). This dolomitization was in general matrix selective (Fig.4.11b) and larger bio-, inter- and intraclasts tend to be preserved as calcite and were later dissolved, resulting in vuggy and moldic porosity (Fig. 4.11c). These dolomites form the best reservoir rocks in the study area due to high porosity and permeability. The reservoir quality is only diminished when secondary anhydrite and late calcite cements plug up the pore space (Fig. 4.19b).

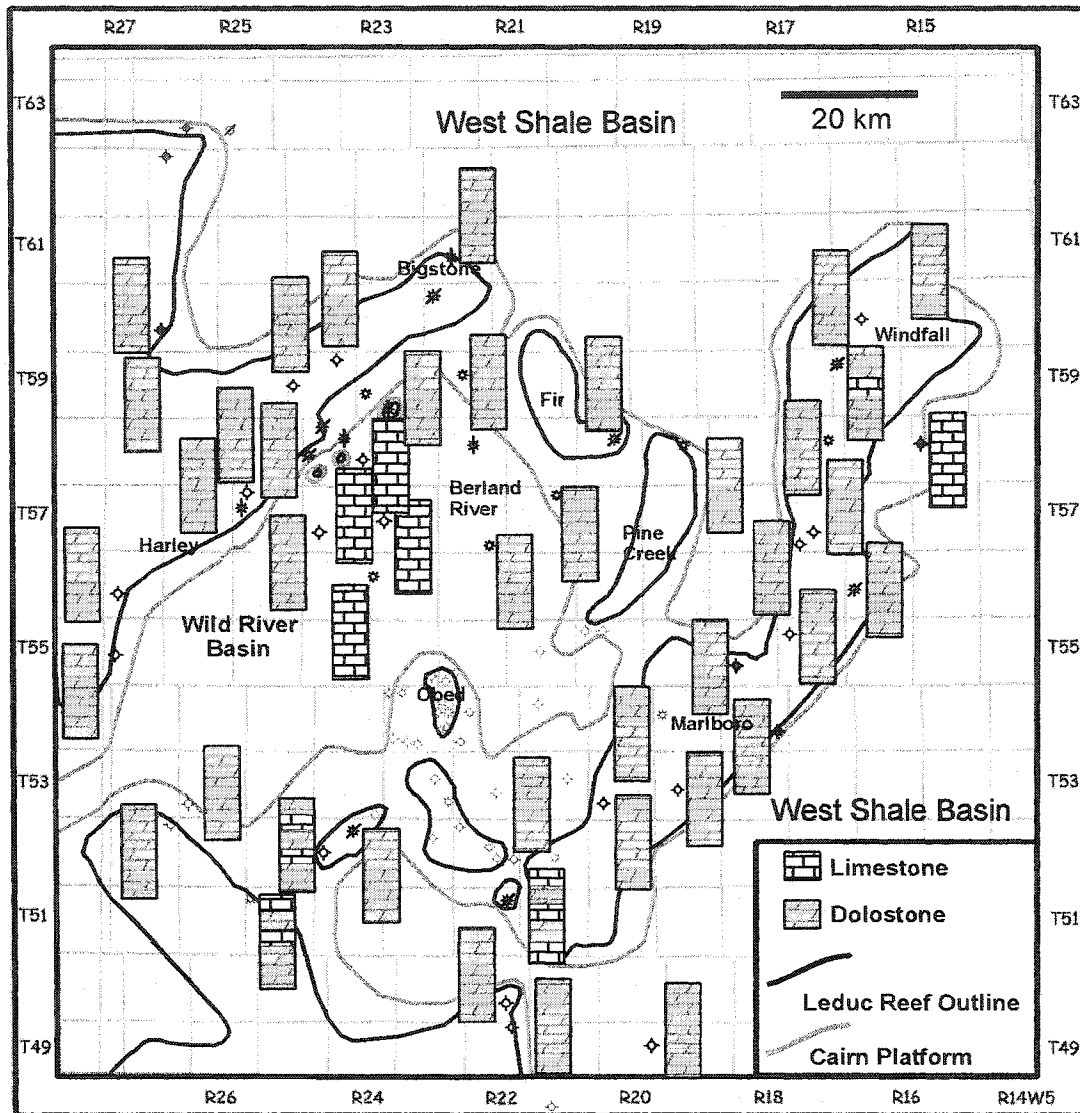


Figure 4.9: Dolomitization pattern and distribution throughout logged core in the SCCC. Limestones only occur on the platform edge and in low-permeability areas in the Wild River Basin, indicating that only the platform interior provided sufficient permeability for dolomitizing fluids.

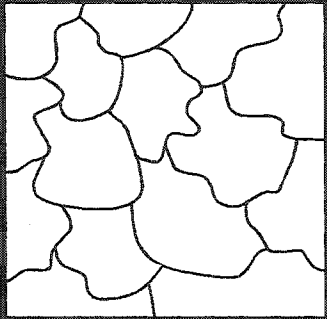
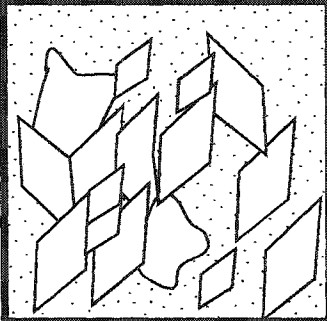
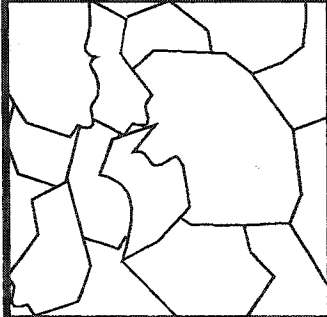
	<p>NON-PLANAR: closely packed anhedral crystals with mostly curved, lobate, serrated or otherwise irregular intercrystalline boundaries.</p> <p>Xenotopic mosaic</p>
	<p>PLANAR-E (euohedral): most dolomite crystals are euohedral rhombs.</p> <p>Idiotopic mosaic</p>
	<p>PLANAR-S (subhedral): most dolomite crystals are subhedral to anhedral with straight, compromise boundaries and many crystal-face junctions.</p> <p>Hypdiotopic mosaic</p>

Figure 4.10: Dolomite classification after Sibley & Gregg (1987). The common replacement/matrix dolomite occurs as planar-s, with most dolomite crystals being subhedral to anhedral, and crystal sizes between 4 μm and 25 μm .

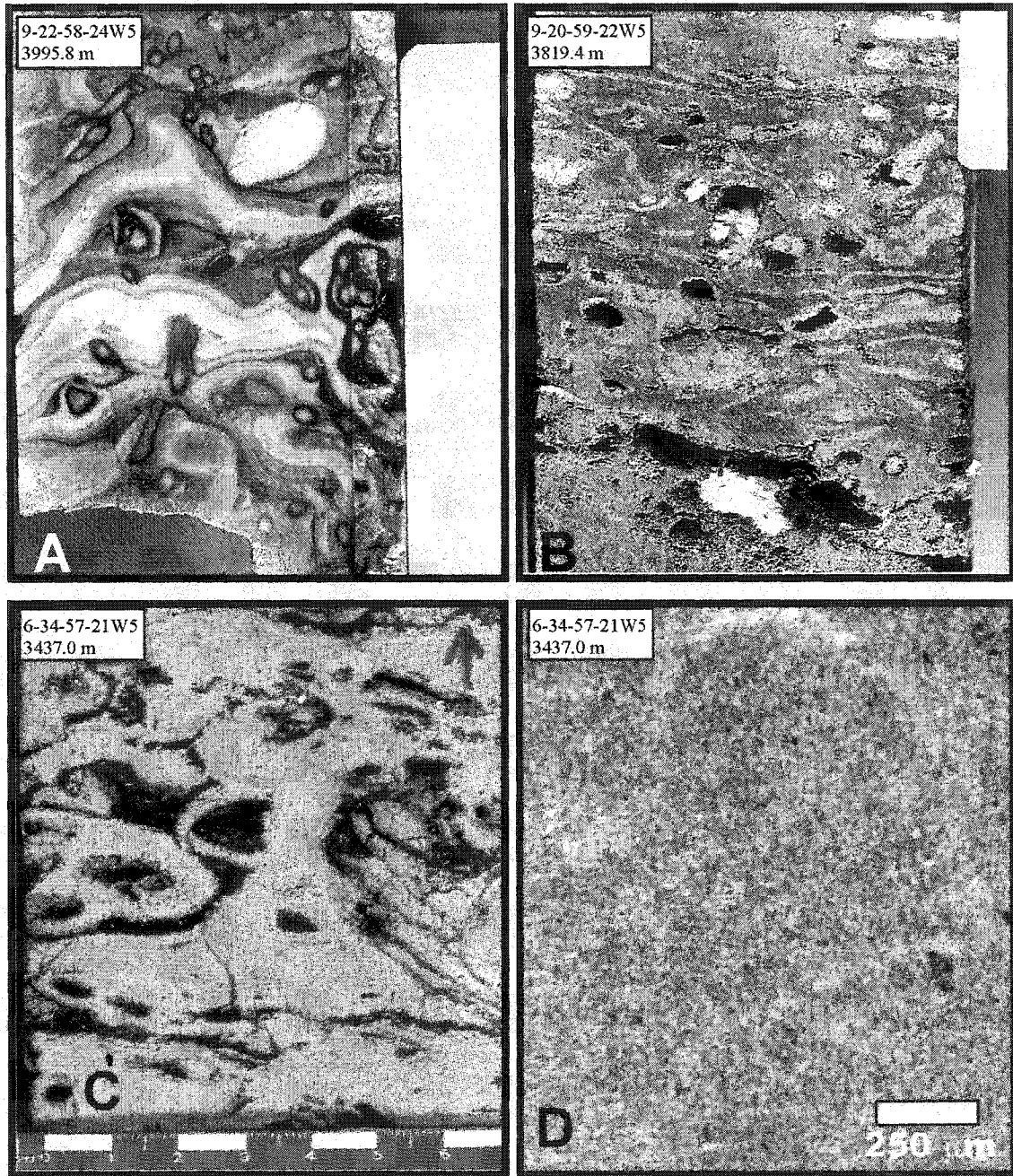


Figure 4.11: Different dolomitization stages from three wells of the SCCC. A) Limestone with perfectly preserved facies features; B) Partially dolomitized *Amphipora/Stachyodes* float- to rudstone. C) Pervasively dolomitized core sample, where the facies features are obliterated. The laminar solution resembles laminar stromatoporoids, thus it is concluded, that this is a stromatoporoid boundstone as seen in A. D) Microphotograph of matrix dolomite with mainly subhedral dolomite crystals, that resemble sugar grains.

The matrix dolomites of the SCCC have many of similarities with other matrix dolomites in different parts of the Alberta Basin in terms of their texture, the facies distribution, structural features, stylolites and the stable and radiogenic isotope data. They are interpreted to be "burial dolomites" that replaced limestones in a shallow burial environment in a depths of 300 to 1000 m during the late Devonian and early Mississippian (Mountjoy and Amthor, 1994), (Fig.4.2). The pervasive matrix dolomitization is a basin wide phenomenon in Alberta and the dolomitizing fluids most likely were slightly modified Devonian seawaters (Amthor et al., 1993; Machel et al., 1994; Mountjoy et al., 1999) (also see isotope data in Chapter 5). The driving forces for the dolomitizing fluids likely were a combination of compaction-driven flow (Illing, 1959; Mattes & Mountjoy, 1980; Machel & Mountjoy, 1986) and convection-driven flow. Compaction-driven flow is a reasonable mechanism because the dolomites are encased in shales and formed when mechanical compaction was taking place. Convection-driven flow is a plausible driving mechanism because it can provide sufficient amounts of magnesium for the dolomite rock volumes of the SCCC. However, the hypothesis of convection driven flow still needs to be proven, so far no evidence of convection-driven flow has been found. Topography-driven flow as described by Garven and Freeze (1984a,b) and Gregg (1985) is not a very likely driving force for the fluids that formed the matrix dolomites of the SCCC. There was little topographic relief during the Late Devonian and Early Mississippian and the isotope data (see Chapter 5) do not support a meteoric component for the matrix dolomitization.

4.2.3 Dissolution

Dissolution took place during at least two stages during the burial history of the SCCC. One major dissolution event took place immediately after replacement dolomitization and led to the formation of highly porous, vuggy dolostones as seen in Figure 4.12. Minor dissolution of calcite and dolomite minerals took place during later stages of burial, however the processes leading to dissolution are summarized in this part to avoid repetitions. Dissolution and secondary porosity development in carbonates is mainly controlled by the generation of acidic fluids (Mazzullo & Harris, 1992). Several processes can lead to the generation of acidic fluids in the burial environment of carbonates. For example, the mixing of two solutions that are both in equilibrium with respect to carbonate minerals but have different $p\text{CO}_2$, temperatures, salinity, degree of calcite saturation, and/or pH may result in under-saturation with respect to $\text{CaMg}(\text{CO}_3)_2$ leading to carbonate dissolution (mixing corrosion). Walls and Burrowes (1990) described microstalactitic cements in Golden Spike (a deep Devonian field south of this study area) and suggested that mixing of vadose and phreatic waters may have been responsible for near surface dissolution in the Leduc Formation, however no such cements have been found in the SCCC. Hutcheon (1992) suggested that in the Western Canada foreland basin, small portions of relatively low-salinity waters from Mesozoic rocks may have been added to greater proportions of the saline water from Paleozoic rocks. Subsequently, the mixture would become undersaturated with respect to dolomite and calcite and lead to burial dissolution of carbonates in the subsurface. However, Creaney and Allan (1992) showed, based on hydrocarbon geochemistry and hydrological studies, that the Devonian strata in most parts of the WCSB (especially in the deeply buried western part) are not in

connection with the overlying Mesozoic strata (Creaney and Allan, 1992) and thus carbonate dissolution in the Leduc dolomites most likely resulted from other processes.

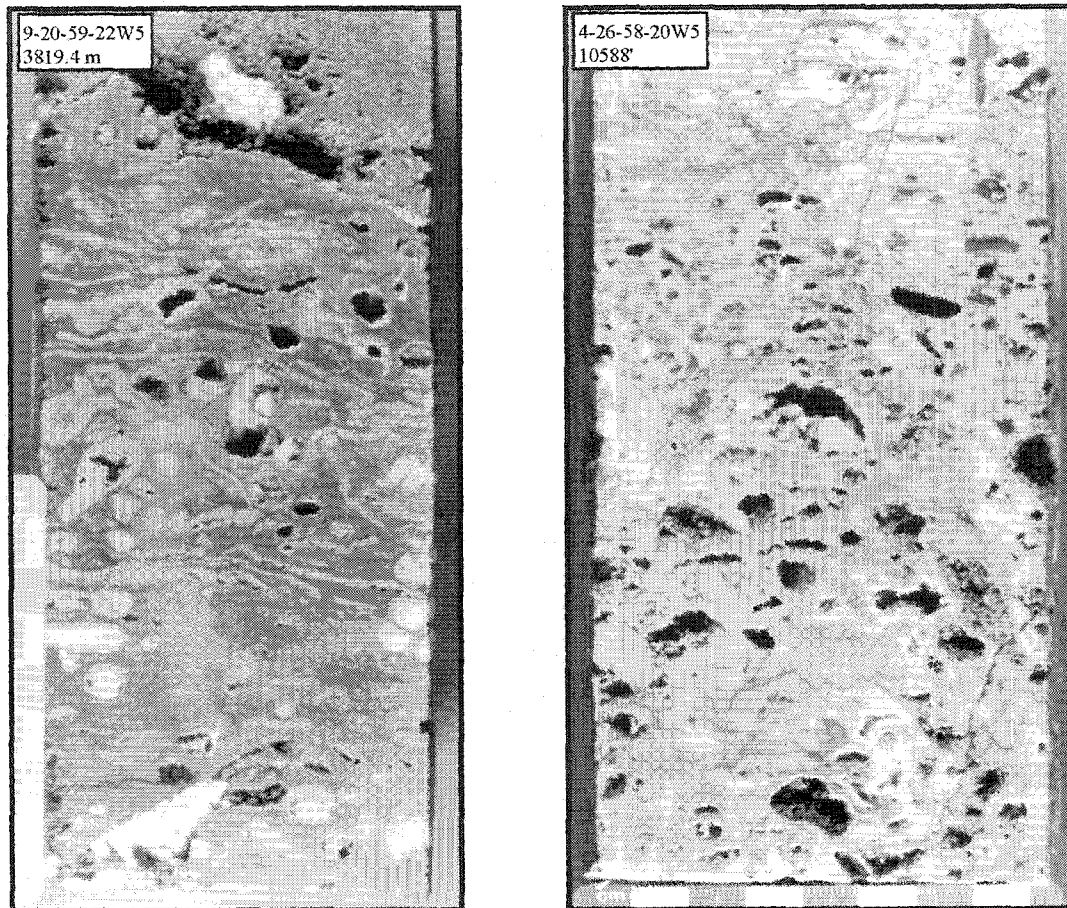


Figure 4.12: Dissolution enhanced vuggy and intercrystalline porosity in pervasively dolomitized core intervals; the porosity reaches up to 25 to 30 % with permeabilities of about 200 md.

Since there is no textural nor geochemical evidence to support extensive meteoric recharge in the dolostones of the study area burial dissolution of the carbonates by reaction with meteoric fluids charged with carbonic and organic acids is very unlikely. Mazzullo and Harris (1992) suggested that the release of hydrogen ions during silicate

hydrolysis of clay minerals during burial (90°C to 150°C) lowers the pH of the formation waters and may induce dissolution. However, the acidic fluids would probably have been neutralized in situ, at least partially, because the surrounding Ireton and Berland shales are carbonate rich. However, some of these fluids may have been migrated through the carbonate complexes and potentially caused carbonate dissolution. Other processes that may generate acidic fluids include the maturation of organic matter, which produces CO₂, H₂S, and kerogen and these may mix with water to form carbonic, sulfuric, and organic acids, respectively. These fluids could have contributed to creating porosity in the carbonates of the SCCC. In addition, fluid inclusion homogenization temperatures (up to 173 °C) (see Chapter 5) show that hot fluids precipitated the late dolomite and calcite cements. When those hot fluids were introduced to the system the temperature decreased, which lead to increased saturation levels of dissolved carbonates and may have caused dissolution (Qing, 1991). Thermochemical sulfate reduction took place in deep parts of the SCCC and is explained in later parts of this chapter (see Section 4.4). The main products of TSR are H₂S (up to 25%), the late stage blocky calcite cement with very light carbon isotopic composition, sulfide minerals and elemental sulphur. These minerals are most abundant in deeper parts of the SCCC and become less abundant northeastward with decreasing burial depth. The TSR acids would have been released during sulphide formation (Machel, 1987a,b) and could have caused considerable dissolution and created and enhanced secondary porosity. Also, during hydrocarbon maturation (Late Cretaceous) the thermal cracking and oxidation of hydrocarbons may generate organic and carbonic acids, which could have contributed to dissolution in the SCCC.

4.2.4 Pressure solution features / stylolites

Pressure solution features are common throughout the study area and occur as small undulose, dark gray to black, seams, fitted fabrics and distinct stylolites with amplitudes in mm- to cm size (Figs. 4.13 and 4.14). The stylolites often occur in areas where two different facies types or two different mineral types (calcite/dolomite) occur together (Fig. 4.13c). They always post-date the matrix dolomites and the early features of near-surface diagenesis, thus placing their origin in stages two (shallow-burial diagenesis) or even three (intermediate burial diagenesis). Stylolites are often associated with dolomite crystals (Fig. 4.14b), pyrite and dark clay minerals (Fig. 4.14c). In addition, carbonate components next to the stylolites are often partly dissolved.

Stylolites are common features in carbonates and are the result of pressure solution/chemical compaction due to overburden. During this process pressure is concentrated on the contacts between grains and crystals and larger entities and increases the solubility of the stressed component due to increased elastic strain, which causes dissolution at the contact (Choquette, 1990). Dolostones are less soluble than limestones and therefore are more resistant to pressure solution and do not compact as much as adjacent limestones (Choquette and Steinen, 1980). According to Logan & Semeniuk (1976), Wanless (1979), Buxton and Sibley (1981) and Bathurst (1991) pressure solution features can be subdivided into three categories: a) stylolites, b) dissolution seams and c) fitted fabrics. Stylolites develop serrated interfaces between two rock masses and have a sutured appearance in cross section.

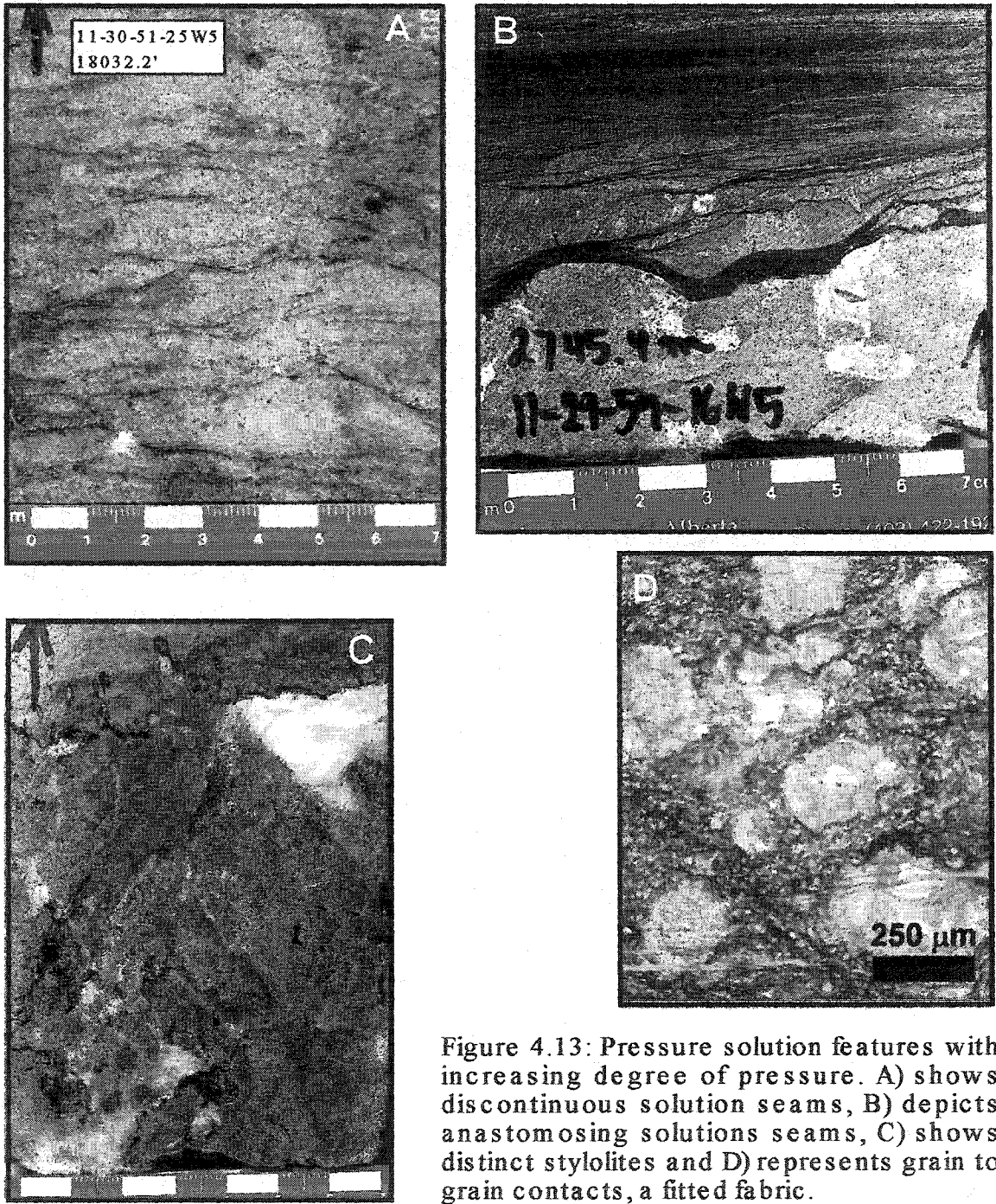


Figure 4.13: Pressure solution features with increasing degree of pressure. A) shows discontinuous solution seams, B) depicts anastomosing solutions seams, C) shows distinct stylolites and D) represents grain to grain contacts, a fitted fabric.

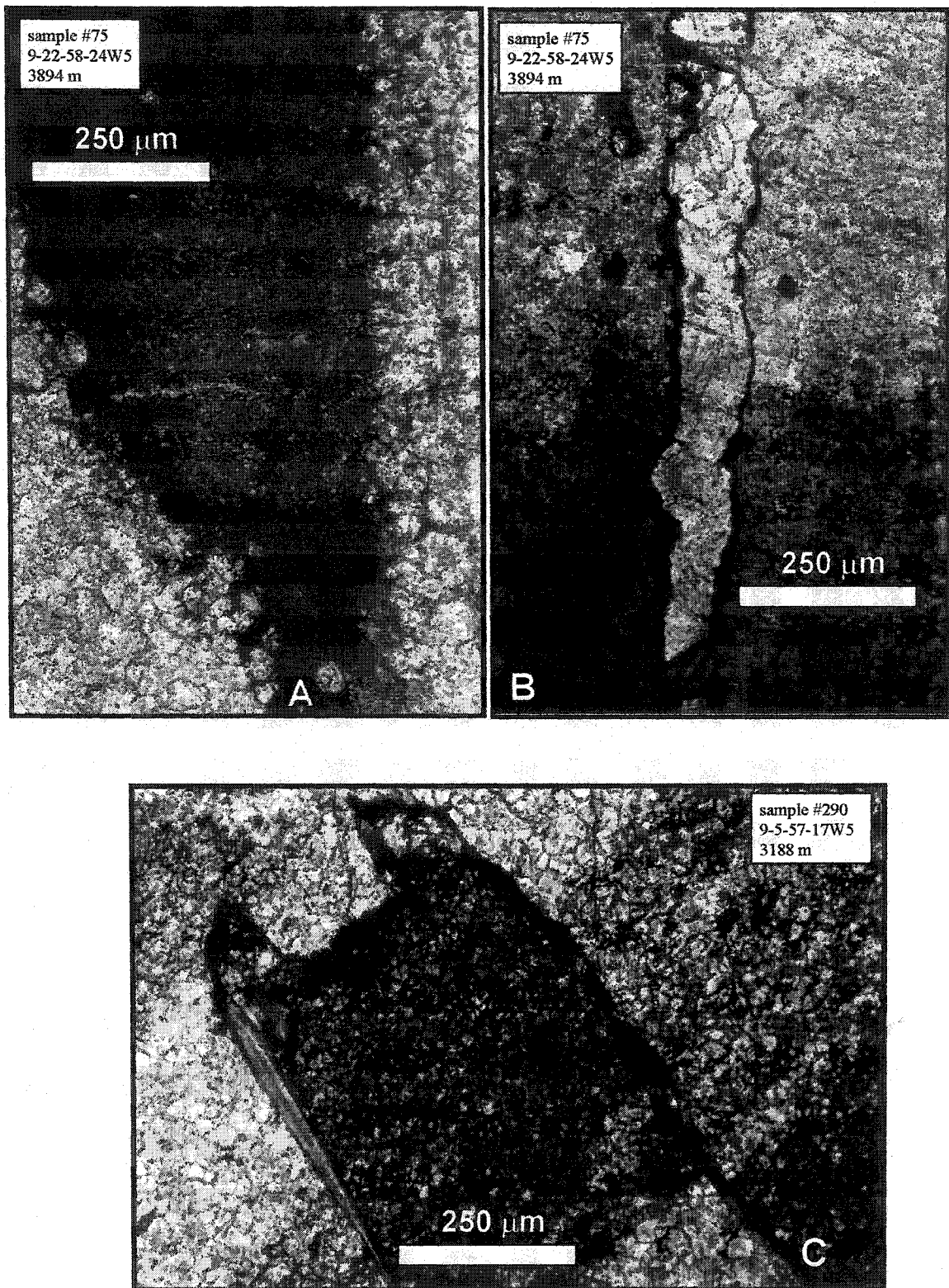


Figure 4.14: Pressure solution features on a microscopic scale. A) shows the ferroan dolomite associated with stylolitization, whereas B) and C) depicts mineralization of pyrite along the solution seams.

Stylolites appear mainly/only in carbonates with a carbonate content of at least 90 to 95% and therefore are most prominent in the limestones of the study area. The second category, "dissolution seams" are smooth, undulose seams of insoluble residue and do not show the distinctive sutures of the stylolites. They generally pass around grains in an anastomosing pattern and do not cut the grains. Dissolution seams often occur in multitudes in and around nodular limestones and give the rocks a flaser appearance. The seams are most common in argillaceous limestone and wackestones of the Ireton Formation, the Blueridge Formation and the informal "Berland Carbonate". The third category is referred to as "fitted fabrics" and usually is a framework of interpenetrating grains, with the surfaces of the grains being sutured or curved into each other. The development of fitted fabrics can be inhibited by early cementation (Bathurst, 1987). In the study area, fitted fabrics are predominantly developed in grainstones of the Swan Hills, Leduc and Nisku Formation reefal and lagoonal carbonates.

The amount of pressure solution is in general dependent on different lithological parameters, like mineralogy, grain size and clay content as well as the preceding diagenesis of the rock (Bathurst, 1987). The onset of pressure solution is still in debate, according to Choquette and James (1987). For limestones a minimum depth of about 500 to 700 m seems necessary, Lind (1993) showed on modern sediments that stylolites develop at a depths below about 600 m even in pressure solution resistant chalks. For dolomites the depth of initiation would be even greater perhaps as much as 1000 m (Mountjoy et al., 1999).

4.2.5 Dolomites associated with stylolites

Small (up to 50 μm) and mostly euhedral dolomite crystals are associated with stylolites on a local scale (Fig. 4.14). In some cases there might be even two generations of stylolite-related dolomite. The second generation nucleates on the first and growth into bigger (100 μm) curved crystals with undulose extinction. The crystals also show a turquoise greenish color (potassium-ferri-cyanide stain) indicating that they contain small amounts of iron. This ferrous dolomite can only be found in the limestones.

Due to their close relationship with the stylolites, the dolomite most likely formed during pressure solution. Wanless (1979) proposed, that the source of Mg^{2+} for this dolomite was high-Mg calcite, which had not been stabilized closer to the surface. This could only be the case, if there had been little or no early meteoric diagenesis, during which the metastable high-Mg calcite would have been rapidly altered to low-Mg calcite.

4.2.6 Pyrite II

Small and rare euhedral pyrite crystals or pyrite accumulations are also common along pressure solution seams and stylolites. They are opaque under the microscope but show their characteristic goldish color, when the section is held up against light. The origin of this pyrite is not quite clear; it is most likely a dissolution remnant along the solution seams.

4.2.7 Fracture 1

Fracturing 1 affects all of the above diagenetic stages and their products. The vertical fractures are usually small (μm size) and are either open and/or filled with calcite cement. The fractures are cross cut by bigger fractures that are filled with saddle dolomite and late stage calcite cement. It is assumed that these fractures formed during moderate tension during and/or after the Antler orogeny.

4.2.8 Calcite cement in small fractures

The calcite cement FC 1 in small fractures consists of veins is blocky spar of 50 to 100 μm crystal sizes. It is coarser than the early diagenetic calcites, but small in comparison to the large late stage calcite cements. The fractures are very small and in most cases only recognizable in thin-sections. They also seem to be restricted to the limestones and/or are overprinted by the later dolomitization processes. The cements are difficult to sample from the host rock, without sample contamination, therefore these cements could not be analyzed geochemically.

Early to intermediate diagenetic products are summarized in Figure 4.15.

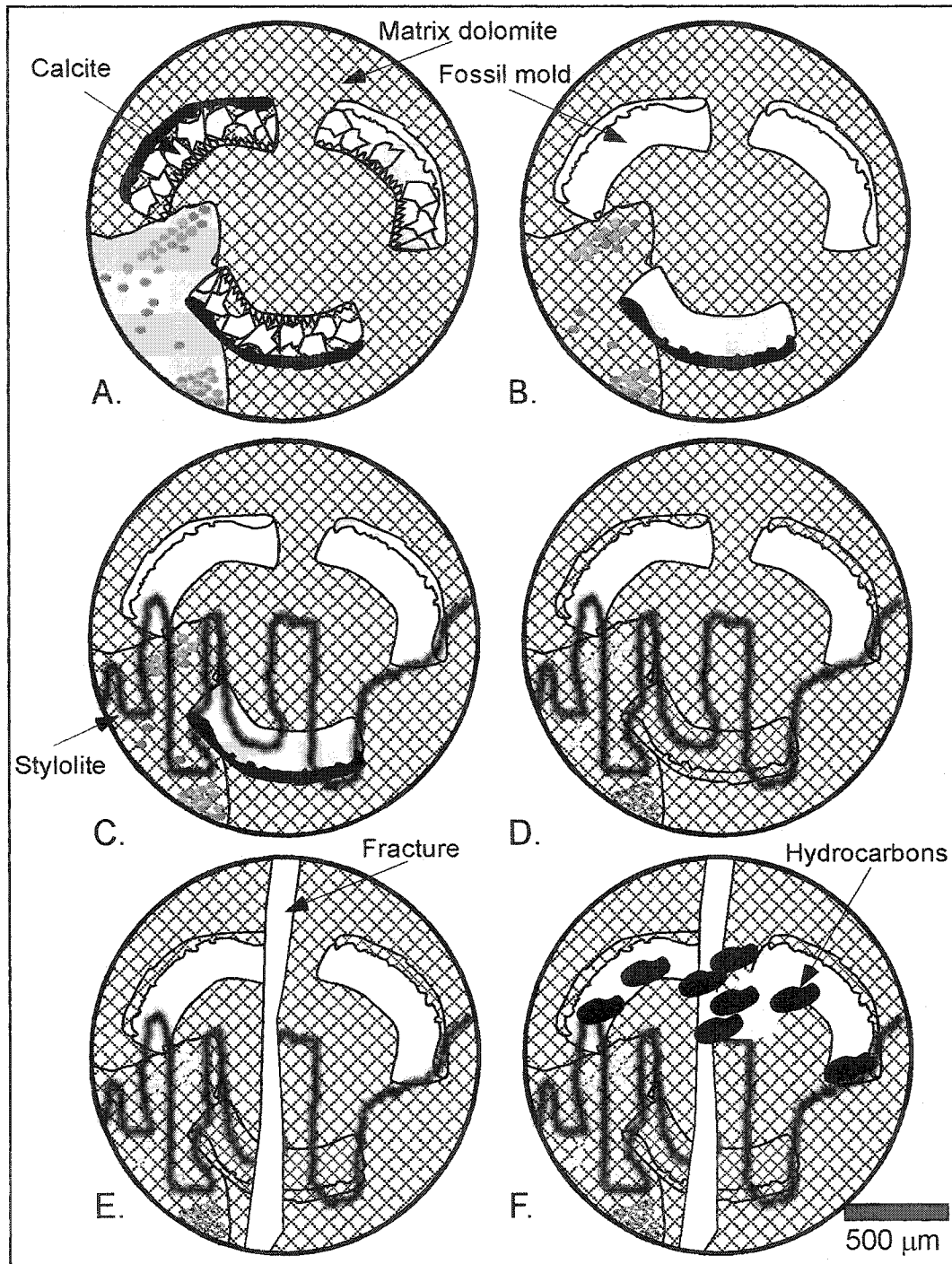


Figure 4.15: Early burial to intermediate diagenetic products on a microscopic scale: A) fabric selective matrix dolomitization, where fossil fragments are preserved as calcite with their specific marine cements; B) first stage of dissolution, where preferentially fossil molds are formed and or/fossils become partially dolomitized; C) stylolitization; D) further discrimination of primary facies features; E) fracturing; and F) infilling of fractures with hydrocarbons.

4.3 Stage 3: Intermediate Burial Diagenesis

The main diagenetic processes during intermediate burial were the maturation and primary migration of hydrocarbons. The main source rocks for the study area most likely are shales in the D3 (Ireton/Duvernay? formations) and D2 (Cynthia Member) intervals (Wendte et al., 1998; Creaney and Allan, 1990; Stoakes and Creaney, 1984). Other diagenetic products of this stage are stylolites, anhydrite, and bitumen.

4.3.1 Secondary anhydrite

Late diagenetic, secondary anhydrites occur as nodular blotches that are floating in the dolostone, and as massive replacements that can be up to m-sizes in thickness, within the dolostone column. The anhydrite is usually milky- white to brownish-gray, the latter resulting from hydrocarbon stain. It can occur in a range of textures and crystal sizes, e.g. felted (mm size) or bladed (cm size). The secondary anhydrite appears as massive intervals within the dolostone-saddle dolomite sequence with patches of dolostone floating in the anhydrite (Fig. 4.22 A). It always postdates saddle dolomite, is intergrown with solid bitumen and is sometimes found with late calcite cement. The amounts of calcite cements are very low in comparison to that of anhydrite, in the latter case. It seems that remnants of late calcite cements are irregular distributed within the massive anhydrite.

Anhydrite nodules form according to Spencer & Lowenstein (1990) in a burial setting, due to dehydration of Gypsum. The dehydration forms porous plastic masses of anhydrite laths, which are easily deformed into nodules. Massive packages of anhydrite with

floating dolomites are interpreted as replacement anhydrites. The occurrence of patches of calcite cements within the massive anhydrite give rise to the assumption, that anhydrite replaces the late calcite cement. The distribution of anhydrite throughout the study area still needs to be mapped, since it appears that anhydrite is to this time moving and influencing the hydrology in the study area (Amoco, pers. comm., 2000). In addition, Spencer & Hutcheon (2001) related the amount of anhydrite in a reservoir to the degree of TSR processes.

4.3.2 Fracture II

A major fracture event happened in the deep burial realm and enlarged the porosity and permeability. The fractures are often completely filled with saddle dolomites and bitumen. The fractures can be up to several cm in size, facilitating a huge pore space for fluid movement and crystal growth.

4.3.3 Hydrocarbons and solid bitumen

Most of the reservoirs in the study area contain high amounts of natural gas with H₂S contents between 0 and 27% (EUB, 2000). Other hydrocarbons present are several varieties of solid secondary bitumen (pyrobitumen). The bitumen can either be stain-like, in which case it comes off easily, or it can be solid blobs of black organic material that adhere to the rocks. It can both be pore lining and pore filling in which case it covers the early calcite cements and predates some dolomite cements, or it can occur along microfractures, especially in the very deep part of the basin as seen in Figure 4.16 (below 3000 m; see deep burial diagenesis).

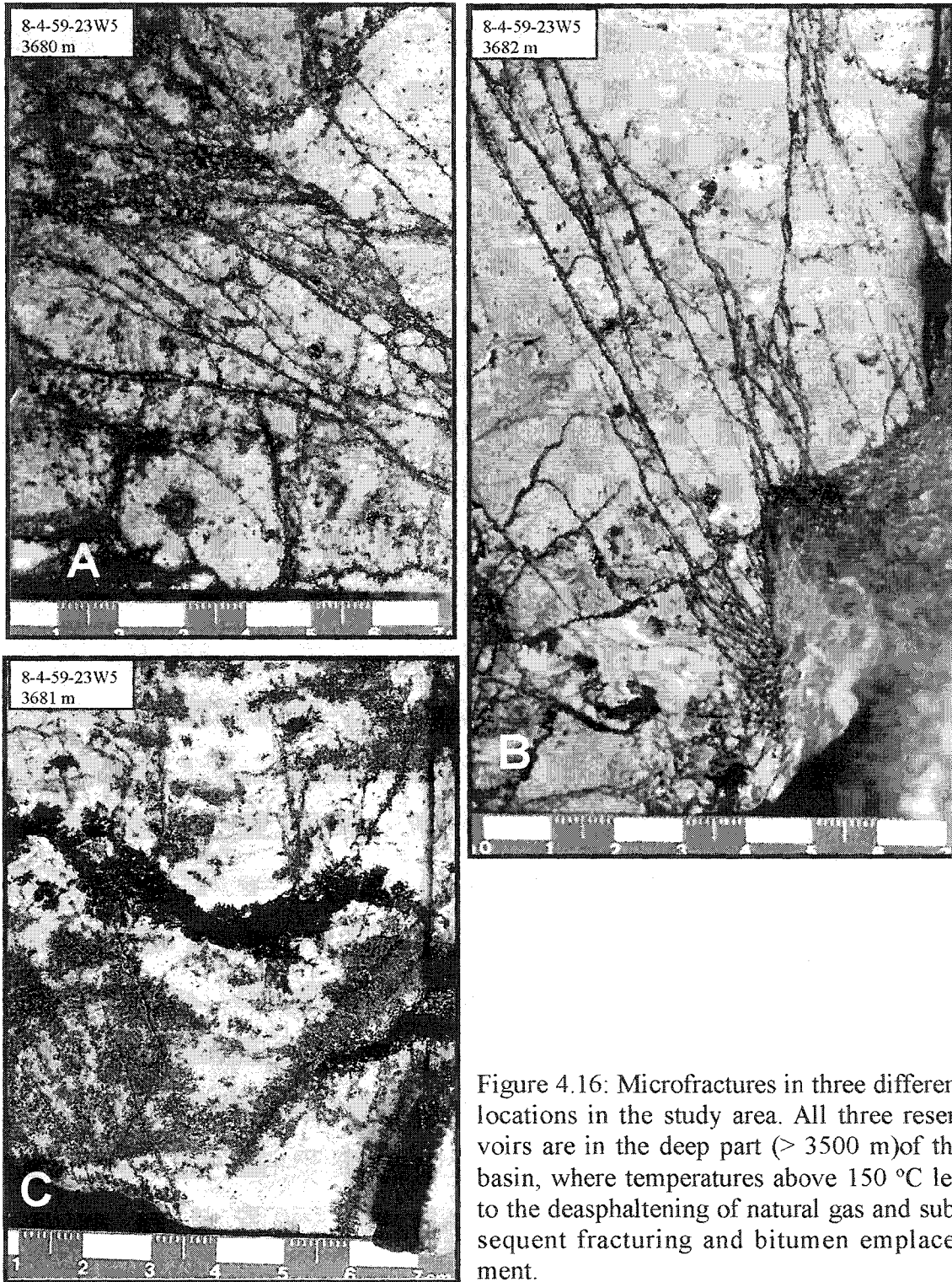


Figure 4.16: Microfractures in three different locations in the study area. All three reservoirs are in the deep part (> 3500 m) of the basin, where temperatures above 150 °C led to the deasphalting of natural gas and subsequent fracturing and bitumen emplacement.

Pyrobitumen, or secondary bitumen is derived from microbial, oxidative or thermal alteration of a preexisting bitumen or liquid hydrocarbon (Curiale, 1993). Pyrobitumen is a frequent component of gas reservoirs in the deep part of the WCSB (Bailey et al., 1974; Rodgers et al., 1974). It has been interpreted as the insoluble residual product that formed during thermally-induced oil to gas reactions, which take place in the reservoir, carrier bed and hydrocarbon source rock (Hill et al., 1996). Stasiuk (1997) has analyzed pyrobitumen from a deep basin Leduc Formation Strachan-Ricinus gas reservoir. He categorized the Leduc reservoir pyrobitumens into two groups: A) a non-graphitizing sulphur-enriched group and B) a graphitizing, sulphur-depleted group, which reflect variations in the gross chemistry of the precursor petroleum source, as well as variations in physical conditions in the Leduc reservoirs oil to gas transformation reactions. He further concluded that the group B pyrobitumens were produced from "graphitizing" petroleum, enriched in saturates and aromatics, during the late oil to condensate to gas stage of thermal maturity (Fig. 4.17). The petroleum sources are supposedly shales of the Duvernay Formation. Group A pyrobitumen was, in contrast, derived from a precursor, which was significantly enriched in NSO compounds. The NSO concentration could have formed either before or during oil to gas transformation. Stasiuk (1997) inferred that the Group A bitumen are the result of crude oil alteration by TSR-related processes, i.e. oxidation of organic matter and reduction of SO_4^{2-} .

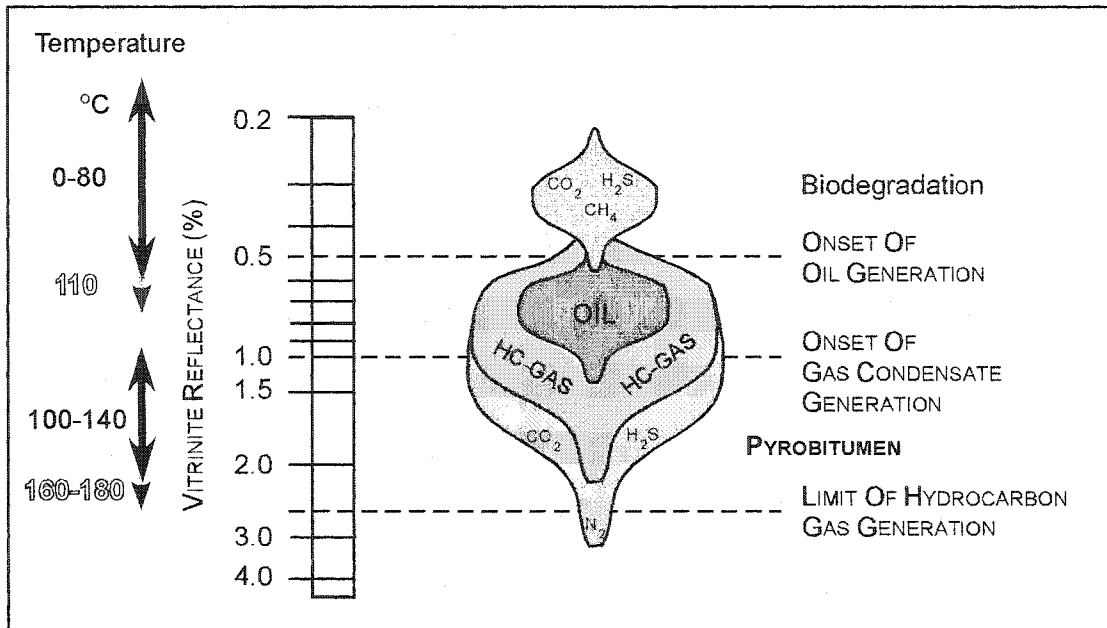


Figure 4.17: Stability fields of various hydrocarbons as well as the onset temperatures for deasphalting of natural gas and the subsequent formation of solid bitumen.

4.4 Stage 4: Deep Burial

Stage 4 took place during the latter part of rapid burial to maximum burial depths of about 7 km in the Paleocene (Fig. 4.2). The major diagenetic process for this realm was thermochemical sulfate reduction (TSR). The onset of TSR is generally constrained to minimum temperatures of 100 – 140°C (Machel, 1998), however TSR in the SCCC probably took place in a temperature range of 125 – 160°C as indicated by fluid inclusion data (see Chapter 5). The main products of TSR are sour gas (H₂S), saddle dolomite, secondary anhydrite, blocky calcite cements as well as minor amounts of pyrite III, chalcopyrite and elemental sulfur (S⁰) (Fig. 4.18).

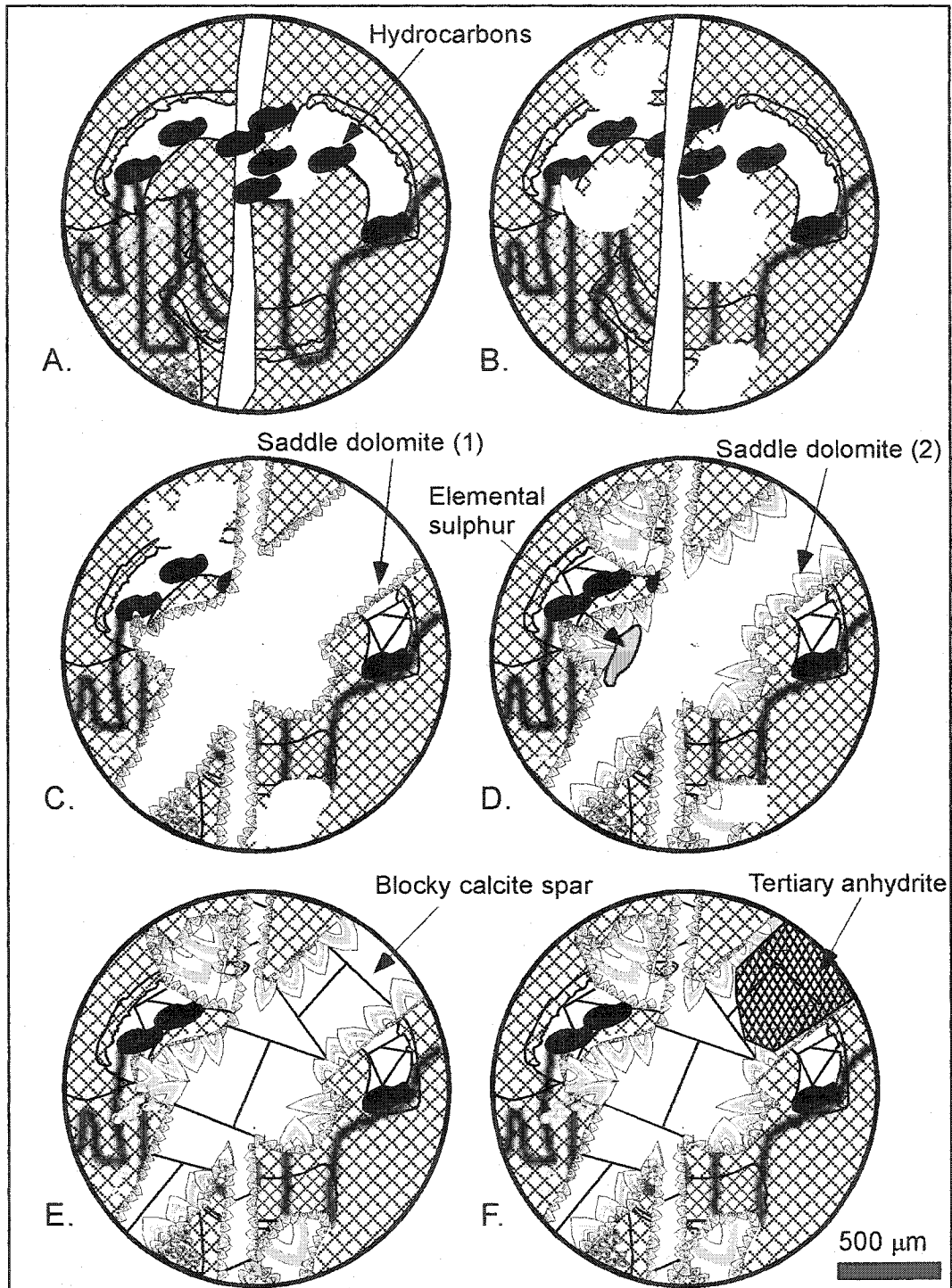


Figure 4.18: Late burial diagenetic products on a microscopic scale; A shows the first hydrocarbons filling in some of the open pore space. B depicts enhanced stages of vuggy porosity and additional hydrocarbon emplacement. C shows the precipitation of saddle dolomite cements during TSR, whereas D represents a second generation of bigger saddle dolomite crystals some of which are covered with elemental sulfur. E shows the emplacement of late stage blocky calcite spar and F represents the replacement of calcite by tertiary anhydrite.

4.4.1 Fracture III

A third fracture event occurred in the deep burial realm, which led to the formation of vertical and subvertical fractures in cm and dm size. The fractures are filled with saddle dolomite or late stage calcite cement (see below). The fracturing and faulting is related to compressional stresses during the Columbian and Laramide orogenies. These orogenies took place during the late Jurassic/Early Cretaceous and the Late Cretaceous to Early Paleocene, respectively and resulted in the Rocky Mountains (Mossop and Shetsen, 1994).

4.4.2 Saddle dolomite (Dolomite Type 3 and 4)

Saddle dolomite is a common cement throughout the study area and occurs as replacement as well. The crystals nucleate on matrix dolomite in vugs, molds and fractures and then grew into open pore spaces as subhedral crystals with curved faces and curved cleavage planes (Fig. 4.19). These crystals are up to several mm in size, they are white and show the characteristic sweeping extinction under the microscope. Saddle dolomites are associated with hydrocarbons, as they are in places covered with solid bitumen. Some of the minerals show zoning and they are bright luminescent. Saddle dolomite is more common in dolostones than in limestones, which perhaps is due to the lower porosities in limestones compared to dolostone at this stage of burial. Saddle dolomite also postdates matrix dolomitization and the fracture event I and II as well as all other hitherto described products. It is always one of the late diagenetic products and saddle dolomite is in many cases associated with epigenetic sulfide mineralization.

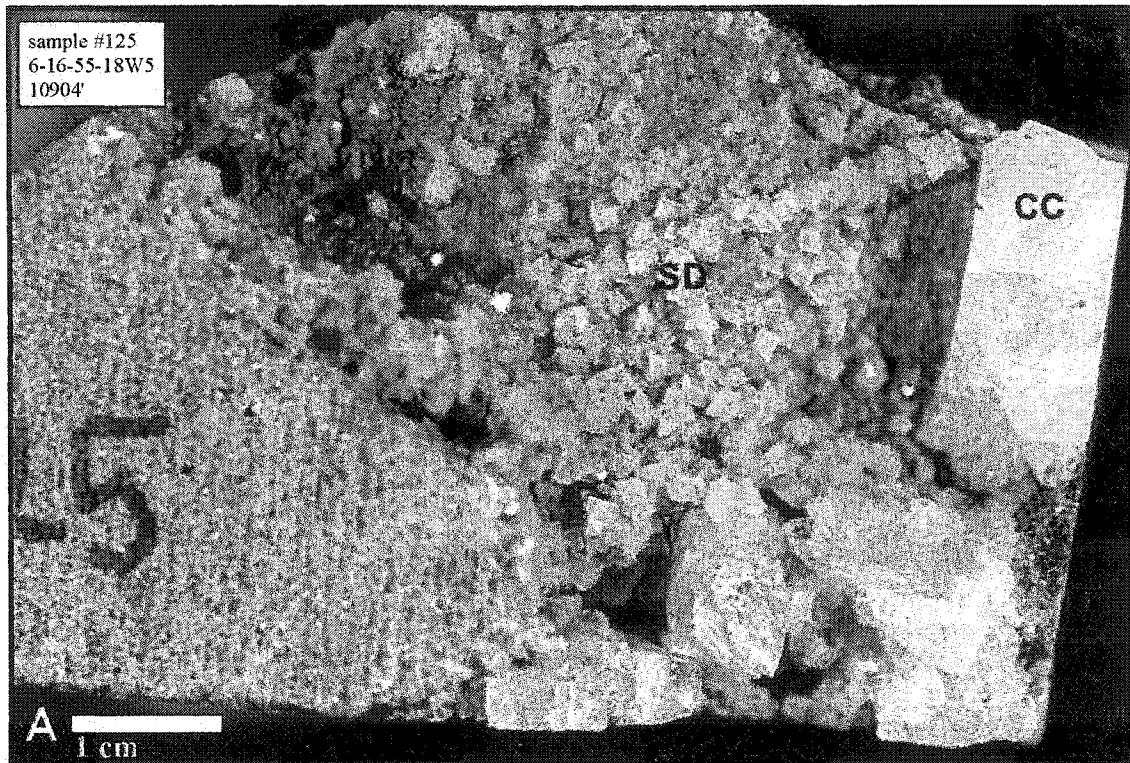


Figure 4.19: A) shows saddle dolomite crystals(SD) in a vug that are covered by solid bitumen and postdated by late blocky calcite spar (CC). B) depicts slightly larger saddle dolomite cements, that are covered with elemental sulfur, indicating that the saddle dolomite formed during TSR.

Radke and Mathis (1980) suggested that saddle dolomite forms within the oil window at temperatures between 60° and 150 °C, because it is often associated with hydrocarbons. It is often described as a product that precipitated from fluids with elevated temperatures (> 60 °C) and high salinities in a deep burial setting (Machel, 1987; Zenger & Dunham, 1988; Amthor & Friedman, 1991). It also has been suggested, that saddle dolomite is a by-product of thermo-chemical sulfate reduction, especially when it is associated with sulfide minerals (Machel, 1987; Mountjoy, 1991).

4.4.3 Calcite cement L (late diagenetic)

This cement occurs as coarse crystals (up to dm in size and m sized vug infills) (Fig. 4.20), which can be translucent or milky white in color and in many cases show distinct crystal planes and is fluid inclusion rich. This cement is the major fracture-filling product and postdates saddle dolomite without exception. It is widespread and a common feature in the SCCC as indicated by the CC in Figure 4.21. These late calcite cements have been described from the Obed Field (Patey, 1995), Simonette Field (Duggan, 1998), the Kaybob and Rosevear Fields (Green, 1999; Kaufman et al., 1990) as well as from outcrops in the Rocky Mountains (Smith, 2001).

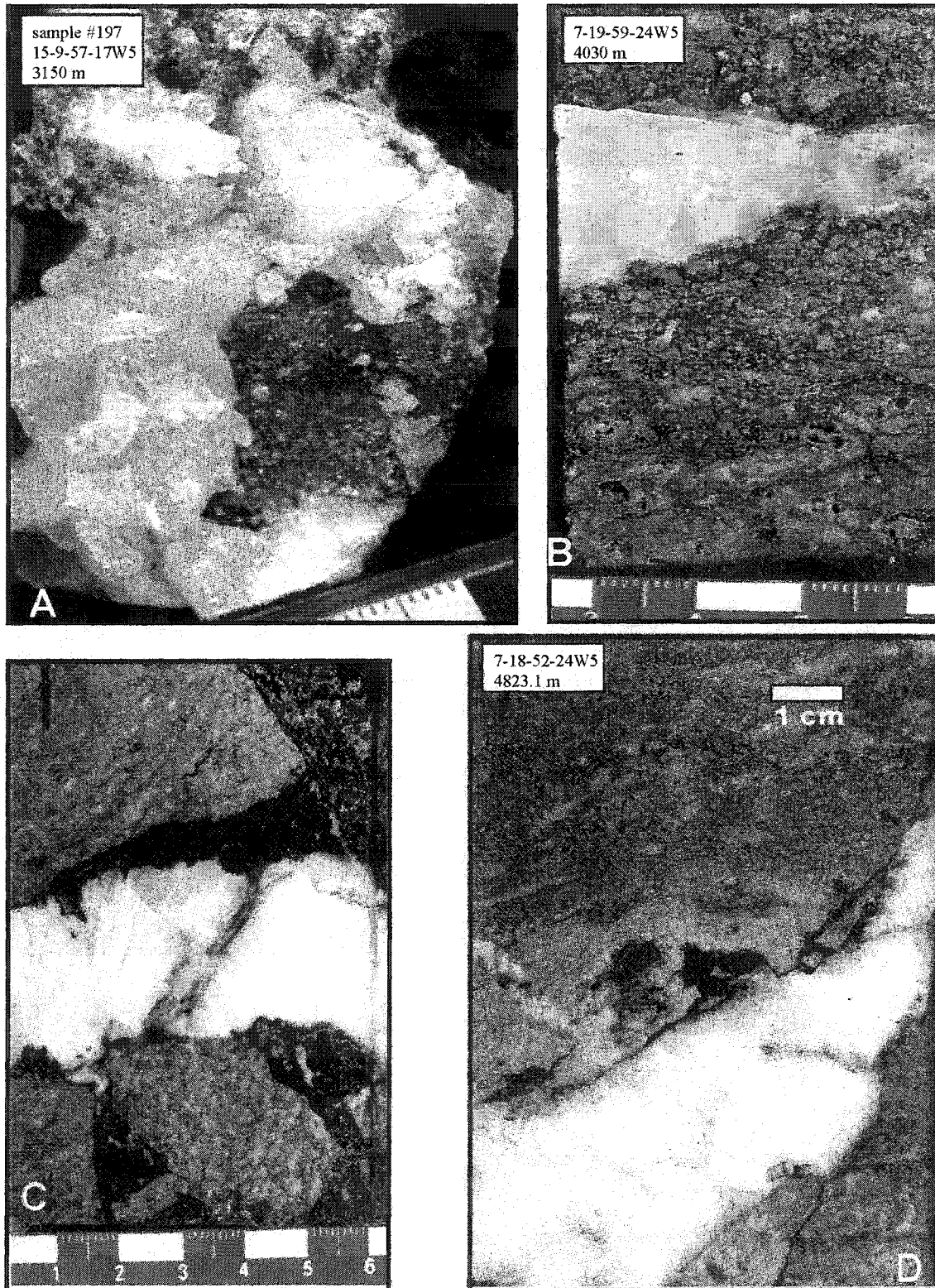


Figure 4.20: Late stage calcite cements occur throughout the study area in abundance and variability where anhydrite is minor or absent. A) and B) show the glassy to limpid calcite that lines vugs and molds. C and D show the common milky-white calcite fracture infill.

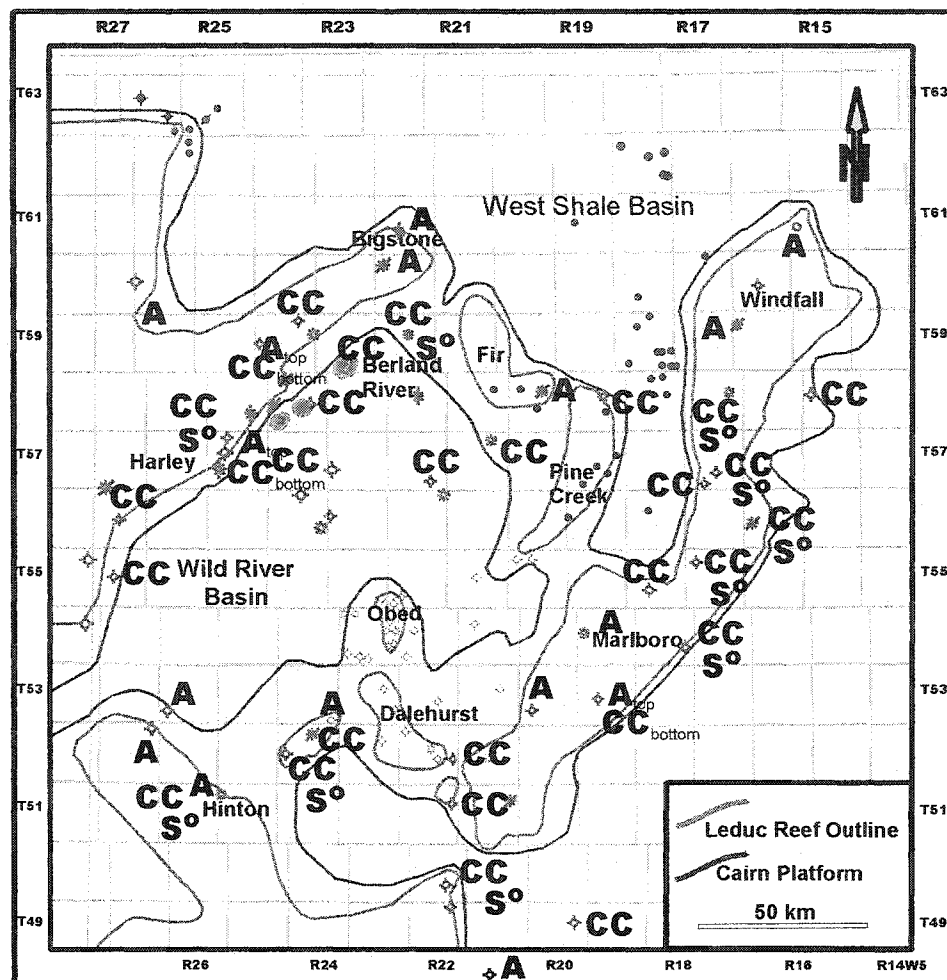


Figure 4.21: Distribution of various diagenetic products throughout the study area. Note that the late calcite (CC) is more common/ abundant where secondary/tertiary anhydrite(A) is rare or absent and vice versa. This may indicate that the tertiary anhydrite replaces the late calcite cement during very late/recent stages of diagenesis. Elemental sulfur (S°) occurs in deep strata and is more common closer to the Rocky Mountain Fold and Thrust Belt.

Paragenetic observations and geochemical data (see Chapter 5) indicate that the late calcite cements formed during maximum burial depths and/or later during uplift and cooling. Geobarometry combined with maturation modeling suggested depth ranges between 4 and 5.5 km for the late calcite cements in the Pine Creek and Kaybob area

(Green 1999). Because the late calcite cements occur over a wide areal and stratigraphic range it is inferred that the flow processes from which they were precipitated are regional processes that affected the deep part of the basin. Mountjoy & Amthor (1994) and Bachu (1995) inferred a basin-wide flow along stratigraphic, fracture and fault conduits during deep burial during the Cretaceous and Paleocene. Machel et al. (1996) interpreted the late calcite cements at Obed as a result of tectonic expulsion of fluids during the late Cretaceous-Early Paleocene Laramide orogeny. It is therefore assumed that the late calcite cements in the SCCC are a result of tectonically induced fluid migration horizontally as well as vertically during times of high tectonic movement, e.g., the Laramide orogeny in the Late Cretaceous and early Paleocene.

4.4.4 Elemental sulfur

Elemental sulfur (S^0) occurs together with saddle dolomites and/or is associated with the late calcite cement. It can either be a yellow, powder like mineral, or a blotchy yellow, chewing gum resembling, and shiny amorphous mineral of several mm in size (Fig. 4.19).

Elemental sulfur usually is formed as an intermediate product from partial reoxidation of H_2S , as shown by the following alternatives (Reactions A to C) (Machel, 1992; 2001):



With sulfate (reaction B and C) being the only common oxidant in high temperature diagenetic settings like the ones in this study area. However, elemental sulfur is a rare

diagenetic product, because as the settings of TSR are typically reducing and/or anoxic elemental sulfur is usually reduced to sulfide by excess organics (Machel, 2001).

4.4.5 Pyrite III/sphalerite

Iron sulfide minerals are always associated with saddle dolomites and clear, limpid, late diagenetic calcite cements. They occur as euhedral minerals in mm size in vugs and fractures, however their total abundance is very low.

Iron sulfide minerals form from the reaction of H₂S with ferrous iron (Riciputi et al., 1996) via reactions such as: $\text{Fe}^{2+} + \text{H}_2\text{S} \rightarrow \text{FeS} + 2\text{H}^+$.

These reactions commonly produce various acid-soluble iron monosulfides, which tend to recrystallize and/or be replaced by pyrite (e.g., Barnes, 1979). Controlling factors of the formation of pyrite and other metal sulfides during diagenesis are the availability of reactive metal, the rate and amount of sulfate supplied to the system, the availability of organic material, and excess of sulfide over ferric iron (Fe³⁺) (Riciputi et al., 1996).

4.4.6 Microfractures

Microfractures are very irregular hair-like features in micron size as shown in Figure 4.16. They only occur in reservoirs that are at depths of about 3500 m or deeper. The fractures are filled with solid bitumen and commonly enhanced the reservoir quality of these traps (Marquez and Mountjoy, 1996).

According to Stasiuk (1997) the gas generation in the relatively well-sealed Leduc reservoirs led to significant overpressures, which eventually generated microfractures. This process also took place in some reservoirs of the SCCC, that are directly in the vicinity of the disturbed belt and which have been buried to maximum depths of about 7000 m.

4.4.7 Hydrogen sulfide (H₂S)

Most reservoirs in the study area contain hydrocarbons with substantial amounts of H₂S up to 35.7 %. H₂S is the most conspicuous and abundant product of TSR (Machel, 2001, and references cited therein). Any reservoir with more than a few percent H₂S presumably underwent TSR, because thermal cracking of hydrocarbons does generally not provide more than about 1-3% H₂S (Orr, 1977). H₂S develops as a separate gas stage in TSR settings once its concentration exceeds its aqueous solubility (initially H₂S forms and is dissolved in the formation water). The amounts of H₂S that can be generated and/or accumulated are dependent on several factors (Krouse & Hutcheon, 2000; Machel, 2001). One limitation is the availability of organic reactants and sulfate. Another limitation is the presence/absence of base metals, since metal sulfides are rapidly formed when Me²⁺ and S²⁻ come into contact and H₂S is effectively removed via the precipitation of metal sulfides. However, this is apparently not important in deep diagenetic carbonate settings, because they do not contain sufficient amounts of base metals and therefore host significant amounts of H₂S. Clastic rocks, in contrast, contain larger amounts of reduced and reducible transition and base metals, thus H₂S can be removed, which probably explains the scarcity of clastic sour gas reservoirs (Machel, 2001).

Another restraining factor on H₂S concentrations is hydrodynamics, or more specifically the solubility of H₂S and hydrodynamic flux. The aqueous solubility of H₂S is much greater than that of most hydrocarbon gases (Orr, 1977; Barker, 1982), thus the potential of migration of H₂S in solution is greater than for sweet gas in regions with strong advection. Hence, the solubility of H₂S probably is not a limiting factor for migration in solution. However, fluxes of formation waters in deep (3000m to 5000m) reservoirs like the SCCC are exceedingly low, which appears to inhibit the significant removal of H₂S via advection even over geologic times in most locations. The occurrence of the deep sour gas fields in the SCCC and other parts of the Alberta Basin support this assumption. However, arguments have been made that H₂S diffusion out of a system can limit the H₂S concentrations significantly in at least some locations (Wade et al., 1989). In addition, Krouse and Hutcheon (2000) strongly relate the H₂S concentration to the amount of available sulfate. A combination of these factors is most likely the reason for the high variability of H₂S concentration in the SCCC (Fig. 4.2) as well as other parts of the Alberta basin.

4.5 STAGE 5: Post-Orogenic Uplift

Stage 5 represents the time between maximum burial and the present reservoir depths (Fig.4.2). Diagenetic products are small amounts of calcite and dolomite cements, which do not affect the present hydrology in the deep part of the basin. Tertiary anhydrite is abundant in some parts of the study area (Fig. 4.21 listed by capital A) and is a major obstacle for the present day reservoir quality (pers. Communication, Chevron 2000).

4.5.1 Tertiary anhydrite

Late diagenetic, tertiary anhydrite occurs mainly in fractures as cement as seen in Figure 4.22 D. The anhydrite is usually milky- white. It can occur in a range of textures and crystal sizes, e.g., felted (mm size) or bladed (cm size). Sometimes it is associated with minor amounts of late calcite cement. In the latter case, the amount of calcite cement is very low in comparison to that of anhydrite. It seems that remnants of late calcite cements are irregular distributed within the massive anhydrite and that the anhydrite is replacing the calcite cement.

4.6 Porosity Evolution

The diagenetic products described above are the result of a plethora of processes, which either resulted in the enhancement and/or reduction of porosity and permeability in the reservoir rocks (Fig. 4.1) and happened during five stages (Fig. 4.23). Each stage contributed to a significant change in the above-mentioned parameters. Facies type, lithology as well as primary porosity and permeability (“poroperm”) are governing factors in the burial fate of the reservoir rocks.

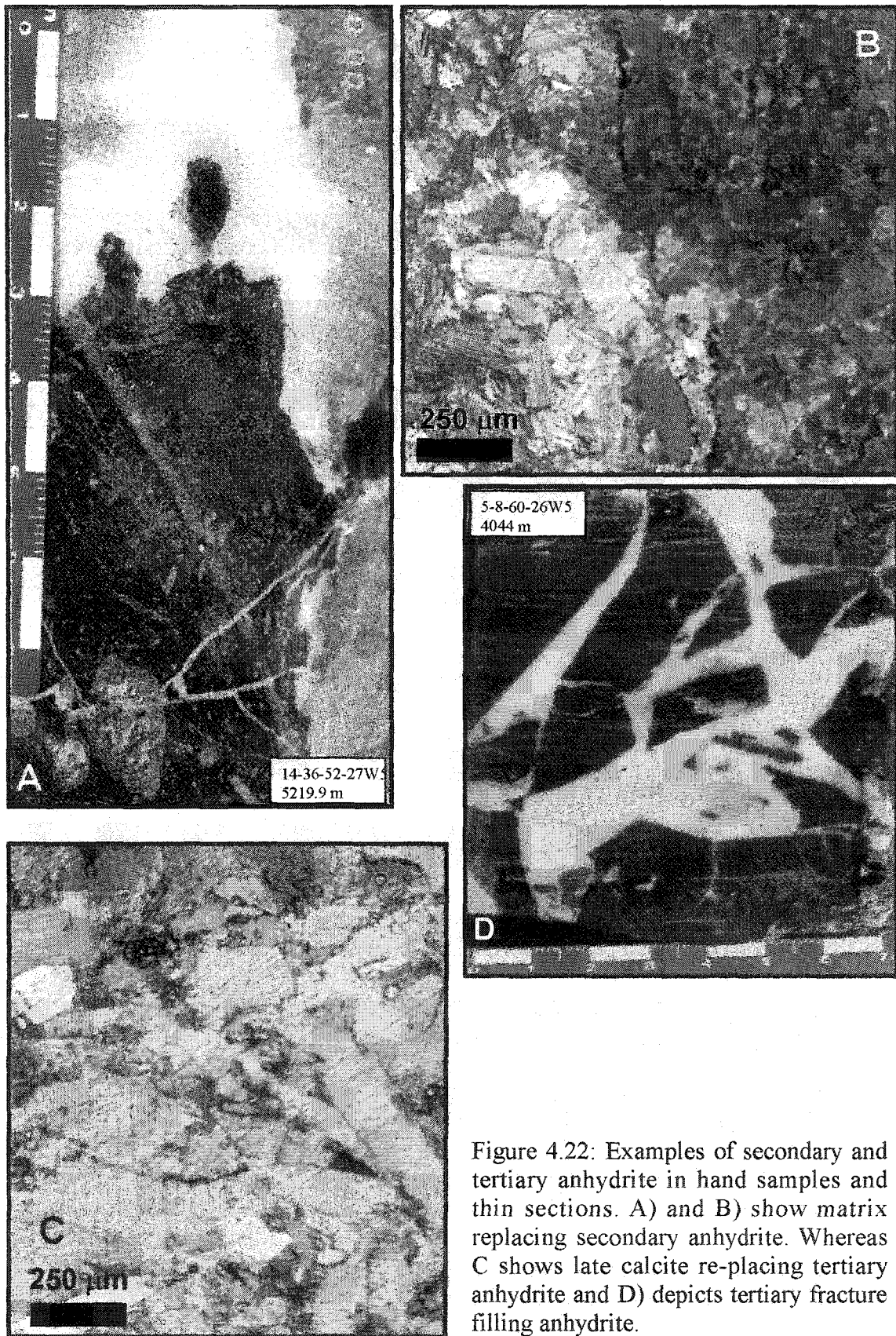


Figure 4.22: Examples of secondary and tertiary anhydrite in hand samples and thin sections. A) and B) show matrix replacing secondary anhydrite. Whereas C shows late calcite re-placing tertiary anhydrite and D) depicts tertiary fracture filling anhydrite.

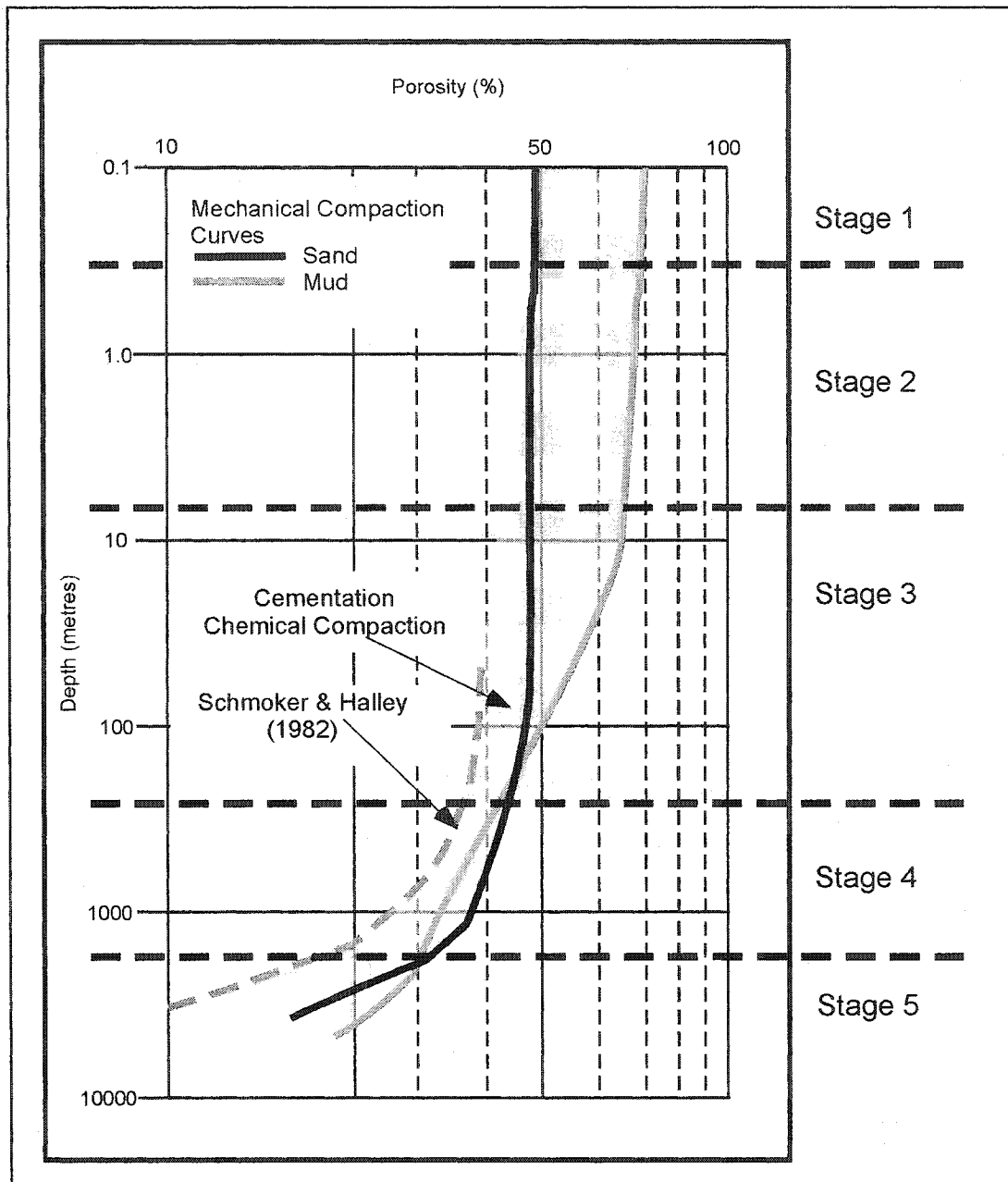


Figure 4.23: The change in porosity of mechanically compacted mud and sand sediments with depths (Goldhammer, 1997). The potential effect of chemical compaction and cementation is shown by the difference between mechanical compaction and subsurface porosity vs. depth data from Florida (Schmoker and Halley, 1982).

During Stage 1 diagenesis, a general decrease in poroperm took place due to marine cementation and beginning physical compaction. The latter process was very efficient in the fine-grained mudstones resulting in a reduction of porosity from 70 % to about 40% within the first 100m of depths (Goldhammer, 1997). In contrast, the more rigid grainstones, packstones and boundstones may retain their primary porosity of about 40 % until depths of ~700 to 1000 m before grain breakage and closer packing result in the first significant reduction of pore space during stage 2 (Lucia, 1999) (Fig. 4/p.116). However, porosity values of about 30 –40 % still provide sufficient pore space and permeability for the dolomitizing fluids, which preferentially move through the reefal carbonates and grainstones and rudstones at the reef flanks.

The primary porosity in these rocks decreases with increasing dolomitization, because the dolomites are using volumetrically more space than the precursor limestones. However, the dolomites are more resistant to pressure solution and compaction during progressive burial, thus they retain a high amount of porosity in comparison to limestones at the same depth (Amthor et al., 1994; Mountjoy et al., 2001). This effect renders them the best reservoir rocks in the study area and in the Alberta Basin. Another important process during Stage 2 is the selective dissolution of calcite fossils that escaped earlier dolomitization and resulted in moldic porosity, though this step did not increase permeability at this stage, because moldic pore spaces are only connected through the interparticle network. However, this might have changed during later stages (3 and 4), when the interparticle pore space was enlarged due to highly reactive formation brines that entered the system with the emplacement of hydrocarbons and subsequently sour gas.

The initial hydrocarbon migration into the reservoirs during the late Cretaceous (Stage 3) appears to have inhibited diagenesis at least for a while, because no apparent products are associated with this stage. This scenario changed when fracturing and further burial into the TSR regime reactivated the system and saddle dolomite, late calcite cement, anhydrite as well as the emplacement of sulfides took place.

Present day porosity and permeability values (Table 4.1 and core analyses in the Appendix) of the reefal dolostones range between 5–25 % and 5-200 md, respectively, with an average reservoir porosity of 7%. The rudstones and grainstones vary between 3-10 % (average 5%) porosity and 0.5 to 100 md permeability. The initially highly porous lime muds of the basin as well as shallow subtidal to intertidal settings are now ranging between less than 1% porosity and less than 0.1 md permeability, which makes them effective seals for the reservoir rocks they encompass.

	Porosity (%)	Average Permeability (md)
WABAMUN	1 to 38 %	0.04
NISKU	1 to 22 %	0.09
LEDUC	4 to 25 %	0.30
WATERWAYS	1 to 19 %	0.20

Table 4.1: Present day guide values for porosity and permeability in the four Upper Devonian carbonate units. Calculated from Drill Stem Test's and core analyses. From Bachu and Underschultz, 1992.

CHAPTER 5: GEOCHEMICAL DATA AND FLUID INCLUSIONS

5.1 Introduction

Stable isotopes ($\delta^{18}\text{O}$, $\delta^{13}\text{C}$, δD , $\delta^{34}\text{S}$), radiogenic isotopes ($^{87}\text{Sr}/^{86}\text{Sr}$), and fluid inclusion investigations are commonly used in the study of carbonates to aid in defining their diagenetic history (Tucker, 1988, and references cited therein). There are some major problems involved with the stable isotope geochemistry in carbonates (Land, 1980) due to the high fractionation effects. The major problem is that the relationship between temperature, $\delta^{18}\text{O}_{\text{water}}$, and $\delta^{18}\text{O}_{\text{dolomite}}$ is imprecisely known and it is therefore important that the interpretation of the data is done in comparison with other geochemical analyses, especially fluid inclusion measurements.

5.1.1 $\delta^{18}\text{O}/\delta^{13}\text{C}/\delta^{34}\text{S}$ of solids

The oxygen isotopic ($\delta^{18}\text{O}$) composition of carbonate minerals is dependent on various processes (Fig. 5.1) and may provide information about temperatures during precipitation, meteoric water influx, or recrystallization. The carbon isotopic ($\delta^{13}\text{C}$) composition provides insights into processes like biodegradation, methane oxidation, fermentation, thermal decarboxylation, as well as sulfate reduction (Figs. 5.1, 5.2, 5.3). Sulfur isotopes ($\delta^{34}\text{S}$) of evaporites, bitumen may provide additional information about anhydrite sources, thermochemical sulfate reduction, and sulfide precipitation, as well as processes like biodegradation and thermochemical sulfate reduction (Fig. 5.4).

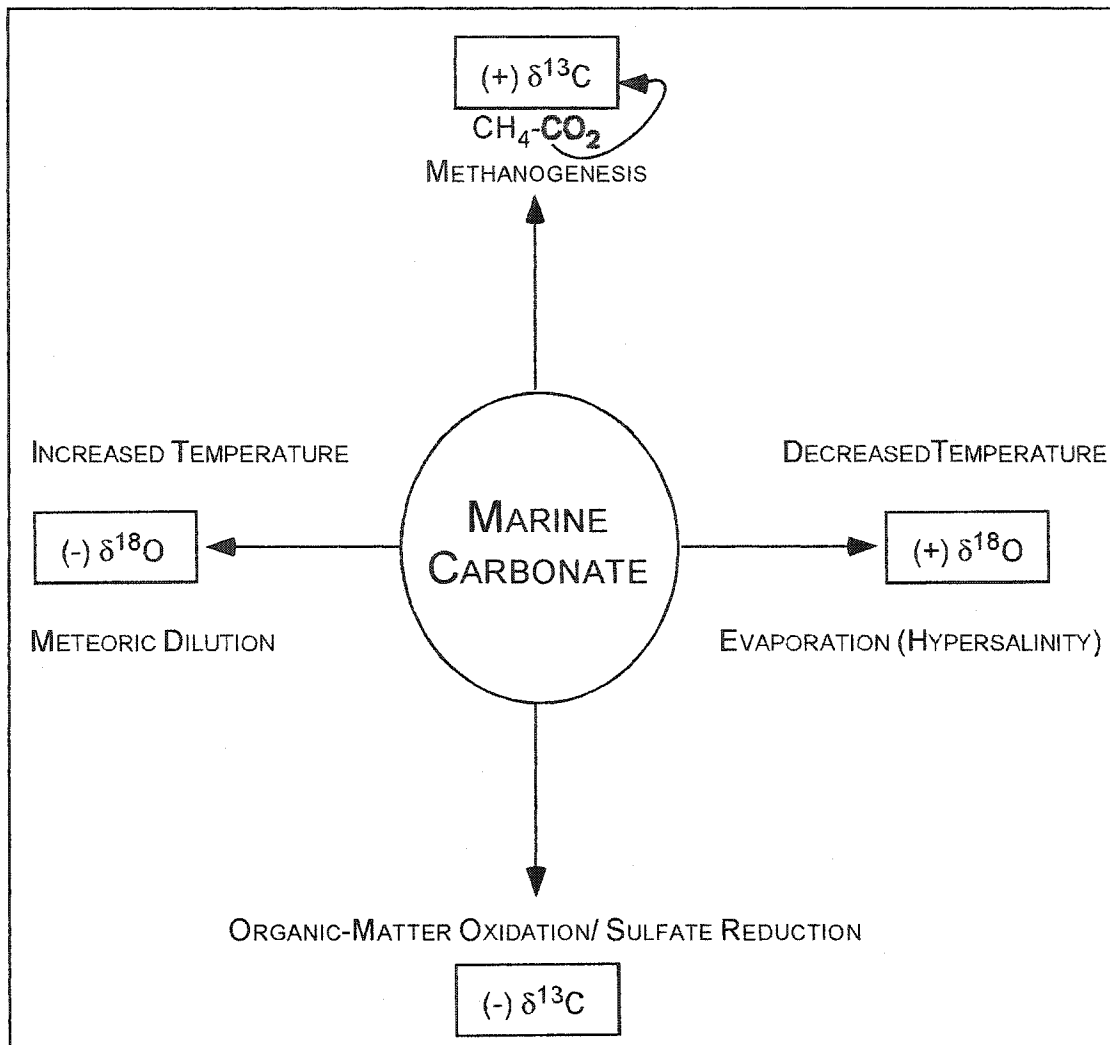


Figure 5.1: Summary of the effects of temperature, evaporation, and dilution of the fluids, plus input of CO₂ derived from methanogenesis, and organic matter oxidation, on the isotopic composition of carbonates. After Lohmann (1988).

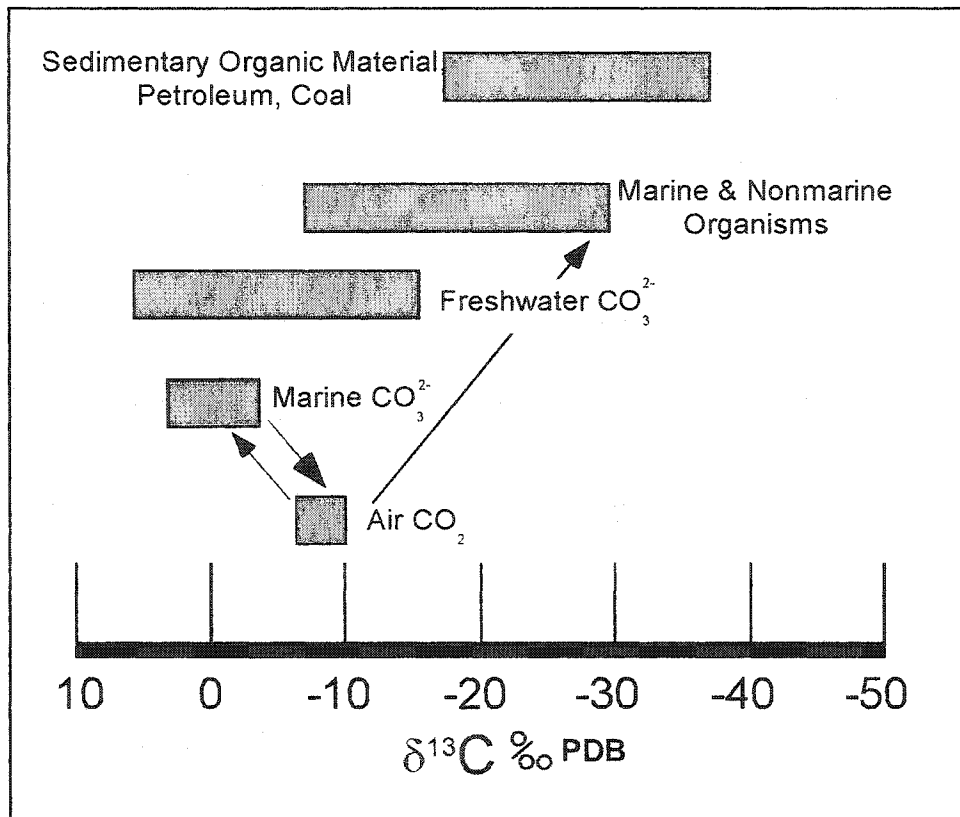


Figure 5.2: $\delta^{13}\text{C}$ compositions of common carbon-bearing compounds. The ultimate source of carbon in submarine cements, shells and soft parts, aquatic algae, kerogen, and oil, is atmospheric CO_2 . Carbon isotopes are fractionated so that ^{12}C is concentrated in organic material and the products of its degradation (microbial methane, kerogen, oil) and ^{13}C is concentrated in inorganic material (after Allan & Wiggins, 1993).

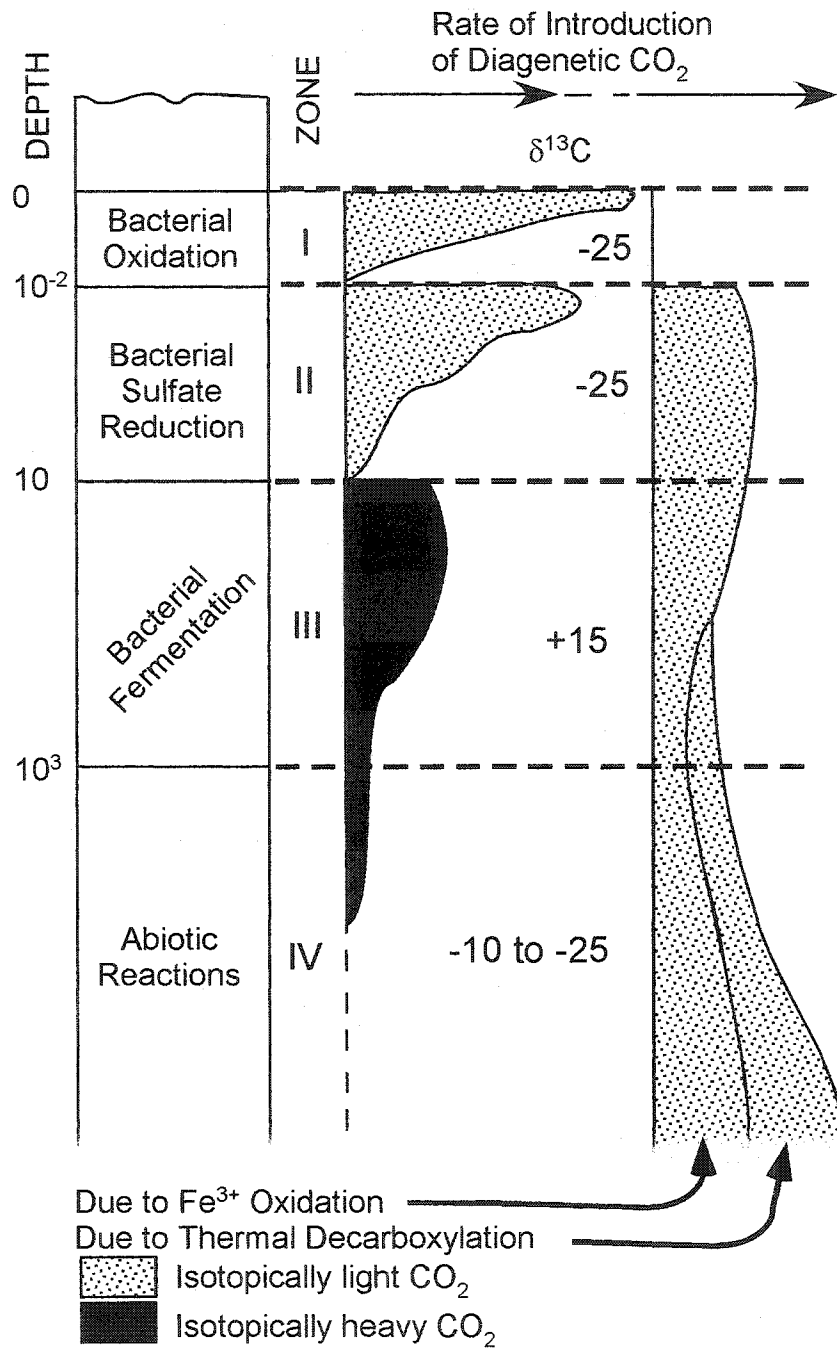


Figure 5.3: Diagenetic CO₂ within different diagenetic zones (after Irwin & Curtis, 1977).

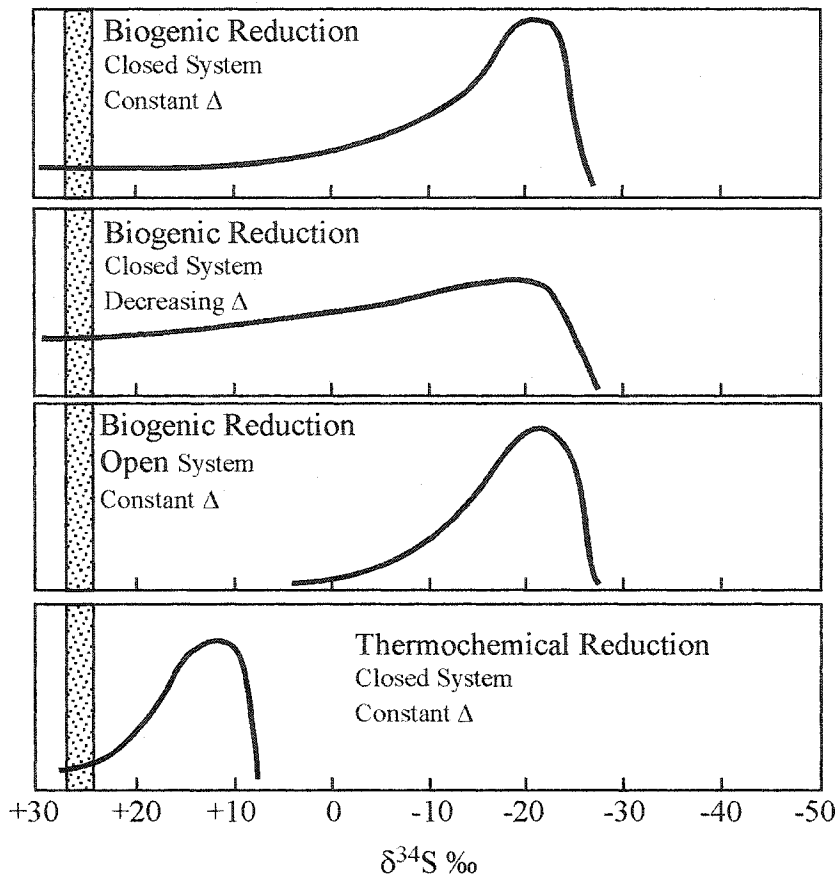


Figure 5.4: Theoretical distribution of $\delta^{34}\text{S}$ values for sulfides formed from Devonian seawater sulfate (+25 ‰) by biogenic and thermochemical sulfate reduction. Models for systems both open and closed to additional input of sulfate are illustrated for biogenic sulfate reduction; the effect of decreasing Δ is also illustrated for biogenic sulfate reduction. The $\Delta_{\text{sulfide-SO}_4}$ value is assumed to be -50 ‰ for biogenic sulfate reduction, and -15 ‰ for thermochemical sulfate reduction. The stippled pattern illustrates the best estimate of Upper Devonian seawater sulfate. Modified after Riciputi et al., 1996.

5.1.2 $\delta^{18}\text{O}$ / δD of fluids

The oxygen ($\delta^{18}\text{O}$) and hydrogen (δD) isotope compositions of the formation fluids may answer questions about fluid origin, e.g., whether it was derived from meteoric, marine or evaporative waters, and regarding interaction with host rock minerals (Table 5.1 and Fig. 5.5).

Water	$\delta^{18}\text{O}$ (‰ SMOW)	δD (‰ SMOW)	Reference
Seawater Devonian	0 to -3	0	
Meteoric Water Devonian	-7 to -3	-40 to -20	(Conolly, 1991)
Clay minerals Devonian	+13 to +17	-80 to -20	(Longstaffe, 1989)
Meteoric water Today(AB)	-18	-130	(Connolly et al., 1990)
SulfateOxygen (TSR)	+ 14.5 to 15	-300 to -120 (from HC)	(Machel, 1985)
Water of Dehydration (Gypsum)	+ 8 / + 4 (to SO ₄ saturation) → + 12	+5 to +15 / +25 → +30 to +45 (Pflaume)	(Machel, 1985)
Metamorph H ₂ O	+3 to +20	-65 to -10	(Barnes, 1979)

Table 5.1: Summary of stable isotope variation in different waters that could have contributed to present day formation brine isotopic compositions. See also Figure 5.5 and text for further explanation.

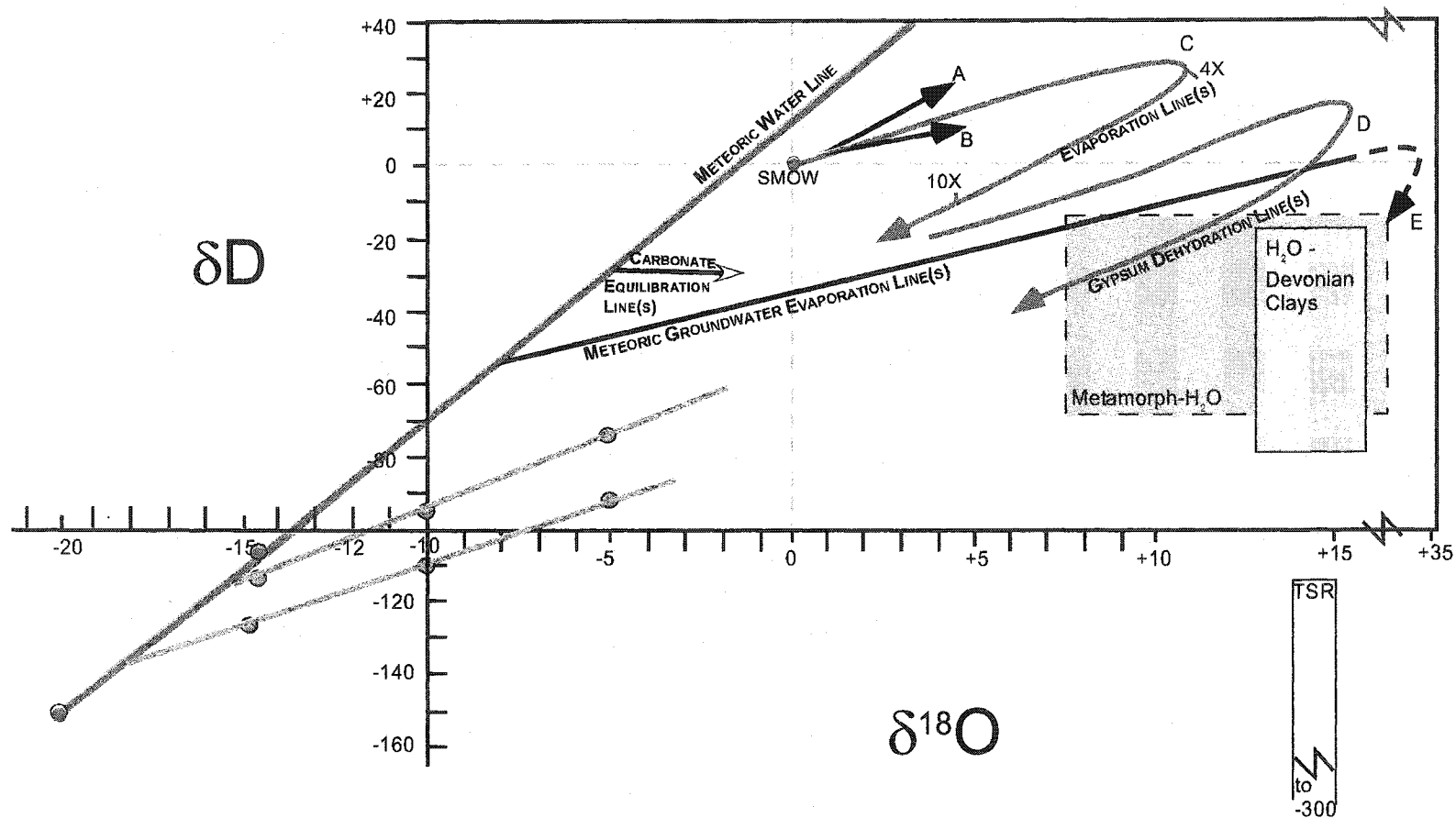


Figure 5.5: Trajectories and fields for the isotopic composition of various waters as well as evaporation lines. The green shaded field represents Devonian meteoric water after Connolly, 1991. The yellow shaded field represents H_2O from Devonian clay minerals after Longstaffe, 1989. The TSR box has been established using Machel (1985). The two green lines represent Devonian Formation brines from Hitchon and Friedman (1969) and Connolly et al. (1990). Vector A represents initial evaporation under relatively humid conditions; vector B is for arid conditions. Curve C is Holser's estimate (Holser, 1979) of evaporating seawater through a concentration of 10 x. The isotopic composition of hydration water in gypsum precipitated at any point on evaporation trajectory C is given by curve D. (Diagram modified after Knauth and Beeunas (1986). See also Table 5.1.

5.1.3 $^{87}\text{Sr}/^{86}\text{Sr}$ isotopes

The isotopic composition of strontium in the hydrosphere depends on the $^{87}\text{Sr}/^{86}\text{Sr}$ ratios of the rocks that interact with the circulating fluids, hence strontium isotope ratios of rocks can be used as tracers for paleo fluid flow (Banner, 1995). In addition, carbonates and evaporites have sustained a record of the changing isotope composition of Sr in the oceans throughout Proterozoic and Phanerozoic time (Faure, 1982; Burke et al., 1982; Banner, 1995; Denison et al., 1997, Veizer et al., 1999). Strontium isotopes can therefore be used as a relative age dating tool (Fig.5.6) under favorable conditions (no external input of strontium and/or rubidium).

Additionally, groundwater and subsurface brines also contain Sr whose isotopic composition is controlled by the lithology/chemical composition of the rocks they have interacted with. The Sr isotopic compositions of oil field brines have therefore been used to identify their provenance and migration, ion exchange reactions with clay minerals during diagenesis and mixing of brines of various origins. The diagenetic products (carbonates and evaporites) that precipitate from these brines have the same $^{87}\text{Sr}/^{86}\text{Sr}$ ratios as the brines, because the precipitation process does not fractionate Sr isotopes. Furthermore, the $^{87}\text{Sr}/^{86}\text{Sr}$ ratios of the carbonates and evaporites are practically unchangeable over time because they do not contain Rb. Therefore, it can be concluded that the carbonates and evaporites retain the value of the $^{87}\text{Sr}/^{86}\text{Sr}$ ratio that existed in the brine from which they were originally precipitated. As a result, Sr isotopes of diagenetic products are a powerful tool in tracing the evolution of pore fluids, their migration behavior, and diagenetic processes.

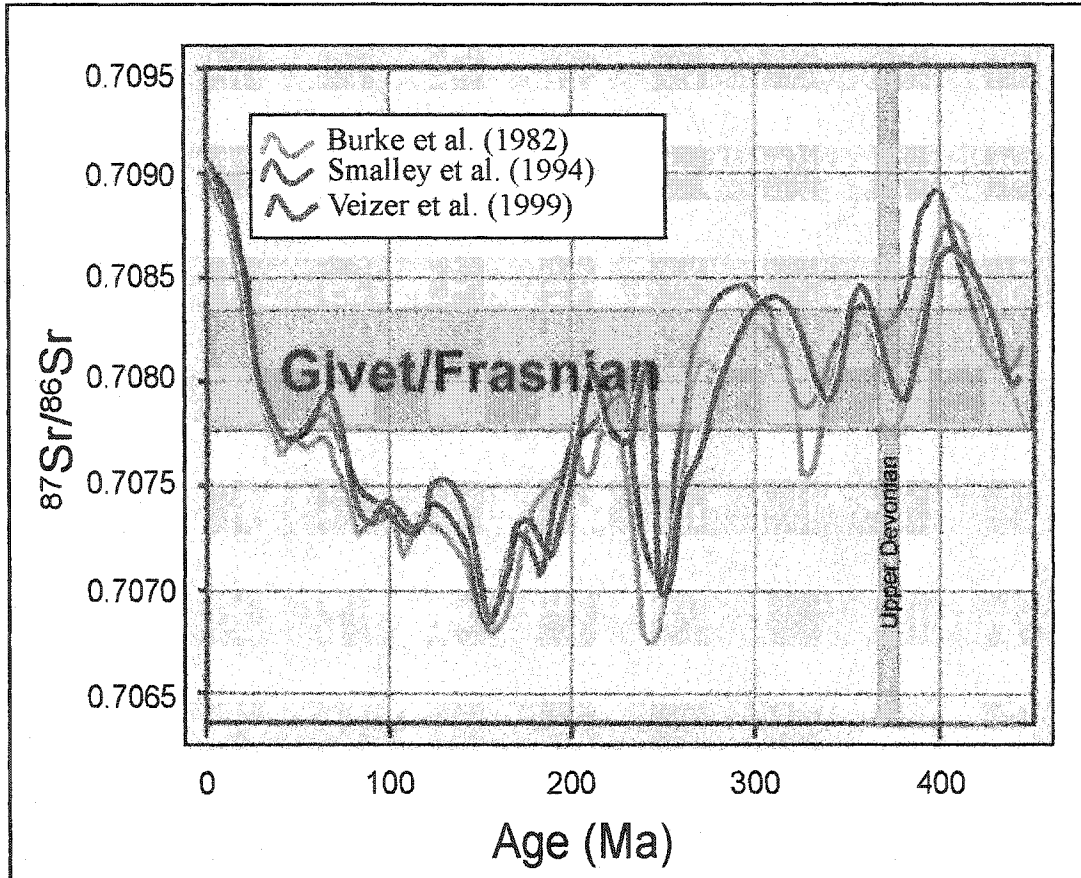


Figure 5.6: Variation of the $^{87}\text{Sr}/^{86}\text{Sr}$ ratio of marine carbonates during Phanerozoic times. The gray shading denotes the Upper Devonian time span as well as its $^{87}\text{Sr}/^{86}\text{Sr}$ range. Modified after Burke et al. (1982), and Smalley et al. (1994), and Veizer et al. (1999).

5.1.4 Fluid inclusions

Fluid inclusions provide the only direct information about ancient temperatures, pressures, and fluid compositions, and can improve the understanding of a diagenetic system (Goldstein & Reynolds, 1994). Fluid inclusions are fluid-filled vacuoles up to 10 μm or more in size in minerals (Roedder, 1981). Fluid inclusions are formed within lattice imperfections of actively growing crystals and are best preserved within pores or fracture fills, which explains why cements are more useful for fluid inclusion studies than

fine-grained matrix dolomites (Allan & Wiggins, 1993). Fluid inclusions conventionally are subdivided into primary and secondary. The original solution of precipitation is only trapped in primary inclusions. Figure 5.7 shows that primary fluid inclusions can be distributed along crystal growth zones or can be randomly spread within a crystal (Roedder, 1981). Secondary fluid inclusions are trapped after a crystal grew, hence, they do not represent the original precipitation conditions and commonly occur along microfractures. It is crucial to determine the timing of entrapment of an inclusion relative to the mineral paragenesis, because only the primary inclusions reflect the original precipitation conditions.

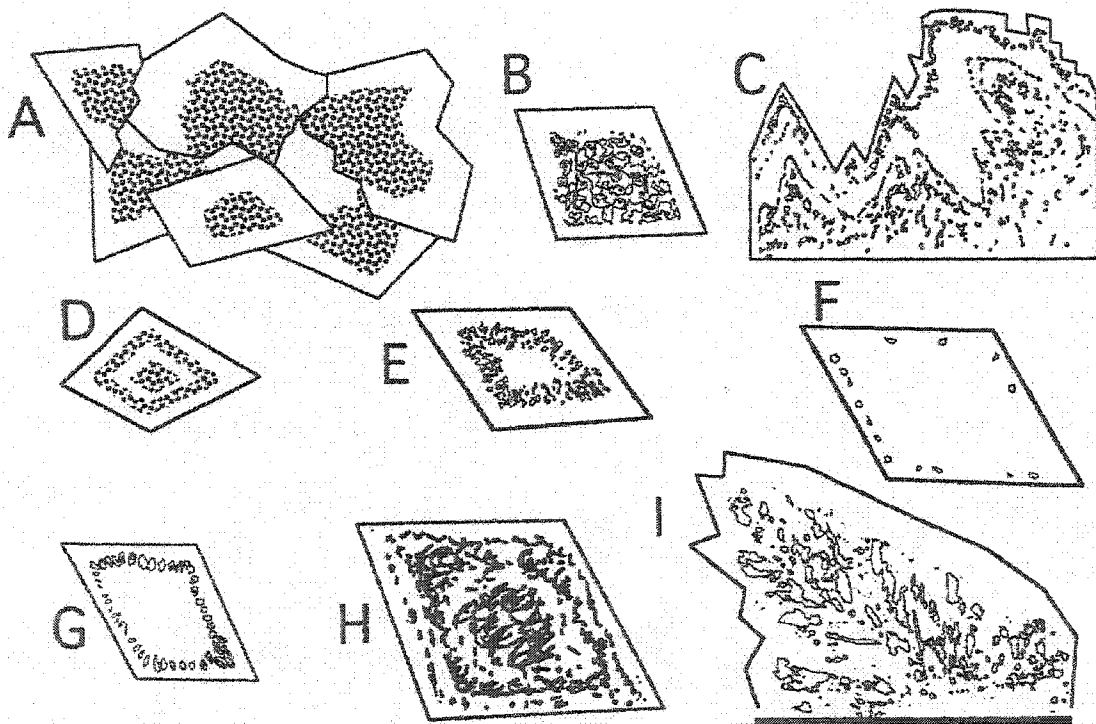


Figure 5.7: Diagram illustrating the occurrence of primary fluid inclusions in carbonate crystals, showing that the inclusion distribution is controlled by growth zonation. A and B show inclusion-rich cores surrounded by clearer rims. C, D, and E show inclusion rich zones that are sharply bounded by clear zones. F and G show single line inclusions along growth zones, whereas H shows a cloudy distribution, however still mimics the growth zonation. I shows the for certain dolomite common “fir-tree pattern” distribution of fluid inclusion (after Goldstein and Reynolds, 1994).

In most cases fluid inclusions are completely filled with a homogenous saline solution during their formation. Such inclusions become two-phased and a vapour bubble is present in addition to the solution upon cooling and exhumation. Upon heating, the liquid-vapour homogenization temperature (T_h), the temperature at which a two-phase inclusion homogenizes to one phase, provides an estimate of the minimum temperature of crystallization of the host crystal (Allan & Wiggins, 1993). In addition, measuring the depression of the freezing point and then the final melting temperature $T_m(\text{ice})$ indicates the major dissolved solids and bulk salinity of the fluid inclusion contents. Specifically, the final melting temperature is a measure of the amount the freezing point of inclusion water is depressed below 0°C by the presence of dissolved salts. However, equal concentrations of different ions depress the freezing point by different degrees, therefore certain assumptions are made about the brine compositions. By convention, salinity is calculated from T_m (Fig. 5.8) by assuming the fluid is a pure NaCl-brine, and salinities are expressed as wt% NaCl equivalents. T_m decreases with increasing fluid inclusion salinity (Fig. 5.8). The composition of the major salts is obtained by measuring the temperature of first melting after supercooling the inclusions to a temperature at which the inclusion contents are entirely frozen, which is known as the eutectic temperature T_e . T_e is rarely reported for carbonate minerals since its measurement is rather difficult, therefore, NaCl-dominated fluids are commonly assumed for carbonate systems (after Allan & Wiggins, 1993) in spite a more complex system is indicated by Spencer (1987).

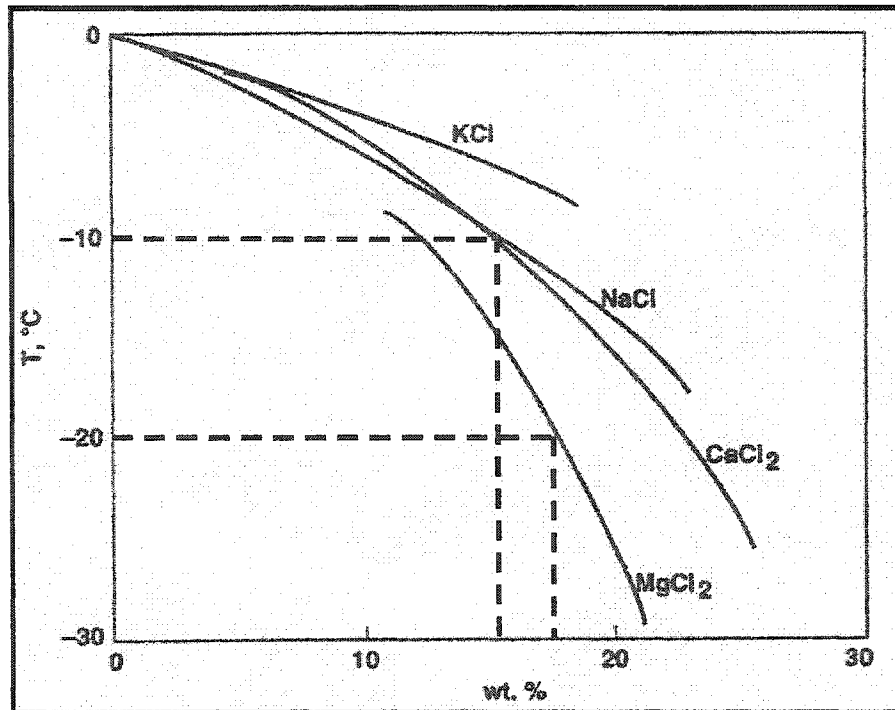


Figure 5.8: Salinity can be calculated from T_m if the composition of the fluid is known. For example, if the fluid is known to contain predominantly NaCl, then a T_m of -10°C would indicate a salinity of approximately 15 wt% NaCl equivalents. A MgCl_2 brine with a T_m of -20°C would have a salinity of approximately 17 wt% MgCl_2 equivalents. Modified from Allan and Wiggins, 1993. The salinities and pressure corrections for this study were done assuming a NaCl-brine composition.

The measured T_h temperatures are only minimum temperatures and after establishing the salinity system, a pressure correction is applied to determine the actual trapping temperature (Fig. 5.9), which is done by estimating the maximum burial depth and including the specific pressure regime (Goldstein and Reynolds, 1994). Crossplots of fluid inclusion T_h and T_m data may reveal information about the fluid inclusion history and hence related information about basin evolution (Roedder, 1981; McLimans, 1987).

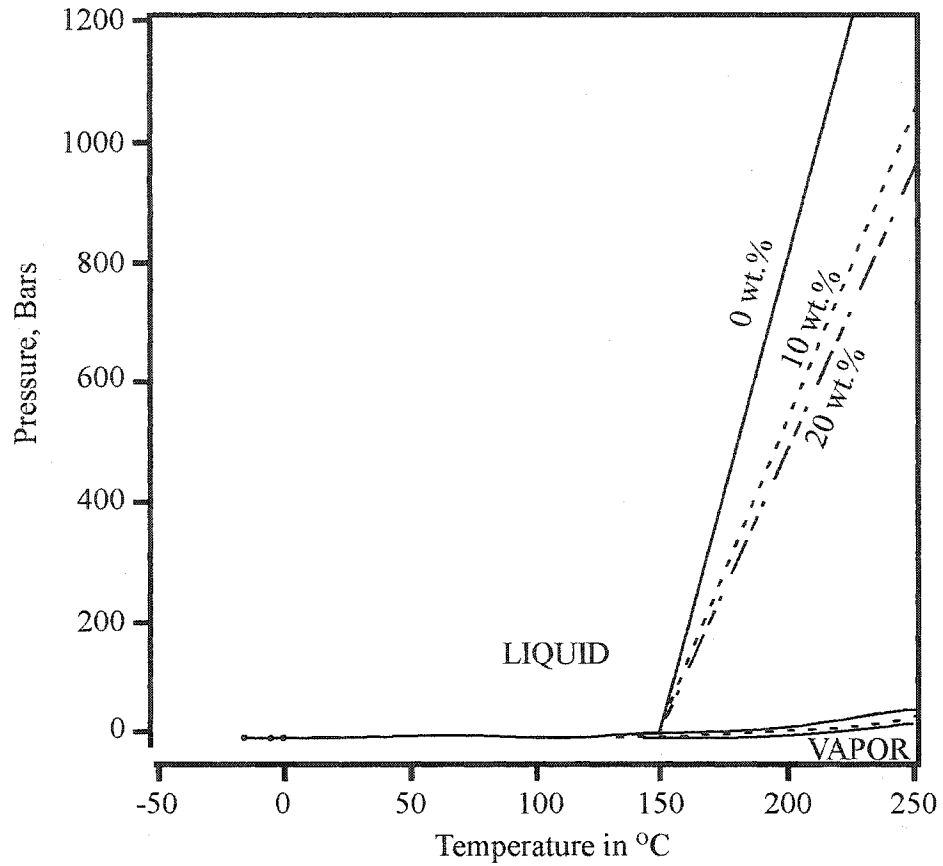


Figure 5.9: P-T plots for H₂O-NaCl systems showing similarity in positions of the liquid-vapor curves, differences in slopes of isochores, and differences in triple points between pure water and water with 10 and 20 wt.% NaCl dissolved. After Goldstein and Reynolds, 1994.

5.2 Analytical Methods

Powder samples for geochemical analyses were obtained using a low speed dental drill assembly. Each of the main diagenetic phases, e.g., matrix dolomite, saddle dolomite, late calcite cement and anhydrite, were extracted separately and a total of 150 powder samples was produced.

Forty carbonate powder samples were selected for carbon and oxygen isotope analyzes using the standard procedure by McCrea (1950). For the carbon and oxygen isotopes of the carbonate minerals a 20 to 30 mg aliquot of powder was reacted with 100 % phosphoric acid at 25°C for 24 hours (calcites) and for 5 days (dolomites). The extracted CO₂-gas was analyzed with a Finnigan-Mat 252 mass spectrometer. The results were reproducible within ± 0.1 ‰ for $\delta^{18}\text{O}$ and $\delta^{13}\text{C}$. The isotope values for the rock samples are reported in δ ‰ PDB (PDB: *Belemnitella americana* of the PeeDee Formation/Cretaceous, South Carolina, USA after McCrea, 1950).

Seven formation brines were retrieved from wellheads and analyzed for δD and $\delta^{18}\text{O}$ following the chromium reduction and the CO₂-H₂O equilibration techniques, respectively at the University of Calgary (Stephen W. Taylor, Lab Manager, Isotope Science Laboratory, Dept. of Physics & Astronomy, University of Calgary; pers. comm. 2002).

Sulfur isotopes of brines, anhydrite, elemental sulfur and bitumen were measured by Continuous-Flow Isotope Ratio Mass Spectrometry at the University of Calgary. The

Oxygen and deuterium isotope values for the brines are reported in δ ‰ SMOW (Standard mean ocean water). The sulphur isotopes are given in δ ‰ CDT (Canyon Diablo Troilite).

All data have been corrected with respect to their standards. In addition, the $\delta^{18}\text{O}$ values of the dolomites have been corrected by -0.82 ‰ due to different fractionation effects between CO_2 and dolomite/calcite during the reaction with phosphoric acid (Sharma & Clayton, 1965).

Strontium isotope ratios of a total of 90 calcite and dolomite samples, 7 brine samples, one magnesite sample, and 3 sandstone/shale sample were measured using 25-mg aliquots of sample powder and/or brine, which were dissolved in 1N hydrochloric acid. Strontium was extracted using conventional cation exchange procedures after Baadsgard (1987). The strontium isotope ratios were measured on a VG 354 thermal ionization mass spectrometer at the University of Alberta. In-run precision was better than 4×10^{-5} (2σ). The average value of the NBS 987 standard during the period of this study was 0.71023. The isotope ratios of the samples were normalized against this value.

The fluid inclusion samples for this study have been chosen to areally cover most of the SCCC. However, the sample number was limited to 10 (185 fluid inclusion measurements) because of time reasons and the data is summarized in Appendix VII. Because of the limited sample number, fluid inclusion studies from Green (1999) in the

northern part of the complex and Smith (2001) in the central Obed area have been incorporated into the interpretation.

Only primary fluid inclusions of nine calcite cements and one dolomite cement have been analyzed for this study. All fluid inclusions are simple two-phase liquid gas (L-G) inclusions. Eight samples are from the Woodbend-Leduc Group, one from the Winterburn Group, and one from the Swan Hills Formation. The final melting temperatures T_h and the homogenization temperature T_h were measured in all samples; the eutectic T_e was measured, where possible. The bulk melting was close to the NaCl-eutectic, and therefore all measured T_h have been pressure corrected using the H₂O-NaCl P-T plot shown in Fig. 5.9.

5.3 Analytical Results

5.3.1 Stable isotopes

Stable isotope compositions of the carbonates from the SCCC were determined for the three main diagenetic carbonate phases: matrix dolomite, saddle dolomite, and late stage calcite cements. The data are presented in a carbon over oxygen plot in Figure 5.10 and shows that the matrix dolomites have stable isotope values of $\delta^{18}\text{O} = -4.9$ to -8.1 ‰ PDB and $\delta^{13}\text{C} = 0$ to 1 ‰ PDB. The saddle dolomites have $\delta^{18}\text{O} = -7.1$ to -9.8 ‰ PDB and $\delta^{13}\text{C} = 0$ to -1 ‰ PDB. The late calcite cements have $\delta^{18}\text{O}$ values between -7.2 to -13.7 ‰ PDB and $\delta^{13}\text{C} = 0$ to -24 ‰ PDB. The data are summarized in Appendix V.

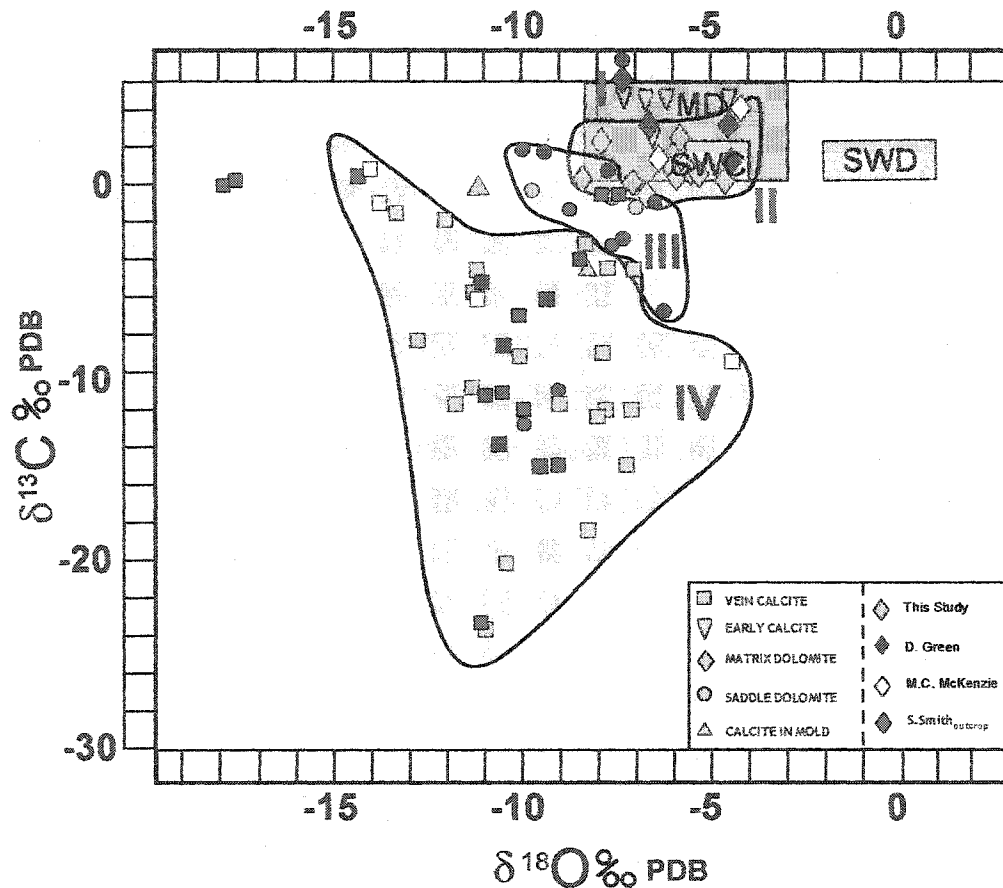


Figure 5.10: Stable isotope data of early calcites, matrix dolomites, late diagenetic saddle dolomites and late calcite cements. The late Devonian sea water calcite field (SWC) and sea water dolomite field (SWD) as well as matrix dolomite field (MD) are plotted for reference as boxes and indicate possible and/or actual ranges. The ranges for SWC and SWD are calculated equilibrium values, the ranges for MD are compiled from various parts of the basin (data taken from Hurley and Lohmann, 1989; Carpenter and Lohmann, 1989; Mountjoy et al., 1992; Amthor et al., 1993, and sources cited therein). The bold roman numerals indicate four major stages of pore fluid evolution that affected the SCCC. Each symbol represents one diagenetic product, and the color fills within the symbol represent the data source.

The sulphur isotopes of elemental sulfur have values of $\delta^{34}\text{S}$ between 18.0 and 18.4 ‰ CDT, the anhydrites range from 18.4 to 26.7 ‰ CDT, and the bitumen vary in between 19.5 and 20.2 ‰ CDT (Fig. 5.11).

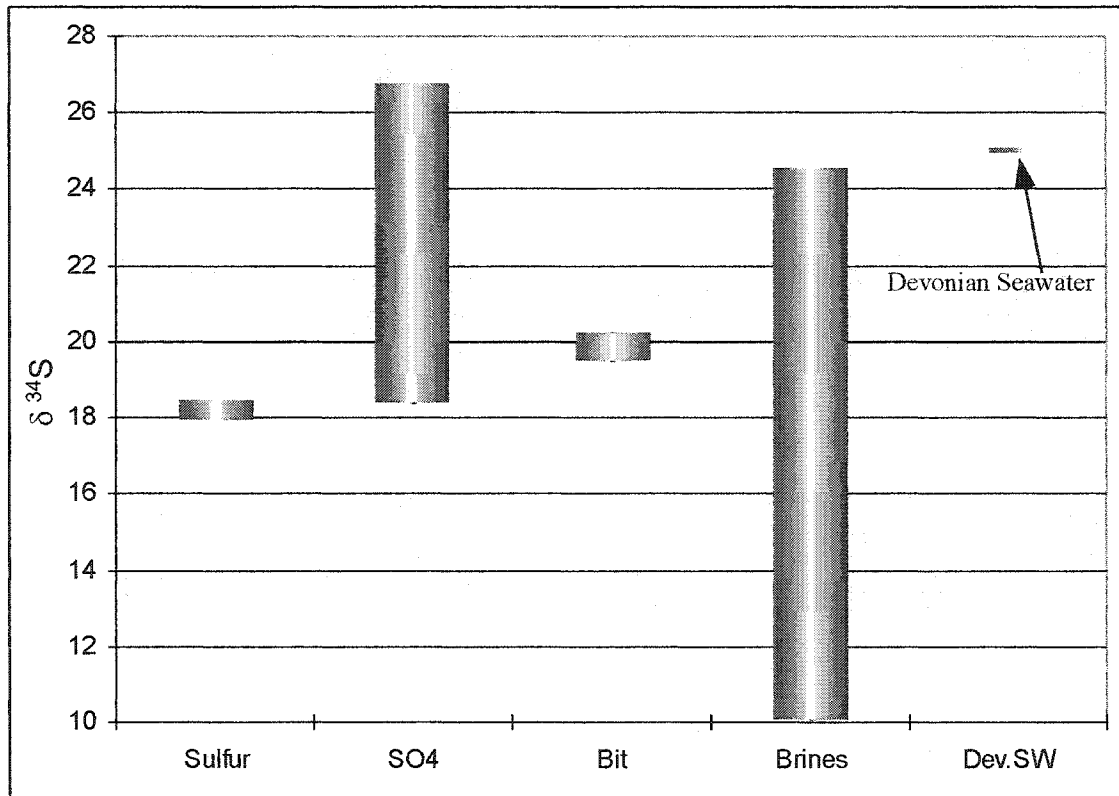


Figure 5.11: Sulfur isotope variations/ranges from elemental sulfur, anhydrite (SO_4), bitumen, and formation brines. The Devonian sea water sulfate isotope value of 25‰ (Claypool et al., 1980) is given as a reference point.

5.3.2 Strontium isotopes

The strontium isotope ratios of this study have a broad range between 0.7080 and 0.7320 (Fig.5.12), whereby the values generally increase with depths and elevated temperatures (the complete data set is shown in Appendix VI). Figure 5.13 and 5.14 show that most of the early diagenetic matrix dolomites of the SCCC range between 0.7080 to 0.7090, and their stable isotope data plot in the seawater calcite field (Fig. 5.13). The saddle dolomites have strontium isotope ratios between 0.7120 and 0.7230, corresponding to more depleted stable isotope values. Strontium isotope ratios of the late stage calcite cements vary between 0.7100 and 0.7320 for the subsurface data of the study area (Fig. 5.13). The late calcite cements from outcrop have distinctly lower Sr isotope ratios (Fig. 5.14).

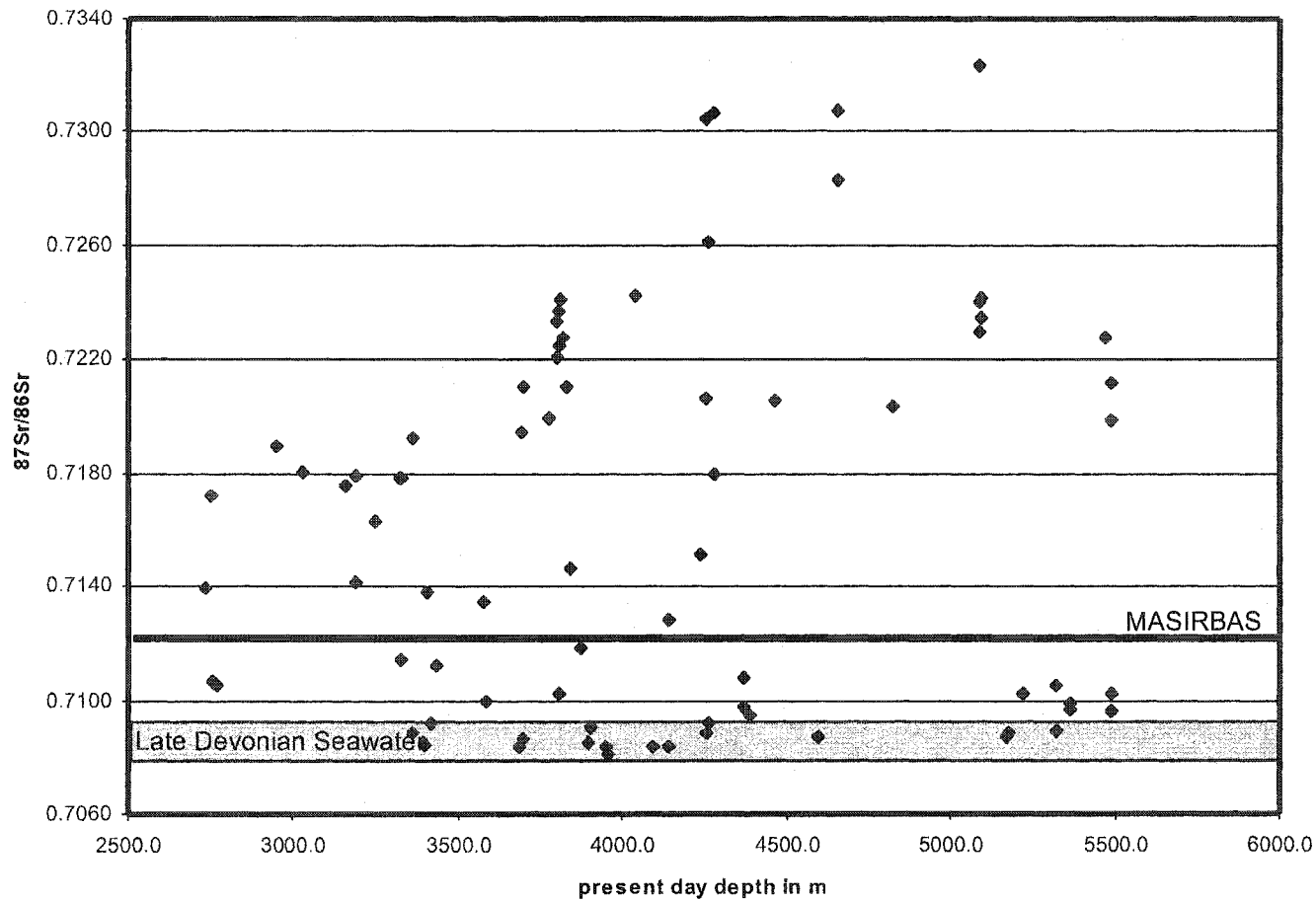


Figure 5.12: Strontium isotope data of this study area plotted over present day depths. The grey area represents the Late Devonian seawater field (Denison et al., 1997) and the thick black line indicates the maximum strontium isotope ratio of the basinal shales (Machel et al., 1996). See text for further explanation.

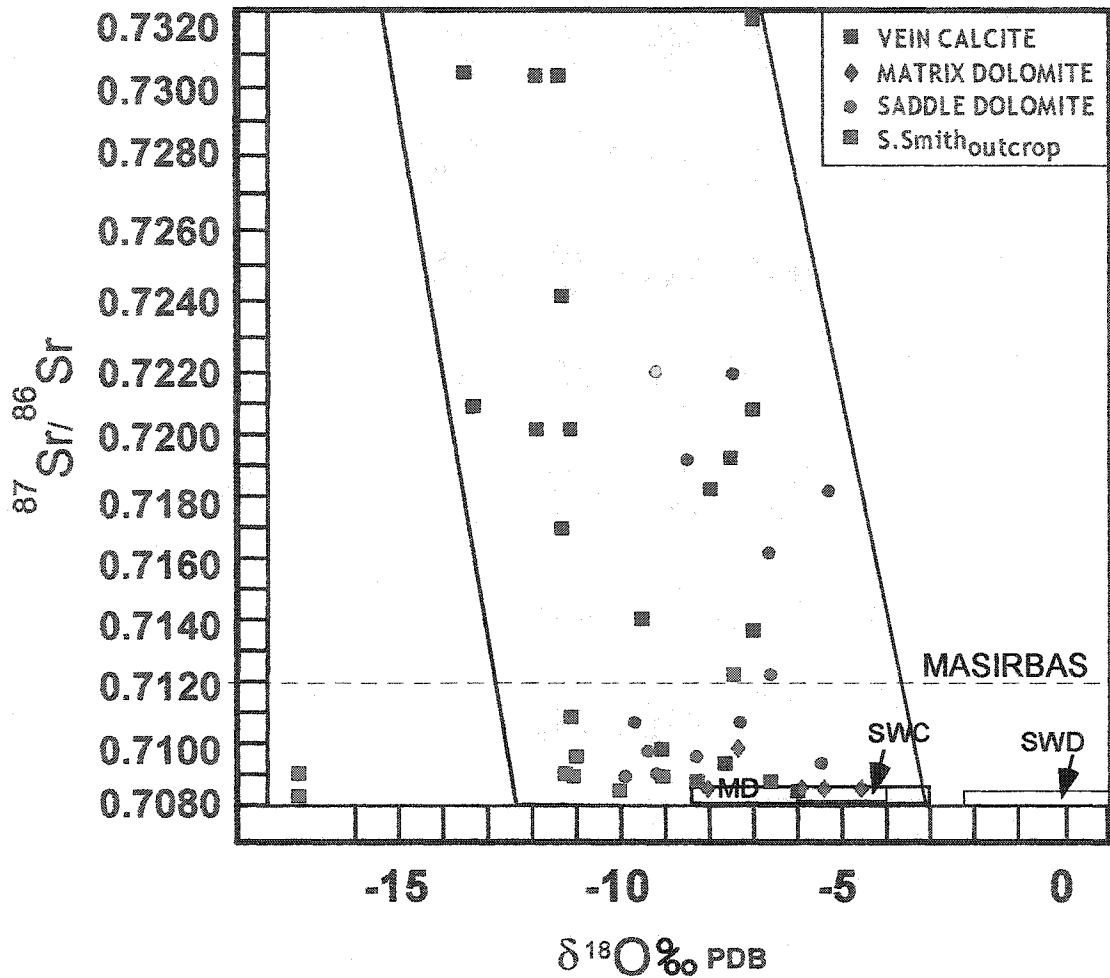


Figure 5.13: Strontium isotope ratios over $\delta^{18}\text{O}$ of matrix dolomites, saddle dolomites and calcite cements. Most of the subsurface late calcite and saddle dolomite values are being much higher than MASIRBAS, the maximum strontium isotope ratio that could derive from the basinal shales (Machel and Cavell, 1999). Red squares represent late cements from outcrops in the Rocky Mountain Front Ranges from Smith (2001).

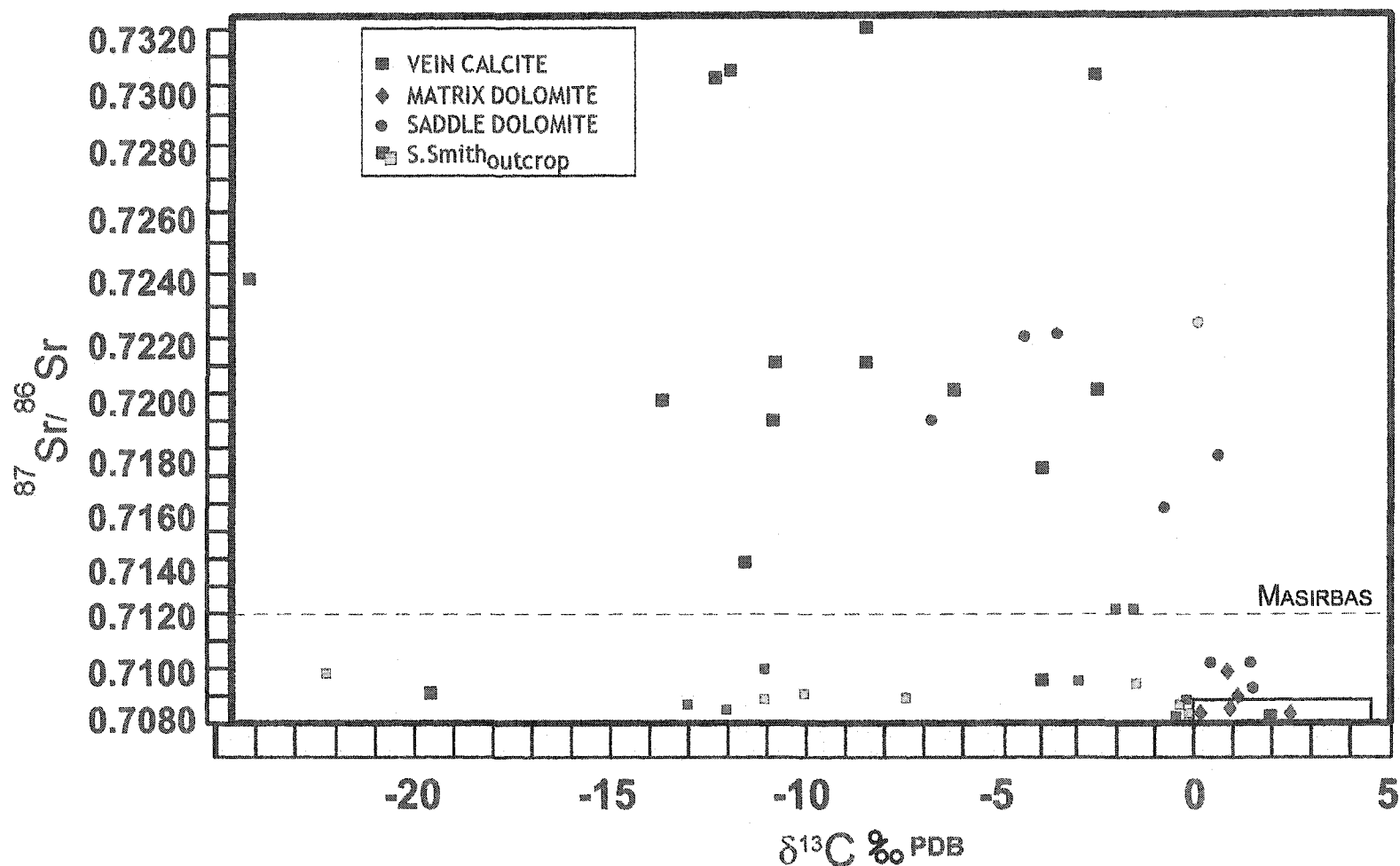


Figure 5.14: Strontium isotope ratios over $\delta^{13}\text{C}$. Red and green squares represent cements from the Front Ranges and Main Ranges of the Rocky Mountains, respectively (from Smith, 2001). This plot shows a complete geochemical decoupling of the Sr from C that has a strongly organogenic (TSR) component in the case of the subsurface samples, and a meteoric component in the case of the outcrop samples.

5.3.3 Fluid inclusion data

Homogenization and freezing data

The uncorrected fluid inclusion data is summarized in Figures 5.15 and 5.16. The complete data set is shown in Appendix VII. The fluid inclusions from calcite cements in well 1-16-55-27W5 (#264) (see Fig. 5.27 for location) are from depths of about 5100 m in the Leduc Formation. The homogenization temperature T_h for this sample vary between 150 – 178 °C (264-1) for one calcite vein, and 136 – 153 °C for another calcite vein (264-2), whereas the final melting temperatures lie between –17.8 to –19.1 °C (= 20.9 to 22.0 wt% NaCl) and –16.4 to –21.5 °C (= 20.1 to 23.6 wt% NaCl), respectively. The initial melting temperatures are $T_e = 55$ °C for 264-1 and $T_e = 50$ °C for 264-2.

Two calcite veins from 14-36-52-27W5 (#15-1, #15-2) (see Fig. 5.27 for location) were sampled at depths of 5221 m from the Leduc Formation. T_h ranges between 143 - 162 °C, T_m ranges between –12.6 to –13.9 °C, and a low T_e at (–45) to (–50) °C was observed for sample 15-1. Sample 15-2 ranges between $T_h = 132 - 164$ °C, $T_m = -12.5 -13.7$ °C and $T_e =$ and -40 to -30 °C.

Saddle dolomite cement at 5-13-54-23W5 (#201) (see Fig. 5.27 for location) was taken from a depth of 4320 m in the Leduc Formation at the Obed field. The fluid inclusions in the dolomite are less than 5 μm in size, but very abundant. T_h ranges between 123 – 145 °C and T_m is between –17.8 and -18 °C (= 21.1 to 21.3 wt% NaCl). T_e could not be measured due to very poor visibility in the sample.

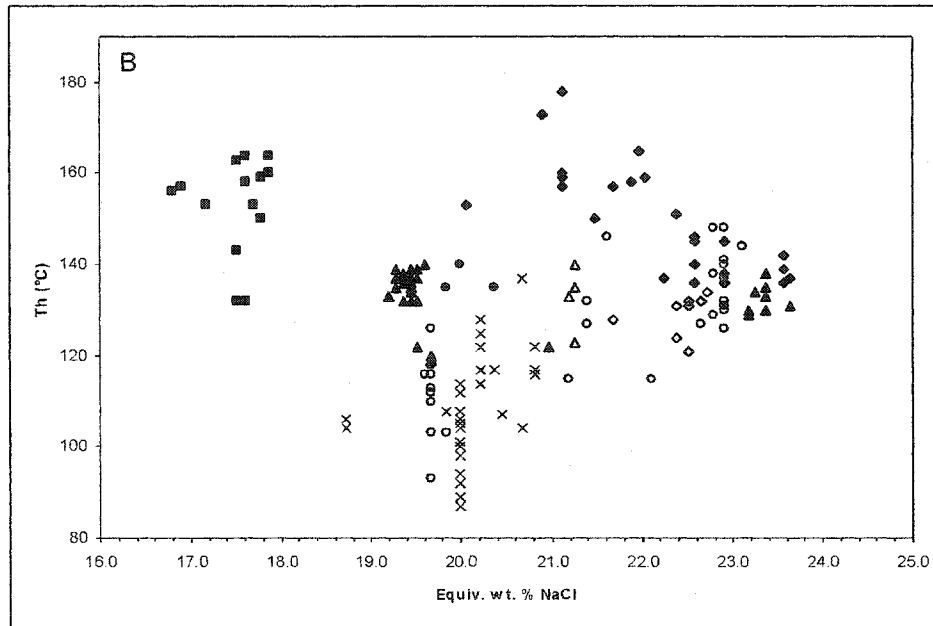
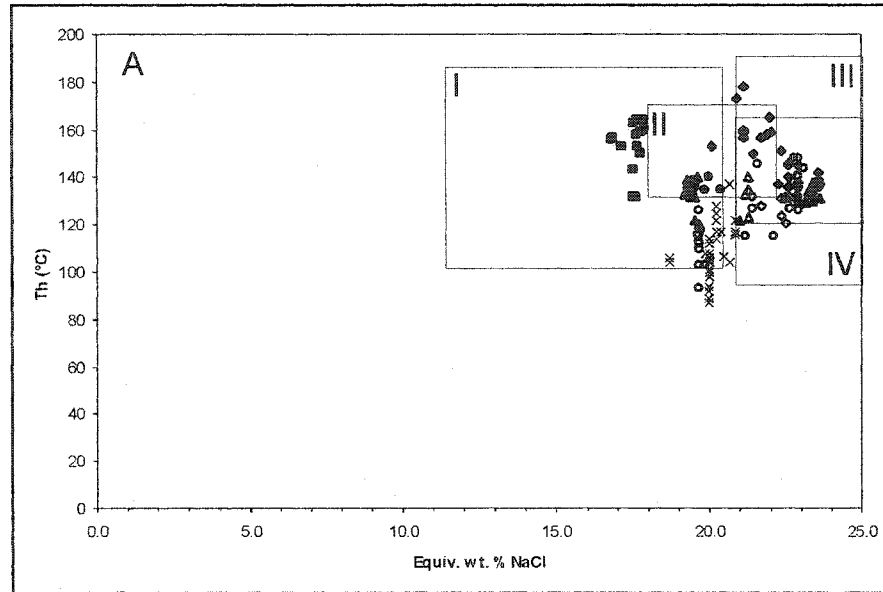


Figure 5.15: Summary plot of fluid inclusion measurements for the SCCC. A total of 9 samples has been analyzed and 179 fluid inclusions were measured. Different symbols indicate different well locations. Figure A shows that the data plot into a narrow range, thus there are only minor differences between different well locations in the SCCC. The boxes in A delineate the fluid inclusion data measured by Smith (2001) and Green (1999). The roman numerals indicate areas of other Th ranges, i.e., I = Outcrop samples from the Front and Main Ranges, II= Obed, III = Pine Creek and Kaybob South, and IV= Simonette. Figure B is a zoom-in, to show minor differences between single well locations, each symbol represents one location. The wells/data are plotted individually in Figure 5.17.

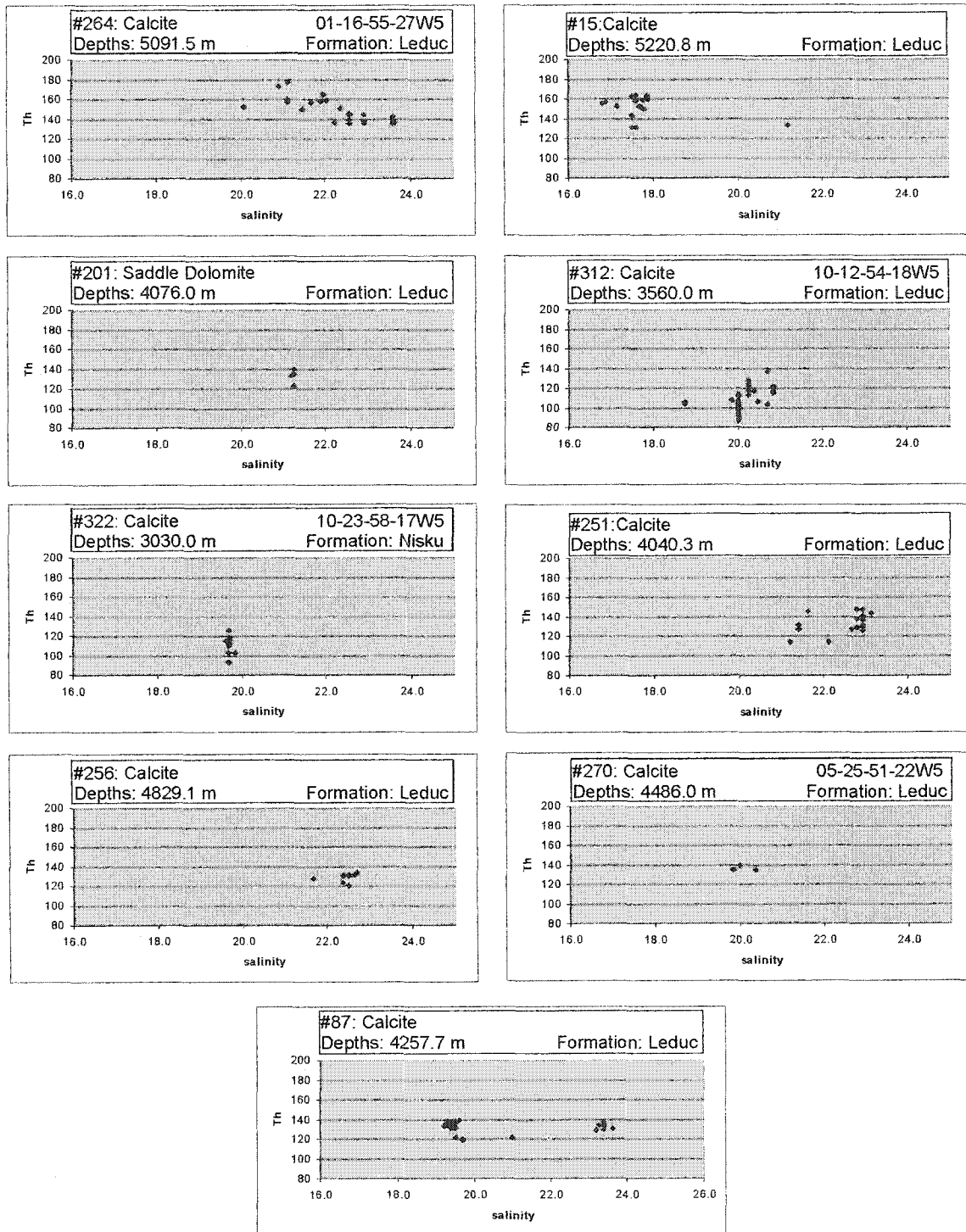


Figure 5.16: Overview over the fluid inclusion data from 9 analysed samples in the SCCC complex (Th in °C, salinity in wt%).

Sample (#312) is from the well location 10-12-54-18W5 at the Edson field (see Fig. 5.27 for location). The sample is from the Swan Hills Formation at a depth of 3560 m. The calcite cements contain relatively small (less $7\mu\text{m}$), irregular shaped inclusions, which were measured from two locations (312-1 and 312-2). The T_h of 312-1 varies between 104°C and 128°C , the T_m is between -14.7°C and -16.1°C and the T_e is around -50°C . Inclusions in 312-2 are homogenizing between 87°C and 114°C and the final melting took place at -16.3°C , the eutectic temperature is between -55°C and -50°C .

The calcite cements were sampled at 10-23-58-17W5 from the Winterburn Group (Nisku Formation) in the Kaybob-South field at a depth of 3030 m (#322) (see Fig. 5.27 for location). The T_h ranges from 93°C to 126°C , T_m is -15.9°C and the T_e ranges from -55 to -50°C .

Sample (#251) is from 7-19-59-24W5 in the Berland-River-West field in the Leduc Formation (see Fig. 5.27 for location). The calcite cement was taken from a depth of 4040 m and fluid inclusions were measured at two locations (251-1, 251-2). The inclusions at 251-1 have T_h between 126°C and 132°C , T_m between -18.2°C and -20.4°C , and a T_e of -50°C . The ones at 251-2 vary between $T_h = 115^\circ\text{C}$ and 148°C , $T_m = -17.9^\circ\text{C}$ and -21.6°C and have a T_e of $\sim -50^\circ\text{C}$.

The calcite cement in sample (#256) is from 7-18-52-24W5 at a depth of 4830 m in the Leduc Formation (see Fig. 5.27 for location). The homogenization temperature is between 115°C and 135°C , the melting temperature is between -16.6°C and -17.2°C ,

the T_e lies at $-50\text{ }^\circ\text{C}$. In addition, a phase melt at $T_{m_{cc}} = -79.4\text{ }^\circ\text{C}$ indicates a CO_2 -methane mixture in these inclusions.

Sample (#270) is also from the Leduc Formation at 5-25-51-22W5 in the Lambert field (see Fig. 5.27 for location). The sample is from a depth of 4468 m and contains calcite cements. The T_h ranges from $135\text{ }^\circ\text{C}$ to $150\text{ }^\circ\text{C}$, the T_m from $-16.5\text{ }^\circ\text{C}$ to -17.2 and the T_e is $-50\text{ }^\circ\text{C}$.

The last sample is from 1-32-57-25W5 (#87) (see Fig. 5.27 for location). The calcite cements are from the Leduc Formation at 4260 m depth. Fluid inclusions were measured from two locations in the section, 87-1 and 87-2. The T_h in 87-1 range between $122\text{ }^\circ\text{C}$ and $135\text{ }^\circ\text{C}$ ($140\text{ }^\circ\text{C}$), the T_m is between $-15.7\text{ }^\circ\text{C}$ and $21.9\text{ }^\circ\text{C}$, and the T_e lies at about -55 to $-50\text{ }^\circ\text{C}$. The T_h in 87-2 varies between $140\text{ }^\circ\text{C}$ and $132\text{ }^\circ\text{C}$, the T_m is between $-15.8\text{ }^\circ\text{C}$ and $-16.3\text{ }^\circ\text{C}$ and the T_e is $-55\text{ }^\circ\text{C}$.

Comparison to other fluid inclusion data

Smith (2001) analyzed fluid inclusions in late calcite cements and saddle dolomite cements from the Obed area, from the Simonette field, and from several outcrop locations in the Front Ranges and the Main Ranges of the Rocky Mountains (see Figure 5.27 for locations of the subsurface locations and Figure 5.15 T_h ranges in different areas). The average uncorrected homogenization temperature for his Obed samples is $146.5\text{ }^\circ\text{C}$ for the calcite cements and $142.1\text{ }^\circ\text{C}$ for the saddle dolomite. The salinities for the Obed samples range between 18.0 and 21 weight% NaCl, with an average of 19 wt% in the calcites and

20.8 wt% in the dolomite sample. Smith's (2001) data for the Simonette field (Swan Hills Formation) ranges between 129.9 °C and 147.9 °C with a mean of 140.4 °C for late calcite cements. The saddle dolomite plots within slightly higher temperatures of 148.2 °C to 154.3 °C. The salinities for the calcite samples have a mean value of 22.7 wt% NaCl.

Green (1999) reported fluid inclusion data from three Devonian aquifers in the Kaybob-South and Pine Creek fields (see Figure 5.27 for locations). He analyzed fluid inclusions in saddle dolomite, anhydrite, calcite and quartz. The T_h and T_m for the saddle dolomites from the Kaybob-South Swan Hills and the Pine Creek Leduc Formation are similar, and are between 130 °C and 160 °C. The mean T_h for the Kaybob-South samples is 146 °C and the one for the Pine Creek is 152 °C. The Wabamun saddle dolomites from Pine Creek have a mean T_h of 151 °C. The salinities range from 21 to 25 wt% NaCl, with generally higher salinities in the Pine Creek area. T_h for calcite samples at the Pine Creek Leduc level is 148 °C and 143 °C for the Kaybob South Swan Hills. Green (1999) noted a salinity trend from the western to the eastern part of the study area, with increasing values towards the west. Green's (1999) quartz and anhydrite inclusions will not be discussed here, because of missing comparable data.

In summary, the temperature and salinity ranges, and variability of Smith's and Green's data are similar to the data of this study. Hence, these data in combination indicate a similar burial history for the whole carbonate complex.

5.3.4 Geochemistry of present-day formation brines

Seven brines samples were taken throughout the study area. Four of the brine samples are from single well locations, whereas three are pipeline mixtures from several well locations (Fig. 5.17).

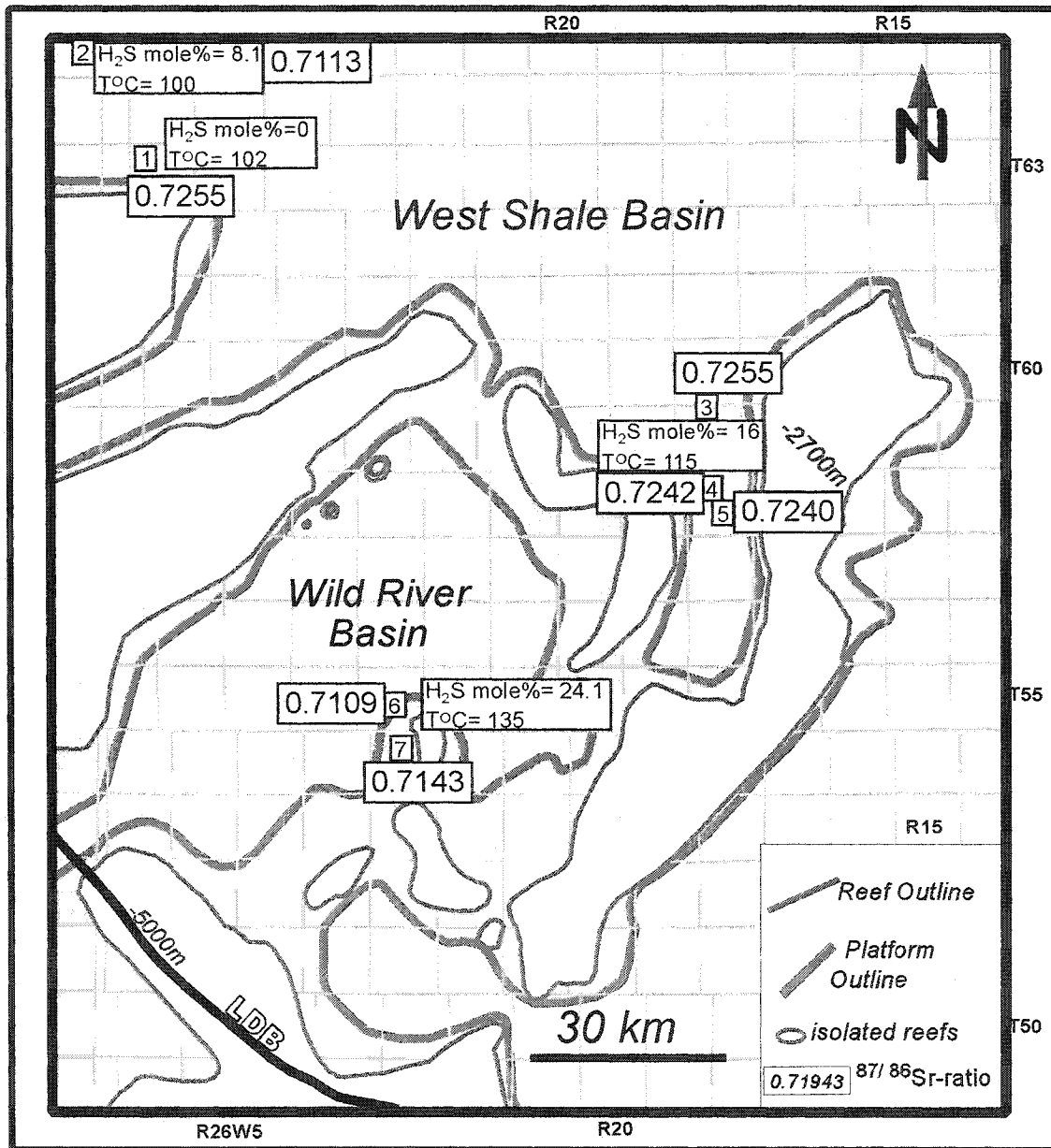


Figure 5.17: Brine sample locations, present day temperatures in the reservoirs, H_2S contents of the hydrocarbons and strontium isotope ratios of the brine samples. Location #1, #2, #6, and #7 are from single wells producing from the Wabamun, the Beaverhill Lake, the Blueridge and the Nisku, respectively. Locations #3, #4, and #5 are from pipelines, all collecting from the Swan Hills Formation.

The isotopic composition of the brines is summarized in Table 5.2 and shown on the oxygen/deuterium plot in Figure 5.18.

#	Sample	$\delta^2\text{H}_{\text{brines}}$	$\delta^{18}\text{O}_{\text{brines}}$	$\delta^{13}\text{C}_{\text{DIC}}$	$\delta^{34}\text{S}_{\text{Ag2S}}$	$^{87}\text{Sr}/^{86}\text{Sr}$	Formation
1	MB- W 1629	-79.0	-1.5	-5.5		0.7255	Wabamun
2	MB- B 614	-58.1	5.0	-11.6	22.9	0.7113	BHLK
3	MB- S 833	-36.9	4.0	-11.2	11.7	0.7255	SWHL
4	MB- S 1135	-42.1	5.4	-13.3	18.8	0.7242	SWHL
5	MB- S 413	-54.6	6.2	-10.8	10.1	0.7240	SWHL
6	MB- 081	-19.6	5.9	-6.9	20.9	0.7109	Nisku
7	MB- N 1526	-41.4	8.7	-20.8	24.5	0.7143	Nisku

Table: 5.2: Summary table of the isotope data for 7 present day brine samples from the SCCC. The # column corresponds to the well location in Figure 5.17. These values in comparison with flinc data provide good guidelines for the oxygen isotope thermometer.

The formation brine δD values range between -79 and -20 ‰ SMOW, their $\delta^{18}\text{O}$ values vary between -1.5 and $+8.7$ ‰ SMOW (Figs. 5.17). The $\delta^{13}\text{C}_{\text{brine}}$ values range from -20.8 to -5.5 ‰ PDB, and their sulfur isotopes (dissolved sulfate) range from 10.1 to 24.5 ‰ CDT (Fig. 5.11). The Sr isotope values of the seven brine samples range between 0.7109 and 0.7255 , the Wabamun and the Swan Hills have the highest values of 0.7255 , whereas the Nisku ($0.7109/0.7143$) and the Beaverhill Lake (0.7113) have distinctly lower values.

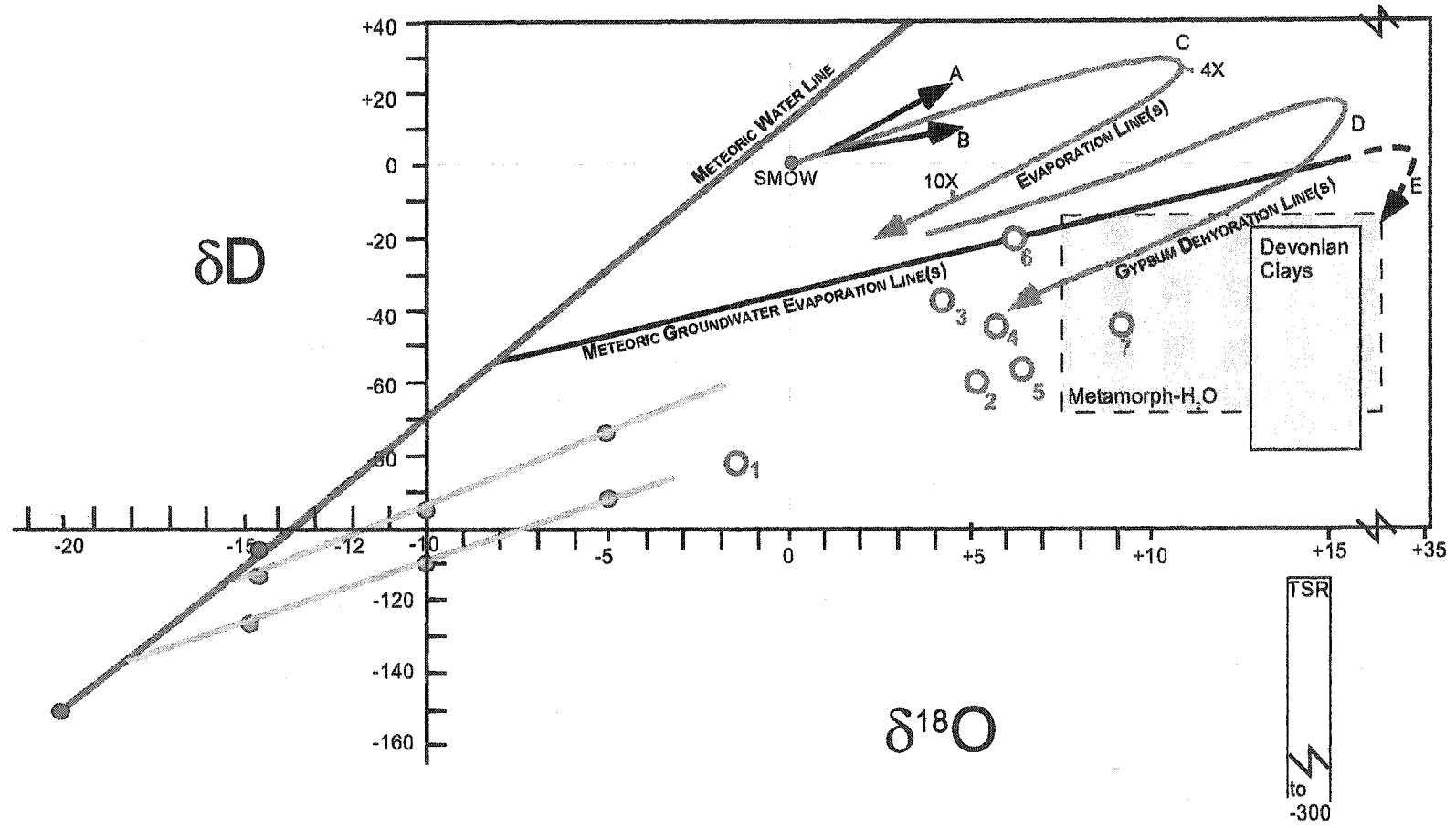


Figure 5.18: Isotopic composition of 7 formation brines from the SCCC (Red Circles numbered 1 to 7) (see Figure 5.17 for well locations). All samples are shifted from the assumed SMOW origin towards the south-east, indicating that processes like evaporation, gypsum dehydration, tectonic expulsion of “metamorphic” fluids and TSR might have overprinted the original waters. See text for further explanation.

5.4 Discussion

5.4.1 Late Devonian marine isotope baselines

Before interpreting the data presented above, it is necessary to define the Late Devonian marine baselines for oxygen, carbon, strontium and, sulfur isotopes. Hurley and Lohmann (1989) compiled oxygen and carbon isotopic compositions of Late Devonian marine calcite cements from around the world and established an average value of $\delta^{18}\text{O} = -5 \pm 1\text{‰}$ PDB and $\delta^{13}\text{C} = 2.5 \pm 1\text{‰}$ PDB (1.5 to 3.5) for Late Devonian marine calcites. Veizer et al. (1999) measured and compiled oxygen and carbon isotopic compositions of marine calcites throughout the Phanerozoic and derived at values of $\delta^{18}\text{O} = -5$ to -8.5‰ and $\delta^{13}\text{C} = 2.5$ to 0‰ PDB (Fig. 5.19) for the Late Devonian, which is in general agreement with Hurley and Lohmann's (1989) results.

The $^{87}\text{Sr}/^{86}\text{Sr}$ ratio of seawater throughout geologic time has been presented as the secular seawater curve by Burke et al. (1982), Denison et al. (1997), and Veizer et al. (1999) (Fig. 5.6 and Fig. 5.20). According to their curves, Late Devonian seawater varied between 0.7079 and 0.7084. Kaufman (1989) analyzed an unaltered brachiopod calcite shell from the Swan Hills field (just northeast of this study area) and measured a strontium isotope ratio of 0.7079, which is in good agreement with the secular seawater curve of Burke et al. (1982). Veizer et al. (1999) derived at a range between 0.7077 and 0.7084 (Figure 5.6b).

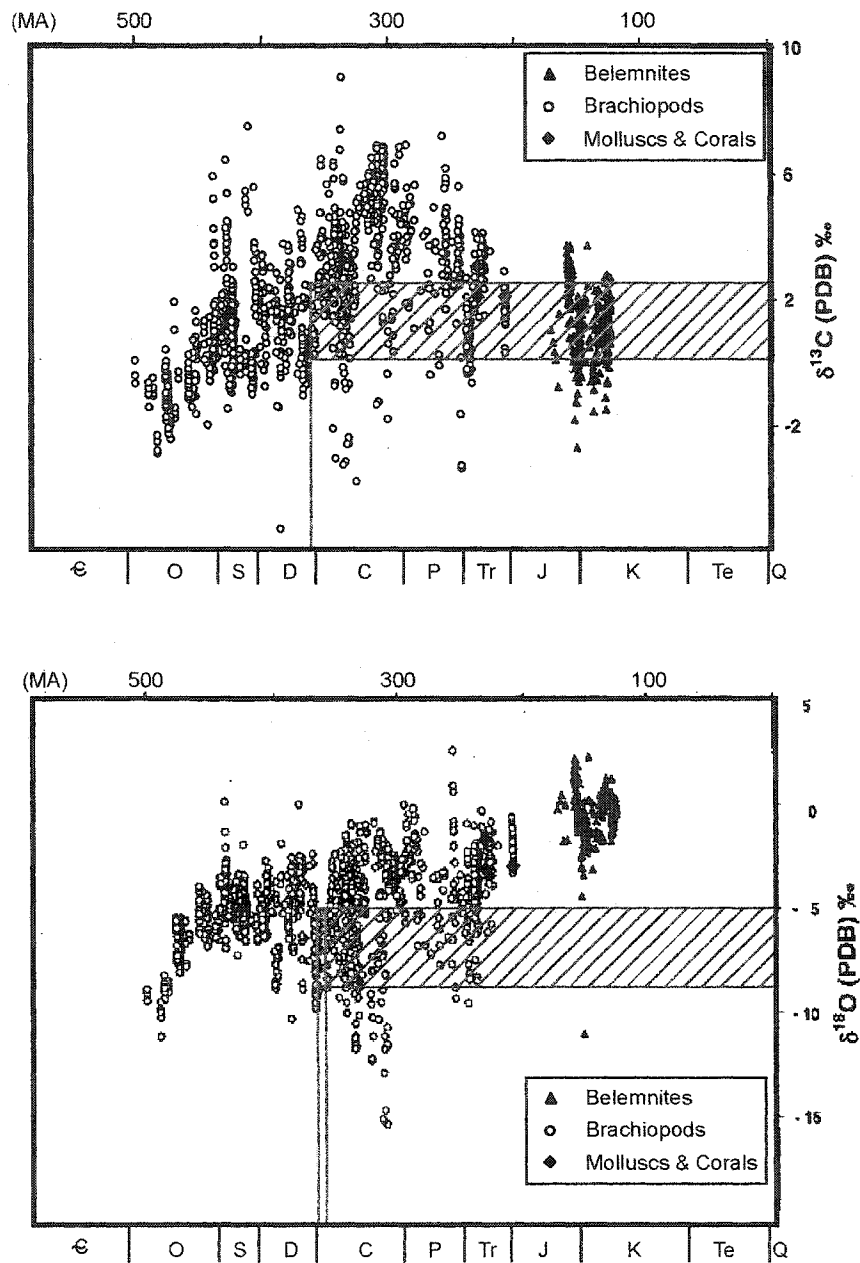


Figure 5.19: Phanerozoic $\delta^{13}\text{C}$ and $\delta^{18}\text{O}$ trend based on brachiopod and belemnite measurements, the red-hatched areas depict a $\delta^{13}\text{C}$ range for Late Devonian carbonates of 2.5 to 0 ‰ PDB and $\delta^{18}\text{O}$ -5 to -8.5 ‰ PDB (after Veizer et al., 1999).

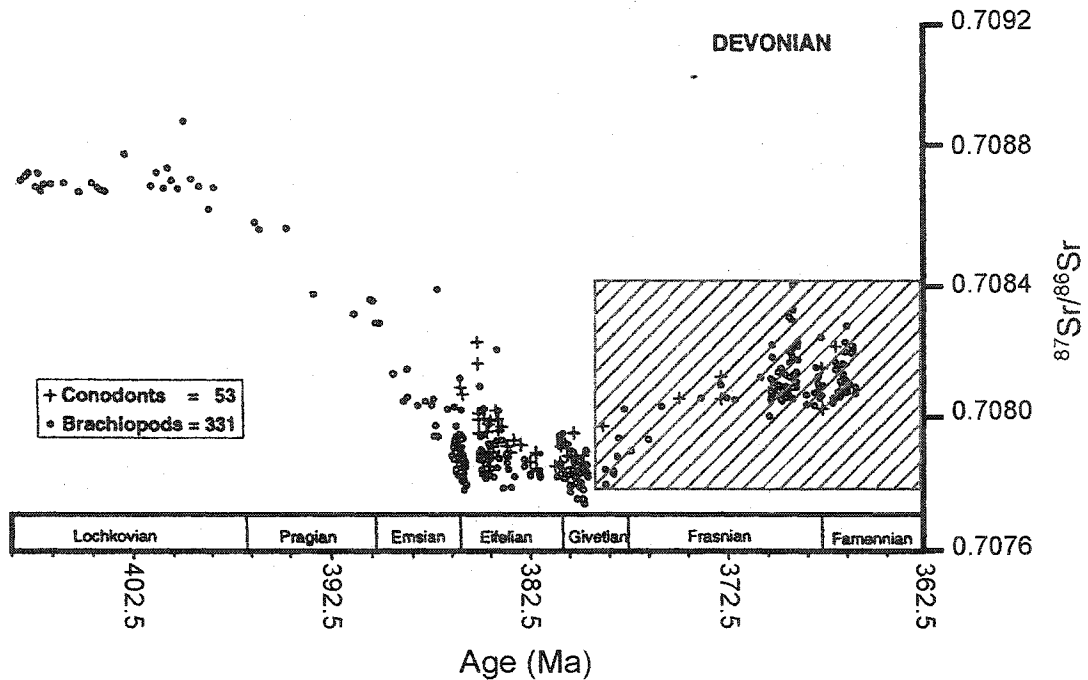


Figure 5.20: $^{87}\text{Sr}/^{86}\text{Sr}$ variations during the Devonian, whereas the hatched box indicates the realm between 0.7077 to 0.7084 as the value for Middle and Upper Devonian carbonates that are part of this study. Modified after Veizer et al., 1999.

The best estimate for primary marine sulfate of the Upper Devonian is $\delta^{34}\text{S} = 25\text{‰}$ CDT and $\delta^{13}\text{C} = 14\text{‰}$. Claypool et al. (1980) report an average $\delta^{34}\text{S}$ value of 25‰ CDT for Late Devonian seawater (Fig. 5.21), which correlates well with the measured primary anhydrite values of 21‰ to 27‰ from Machel and Burton (1991) for the Upper Devonian in the WCSB.

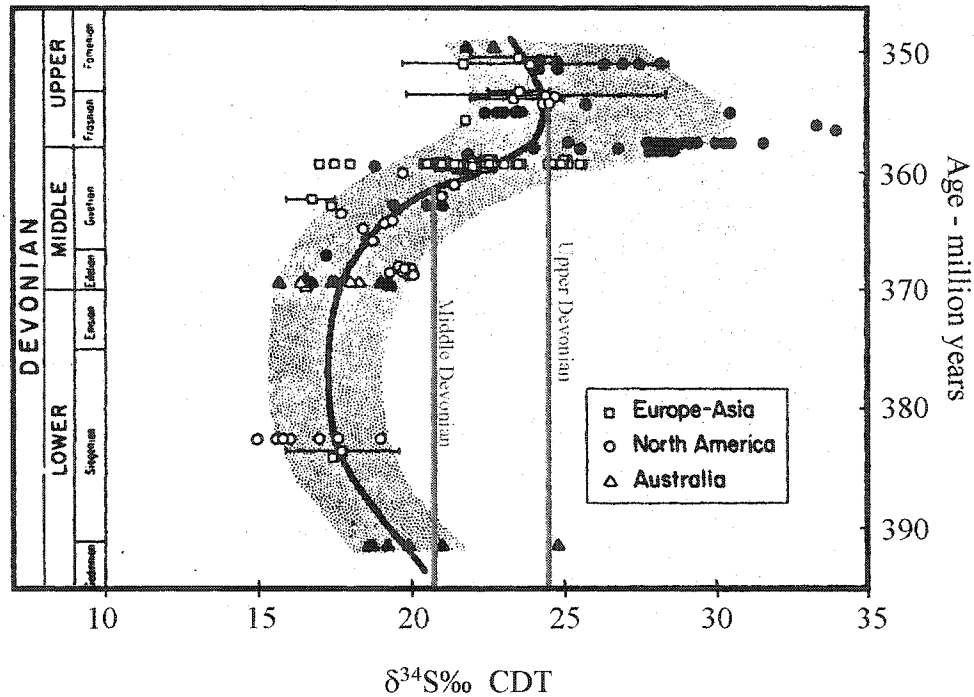


Figure 5.21: Sulfur isotopes in evaporites of Devonian age. Modified from Claypool, et al., 1980.

5.4.2 Interpretation of stable isotope data of the solids

The early marine calcite cements in the study area have stable isotope values between $\delta^{18}\text{O} = -6.0 \pm 1\text{‰ PDB}$ and $\delta^{13}\text{C} = 2 \pm 1\text{‰ PDB}$ and $^{87}\text{Sr}/^{86}\text{Sr}$ -ratios between 0.7080 and 0.7082 (values from Green 1999, Kaufman et al., 1989). These values fall within the range of late Devonian seawater calcites as established by Mountjoy and Amthor (1993) and Denison (1997) and the studies referenced above. The very slight deviation from Devonian seawater calcites reflects minor recrystallization (Machel, 1997) during burial diagenesis. Assuming an original $\delta^{18}\text{O}_{\text{calcite}}$ of $-5 \pm 1 \text{‰ PDB}$ and a $\delta^{18}\text{O}_{\text{seawater}}$ between -3 and 0 ‰ SMOW the temperature range of formation lies between 22 °C and 32 °C (Fig.

5.22), which is in good agreement with the paleogeography and the assumed semi-arid climate for the late Devonian of Western Canada.

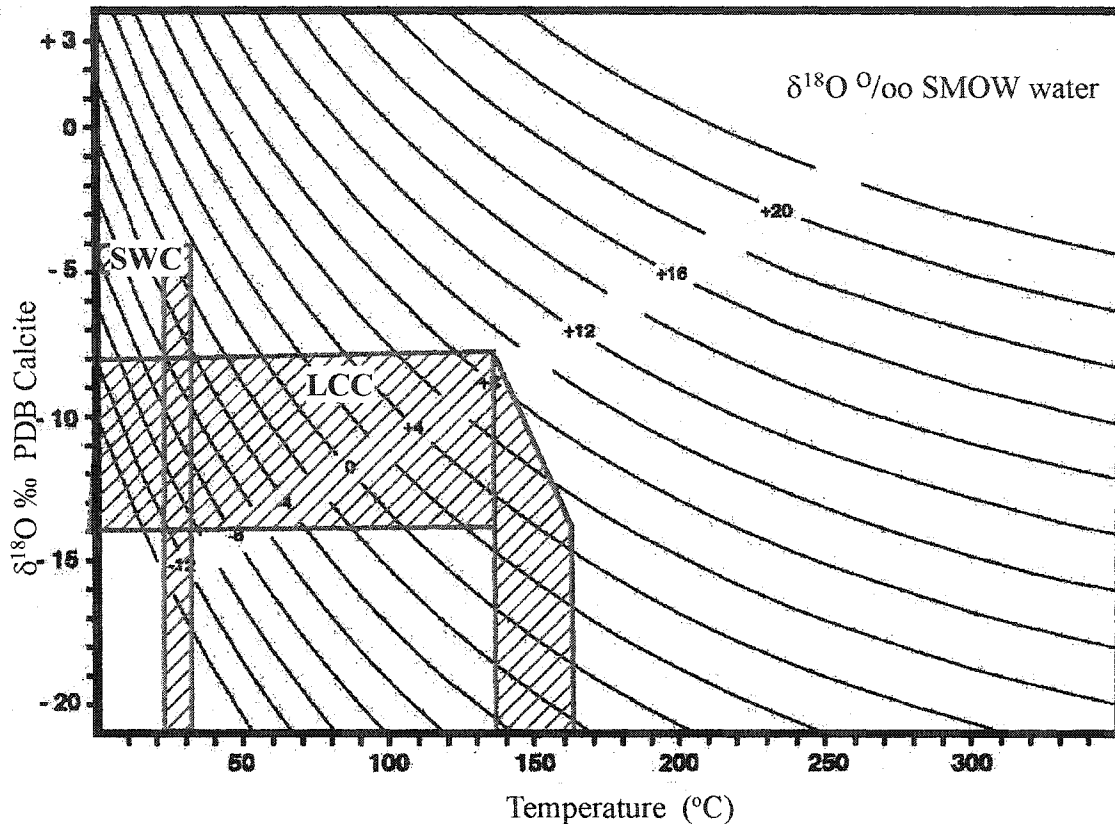


Figure 5.22: Plot of equilibrium relationships between temperature and isotope composition of water and calcite after Friedman and O'Neill (1977). The seawater calcite (SWC) isotope range has been established by measurements of early marine cements, fossils and limematrix, and a Devonian seawater value is assumed between 0 and -3 ‰ SMOW. The isotope measurements of late stage calcite cements (LCC) yielded values between -8 and -14 ‰ PDB and ‰ SMOW for the formation fluid was assumed using the present day formation brines.

The matrix dolomites have slightly lower oxygen values than calculated equilibrium values for Late Devonian seawater (Fig. 5.10), which is probably due to recrystallization during burial and elevated temperatures. The carbon values for the matrix dolomites are in the realm of Late Devonian seawater, which supports the theory that they have formed

from slightly modified Devonian seawater during early to intermediate burial (Amthor et al., 1993). The range of -3 to 0 ‰ SMOW is here considered representative of seawater in the study area during the late Devonian based on two lines of evidence: (1) this range covers the minimum to maximum of Late Devonian seawater as determined from calcites and brachiopods (Kaufman, 1989); (2) there are no indications of syndepositional or early post-depositional evaporation, which could have increased $\delta^{18}\text{O}$ values by up to 10‰ (Knauth & Beeunas, 1986; see also Fig. 5.5). Thus stable isotopes can be used to estimate the temperature at the time of dolomite formation, using the $\delta^{18}\text{O}_{\text{water}}$ of -3 to 0‰ SMOW as a Devonian seawater value and the equation (1) by Land (1983):

$$[3.2 \times 10^6 T (\text{°K})^{-2}] - 3.3 = \delta^{18}\text{O}_{\text{dolomite}} - \delta^{18}\text{O}_{\text{water}} \quad (1)$$

Plotting the ranges of the stable isotope data relative to the equilibrium relationships between temperature and isotope composition of water and dolomite after equation (1), a temperature range of formation for the matrix dolomites of 50 °C to 90°C is revealed (Fig. 5.23). Presuming a geothermal gradient of ~ 30°C/km and a surface temperature of about 25 °C (Hudson & Anderson, 1989), temperatures of this range could have been reached during the Late Devonian and Early Mississippian at depths of around 1000m to 1500m.

The carbon isotope compositions of the matrix dolomites range from 0 to 1 ‰, well in the range of the marine baseline. They indicate that no carbon-altering process had overprinted the rocks (Allan & Wiggins, 1993). The strontium isotope ratio of the matrix dolomites falls within the established range of Late Devonian seawater. The stable and Sr-isotope data together support the previous interpretation that the dolomitizing fluids

for the matrix dolomite in the study area was slightly modified Late Devonian seawater at depths of about 1000 m to 1500 m (Amthor et al., 1993; Mountjoy and Amthor, 1994).

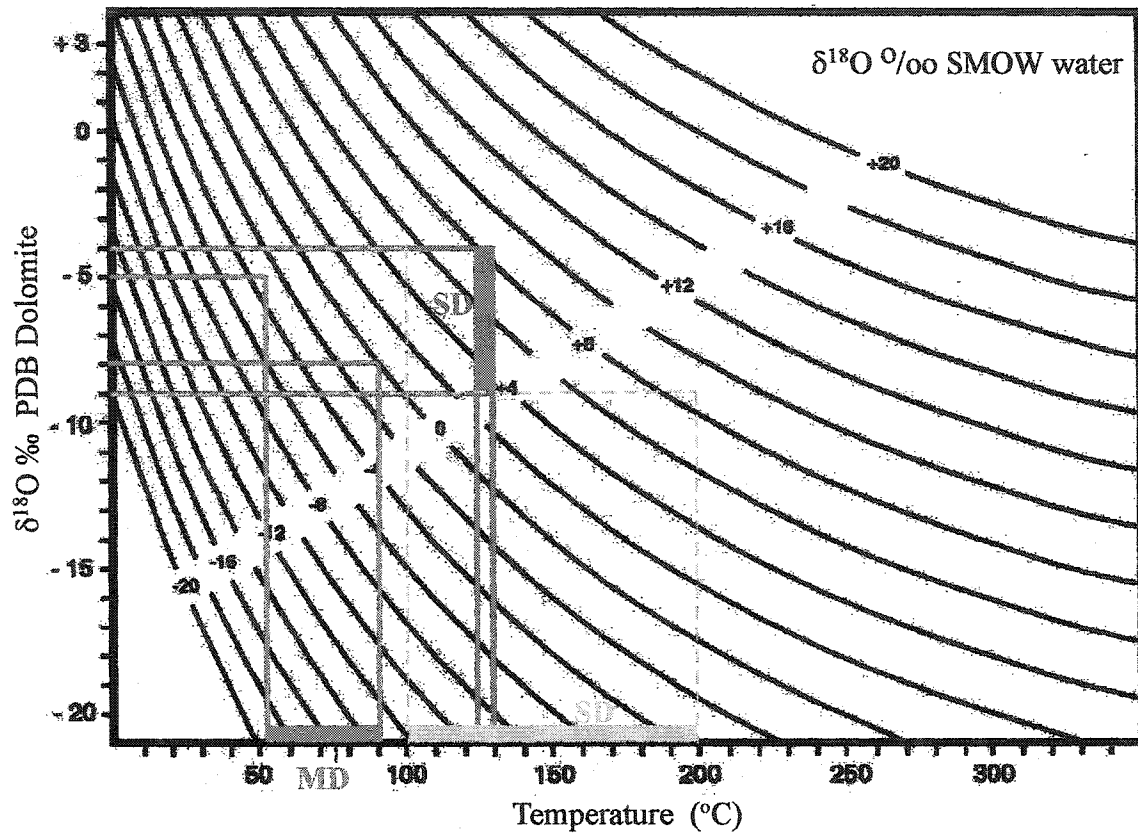


Figure 5.23: Plot of equilibrium relationships between temperature and isotope composition of water and dolomite, after Land (1985). The matrix dolomites (MD) have an isotope range between -5 and -8 ‰ PDB and a Devonian seawater value is assumed between 0 and -3 ‰ SMOW, thus the matrix dolomites would have formed at a temperature between 50 and 90 °C (blue). The isotope measurements of saddle dolomite (SD) yielded values between -4 and -9 ‰ PDB and a temperature range between 125 and 130 °C was measured on fluid inclusions for the study area, which leads to a composition of +3.5 to 9 ‰ SMOW for the fluid that formed saddle dolomite (red box). However, if the present formation brines are assumed as the fluid(s) that formed the saddle dolomite, a temperature range of about 100 to 200 °C is obtained (green box).

The stable isotope data of the saddle dolomites ($\delta^{18}\text{O} = -4$ to -9 ‰ PDB and $\delta^{13}\text{C} = 0$ to -1 PDB ‰) paired with strontium isotope ratios between 0.7120 and 0.7230, differ significantly from those of the earlier described diagenetic phases and indicate a major

change in pore fluid composition. The oxygen values are more depleted, which can be explained by the deeper burial and correspondingly higher temperatures. There are no indications for the involvement of meteoric water, which is another possible process causing the depletion in oxygen isotope values in the solids. The estimation of the temperature for the saddle dolomite formation is in this case more complicated, since the pore fluids seem to have changed, and constraining an $\delta^{18}\text{O}_{\text{water}}$ becomes more difficult. Present day formation brines yield $\delta^{18}\text{O}_{\text{water}}$ between 5 and 8.7 ‰ SMOW (Fig. 5.18). Using these values on the equilibrium relationship plot in Figure 5.23, the saddle dolomites could have formed in a temperature range of 100 °C to 200°C. The strontium isotopes of the saddle dolomite also deviate significantly from the marine baseline, which suggests an alteration/mixing of pore fluids with increasing burial depth and at least one fluid with a higher radiogenic strontium signal than Late Devonian seawater (further discussed below).

The isotopic alterations of the pore fluids are more dramatic for the late calcite cements ($\delta^{18}\text{O}$ values between -7 to -14 ‰ PDB and $\delta^{13}\text{C} = 0$ to -24 ‰ PDB, Sr between 0.7100 and 0.7320). The highly depleted oxygen isotopes are best explained by increased temperature during deeper burial. Using the oxygen isotope thermometer and an assumed $\delta^{18}\text{O}_{\text{water}}$ between + 5 and +8.7 ‰ SMOW according to the present day formation brines, the temperature range of the late calcite cements lies within 135 °C and 165 °C (Fig 5.22). The carbonates of SCCC have not been uplifted to the surface and, as in the case of the dolomites, there are no indications for any influence of meteoric water. An influence of meteoric water is also precluded by the stable isotope composition of the present

formation brines (Fig. 5.18), which indicate that these brines have evolved from seawater evaporation and water-rock interaction (recrystallization), gypsum dewatering, and some input of metamorphic water (further discussed below).

The carbon isotopes of the late burial calcites are highly depleted in ^{13}C . The SCCC passed through the liquid oil window, and hydrocarbons were introduced to the system so that the onset temperatures (100 – 140 °C) for thermochemical sulfate reduction (TSR) were reached and/or exceeded. Based on many other geochemical studies in the WCSB it is well known that H_2S is one major product of TSR (Krouse et al., 1988; Machel et al., 1995) and is produced via the reduction of anhydrite as represented by the following simplified reaction:



Other products of TSR are saddle dolomite, late calcite cements, as well as minor amounts of Fe-sulfides. The depleted $\delta^{13}\text{C}$ -values of the carbonates (especially calcite cements) are due to the incorporation of isotopically light carbon that was formed via the oxidation of organic carbon in crude oils and/or condensates in the presence of sulfate during TSR reactions (Machel et al., 1995, and references cited therein).

5.4.3 Interpretation of strontium isotope data of the solids

Strontium isotopes can be used to reconstruct paleomigration pathways in conjunction with changes in pore water evolution (Banner et al., 1995; Carpenter and Lohman, 1989; Faure & Powell, 1972). $^{87}\text{Sr}/^{86}\text{Sr}$ -isotope ratios of the matrix dolomites range from from 0.7079 to 0.7085. Using the secular seawater curve in Figure 5.6 and the data from Figure

5.20, the matrix dolomites plot in the range of Devonian seawater, supporting the previous interpretation that the matrix dolomites were formed from slightly modified Devonian seawater. The saddle dolomites have significantly higher $^{87}\text{Sr}/^{86}\text{Sr}$ values that range from 0.7120 to 0.7230, indicating a significant change in the chemical composition of the pore waters. The late calcite cements have $^{87}\text{Sr}/^{86}\text{Sr}$ -isotope ratios between 0.7103 and 0.7323, which places them among the most radiogenic isotopes in the Alberta Basin (Mountjoy et al., 1992; Mountjoy et al., 1999). Furthermore, the high strontium isotope values are restricted to certain areas and depths. The highest enrichments (0.7323) in ^{87}Sr occur adjacent to the deformed belt at the greatest depths (approximately 5000 m), and the values decrease gradually northeastward to 0.7132 within the Leduc Formation and with increasing distance from the disturbed belt (Figs. 5.24 and 5.25).

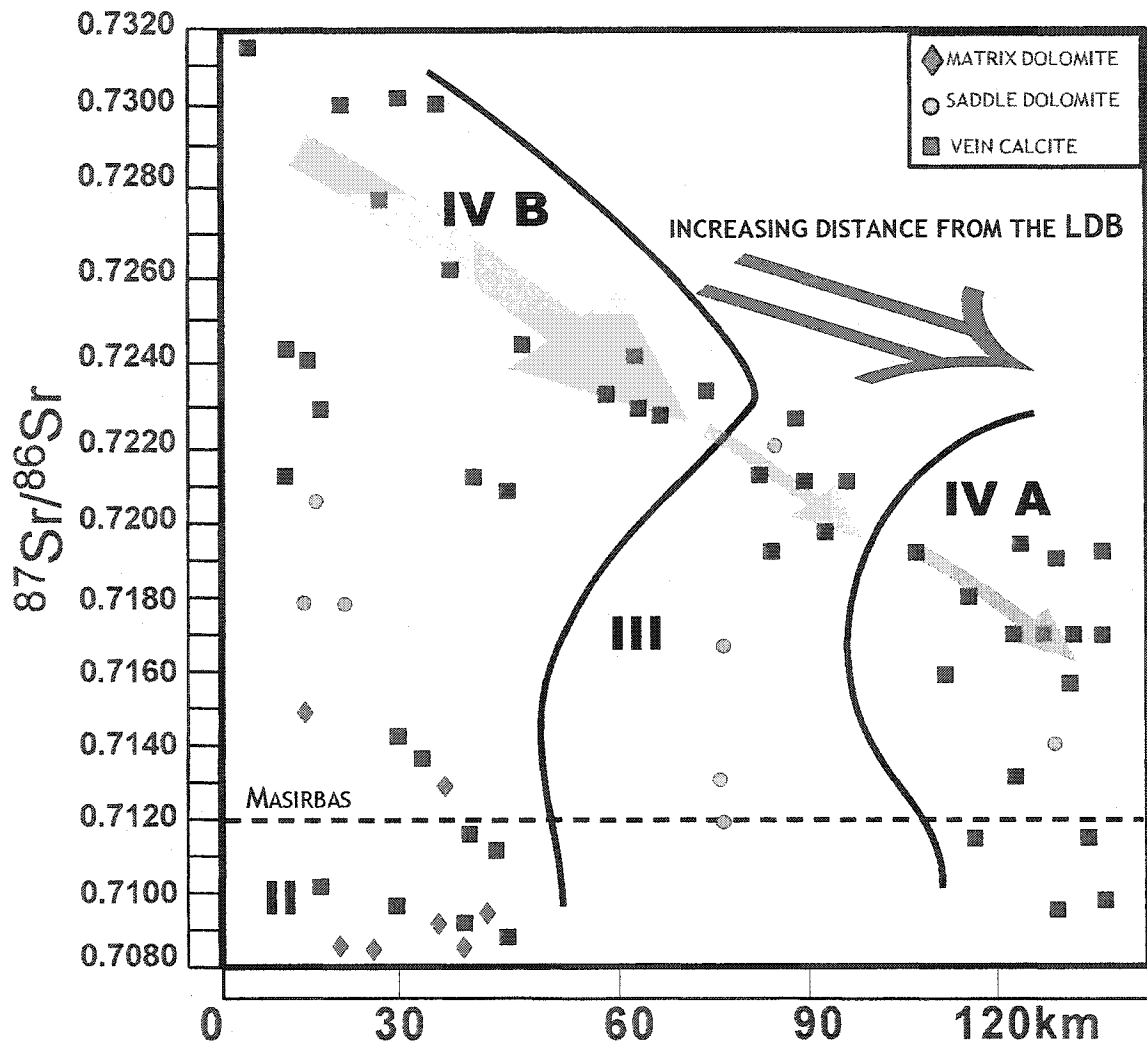


Figure 5.24: Strontium isotope values in relation to the distance from the Rocky Mt. fold and thrust belt (LDB). The values decrease gradually with increasing distance. The bold roman letters denote major diagenetic stages during the history of the SCCC.

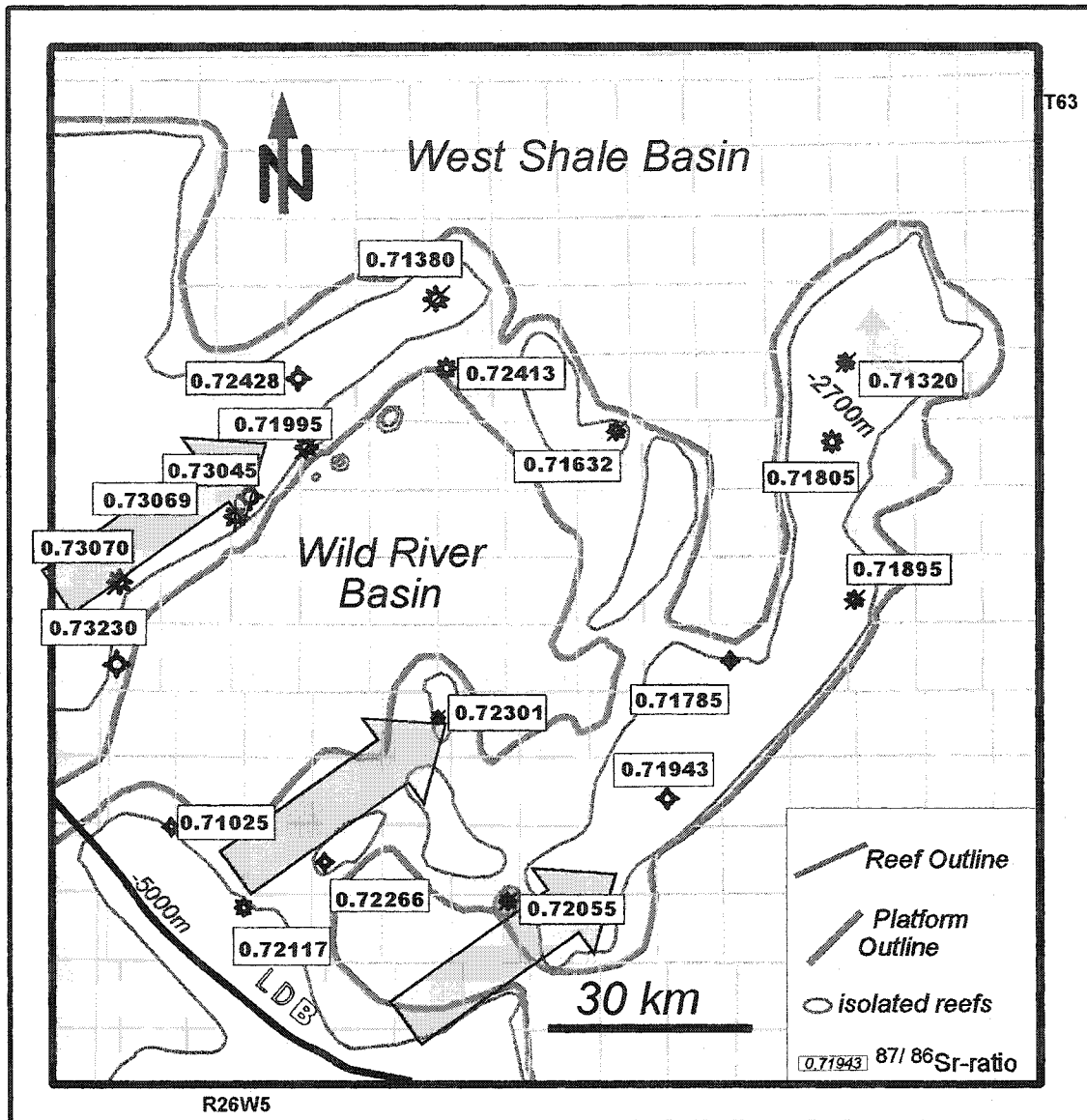


Figure 5.25: Strontium isotope distribution of late calcite cements across the study area. The highest values occur close to the disturbed belt (left) and decrease with increasing distance toward the NE. This suggests that the radiogenic Sr was pushed from the fold and thrust belt along preferential pathways through the Devonian carbonate aquifers into the Alberta basin in a NE direction, as indicated by the arrows.

The basinal shales and marls that surround and overlie the reefs are possible sources for the elevated ^{87}Sr -contents because they contain clay minerals that can release radiogenic strontium into the pore fluids during burial and compaction. The basin-internal shales have been investigated in other studies (Cavell and Machel, 1997; Skilliter, 1999) to test this hypothesis. These studies found that the maximum Sr-isotope ratio of acid-extractable Sr for the basinal shales is 0.7120, a value that was called MASIRBAS (Maximum Strontium Isotope Ratio of Basinal Shale). Hence, strontium isotope ratios that are higher than MASIRBAS could not have been sourced from the basin internal Devonian shales. Therefore, an external fluid source is required to account for the higher Sr isotope values in the saddle dolomites and late calcite cements within the study area, and elsewhere in the deep part of the Alberta Basin (Green, 1999; Buschkuehle & Machel, 1998; McKenzie, 1999; Machel & Cavell, 1999, Buschkuehle & Machel, 2000 a, b, Buschkuehle & Machel, 2002). One likely source of the highly radiogenic Sr are Precambrian metasediments of the Miette Group that are presently exposed in the Main Ranges of the Rocky Mountains, because they can source fluids with isotope ratios as high as 0.7757 (Machel & Cavell, 1999). Another possible source is the Precambrian basement, which underlies the Paleozoic succession in the Alberta Basin.

The driving force behind the ^{87}Sr -enriched pore fluid flow in the SCCC could have been the Laramide orogeny, whereby fluids were injected into the Foreland basin due to tectonic loading and compression. This tectonically induced “squeegee-type” flow (sensu Oliver, 1986) appears to have been most effective directly adjacent to the deformation front. Excess pore pressures must have dissipated within a relatively short distance

because their effects, as recorded in Sr-enrichments, are restricted to about 80 to 100 km away from the disturbed belt (Fig. 5.24, Fig. 5.25) (Buschkuehle et al., 1998a, b; Buschkuehle, et al., 1999; Buschkuehle & Machel, 2000a, b; Buschkuehle & Machel, 2002). Another possible flow mechanism could have been the migration/circulation of fluids from the Precambrian basement into the Devonian succession along faults, reactivated during the Laramide orogeny in the Late Cretaceous and Early Tertiary (Green, 1999; Machel and Cavell, 1999; Duggan et al., 2001; Buschkuehle, 2001). In the eastern part of the study area, e.g. the Windfall field and the Marlboro field (Fig. 5.26), faults, which have been documented through seismic and cross sections, seem to have been likely fluid migration pathways (Green, 1999). In addition the underlying sediments in that area, e.g. Cambrian sandstones and Middle Devonian carbonates, have similar $^{87}\text{Sr}/^{86}\text{Sr}$ -isotope ratios, 0.7160 to 0.7200 and 0.7180, respectively, as the calcite cements in the overlying Upper Devonian strata (see Appendix VI). However, the overall NE-trend in $^{87}\text{Sr}/^{86}\text{Sr}$ (Fig. 5.25) cannot be explained by fluids that ascended from the basement via faults. Hence, the data indicate squeegee-type fluid flow through the Devonian aquifers that was augmented by fault-controlled flow in some locations.

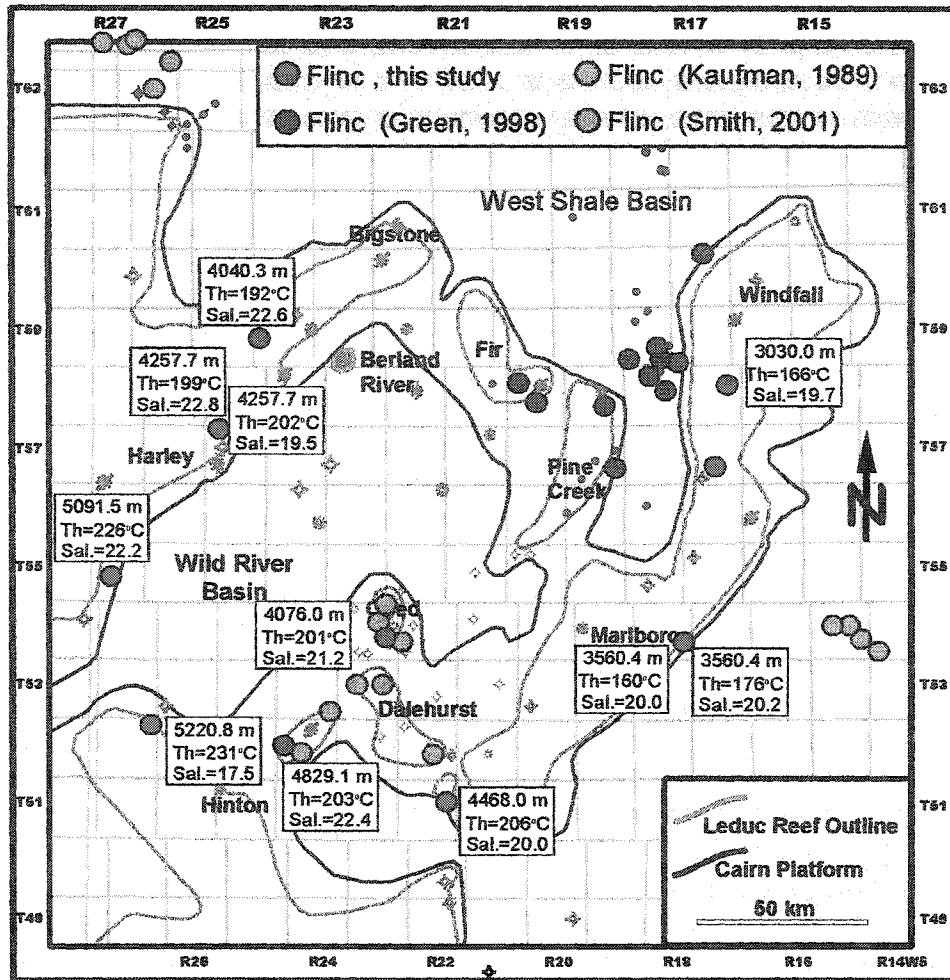


Figure 5.26: Summary and location map of the fluid inclusion data for the SCCC. Note that the deepest sample in the Hinton area has the lowest salinity indicating a process of dilution in the deep part of the Alberta Basin. Temperatures (Th) are corrected for pressure, assuming an additional 2000 m of overburden and therefore represent maximum values.

5.4.4 Interpretation of the geochemistry of present-day formation brines

In general Devonian brines in the WCSB are saline with up to 300g/l Total Dissolved Solids (TDS) and dominated by Na-Ca-Cl (e.g., Michael, 2002). The non-hydrocarbon gases are mainly H₂S, often up to 30 mole% but as high as 90 mole%, including CO₂ and smaller amounts of N₂ and He (Hutcheon et al., 2000).

The brines from the SCCC differ significantly from the brines in shallower areas of the basin that have been collected by Connolly (1990) and Hitchon & Friedman (1969), as seen in Figure 5.18. The brines from the SCCC have higher $\delta^2\text{H}$ as well as higher $\delta^{18}\text{O}$, and they are more radiogenic than brines from the shallow basin. In addition, the SCCC brines have $\delta^{18}\text{O}$ values similar to values calculated for fluid inclusions in TSR-calcites by Hutcheon et al. (2000), suggesting that the isotopic composition of the present day formation waters may be influenced partly by thermochemical sulfate reduction. Also, the brines in the area of the SCCC have significantly lower salinities than the brines in shallower parts of the basin. Figure 5.27 shows the correlation between salinity and facies distribution in the Woodbend-Beaverhill Lake aquifer. The salinity seems to increase with decreasing distance from the LDB. In addition, the 200g/l contour line mimics the edges of the carbonate platform margins, suggesting charging of a “light brine” into the platform from downdip (Michael, 2002).

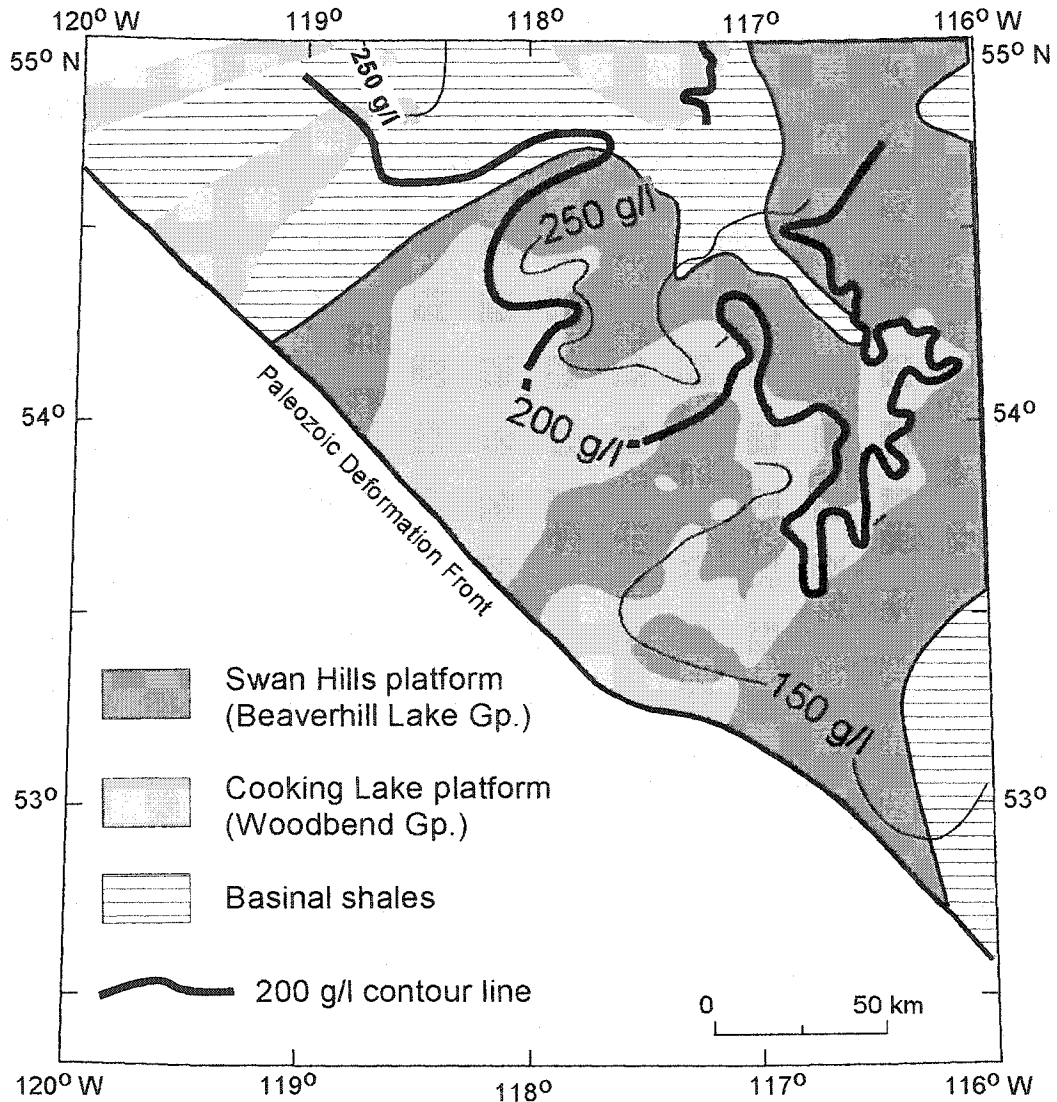


Figure 5.27: Salinity distribution of present day brines within the Woodbend-Beaverhill Lake carbonate platforms in the deep part of the Alberta Basin. The salinities of Upper Devonian brines range up to 300 g/l with a general increase to the northeast (from Michael, 2002).

According to Connolly et al. (1990) the formation waters in the Alberta Basin generally have higher $^{87}\text{Sr}/^{86}\text{Sr}$ -ratios than their host rocks. Only Cambrian shales and the Precambrian basement rocks have greater ratios. However, in this study the diagenetic products are equal or above the $^{87}\text{Sr}/^{86}\text{Sr}$ -ratios of the formation waters.

Sr is more mobile during weathering than Rb, which results in a generally lower $^{87}\text{Sr}/^{86}\text{Sr}_{\text{WATER}}$ in comparison to the $^{87}\text{Sr}/^{86}\text{Sr}_{\text{ROCKS}}$ (Stanley & Faure, 1979). Furthermore the $^{87}\text{Sr}/^{86}\text{Sr}_{\text{ROCKS}}$ must be higher than those of the waters in order to raise the $^{87}\text{Sr}/^{86}\text{Sr}_{\text{WATER}}$. This suggests that the formation waters at some point must have interacted not only with Devonian shales, but more importantly with the Cambrian shales and/or Precambrian basement to obtain a $^{87}\text{Sr}/^{86}\text{Sr}$ -ratio that could lead to the precipitation of highly radiogenic calcite and dolomite cements in the study area.

As shown in Figure 5.18, the isotopic data for the present day brines plot far to the right of the modern Meteoric Water Line, which suggests that meteoric water has not infiltrated the deep Devonian aquifers, which supports the earlier conclusions. A sufficient explanation of the data shown in Figure 5.18 needs a mechanism or way for natural waters to become more ^{18}O enriched than SMOW and meteoric waters. Possible origins of this ^{18}O -rich water are: 1) connate evaporitic brines of marine origin, 2) water derived from the dehydration of gypsum and/or other hydrous minerals, 3) waters that have interacted with the underlying Precambrian basement and adjacent Precambrian metasediments, 4) waters derived from thermochemical sulfate reduction, and 5) mixtures

of waters that derived from a combination of the above mentioned processes (Knauth and Beeunas, 1986).

1) *Connate marine evaporitic brine*

According to Knauth and Beeunas (1986), enriched residual fluids are the result of lighter isotopes being preferentially removed during the early phases of seawater evaporation. The humidity and other local climatic parameters control the trajectory taken by a residual brine. The trajectories for high and low humidities are shown as curves A and B, respectively in Figure 5.12. Lloyd (1966) deemed $\delta^{18}\text{O}$ enrichments of more than +6‰ in coastal environments as unlikely, because atmospheric moisture exchanges oxygen with the evaporating fluid. In the case of extreme evaporation to halite facies and beyond, there is less understanding of the trajectory taken by evaporating seawater. Holser (1979) indicated that progressive enrichment of the heavier isotopes does not continue indefinitely, but that the trajectory hooks around at an evaporation ratio of about 4x (see Curve C in Fig. 5.12). If the present day formation brines had solely evolved via the evaporation of seawater, the data points should plot within the range and/or extension of Curve C. However, the data is shifted downward, indicating that after evaporation other processes have changed the formation fluids.

2) *Water derived from the dehydration of gypsum and/or other hydrous minerals*

Many of the examined cores contain anhydrite. The anhydrite content ranges from trace amounts to nearly 100% in certain core intervals. The origin of anhydrite in evaporites remains controversial. While many researchers consider it to be a primary phase

deposited at the time of sedimentation, others argue that the primary calcium sulfate phase is gypsum, and that the gypsum dehydrates during burial to form anhydrite. At temperatures below 50°C gypsum is the thermodynamically stable phase and should precipitate instead of anhydrite (Hardie, 1967). Kinetic factors, however, are of extreme importance in the precipitation of evaporites and may govern completely the precipitation of sulfate phases in these types of environments (Cody and Hull, 1980). If any or all of the anhydrite in and near the SCCC originated by dehydration of gypsum, the water released during burial must have mixed with the formation water. The water of dehydration would plot along curve D. Sample #3 and #6 fall within the range, however 2,4,5, and 7 are below that line suggesting additional processes overprinting the fluids.

3) Waters that have interacted with the underlying Precambrian basement and adjacent Precambrian metasediments

Water that has passed through a metamorphic system would be highly enriched in $\delta^{18}\text{O}$ and highly depleted in δD , the $\delta^{18}\text{O}$ ranging from about +3‰ to +20‰ SMOW and δD ranging from about -65‰ and -10‰ (Barnes, 1979). The brine samples of this study plot near or within the metamorph-H₂O field, as seen in Fig. 5.12, which suggests an influx of metamorphic water. Other authors (Land, 1997; Schroyen and Muechez, 1998) have advocated that material transfer may happen from the crystalline basement into the overlying deep burial diagenetic setting, whereby prograde metamorphism and devolatilization reactions liberate water and CO₂, which are added to the sedimentary basin above. These metamorphic fluids most likely became injected into the system during the Laramide orogeny in the deep part of the WCSB.

4) Waters derived from thermochemical sulfate reduction

As mentioned in previous chapters, thermochemical sulfate reduction is a process that strongly influenced and overprinted the reservoirs in the SCCC. Water may form as a by-product of TSR and could result in a local dilution of the formation water at or near the reaction site. However, the SCCC brine values are only slightly shifted towards the TSR-water field (Fig. 5.12), indicating that the TSR waters had but a minor influence on the oxygen and deuterium isotopic composition of the formation waters. However, the highly depleted carbon isotopes of the brines clearly indicate that TSR had happened.

5) Mixtures of waters that derived from a combination of the above mentioned processes.

After having described the above mentioned mechanisms it becomes apparent that the isotopic composition of the present day formation brines most likely reflects a combination of evaporation, gypsum dehydration during burial, tectonic injection of metamorphic water, and to a minor degree TSR.

5.4.5 Interpretation of fluid inclusion data

Figure 5.26 shows the regional distribution of the fluid inclusion data and Figure 5.28 the present day pressure distribution of various fields in the SCCC. The fluid inclusion homogenization temperatures measured in this study have been pressure-corrected using the NaCl-H₂O system, because the bulk melting was close to the NaCl-eutectic. The pressure correction seemed to be necessary for two reasons. First, the inclusions were not trapped at boiling; second, the late calcite cements formed during or near maximum burial, and the study area has been uplifted by 1.5 to 2 km since that time (Nurkowski,

1984), which includes a pressure re-equilibration. The pressure-elevation plot in Figure 5.28 shows hydrocarbon accumulations overlying a regional water column in the study area, as well as very high overpressures in isolated parts of the Wild River basin (Wendte, et al., 1998). These data show that most of the SCCC is near or at hydrostatic pressures, which justifies a pressure correction up to hydrostatic pressures corresponding to maximum burial. The abnormally high pressures noted in some reservoirs (Wild River area, Fig. 5.28) are from isolated reefs in the Wild River Basin and not applicable to the platform.

The raw and the pressure corrected data are shown in Figure 5.29. The data follow close to a geothermal gradient of 30°C/km, which has been assumed in previous studies (Mountjoy et al., 1997) to be in effect during the Mesozoic orogenies, in the deep foreland basin. In addition, the fluid inclusion temperatures decrease updip (Fig. 5.26), indicating that hot fluids cooled as they flowed in a northeastward direction, which is in excellent agreement with the observed updip flow from Michael (2002) for the study area in the Upper Devonian succession, and further supports the notion of squeegee-type flow as indicated by Sr-isotope data.

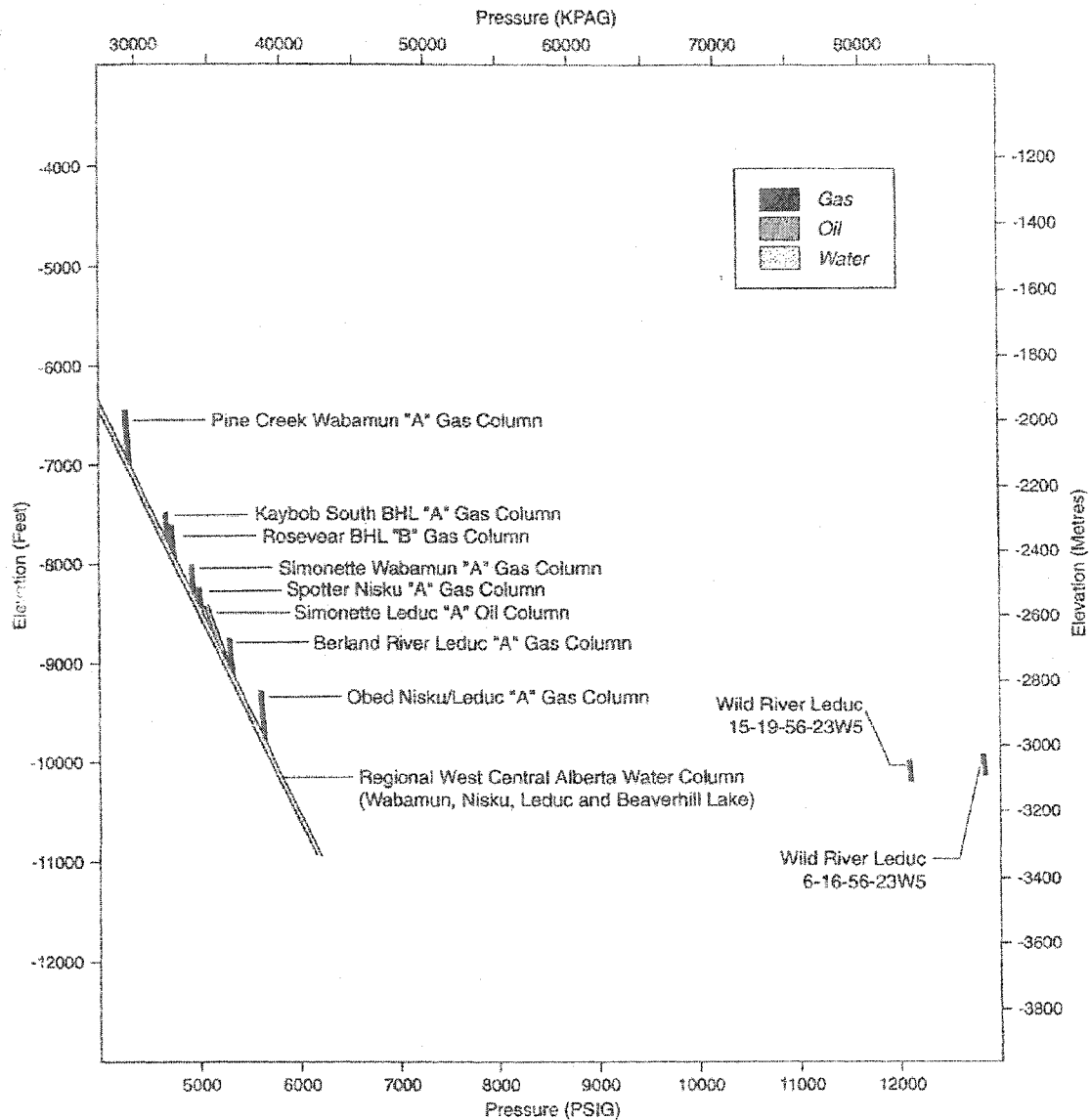


Figure 5.28: Elevation-pressure plot showing hydrocarbon accumulations in the Swan Hills, Leduc, Nisku and Wabamun formations overlying a regional water column in the study area (from Wendte, 1998). Overpressured gas accumulations occur in isolated limestone reefs in the Wild River area, indicating permeability barriers and pressure differences that require pressure corrections of the fluid inclusion data.

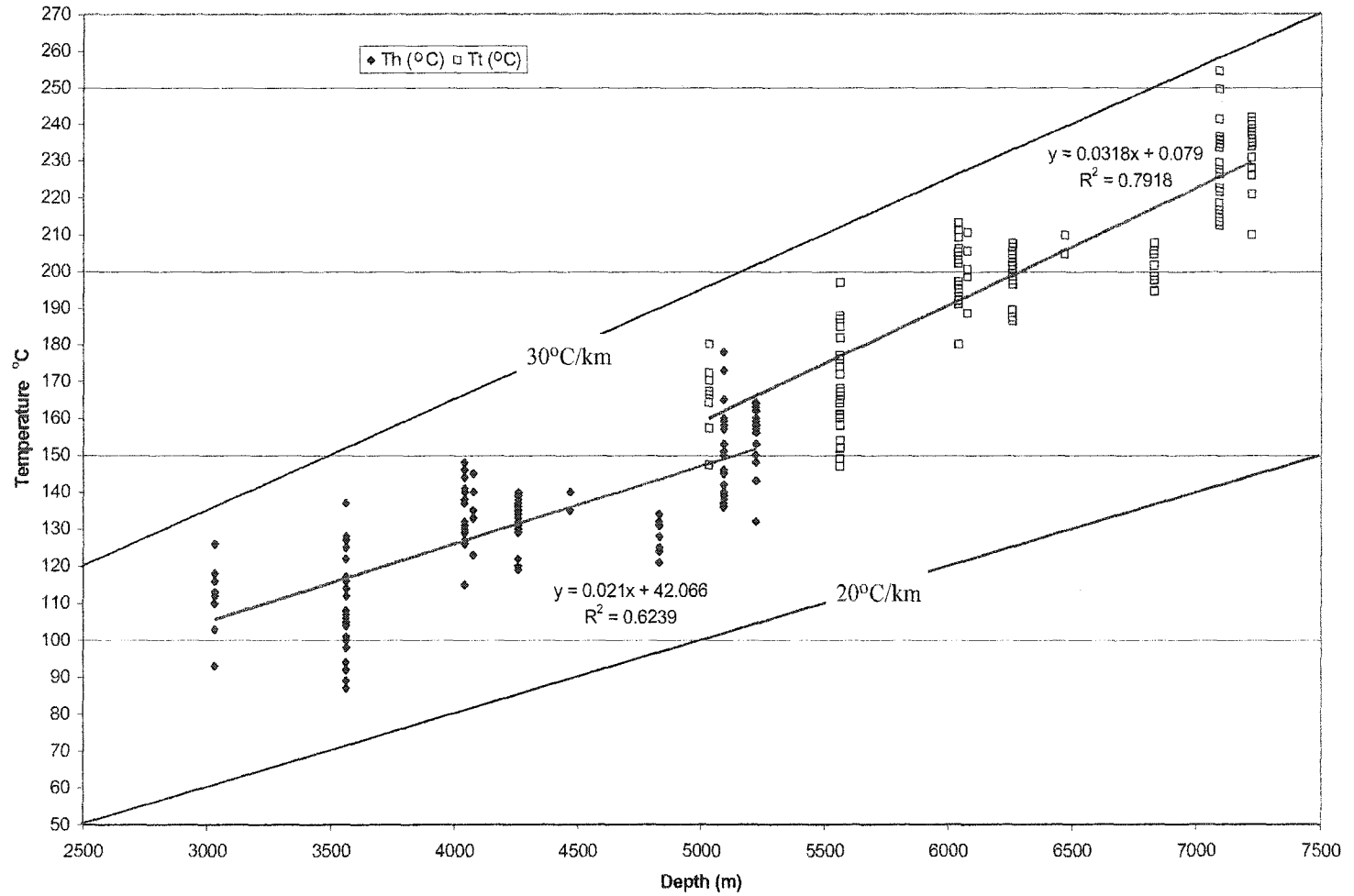


Figure 5.29: Fluid inclusion homogenization temperatures (uncorrected Th and corrected for pressure Tt) versus depths for all inclusions that were measured for this study. A pressure correction has been applied equivalent to hydrostatic pressures at 2 km deeper than present. The corrected temperatures Tt follow close to a 30°C/km geothermal gradient, which is in good agreement with the data from Mountjoy et al., 1997.

Assuming that the $\delta^{18}\text{O}$ values of the calcite and saddle dolomite cements reflect isotopic equilibrium with waters from which the inclusions formed, the homogenization temperatures can be used to estimate the $\delta^{18}\text{O}$ of the water at the time of the cement formation using the equation from Land (1985) for the saddle dolomite

$$[3.2 \times 10^6 T (^{\circ}\text{K})^{-2}] - 3.3 = \delta^{18}\text{O}_{\text{dolomite}} - \delta^{18}\text{O}_{\text{water}} \quad (1)$$

and from O'Neil et al. (1969)

$$[2.78 \times 10^6 T (^{\circ}\text{K})^{-2}] - 2.89 = \delta^{18}\text{O}_{\text{cc}} - \delta^{18}\text{O}_{\text{water}} \quad (2)$$

for the calcite cements. Accordingly, the equilibrium $\delta^{18}\text{O}_{\text{water}}$ of the saddle dolomite was + 4 ‰_{SMOW} using the equilibrium relationship plot from Land (1985) (Figure 5.23). The $\delta^{18}\text{O}_{\text{water}}$ for the calcite cements scatters between 5‰_{SMOW} and 7‰_{SMOW} for a low temperature range around 125°C and 8‰_{SMOW} to 10‰_{SMOW} for a temperature at around 163 °C using the equilibrium relationship plot by O'Neil et al. (1969) (Figure 5.30). In addition, if one takes the measured isotope values of the late calcite cements and $\delta^{18}\text{O}_{\text{water}}$ from present day brines, a temperature range between 95°C and 230°C is created, which coincides perfectly with the corrected fluid inclusion homogenization temperatures (Fig. 5.29). Conversely, the uncorrected Th values paired with present day formation fluids result in $\delta^{18}\text{O}$ values that are too low (blue field in Fig. 5.30), further supporting the need for pressure correction of the Th-data.

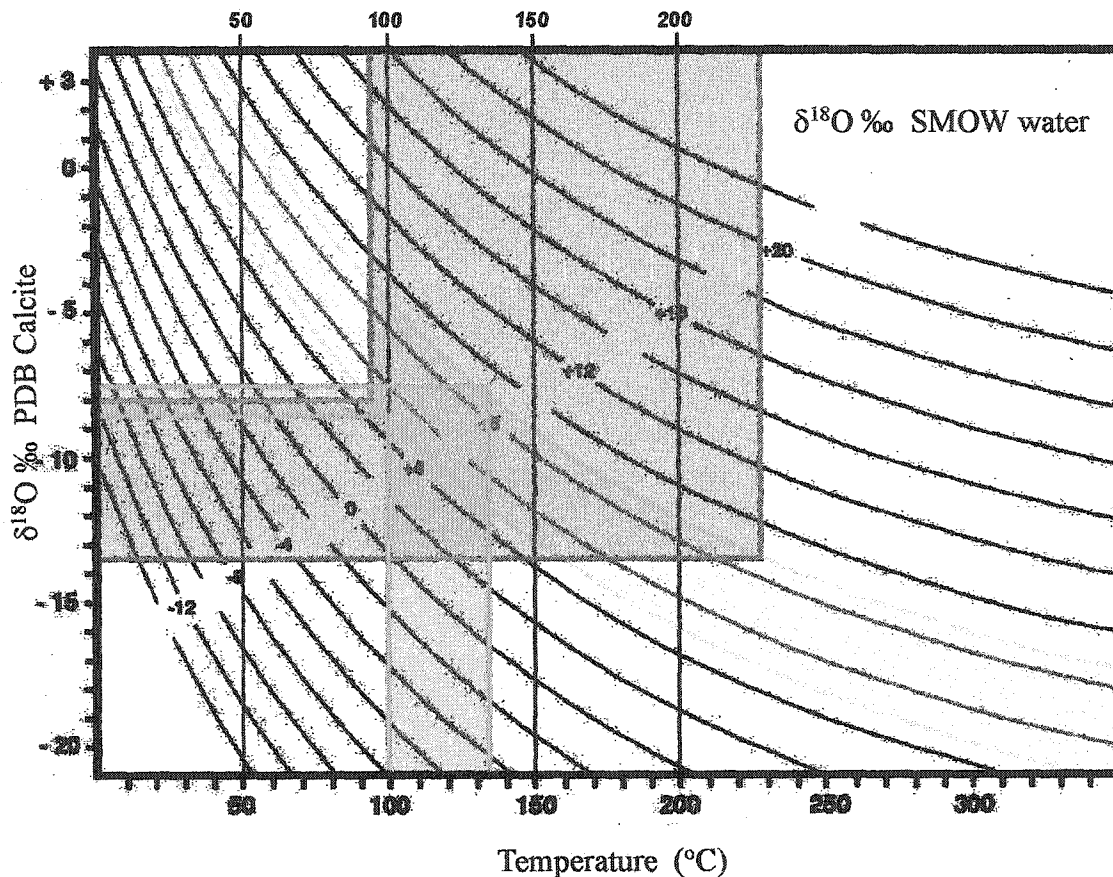


Figure 5.30: Plot of equilibrium relationships between analytical calcite, equilibrium calcite, present day temperatures, present day brines and fluid inclusion data. The yellow field represents oxygen isotopic composition of present day brines. The red area took the analytical calcite cement values and assumed a $\delta^{18}\text{O}\text{‰ SMOW}$ from present day brines, which leads to a temperature range of 95 to 220°C. The blue area took the present day temperature and the present day isotopic composition of brines, which leads to an isotopic equilibrium calcite near the lowest analyzed values.

The eutectic temperatures of the samples vary between $-45\text{ }^{\circ}\text{C}$ and $-55\text{ }^{\circ}\text{C}$, which usually would indicate a complicated cation composition of the inclusion fluid. However, the average T_e of $-51.3\text{ }^{\circ}\text{C}$ corresponds well with the eutectic temperature of the NaCl-CaCl-H₂O-system of Davies et al. (1990). Hence, the salinities were calculated for the NaCl-H₂O-system, notwithstanding that the T_e indicate a more complicated system. It would have been difficult to determine reliable temperatures for intermediate melting of other

phases, which would be needed for the determination of the bulk salinity (Goldstein & Reynolds, 1994). A more complex composition would generally result in slightly lower salinities than those calculated under the assumption of the NaCl-H₂O-system.

5.4.6 Interpretation of the sulfur isotopes of fluids and solids

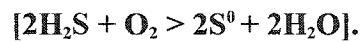
The isotopic compositions of the fluids as well as the solids are summarized in Figure 5.11 and show a wide range of variation. Upper Devonian seawater sulfate had an isotopic sulfur composition of 25‰ $\delta^{34}\text{S}$ and 14‰ $\delta^{18}\text{O}$ (Claypool et al., 1980; Machel & Burton, 1991). The Middle Devonian seawater sulfate $\delta^{34}\text{S}$ was about 21 ‰ CDT. The isotopic range of sulfur isotopes from diagenetic anhydrite varies between 26.7 ‰ $\delta^{34}\text{S}$ and 18.4 ‰ $\delta^{34}\text{S}$ (Fig. 5.11). This variation is most likely due to mixing with sulfate from the underlying Middle Devonian, which could have been injected via faults (Machel & Burton, 1991) and subsequent precipitation as anhydrite.

The sulfur isotopic compositions of the elemental sulfur samples as well as the bitumen are close together, between 18 ‰ $\delta^{34}\text{S}$ and 20.2 ‰ $\delta^{34}\text{S}$. These values probably originated from TSR, which imparts a 10-15 ‰ negative fractionation relative to the source sulfate in the 150 – 200°C temperature range (Machel, et al., 1995).

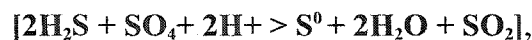
Mixing and TSR processes can also best explain the isotopic compositions of the formation brines. The samples cluster in two groups, whereby the samples out of the Middle Devonian Swan Hills Formation generally have lower ‰ $\delta^{34}\text{S}$ -values than the ones from the Upper Devonian, which corresponds to the isotopic composition of Middle

Devonian seawater ($\sim 20\text{‰ } \delta^{34}\text{S}$). The rather low isotopic compositions ($11.7\text{‰ } \delta^{34}\text{S}$ / $10.1\text{‰ } \delta^{34}\text{S}$) indicate a kinetic fractionation of inorganic compounds by -15‰ to -10‰ , which falls in a temperature range of 150°C to 200°C (Machel, et al., 1995). These values coincide well with the pressure-corrected fluid inclusion temperatures, supporting the notion that the present day formation fluids are similar to the fluids from which the saddle dolomites and calcite cements precipitated.

Another process that could lead to this isotopic variation is oxidation of H_2S by oxygen:



However, this process is highly unlikely in the SCCC because it is too deep to contain any molecular oxygen. Rather, H_2S could have been oxidized by excess sulfate:



which would be the other viable process to explain the isotopic variation in the brines. The schematic evolution of concentration and sulfur isotope ratios are shown in Figure 5.31.

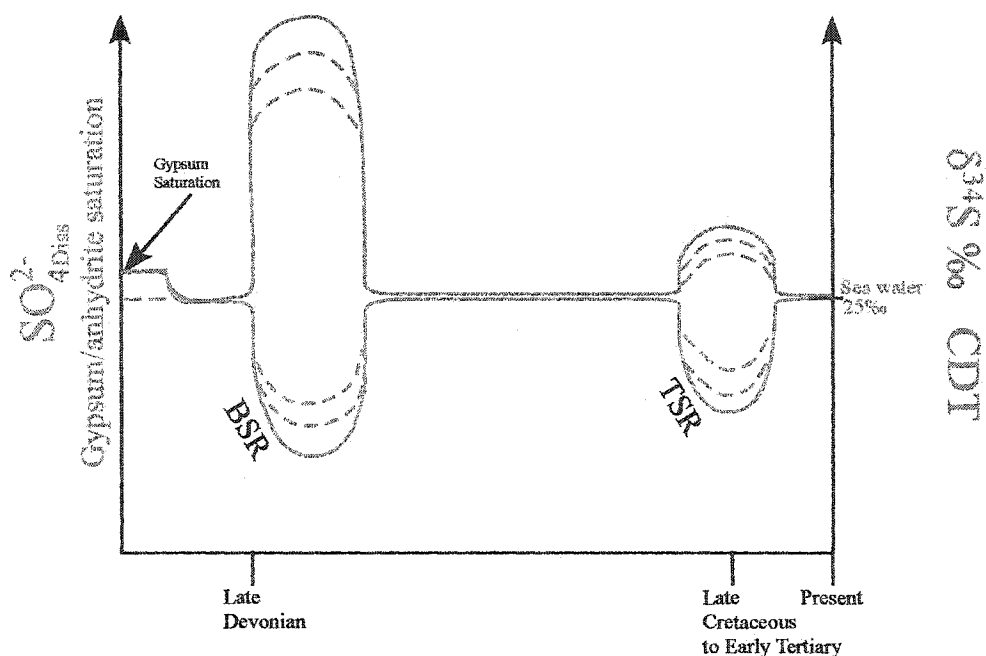


Figure 5.31: Schematic evolution of concentration and sulfur isotope ratios of sulfate dissolved in SCCC pore waters through time. During the late Devonian to Mississippian, bacterial sulfate reduction temporarily depleted the sulfate concentration in the pore waters, and the $\delta^{34}\text{S}$ values of the remaining dissolved sulfate increased dramatically as a result of closed-system Raleigh fractionation. H_2S and/or iron sulfide formed from the H_2S at that time would have correspondingly negative $\delta^{34}\text{S}$ values, but getting heavier with increasing sulfate depletion in the pore waters (see also Figure 5.4). After bacterial sulfate reduction ceased, both sulfate concentration and the $\delta^{34}\text{S}$ values approached the original values due to gypsum/anhydrite dissolution. These patterns repeated themselves during thermochemical sulfate reduction in the Late Cretaceous/Early Tertiary, but were much attenuated because of the lower rate (concentration) and the smaller kinetic isotope fractionation ($\delta^{34}\text{S}$) of TSR compared to BSR. The extent of concentration depletion and isotope enrichment is variable and depends on the rate of sulfate reduction relative to gypsum/anhydrite dissolution (illustrated by dashed contours).

CHAPTER 6: SUMMARY AND CONCLUSION

6.1 Restatement of Objectives and Review

The major objectives of this study were to describe the stratigraphy, diagenesis, and geochemistry of the Upper Devonian rocks in the Southesk-Cairn Carbonate Complex (SCCC) of west-central Alberta; to determine the causes for the present porosity and permeability distribution in the carbonates; and to identify the directions, mechanisms, and approximate fluxes of paleo fluid flow. Understanding of paleo hydrogeology in the SCCC is of particular importance for both science and the petroleum industry. The scientific aspect of this study includes information about pore fluid changes, the mineral products that form from the fluids, and their timing of formation. The petroleum industry will benefit from better understanding by enhanced exploration and exploitation.

In Chapter 1, the study area and the problems related to fluid flow and fluid processes in areas adjacent to a mountain thrust and fold belts are described. Chapter 2 gives an overview of the geologic framework, the basin definition, history and paleogeography of the SCCC area adjacent to the Rocky Mountain Fold and Thrust Belt. In Chapter 3 the dual stratigraphic nomenclature is defined, because the study area deals with subsurface rocks and outcrop data, for which different stratigraphic terms are in use. In addition, the new, informal unit "Berland Shale" was introduced. Furthermore, the lithological features of the four Devonian Groups (Beaverhill Lake, Woodbend, Winterburn and Wabamun) are described, as well as the facies development and the related dolomitization patterns. Chapter 4 contains the description of the diagenetic products and

processes, which are interpreted to having been formed in five major stages of burial and pore-water evolution. In Chapter 5 the isotopic data and fluid inclusion homogenization temperatures are presented, analyzed and integrated into the analysis of the burial history. This final chapter integrates observations and interpretations from the previous ones into a synopsis of the dolomitization processes, tectonic expulsion, paragenetic sequence, burial history, and the evolution of pore fluids in the west-central part of the deep Alberta Basin.

6.2 Dolomitization

Dolomitization is one of the most important diagenetic processes in the study area and is governed by various factors such as: sedimentary facies, recrystallization, chemical compaction, TSR reactions, and faulting. Figure 6.1 shows in summary the different dolomitization models that have been invoked for the formation of various types of dolomite. There are at least four different types of dolomite in the study area and each is related to a different dolomitization process. The first two types, Dolomite 1 and 2 are mainly controlled by facies, whereas the others, Dolomite 3 and 4, are due to structural and burial-diagenetic development. The following interpretations are based on petrography and facies analyses, as well as on diagenetic and structural features, and geochemical data of some of these dolomite types. They reveal that dolomitization took place in a variety of environments, ranging from near surface to deep burial.

DOLOMITIZATION MODEL	SOURCE OF Mg ²⁺	DRIVING MECHANISM	HYDROGEOLOGICAL MODEL	DOLOMITE PATTERNS
A. Reflux Dolomitization	Seawater	density-driven flow storm recharge evaporative pumping		
B1. Seawater Dolomitization	Seawater	slope convection ($K_v > K_h$)		
B2. Seawater Dolomitization	Seawater	slope convection ($K_v < K_h$)		
C1. Burial Dolomitization	buried (connate) seawater	compaction-driven flow		
C2. Burial Dolomitization	basinal brines	tectonic expulsion		
C3. Burial Dolomitization	basinal brines	flow along faults (reactivation)		

Figure 6.1: Dolomitization models and predicted dolomite distribution patterns (in grey) in carbonate build-ups. Models A to C1 and C3 are kilometer scale, Model C2 is basin-scale. Arrows denote flow direction. K_v and K_h = vertical and horizontal hydraulic conductivity, respectively. (Compiled and modified from Amthor et al., 1993, Garven, 1995; Braithwaite and Rizzi, 1997; and Morrow, 1998.)

Dolomite 1: Very fine-grained laminated dolomites, which are associated with anhydrite, occur locally in the Blueridge Member of the Winterburn Group and in the Wabamun Group. These dolomites are interpreted as shallow marine dolomites that are associated with subtidal to supratidal cycles according to their textural and mineralogical association and are equivalent to Dolomite A in Fig. 6.1. The dolomitizing fluid probably was a hypersaline brine that formed from Devonian seawater due to evaporation and was driven by density differences down into the sedimentary column, where it dolomitized the preexisting limestones (Fig. 6.1A). However, reflux probably was restricted in time and space in the SCCC, whereas equivalent dolomites formed on a much larger scale on the Grosmont platform in the eastern part of the Alberta Basin (Cutler, 1983).

Dolomite 2: The second dolomite type is pervasive, replacive matrix dolomite that is a common phenomenon in the Alberta Basin. Numerous authors have discussed the formation of the huge amounts of replacement dolomite in the Alberta Basin, and several models have been suggested to explain them (Machel and Mountjoy, 1987). In the study area, pervasive matrix dolomites occur only in certain facies types such as reefal and platform grain- to boundstones. However, matrix dolomitization requires large amounts of Mg-bearing fluids, which in turn require the presence of aquifers, and only the above mentioned facies types provide sufficient primary permeability. Therefore, the primary permeability distribution is a major controlling factor for dolomitization. Furthermore, the isotope data indicate that the dolomitizing fluids were slightly modified Devonian seawater. Most of the chemical modification of the seawater was due to water-rock interactions that occurred while the water moved through the interbedded and enclosed

argillaceous sediments. The driving forces for the fluids cannot be definitely identified. However, it is assumed that the seawater was driven probably by a combination of convection and compaction through the Devonian strata, when they were buried between 500 and 1500 m, which was previously suggested for the bulk of the replacive dolostones in this basin (Amthor et al., 1993; Machel et al., 1994; Mountjoy et al., 1999). Several authors have invoked the reflux dolomitization model for the matrix dolomites (Shields and Brady, 1995; Potma et al., 2001), however stratigraphic, paleo-geographic, structural and geochemical data, as well as hydrological constraints and mass balance calculations render this explanation for the matrix dolomites in most parts of the Alberta Basin unlikely (Machel et al., 1996; Machel et al., 2002).

Dolomite 3: The third dolomite type in the study area is a coarse crystalline saddle dolomite cement that occurs with calcite in vugs and fractures in certain locations in the study area and probably formed similar to the situation shown in C3 in Figure 6.1. Spatial relationships and geochemical data suggest that this dolomite formed from saline, basinal brines. It is most likely that these cements are the product of a fault-related dolomitization process, where Mg-bearing fluids with elevated temperatures moved through fractures and precipitated the coarse-crystalline dolomite cement. This dolomite formation occurred on a local scale, however, it has been described from all four Devonian groups and numerous areas in the Alberta Basin. It is related due to faulting and re-activation of faults during maximum burial in the Late Cretaceous to early Tertiary during the Laramide orogeny (Green, 1999; Mountjoy et al. 1999).

Dolomite 4: This type is also coarse saddle dolomite cement, but always associated with hydrocarbons, elemental sulfur and anhydrite. Geochemical and fluid inclusion data suggest elevated temperatures during its precipitation. The brines that precipitated this dolomite were formation waters depleted in ^{13}C and enriched in radiogenic strontium. Thus, this dolomite type is clearly related to TSR and the injection of metamorphic fluids.

6.3 Tectonic Expulsion of Formation Fluids

Most of the late diagenetic calcite and dolomite cements in the study area have highly radiogenic strontium isotope ratios, which shows that the chemical composition of the pore waters evolved significantly over time. Furthermore, the strontium isotope signals show a distinctive spatial distribution. The highest $^{87/86}\text{Sr}$ -ratios occur adjacent to the deformed belt at depths of approximately 5000 m, and the values decrease gradually northeastward within the Leduc Formation and with increasing distance from the disturbed belt.

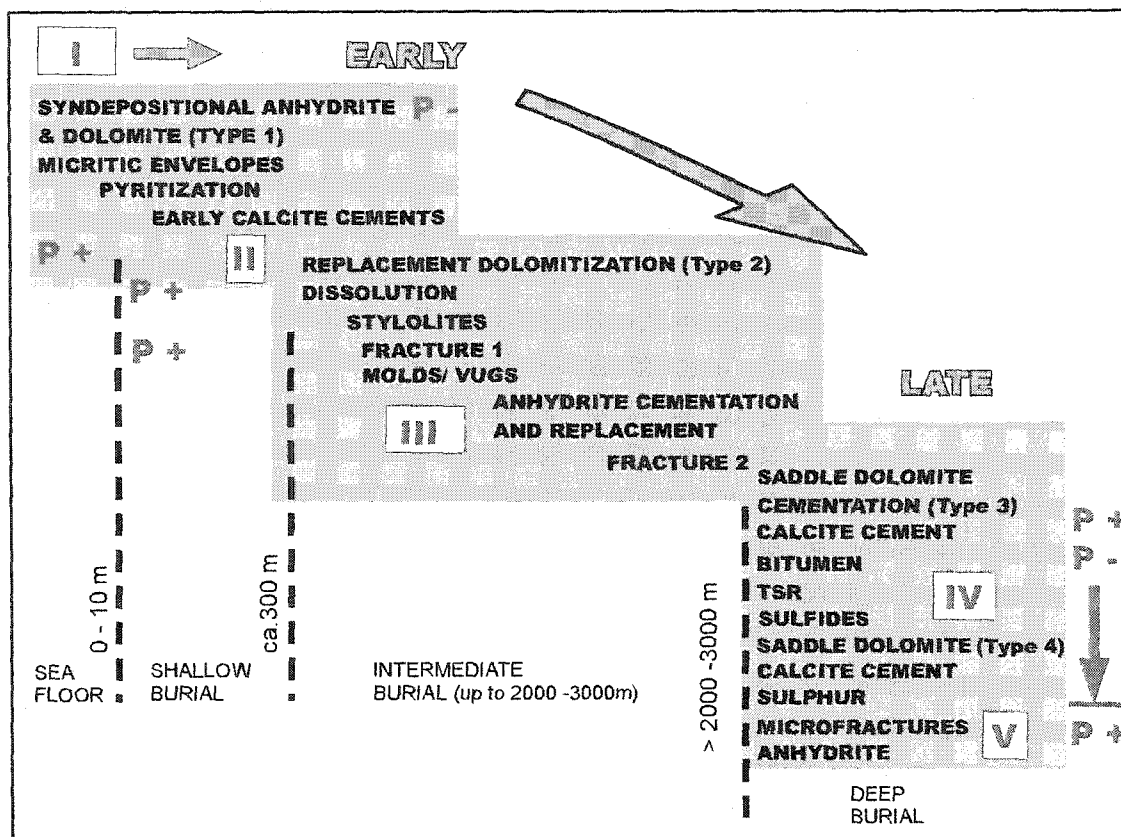
The maximum Sr-isotope ratio of acid-extractable strontium for the basinal shales was defined as MASIRBAS (**M**aximum **S**trontium **I**sotope **R**atio of **B**asinal **S**hales) (Machel and Cavell, 1999). However most of the afore-mentioned diagenetic products have values greater than MASIRBAS and could not have been sourced from the basin internal Devonian shales. Therefore, an external fluid source is required to account for the high-Sr isotope values in the late calcite cements within the study area and elsewhere in the deep part of the Alberta Basin. This further suggest that the fluids must have interacted/mixed

with fluids from Precambrian metasediments of the Miette Group that are presently exposed in the Main Ranges of the Rocky Mountains and /or from the Precambrian basement, because the acid-exchangeable strontium of these two successions has ratios that can source a highly radiogenic fluid (Machel and Cavell, 1999).

The driving force behind the pore fluid flow that carried the radiogenic Sr into the foreland basin could have been tectonic compression during the Laramide orogeny, when fluids were being injected into the Foreland basin due to tectonic loading. This tectonically induced “squeegee-type” flow appears to have been most effective directly adjacent to the deformation front. Excess pore pressures must have dissipated within a relatively short distance because their effects are restricted to about 80 to 100 km away from the disturbed belt. Another possible flow mechanism could have been the migration of fluids from the Precambrian basement along reactivated faults into the Devonian succession. This reactivation could also have been caused by the Laramide orogeny, which was effective during the Late Cretaceous and Early Tertiary. In the northeast part of the study area faults seem to have been the most likely migration pathways (Green, 1999).

6.4 Fluid Evolution, Flow Mechanisms and Paragenetic Sequence of the SCCC

The carbonates of the Southesk-Cairn Carbonate Complex underwent a complex diagenetic history, which can be divided into five stages of burial with corresponding stages of pore water evolution (Fig. 6.2 and Fig. 6.3).



Stage	Time	Diagenetic Realm	Major Diagenetic Phase	Fluid	Flow Driving Mechanism	Fluid Flux
I	Middle to Late Devonian	Seafloor to shallow burial	Early marine calcite cements, laminated dolostone/anhydrite	Seawater and evaporated seawater	Circulation, tidal pumping, density-driven flow	High
II	Late Devonian to Early Mississippian	Intermediate burial	Matrix dolomitization	Modified seawater (dissolution)	Multitude of conceptual models and interpretations	Medium - high
III	Cretaceous	Deep burial	Hydrocarbons & recrystallization	Brine	Compaction, ... ?	Low (?)
IV	Late Cretaceous/ Early Tertiary	Maximum burial	TSR & Dolomite cements & Calcite cements	Strontium-charged brine	Tectonically-driven, topography (?)	Medium in pulses
V	Tertiary till present	Uplift to present depth	Minor anhydrite cements	Diluted brine (TSR?/Mixing?)	Topography (?)	Very low

Figure 6.2: Diagenetic paragenesis of the Southesk-Cairn Complex. Roman numbers indicate diagenetic and fluid stages; The table shows the timing, the fluid, the driving mechanisms and the fluxes behind each fluid stage. P+ indicates increase in porosity, whereas P- indicates decrease in porosity.

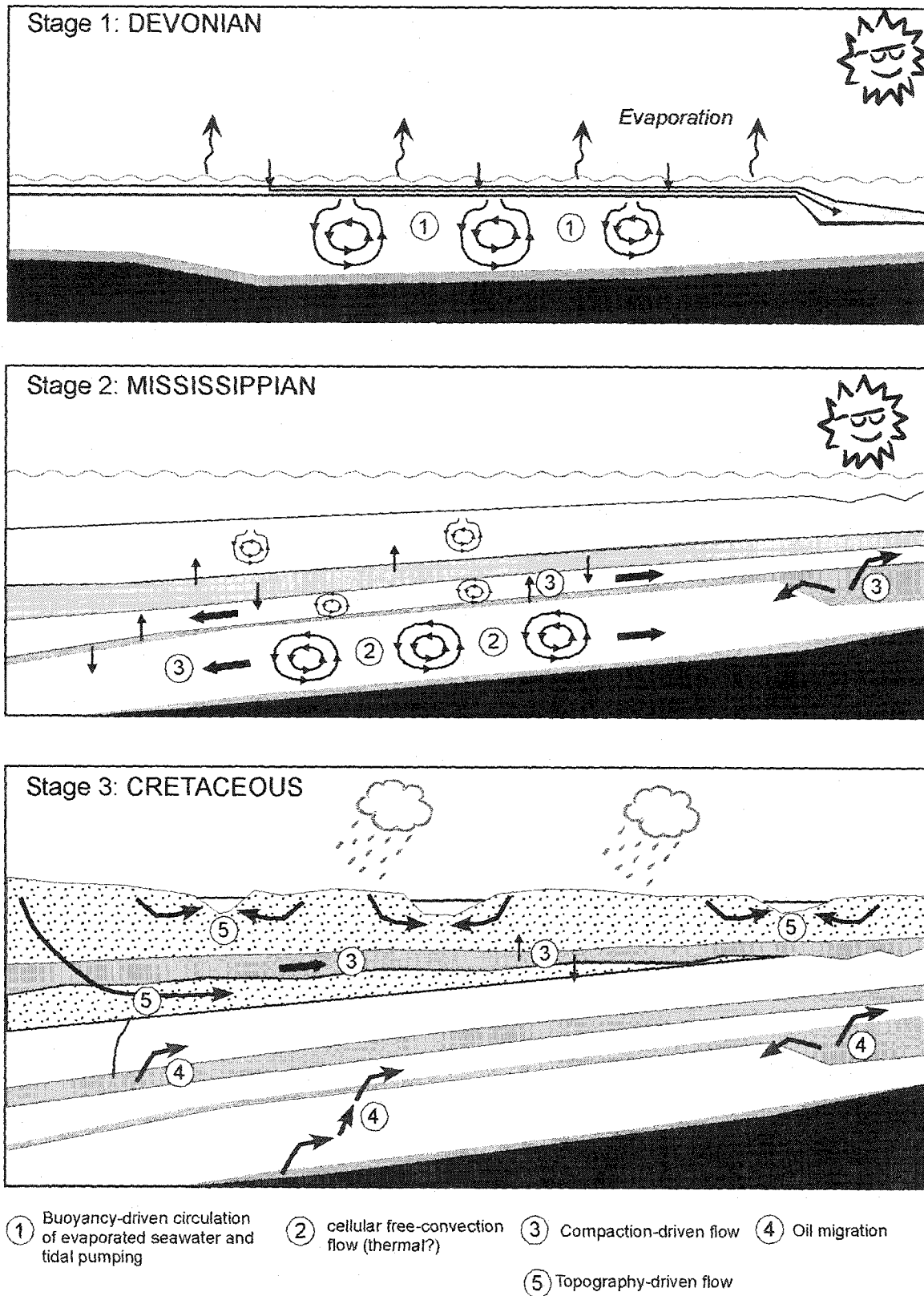
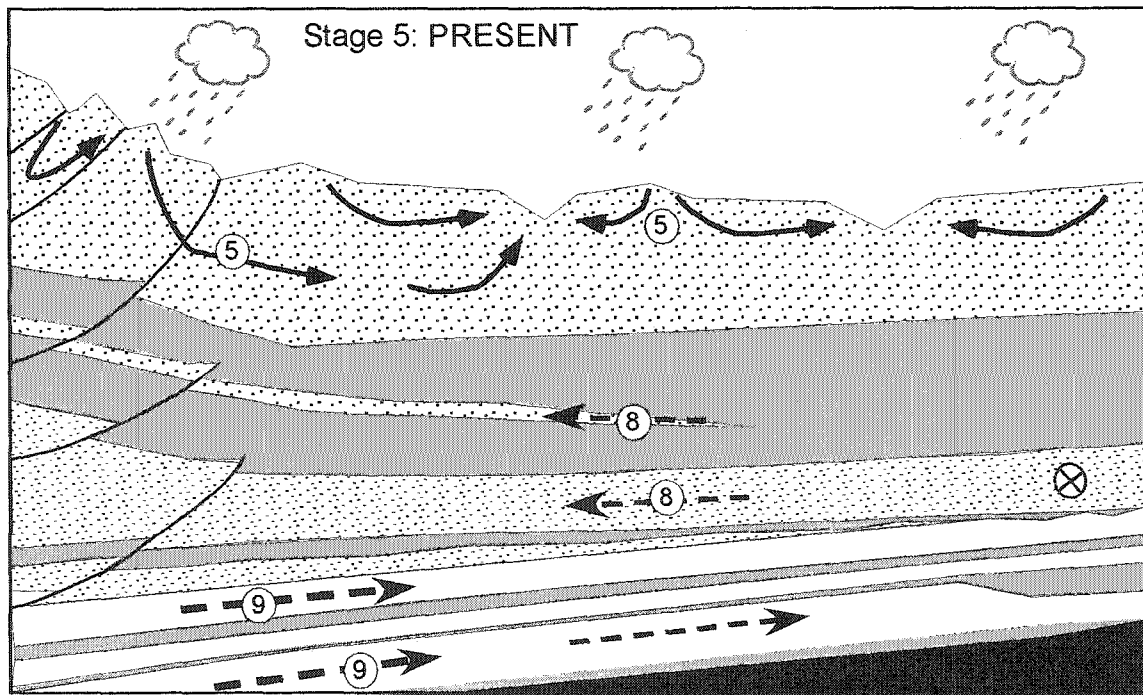
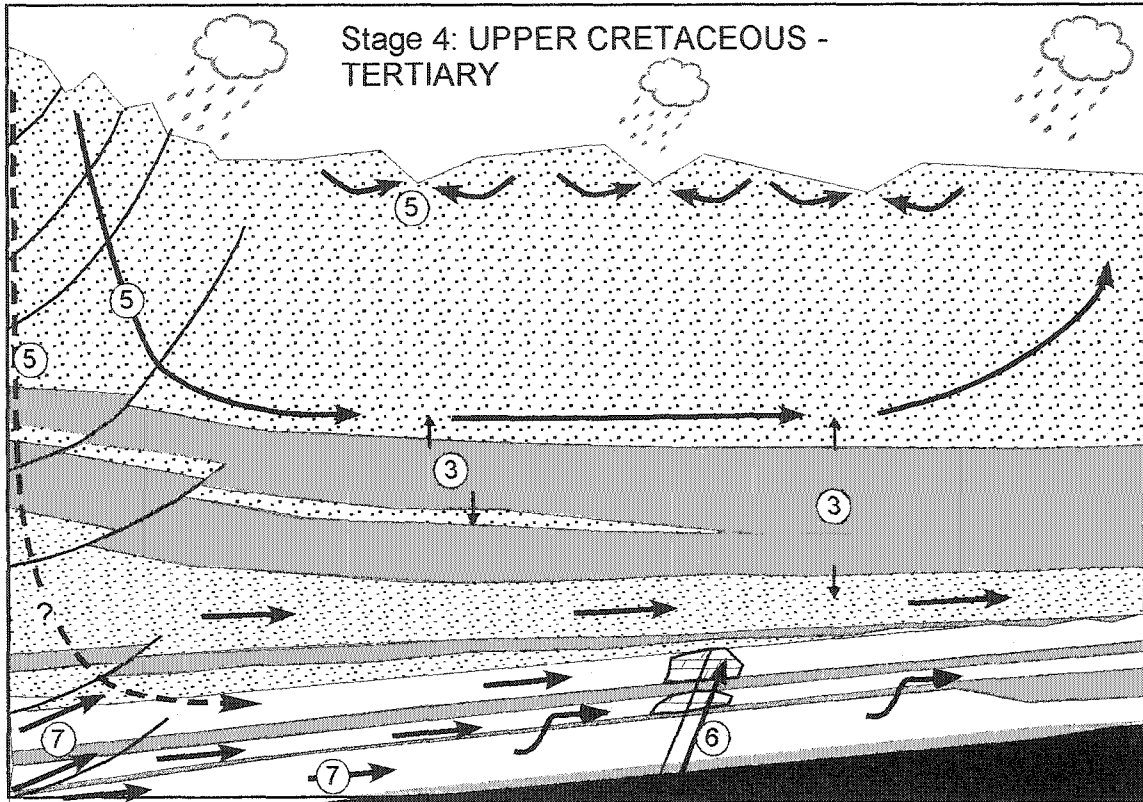


Figure 6.3: Conceptual evolution of flow patterns in the deep Alberta Basin from the Devonian to the present. See text for discussion (continued on next page).



- | | | | | | |
|---|------------------------|---|-------------------------------------|---|-------------------------------------|
| ③ | Compaction-driven flow | ⑥ | Expulsion of fluids along faults | ⑧ | Flow driven by erosional rebound |
| ⑤ | Topography-driven flow | ⑦ | Flow driven by tectonic compression | ⑨ | Remnant of tectonically-driven flow |

Figure 6.3: (Continued from previous page.)

The first stage includes all processes on the marine seafloor and its syndepositional features, like micrite rims, early marine calcite cements, and the formation of microbial pyrite in microenvironments. These products are best preserved in the un-dolomitized, yet rare limestones. Furthermore, early diagenetic anhydrite and Dolomite Type 1 formed locally in shallow marine subtidal to intertidal facies zones during the deposition of the Blueridge Member and during the Early Wabamun time. The initial porosity and permeability was relatively high during this stage, but generally decreased fast due to ongoing cementation. The first fluid that was involved in these strata in the basin history was Upper Devonian seawater, the chemical composition of which has been defined in this study and in previous studies. The driving forces for fluid flow most likely were circulation (free convection), tidal pumping, and evaporative reflux during the Blueridge and Wabamun deposition (Fig. 6.3 Stage 1).

Stage 2 took place during shallow to intermediate burial between 300 m and 1500 m during the Late Devonian to Early Mississippian. The major diagenetic phase during this stage is Dolomite Type 2, i.e., approximately 85% of the carbonates in the SCCC became pervasively dolomitized during this time. This dolomitization process was facies-dependent, as well as matrix-selective. Larger bioclasts and lithoclasts were preserved as calcite and later dissolved at most locations, which led to the formation of moldic and vuggy porosity. The matrix dolomites form the best reservoir rocks in the study area due to their high primary and enhanced secondary porosity and permeability. Other products/processes during this stage were physical and chemical compaction, the formation of stylolite-related dolomites and pyrite, as well as a first fracture phase and associated

calcite cements, and secondary replacive anhydrite. The major fluid, facilitating these diagenetic processes was slightly modified Devonian seawater, as indicated by isotope data. The fluid was forced through the rocks by compaction (sedimentary-loading) and presumably convection flow (Fig. 6.3 Stage 2). The ultimate driving mechanism is not yet identified. During this stage the Devonian seawater became increasingly modified due to water-rock interactions with the intervening argillaceous sediments and gypsum dehydration.

Stage 3 took place during intermediate to deep burial. The main diagenetic processes during Stage 3 were oil maturation and primary migration during the Late Cretaceous, after the source rocks had reached the liquid oil window (Fig. 6.3, Stage 3). The main source rocks in the study area are probably shales within the D3 (Duvernay Formation) and D2 intervals (Nisku equivalents/Cynthia Member). The formation fluids significantly changed in their composition during this time due to water-rock-hydrocarbon interaction.

Stage 4 took place during the latter part of rapid burial to maximum burial depths of about 7 km in the Paleocene (Fig. 6.3, Stage 4). The major diagenetic processes were thermochemical sulfate reduction (TSR), hydrocarbon maturation and late calcite cementation. The onset of TSR is usually constrained to minimum temperatures of 100-140°C, and the formation of TSR calcite took place in a temperature range of about 140-220 °C, as indicated by fluid inclusion data. Products of stage 4 diagenesis are sour gas (up to 35 mole% H₂S), abundant saddle dolomite cements, blocky calcite cements, pyrite and chalcopyrite as well as anhydrite.

Radiogenic strontium was introduced to the fluid, as shown by the saddle dolomite and late calcite cements. The radiogenic strontium signal increases with increasing burial and calcite cementation; however, it was not equally distributed over the area, since high strontium signals can be found in different strata and in different locations, thus indicating that these fluids followed preferential pathways. Rather, the Sr isotope data suggest lateral expulsion of formation waters with a metamorphic or hydrothermal component from the area of the Rocky Mountain into the plains region. In addition, formation waters entered the Devonian strata at least in certain areas via faults (Fig. 6.3, Stage 4). A deeply penetrating topographic flow system must have been active during the Late Cretaceous/Tertiary due to the high topographic relief that was created by the Laramide orogeny. However, the big shale packages in the stratigraphic column most likely prevented this flow system from reaching the Devonian strata, as is also indicated by diagenetic and isotope data presented in this study. Hence, topography-driven flow probably did not reach down to the Devonian strata during that time (Fig. 6.3, Stage 4).

Stage 5 represents the time interval between maximum burial and the present, in which about 2000 m of the overlying sediments were eroded in the area of the SCCC. Except for small amounts of calcite cements, anhydrite cements seem to dominate this stage, because they are abundant in late stage fracture fills and are always postdating hydrocarbons. The continuous water-rock interactions led to the composition of the present-day formation waters, which have geochemical compositions distinctly different from the Devonian seawater. In addition, the brines in the deep part of the SCCC differ distinctly from brines in other parts of the Alberta Basin; they have higher oxygen ratios

and higher deuterium ratios, which is partly the result of TSR, the latter being one of two processes exclusively restricted to the deep part of the basin. One other observation from the fluid inclusion and DST-Geochemistry data is that some of the formation brines were slightly diluted adjacent to the disturbed belt, which may also indicate the introduction of less saline waters from the fold and thrust belt into the foreland basin. The present-day flow pattern in the Devonian show the updip displacement of a high-salinity brine (>200g/l) by a less saline brine (Fig. 6.4). However, flow is almost stagnant due to the combination of density differences between light and heavy brine and a weak flow-driving mechanism, which may be a remnant of tectonic expulsion and high topographic relief during the Laramide orogeny (Fig. 6.2, Stage 5).

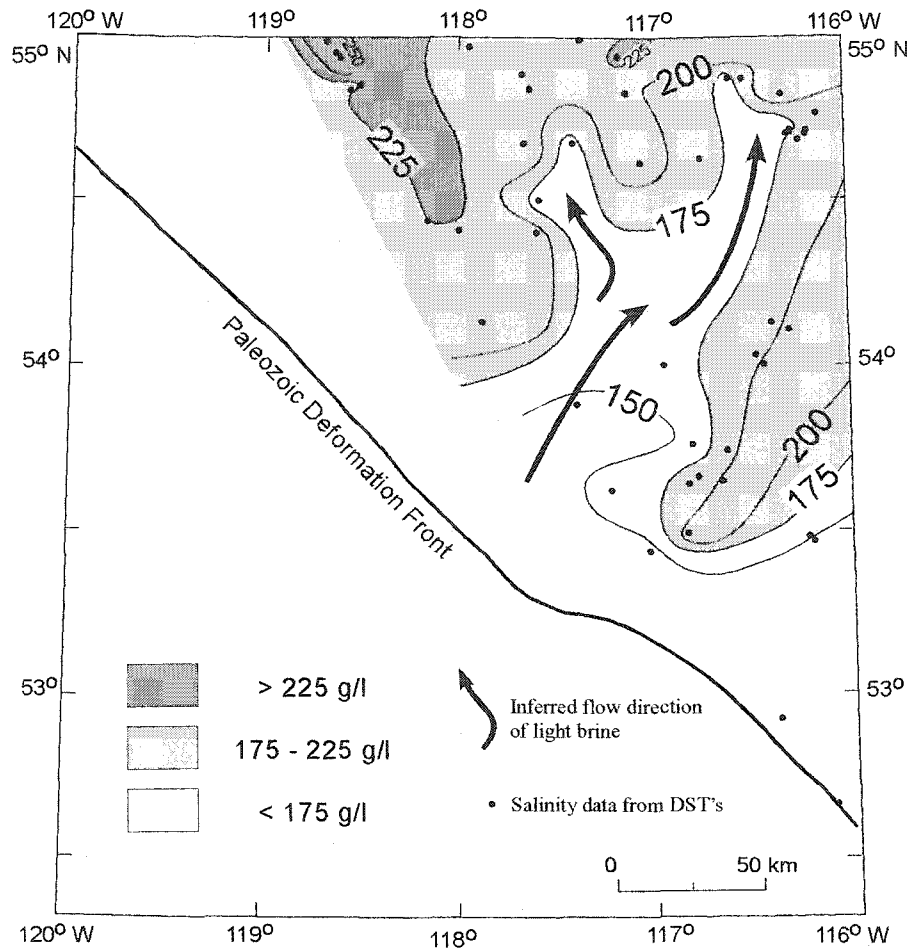


Figure 6.4: Present salinity distribution and inferred flow directions in the Winterburn aquifer within the study area (from Michael, 2002).

6.5 Fluid Flow in the Alberta Basin

Regional fluid flow in the southern Rocky Mountains and its foreland basin south of the Peace River Arch is characterized by major fluid events that correspond to some degree to the diagenetic stages and fluid events in the SCCC. (1) A basin-scale flow of dolomitizing fluids along Upper Devonian conduits during the Late Devonian/Early Mississippian as described by Anthor (1993) is equal to this studies Stage 2; the driving force was most likely a combination of compaction-driven flow and density-driven cellular flow. The flow intensity was controlled mainly by permeability; hence it had the highest fluxes where the permeability was highest. (2) A pre-Laramide (Antler/Columbian orogeny) west-to-east brine migration with mineralization, as discussed by Nesbitt and Muehlenbachs (1994,1995) could not be detected in the SCCC. (3) Laramide tectogenesis, including thrusting, with pulses of tectonic expulsion of fluids into the foreland basin (squeegee model) within thrust sheets (which may have been hydrodynamically relatively isolated from each other) and/or flow along relatively permeable thrust faults (Machel and Cavell, 1999; Green 1999). The flow was generally in a northeastward direction and the pathways were locally isolated. The brines carried a hydrothermal and/or metamorphic component. These flow patterns are equivalent to Stage 4. (4) Post-Laramide meteorically recharged deep convection in the disturbed belt that did/does not feed into the deep Devonian aquifers (Bachu, 1995; Nesbitt & Muehlenbachs, 1994,1995). In the SCCC, the present day formation brines are almost stagnant, however have a potential for updip flow (Bachu, 1995; Michael, 2002) equivalent to Stage 5.

6.6 Future Work

Future work on the Devonian carbonates of the SCCC should include a detailed mapping of the Berland shale unit within the Wild River Basin, which may lead to the potential discovery of new hydrocarbon accumulations, since the Berland shale might contain hydrocarbons in higher permeability areas.

Furthermore, high-resolution structural mapping for the location of faults, the offset along these faults, and the spatial distribution of late diagenetic products associated with these faults, is needed. A better understanding of the locations of faults will simplify the lingering debate (Mountjoy, et al. 1999; Machel and Cavell, 1999) about fault-controlled mineralization, which is supposed to be rather local versus the mineralization that is associated with the tectonic expulsion hypothesis by Oliver (1986), which is a regional scale process.

The analyses of formation waters in the deep part of the basin should be extended to include each aquifer in the study area to better understand the processes that lead to the present brine composition. The aquifers to be included are the Swan Hills Formation, the Leduc Formation, the Berland Shale Unit, the Nisku Formation, the Blueridge Member, and pools in the Wabamun Group. Potential-mixing relations within the water/carbonate systems can be tested using a plot of $^{87}\text{Sr}/^{86}\text{Sr}$ ratios vs. Sr-concentrations; the latter needs to be measured in future work. A more detailed fluid inclusion study, especially on the very small inclusions in the matrix dolomite, could provide further information on dolomitization processes, the timing of the processes and the origin of fluids, similar to

the approach taken by Yang et al. (1995) and Nesbitt et al. (in press). Also, fluid inclusions in anhydrite and other diagenetic products need to be analyzed to further constrain the origin and timing of mineralization. In addition, more work on hydrocarbon and gas-rich inclusions in the late stage cements could provide information on the history of hydrocarbon maturation and the thermal history of this part of the basin. The geochemical investigation on the rare sulfide minerals could provide information on the timing of fluid migration and mineralization using common age dating systems. In addition, trace element analyses could provide information about dolomite stoichiometry, equilibrium coefficients, fluid composition and flow directions, and therefore, would further enhance the understanding of the diagenetic processes in the study area.

7. REFERENCES

- Allan J.R. and Wiggins, W.D., 1993. Dolomite reservoirs – geochemical techniques for evaluating origin and distribution. AAPG Continuing Education Course Note Series No. 36, 129p.
- Amthor, J.E. and Friedman G.M., 1991. Early-to-late diagenetic dolomitization of platform carbonates; Lower Ordovician Ellenburger Group, Permian Basin, West Texas and southeastern New Mexico. AAPG Bulletin. 75; 3, Pages 534. 1991.
- Amthor, J.E., Mountjoy, E.W., and Machel, H.G., 1993. Subsurface dolomites in Upper Devonian Leduc Formation buildups, central part of Rimbey-Meadowbrook reef trend, Alberta, Canada. Bulletin of Canadian Petroleum Geology, v. 41, p. 164-185.
- Anderson, J.H., 1985. Depositional facies and carbonate diagenesis of the downslope reefs of the Nisku Formation (U. Devonian), central Alberta. Ph.D. thesis, Univ. of Texas, Austin, 393 pp.
- Anderson, J.H. and Machel, H.G., 1989. The Upper Devonian Nisku reef trend Alberta. In: Geldsetzer, H.H.J., James, N.P., and Tebbutt, G.E. (eds.), Reefs, Canada and adjacent area. Canadian Society Petroleum Geologists Memoir, No. 13, p. 391-398.
- Andrews, G.D., 1987. Devonian Leduc outcrop reef-edge models and their potential seismic expression. In: McMillan, N.M., Embry, A.F., and Glass, D.J. eds., Devonian of the World, Proc. 2nd International Symposium on the Devonian System: C.S.P.G. Memoir #14, II, p. 427-450.
- Andrichuk, J.M., 1958. Stratigraphy and facies analysis of Upper Devonian reefs in Leduc, Stettler, and Redwater areas, Alberta. AAPG Bulletin, v. 41, p. 1-93.
- Anfort, S.J., Bachu, S. and Bentley, R.L., 2001. Regional-scale hydrogeology of the Upper Devonian-Lower Cretaceous sedimentary succession, south-central Alberta basin, Canada. American Association of Petroleum Geologists Bulletin, v. 85, No.4, pp. 637-660
- Baadsgard, H., 1987. Rb-Sr and K-Ca isotope systematics in minerals from potassium horizons in the Prairie Evaporite Formation, Saskatchewan, Canada. Chemical

- Geology (isotope Geoscience Section), v.66, p. 1-15.
- Bachu, S., 1995. Synthesis and model of formation-water flow, Alberta Basin, Canada. American Association of Petroleum Geologists Bulletin, v. 79, p. 1159- 1178.
- Bachu, S., 1997. Flow of formation waters, aquifer characteristics, and their relation to hydrocarbon accumulations, northern Alberta Basin. American Association of Petroleum Geologists Bulletin, v. 81, No. 5, pp. 712-733.
- Bachu, S., 1999. Flow systems in the Alberta Basin: patterns, types and driving mechanisms. Bulletin Canadian Petroleum Geology, v. 47, p. 455-474.
- Bachu, S., Hitchon, B., and Mortensen, P., 1986. Preliminary Analysis of Transport Processes in the Basal Cambrian Aquifer of South-Central Alberta. ARC/NWWA, Proc. Third Canadian/American Conf. Hydrogeology, Banff, AB, Canada, June 22-26, 1986, 118-126.
- Bachu, S. and Underschultz, J.R., 1992. Regional-Scale Porosity and Permeability Variations, Peace River Arch, Alberta, Canada. American Association of Petroleum Geologists Bulletin, v. 76, No. 4, p. 547-562.
- Bachu, S. and Underschultz, J.R., 1993. Hydrogeology of Formation waters, Northeastern Alberta Basin. American Association of Petroleum Geologists Bulletin, v. 77, No. 10, p. 1745-1768.
- Bailey, N.J.L., Evans, C.R., and Milner, C.W.D., 1974. Applying Petroleum Geochemistry to Search for Oil; examples from Western Canada Basin. In: Advances in Petroleum Geochemistry. AAPG Bulletin. 58; 11, Part 1, Pages 2284-2294.
- Banner, J.L., 1995. Application of the trace element and isotope geochemistry of strontium to studies of carbonate diagenesis. Sedimentology, v.42, p.805-824.
- Barker, C., 1982. Organic geochemistry. American Association of Petroleum Geologists Education Short Course Note Series #10, 159 pp.
- Barnes, H.L., [ed.] 1979. Geochemistry of hydrothermal ore deposits. New York: Wiley-Interscience
- Bathurst, R.G.C., 1975. Carbonate sediments and their diagenesis. Developments in Sedimentology No. 12 (2nd enlarged edition), Elsevier, Amsterdam, 658 p.
- Bathurst, R.G.C., 1987. Diagenetically enhanced bedding in argillaceous platform

- limestones: stratified cementation and selective compaction. *Sedimentology*, v. 34, p. 749–778.
- Bathurst, R.G.C., 1991. Pressure-Dissolution and Limestone Bedding: the Influence of stratified cementation. In: Einsele, G., Ricken, W. & Seilacher, A. (eds.): *Cycles and events in Stratigraphy*. P. 450-463, Springer (Berlin).
- Bebout, D.G. and Maiklem, W.R., 1973. Ancient anhydrite facies and environments, Middle Devonian Elk Point basin, Alberta. *Bulletin of Canadian Petroleum Geology*, v. 21, p. 287-343.
- Belyea, 1954. Some reef-shale relationships on Wapiabi Creek, Alberta. *Alberta Soc. Petroleum Geologists News Bull.*, v.2, no.9, p.6.
- Belyea, H.R., 1964. Upper Devonian, Part II – Woodbend, Winterburn and Wabamun Groups. In: R.G. McCrossan and R.P. Glaister (eds.): *Geological history of western Canada*. Alberta Society of Petroleum Geologists, v. 77, p. 1745-1768.
- Belyea, H.R. and McLaren, D.J., 1956. Devonian sediments of the Bow Vally and adjacent areas. 6th Annual Filed Conference Guidebook, Alberta Society of Petroleum Geologists, p. 74-106.
- Belyea & McLaren, 1957. Upper Devonian nomenclature in southern Alberta. *Alberta Society of Petroleum Geologists*, v. 5, p. 166-182.
- Belyea, H.R. and McLaren, D.J., 1964. Devonian correlations near Sunwapta Pass, Banff National Park, Alberta. *Bulletin of Canadian Petroleum Geology*, v. 12, p. 779-807.
- Berner, R.A., 1970. Sedimentary pyrite formation. *Amer. Journ. Sci.*, 286, p. 1-23
- Berner, R.A., 1984. Sedimentary pyrite formation: An update. *Geochim. Cosmochim. Acta*, 48, p. 605-615.
- Braithwaite, C.J.R., and Rizzi, G., 1997. The geometry and petrogenesis of hydrothermal dolomites at Navan, Ireland. *Sedimentology*, 44, p. 421-440.
- Burke, W.H., Denison, R.E., Hetherington, E.A., Koepnick, R.B., Nelson, H.F., and Otto, J.B., 1982. Variations of seawater $^{87}\text{Sr}/^{86}\text{Sr}$ throughout Phanerozoic time. *Geology*, v. 10, 516-519.
- Buschkuehle, B. E. and Machel, H.G., 2002. Diagenesis and paleofluid flow in the Devonian Southesk-Cairn carbonate complex in Alberta, Canada. *Marine and*

- Petroleum Geology, 19, p. 219-227.
- Buschkuehle, B. E. and Machel, H.G., 2000. Diagenese und Paleoporenwasserfluss in tiefen devonischen Gasfeldern von Alberta, Canada. Zbl. Geol. Palaeont. Teil 1, Heft1/2, 15-32.
- Buschkuehle, B. E. and Machel, H.G., 2000a. Geochemical evolution of diagenetic fluids in a deep Devonian carbonate complex, west-central Alberta, Canada. Geocanada 2000, Abstracts, on CD only.
- Buschkuehle, B. E. and Machel, H.G., 2000b. Diagenesis of the Southesk Cairn carbonate complex with implications for paleo fluid flow- Upper Devonian, Western Canada Sedimentary Basin. 2000 AAPG Annual Convention, April 16-19, New Orleans, Official Program, v.9, p. A21.
- Buschkuehle, B.E., Cavell, P.A., Machel, H.G., and Skilliter, C.C., 1999. Indications for tectonically induced fluid flow into the Rocky Mountain Foreland basin with implications for petroleum exploration. CSPG Sedimentology Division, February 1999, CSPG Reservoir, vol.26-2, p.14-15.
- Buschkuehle, B.E., Machel, H.G. and Cavell, P.A., 1998a. Paleofluid flow within the Middle and Upper Devonian Southesk-Cairn carbonate complex, Rocky Mountain foreland basin, as determined from carbonate cements. CSPG/CSEG/CWLS Joint Annual Convention, Geo-Triad '98, Abstracts, p. 121-122.
- Buschkuehle, B.E., Machel, H.G. and Cavell, P.A., 1998b. Paleoporenwasserfluß in devonischen Karbonaten des Southesk-Cairn Karbonatkomplexes, Rocky Mountain Vorlandbecken, Alberta, Canada. Terra Nostra, Schriften der Alfred Wegener Stiftung, 98/3, p. V51.
- Butler, G.P., 1969. Modern evaporite deposition and geochemistry of coexisting brines, the sabkha, Trucial Coast, Arabian gulf. Journal of Sedimentary Petrology, v. 39, p. 70-89.
- Butler, G.P., 1970. Holocene gypsum and anhydrite of the Abu Dhabi sabkha, Trucial Coast: An alternative explanation of origin. Third Symposium on Salt, N. Ohio Geological Society, v. 1, p. 120-152.
- Butler, G.P., 1973. Modern evaporite deposition and geochemistry of coexisting brines,

- the sabkha, Trucial Coast, Arabian Gulf [with comment]. In: *Marine Evaporites; Origin, Diagenesis, and Geochemistry*. Pages 91-103.
- Buxton, T.M. & Sibley, D.F., (1981). Pressure solution features in shallow buried limestone. *J. Sedim. Petrol.*, 51, p. 19 – 26.
- Carpenter, S.J. and Lohmann, K.C., 1989. $\delta^{18}\text{O}$ and $\delta^{13}\text{C}$ variations in Late Devonian marine cements from the Golden Spike and Nevis reefs, Alberta Canada: *Journal of Sedimentary Petrology*, v. 59, p 792.
- Cavell, P.A. and Machel, H.G., 1997. Concentrations and isotopic compositions of strontium leached from Upper Devonian shales of the Alberta Basin - implications for regional paleofluid flow. *CSPG-SEPM Joint Convention*, June 1 - 6, Program with Abstracts, p. 57
- Chevron Standard Limited Exploration Staff, 1979. The geology, geophysics and significance of the Nisku reef discoveries, West Pembina area, Alberta, Canada. *Bulletin of Canadian Petroleum Geology*, v. 27, p. 326-359.
- Choquette, P.W., 1990. Microfabrics and pore-system development in "lime-mud" shelf dolomites; physical evidence from limestone-to-dolomite transitions. In: *Carbonate microfabrics symposium and workshop*. Drews-Sandy (editor), Pages 48.
- Choquette, P.W., and James, N.P., 1987. Diagenesis in limestones – 3. The deep burial environment. *Geoscience Canada*, v. 14, p. 3-35.
- Choquette, P.W., and James, N.P., 1990. Limestones – The burial diagenetic environment. In: McIlreath, I.A. and Morrow, D. W. (eds.), *Diagenesis*. *Geoscience Canada Reprint series*, 4, p. 75 to 111.
- Choquette, P.W. and Steinen, R. P., 1980. Mississippian non-supratidal dolomite, Ste. Genevieve Limestone, Illinois Basin: evidence for mixed-water dolomitization. In: Zenger, D.H., Dunham, J.B. and Ethington, R.L. (eds.), *Concepts and Models of Dolomitization - a symposium : Society of Economic paleontologists and Mineralogists*, Special Publication 28, p.163-196.
- Claypool G.E., Holser, W.T., Kaplan, I.R., Sakai, H., and Zak, I., 1980. The age curves of sulfur and oxygen isotopes in marine sulfate and their mutual interpretation. *Chemical Geology*, 28, p. 199-260.

- Cody and Hull, 1980. Experimental growth of primary anhydrite under sedimentological conditions. In: The Geological Society of America, 93rd annual meeting. Abstracts with Programs - Geological Society of America. 12; 7, Pages 404.
- Cody, J.D. and Hutcheon, I.E., 1994. Regional water and gas geochemistry of the Mannville Group and associated horizons, southern Alberta. *Bulletin of Canadian Petroleum Geology*, v.42,p. 449-464.
- Connolly, C.A., Walter, L.M., Baadsgaard, H., and Longstaffe, F.J., 1990a. Origin and evolution of formation waters, Alberta Basin, Western Canada Sedimentary Basin: I. Chemistry. *Applied Geochemistry*, v. 5, p. 375-395.
- Connolly, C.A., Walter, L.M., Baadsgaard, H., and Longstaffe, F.J., 1990b. Origin and evolution of formation waters, Alberta Basin, Western Canada Sedimentary Basin: II. Isotope Systematics and Water Mixing. *Applied Geochemistry*, v. 5, p. 397-413.
- Creaney, S. and Allen, J., 1990. Hydrocarbon generation and migration in the Western Canada Sedimentary Basin. In: Brooks, J. (ed), *Classic Petroleum Provinces*, Geological Society Special Publication No. 50, p. 189-202.
- Creaney, S. and Allen, J., 1992. Petroleum systems in the foreland basin of western Canada. In: R.W. Macqueen and D.A. Leckie (eds.): *Foreland basins and foldbelts*. AAPG Memoir 55, p. 279-308.
- Curiale, J.A., 1993. Occurrence and significance of metals in solid bitumens; an organic geochemical approach. In: *Bitumens in ore deposits*. Parnell-J (editor); Kucha-H (editor); Landais-P (editor); Special Publication of the Society for Geology Applied to Mineral Deposits. 9; Pages 461-474.
- Cutler, W.G., 1983. Stratigraphy and sedimentology of the Upper Devonian Grosmont Formation, Alberta, Canada. *Bulletin of Canadian Petroleum Geology*, v. 31, p. 282-325.
- Davies, D.W, Lowenstein, T.K., and Spencer, R.J., 1990. Melting behaviour of fluid inclusions in laboratory-grown halite crystals in the systems NaCl-H₂O, NaCl-KCl-H₂O, NaCl-MgCl₂-H₂O. *Geochim. Cosmochim. Acta*, 54, p.591-601.
- Dembicki, E.A. and Machel, H.G., 1996. Recognition and delineation of Paleokarst zones by the use of wireline logs in the bitumen-saturated Upper Devonian Grosmont

- Formation of northeastern Alberta, Canada. *American Association of Petroleum Geologists Bulletin*, v. 80, p. 695-712.
- Deming, D., Nunn, J.A., and Evans, D.G. 1990. Thermal effects of compaction-driven groundwater flow from overthrust belts. *Journal of Geophysical Research*, v. 95(B5), p. 6669-6683.
- Denison, R.E., Koepnick, R.B., Burke, W.H., Hetherington, E.A. & Fletcher, A., 1997. Construction of the Silurian and Devonian seawater $^{87}\text{Sr}/^{86}\text{Sr}$ curve. *Chemical Geology*, v.140, p.109-121.
- Dewit, R. and McLaren, D.J., 1950. Devonian sections in the Rocky Mountains between Crowsnest Pass and Jasper, Alberta.-*Geological Survey of Canada, Paper 50-23*
- Dix, G.R., 1993. Patterns of burial- and tectonically controlled dolomitization in an Upper Devonian fringing-reef complex: Leduc Formation, Peace River Arch area, Alberta, Canada. *Journal of Sedimentary Petrology*, v. 63, p. 628-640.
- Drivet, E., 1993. Diagenesis and reservoir characteristics of Upper Devonian Leduc dolostones, southern Rimbey-Meadowbrook reef trend, central Alberta. Unpublished M.Sc. Thesis, McGill University, Montreal, 112 p.
- Duggan, J.P., 1997. Sedimentology and diagenesis of Swan Hills Simonette oil field, west-central Alberta basin. Unpublished M.Sc. Thesis, McGill University, Montreal, 177 p.
- Duggan, J.P., Mountjoy, E.W., and Stasiuk, L.D. 2001. Fault-controlled dolomitization at Swan Hills Simonette oil field (Devonian), deep basin west-central Alberta, Canada. *Sedimentology*, 48: 301-323.
- Dunham, R. J., 1962. Classification of carbonate rocks according to depositional texture. In: *Classification of carbonate rocks*, Ham, W.E. (ed.), *Mem. Am. Ass. Petrol. Geol.*, 1, p. 108-121.
- Edwards, D.J., Lyatsky, H.V., and Brown, R.J., 1995. Basement fault control on Phanerozoic stratigraphy in the Western Canada sedimentary province; integration of potential-field and lithostratigraphic data. In: *Lithoprobe; Alberta basement transects*. Ross, G.M. (editor); *Lithoprobe Report*. Pages 181-244. 1995.
- Eliuk, L. S., 1989. Cripple Creek margin, North Fairholme reef complex, Frasnian age, Alberta. In: *Reefs, Canada and adjacent areas*, Geldsetzer, H.H.J, James, N.P. and C

- Tebbutt (eds.), Canadian Society of Petroleum Geologist, Memoir 13, p. 422-428
- Embry, A.F. and Klovan, J.E., 1971. A late Devonian reef tract on northeastern Banks Island, Northwest territories. *Bull. Can. Petrol. Geol.*, 19, p. 730-781.
- EUB, 1998. Alberta's reserves. Statistical series 99-18.
- Faure, G., 1982. The marine-strontium geochronometer. In: G.S. Odin (ed.): *Numerical dating in stratigraphy*, v. 1, p. 73-79
- Faure, G. and Powell, J.L. 1972. *Strontium isotope geology*. Springer Verlag, 188 pp.
- Fluegel, E., 1982. *Microfacies Analysis of Limestones*. Springer Verlag, 453 p.
- Garven, G. and Freeze, R.A., 1984a. Theoretical analysis of the role of groundwater flow in the genesis of stratabound ore deposits. 1. Mathematical and numerical model. *American Journal of Science*, v. 284, p. 1085-1124.
- Garven, G. and Freeze, R.A., 1984b. Theoretical analysis of the role of groundwater flow in the genesis of stratabound ore deposits. 2. Quantitative results. *American Journal of Science*, v. 284, p. 1125-1174.
- Garven G., 1995. Continental-scale groundwater flow and geologic processes. In: Wetherill, G.W., Albee, A.L., and Burke, K.C. (eds.), *Annual Review of Earth and Planetary Sciences*, 23, p.89-118.
- Goldhammer, R.K., 1997: Compaction and decompaction algorithms for sedimentary carbonates. *J. Sediment. Res.*, 67,1, p. 26-56.
- Goldstein, R.H. and Reynolds, T.J., 1994. Systematics of fluid inclusions in diagenetic minerals. *SEPM Short course* 31, 199 p.
- Green D.G., 1999. Dolomitization and deep burial of the Devonian of west-central Alberta deep basin: Kaybob South and Fox Creek (Swan Hills Formation) and Pine Creek fields (Leduc and Wabamun Formations). Unpub. Ph.D. thesis, McGill University, Montreal, 267 pp.
- Gregg, J.M., 1985. Regional epigenetic dolomitization in the Bonnetterre Dolomite (Cambrian), southeastern Missouri. *Geology*, v. 13, p. 503-506.
- Gregg, J.M. and Sibley, D.F., 1984. Epigenetic dolomitization and the origin of xenotopic dolomite texture. *Journal of Sedimentary Petrology*, v. 54, p.908-931.
- Haquebard, P., 1977. Rank of coals as an index of organic metamorphism for oil and gas in Alberta. In: *The origin and migration of petroleum in the Western Canada*

- Sedimentary Basin, Alberta. Geological Survey of Canada, Bulletin 262.
- Hanor, J.S., 1980. Dissolved methane in sedimentary brines: potential effect on the PVT properties of fluid inclusions. *Economic Geology*, v. 75, p. 603-609.
- Hardie, L.A., 1967. The gypsum-anhydrite equilibrium at one atmosphere pressure. *American Mineralogist*. 52; Pages 171-200. 1967. Mineralogical Society of America. Washington, DC, United States.
- Hearn, M.R. 1996. Stratigraphic and diagenetic controls on aquitard integrity and hydrocarbon entrapment, Bashaw reef complex, Alberta, Canada. Unpublished M.Sc. thesis, University of Alberta, 135 p.
- Hedinger, A. S. and Workum, R.H., 1989. Uppermost Frasnian reefs, Jasper Basin, Alberta. In: Reefs, Canada and adjacent areas, Geldsetzer, H.H.J, James, N.P. and G.E. Tebutt (eds.), *Canadian Society of Petroleum Geologist, Memoir 13*, p. 466-470.
- Hitchon, B., 1969a. Fluid flow in the Western Canadian Sedimentary Basin: 1. Effect of Topography. *Water Resources Research*, v. 5(1/2), p. 187-195.
- Hitchon B., 1969b. Fluid flow in the Western Canadian Sedimentary Basin 2: Effect of geology. *Water Resources Research*, v. 5, p. 460-469.
- Hitchon, B., 1984. Geothermal gradients, hydrodynamics, and hydrocarbon occurrences, Alberta, Canada. *AAPG Bulletin*, v. 68, p. 713-743.
- Hitchon, B. and Friedman, I., 1969. Geochemistry and origin of formation waters in the Western Canada Sedimentary Basin. I. Stable isotopes of hydrogen and oxygen. *Geochimica et Cosmochimica Acta*, v. 33, p. 1321-1349.
- Hitchon, B., S. Bachu, and Underschultz, J.R., 1990. Regional subsurface hydrogeology, Peace River Arch Area, Alberta and British Columbia. *Bulletin of Canadian Petroleum Geology*, v. 38A, 196-217.
- Hill et al., 1996 see Stasiuk 1997
- Holser, W.T., Kaplan, I.R., Sakai, H., and Zak, I., 1979. Isotope geochemistry of oxygen in the sedimentary sulfate cycle. *Chemical Geology*, 25, p. 1 - 17.
- Hudson, J.D. and Anderson, T.F., 1989. Ocean temperatures and isotopic compositions through time. In: *Environments and physiology of fossil organisms*. Clarkson E.N.K.; Curry, G.B. [eds.] *Transactions of the Royal Society of Edinburgh: Earth*

- Sciences. 80; 3-4, Pages 183-192.
- Huebscher, H., 1996. Regional controls on the stratigraphic and diagenetic evolution of Woodbend Group carbonates, north-central Alberta, Canada. Unpublished Ph.D. thesis, University of Alberta, Edmonton, 231 p.
- Huebscher, H. and Machel, H.G., 1997a. Paleokarst in the Grosmont Formation, northeastern Alberta. In: Wood, J. and Martindale, B. (compilers), CSPG-SEPM Joint Convention, Core Conference, p. 129-151.
- Hurley N.F. and Lohmann, K.C., 1989. Diagenesis of Devonian reefal carbonates in the Oscar Range, Canning Basin, Western Australia. *Journal of Sedimentary Petrology*. 59; 1, Pages 127-146.
- Hutcheon, I.E, Krouse, H.R. and Abercrombie, H, 1995. Geochemical transformations of sedimentary sulfur: controls of the origin and distribution of elemental sulfur, H₂S and CO₂ in Paleozoic reservoirs of western Canada. In: Vairavamurthy, M.A., Schoenen, M.A.A. [eds.], *Geochemical Transformations of Sedimentary Sulfur*. ACS Symposium Series, vol. 612, pp. 426-438.
- Hutcheon, I. E., 2000. Principles of diagenesis and what drives mineral change; chemical diagenesis. In: *Fluids and basin evolution*. Kyser, K. (editor); Short Course Handbook. 28; Pages 93-114. Mineralogical Association of Canada.
- Hutcheon, I. E., Cody, J., and Yang, C., 2000. Fluid flow in the Western Canada Sedimentary Basin; a biased perspective based on geochemistry. In: *Fluids and basin evolution*. Kyser, K. (editor); Short Course Handbook. 28; Pages 197-210. 2000.
- Illing, L.V., 1959. Deposition and diagenesis of Upper Paleozoic carbonate sediments in Western Canada. 5th World Petroleum Congress, New York, Proceedings Section 1, p. 23-52.
- Imperial Oil Ltd., Geological Staff, 1950. Devonian nomenclature in the Edmonton area. *AAPG Bulletin*, v. 34, p. 1807-1825.
- Irwin, H., Curtis, M.L., and Coleman, C., 1977. Isotopic evidence for the source of diagenetic carbonate during burial of organic-rich sediments: *Nature*, Vol. 269, p. 209-213.
- James, N.P., 1984. Reefs. In: *Facies Models*, Walker, R.G. (ed), Geoscience Canada, p.

229-244.

- James, N.P. and Choquette, P.W., 1990. Limestones – the sea-floor diagenetic environment. In: I.A. McIlreath and D.W. Morrow (eds.): Diagenesis. Geological Association of Canada, Geoscience Series, v. 10, No. 4, p. 13-34.
- Kalkreuth, W. and McMechan, M., 1988. Burial history and thermal maturity, Rocky Mountain Front Ranges, foothills, and foreland, British Columbia and adjacent Alberta, Canada. AAPG Bulletin, v. 72, p. 1395-1410.
- Kaufman, J., 1989. Sedimentology and diagenesis of the Swan Hills Formation (Middle-Upper Devonian), Rosevear Field, Alberta, Canada. Unpublished Ph.D. thesis, State University of New York at Stony Brook. 412 p.
- Kaufman, J., Meyers, W.J., and Hanson, G.N., 1990. Burial cementation in the Swan Hills Formation (Devonian), Rosevear Field, Alberta, Canada: Journal Sedimentary Petrology, v. 60, p. 918-939.
- Kendall, A.C. & Tucker, M. E., 1973. Radial fibrous calcite: a replacement after acicular carbonate. Sedimentology, v. 20, p.365-389.
- Kendall, A.C., 1985. Radial fibrous calcite: A reappraisal. In: Carbonate Cements. Schneidermann, N. & Harris, P.M. (eds.), Society of Economic Paleontologists and Mineralogists, Spec. Publ. No. 36, p. 59 – 77.
- Klovan, J.E., 1964. Facies analysis of the Redwater reef complex, Alberta, Canada. Bulletin of Canadian Petroleum Geology, v. 12, p.171-189.
- Knauth, L.P. and Beeunas, M.A., 1986. Isotope geochemistry of fluid inclusions in Permian halite with implications for the isotopic history of ocean water and the origin of saline formation waters. Geochimica et Cosmochimica Acta. 50; 3, Pages 419-433.
- Krebs, W., 1972. Facies and development of the Meggen Reef (Devonian, West Germany). Geol. Rundsch., 61, 647-671.
- Krouse, H.R., 1977. Sulfur isotope studies and their role in petroleum exploration. J. Geochem. Explor. 7, 189-211.
- Krouse, H.R., Viau, C.A., Eliuk, L.S, Ueda, A.; and Halas, S., 1988. Chemical and isotopic evidence of thermochemical sulphate reduction by light hydrocarbon gases in deep carbonate reservoirs. Nature (London). 333; 6172, Pages 415-419.

- Land, L.S., 1980. The isotopic and trace element geochemistry of dolomite: The state of the art. In: D.H. Zenger, J.B. Dunham and R.G. Ethington (eds.): Concepts and models of dolomitization. Soc. Econ. Paleont. Miner., Special Publication 28, p. 87-110.
- Land, L.S., 1983. The application of stable isotopes to the studies of the origin of dolomite and to problems of diagenesis of clastic sediments. In: M.A. Arthur (ed.): Stable isotopes in Sedimentary Geology. Soc. Econ. Paleont. Miner. Short Course 10, p. 4.1-4.22.
- Land, L.S., 1985. The origin of massive dolostone. *Journal of Geological Education*, v. 33, p. 112-125.
- Land, L.S., 1997. Mass transfer during burial diagenesis in the Gulf of Mexico sedimentary basin; an overview. In: Basin-wide diagenetic patterns; integrated petrologic, geochemical, and hydrologic considerations. Montanez, I.P., Gregg, J.M., Shelton, K.L. [eds.], Special Publication - SEPM (Society for Sedimentary Geology). 57; Pages 29-39.
- Lind, I.L., 1993. Stylolites in chalk from Leg 130, Ontong Java Plateau. In: W.H. Berger, J.W. Kroenke, and L.A. Mayer (eds.): Proceedings of the Ocean Drilling Program, Scientific Results, v. 130, p. 445-451.
- Lloyd, R.M., 1966. Oxygen isotope enrichment of sea water by evaporation. *Geochimica et Cosmochimica Acta*. 30; 8, Pages 801-814.
- Logan, B.W. and Semeniuk, V., 1976. Dynamic metamorphism; processes and products in Devonian carbonate rocks, Canning Basin, Western Australia. *Spec. Publ. Geol. Soc. Austr.*, v.16, p.1-138.
- Lohmann, K.C., 1988. Application of carbon and oxygen isotopic techniques for unraveling the diagenetic history of carbonate sequences: in Allan, J.R. and Harris, P.M., eds., *Stable Isotope, Trace Element, and Fluid Inclusion Workshop*, Chevron Oil Field Research Co., unpublished report, p. 1-49.
- Longman, M.W., 1980. Carbonate diagenetic textures from nearshore diagenetic environments. *AAPG Bulletin*, v. 64, p. 461-487.
- Longstaffe, F.J., 1989. Stable isotopes as tracers in clastic diagenesis. In: Hutcheon I.E. (ed.), *Short course in burial diagenesis*. Min. Ass. Of Canada, p.201-277.

- Lowenstein, T.K., and Spencer, R.J., 1990. Syndepositional origin of potash evaporites; petrographic and fluid inclusion evidence. *American Journal of Science*. 290; 1, Pages 1-42. 1990.
- Lucia, F.J., 1999. Carbonate reservoir characterization. Springer Verlag, Berlin, Heidelberg, 226 p.
- Luo, P. and Machel, H.G., 1995. Pore size and pore-throat types in a heterogeneous dolostone reservoir, Devonian Grosmont Formation, Western Canada Sedimentary Basin. *American Association of Petroleum Geologists Bulletin*, v. 79, p. 1698-1720.
- Machel, H.G., 1984. Facies and dolomitization of the Upper Devonian Nisku Formation in the Brazeau, Pembina and Bigoray areas, Alberta, Canada. In: Carbonates in subsurface and outcrop, a core workshop. Canadian Society of Petroleum Geologists, p. 191-224.
- Machel H.G., 1985. Facies and diagenesis of the Upper Devonian Nisku Formation in the subsurface of central Alberta. Unpublished Ph.D. thesis, McGill University Montreal, 392 p..
- Machel, H.G, 1987a. Some aspects of diagenetic sulphate-hydrocarbon redox reactions. In: Marshall, J.D. (ed.), *The diagenesis of sedimentary sequences*. G.S.A. Spec. Publ. No. 36, p. 15-28.
- Machel, H.G, 1987b. Saddle dolomite as a by-product of chemical compaction and thermo-chemical sulfate reduction. *Geology*, v. 15, p. 936-940.
- Machel, H.G., 1990. Burial, porosity and permeability development in carbonates. In: Bloy, G.R. and Hadley, M.G. (eds.), *The development of porosity in carbonate reservoirs*. Canadian Society Petroleum Geologists Short Course Notes, p. 2-1 - 2-18.
- Machel, H.G., 1992. Anomalous magnetization as indicator for hydrocarbon seepage; with application to hydrocarbon exploration. *CSPG Reservoir*. 19; 10, Pages 2. 1992. Canadian Society of Petroleum Geologists. Calgary, AB, Canada.
- Machel, H.G., 1997. Recrystallization versus neomorphism, and the concept of 'significant recrystallization' in dolomite research. *Sedimentary Geology*, v. 113, p. 161-168.

- Machel, H.G. (1998): Comment on "The Effects of Thermochemical Sulfate Reduction upon Formation Water Salinity and Oxygen Isotopes in Carbonate Reservoirs" by R.H. Worden, P.C. Smalley, and N.H. Oxtoby. *Geochimica and Cosmochimica Acta*, v. 62(2), 337-341.
- Machel, H.G., 1998. Indications for tectonically induced fluid flow into the Rocky Mountain foreland basin - with implications for petroleum exploration. *Reservoir*, May 1998, p. 7.
- Machel, H.G., 1999. Effects of groundwater flow on mineral diagenesis, with emphasis on carbonate aquifers. *Hydrogeology Journal*, v. 7, p. 94-107.
- Machel, H.G., 2000. The Devonian petroleum system of the Western Canada Sedimentary Basin. *Marine Origin Petroleum Geology*, in press.
- Machel, H.G., Krouse, H.R., and Sassen, R., 1995. Products and distinguishing criteria of dolomitization - a reappraisal: *Earth Science Reviews*, 23: 175-222.
- Machel, H.G. and Mountjoy, E.W. (1986): Chemistry and environments of dolomitization - a reappraisal: *Earth Science Reviews*, 23: 175-222.
- Machel, H.G. and Burton, E.A., 1991. Burial-diagenetic sabkha-like gypsum and anhydrite nodules. *J. Sedim. Petrol.*, 61, 394-405.
- Machel, H.G., Mountjoy, E.W., and Amthor, J.E., 1994. Dolomitisierung von devonischen Riff- und Plattformkarbonaten in West-Kanada. *Zentralblatt für Geologie und Paläontologie*, Teil I, 1993 (7/8), p. 941-957.
- Machel, H.G. and Huebscher, H., 2001. The Devonian Grosmont heavy oil reservoir in Alberta, Canada. *Zentralblatt Geologie und Paläontologie*, Teil 1, vol. 1/2 p. 55-84.
- Machel, H.G. and Hunter, I.G., 1994. Facies models for Middle to Late Devonian shallow - marine carbonates, with comparisons to modern reefs: *A guide for facies analysis: Facies*, v.30, p.155-176
- Machel, H.G., Cavell, P.A., and Patey, K.S., 1995a. Carbonate cementation and recrystallization during tectonic expulsion of fluids into the Western Canada Sedimentary Basin. 10th Bathurst Meeting of Carbonate Sedimentologists, London, 2-5 July, Abstract Volume for Talks and Posters, p.37.
- Machel, H.G., Cavell, P.A., and Patey, K.S., 1995b. Carbonate diagenesis during tectonic expulsion of fluids into the Western Canada Sedimentary Basin. In Ross, G.M.

- (ed.), 1995 Alberta Basement Transects Workshop, Lithoprobe Report # 47, p. 254-263.
- Machel, H.G., Cavell, P.A. and Patey, K.S., 1996. Isotopic evidence for carbonate cementation and recrystallization, and for tectonic expulsion of fluids into the Western Canada Sedimentary Basin. *Geological Society of America Bulletin*, 108, p. 1108-1119.
- Machel, H.G., Cavell, P.A., and Buschkuehle, B.E., 1998. Hinweise auf tektonisch induzierten Fluß von Formationswässern in das Rocky Mountain Vorlandbecken aufgrund der Gehalte an stabilen und Sr-isotopen. *Terra Nostra*, Schriften der Alfred Wegener Stiftung, 98/3, p. V215-V216.
- Machel, H.G., and Cavell, P.A., 1999. Low-Flux, Tectonically Induced Squeegee Fluid Flow ("Hot Flash") into the Rocky Mountain Foreland Basin. *Bulletin of Canadian Petroleum Geology*, v. 47, p. 510-533.
- Machel, H.G., Cavell, P.A., Buschkuehle, B.E., and Michael, K., 2000. Tectonically induced fluid flow in Devonian carbonate aquifers of the Western Canada Sedimentary Basin. *Journal of Geochemical Exploration*, 69-70, p. 213-217.
- Machel, H.G., Buschkuehle, B.E. and Michael, K., 2001. Squeegee flow in Devonian carbonate aquifers in Alberta, Canada. In: Cidu, R. (ed.), *Water-Rock Interaction*, Vol. 1. Proceedings of the Tenth International Symposium on Water-Rock-Interaction WRI-10, Villasimius, Italy, p. 631- 634.
- Machel, H.G. and Lonnee, J., 2002. Hydrothermal dolomite - a product of poor definition and imagination. *Sedimentary Geology*, 152, p. 163-171.
- Machel, H.G., Mountjoy, E.W., Jones, G.D. and Rostron, B.J., 2002. Toward a sequence stratigraphic framework for the Frasnian of the Western Canada Basin – Discussion. *Bulletin of Canadian Petroleum Geology*, vol. 50, no.2, p. 332-338.
- Mackenzie, W.S., 1965. Upper Devonian stratigraphy, northwest margin of the Southesk Reef, eastern Rocky Mountains, Alberta.- *Geological Survey of Canada*, Paper 64-19
- Mackenzie, W.S., 1969. Stratigraphy of the Devonian Southesk Cairn carbonate complex and associated strata , eastern Jasper National Park, Alberta.- *Geological Survey of Canada*, Bulletin 184.

- McKenzie, M.C., 1999. Carbonates of the Upper Devonian Leduc Formation, southwestern Peace River Arch, Alberta: Indications for tectonically induced fluid flow. Unpublished M.Sc. thesis, University of Alberta, Edmonton, 131 p.
- Marquez, X., 1994. Reservoir geology of Upper Devonian Leduc buildups, deep Alberta Basin. Unpublished Ph.D. thesis, McGill University, Montreal, 285p.
- Marquez, X. and Mountjoy, E.W., 1996. Origin of microfractures in the Upper Devonian Leduc Strachan reservoir, deep Alberta Basin. *American Association of Petroleum Geologist, Bulletin*, v.80, p. 570-588
- Mattes, D.H. and Mountjoy, E.W., 1980. Burial dolomitization of the Upper Devonian Miette buildup, Jasper National Park, Alberta. In: D.H. Zenger, J.B. Dunham and R.L. Ethington (eds.): *Concepts and Models of Dolomitization*. Spec. Publ. Soc. Econ. Paleont. Miner., v. 28, p. 259-297.
- Mazzullo, S.J., and Harris, P.M., 1992. Mesogenetic dissolution; its role in porosity development in carbonate reservoirs. *AAPG Bulletin*. 76; 5, Pages 607-620. 1992. American Association of Petroleum Geologists. Tulsa, OK, United States.
- McCrea, J.M., 1950. On the isotopic chemistry of carbonates and a paleothermometer scale. *Journal of Chemical physics*, v. 5, p. 48-51.
- McGillivray, J.G. and Mountjoy, E.W., 1975. Facies and related reservoir characteristics, Golden Spike reef complex, Alberta. *Bulletin of Canadian Petroleum Geology*, v. 23, p. 753-809.
- McLaren, D.J., 1953. Reef development in the Devonian of the Canadian Rocky Mountains. *Bulletin of the Canadian Institute of Mining and Metallurgy*, v. 46, p. 706-710.
- McLaren, D.J., 1956. Devonian formations in the Alberta Rocky Mountains between the Bow and Athabasca Rivers. *Geological Survey of Canada, Bulletin* 35, 59p.
- McLaren, D.J. and Mountjoy, E.W., 1962. Alexo equivalents in the Jasper area. *Geological Survey of Canada, Paper* 62-63, 36p.
- McLimans, R.K., 1987. The application of fluid inclusions to migration of oil and diagenesis in petroleum reservoirs. *Applied Geochemistry*, v. 2, p. 585-603.
- McNamara, L.B. and Wardlaw, N.C., 1991. Geological and statistical description of the Westerosé reservoir, Alberta. *Bulletin of Canadian Petroleum Geology*, v. 39, p.

332-351.

- Michael, K., 2002. Flow of formation water in the Alberta Basin adjacent to the Rocky Mountains thrust and fold belt, west-central Alberta, Canada. Unpubl. Ph.D. Thesis, University of Alberta, 332 p.
- Michael, K., Bachu, S., & Machel, H.G., 2000. Flow of variable-density brines in deep Devonian aquifers, West-Central Alberta. Geocanada 2000, Calgary Canada, May 29 – June 2, 2000, extended abstract # 339, publ. on CD-ROM.
- Moore, P.F., 1989. The Lower Kaskaskia Sequence - Devonian. In: Western Canada Sedimentary Basin, A case History; B.D. Ricketts (ed.), Canadian Society of Petroleum Geologists, p. 139-164.
- Morris, G.A. and Nesbitt, B.E., 1998. Geology and timing of paleohydrogeological events in the MacKenzie Mountains, Northwest Territories, Canada. In: Parnell, J. (ed.), Dating and duration of fluid flow and fluid-rock interaction. Geological Society, London, Special Publication 144, p. 161-172.
- Morrow, D.W., Potter, J., Richards, B., and Goodarzi, F., 1993. Paleozoic burial and organic maturation in the Liard Basin region, northern Canada. Bulletin of Canadian Petroleum Geology, v. 41, p. 17-31.
- Morrow, D.W. and Aulstead, K.L., 1995. The Manetoe dolomite: A Cretaceous-Tertiary or a Paleozoic event? Fluid inclusion and isotopic evidence. Bulletin of Canadian Petroleum Geology, v.43, p. 267-280.
- Morrow, D.W., 1998. Regional subsurface dolomitization: models and constraints. Geoscience Canada, v. 25, p. 57-70.
- Mossop, G. and Shetsen, I., 1994. Geological Atlas of the Western Canada Sedimentary Basin, 510p.
- Mountjoy, E.W., 1960. Structure and stratigraphy of the Miette and adjacent areas, eastern Jasper Nationalpark, Alberta. [Ph.D. dissert.]: Toronto, Canada, University of Toronto, 249 p.
- Mountjoy E.W., 1965. Stratigraphy of the Devonian Miette reef complex and associated strata, eastern Jasper National Park, Alberta. Geological Survey of Canada, Bulletin 110, 132 p.
- Mountjoy, E.W., 1967. Factors governing the development of the Frasnian Miette and

- Ancient Wall reef complexes (banks or biostromes), Alberta. In: International Symposium on the Devonian System. Alberta Society of Petroleum Geologists, v.2, p. 387-408.
- Mountjoy, E.W., 1978. Upper Devonian reef trends and configuration of the western portion of the Alberta Basin. In: I.A. McIlreath and P.C. Jackson (eds.): The Fairholme Carbonate Complex. Canadian Society of Petroleum Geologists guidebook, p. 1-30.
- Mountjoy, E.W., 1980. Some questions about the development of Upper Devonian carbonate build-ups (reefs), Western Canada.- Bulletin of Canadian Petroleum Geology, v.28, p.315-344.
- Mountjoy, E.W. 1987. The Upper Devonian Ancient Wall reef complex, Jasper National Park. Canadian Society of Petroleum Geologists Fieldtrip Guidebook, Excursion A5, 50 p..
- Mountjoy, E.W., Qing, H., and McNutt, R.H., 1992. Strontium isotopic composition of Devonian dolomites, Western Canada sedimentary basin; significance of sources of dolomitizing fluids. Applied Geochemistry. 7; 1, Pages 59-75. 1992. Pergamon. Oxford-New York-Beijing, International.
- Mountjoy, E.W., Green, D.G., Duggan, J. and Smith, S., 1997. Burial fluids and heat flow regimes in the deep Alberta Basin; new C, O and Sr isotope and fluid inclusion evidence from late cements. In: Lithoprobe; Alberta basement transects. Ross, G.M. (compiler) Lithoprobe Report. 59; Pages 183.
- Mountjoy E.W., Machel, H.G., Green, D., Duggan, J. and A.E. Williams-Jones, 1999. Devonian matrix dolomites and deep burial carbonate cements: A comparison between the Rimbey-Meadowbrook reef trend and the deep basin of west-central Alberta. Bulletin of Canadian Petroleum Geology, vol, 42, No.4, p.487-509
- Mountjoy, E.W. and Amthor, J.E., 1994. Has burial dolomitization come of age? Some answers from the Western Canada Sedimentary Basin. International Association of Sedimentology, Special Publication No. 21, p. 203-229.
- Mountjoy E.W, and Geldsetzer, H.H.J., 1981. Devonian stratigraphy and sedimentation, Southern Rocky Mountains. In: Field guides to geology and mineral deposits; Calgary '81 annual meeting. Thompson, R.I., and Cook, D.G. [eds.], Pages 195-

224. Geol. Assoc. Can., Canada.
- Nesbitt, B.E. and Muehlenbachs, K., 1994. Paleohydrogeology of the Canadian Rockies and origins of brines, Pb-Zn deposits and dolomitization in the Western Canada Sedimentary Basin. *Geology*, 22: 243-246.
- Nesbitt, B.E. and Muehlenbachs, K., 1994. Paleohydrogeology of the Canadian Rockies and origins of brines, Pb-Zn deposits and dolomitization in the Western Canada Sedimentary Basin: Comment and Reply. *Geology*, 22: 1149-1151.
- Nesbitt, B.E. and Muehlenbachs, K., 1995. Geochemistry of syntectonic, crustal fluid regimes along the Lithoprobe Southern Canadian Cordillera Transect. *Canadian Journal of Earth Sciences*, 32: 1699-1718.
- Nurkowski, J.R., 1984. Coal Quality, Coal Rank Variation and Its Relation to Reconstructed Overburden, Upper Cretaceous and Tertiary Plains Coals, Alberta, Canada. *AAPG Bulletin*, v. 86, p. 285-295.
- Oldale, H.S., and Munday, R.J., 1994. Devonian Beaverhill Lake Group of the Western Canada Sedimentary Basin. In: G.D. Mossop and I. Shetsen (comps.): *Geological Atlas of the Western Canada Sedimentary Basin*. Can. Soc. Petr. Geol. and Alberta Research Council, p. 149-163.
- Oliver, J., 1986. Fluids expelled tectonically from orogenic belts: their role in hydrocarbon migration and other geologic phenomena. *Geology*, v. 14, p. 99-102. *Geology*, v. 38A, p. 25-35.
- O'Neil, J.R., Clayton, R.N. and Mayeda, T.K., 1969. Oxygen isotope fractionation in divalent metal carbonates. *J. Chem Phys* 51, p. 5547-5558.
- Orr, W., 1977. Geologic and geochemical controls on the Distribution of hydrogen sulfide in natural gas. In: R. Campos and I Goni (eds.): *Advances in organic geochemistry*, p. 572-597.
- Patey, K.S., 1995. Upper Devonian carbonates in the Obed area. Unpub. M.Sc. thesis, University of Alberta, Edmonton, Alberta. 147p.
- Potma, K., Weissenberger, J.A.W., Wong, P.K., and Gilhooly, M.G., 2001. Toward a sequence stratigraphic framework for the Frasnian of the Western Canada Basin. *Bulletin Canadian Petroleum Geology*, 49, p. 37-85.
- Price, R.A., 1964. The Devonian Fairholme-Sassenach succession and evolution of reef-

- front geometry in the Flathead-Crowsnest Pass area, Alberta and British Columbia. *Bulletin of Canadian Petroleum Geology*. 12; p. 427-451.
- Price, R.A., 1994. Cordilleran tectonics and the evolution of the Western Canada Sedimentary Basin. In: *Geologic Atlas of the Western Canada Sedimentary Basin*; G.D. Mossop & I. Shetsen (comps.), Canadian Society of Petroleum Geologists and Alberta Research Council, p. 13-24.
- Qing, H., 1991. Diagenesis of Middle Devonian Presqu'ile dolomite, Pine Point NWT and adjacent subsurface. Unpublished Ph.D. thesis, McGill University, Montreal, 287p.
- Qing, H., and Mountjoy, E.W., 1992. Large-scale fluid flow in the Middle Devonian Presqu'ile barrier, Western Canada Sedimentary Basin. *Geology*, v. 20, p. 903-906.
- Qing, H., and Mountjoy, E.W., 1994. Formation of coarsely crystalline, hydrothermal dolomite reservoirs in the Presqu'ile Barrier, Western Canada Sedimentary Basin. *American Association Petroleum Geologists Bulletin*, v. 78, p. 55-77.
- Radke, B.H. and Mathis, R.L., 1980. On the formation and occurrence of saddle dolomite. *Journal of Sedimentary Petrology*, v. 50, p. 1149-1168.
- Raymond, P.E., 1930. The Paleozoic formations in Jasper Park, Alberta. *American Journal of Science*. 20; Pages 289-300. 1930.
- Riciputi, L.R., Cole, D.R., and Machel, H.G., 1996. Sulfide formation in reservoir carbonates of the Devonian Nisku Formation, Alberta, Canada: An ino microprobe study. *Geochimica et Cosmochimica Acta*, vol. 60, No.2, pp. 325-336.
- Rickard, D.T., Willden, M.Y., Marinder, N.E. and Donnelly, T.H., 1979. Studies on the genesis of the Laiswell sandstone lead-zinc deposit, Sweden. *Economic Geology*, v.74, p. 1255-1285.
- Rock, L., 1999. Sedimentology, diagenesis and reservoir characteristics of the Devonian Simonette (Leduc Formation) and Ante Creek (Swan Hills Formation) fields: a comparison between a limestone and dolomite field, west-central Alberta. Unpublished M.Sc. Thesis, McGill University, Montreal, 168 p.
- Roedder, E., 1981. Origin of fluid inclusions and changes that occur after trapping. In:

- L.S. Hollister and M.L. Crawford (eds.): Mineralogical Association of Canada Short Course in Fluid Inclusions: Applications to Petrology, v. 6, p. 101-137.
- Ross, R.M., 1990. Deep crust and basement structure of the Peace River Arch region: constraints on mechanisms and formation. *Bulletin of Canadian Petroleum Geology*, v. 38A, p. 25-35.
- Rostron, B.J., and Tóth, J., 1997. Cross-Formational Fluid Flow and the Generation of a Saline Plume of Formation Waters in the Mannville Group, West-Central Alberta. In: S.G. Pemberton and, D.P. James (eds): *Petroleum Geology of the Cretaceous Mannville Group, Western Canada*. CSPG Memoir 18, Calgary, AB, p. 169-190.
- Rostron, B.J., Toth, J. and Machel, H.G., 1997. Fluid Flow, hydrochemistry, and petroleum entrapment in Devonian reef complexes, south-central Alberta, Canada. In: *Basin-wide diagenetic patterns: Integrated Petrologic, Geochemical, and hydrologic considerations*. I.P. Montanez, J.M. Gregg and K.L. Shelton (eds.). Society of Economic Paleontologists and Mineralogists, Special Publication, no. 57, p. 139-155
- Shields, M.J. and Brady, P.V., 1995. Mass Balance and fluid flow constraints on regional-scale dolomitization, Late Devonian, Western Canada Sedimentary Basin. *Bulletin of Canadian Petroleum Geology*, v. 43, p. 371-392.
- Schmoker, J.W. and Halley, R.B., 1982. Carbonate porosity versus depth – a predictable relation for south Florida. *AAPG Bulletin*, v. 66, p. 2561-2570.
- Schroeder, J.H., 1972. Fabrics and Sequences of submarine carbonate cements in Holocene Bermuda cup reefs: *geol. Rundschau*, v. 61, p. 708 – 730.
- Schroyen, K. and Muechez, P., 2000. Evolution of metamorphic fluids at the Variscan fold-and-thrust belt in eastern Belgium. In: P. Muechez and T. Bechstaedt (eds.): *Paleofluid flow and diagenesis during basin evolution*. *Sedimentary Geology*, v. 131, no. 3-4, p. 163-180.
- Sharma, T. and Clayton, R.N., 1964. Measurement of O¹⁸/O¹⁶ ratios of total oxygen of carbonates. *Geochimica et Cosmochimica Acta*, v. 29, p. 1347-1353.
- Sibley, D.F. and Gregg, J.M., 1987. Classification of dolomite rock texture. *J.sediment. Petrol.* 57, 967-975.
- Skilliter, C.C., 1999. Stratigraphic and Geochemical Investigation of Middle to Upper

- Devonian "aquitards" in west-central Alberta, Canada. Abstract in AAPG Bulletin, in press.
- Smalley, P.C., Higgins, A.C., Howarth, R.J., Nicholson, H., Jones, C.E., Swinburne, N.H.M., and Bessa, J., 1994. Seawater Sr isotope variations through time: A procedure for constructing a reference curve to date and correlate marine sedimentary rocks. *Geology*, 22, p. 431-434.
- Smith, S.G.W., 2001. The origin and timing of late-stage carbonate cements in Devonian carbonates of the deep Alberta basin: based on fluid inclusion and isotopic evidence. Unpublished M.Sc. Thesis, McGill University, Montreal, 116 p.
- Spencer, R.J., 1987. Origin of Ca-Cl brines in Devonian formations, Western Canada Sedimentary Basin. *Applied Geochemistry*, v. 2, p. 373-384.
- Stanley, K.O., and Faure, G., 1979. Isotopic composition and sources of strontium in sandstone cements; the High Plains sequence of Wyoming and Nebraska. *Journal of Sedimentary Petrology*, v. 49, p. 45-53.
- Stasiuk, L.D., 1997. The origin of pyrobitumen in Upper Devonian Leduc Formation gas reservoirs, Alberta, Canada: An optical and EDS study of oil to gas transformation. *Marine and Petroleum Geology*, 14, 7-8, p.915-929.
- Stephenson, R.A., Zelt, C.A., Jajnal, Z., Morel-a-L'Huissier, P., Mereu, R.F., Northey, d.J., West, G.F. and Kanasewich, E.R., 1989. Crust and upper mantle structure and the origin of the Peace River Arch. *Bulletin of Canadian Petroleum Geology*, v.37, p. 224-235.
- Stoakes, F.A., 1980. Nature and control of shale basin fill and its effect on reef growth and termination: Upper Devonian Duvernay and Ireton formations of Alberta, Canada. *Bulletin of Canadian Petroleum Geology*, v. 28, p.345-410.
- Stoakes, F.A., 1992. Winterburn megasequence. In: J.C. Wendte, F.A. Stoakes and C.V. Campbell (eds.): Devonian-Early Mississippian carbonates of the Western Canada Sedimentary Basin: a sequence-stratigraphic framework. Society for Sedimentary Geology, Short Course No. 28, p. 207-224.
- Stoakes, F.A. and Creaney, S., 1984. Sedimentology of a carbonate source rock: the Duvernay Formation of Central Alberta.- In: Eliuk, L. (ed.), Carbonates in subsurface and outcrop. Canadian Society Petroleum Geology Core Conference

- 1984, p. 132-147.
- Switzer, S.B., Holland, W.G., Christie, P.S., Graf, G.C., Hedinger, A.S., McAnley, R.J., Wierzbicki, R.A., and Packard, J.J., 1994. Devonian Woodbend - Winterburn Strata of the Western Canada Sedimentary Basin. In: G.D. Mossop and I. Shetsen (comps.): Geological Atlas of the Western Canada Sedimentary Basin. Canadian Society of Petroleum Geologists and Alberta Research Council, p. 165-202
- Taylor, P.W., 1957. Revision of Devonian nomenclature in the Rocky Mountains [Alberta]. Journal of the Alberta Society of Petroleum Geologists. 5; 8, Pages 183-195. Canadian Society of Petroleum Geologists. Calgary, AB, Canada.
- Tóth, J., 1978. Gravity-induced cross-formational flow of formation fluids, Red Earth Region, Alberta, Canada: analysis, patterns and evolution. Water Resources Research, v. 14(5), p. 805-843.
- Tucker, M.E., 1985. Shallow-marine carbonate facies and facies models. In: P.J. Benchley and B.P.J. Williams (eds.): Sedimentology: Recent Developments and Applied Aspects, Spec. Publ. Geol. Soc. Lond. 18, p. 139-161.
- Tucker, M.E., and Wright, V.P., 1990. Carbonate Sedimentology. Blackwell Scientific Publications. 482 p.
- van Buchem, F.S.P., Chaix, M., Eberli, G.P., Whalen, M.T., Masse, P., and Mountjoy, E.W., 2000. Outcrop to surface correlation of the Upper Devonian (Frasnian) in the Alberta Basin (W. Canada) based on the comparison of Miette and redwater carbonate Buildup margins. In: P.W. Homewood and G.P. Eberli (eds.): Genetic stratigraphy on the exploration and production scales – case studies from the Pennsylvanian of the Pardo basin and the Upper Devonian of Alberta. Bulletin, Centre Recherche Elf Exploration-Production, Memoire 24, p. 225-267.
- Veizer, J., Ala, D., Azmy, K., Bruckschen, P., Buhl, D., Bruhn, F., Carden, G., Diener, A., Ebner, S., Godderis, Y., Jasper, T., Korte, C., Pawellek, F., Podlaha, O.G., and Strauss, H., 1999. $^{87}\text{Sr}/^{86}\text{Sr}$, $\delta^{13}\text{C}$ and $\delta^{18}\text{O}$ evolution of Phanerozoic seawater. Chemical Geology. 161; 1-3, Pages 59-88. 1999.
- Wade, W.J., Hanor, J.S., and Sassen, R., 1989. Controls on H_2S concentration and hydrocarbon destruction in the eastern Smackover Trend. In: Gulf Coast Association of Geological Societies, 39th annual meeting; and Gulf Coast Section

- SEPM, 36th annual meeting. Transactions - Gulf Coast Association of Geological Societies. 39; Pages 309-320.
- Walls R.A. and Burrowes G.O., 1990. Diagenesis and reservoir development in Devonian limestone and dolostone reefs of Western Canada. In: The development of porosity in carbonate reservoirs; short course notes. Bloy-Graeme-R (compiler); Hadley-Mark-G (compiler); Pages 5.1-5.17. 1990. Can. Soc. Pet. Geol., Canada. 1990.
- Walls, R.A., 1983. Golden Spike reef complex, Alberta. In: P.A. Scholle, D.G. Bebout and C.H. Moore (eds.): Carbonate Depositional Environments. AAPG Memoir, v. 33, p. 445-453.
- Walls, R.A., Mountjoy, E.W., and Fritz, P., 1979. Isotopic composition and diagenetic history of carbonate cements in Devonian Golden Spike reefs, Alberta, Canada. Geol. Soc. America Bull., Pt. 1, v.90, p. 963-982.
- Walkden, G.M., and Berry, J.R., 1984. Syntaxial overgrowths in muddy crinoidal limestones; cathodoluminescence sheds new light on an old problem. Sedimentology. 31 (2), p. 251-267.
- Wanless, H.R., 1979. Limestone response to stress: pressure solution and dolomitization. J. Sedim. Petrol., 49, 437-462.
- Waring, W.W., and Layer, D.B., 1950. Devonian dolomitized reef, D-3, reservoir, Leduc field, Alberta, Canada. Bulletin of the American Association of Petroleum Geologists. 34 (2), p. 295-312.
- Watts, N.R., 1987. Carbonate sedimentology and depositional history of the Nisku Formation in south-central Alberta. In: F.F. Krause and O.G. Burrowes (eds.): Devonian lithofacies and reservoir styles in Alberta. Manual of the 13th CSPG Core Conference, p. 87-152.
- Weihmann, I., 1980. Grassi Lakes - Whiteman Gap field trip guidebook. Can. Soc. Pet. Geol., Canada, p. 59.
- Weissenberger, J.A.W. and McIlreath, I.A., 1989. Southesk-Cairn reef complex, Upper I
- Weissenberger, J.A.W., 1994. Frasnian reef and basal strata of west-central Alberta: combined sedimentological and biostratigraphic analysis. Bulletin of Canadian Petroleum Geology, v.42, p.1-25.

- Weller, H., 1991. Facies and development of the Devonian (Givetian/Frasnian) Elbingerode Reef Complex in the Harz area (Germany). *Facies*, 25, p.1-50.
- Wendte J., 1992. Platform evolution and its control on reef inception and localization. In: J.C. Wendte, F.A. Stoakes and C.V. Campbell (eds.): Devonian-Early Mississippian carbonates of the Western Canada Sedimentary Basin: a sequence-stratigraphic framework. Society for Sedimentary Geology, Short Course No. 28, p. 41-88.
- Wendte, J. 1994. Platform evolution and its control on Late Devonian Leduc reef inception and localization. *Bulletin Canadian Petroleum Geology*, v. 42, p. 499-528.
- Wendte J., Stoakes, F.W., and Campbell, C.v., 1992. Devonian-Early Mississippian carbonates of the Western Canada Sedimentary Basin: a sequence stratigraphic framework. *Tulsa, SEPM Short Course 28*, 255 p.
- Wendte, J., Dravis, J.J., Stasiuk, L.D., Qing, H., Moore, S.L.O. and Ward, G., 1998. High-temperature saline (thermoflux) dolomitization of Devonian Swan Hills platform and bank carbonates, Wild River area, west-central Alberta. *Bulletin Canadian Petroleum Geology*, v. 46, p. 210-265.
- Whalen M.T., Eberli, G.P., van Buchem, F.S.P., Mountjoy, E.W. and Homewood, P.W., 2000. Bypass margins, basin-restricted wedges, and platform-to-basin correlation, Upper Devonian, Canadian Rocky Mountains: implications for sequence stratigraphy of carbonate platform systems. *Journal of Sedimentary Research*, v. 70, p. 913-936.
- Wilkinson, P.K., 1995. Is Fluid Flow in Paleozoic Formations of West Central Alberta Affected by the Rocky Mountain Thrust Belt? M.Sc. Thesis (unpubl.), University of Alberta, Edmonton, 102p.
- Witzke, B.J. and Heckel, P.H., 1988. Paleoclimatic indicators and inferred Devonian paleo latitudes of Euramerica. In: N.J McMillan, A.F. Embry and D.J. Glass (eds.): Devonian of the World. Second Symposium on the Devonian System, Canadian Society of Petroleum Geologists Memoir 14, v.1, p. 49-68.
- Worden, R.H., Smalley, P.C., and Oxtoby, N.H., 1996. The effects of thermochemical sulfate reduction upon formation water salinity and oxygen isotopes in carbonate

- reservoirs. *Geochimica and Cosmochimica Acta*, v. 60, p. 3925-3931.
- Worden, R.H., Smalley, P.C., and Oxtoby, N.H., 1998. Reply to the comment by H.G. Machel on "The Effects of thermochemical sulfate reduction upon formation water salinity and oxygen isotopes in carbonate reservoirs". *Geochimica and Cosmochimica Acta*, v. 62(2), p. 343-346.
- Workum, R.H., 1978. Cripple Creek, a leeward Leduc reef margin. In: *The Fairholme Carbonate Complex at Hummingbird and Cripple Creek*, I.A. McIlreath and P.C. Jackson (eds.), Canadian Society of Petroleum Geologists, Guidebook.
- Workum, R.H. and Hedinger, A.S., 1987. Geology of the Devonian Fairholme Group, Cline Channel, Alberta. Second International Symposium on the Devonian System, Calgary, Field Excursion A-6 Guidebook, 45 p.
- Wright, G.N., McMechan, M.E., and Potter, D.E.G., 1994. Structure and Architecture of the Western Canada Sedimentary Basin. In: *Geologic Atlas of the Western Canada Sedimentary Basin*; G.D. Mossop & I. Shetsen (comps.), Canadian Society of Petroleum Geologists and Alberta Research Council, p. 25-40.
- Yang, C., Hutcheon, I., and Krouse, H.R., 2001. Fluid inclusion and stable isotope studies of thermochemical sulphate reduction from Burnt Timber and Crossfield East gas fields in Alberta, Canada. *Bulletin of Canadian Petroleum Geology*, v. 49, p. 149-164.
- Zenger, D.H., and Dunham, J.B., 1988. Dolomitization of Siluro-Devonian limestones in a deep core (5,350 M), southeastern New Mexico. In: *Sedimentology and geochemistry of dolostones, based on a symposium*. Shukla, V., and Baker, P.A. [eds.]; Special Publication - Society of Economic Paleontologists and Mineralogists. 43; Pages 161-173. 1988.
- Ziegler, P.A., 1988. Laurussia – The old red continent. In: N.J. McMillan, A.F. Embry and D.J. Glass (eds.): *Devonian of the World. Second Symposium on the Devonian System*, Canadian Society of Petroleum Geologists Memoir 14, v.1, p. 15-48.

APPENDIX I

List of the 52 logged core locations, cored formations, core lengths, and general lithology.

#	Location	Stratigraphic Interval	Lengths	Log	Remarks
#1	06-29-60-22W5	Leduc	14.7m	x	Lobstick? Uppermost Nisku
#2	09-20-59-22W5	Leduc	15.8m	x	dolomitized
#3	09-22-58-24W5	Leduc	17.9m	x	fossilif. limestone
#4	01-32-57-25W5	Leduc	23m	x	limestone
#5	10-20-57-25W5	Winterburn Leduc	13.7m 17.6m	xx	Upper Bluebridge (Silty dolomite/ anhydrite)Lobstick?
#6	10-15-56-27W5	Leduc	2.1m	x	dolomite/ fault?
#7	01-16-55-27W5	Leduc	3.4m	x	big vugs/ veins
#8	15-19-56-23W5	Leduc	43.5m	x	partial Leduc reef down into Cairn limestone
#9(X1)	05-13-58-24W5	Leduc	54.9m	x	Leduc debris on top of Cairn ? (lots of solid bitumen !)
#10	05-08-60-26W5	Nisku	16.5m	x	Simonette/Dolostone + massive Anhydrite/Sulfur
#11	15-18-58-24W5	Calmar/Nisku(3773-3782m)	9.0m	x	Dolomud-to wackestone/cc/anhydr.
		Leduc (3871 to 3879 m)	5.6m	x	Dolofloatstone/ Reservoir/ Bitumen/SD/CC
#12	16-32-58-24W5	Calmar/Nisku(3698-3716m)	16.8m	x	Limy Dolostone on Top/ Dolofloatstone+ A/CC/Bit
		Leduc (3823-3841m)	16.6m	x	vuggy Floatstone/CC!!/S
#13	08-04-59-23W5	Leduc (3668.3 -3688.7m)	11m	x	Bit-stained/ microfractured/CC/SD
#14	07-35-59-24W5	Leduc	1.6m	x	Dolostone (no litholog)
#15	07-19-59-24W5	Leduc	14.9m	x	partly vuggy Dolostone/ A/CC/SD
#16	15-9-57-17W5	Nisku-Leduc	18.0m	x	Dolomite/ fractures & vugs
#17	1-18-56-16W5	Leduc	15.4m	x	Dolomite/ high Porosity
#18	6-16-55-18W5	Leduc?	18.0m	x	Dolomite (partly brecciated)
#19	2-19-54-19W5	Leduc	18.0m	x	dirty Lobstick?
#20	9-17-53-19W5	Leduc	13.1m	x	Lobstick? (Dolomite)/ porous
#21	7-35-49-22W5	Leduc	7.9m	x	Dolostone/ porous)
#22	14-8-48-21W5	Leduc	17.0m	x	Dolomite/ distinct sulfur smell
#23	11-9-61-22W5	Leduc	29.0m	x	Dolomite/ increasing porosity towards the bottom/ bitumen
#24	4-26-58-20W5	Leduc	34.7m	x	Wabamun? Dolomite / porosity changes with facies
#25	11-30-51-25W5	Leduc	30.5m	x	Dolomite / Limestone
#26	14-36-52-27W5	Leduc	24.2m	x	Dolomite/ (parts highly porous)
#27	07-07-53-26W5	Leduc?	4.60m	x	Dolomite (partly high porous)
#28	10-32-44-19W5	Leduc	54.4m	x	Dolomite/ porous/ Bitumen!!
#29	07-18-52-24W5	Leduc	41.6m	x	Dolomite/Limestone!/? (Core Display)
#30	14-36-52-27W5	Leduc	24.2m		Dolomite/ AA!!!!/S/CC
#31	01-16-55-27W5	Leduc	3.7m		vuggy Dolostone, SD, CC
#32	03-26-49-20W5	Swan Hills	3.6m	x	vuggy dolostone, CC.A, Py
#33	05-25-51-22W5	Leduc	29.5m	x	Limestone, Bit, marine cements (core

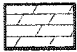
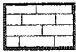
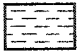
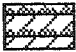




















					display)
#34	10-13-52-22W5	Leduc	24.9m	x	Dolostone, AAA!!,small CC-cem
#35	15-29-55-17W5	Leduc	3.8m	x	Dolostone/Anhy/ no calcite
#36	10-08-53-20W5	Leduc	4.6m	x	Dolostone, A in veins, small cc in vug
#37	10-27-52-24W5	Leduc	18.3m	x	Dolostone, S!!!, cc in small vugs, no vein cc
#38	10-09-57-24W5	Swan Hills	18.3m		Dolostone, no S, A-nodules, CC-cement, Dol-cem
#39	10-17-57-23W5	Ireton	9.1m		shaly limestone, basinal facies
#40	09-05-57-17W5	Leduc	3.0m	x	Dolomudstone, big calcite
#41	06-34-57-21W5	Leduc	15.3m	x	Dolostone, lots of cc-vug infill, Bit, micfrac, SD (core display)
#42	02-14-50-22W5	Wabamun(3904.5-3918.2m) Leduc (4581.1-4599.4m)	13.7m 18.3m	x	Dolomudstone, small cc in vugs Dolostone, huge A-vugs, cc, microfracs, S, Bit
#43	16-22-58-19W5	Leduc	18.3m	x	vuggy Dolostone, Sd, CC, Bit, elong. x-tal?
#44	11-07-59-23W5	Leduc	5.3m	x	is this one logged?????
#45	10-20-58-15W5	BH LK	18.3m	x	Limestone, micfracs, Bit, A?,
#46	10-12-54-18W5	SW HL	24.7m	x	Dolostone, A, CC, S (core display)
# 47	16-18-61-15W5	Leduc,G-W	41.5m	x	Vuggy Dolostone, two types of A
#48	02-02-57-22W5	Nisku	9.5m		vuggy Dolostone, A, CC, SD, Bit
#49	15-09-57-17W5	Nisku/Leduc	18.0m		Float-to Wackestone, Dolostone, CC, Some A on Top, SD, Frac with CC
#50	11-29-59-16W5	BLRD, Calmar, Nisku	37.5m	x	Silty dolostone, LST, Vuggy Dolostone, A, PS, CC, Mudstone
#51	13-15-60-16W5	Nisku	2.1m		vuggy dolostone
#52	10-23-58-17W5	Nisku	2.6m		vuggy Dolostone, vein CC!!!

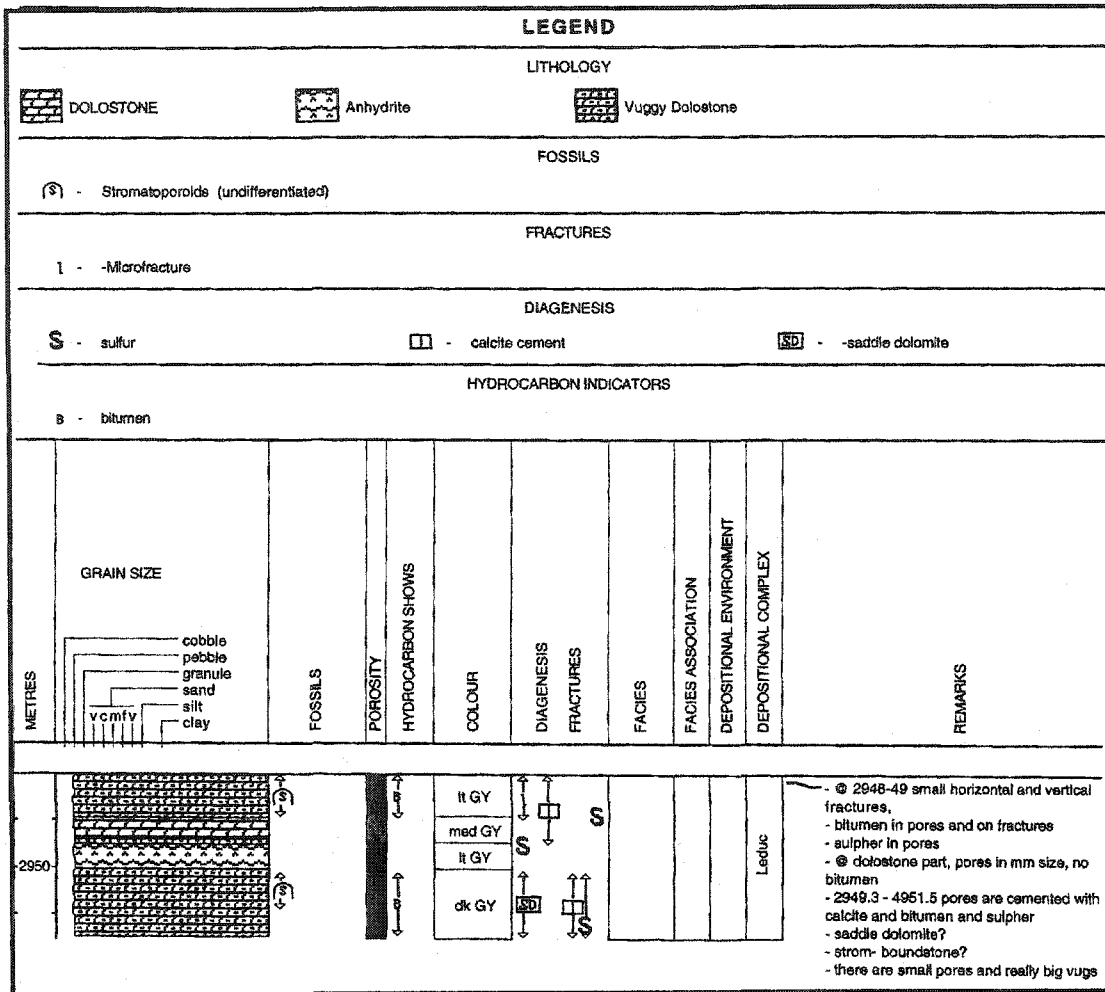
APPENDIX II

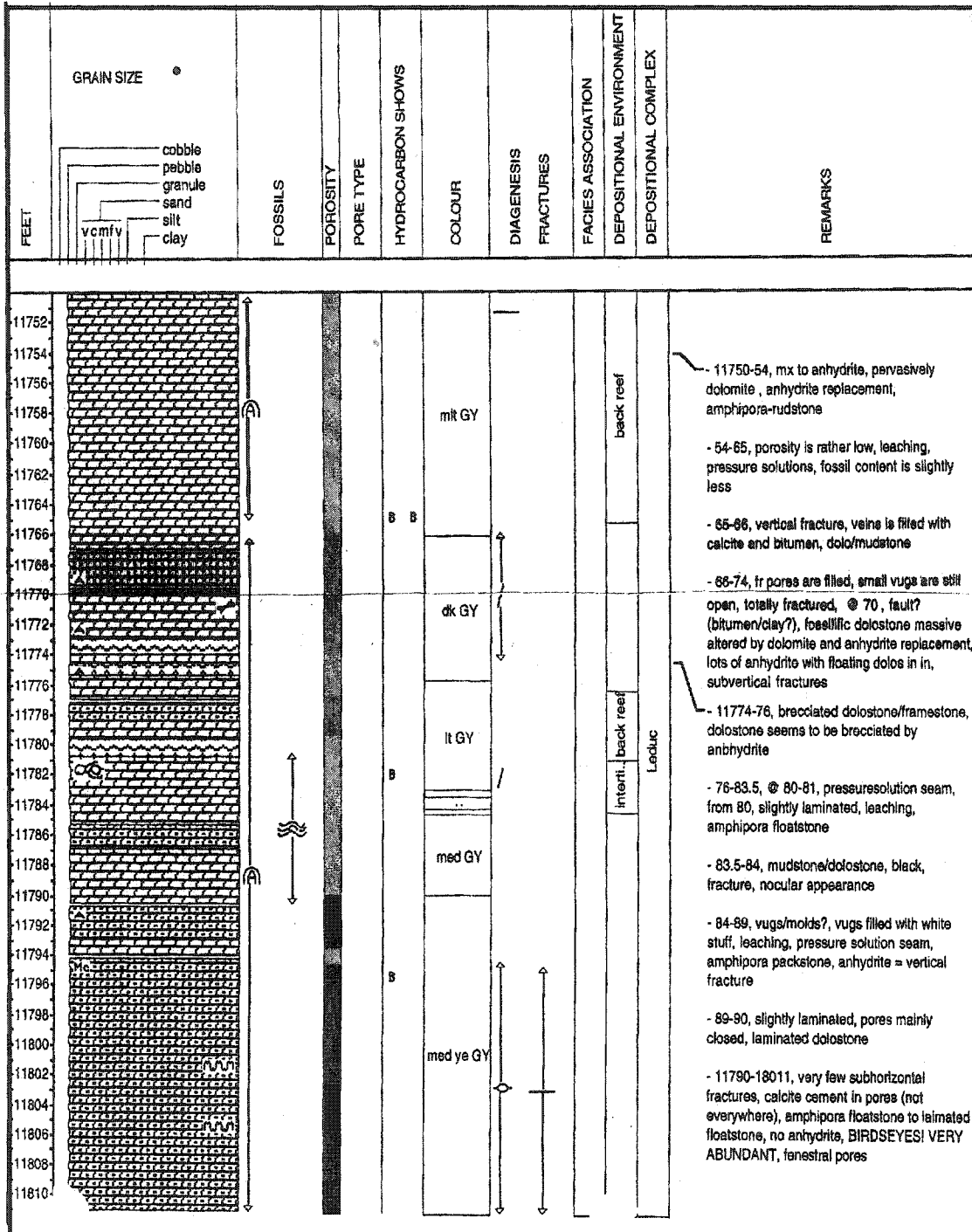
Schematic lithologs of 48 cores from the Southesk-Cairn carbonate complex. The cores were originally logged using the "Macintosh Apple-core®" logging program (Copyright by Mike Ranger, Calgary). The logs were later modified and generalized to fit the thesis format; detailed core descriptions are available upon request. The drill cores were investigated with respect to their gross facies distribution using the carbonate facies model for Middle and Upper Devonian shallow-marine carbonates by Machel and Hunter (1994); see also Chapter 3, Figure 3.13. All core were also closely investigated for diagenetic features. For lithologic patterns, symbols, and abbreviations, refer to legend on the next page.

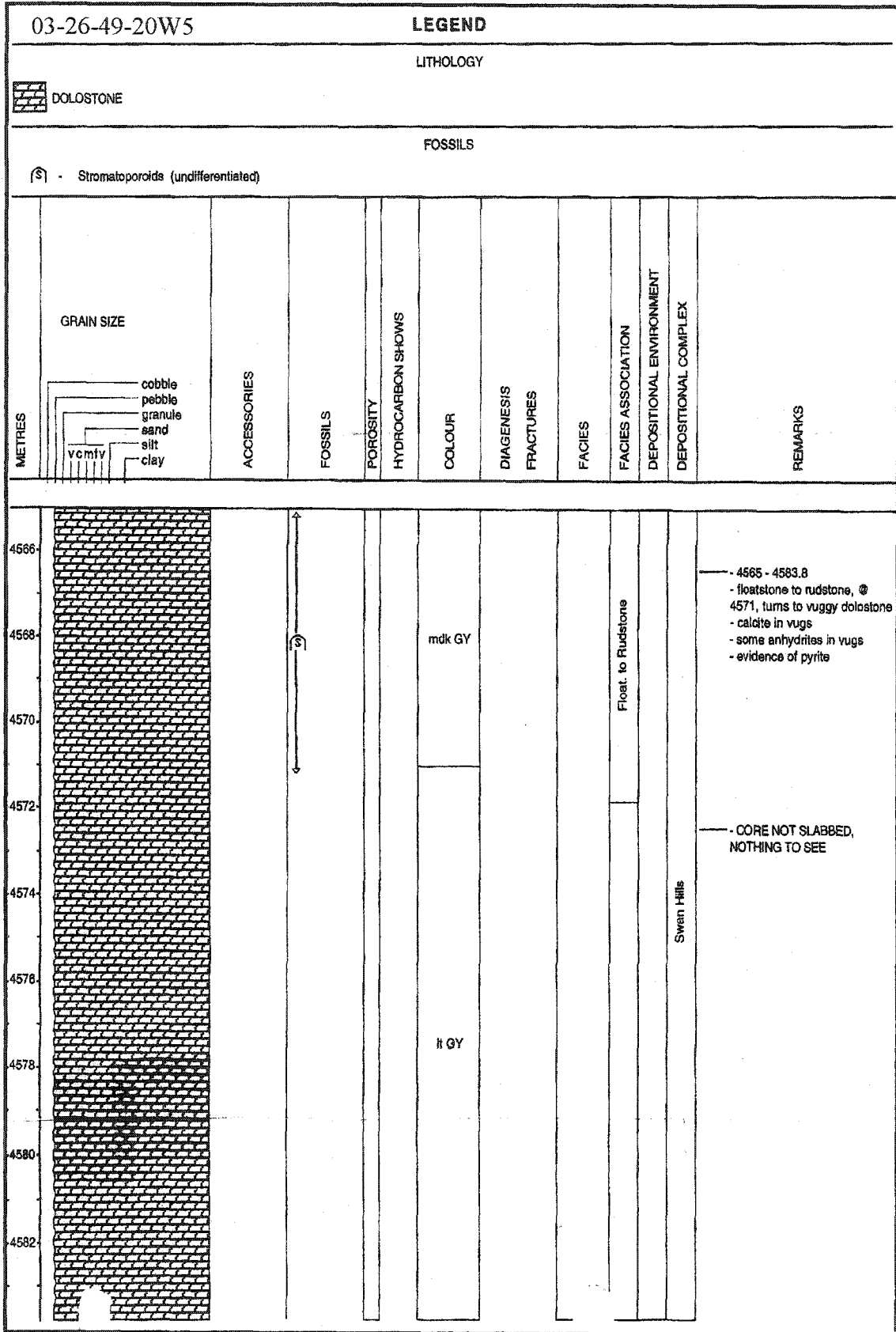
References

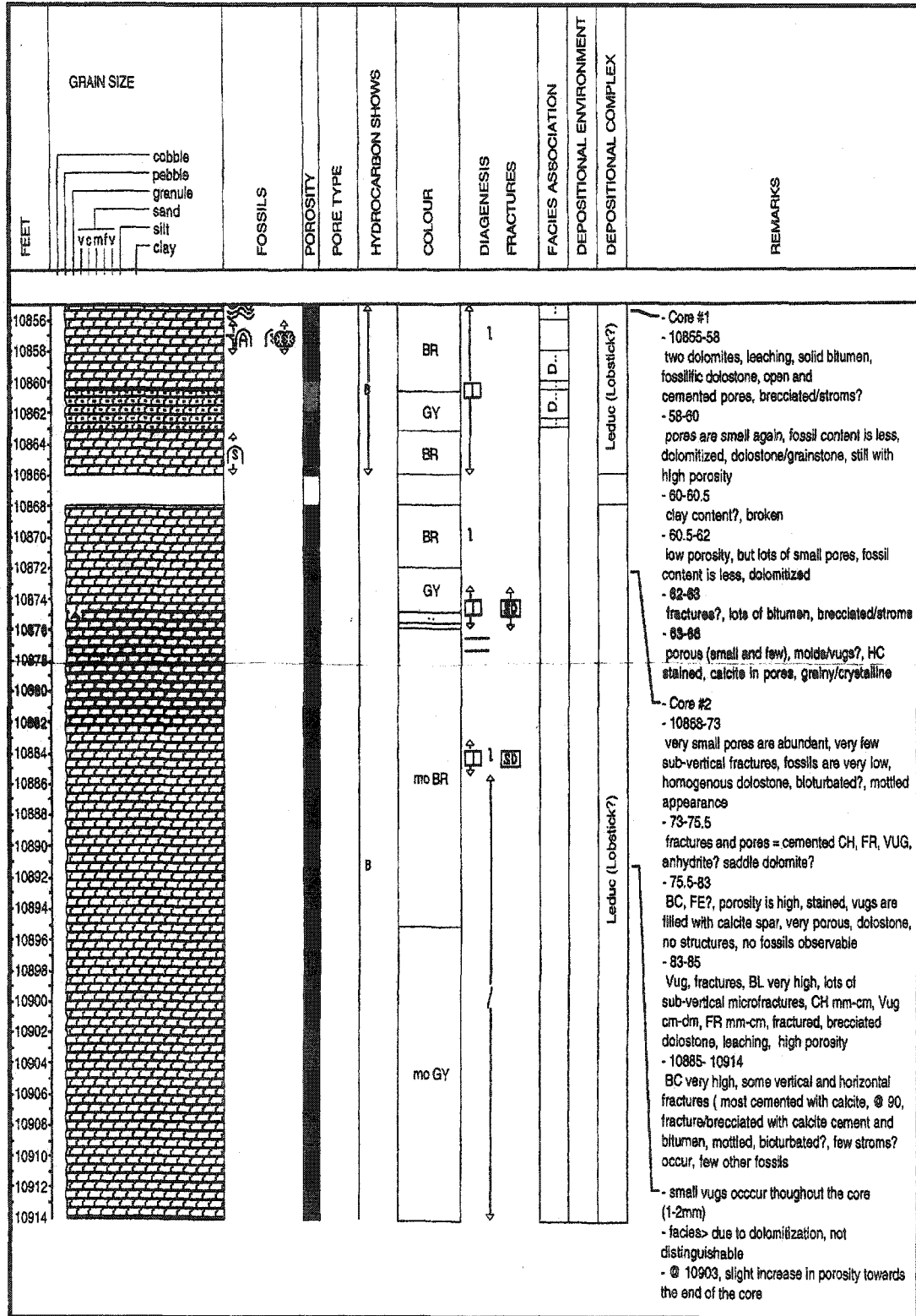
Machel, H.G. and Hunter, I.G., 1994. Facies models for Middle to Late Devonian shallow - marine carbonates, with comparisons to modern reefs: A guide for facies analysis: *Facies*, v.30, p.155-176

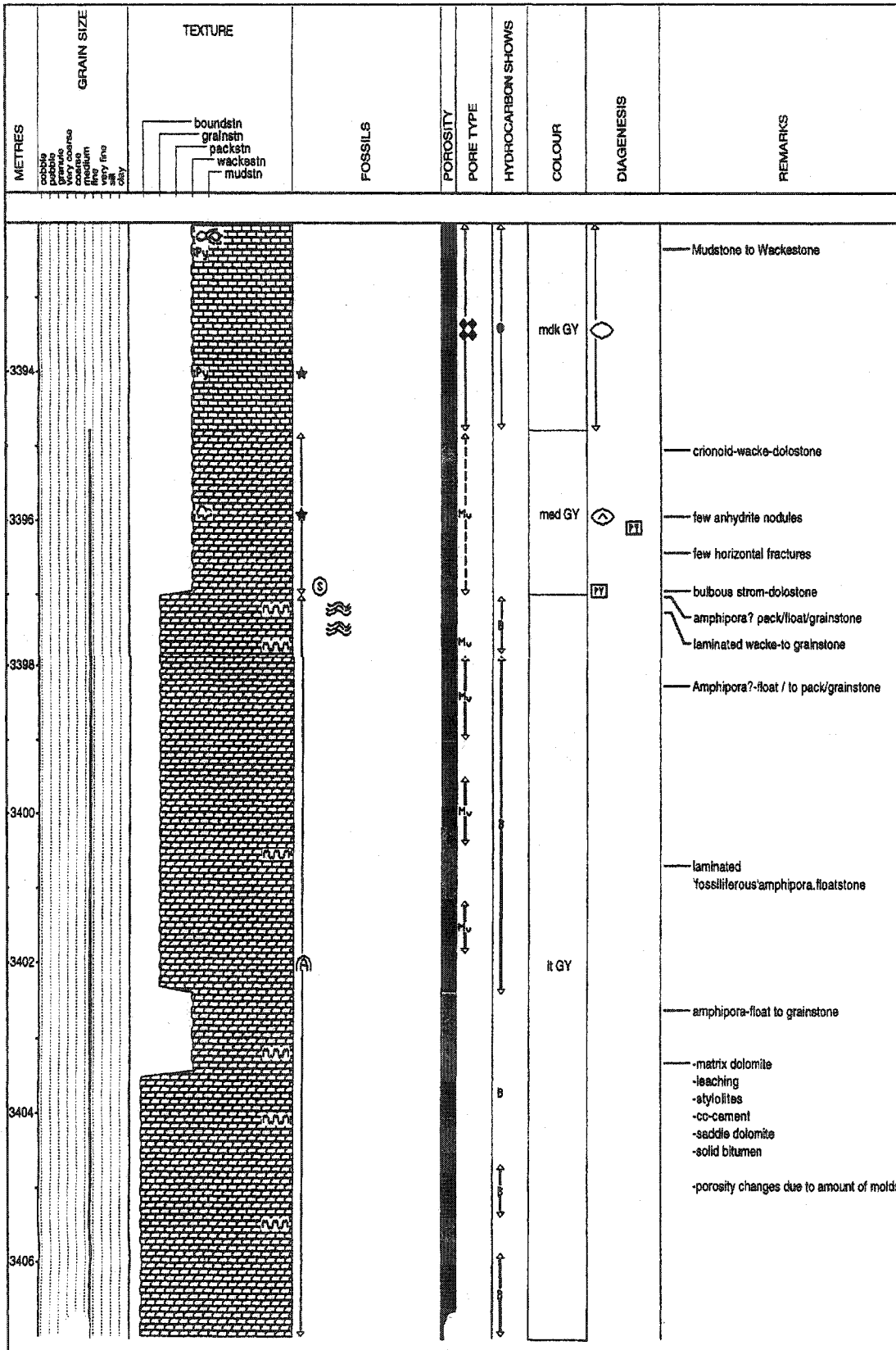
LEGEND			
Lithology			
	Dolostone		Limestone
	Shale/Mudstone		Anhydrite
			Vuggy Dolostone
Fossils			
	Stromatoporoid (undifferentiated)		Amphipora
	Lamination		Brachiopods
			Corals (colonial)
			Gastropods
			Crinoids
			Bulbous Stromatoporoid
Accessories			
Py	Pyrite		Clay Seams
			Stylolites
			Anhydrite Crystals
	Calcite Cement		Anhydrite (Nodules)
			Anhydrite Cement
		B	Bitumen
S	Elemental Sulfur		Saddle Dolomite
			Geopetal
	Fracture (General)		Fracture (Horizontal)
			Microfractures

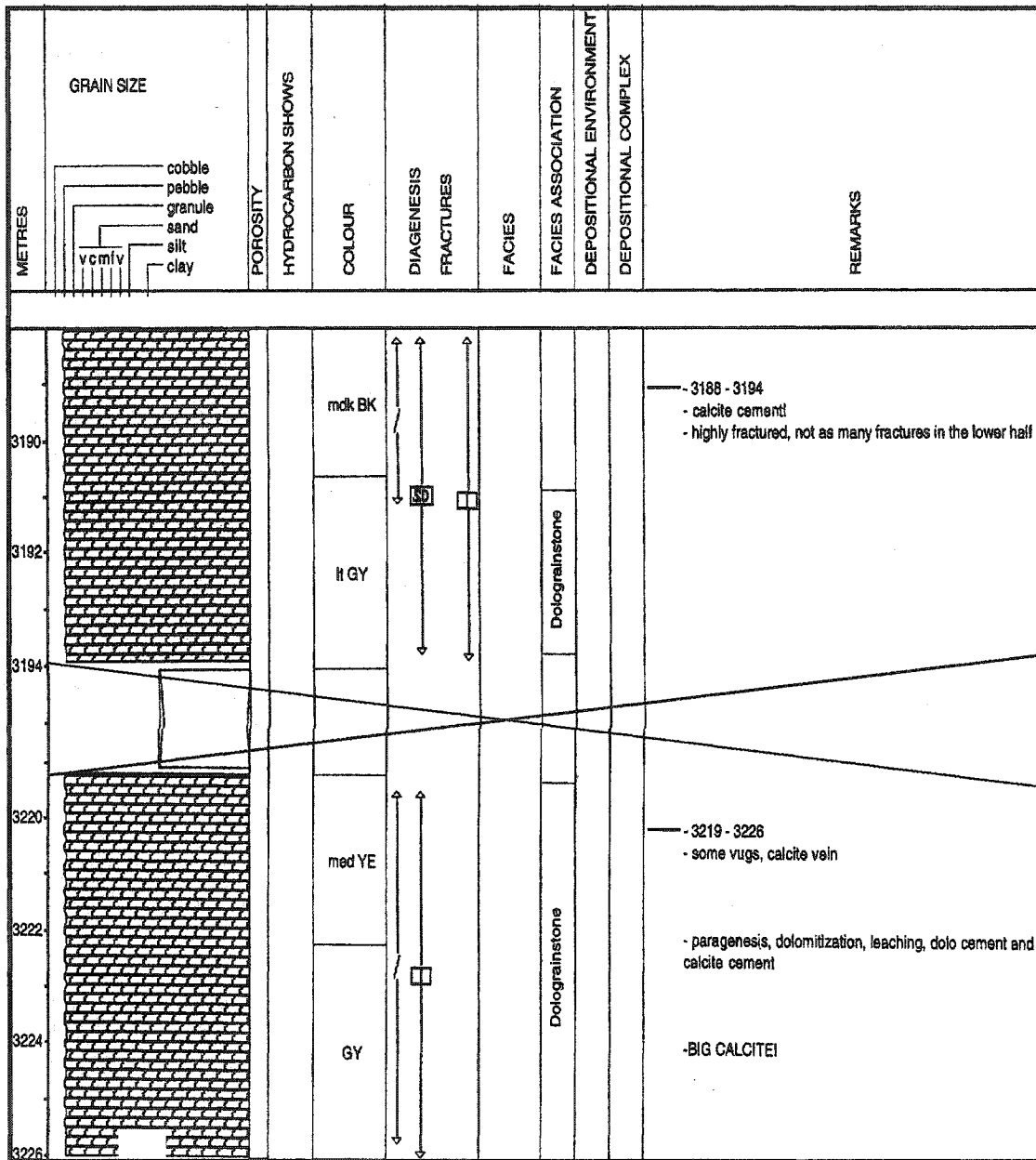


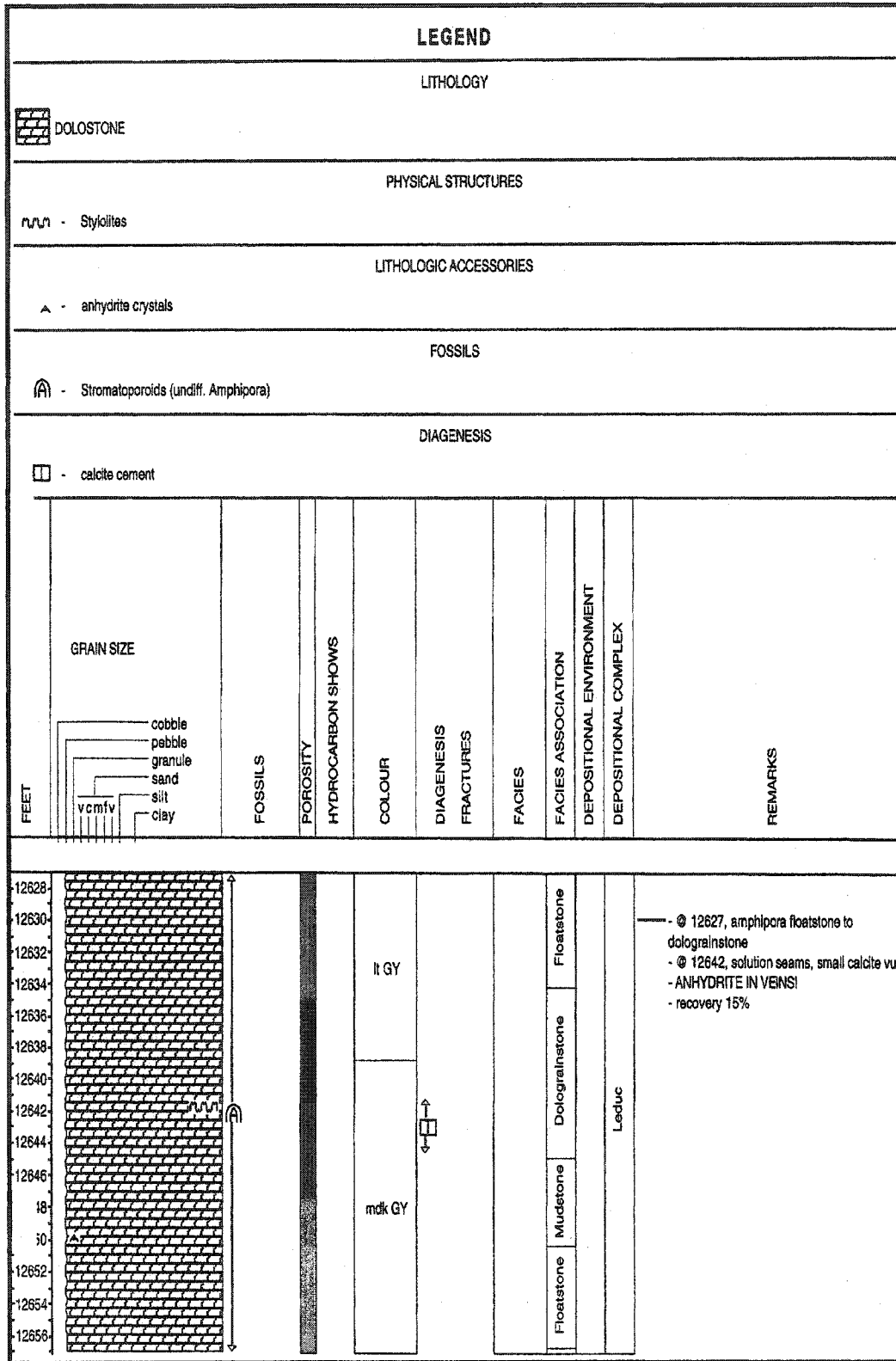


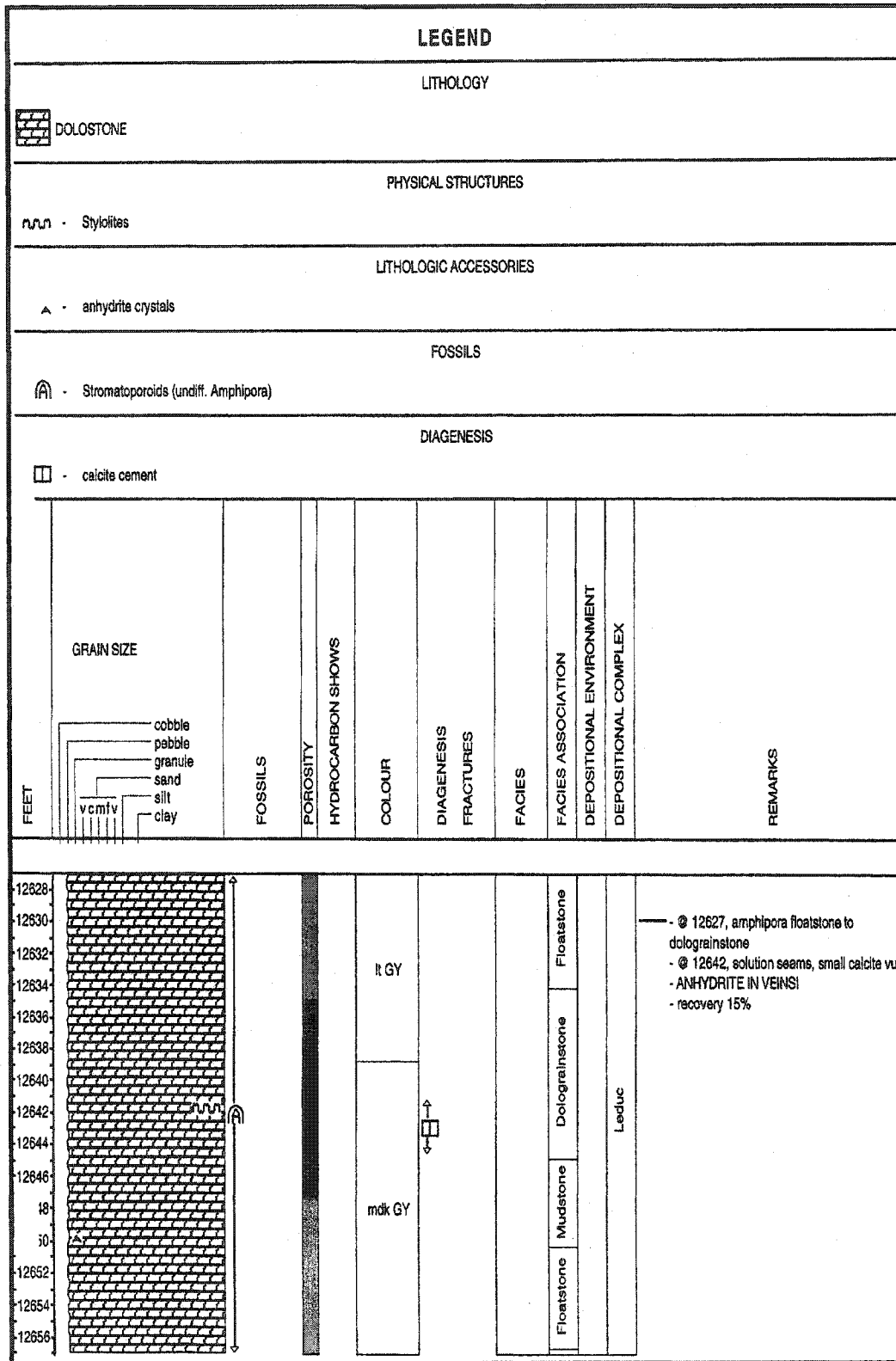


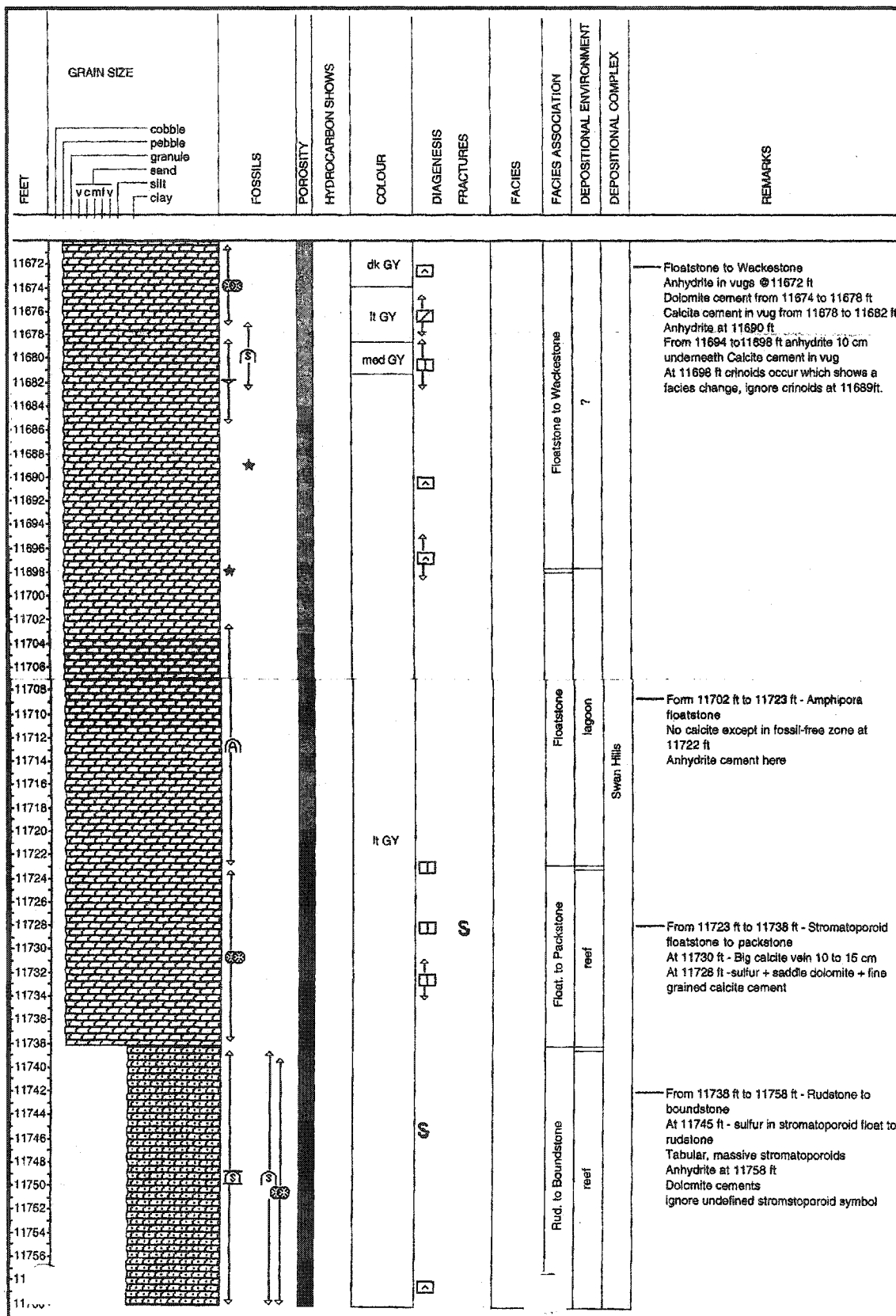


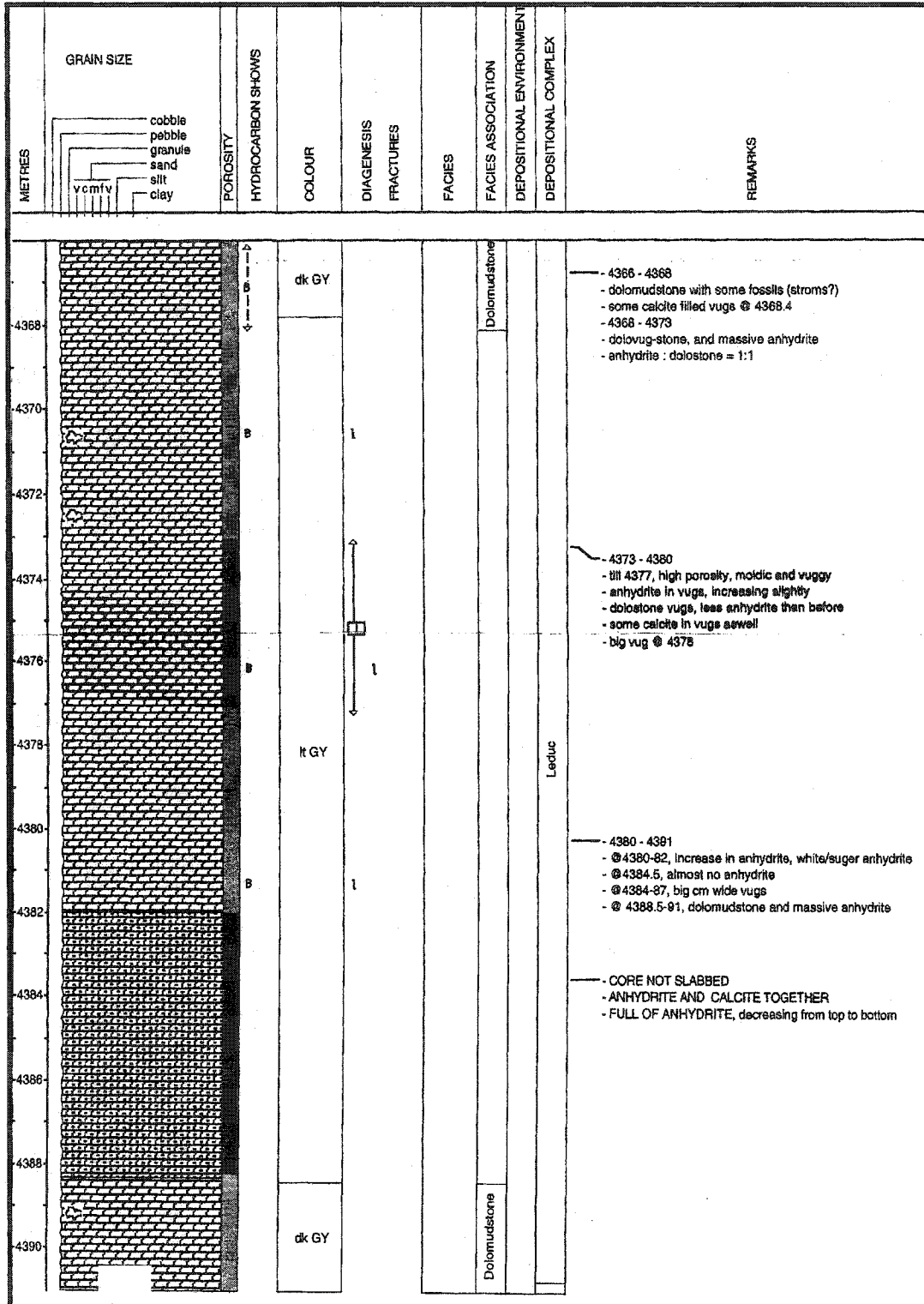




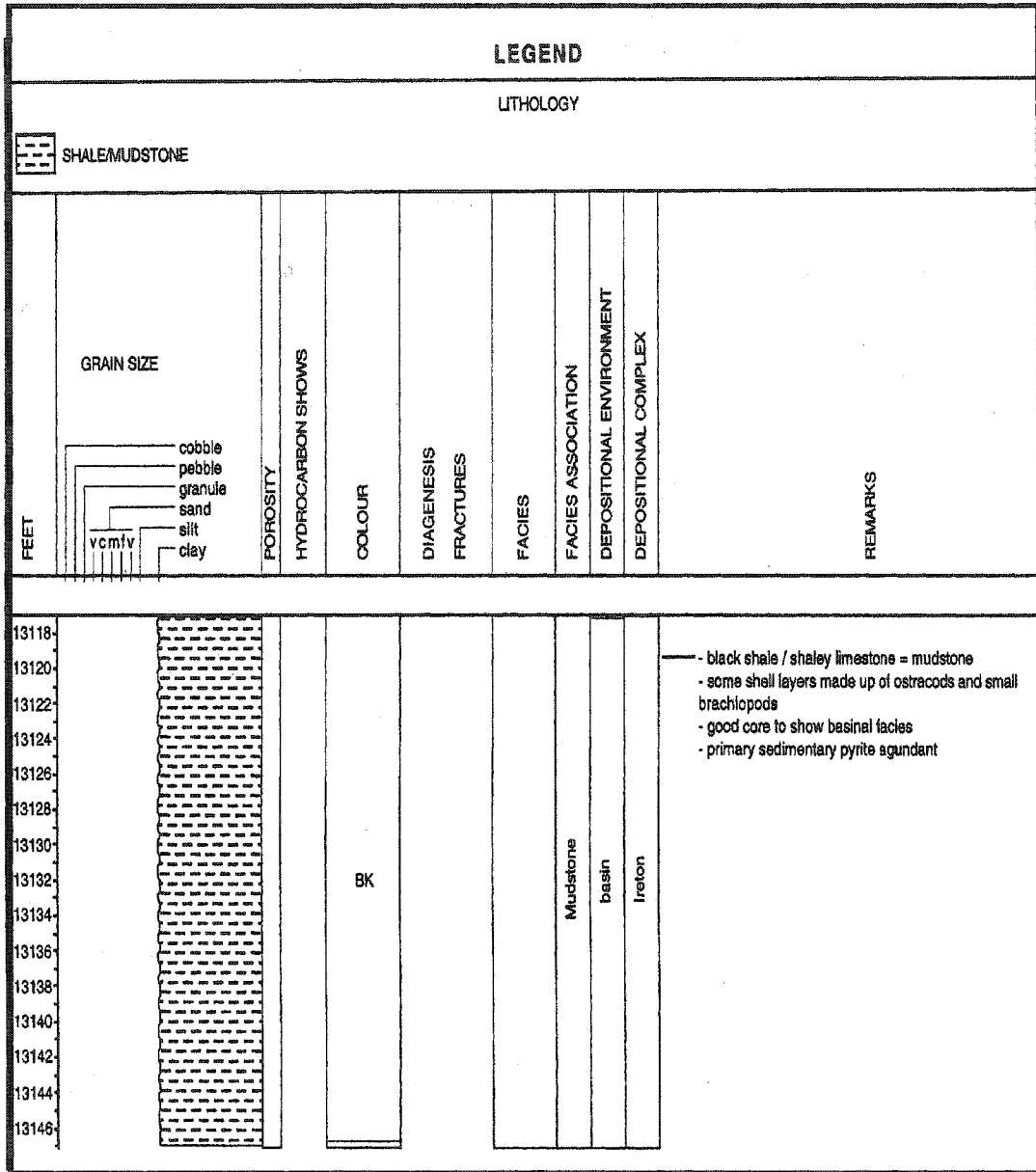


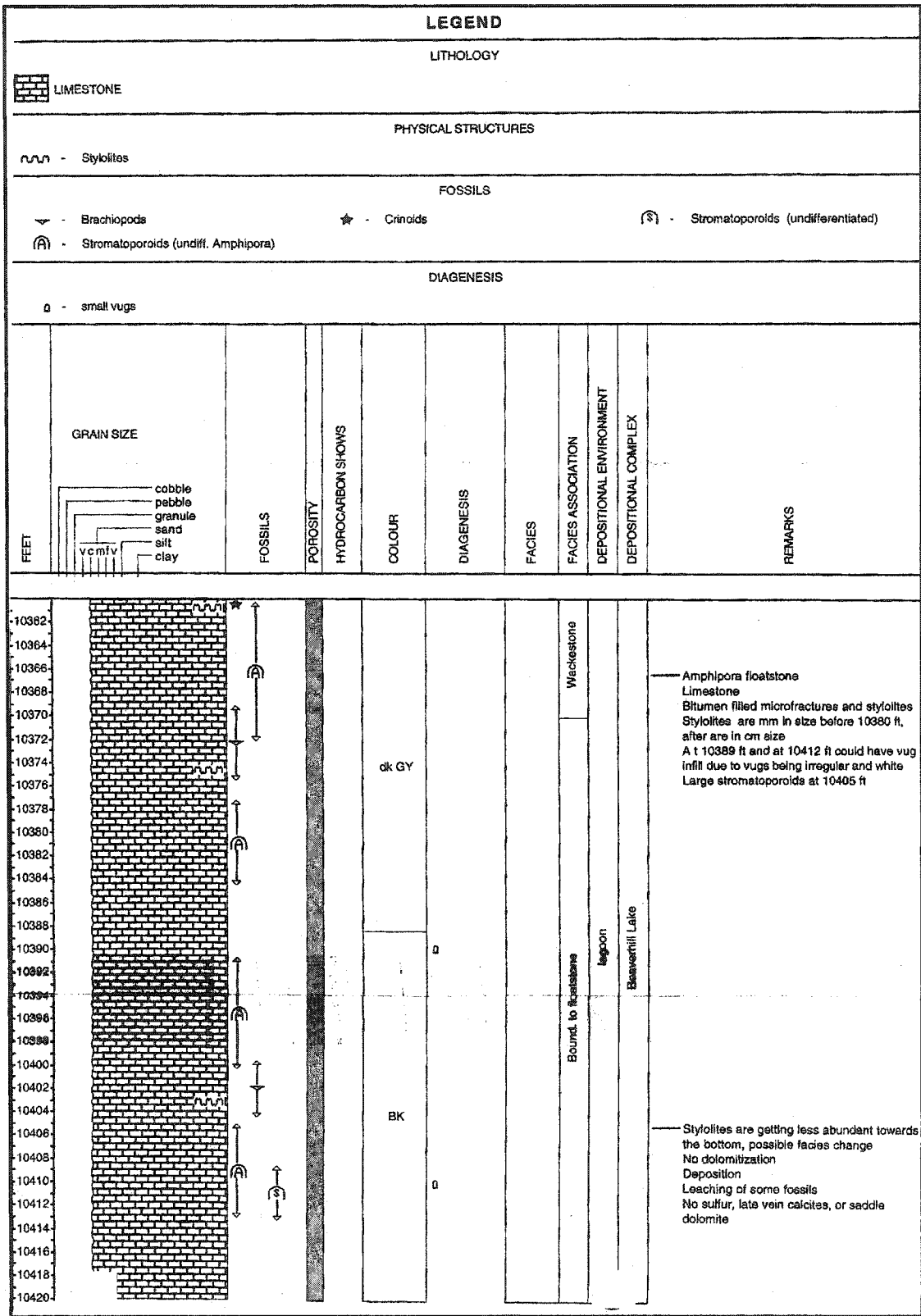


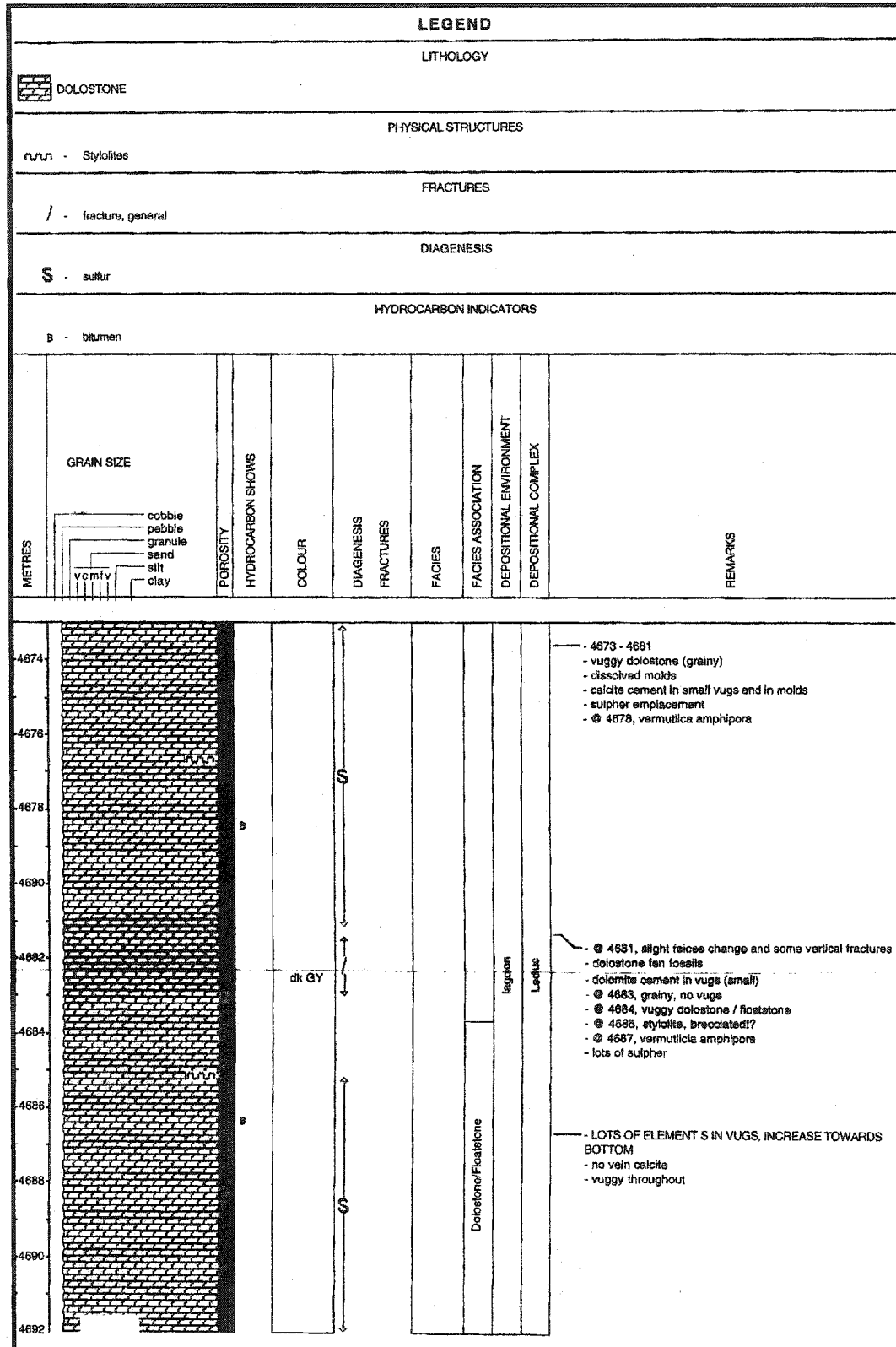


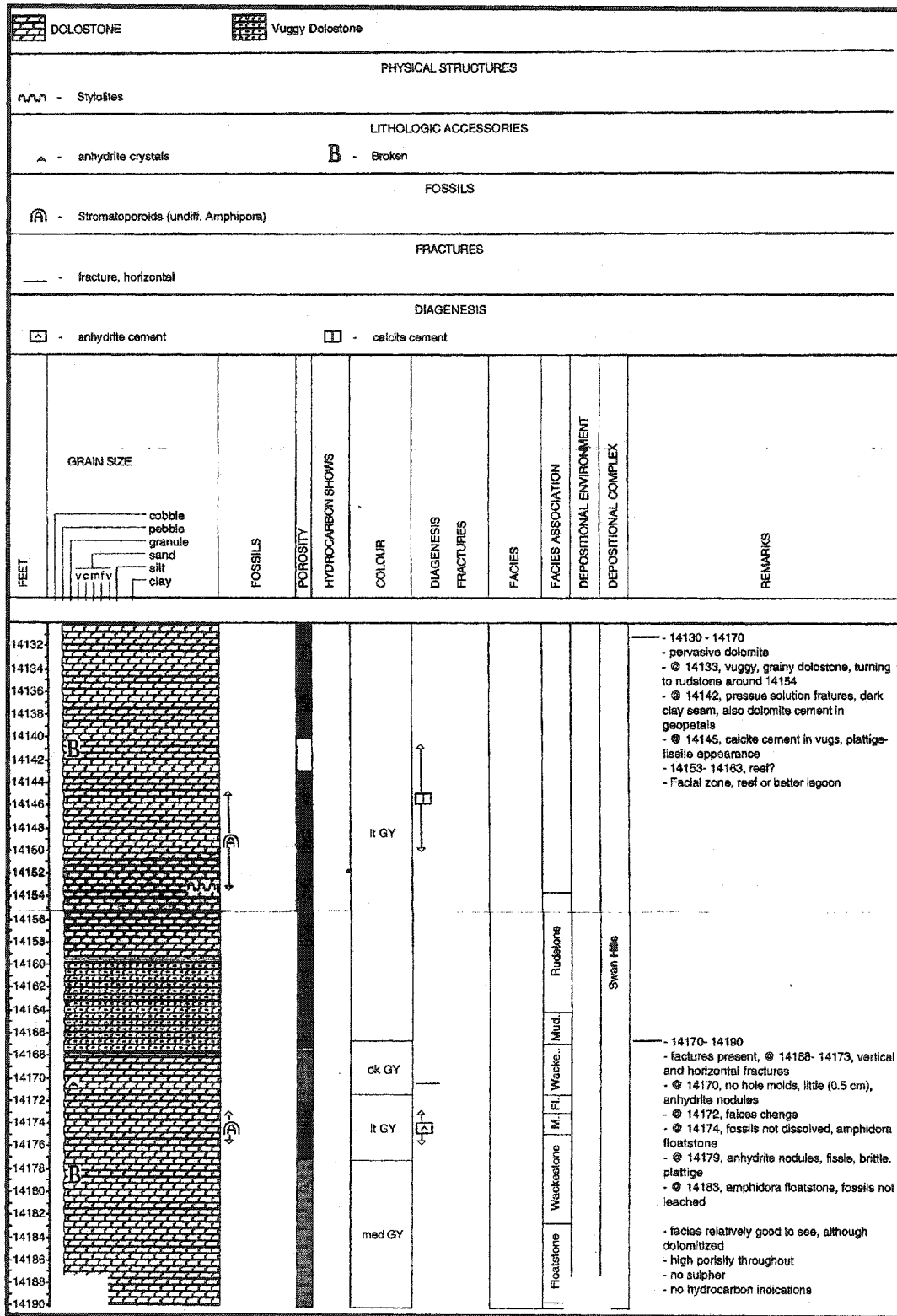


FEET	GRAIN SIZE	TEXTURE	POROSITY	PORE TYPE	HYDROCARBON SHOWS	COLOUR	DEPOSITIONAL ENVIRONMENT	DEPOSITIONAL COMPLEX	REMARKS
15262 15264 15266 15268 15270 15272 15274	cobbic pebbly granule coarse coarse medium fine very fine silt clay	boundstn grainstn packstn wackestn mudstn				GY	homogenous dolostone	LEDUC	all core is broken / recovery is not good small pores (less 1mm) > intermediate porosity? broken rocks = high porosity? no hydrocarbon shows observable white veins and chunks of calcite towards the bottom

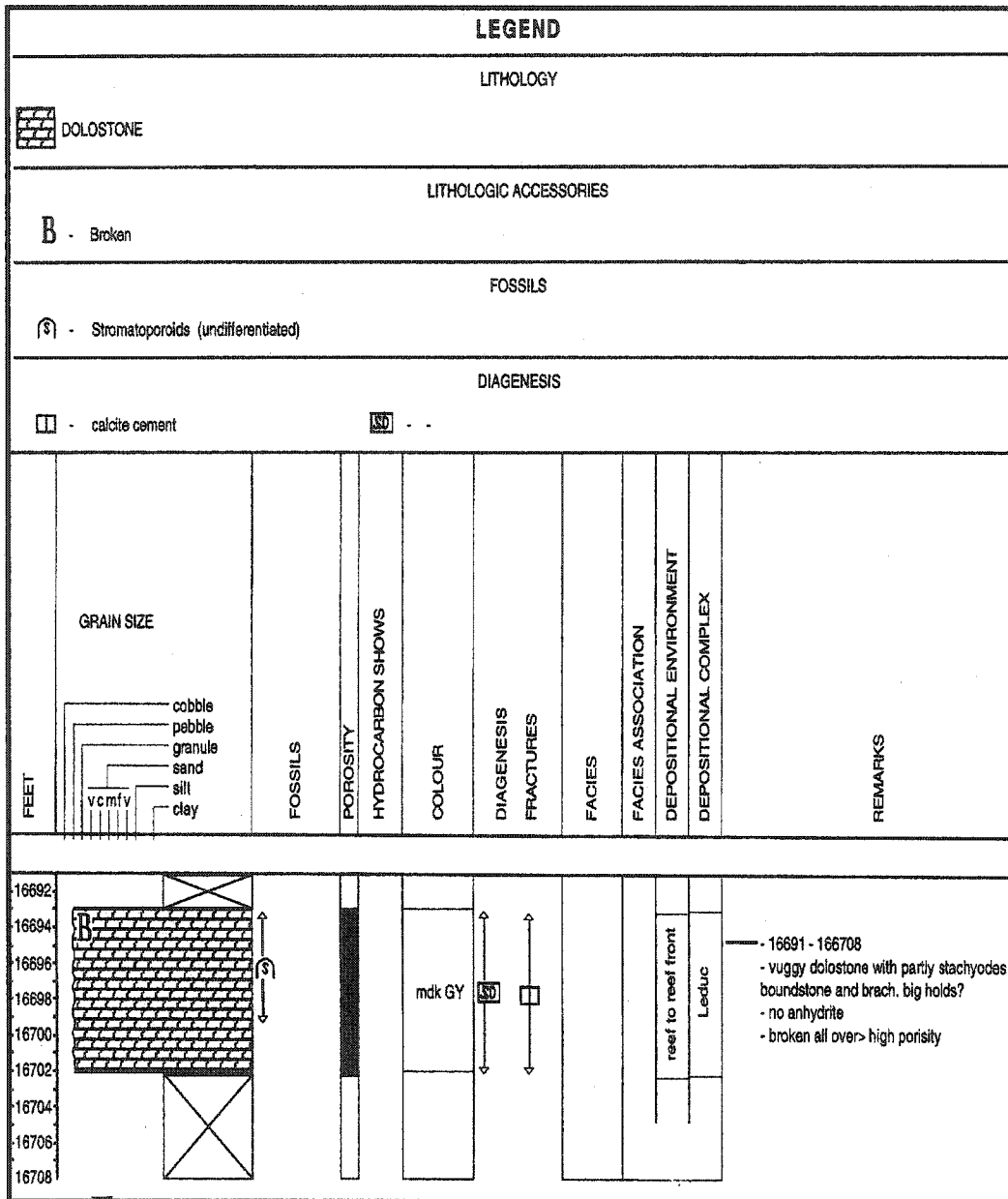




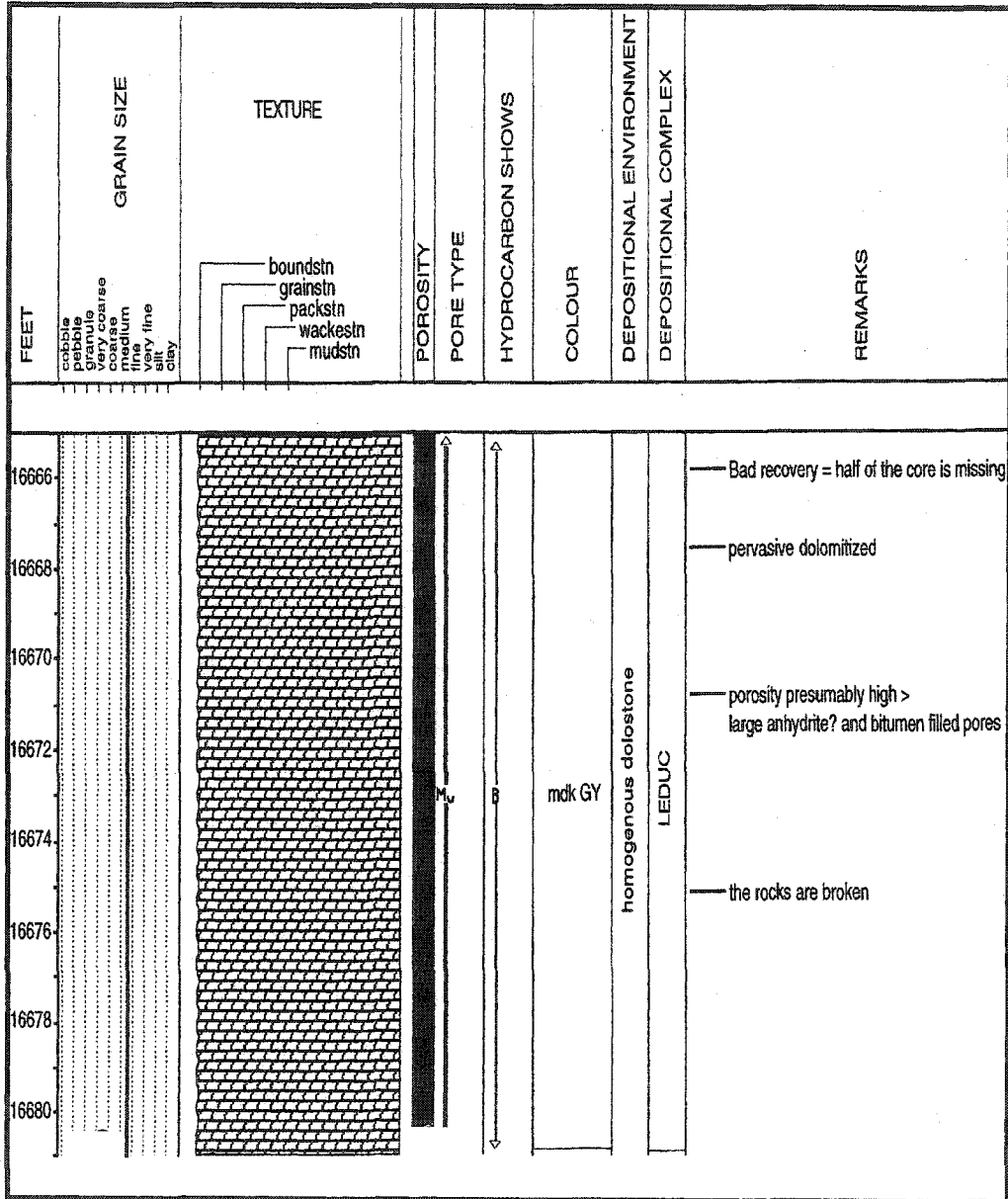




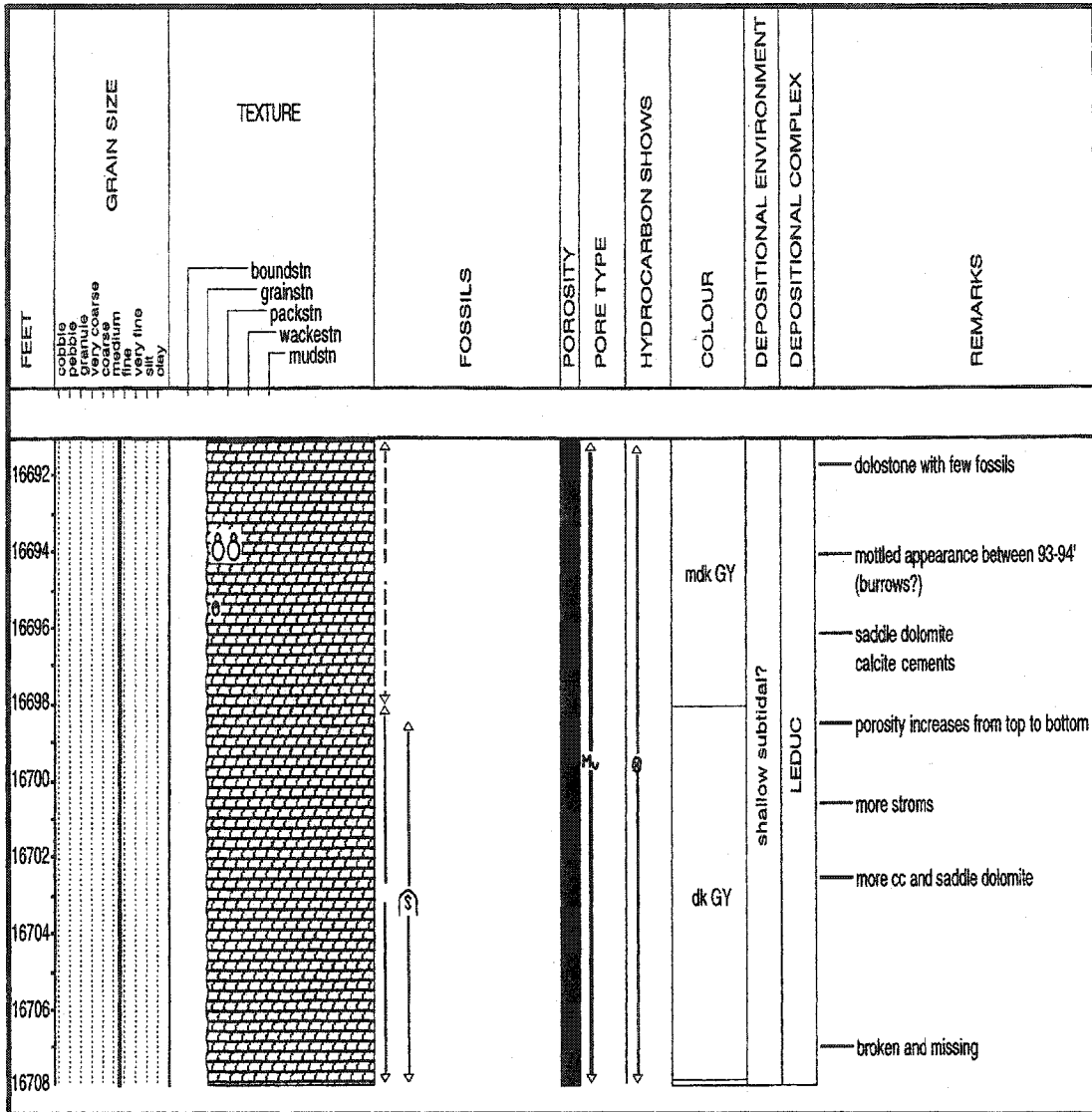
1-16-55-27W5

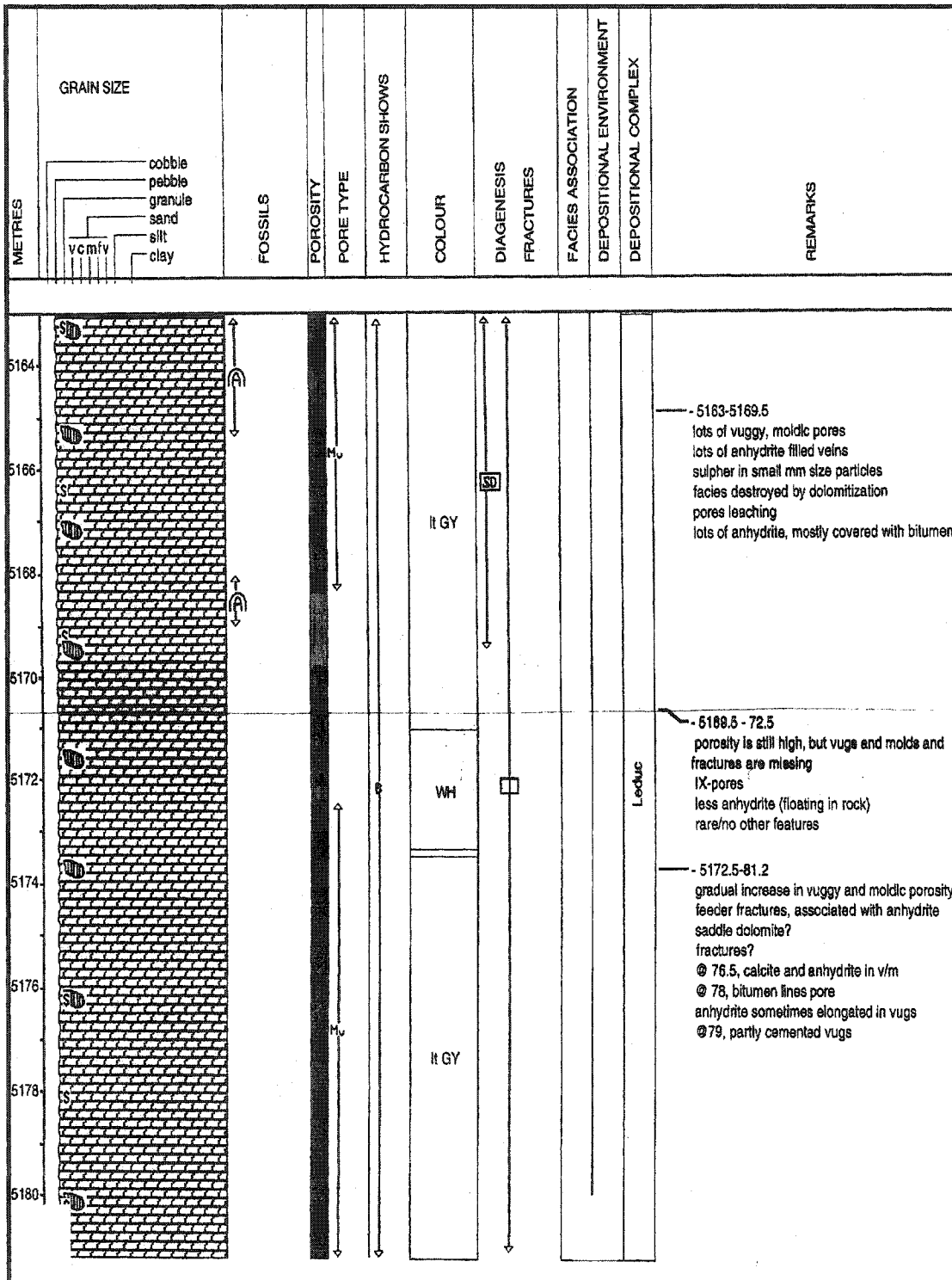


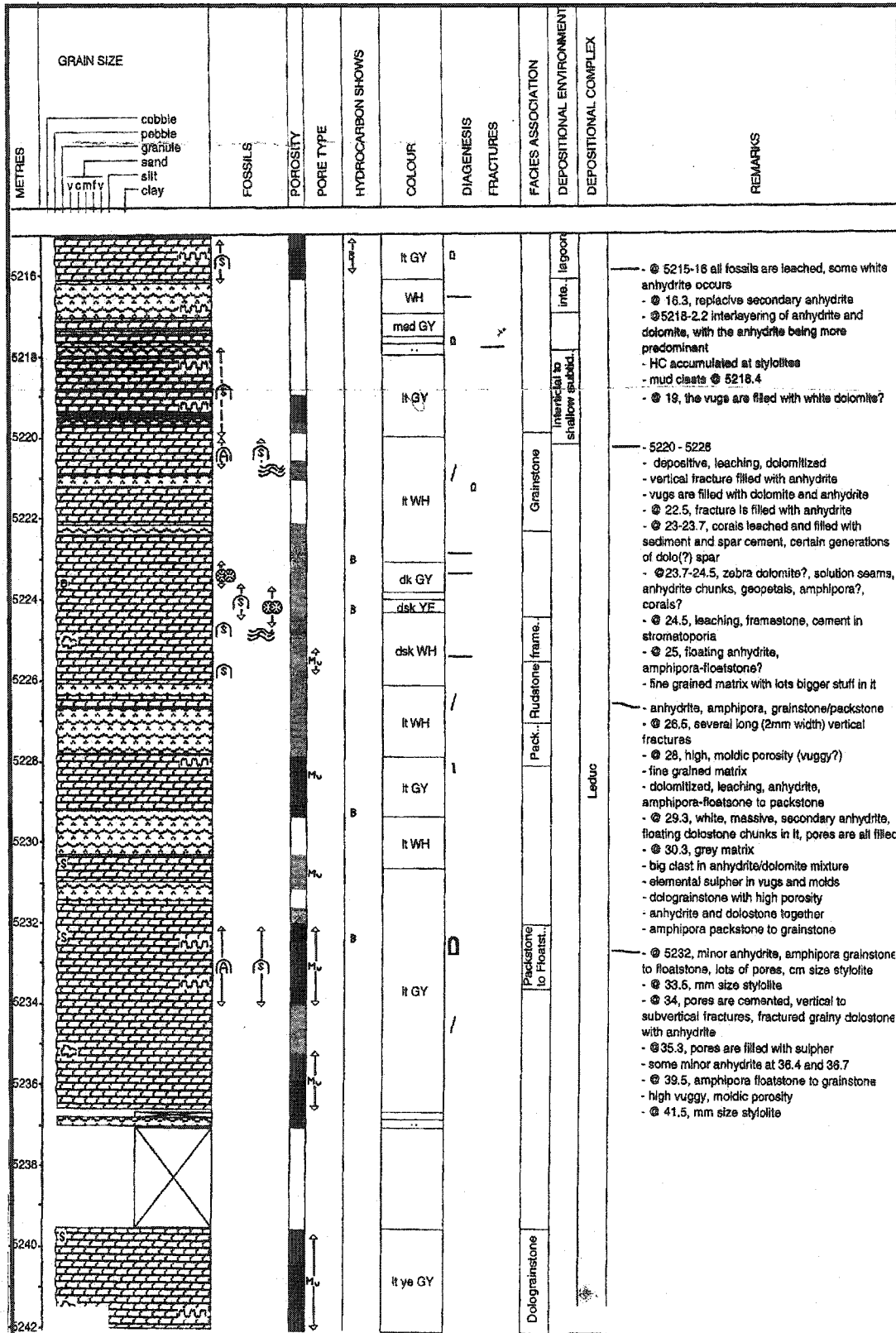
1-16-55-27W5
Core #1



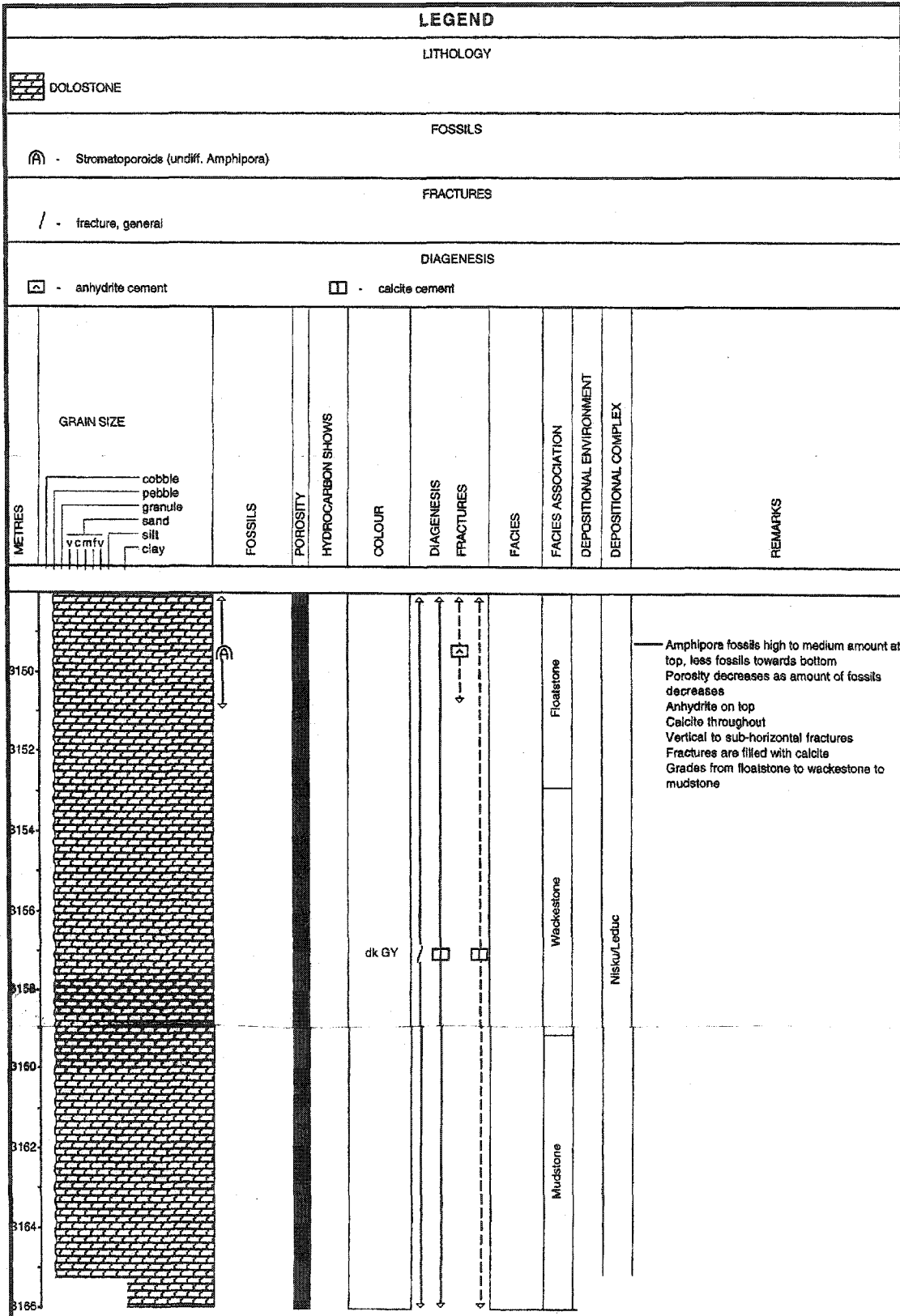
1-16-55-27W5
core #2

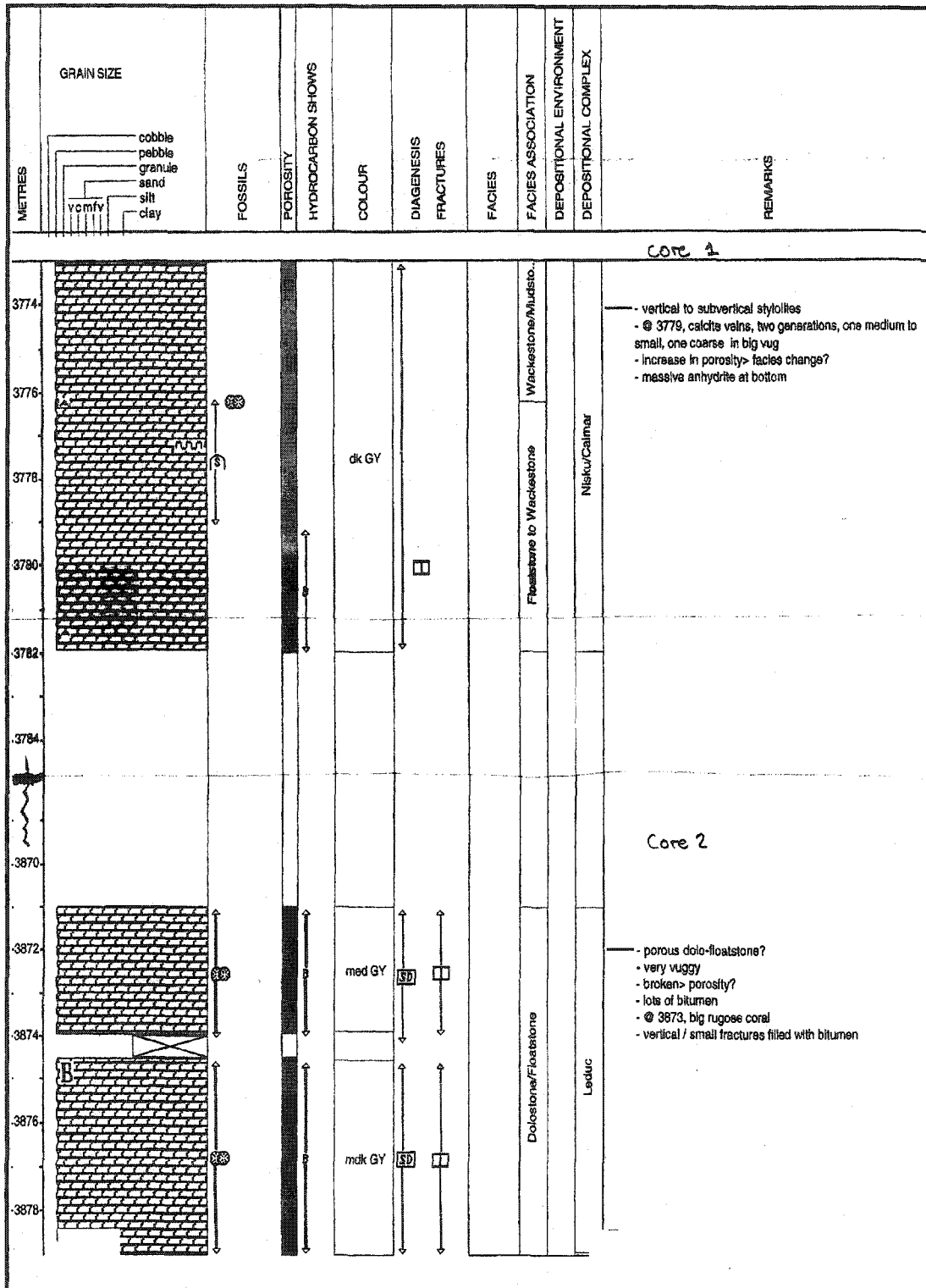


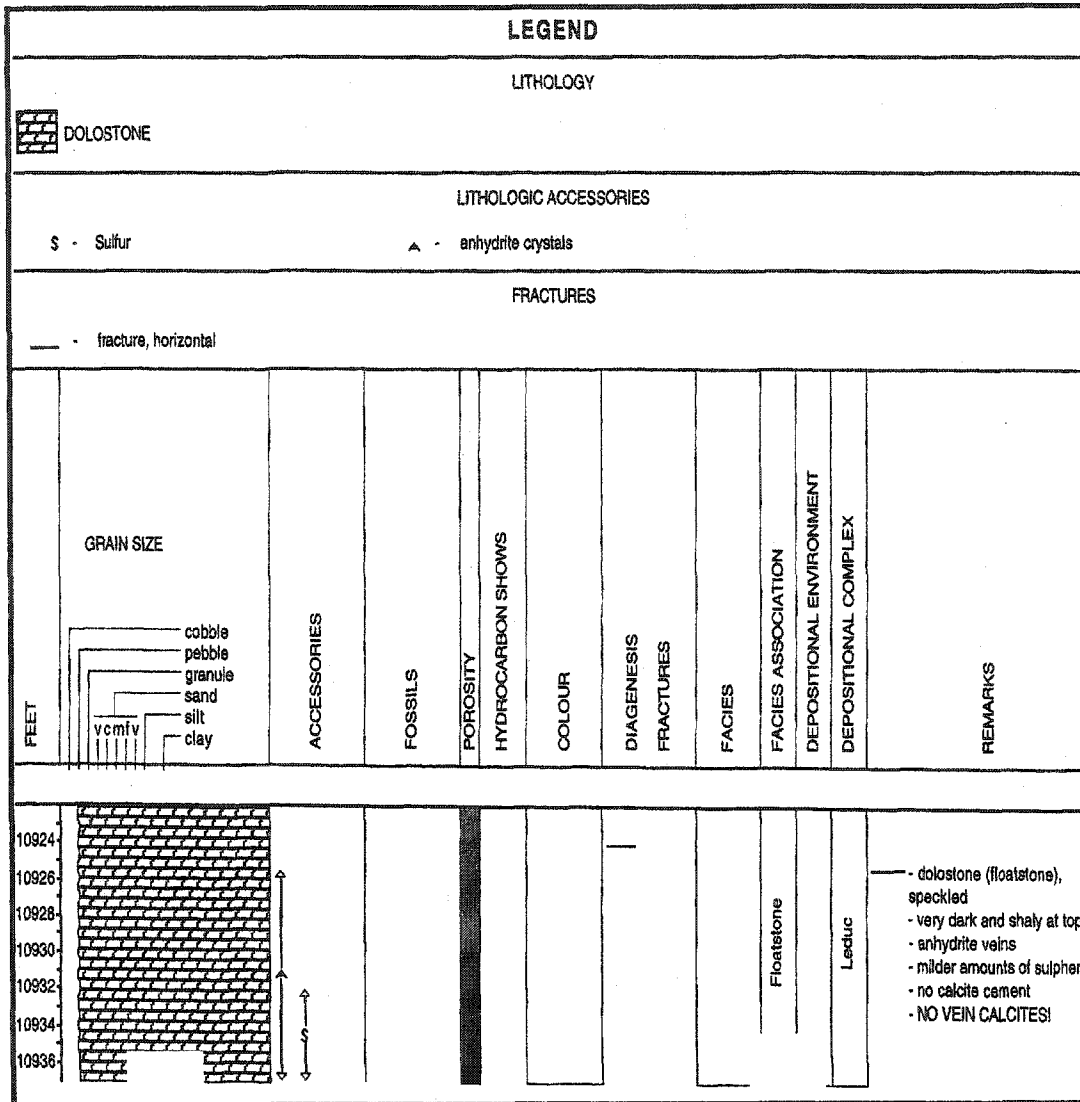


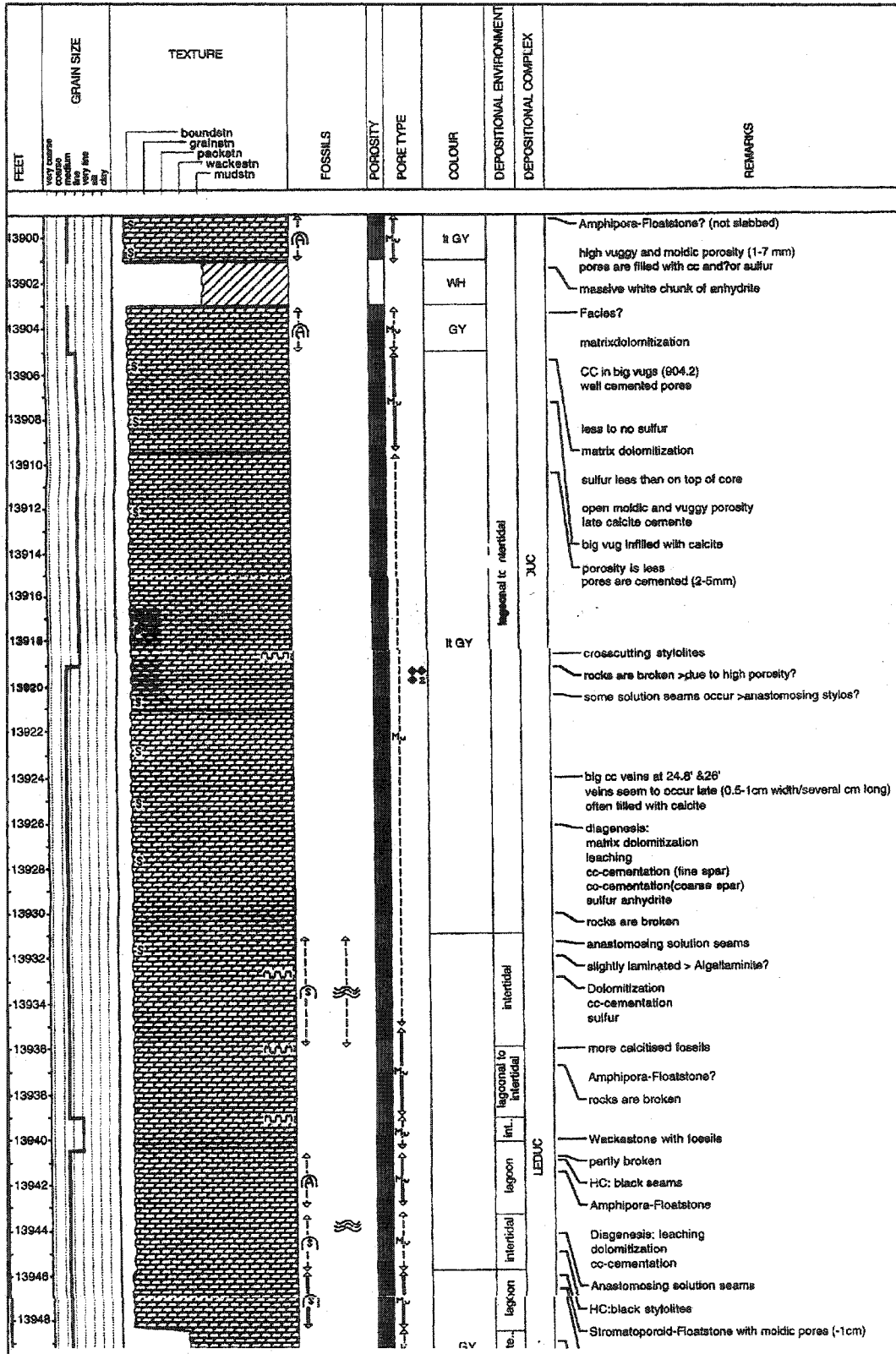


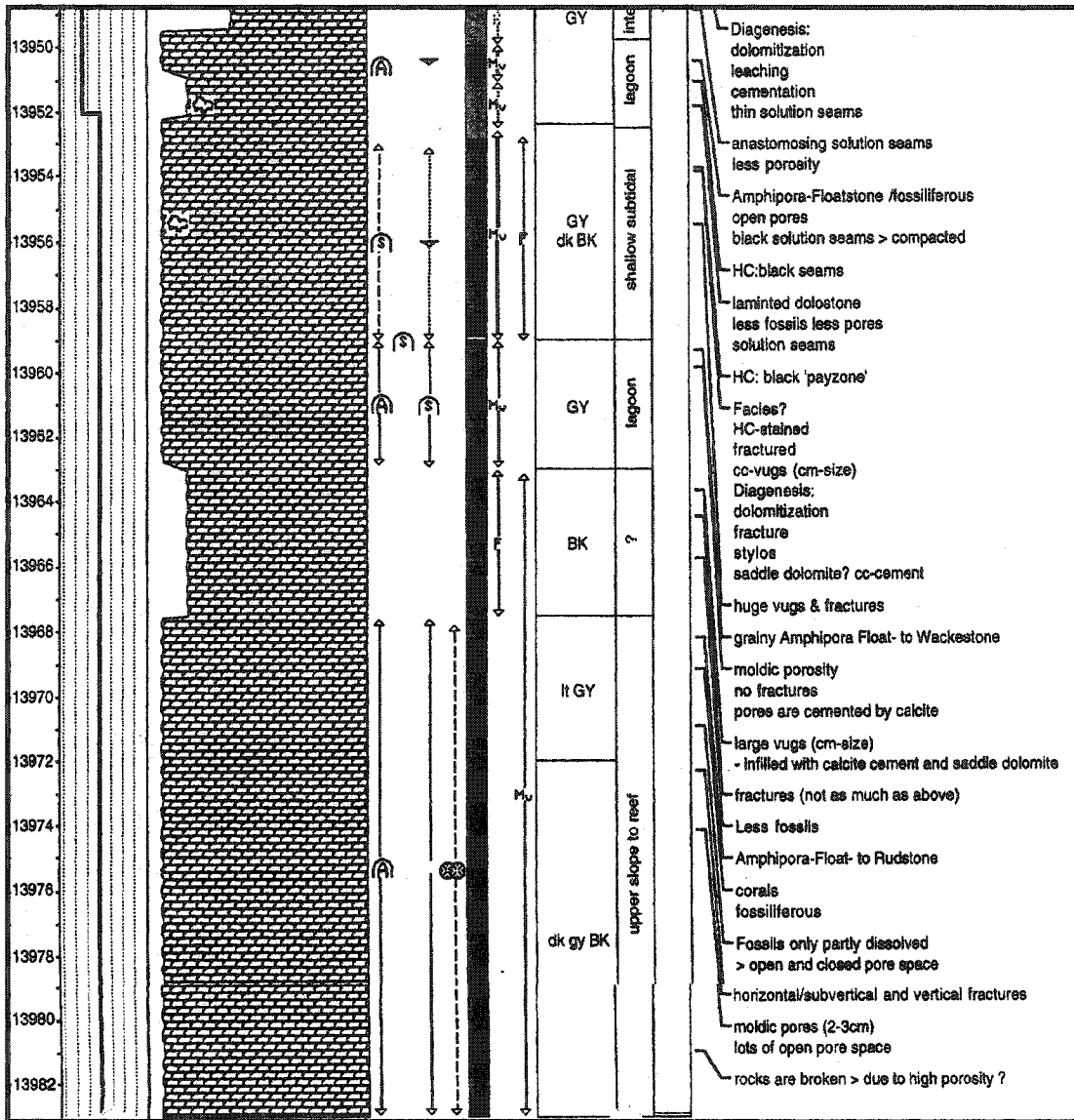
15-9-57-17W5

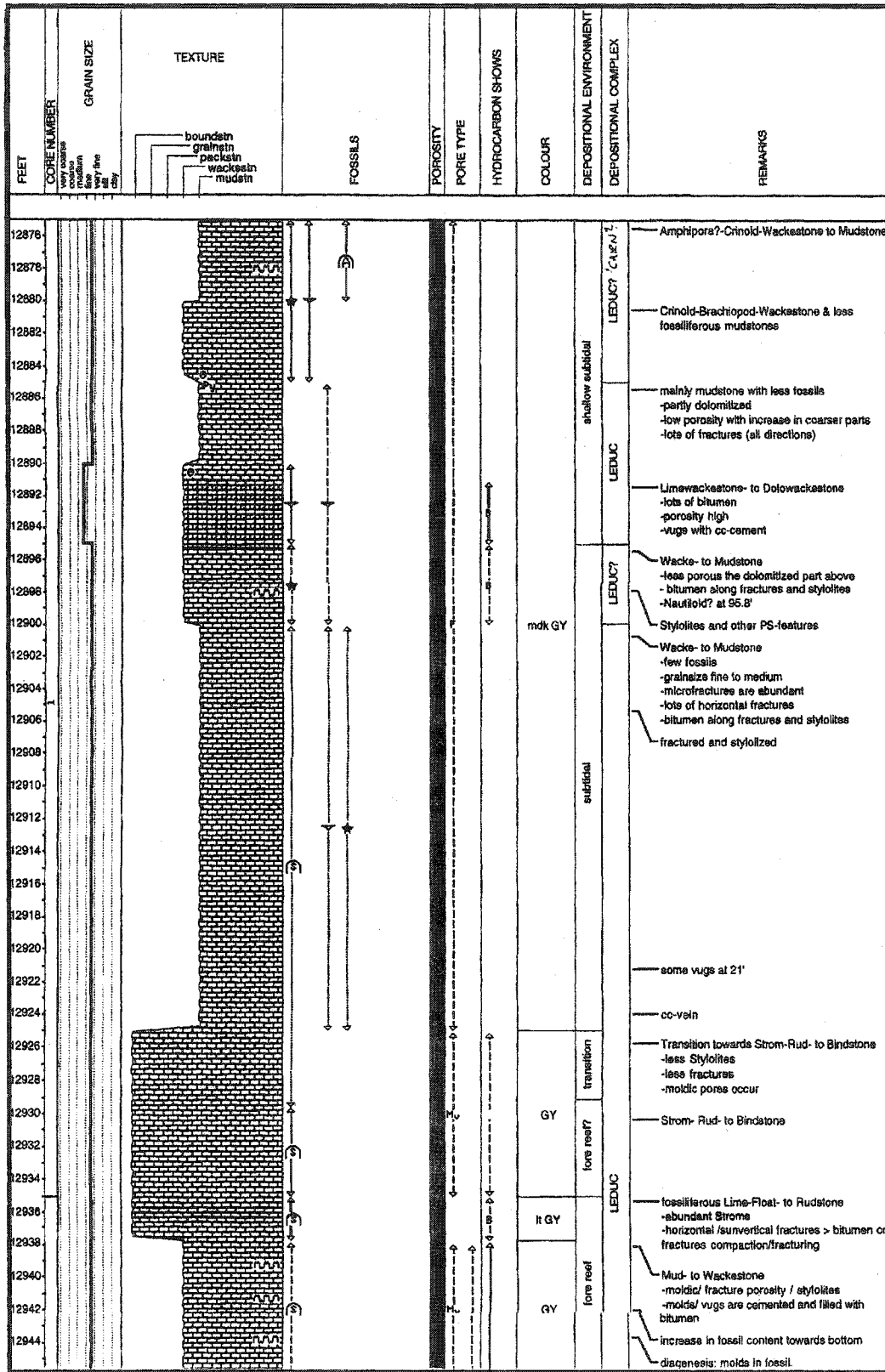


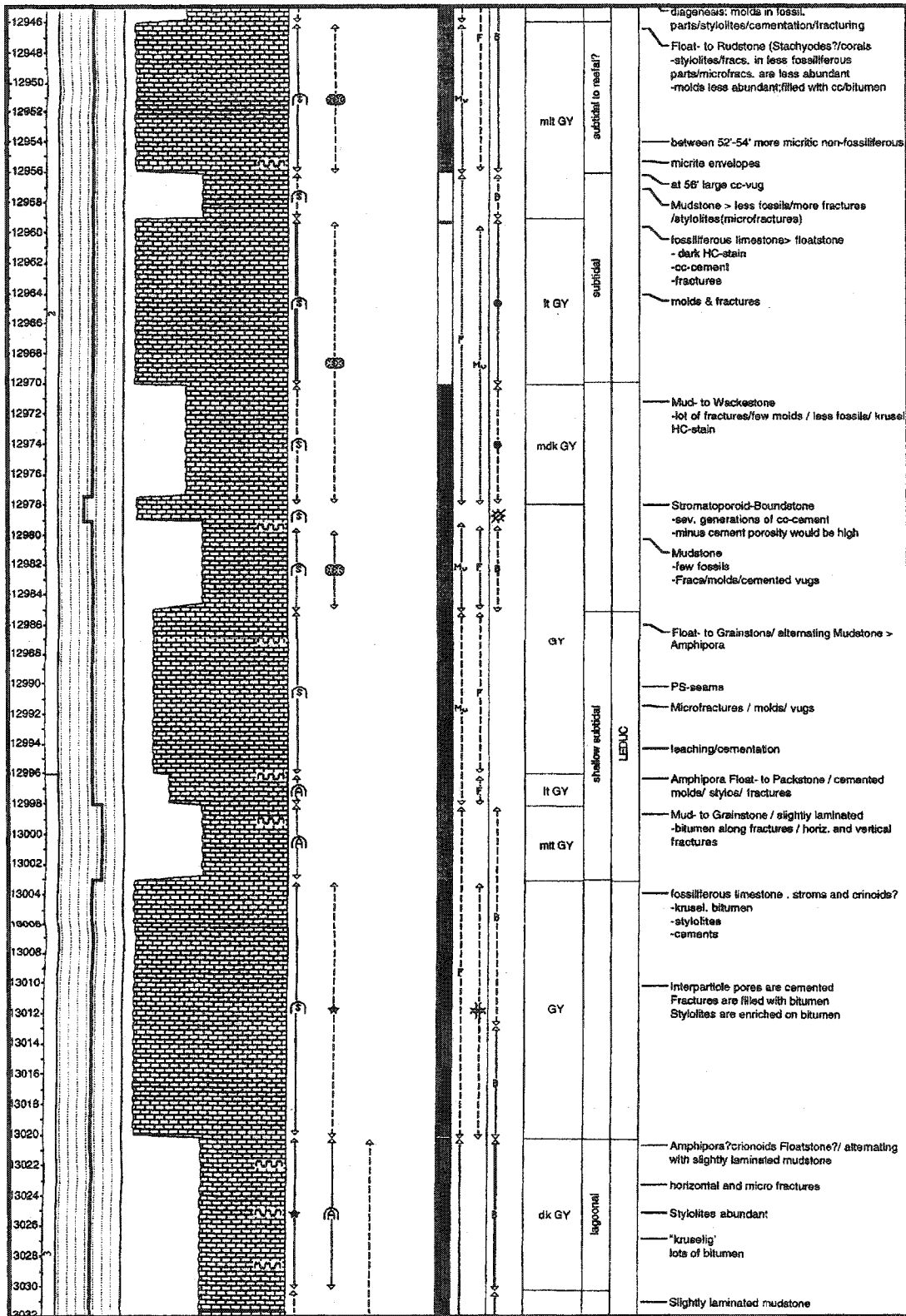


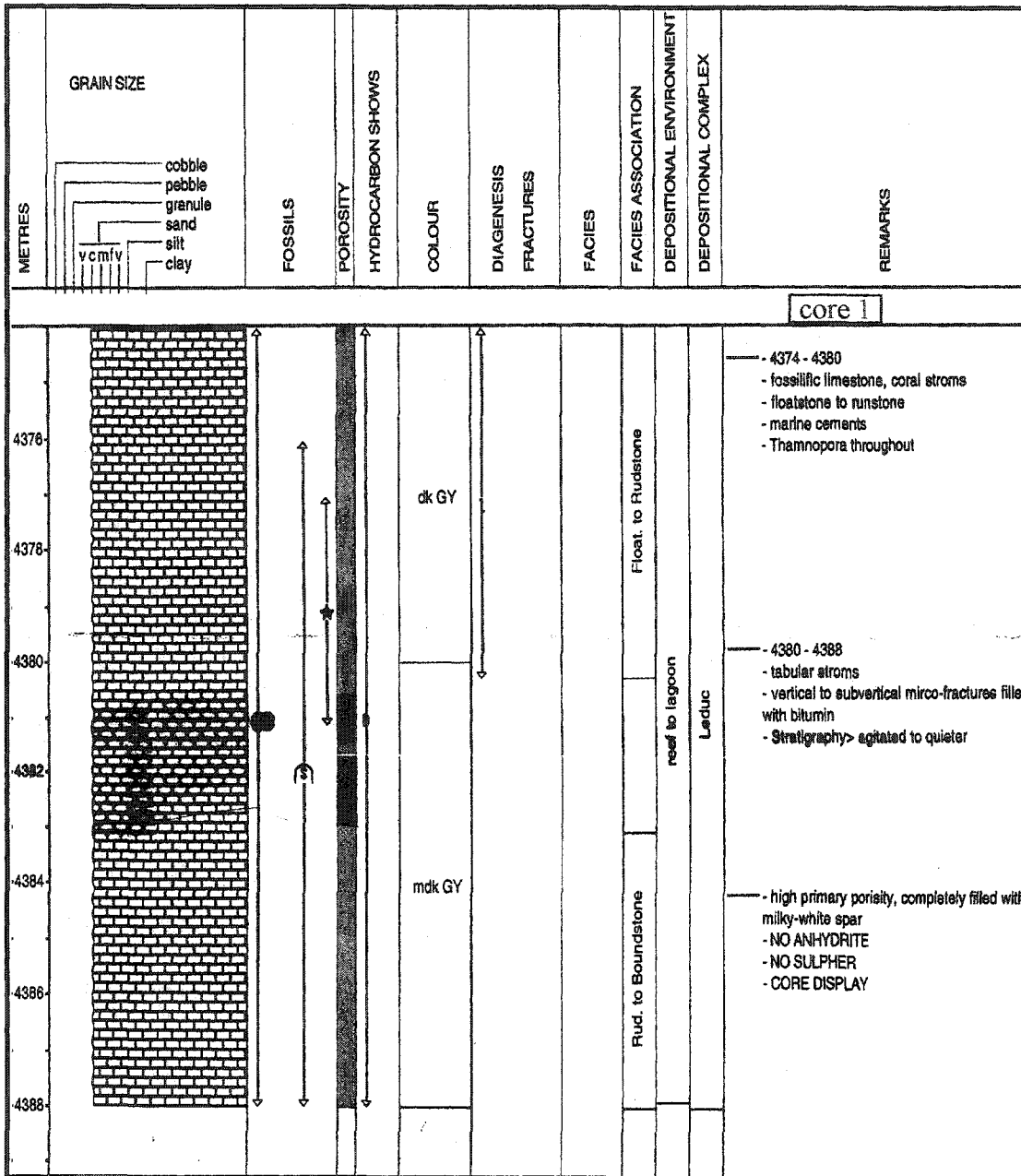


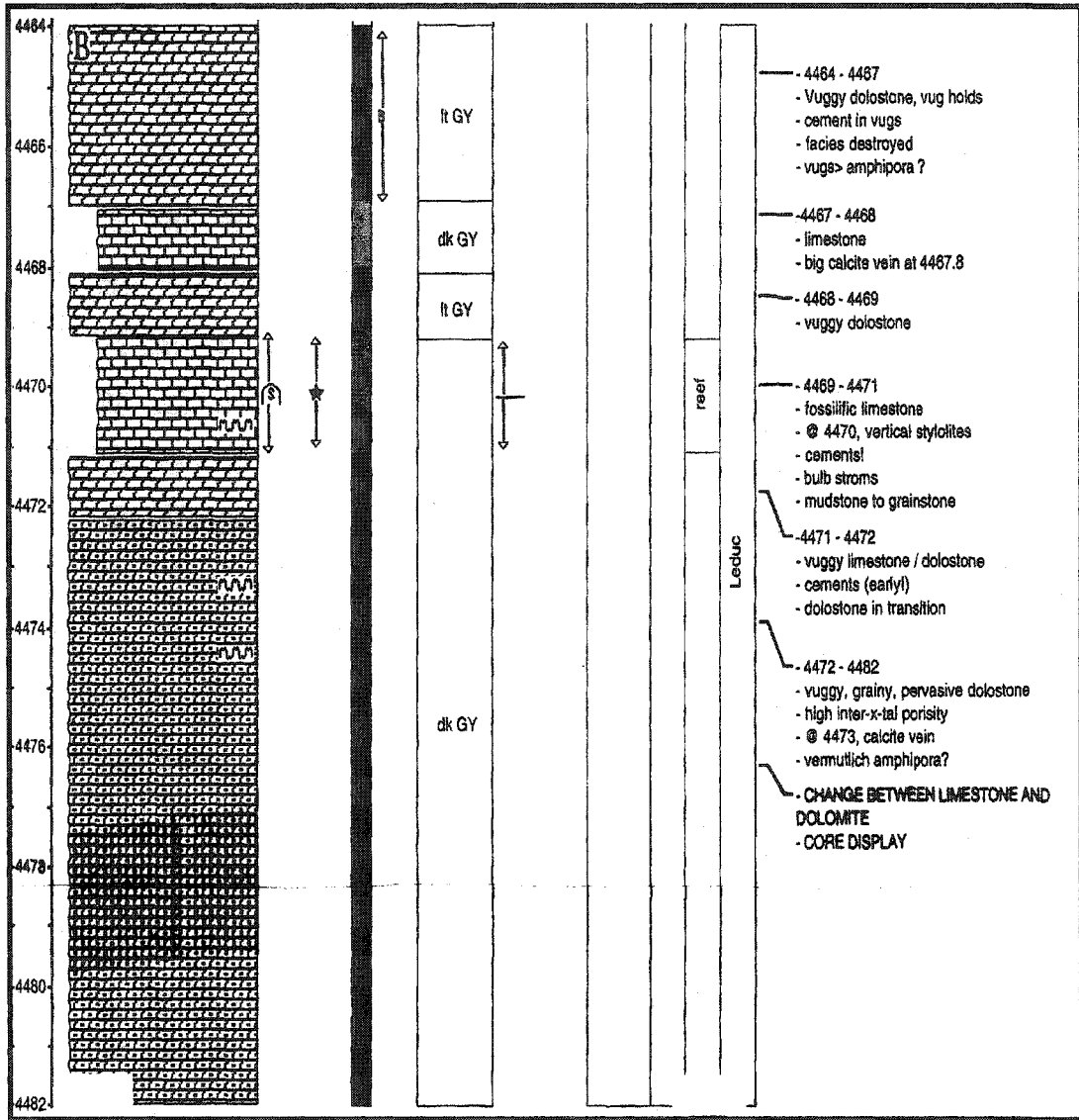


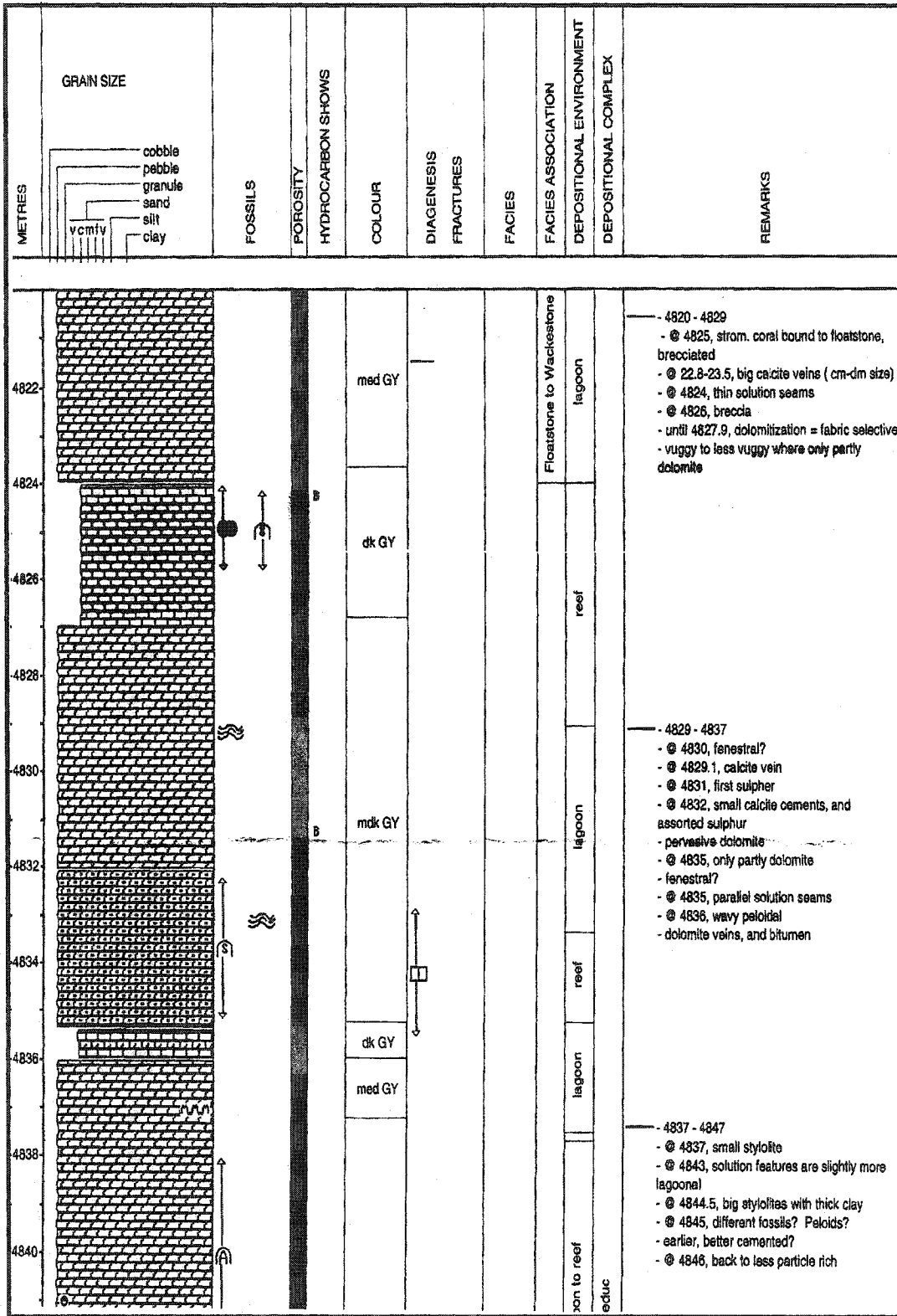


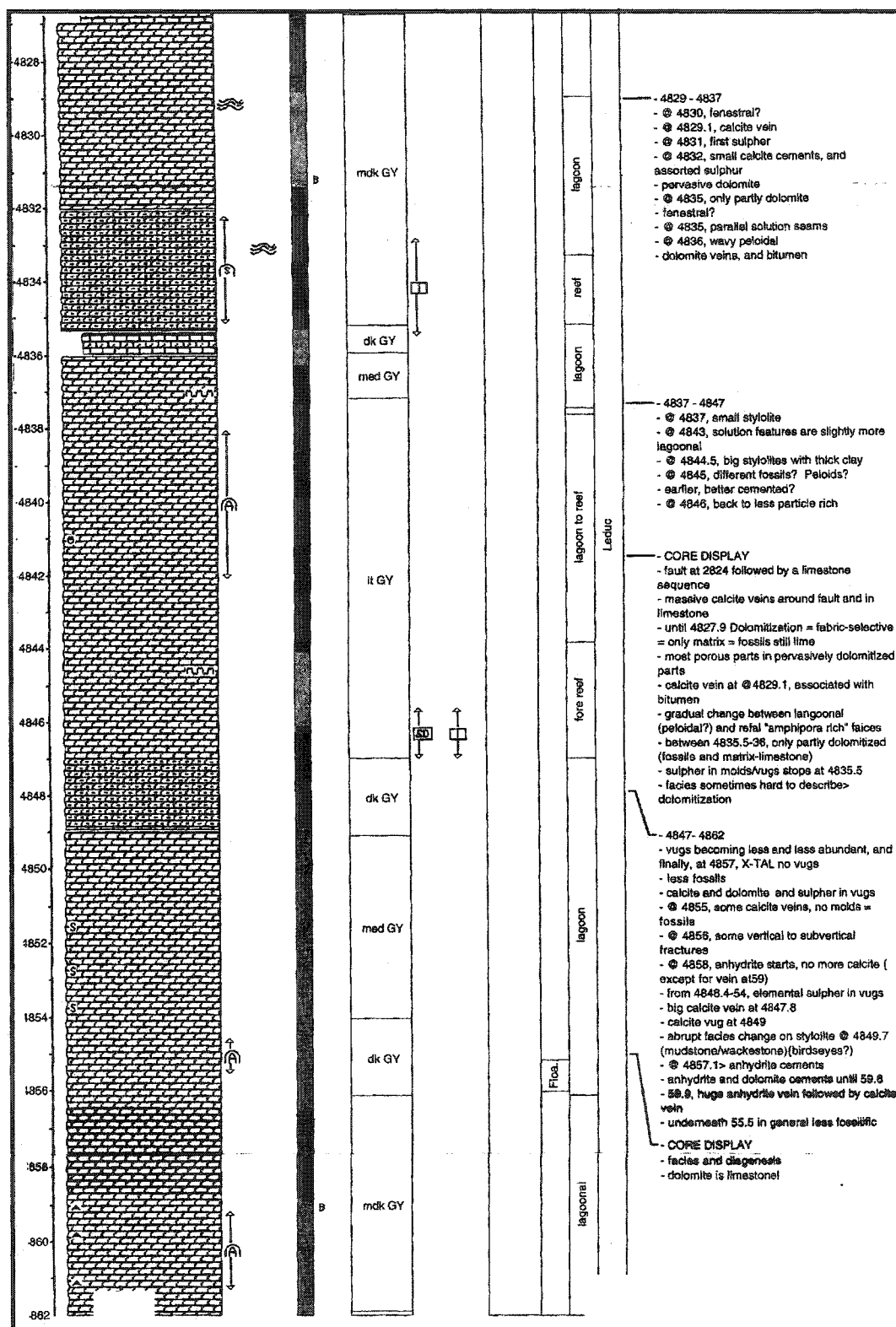












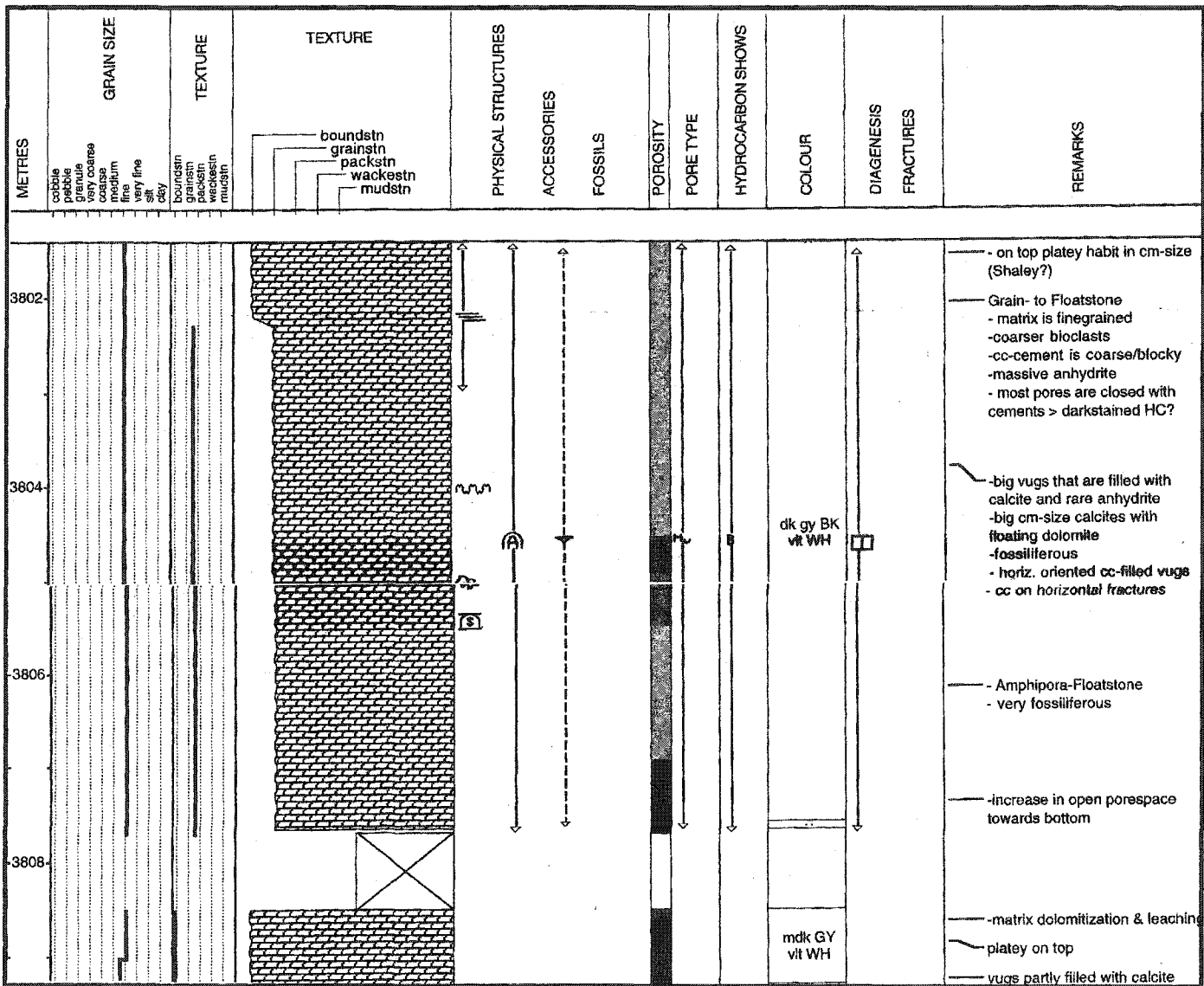
- 4829 - 4837
 - @ 4830, fenestral?
 - @ 4829.1, calcite vein
 - @ 4831, first sulphur
 - @ 4832, small calcite cements, and assorted sulphur
 - pervasive dolomite
 - @ 4835, only partly dolomite
 - fenestral?
 - @ 4835, parallel solution seams
 - @ 4836, wavy peloidal
 - dolomite veins, and bitumen

- 4837 - 4847
 - @ 4837, small stylonite
 - @ 4843, solution features are slightly more lagoonal
 - @ 4844.5, big stylonites with thick clay
 - @ 4845, different fossils? Peloids?
 - earlier, better cemented?
 - @ 4846, back to less particle rich

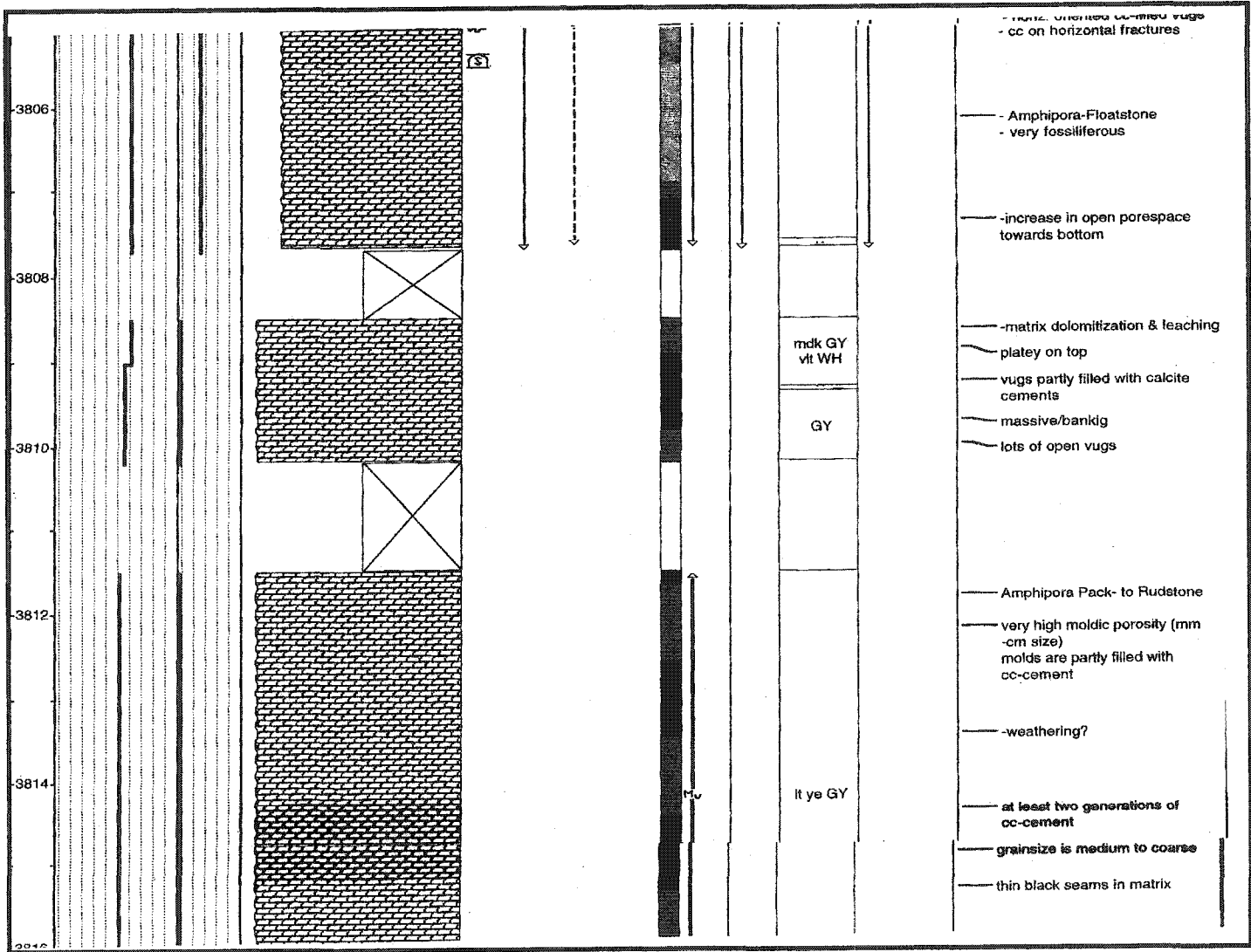
- CORE DISPLAY
 - fault at 2824 followed by a limestone sequence
 - massive calcite veins around fault and in limestone
 - until 4827.9 Dolomitization = fabric-selective
 - = only matrix = fossils still lime
 - most porous parts in pervasively dolomitized parts
 - calcite vein at @ 4829.1, associated with bitumen
 - gradual change between lagoonal (peloidal?) and reef "amphipora rich" facies
 - between 4835.5-36, only partly dolomitized (fossils and matrix-limestone)
 - sulphur in molds/vugs stops at 4835.5
 - facies sometimes hard to describe - dolomitization

- 4847 - 4862
 - vugs becoming less and less abundant, and finally, at 4857, X-TAL no vugs
 - less fossils
 - calcite and dolomite and sulphur in vugs
 - @ 4855, some calcite veins, no molds = fossils
 - @ 4856, some vertical to subvertical fractures
 - @ 4858, anhydrite starts, no more calcite (except for vein at 59)
 - from 4848.4-54, elemental sulphur in vugs
 - big calcite vein at 4847.8
 - calcite vug at 4849
 - abrupt facies change on stylonite @ 4849.7 (mudstone/wackestone)(birdseyes?)
 - @ 4857.1 - anhydrite cements
 - anhydrite and dolomite cements until 59.8
 - 59.8, huge anhydrite vein followed by calcite vein
 - underneath 55.5 in general less fossiliferous

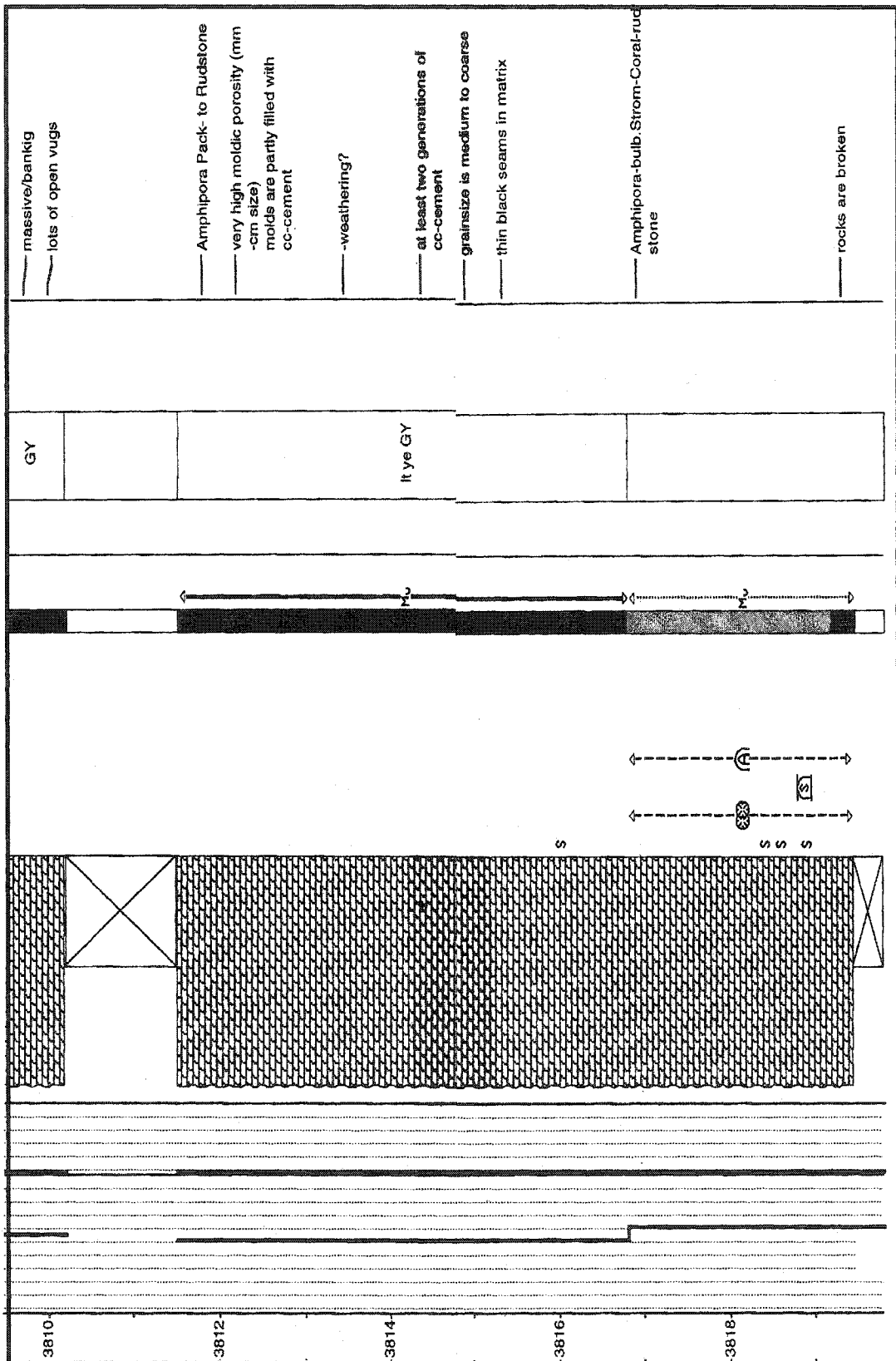
- CORE DISPLAY
 - facies and diagenesis
 - dolomite is limestone!

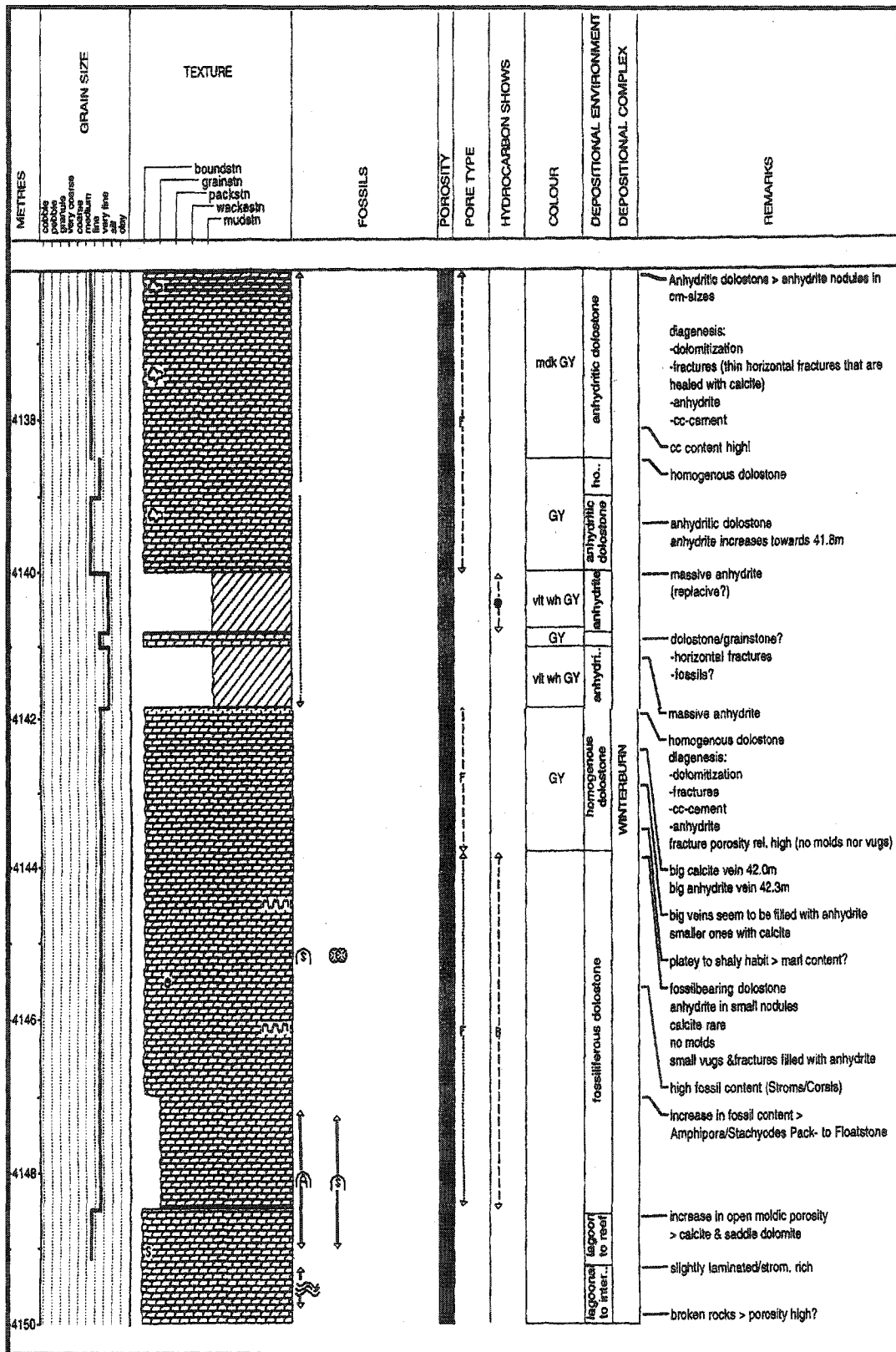


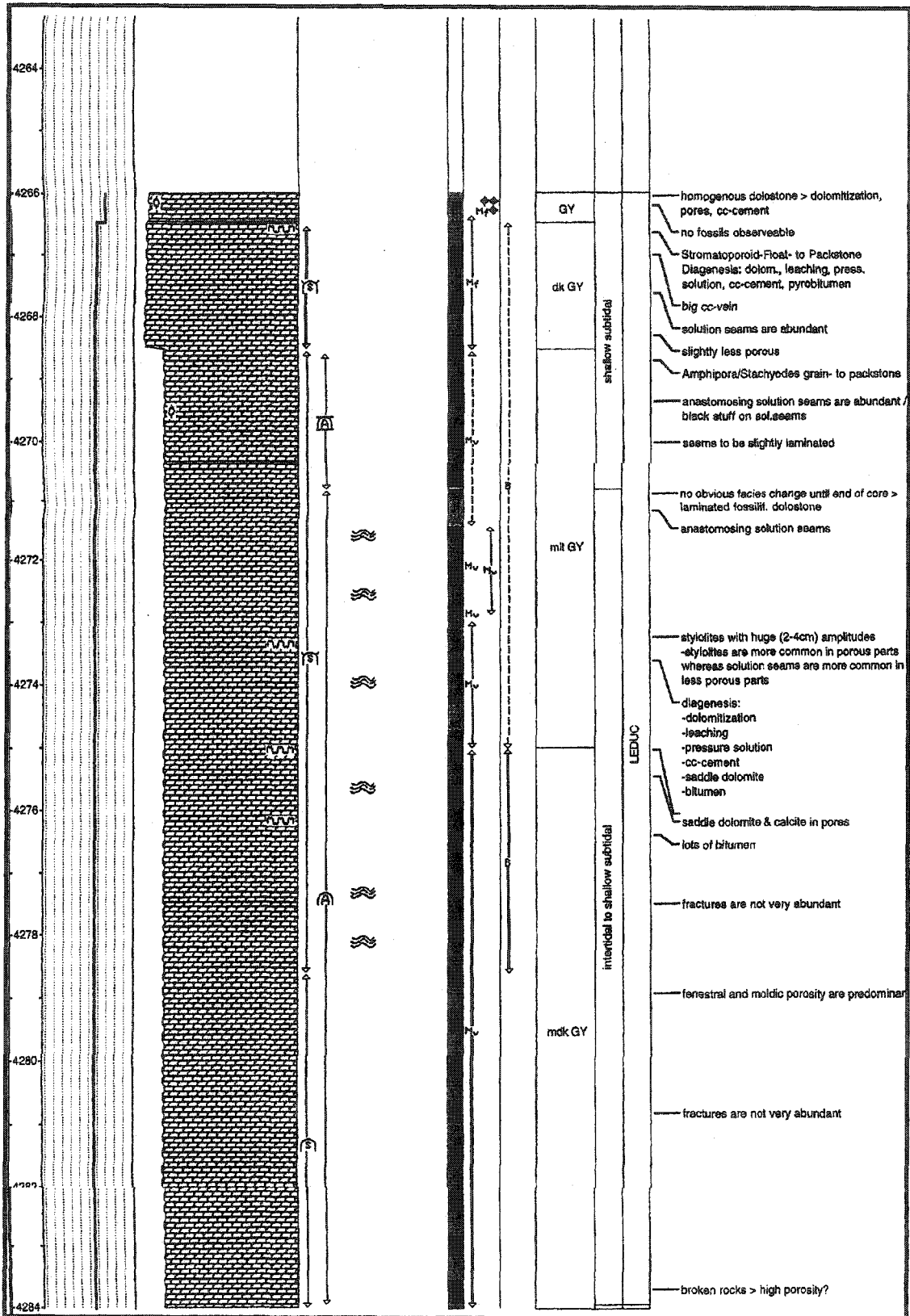
1_09-20-59-22WS

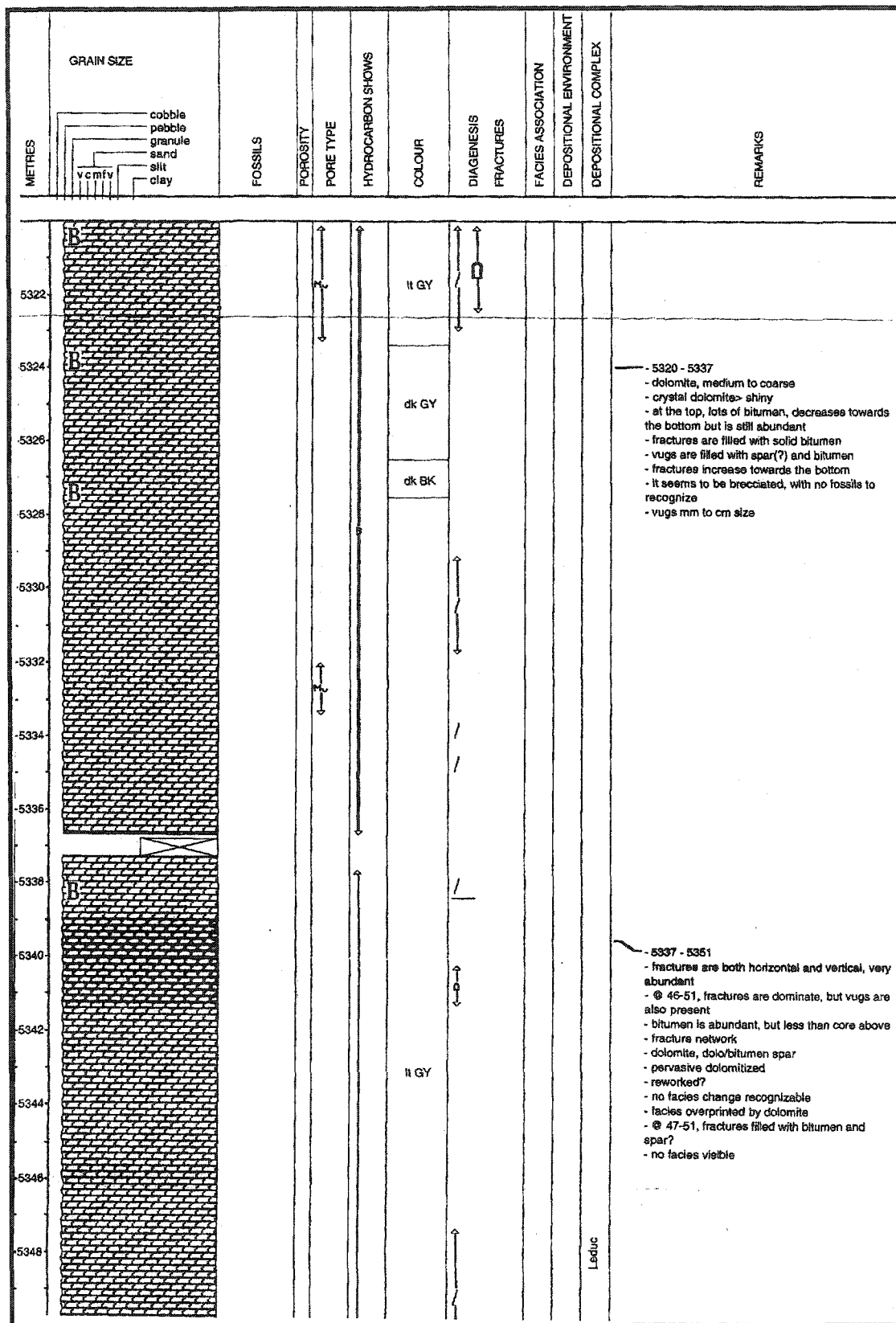


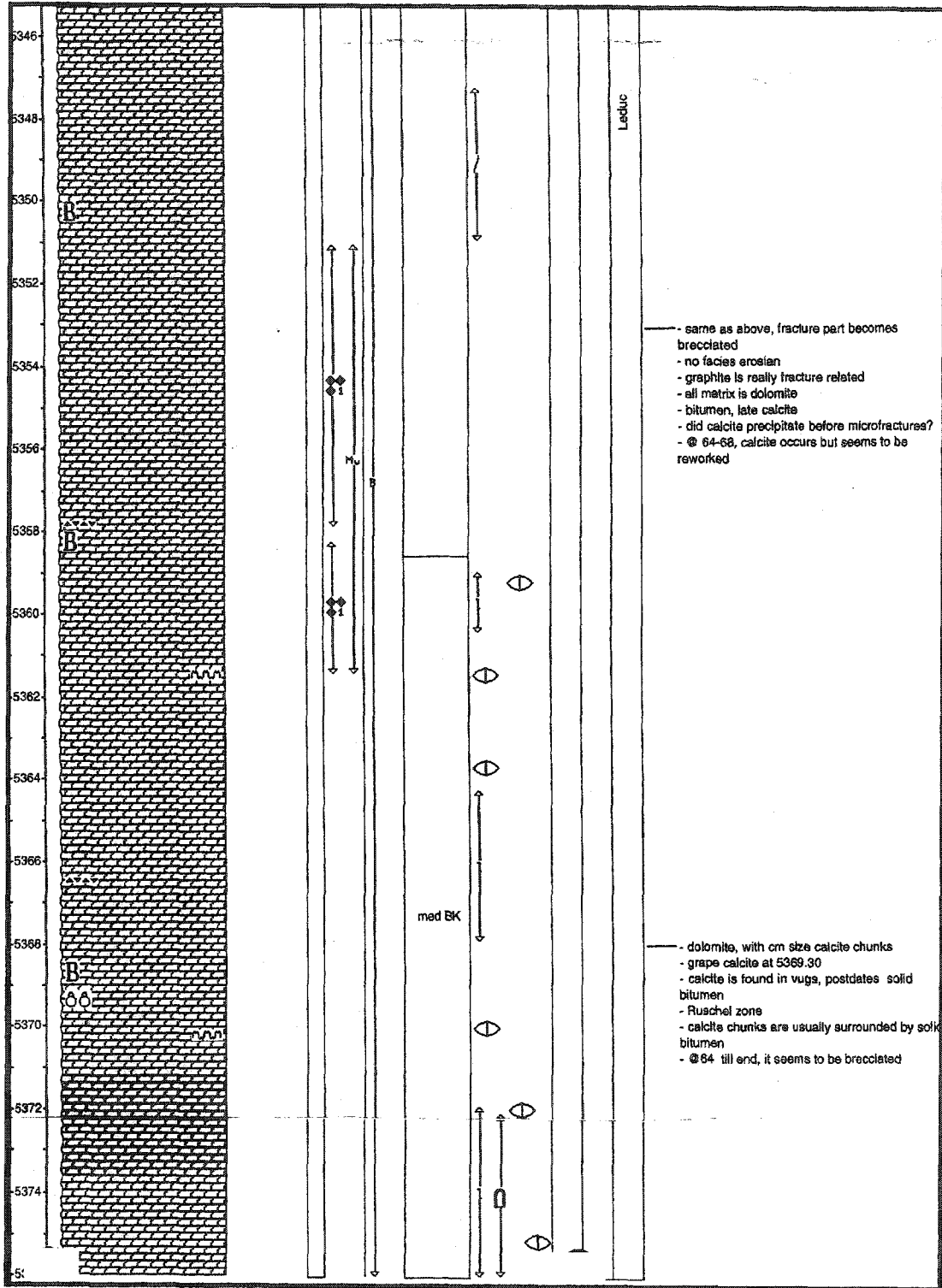
2_09-20-59-22W5

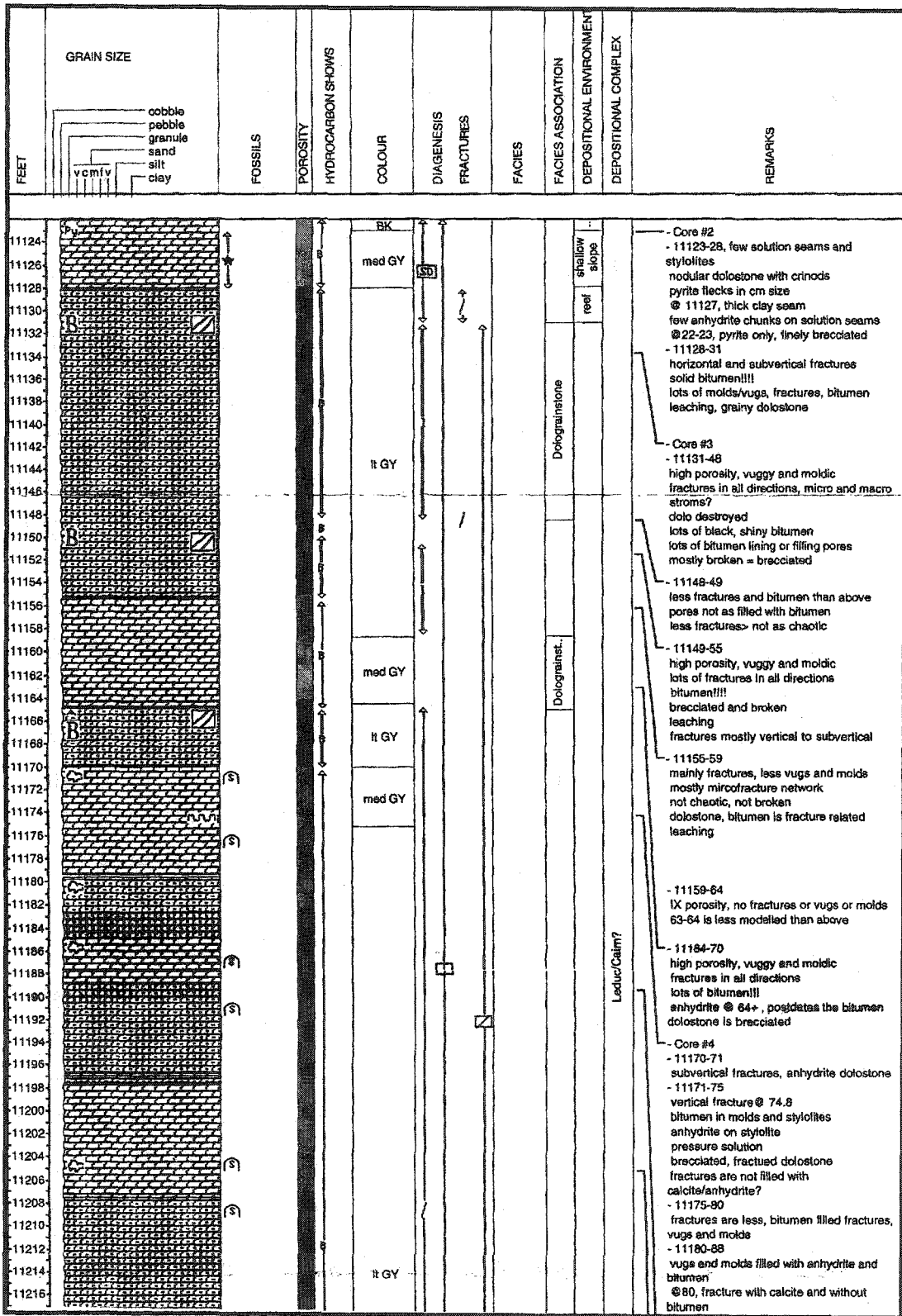


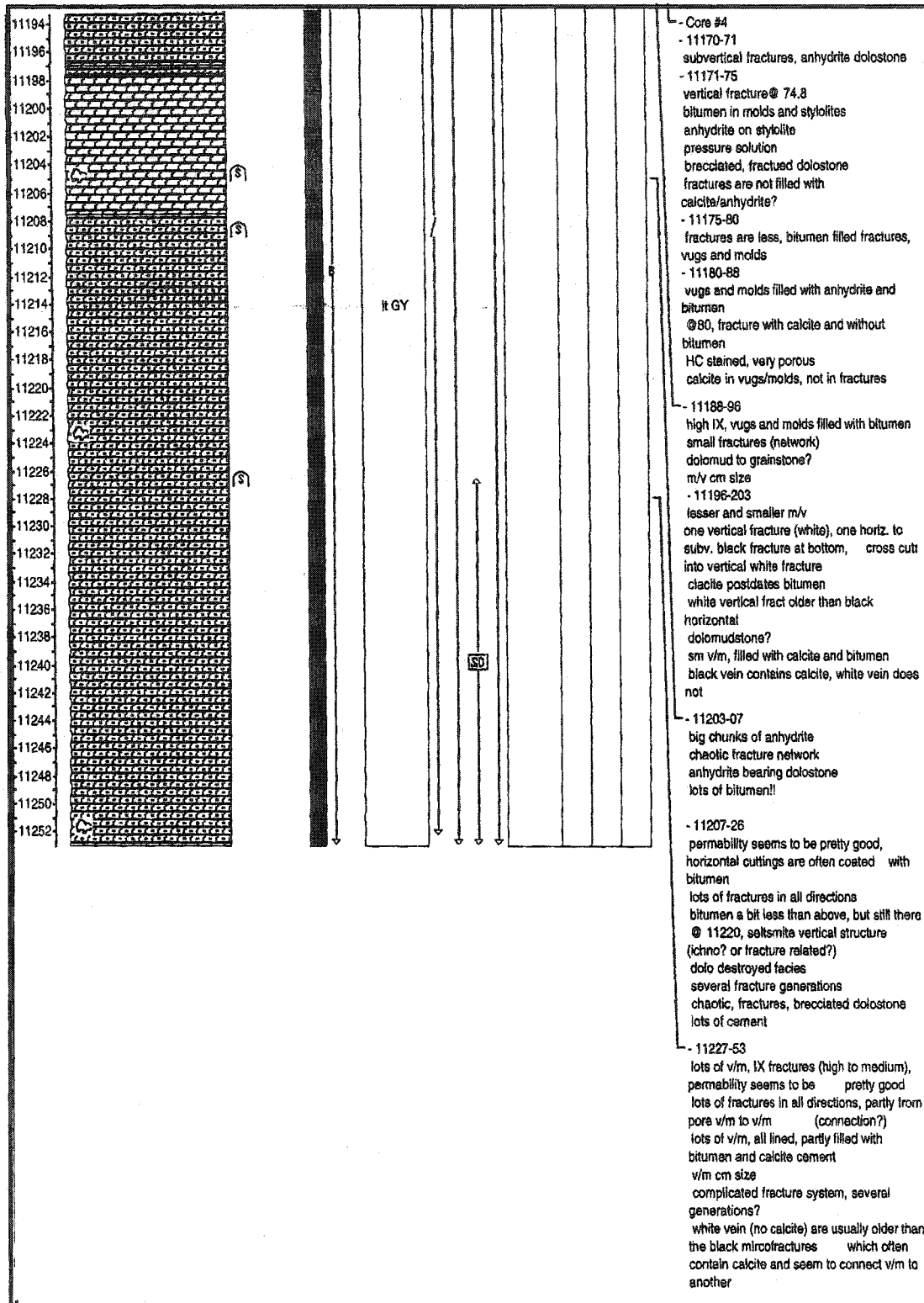


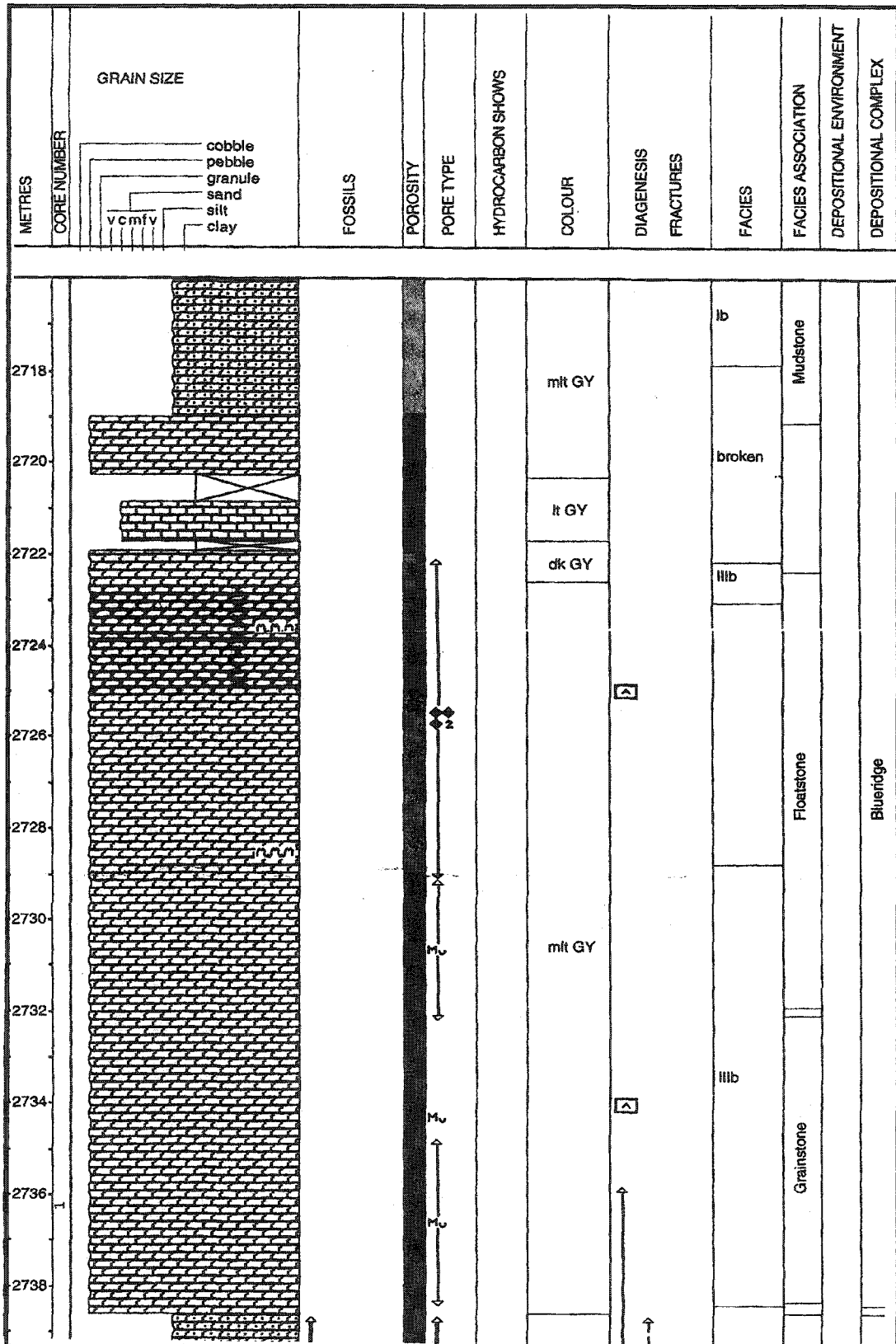


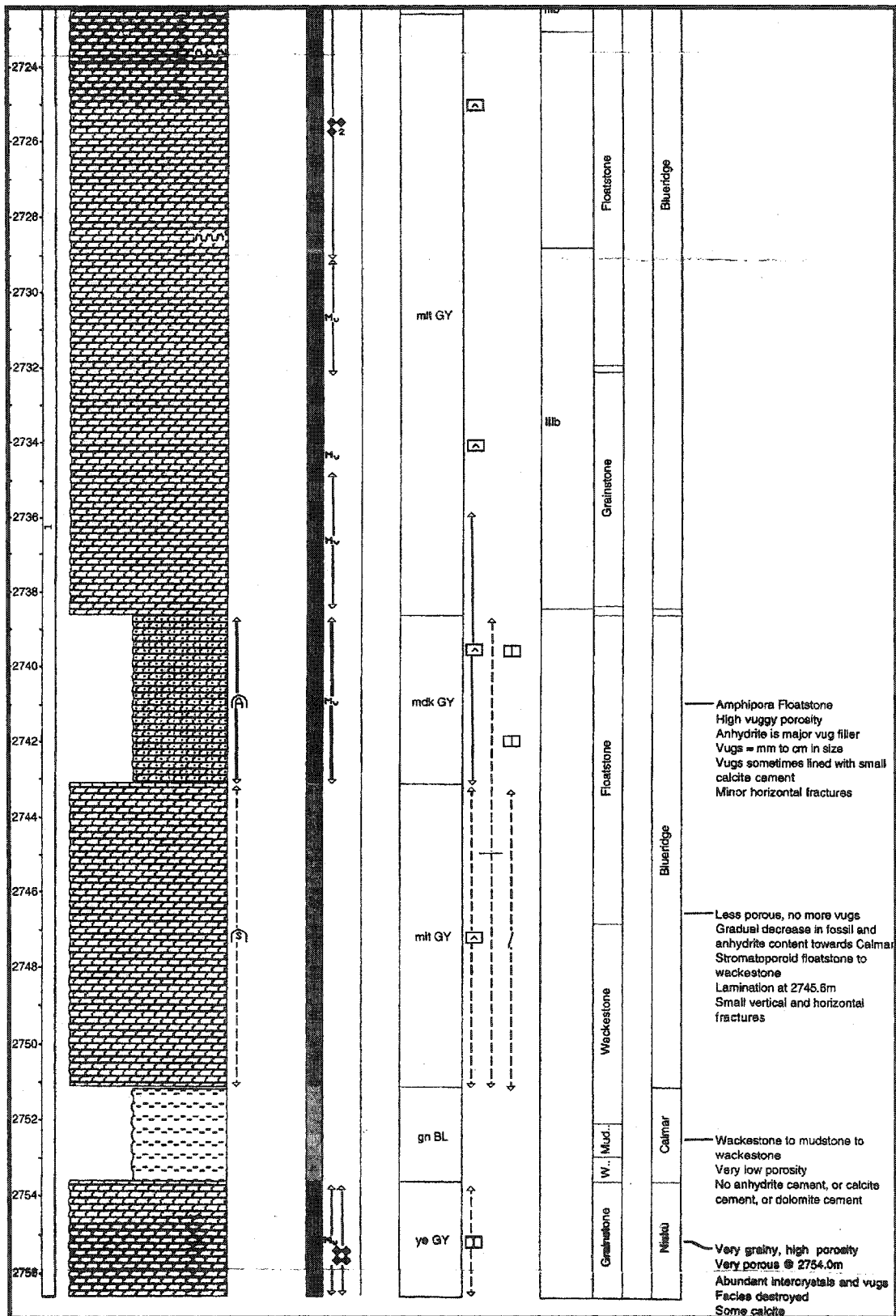


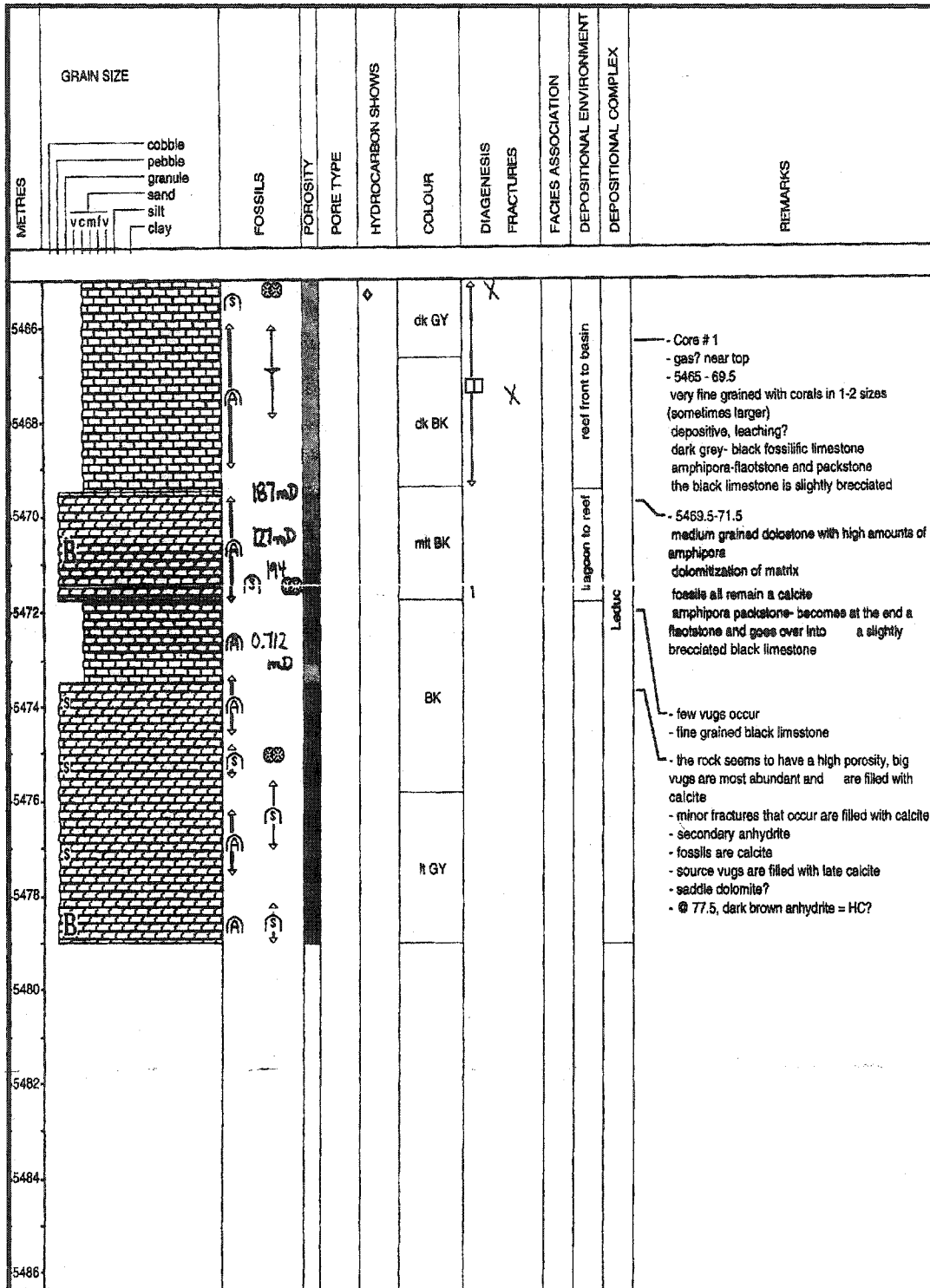


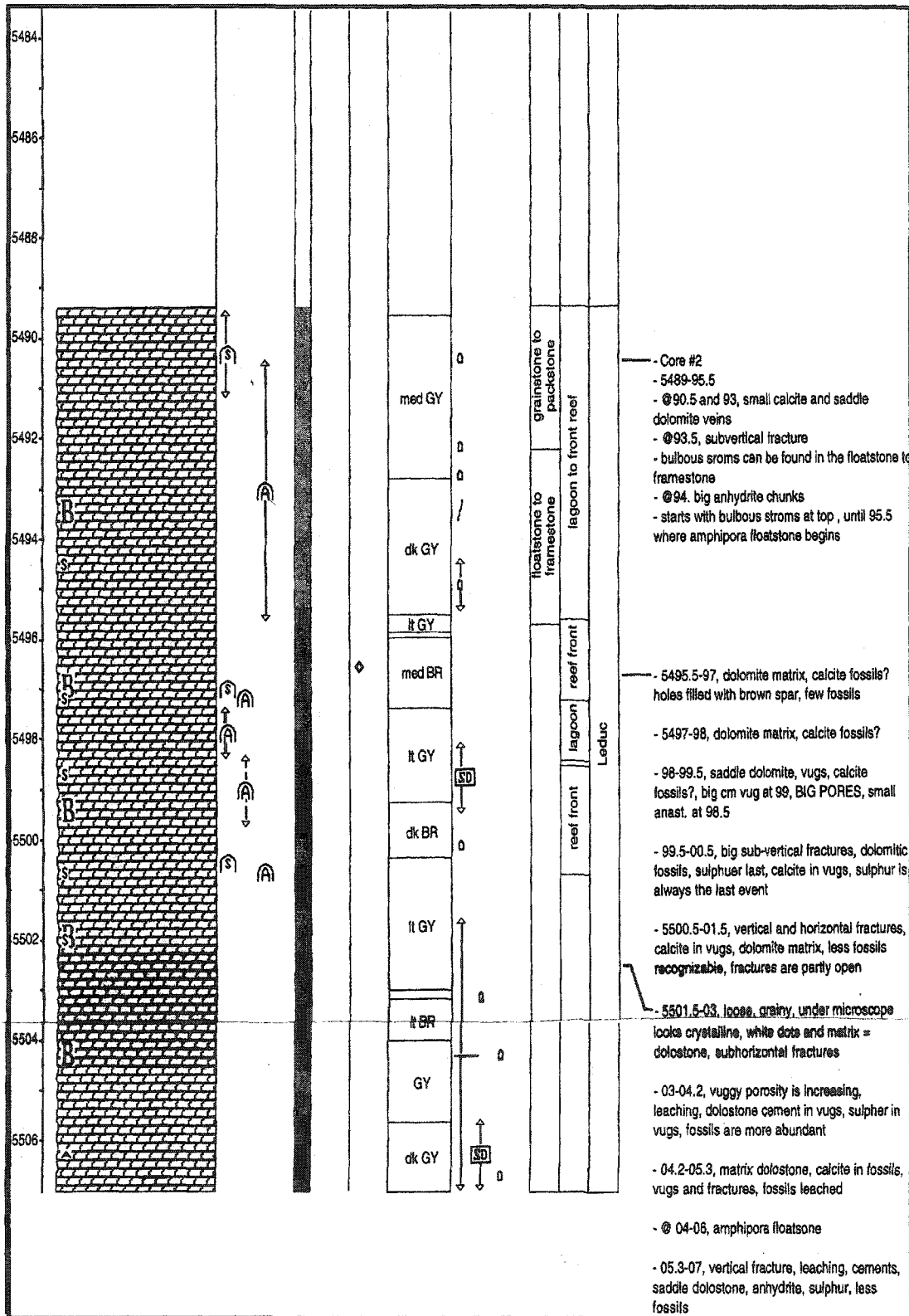






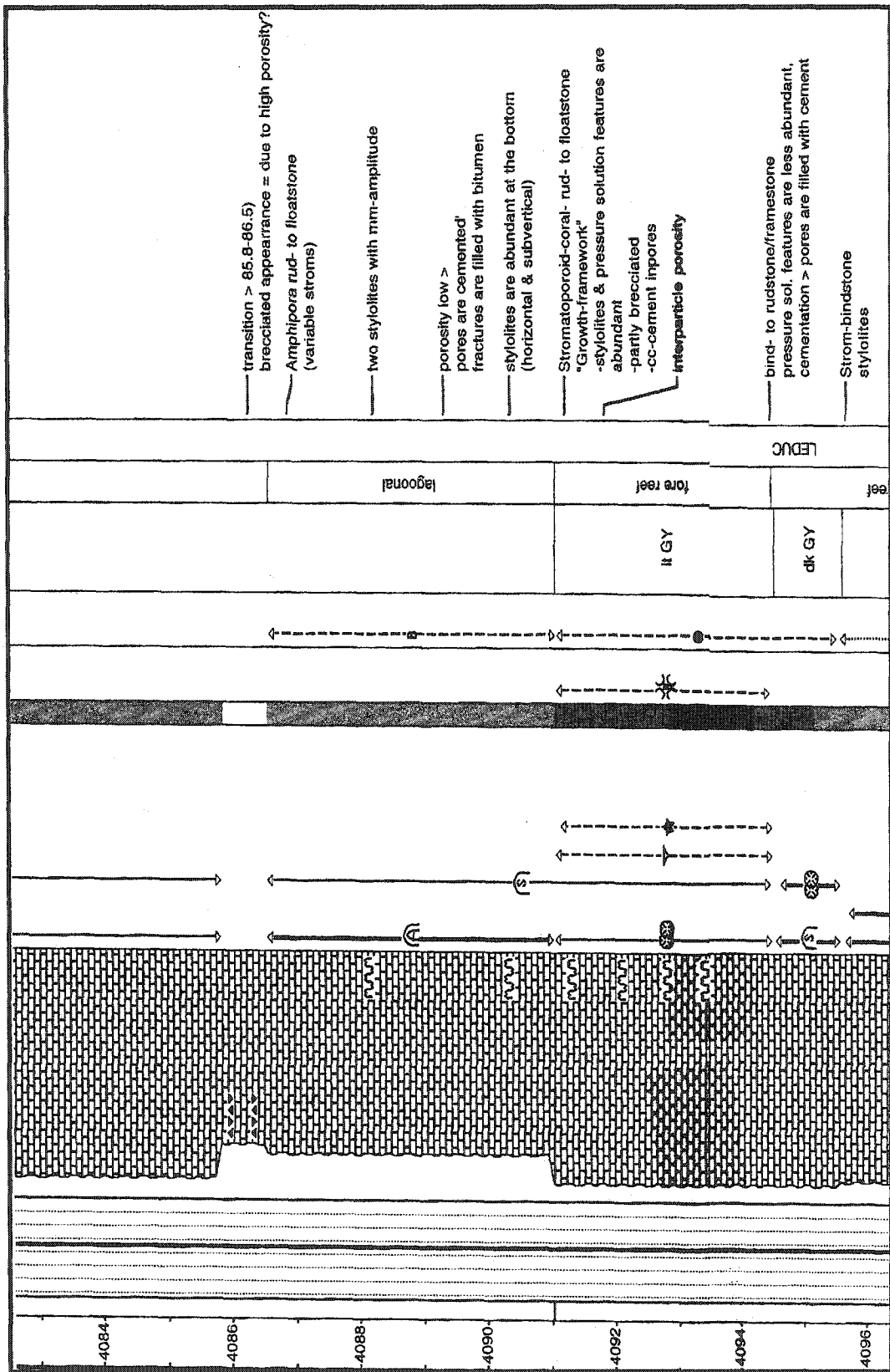


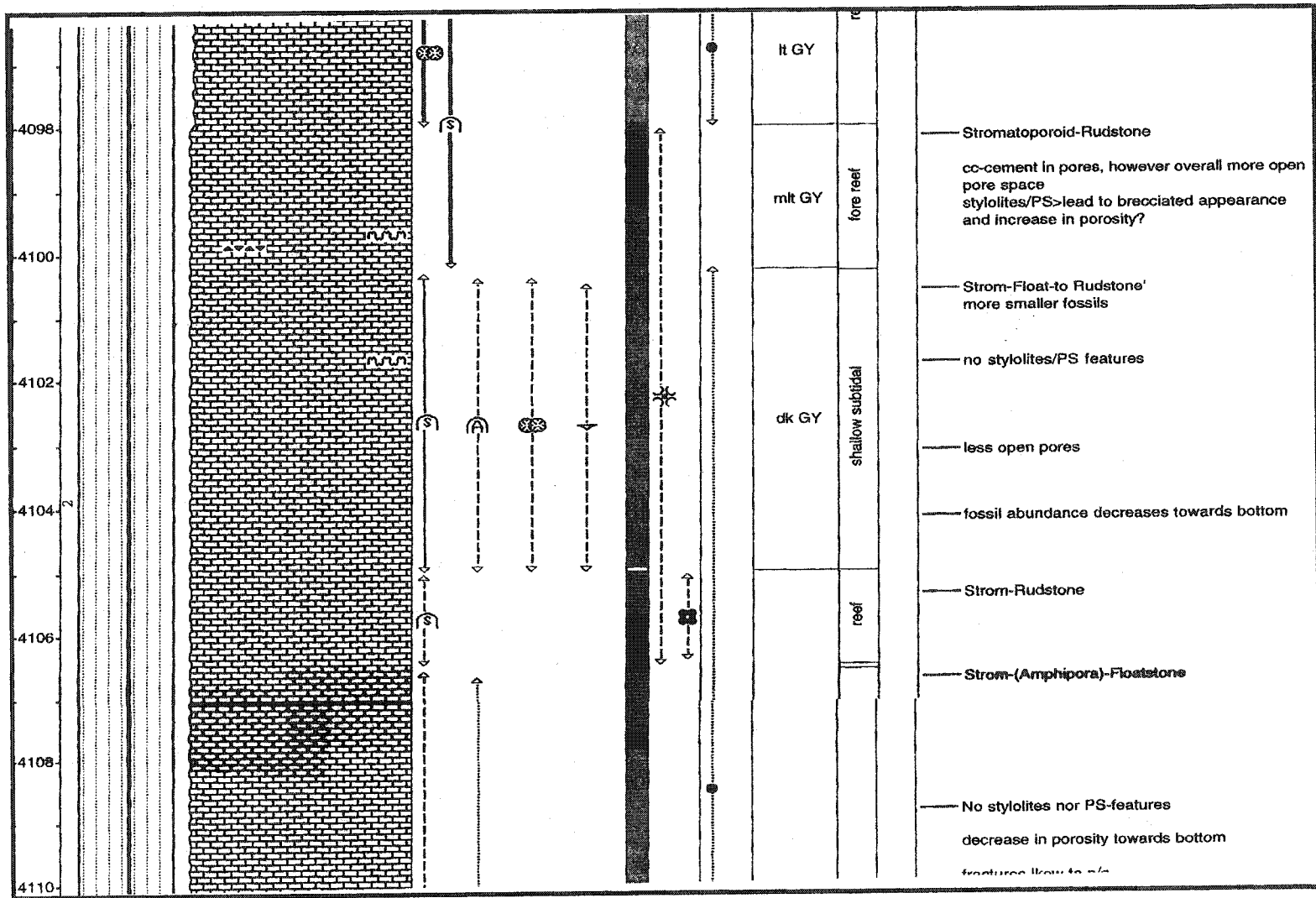




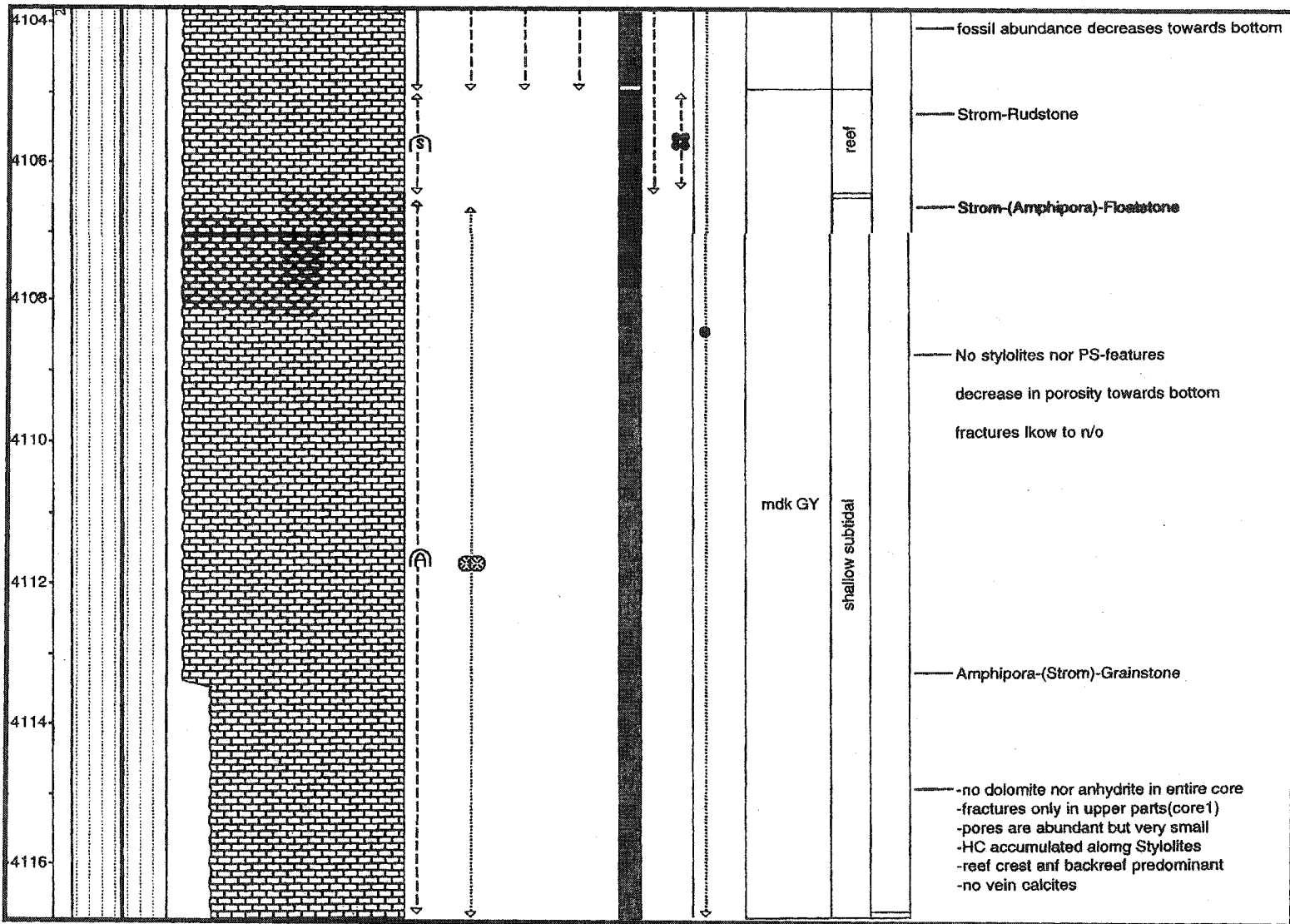
METRES	CORE NUMBER	GRAIN SIZE	TEXTURE	FOSSILS	POROSITY	PORE TYPE	HYDROCARBON SHOWS	COLOUR	DEPOSITIONAL ENVIRONME	DEPOSITIONAL COMPLEX	REMARKS
4074 4076 4078 4080 4082 4084		very coarse coarse medium fine very fine silt clay	boundstn grainstn packstn wackestn mudstn					mdk GY	reef back reef?	<ul style="list-style-type: none"> Amphipora pack- to rudstone, partly laminated, partly branching stroms (74.65) porosity low, microfractures are filled with bitumen, molds are filled with calcite cc-filled mold at 75.45 diagenesis: deposition, leaching, cc-cementation, fracturing, bitumen emplacement strom. bind- to rudstone, bulbous massive stroms, corals (thamnopora, Alveolites) micrite envelopes almost all porespace is cemented, microfractures occur and contain HC Diagenesis: <ul style="list-style-type: none"> -deposition -recryst.? -some leaching -cementation strom bind- to rudstone porosity slightly higher > less cement in molds 	

1_15-19-56-23WS

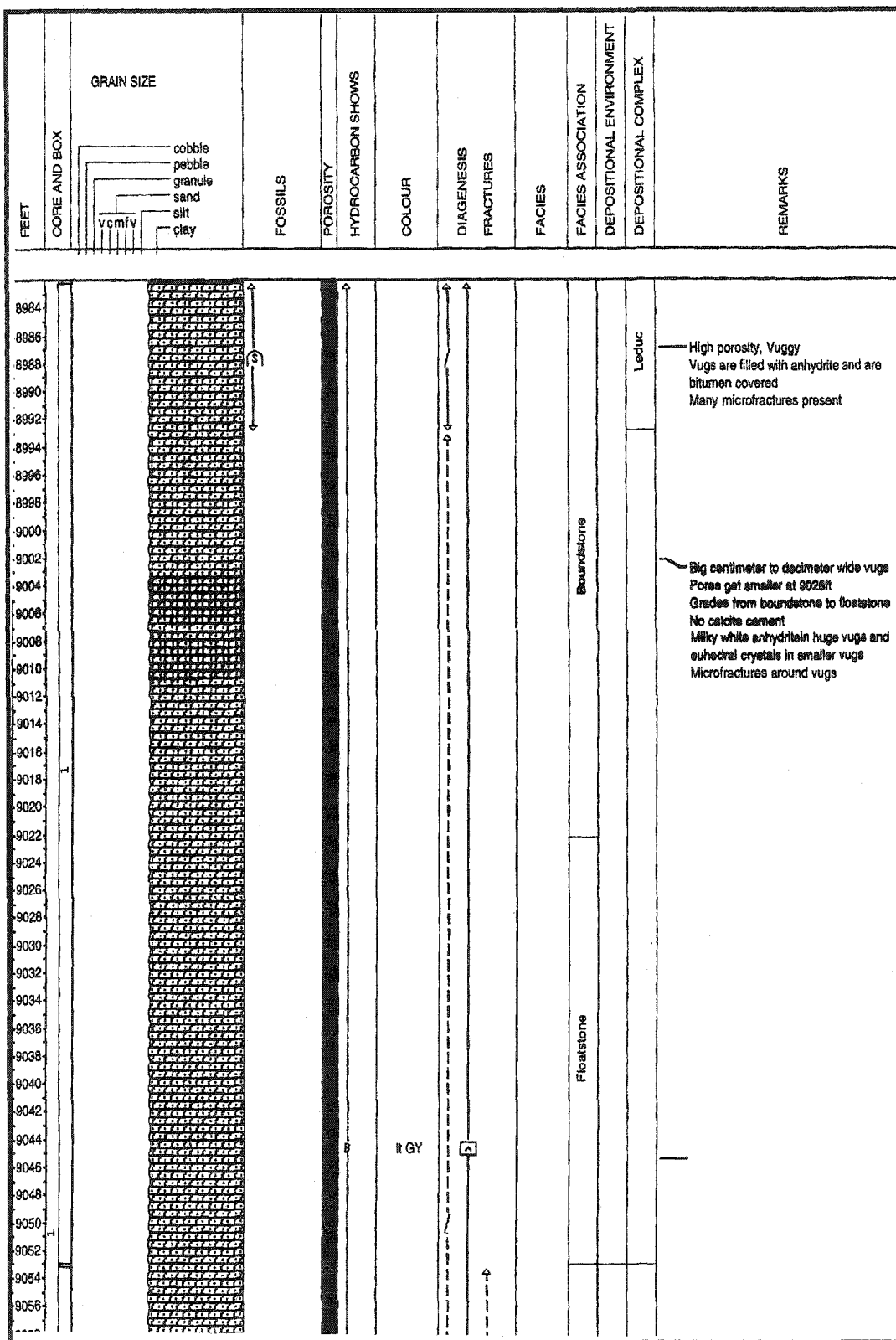


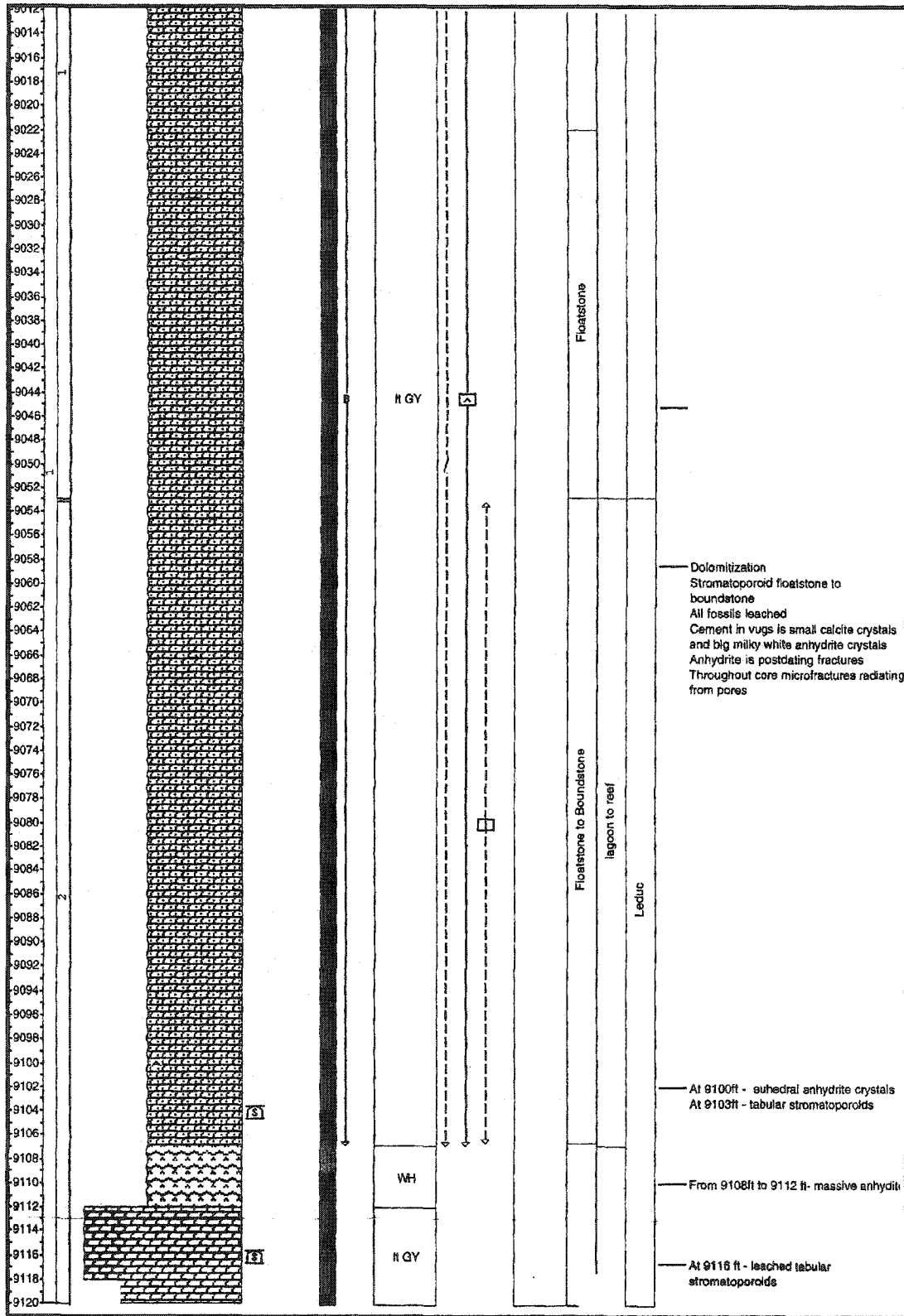


3_15-19-56-23W5

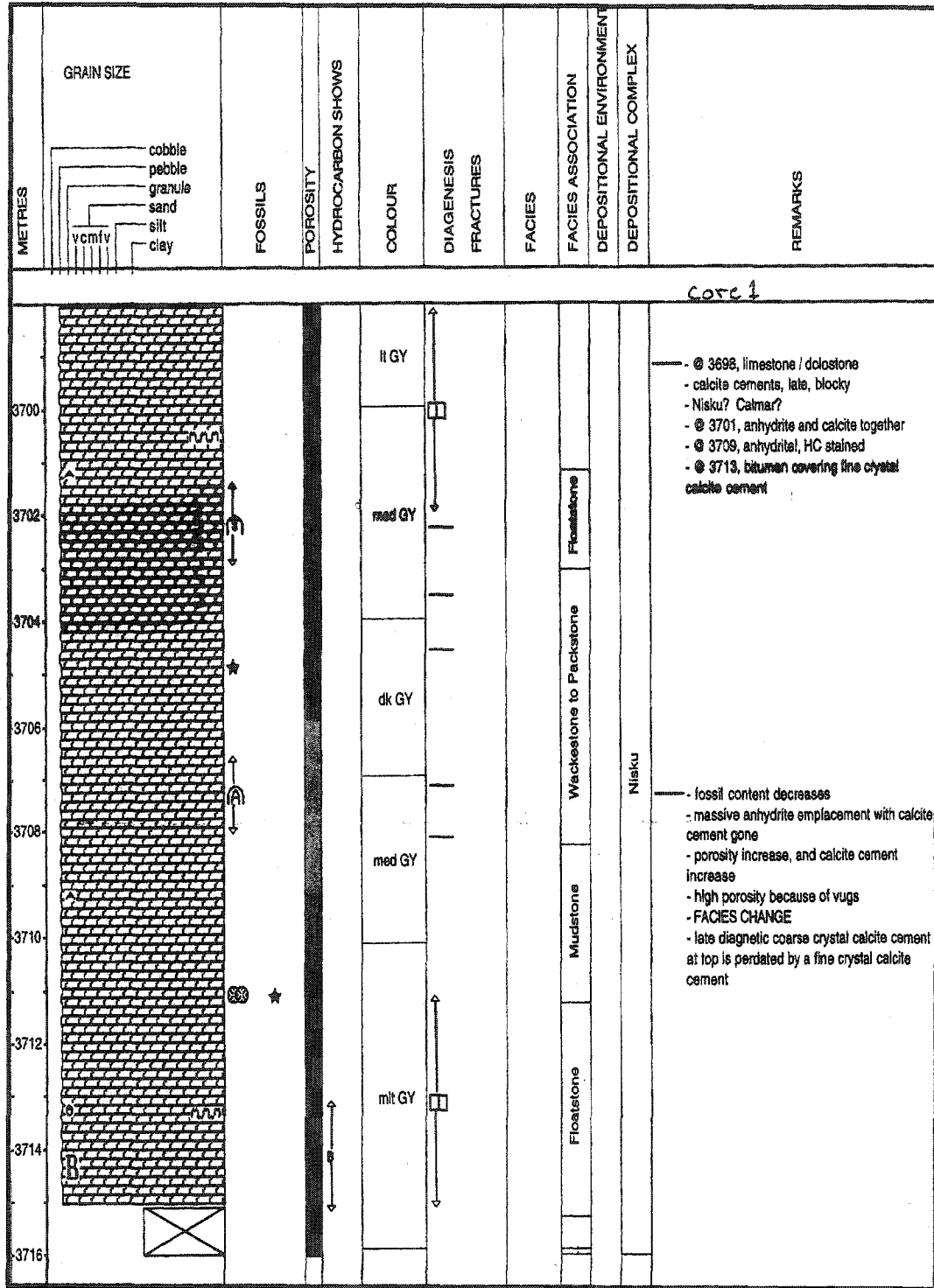


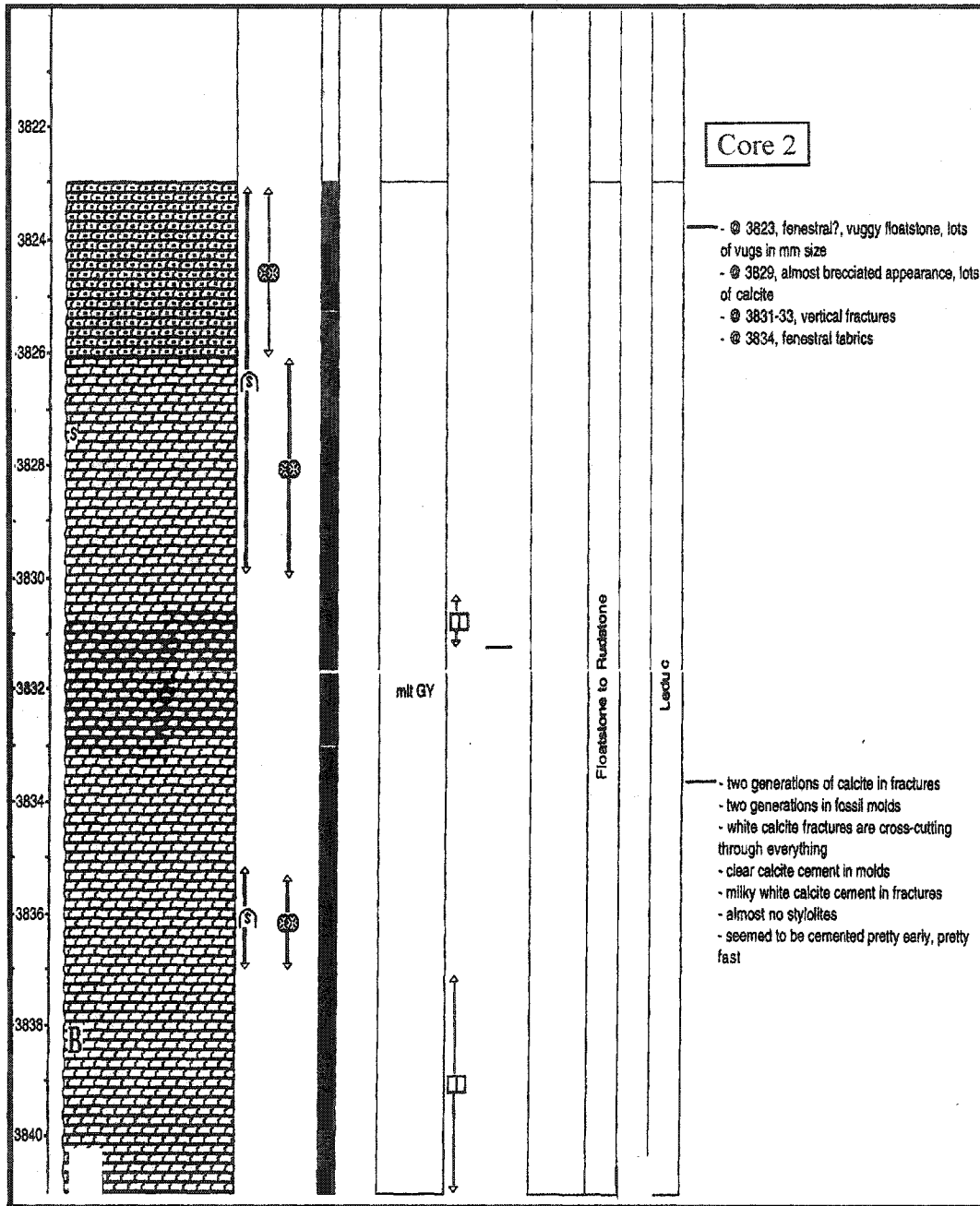
4_15-19-56-23W5



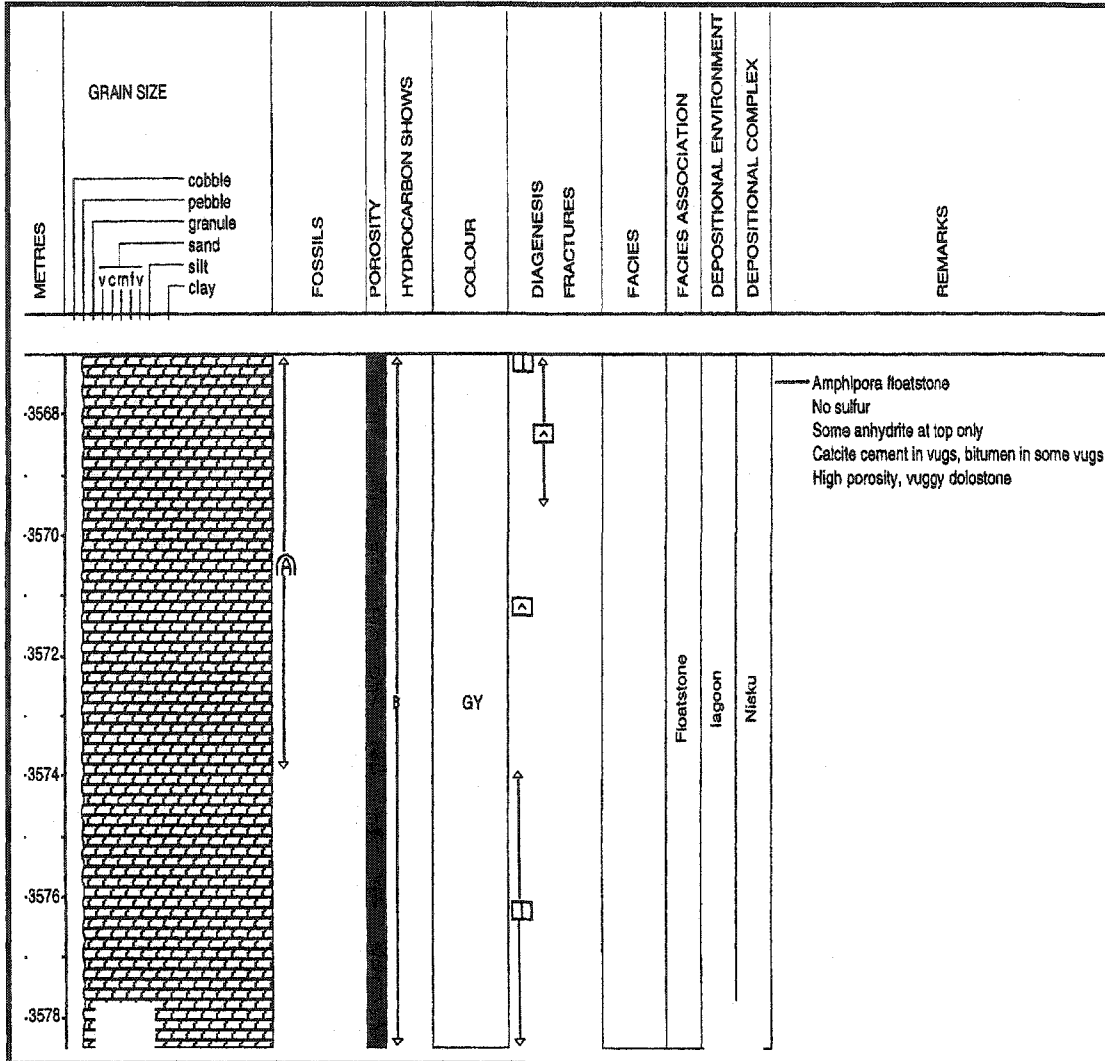


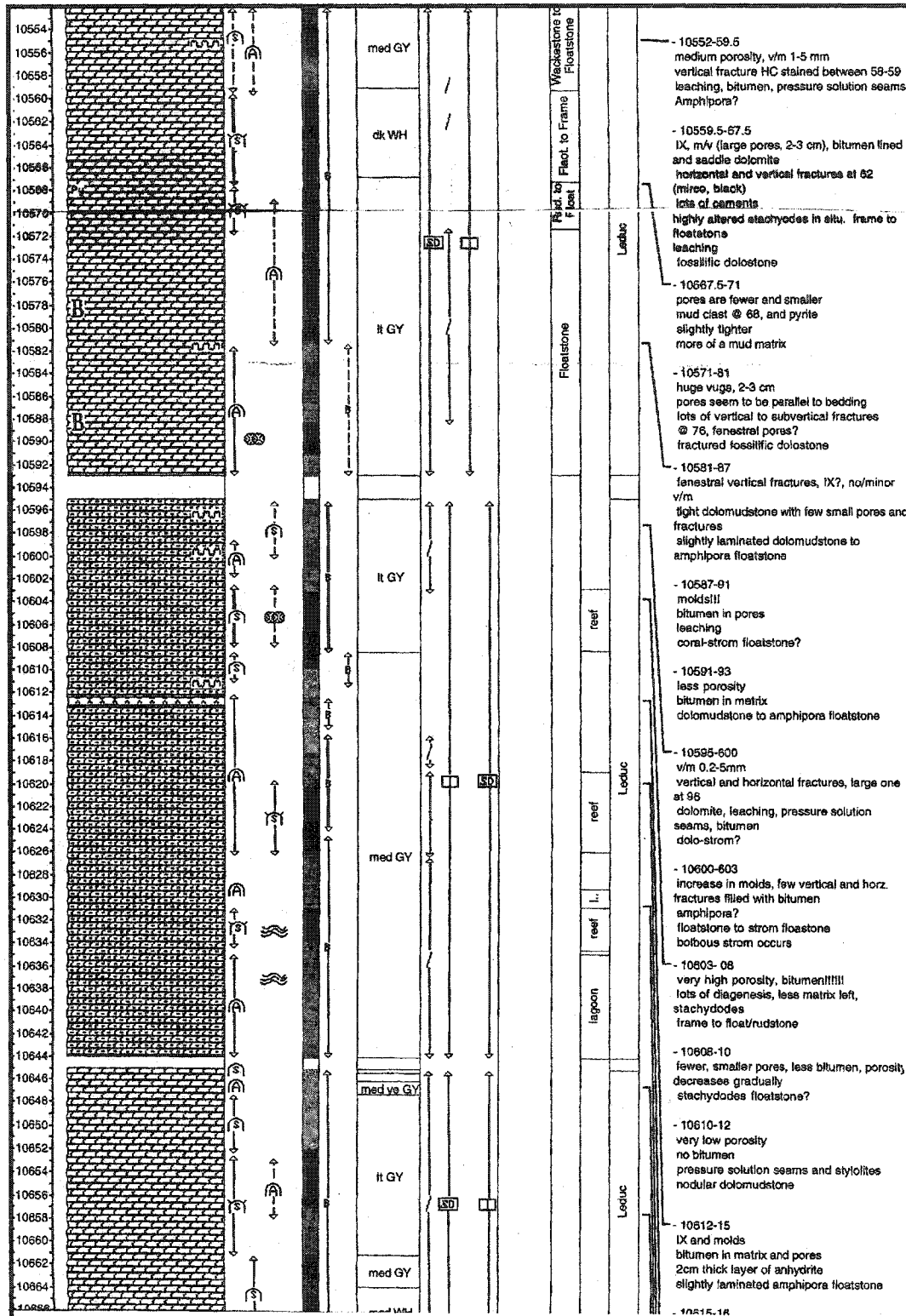
36294									
36296									
36298									
36300									
36302									
36304									
36306									
36308									
36310									
36312									
36314									
36316									
36318									
36320									
36322									
36324									
36326									
36328									
36330									
36332									
36334									
36336									
36338									
36340									
36342									
36344									
36346									
36348									
36350									
36352									
36354									
36356									
36358									
36360									
36362									
36364									
36366									
36368									
36370									
36372									
36374									
36376									
36378									
36380									
36382									
36384									
36386									



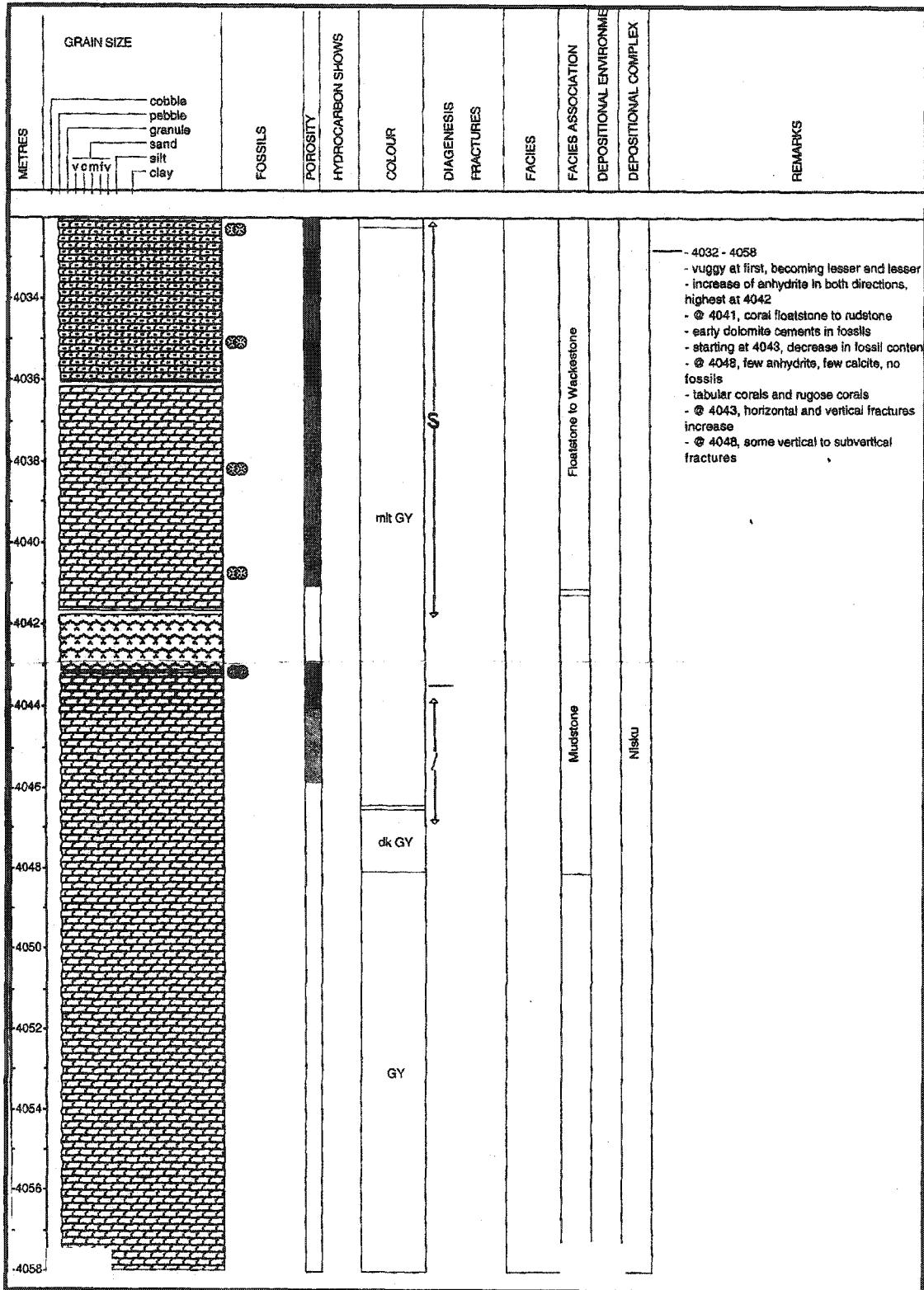


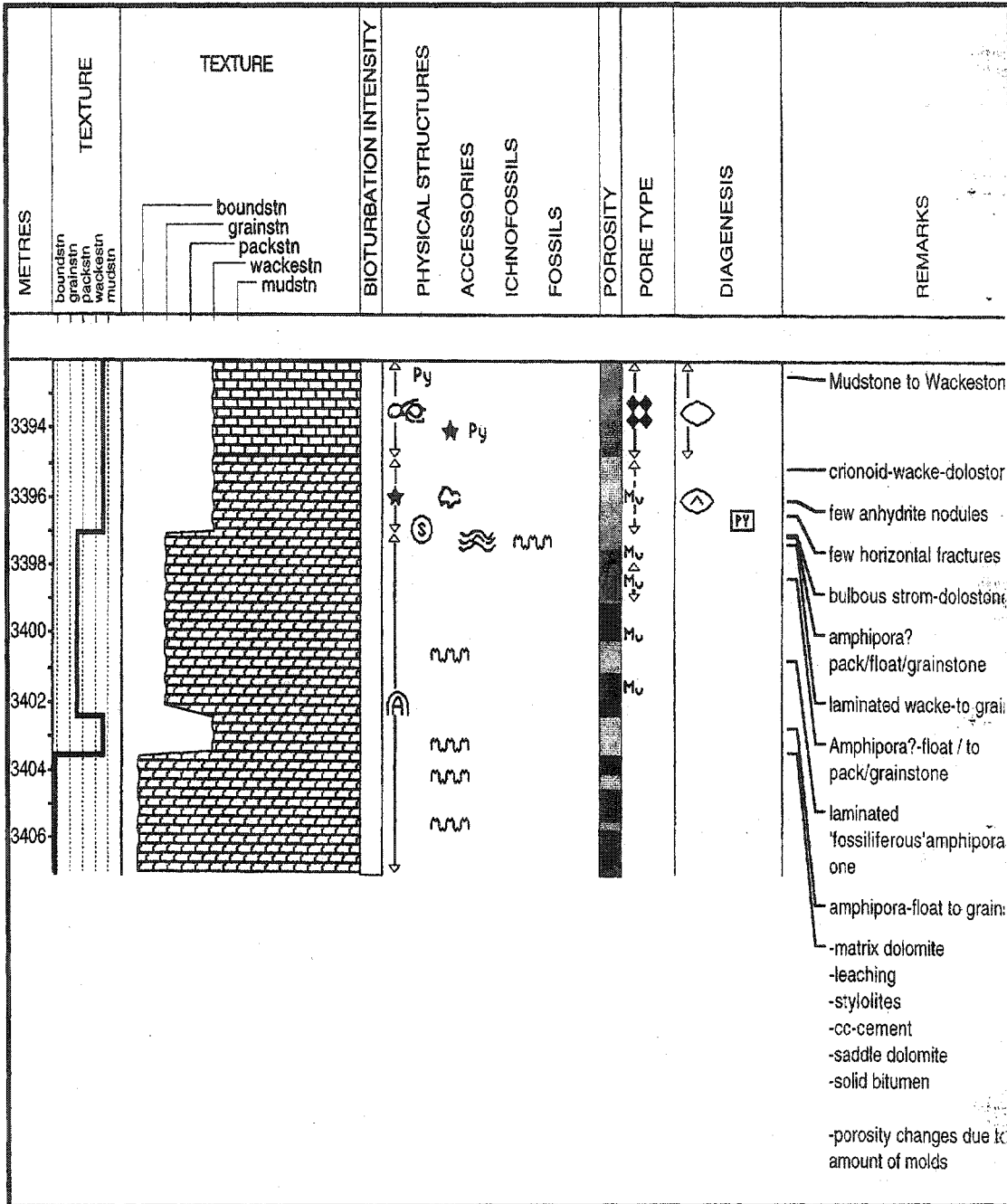
2-2-57-22W5

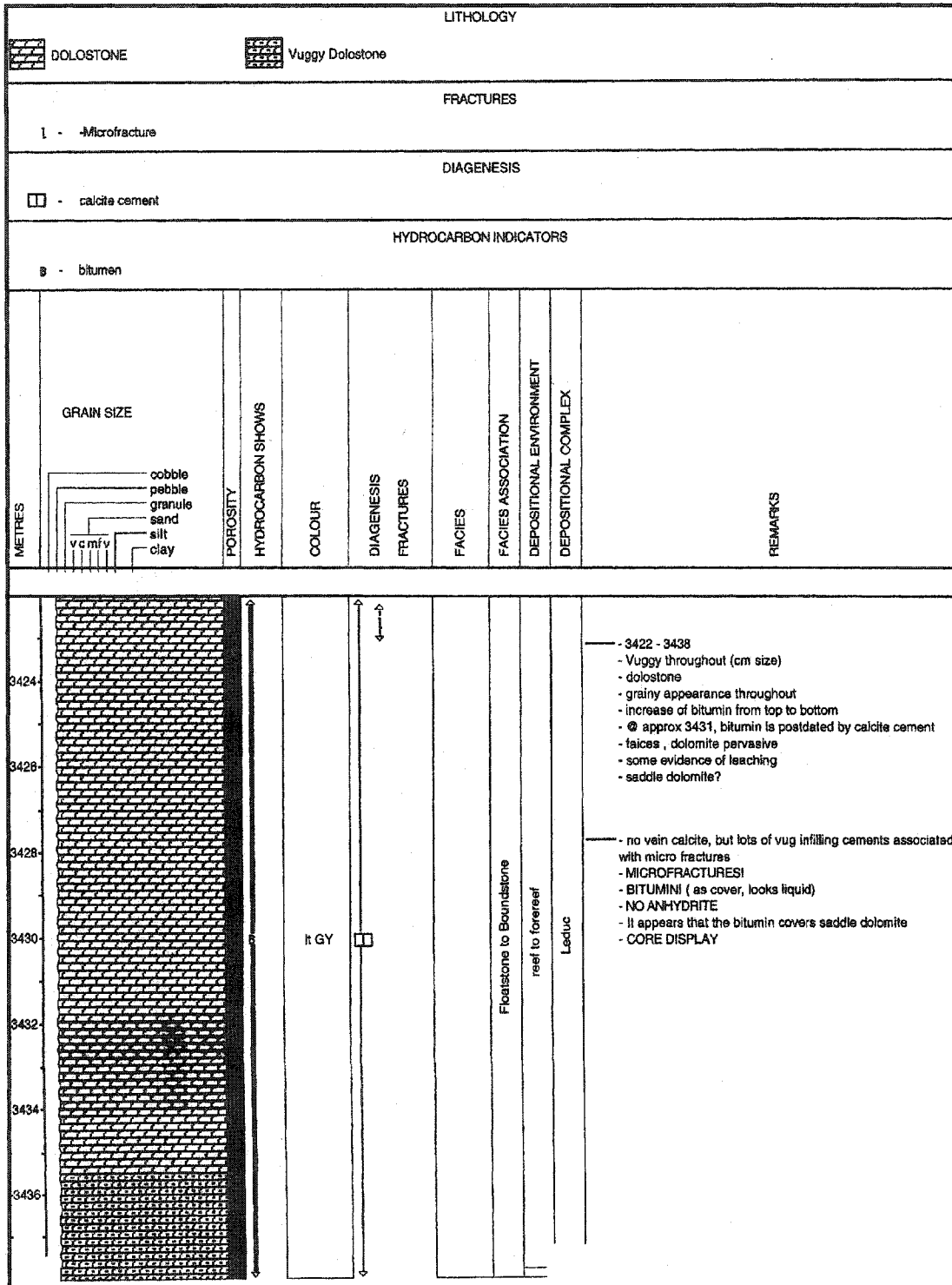


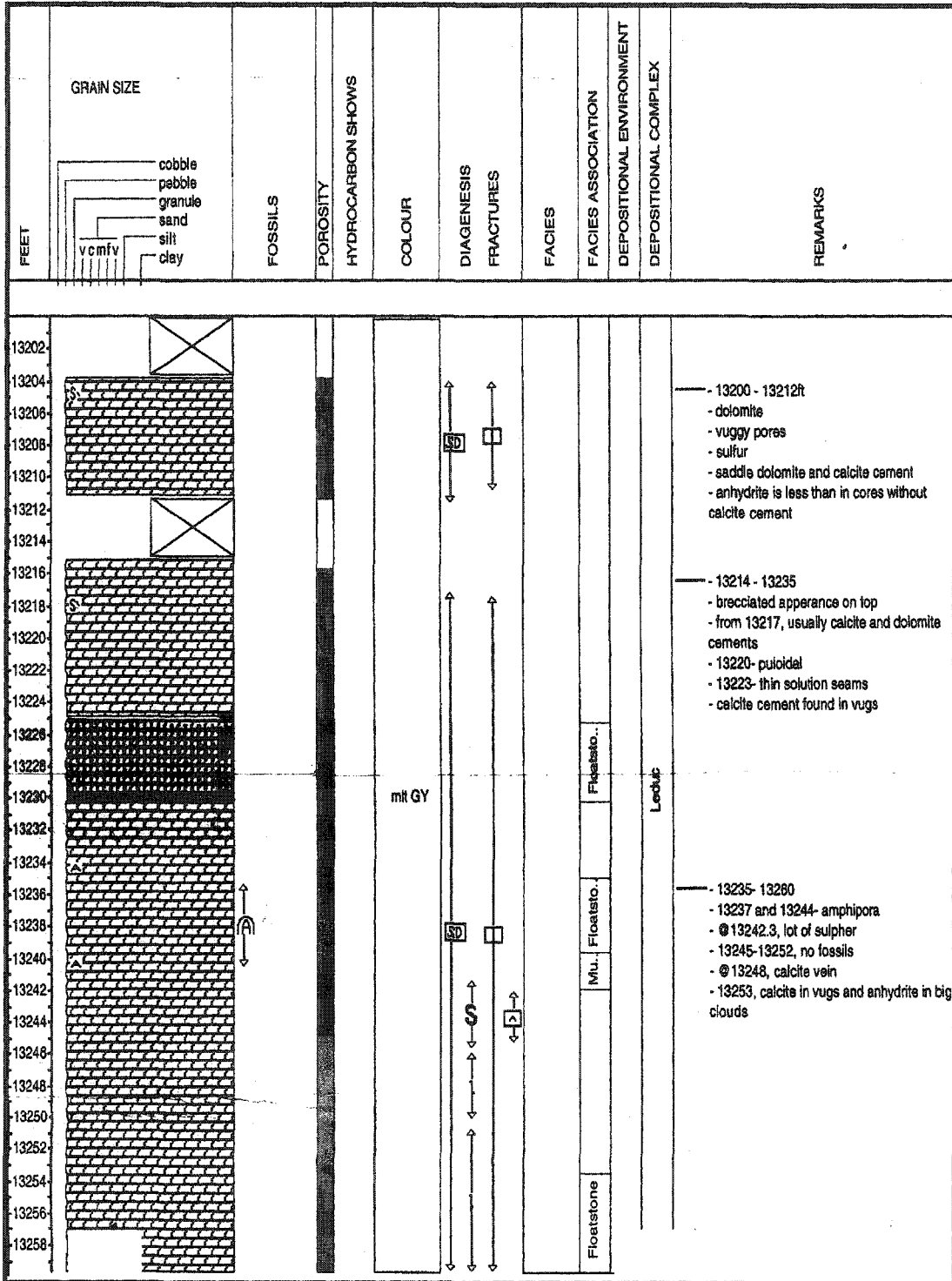


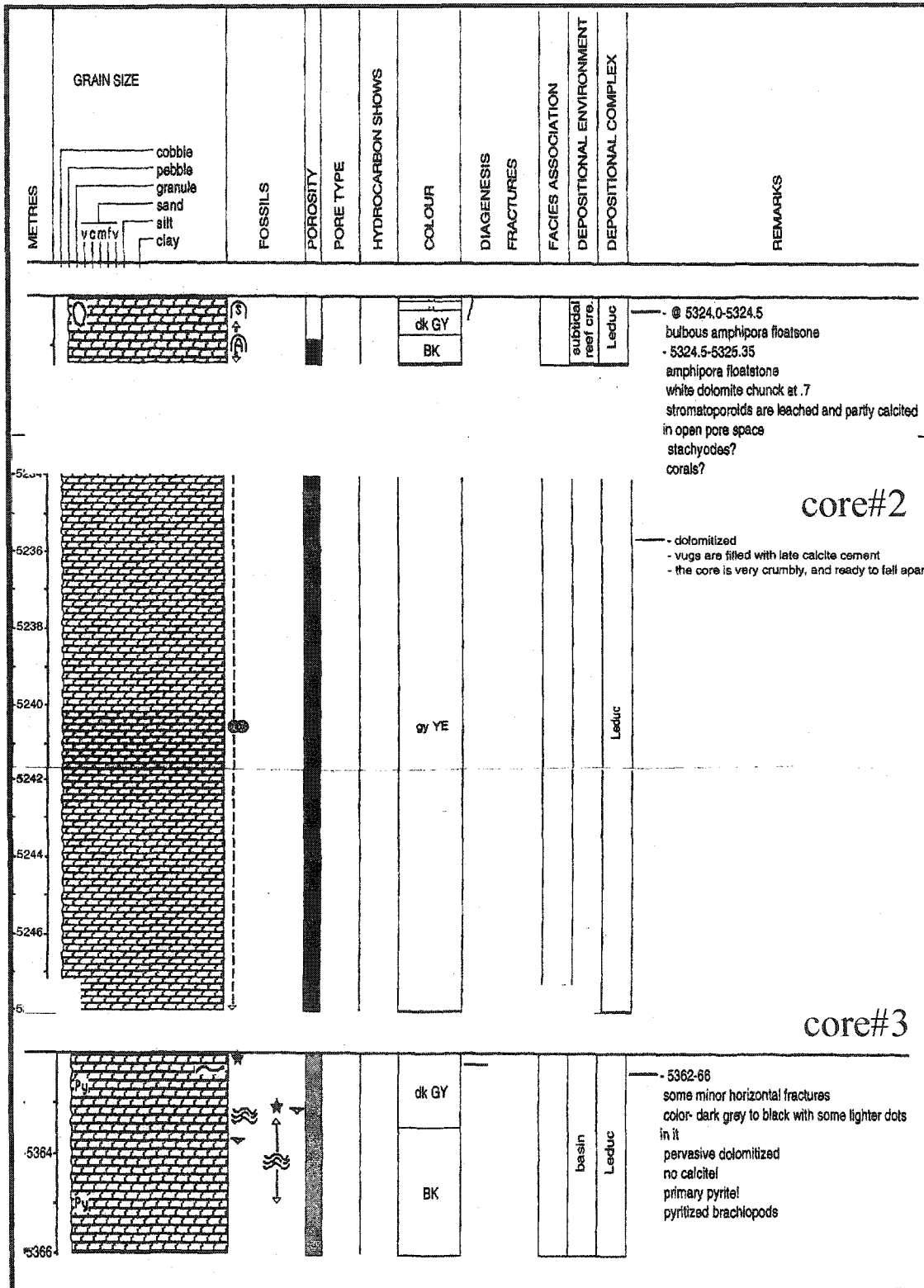
5-8-60-26W5

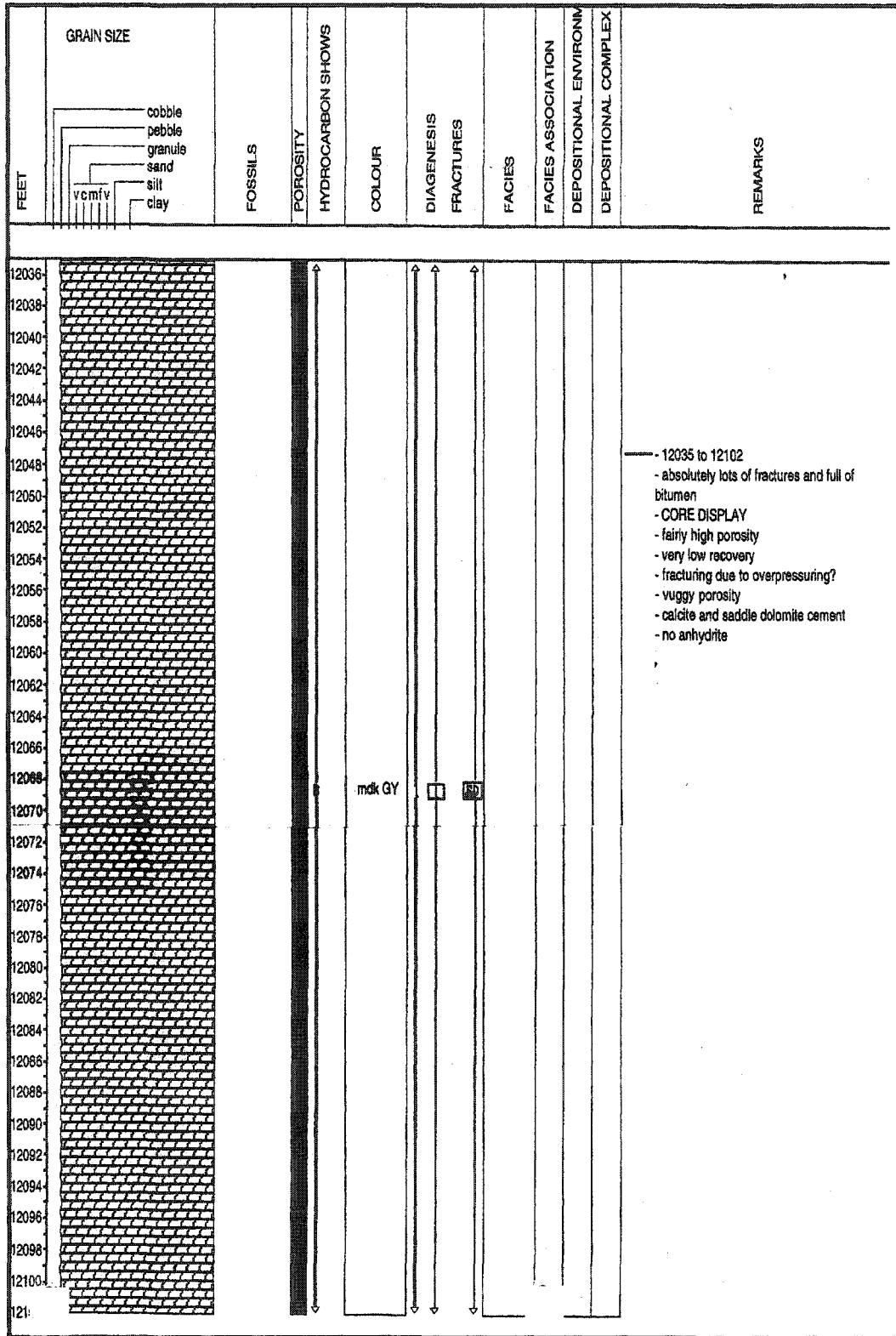


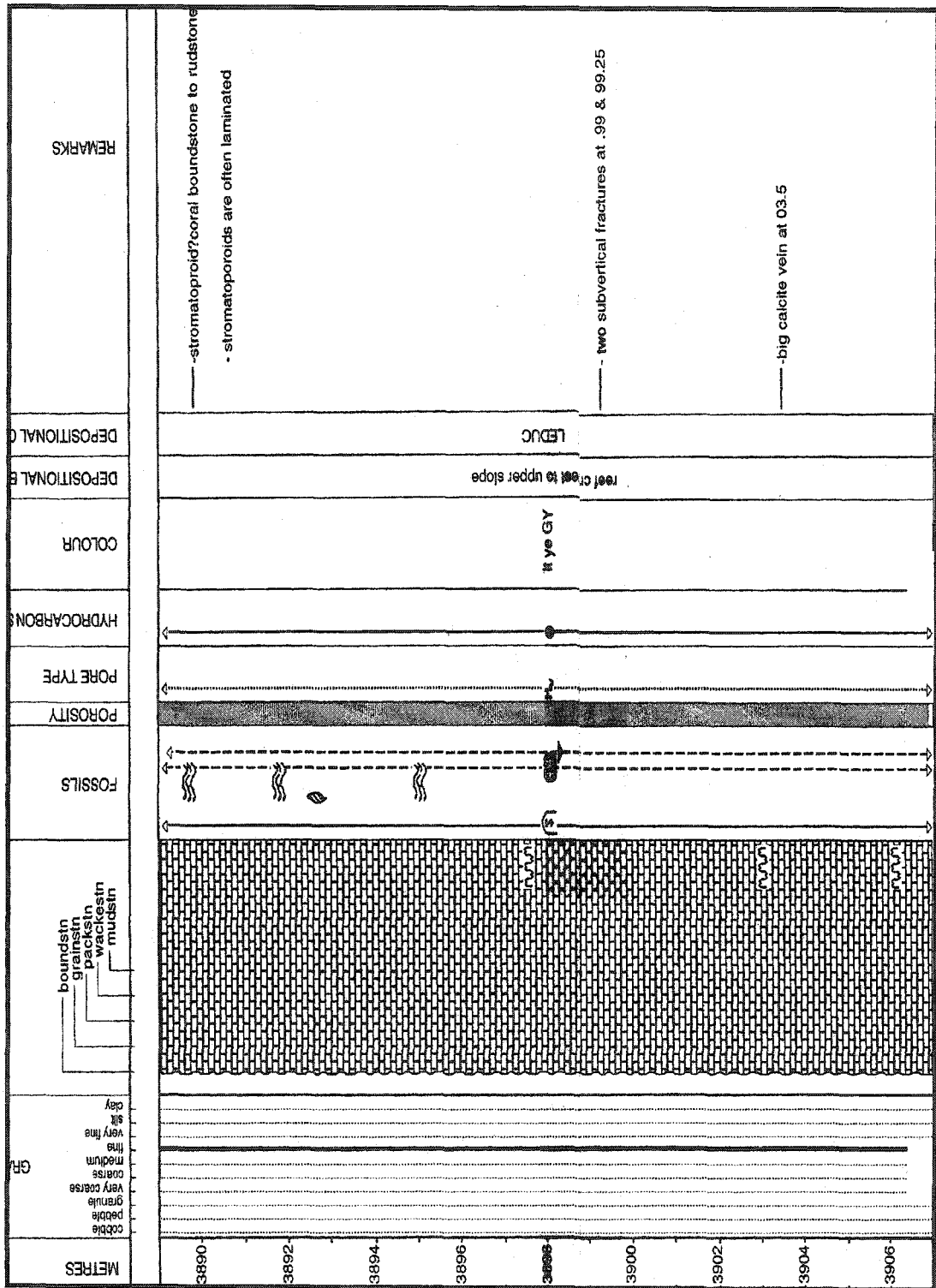




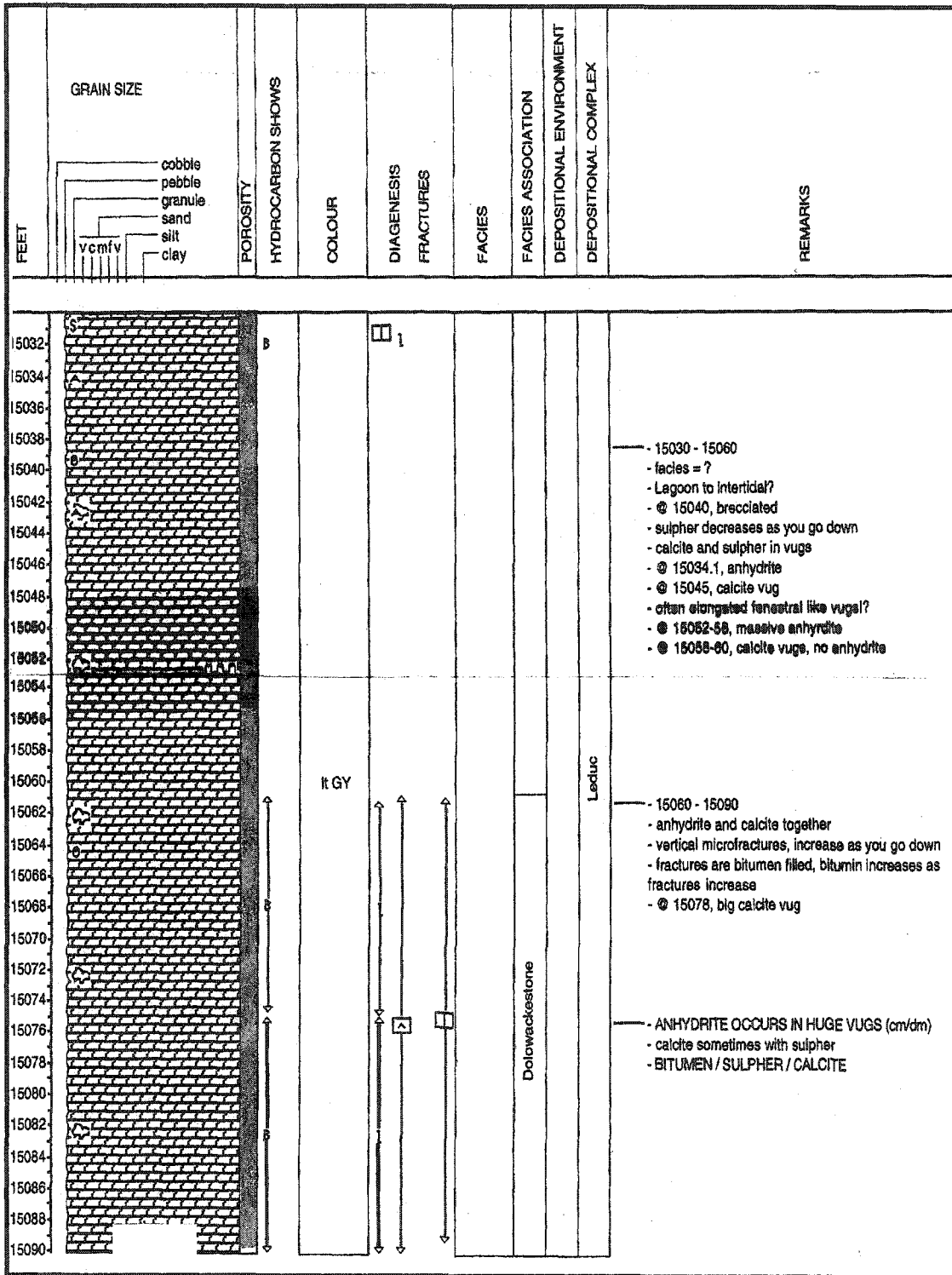




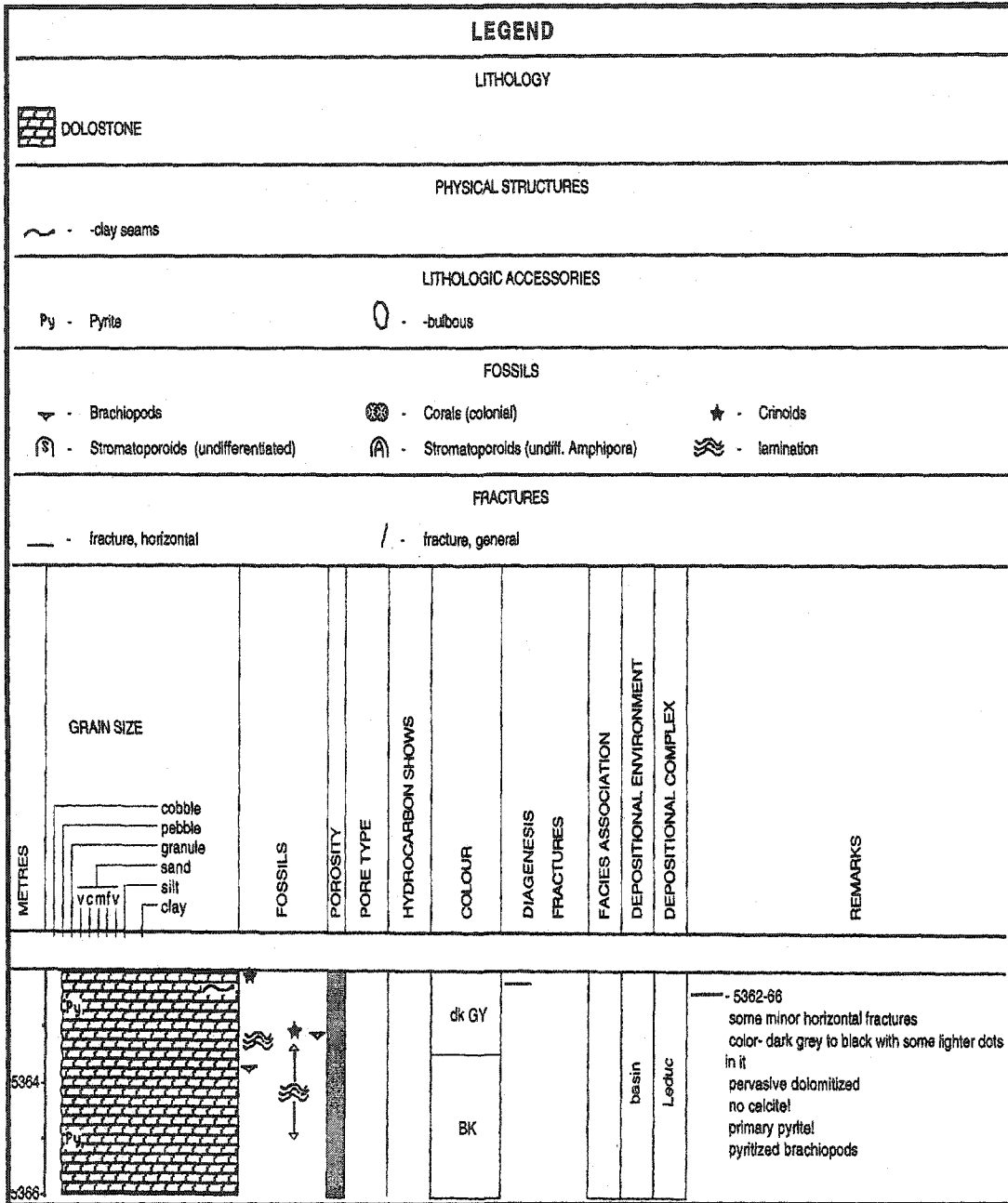




2-14-50-22W5
core#2



7-7-53-26W5
core#3



APPENDIX III

Sample list of sample numbers, core locations, sample depths, and general lithology/
diagenetic feature of sample.

#	Sample #	Location	Core Box	Depths	Remarks
1	MB97/001	10-32-44-19W5	1/2/12	5323.7m	Leduc/vugs
2	MB97/002	10-32-44-19W5	1/3/12	5324.6m	pyrobitumen
3	MB97/003	10-32-44-19W5	1/5/12	5326.6m	pyrobitumen
4	MB97/004	10-32-44-19W5	1/12/12	5363.0m	dolostone
5	MB97/005	10-32-44-19W5	2/6/07	5344.7m	dolostone
6	MB97/006	10-32-44-19W5	4/3/04	5353.9m	brecc. Dolostone
7	MB97/007	10-32-44-19W5	5/2/08	5358.7m	cc-xtal in brecc.dolostone
8	MB97/008	10-32-44-19W5	5/4/08	5362.3m	grainy dolostone
9	MB97/009	10-32-44-19W5	5/5/08	5363.0m	cc-xtal/chunk
10	MB97/010	10-32-44-19W5	5/5/08	5363.9m	cc-xtal/chunk
11	MB97/011	10-32-44-19W5	5/8/08	5367.5m	cc/bitumen
12	MB97/012	10-32-44-19W5	6/3/05	5371.6m	cc/dolostone
13	MB97/013	10-32-44-19W5	6/5/08	5374.4m	cc-xtal/chunk
14	MB97/014	07-07-53-26W5	2/1/01	5324.7m	anhydrite/dolomite?
15	MB97/015	14-36-52-27W5	1/5/14	5220.8m	fracture filling anhydrite
16	MB97/016	14-36-52-27W5	1/7/14	5223.5m	cements in coral/digg. Generations
17	MB97/017	14-36-52-27W5	1/8/14	5224.5m	stromatoporoid
18	MB97/018	14-36-52-27W5	1/9/14	5226.7m	vein anhydrite
19	MB97/019	14-36-52-27W5	1/10/14	5228.0m	porous dolomite
20	MB97/020	14-36-52-27W5	1/13/14	5231.2m	vein anhydrite
21	MB97/021	14-36-52-27W5	1/14/14	5233.4m	porous dolomite & elemental sulfur
22	MB97/022	14-36-52-27W5	2/3/03	5237.0m	massive anhydrite
23	MB97/023	11-30-57-25W5	01/03	17937.2'	Leduc/amphipora pack-floatstone
24	MB97/024	11-30-57-25W5	01/04	17938.7'	white xtal in foss. Dolostone
25	MB97/025	11-30-57-25W5	01/05	17.946.3'	vug filling white xtals in dolostone
26	MB97/026	11-30-57-25W5	01/07	17952.4'	white vug filling xtal in limestone
27	MB97/027	11-30-57-25W5	01/09	17958.1'	white anhydrite
28	MB97/028	11-30-57-25W5	01/11	17964.9'	yellowish brown anhydrite
29	MB97/029	11-30-57-25W5	01/13	17973.7'	yellow dolomite/anhydrite
30	MB97/030	11-30-57-25W5	01/13	17973.8'	saddle dolomite
31	MB97/031	11-30-57-25W5	01/15	18011.8'	vug filling xtals
32	MB97/032	11-30-57-25W5	02/15	18014.0'	elemental sulfur
33	MB97/033	11-30-57-25W5	04/15	18028.0'	white xtals/stuff
34	MB97/034	11-30-57-25W5	01/14	17932.8'	black bitumen ? In/before vein
35	MB97/035	11-30-57-25W5	01/07	17953.7'	black bitumen ? In/before vein
36	MB97/036	11-30-57-25W5	02/01	18013.0'	vein cc
37	MB97/037	11-30-57-25W5	02/02	18014.5'	saddle dolomite
38	MB97/038	11-30-57-25W5	02/03	18020.5'	vein cc
39	MB97/039	11-30-57-25W5	02/03	18021.0'	saddle dolomite
40	MB97/040	11-30-57-25W5	02/06	18030.8'	fracture / fillings
41	MB97/041	11-30-57-25W5	02/07	18036.4'	porous dolostone
42	MB97/042	11-30-57-25W5	02/09	18044.5'	vug with sulfur filling
43	MB97/043	11-30-57-25W5	14/15	18064.8'	anhydrite
44	MB97/044	11-30-57-25W5	14/15	18065.8'	vug sulfur
45	MB97/045	11-30-57-25W5	15/15	18066.7'	white crystals/stuff?
46	MB97/046	11-30-57-25W5	15/15	18069.0'	vugs
47	MB97/047	06-29-60-22W5	01/01/10	3392.9m	"berland" nodular limestone
48	MB97/048	06-29-60-22W5	01/02/10	3394.5m	limestone
49	MB97/049	06-29-60-22W5	01/03/10	3395.2m	dolostone
50	MB97/050	06-29-60-22W5	01/04/10	3396.6m	anhydrite underneath bulb. Strom
51	MB97/051	06-29-60-22W5	01/05/10	3398.0m	porous dolostone
52	MB97/052	06-29-60-22W5	01/06/10	3399.6m	dolostone
53	MB97/053	06-29-60-22W5	01/07/10	3401.9m	dolostone
54	MB97/054	06-29-60-22W5	01/09/10	3403.9m	tight dolostone
55	MB97/055	06-29-60-22W5	01/10/10	3405.3m	porous dolostone
56	MB97/056	06-29-60-22W5	01/10/10	3406.7m	fractures (fillings?)

57	MB97/001/9-20	09-20-59-22W5	03/05/06	3818.6m	vug lining cc xtal
58	MB97/002/9-20	09-20-59-22W5	01/01/05	3802.3m	dolostone with cc
59	MB97/003/9-20	09-20-59-22W5	01/02/05	3803.0m	cc in dolostone
60	MB97/004/9-20	09-20-59-22W5	01/03/05	3804.9m	anhydrite?
61	MB97/005/9-20	09-20-59-22W5	01/03/05	3805.6m	late cc & pyrobitumen
62	MB97/006/9-20	09-20-59-22W5	01/04/05	3806.6m	late cc in big vein
63	MB97/007/9-20	09-20-59-22W5	n/a	n/a	n/a
64	MB97/008/9-20	09-20-59-22W5	03/01/06	3811.8m	porous dolostone
65	MB97/009/9-20	09-20-59-22W5	03/01/06	3812.4m	cc xtals in pore
66	MB97/010/9-20	09-20-59-22W5	03/03/06	3815.9m	porous dolostone
67	MB97/011/9-20	09-20-59-22W5	03/05/06	3818.1m	tight/non-porous dolostone
68	MB97/012/9-20	09-20-59-22W5	03/05/06	3818.2m	vein cc
69	MB97/013/9-20	09-20-59-22W5	03/06/06	3818.7m	vein cc & sulfur
70	MB97/014/9-20	09-20-59-22W5	03/06/06	3819.3m	cc & sulfur in vug
71	MB97/071	09-22-58-24W5	01/04/13	3894.0m	Leduc dolomite? anhydrite vein
72	MB97/072	09-22-58-24W5	01/06/13	3896.6m	calcite "nodule"
73	MB97/073	09-22-58-24W5	01/08/13	3899.25m	cc in vein
74	MB97/074	09-22-58-24W5	01/10/13	3903.3m	fracture network
75	MB97/075	09-22-58-24W5	01/11/13	3904.5m	fracture cc
76	MB97/076	09-22-58-24W5	01/12/13	3905.75m	coral / facies
77	MB97/077	01-32-57-25W5	01/01/06	13899.0'	sulfur/cc in strom. Lam. Dolostone
78	MB97/078	01-32-57-25W5	01/01/06	13902.5'	anhydrite
79	MB97/079	01-32-57-25W5	01/02/06	13904.0'	calcite filled vug
80	MB97/080	01-32-57-25W5	01/02/06	13907.1'	cc molds
81	MB97/081	01-32-57-25W5	01/03/06	13909.1'	algal laminite
82	MB97/082	01-32-57-25W5	01/05/06	13923.5'	sulfur
83	MB97/083	01-32-57-25W5	01/06/06	13925.0'	cc vein
84	MB97/084	01-32-57-25W5	02/02/11	13936.7'	porous dolostone
85	MB97/085	01-32-57-25W5	02/06/11	13955.5'	diff. Cement generations
86	MB97/086	01-32-57-25W5	02/06/11	13958.8'	cc vug
87	MB97/087	01-32-57-25W5	02/08/11	13965.2'	cc & saddle dolomite
88	MB97/088	01-32-57-25W5	02/09/11	13973.5'	horiz. Cc vein in amphipora packstone
89	MB97/089	01-32-57-25W5	02/10/11	13977.2'	big cc vug
90	MB97/090	01-32-57-25W5	02/11/11	13980.1'	fracture cc
91	MB97/091	10-20-57-25W5	01/01/13	4136.5m	Winterburn/Anhydrite
92	MB97/092	10-20-57-25W5	01/03/13	4138.5m	Winterburn/Anhydrite
93	MB97/093	10-20-57-25W5	01/05/13	4141.7m	Winterburn/ no Anhydrite
94	MB97/094	10-20-57-25W5	01/06/13	4142.0m	Winterburn/ big vein cc/ /Anhydrite
95	MB97/095	10-20-57-25W5	01/07/13	4143.5m	Winterburn/ big vein cc/ /Anhydrite
96	MB97/096	10-20-57-25W5	01/13/13	4149.8m	pore cc
97	MB97/097	10-20-57-25W5	02/01/13	4266.1m	Leduc/ facies
98	MB97/098	10-20-57-25W5	02/01/13	4266.75m	leduc / bitumen & cc
99	MB97/099	10-20-57-25W5	02/02/13	4266.6m	grainstone facies
100	MB97/100	10-20-57-25W5	02/04/13	4270.85m	pores/dolostoe/bitumen
101	MB97/101	10-20-57-25W5	02/05/13	4272.75m	pore cc
102	MB97/102	10-20-57-25W5	02/06/13	4273.25m	pore cc
103	MB97/103	10-20-57-25W5	02/07/13	4276.0m	vuggy dolostone / stylolite
104	MB97/104	10-20-57-25W5	02/08/13	4277.0m	porous dolostone / bitumen
105	MB97/105	10-20-57-25W5	02/09/13	4278.45m	vein calcite
106	MB97/106	10-20-57-25W5	01/12/13	4282.5m	cc/saddle dolomite in porous rock
107	MB97/107	10-20-57-25W5	02/01/13	4266.75m	cc underneath stylolite
108	MB97/108	10-15-56-27W5	01/03/03	15274.0'	white chunk in dolomite
109	MB97/109	01-16-55-27W5	01/01/01	16665.0'	white anhydrite
110	MB97/110	01-18-56-16W5	01/01/03	2948.0m	dolomite & solid bitumen
111	MB97/111	01-18-56-16W5	01/01/03	2948.5m	white pore/fracture cc?
112	MB97/112	01-18-56-16W5	01/01/03	2948.7m	cc pore/vug
113	MB97/113	01-18-56-16W5	01/02/03	2949.2m	cc pore/vug

114	MB97/114	01-18-56-16W5	01/02/03	2949.85m	sulfur/cc
115	MB97/115	01-18-56-16W5	01/02/03	2949.6m	anhydrite
116	MB97/116	01-18-56-16W5	01/03/03	2951.2m	cc/sulfur
117	MB97/117	06-16-55-18W5	02/01/02	10857.0'	brecc. Dolostone - rudstone?
118	MB97/118	06-16-55-18W5	02/02/02	10861.2'	porous dolostone with cc & bitumen
119	MB97/119	06-16-55-18W5	02/02/02	10862.8'	porous dolostone & bitumen & fossils
120	MB97/120	06-16-55-18W5	03/02	10873.5'	frac. Fillings
121	MB97/121	06-16-55-18W5	03/04	10881.2'	calcite nodule
122	MB97/122	06-16-55-18W5	03/04	10889.0'	vugs with cc & dolomite
123	MB97/123	06-16-55-18W5	03/05	10890.1'	veins/cc/bitumen
124	MB97/124	06-16-55-18W5	03/08	10902.0'	cc-chunk
125	MB97/125	06-16-55-18W5	03/08	10904.0'	cc-vugs/veins
126	MB97/126	02-09-54-19W5	01/01/13	11752.0'	anhydrite in amphipora floatstone
127	MB97/127	02-09-54-19W5	01/02/13	11760.0'	anhydrite in frac
128	MB97/128	02-09-54-19W5	01/03/13	11764.0'	amphipora floatstone
129	MB97/129	02-09-54-19W5	01/05/13	11773.0'	fracture anhydrite
130	MB97/130	02-09-54-19W5	01/07/13	11783.0'	anhydrite
131	MB97/131	02-09-54-19W5	01/08/13	11786.0'	fracture anhydrite
132	MB97/132	02-09-54-19W5	01/10/13	11794.0'	anhydrite in porous dolostone
133	MB97/133	15-19-56-23W5	01/05/14	4079.3m	stroms & molds
134	MB97/134	15-19-56-23W5	01/05/14	4079.4m	stroms & molds
135	MB97/135	15-19-56-23W5	01/12/14	4087.96m	molds/vugs/stylos/bitumen
136	MB97/136	15-19-56-23W5	02/03/11	4094.0m	facies & porosity
137	MB97/137	15-19-56-23W5	02/11/11	4105.7m	facies & porosity
138	MB97/138	15-19-56-23W5	03/08/09	4112.2m	facies
139	MB97/139	05-13-58-24W5	01/01/13	12878.0'	stylolite & bitumen in limemudstone
140	MB97/140	05-13-58-24W5	01/05/13	12895.0'	finegrained mudstone
141	MB97/141	05-13-58-24W5	01/06/13	12900.0'	stylolite/bitumen
142	MB97/142	05-13-58-24W5	01/11/13	12925.5'	stylolite/white veins
143	MB97/143	05-13-58-24W5	01/13/13	12935.0'	cc filled mold
144	MB97/144	05-13-58-24W5	02/02/13	12944.0'	cc-cements in stroms
145	MB97/145	05-13-58-24W5	02/04/13	12953.0'	cc-cements in stroms
146	MB97/146	05-13-58-24W5	02/08/13	12970.0'	krusel bitumen in limestone
147	MB97/147	05-13-58-24W5	02/09/13	12978.0'	cements
148	MB97/148	05-13-58-24W5	02/10/13	12980-81'	stylolite
149	MB97/149	05-13-58-24W5	03/01/13	12995.0'	facies/ amphipora
150	MB97/150	05-13-58-24W5	03/02/13	13003.0'	facies & cements
151	MB97/151	05-13-58-24W5	?	13013.0'	facies?
152	MB97/152	05-13-58-24W5	03/06/13	13025.0'	krusel & facies
153	MB97/153	05-13-58-24W5	03/09/13	13040-41	stromes & birdeyes facies
154	MB97/154	05-13-58-24W5	03/10/13	13045.0'	birdseyes
155	MB97/155	09-17-53-19W5	sample bag	sample bag	crystals
156	MB97/156	09-17-53-19W5	01/03/12	12110-11'	anhydrite
157	MB97/157	09-17-53-19W5	01/04/12	12115.0'	dolomite vug
158	MB97/158	09-17-53-19W5	01/05/12	12117.0'	big cc vein
159	MB97/159	09-17-53-19W5	01/06/12	12121.0'	xtals in pores
160	MB97/160	09-17-53-19W5	01/08/12	12128.0'	black bitumen on clay seam?
161	MB97/161	09-17-53-19W5	01/09/12	12130.0'	xtals in pores
162	MB97/162	09-17-53-19W5	01/10/12	12137-38'	sulfur/dolomite/cement
163	MB97/163	09-17-53-19W5	01/12/12	12143.0'	cc-vein/vug
164	MB97/164	14-08-48-21W5	?	5176.7m	anhydrite xtals
165	MB97/165	14-08-48-21W5	02/01/13	5163.3m	anhydrite in dolostone
166	MB97/166	14-08-48-21W5	02/01/13	5164.0m	sulfur/anhydrite/bitumen
167	MB97/167	14-08-48-21W5	02/03/13	5167.4m	anhydrite
168	MB97/168	14-08-48-21W5	02/07/13	5172.5m	dolostone
169	MB97/169	14-08-48-21W5	02/10/13	5176.6m	pore/anhydrite
170	MB97/170	14-08-48-21W5	02/11/13	5178.2m	anhydrite/dolostone

171	MB97/171	14-08-48-21W5	02/13/13	5180.0m	anhydrite/pores/cc
172	MB97/172	11-09-61-22W5	02/02/02	11128.0'	pyrite & bitumen
173	MB97/173	11-09-61-22W5	03/03/11	11139.0'	bituminous dolostone
174	MB97/174	11-09-61-22W5	03/05/11	11146.0'	cements
175	MB97/175	11-09-61-22W5	03/08/11	11161.0'	krusel dolostone
176	MB97/176	11-09-61-22W5	03/09/11	11164.0'	cements
177	MB97/177	11-09-61-22W5	04/01/22	11170.0'	anhydrite
178	MB97/178	11-09-61-22W5	04/02/22	11174.8'	veins
179	MB97/179	11-09-61-22W5	04/04/22	11182.4'	cements & bitumen
180	MB97/180	11-09-61-22W5	04/06/22	11191.0'	bitumen
181	MB97/181	11-09-61-22W5	04/10/22	11204.0'	anhydrite / cements
182	MB97/182	11-09-61-22W5	04/11/22	11210-11'	layered things & cements
183	MB97/183	11-09-61-22W5	04/14/22	11221.0'	anhydrite & cements
184	MB97/184	11-09-61-22W5	04/15/22	11226.0'	facies & cements
185	MB97/185	11-09-61-22W5	04/19/22	11240.0'	cement & bitumen
186	MB97/186	11-09-61-22W5	04/22/22	11252.0'	cements / pores
187	MB97/187	04-26-58-20W5	03/02/05	10561.5'	stachyodes / cements
188	MB97/188	04-26-58-20W5	03/03/05	10565.0'	bitumen & cements
189	MB97/189	04-26-58-20W5	05/03/11	10604.6'	cements
190	MB97/190	04-26-58-20W5	05/04/11	10605.1'	cements
191	MB97/191	04-26-58-20W5	05/04/11	10607.8'	anhydrite
192	MB97/192	04-26-58-20W5	05/08/11	10632.2'	cements
193	MB97/193	04-26-58-20W5	06/01/05	10648.0'	cc-xtal
194	MB97/194	04-26-58-20W5	06/03/05	10657.8'	cements
195	MB97/195	2/15-09-57-17W5	01/01/16	3145.3m	replacive xtal anhydrite
196	MB97/196	2/15-09-57-17W5	01/02/16	3147.0m	cc / anhydrite?
197	MB97/197	2/15-09-57-17W5	01/05/16	3149.5m	cc vug
198	MB97/198	2/15-09-57-17W5	01/08/16	3153.2m	cc vein
199	MB97/199	2/15-09-57-17W5	01/11/16	3156.2m	cc-vug / sulfur
200	MB97/200	2/15-09-57-17W5	01/11/16	3162.75m	cc-vug / vein
201	MB97/201	05-13-54-23W%	01/05/07	13368.0'	saddle dolomite
202	205	11-29-59-16W5		113 2716.3 m	little cement on top of core
203	206	11-29-59-16W5		111 2721.0 - 27121.5 m	limestone interval
204	207	11-29-59-16W5	core #4, 9116	2732.0 m	Anhydrite
205	208	11-29-59-16W5	core #4, 121116	2734.4 m	calcite and saddle dolomite
206	209	11-29-59-16W5		2736.29 m	calcite, big calcite
207	210	11-29-59-16W5	15116	2737.5 m	Anhydrite
208	211	11-29-59-16W5		2735.4 m	saddle dolomite
209	212	11-29-59-16W5	1117	2738.6 m	Blue Ridge
210	213	11-29-59-16W5	3117	2740.8 m	Anhydrite
211	214	11-29-59-16W5	12117	2751.05 m	Calmar
212	215	11-29-59-16W5	15117	2754.8 m	Nisku
213	216	11-29-59-16W5	17117	2756.5 m	Nisku
214	217	5-8-60-26W5	core #6, 1111	4032.2 m	calcite / Anhydrite cements
215	218	5-8-60-26W5	3111	4035.5 m	sulphur and cement
216	219	5-8-60-26W5	8111	4042.2 m	massive Anhydrite
217	220	5-8-60-26W5	8111	4043.0 m	facies / early cement
218	221	5-8-60-26W5	core #8,112	4048- 4058 ? m	cement
219	222	15-18-58-24W5	118	3773.0 m	Calmar dolostone
220	223	15-18-58-24W5		3775.0 m	Anhydrite at top, Nisku
221	224	15-18-58-24W5	618	3379.0 m	Calcite cement postdating hydrocarbons
222	225	15-18-58-24W5	618	3779.2 m	big calcite vug
223	226	15-18-58-24W5		3780 m	Anhydrite
224	227	15-18-58-24W5	618	3875 m	cements
225	228	15-18-58-24W5		3878.8 m	Bitumen
226	229	16-32-58-24W5	core #1, 1113	3699.1 m	late / coarse calcite cement

227	230	16-32-58-24W5	core #1, 4113	3703.1 m	Anhydrite
228	231	16-32-58-24W5		3711(~) m	two types of calcite cement
229	232	16-32-58-24W5		3714 m	cements / bitumen
230	233	16-32-58-24W5		3827 m	sulfur / cements
231	234	16-32-58-24W5		3829 m	cements / matrix
232	235	16-32-58-24W5		3830.8 m	fractures
233	236	16-32-58-24W5		3833.0 m	cements / calcite
234	237	16-32-58-24W5		3838.8 m	late calcite cement
235	238	16-32-58-24W5		3835.7 m	FACIES and cement
236	239	16-32-58-24W5		3712.0 m	calcite cement
237	240	7-35-59-24W5		3840 - 3858 m	cements
238	241	8-4-59-23W5		12035 ? m	Bitumen
239	242	8-4-59-23W5		12072 ? m	saddle dolomite and Bitumen
240	243	8-4-59-23W5		12083 m	cements / calcite
241	244	8-4-59-23W5		12100 m	cements / Bitumen
242	245	7-19-59-24W5		13200m	Anhydrite
243	246	7-19-59-24W5		13217 m	calcite crystals in vug
244	247	7-19-59-24W5		13219 m	vein calcite
245	248	7-19-59-24W5		13225 m	sulfur
246	249	7-19-59-24W5		13233 feet	vein calcite
247	250	7-19-59-24W5		13242 feet	sulfur / cements
248	251	7-19-59-24W5		13252 feet	vein calcite
249	252	7-18-52-24W5		4822.9 m	big (decimeter) calcite vein
250	253	7-18-52-24W5		4824.0 m	fault/ limestone/ dolostone
251	254	7-18-52-24W5		4824.5 m	vein in limestone
252	255	7-18-52-24W5		4827.3 m	calcite stromatoporoid in dolomite matrix
253	256	7-18-52-24W5		4829.1 m	vein and bitumen
254	257	7-18-52-24W5		4834.6 m	cc and sulfur
255	258	7-18-52-24W5		4845.6 m	saddle dolomite and calcite cement
256	259	7-18-52-24W5		4847.5 m	calcite vein
257	260	7-18-52-24W5		4860.0 m	calcite vein / underneath anhydrite
258	261	14-36-52-24W5		5215.5 m	stromatoporoids
259	262	14-36-52-24W5		5223.5 m	cements
260	263	14-36-52-24W5		5240.5 m	Anhydrite
261	264	1-16-55-27W5		~ 16700 ~ m ?	calcite vein
262	265	1-16-55-27W5		~ 16699 ~ m ?	saddle dolomite - vugs
263	266	5-25-51-22W5		~4377.5 m	FACIES
264	267	5-25-51-22W5		4380 m	FACIES and cements
265	268	5-25-51-22W5		4387 m	FACIES and cements
266	269	5-25-51-22W5		4467.2 m	vug - infill
267	270	5-25-51-22W5		4468 m	calcite vein
268	271	5-25-51-22W5		4473 m	calcite on stylolite
269	272	5-25-51-22W5		4480 m	saddle dolomite
270	273	3-26-49-20W5		~ 4577 m	calcite / pyrite / dolomite
271	274	10-13-52-22W5		4366.5 m	calcite vein
272	275	10-13-52-22W5		4368.7 m	vug and cement
273	276	10-13-52-22W5		~4388.0 m	elongated clear mineral
274	277	10-13-52-22W5		~4377 m	Anhydrite
275	278	15-29-55-17W5		10930 feet	
276	279	10-8-53-20W5		12657 feet	anhydrite
277	280	10-27-52-24W5		4673.5 m	stylolite / sulfur / cements
278	281	10-27-52-24W5		4681.2 m	calcite vugs
279	282	10-27-52-24W5		4682.0 m	vug with early to intermediate cements
280	283	10-27-52-24W5		4685.5 m	cements
281	284	10-27-52-24W5		4687.5 m	vugs / sulfur
282	285	10-9-57-24W5		14147 m	vein calcite
283	286	10-9-57-24W5		14163 m	vein calcite

284	287	10-9-57-24W5		14169 m	vein / vug calcite
285	288	10-9-57-24W5		14180 m	vein / vug fill
286	289	10-17-57-23W5		13128 m	black limestone and pyrite
287	290	9-5-57-17W5		3188 m	vein calcite
288	291	9-5-57-17W5		~3194 m	cements
289	292	9-5-57-17W5		~3221 m	cements
290	293	6-34-57-21W5		3437.0 m	reservoir
291	294	6-34-57-21W5		3432 m	bitumen and late calcite cement
292	295	6-34-57-21W5		3430 m	bitumen
293	296	2-14-50-22W5		~12856 m	calcite vug in dolomite mudstone = Wabamun?
294	297	2-14-50-22W5		~15032 m	sulfur / cements
295	298	2-14-50-22W5		15078 m	calcite vug
296	299	2-14-50-22W5		15042 m	cements / diagenesis
297	300	16-22-58-19W5		11045 m	cemented vug / crystal ?
298	301	16-22-58-19W5		11062.3 m	vug filling crystal / anhydrite ?
299	302	16-22-58-19W5		11035 m	calcite vug / after bitumen
300	303	16-22-58-19W5		11074 m	calcite vug / after bitumen
301	304	16-22-58-19W5		11087 m	bitumen / calcite
302	305	16-22-58-19W5		11035 m	cements
303	306	10-20-58-15W5		10.411 feet	white vugs in limestone
304	307	10-20-58-15W5		10.397 feet	fossils in limestone
305	308	10-20-58-15W5		10.389 feet	white vugs in limestone
306	309	10-20-58-15W5		10.378.3 feet	stromatoporoids and cements
307	310	10-20-58-15W5		10.374 feet	vug cement
308	311	10-12-54-18W5		11.673 feet	calcite vug at top
309	312	10-12-54-18W5		11.678 feet	late vein calcite and (saddle dolomite NO !)
310	313	10-12-54-18W5		11.698 feet	anhydrite
311	314	10-12-54-18W5		11.727 feet	vein - calcite
312	315	10-12-54-18W5		11.743 feet	sulfur
313	316	16-18-61-15W5		8991 feet	bitumen / anhydrite in dolostone
314	317	16-18-61-15W5		9023 feet	vugs / bitumen
315	318	16-18-61-15W5		~ 9045 feet	vugs
316	319	16-18-61-15W5		9053 feet	anhydrite and cements
317	320	16-18-61-15W5		9083 feet	anhydrite ?
318	321	16-18-61-15W5		9120 feet	anhydrite
319	322	10-23-58-17W5		3030 m	calcite vein and sulfur
320	323	10-23-58-17W5		3033 m	calcite
321	324	2-2-57-22W5		3567.5 m	calcite and other cements
322	325	2-2-57-22W5		3568 m	anhydrite
323	326	2-2-57-22W5		3578 m	vuggy dolostone
324	327	13-15-60-16W5		2550 - 2568 m	dolostone
325	328	13-15-60-16W5		2507 - 2516 m	crinoid grainstone
326	329	15-9-57-17W5		~3145 m	dolomite cement / anhydrite
327	330	15-9-57-17W5		~3149.5 m	cement / calcite vein
328	331	15-9-57-17W5		~3150 m	vein - calcite
329	332	15-9-57-17W5		~3157 m	cements
330	333	15-9-57-17W5		~3162 m	vein - calcite

APPENDIX IV

Formation tops picked from electric logs that were used for cross sectioning, isopach map, and structure map construction. Abbreviations are as follows:

KB (m)	Depth of Kelly Bushing
(m)	meters
Twab(md)	Top Wabamun in measured depths
Twint(md)	Top Winterburn in measured depths
Tire (md)	Top Ireton in measured depths
Tduv (md)	Top Duvernay in measured depths
Tled (md)	Top Leduc in measured depths
Tcklk (md)	Top Cooking Lake in measured depths
Tswhl (md)	Top Swan Hills in measured depths
Tgil (md)	Top Gilwood in measured depths
Twab(ss)	Top Wabamun in subsea elevation
Twint(ss)	Top Winterburn in subsea elevation
Tire (ss)	Top Ireton in subsea elevation
Tduv (ss)	Top Duvernay in subsea elevation
Tled (ss)	Top Leduc in subsea elevation
Tcklk/swhl (ss)	Top Cooking Lake/Swan Hills in subsea elevation
Tswhl/Bhlk(ss)	Top Swan Hills/Beaverhill Lake in subsea elevation
Tcklk/swhl (ss)	Top Cooking Lake/Swan Hills in subsea elevation

Location	KB (m)	T _{web} (md)	T _{sub} (md)	T _{iso} (md)	T _{div} (md)	T _{lid} (md)	T _{shk} (md)	T _{ent} (md)	T _g (md)	T _{web} (ss)	T _{sub} (ss)	T _{iso} (ss)	T _{div} (ss)	T _{lid} (ss)	T _{shk} (ss)	T _{ent} (ss)	T _g (ss)	T _{web} (iso)	T _{sub} (iso)	T _{iso} (iso)	T _{div} (iso)	T _{lid} (iso)	T _{shk} (iso)	T _{ent} (iso)	T _g (iso)	
9-23-57-25W5	1107.7	3691	3899.0	4030.7	4298.0	4770.0	4920	2594.3	-2782.3	-2923.3	-3161.3	-3191.3	196.0	141.0	238.0	30.0	150.0									
10-4-56-26W5	1165.6	4196	4407.0	4552.7	4770.0	4656.0	4820	-5001.4	-3241.4	-3386.4	-3442.5	-3604.4	217.0	145.0	218.0		150.0									
5-27-56-27W5	1213.5	4265	4482.0	4627.7	4790.0	4656.0	4820	-5001.4	-3241.4	-3386.4	-3442.5	-3604.4	217.0	145.0	218.0		150.0									
1-16-55-27W5	1277.7	4526	4790.0	4954.0	5047.0	5058	5258	-3248.3	-3452.3	-3676.3	-3769.3	-3901.3	204.0	224.0	93.0	132.0	79.0									
7-36-54-28W5	1360.3	4593	4671.0	4708.0	4708.0	4708.0	4708.0	-3358.9	-3436.9	-3473.9	-3473.9	-3543.1	78.0	37.0												
10-15-56-27W5	1234.1	4593	4671.0	4708.0	4708.0	4708.0	4708.0	-3358.9	-3436.9	-3473.9	-3473.9	-3543.1	78.0	37.0												
6-1-57-27W5	1131.9	4105	4319.0	4511.0	4675.0	4511.0	4612	-2973.1	-3157.1	-3379.1	-3543.1	-3860.1	214.0	192.0	184.0	137.0										
13-13-58-25W5																										
D-D Location	KB (m)	T _{web} (md)	T _{sub} (md)	T _{iso} (md)	T _{div} (md)	T _{lid} (md)	T _{shk} (md)	T _{ent} (md)	T _g (md)	T _{web} (ss)	T _{sub} (ss)	T _{iso} (ss)	T _{div} (ss)	T _{lid} (ss)	T _{shk} (ss)	T _{ent} (ss)	T _g (ss)	T _{web} (iso)	T _{sub} (iso)	T _{iso} (iso)	T _{div} (iso)	T _{lid} (iso)	T _{shk} (iso)	T _{ent} (iso)	T _g (iso)	
5-8-60-29W5	1174.1	3717	3947.0	4075.0	4075.0	4037.0	4037.0	2542.9	-2772.9	-2900.9	-2924.0	-2924.0	230.0	243.0												
5-27-59-29W5	1113.0	3677	3920.0	4037.0	4037.0	4037.0	4037.0	2542.9	-2772.9	-2900.9	-2924.0	-2924.0	230.0	243.0												
14-19-54-25W5	1262.0	3791	FAULT ?																							
10-20-59-25W5	1257.3	3709	3937.0	4017.7	4090.0	4090.0	4090.0	-2451.7	-2679.7	-2759.7	-2832.7	-2832.7	226.0	80.0	73.0											
7-18-59-24W5	1189.9	3581.4	3822.0	3922.0	3922.0	3922.0	3922.0	-2381.5	-2632.1	-2719.1	-2744.1	-2744.1	218.0	134.0	25.0											
16-32-58-24W5	1045.9	3413	3631.0	3765.0	3760.0	3760.0	3760.0	-2381.5	-2632.1	-2719.1	-2744.1	-2744.1	218.0	134.0	25.0											
16-34-58-24W5	1042.4	3406	3598.0	3735.0	3760.0	3760.0	3760.0	-2381.5	-2632.1	-2719.1	-2744.1	-2744.1	218.0	134.0	25.0											
09-23-57-24W5	1036.4	3504	3701.0	3849.0	3853.0	4121.0	4118	-2464.6	-2661.6	-2809.6	-2815.6	-3081.6	197.0	148.0	6.0	266.0										
11-11-57-22W5	1117.7	3365	3577.0	3788.0	3923.0	3923.0	3923.0	-2247.3	-2459.3	-2670.3	-2668.3	-2868.3	212.0	211.0	198.0	132.0										
2-2-57-22W5	1037.2	3283	3497.0	3720.0	3923.0	3923.0	3923.0	-2245.8	-2459.8	-2682.8	-2685.8	-2865.8	214.0	223.0	203.0											
11-25-56-22W5	925.4	3165	3363.0	3566.0	3761.0	3761.0	3761.0	-2239.6	-2437.6	-2660.6	-2663.6	-2853.6	198.0	223.0	195.0	142.0										
13-22-56-21W5	1115.3	3390	3563.0	3760.0	3970.0	3970.0	4112	-2264.7	-2447.7	-2664.7	-2667.7	-2854.7	183.0	217.0	190.0	142.0										
6-18-58-20W5	1120.7	3260	3513.0	3718.0	3659.0	3659.0	3659.0	-2169.3	-2392.3	-2597.3	-2738.3	-2769.3	223.0	205.0	141.0	61.0										
7-25-55-21W5	1356.5	3602	3813.0	4002.0	4114.0	4243.0	4386	-2243.5	-2454.5	-2643.5	-2755.5	-2884.5	223.0	205.0	141.0	126.0	143.0									
9-31-55-20W5	1378.2	3562	3745.0	3933.0	4070.0	4236.0	4312	-2163.8	-2366.8	-2554.8	-2691.8	-2857.8	183.0	188.0	137.0	166.0	76.0									
11-19-55-20W5	1314.0	3548	3758.0	3907.0	3922.0	4199.0	4094	-2234.0	-2444.0	-2593.0	-2608.0	-2865.0	210.0	149.0	15.0	277.0										
2-11-55-20W5	1136.5	3313	3535.0	3680.0	3908.0	3908.0	4094	-2181.1	-2405.1	-2541.1	-2751.1	-2797.5	224.0	198.0	254.0	160.0	180.0									
7-29-54-20W5	1139.4	3223	3550.0	3710.0	3710.0	3710.0	3710.0	-2163.6	-2410.6	-2570.6	-2570.6	-2797.5	222.0	160.0	77.0											
10-23-54-20W5	1099.7	3286	3520.0	3757.0	3834.0	3834.0	3834.0	-2199.3	-2430.3	-2667.3	-2744.3	-2868.4	234.0	237.0	47.0											
2-19-54-19W5	1040.6	3176	3412.0	3680.0	3727.0	3727.0	3727.0	-2135.4	-2371.4	-2639.4	-2686.4	-2686.4	226.0	268.0	47.0											
2-13-54-19W5	969.0	3032	3258.0	3508.0	3307.0	3514.0	3590	-2043.0	-2269.0	-2263.9	-2360.9	-2567.9	226.0	236.0	207.0	76.0										
6-5-55-17W5	946.1	2821	3062.0	3210.0	3287.0	3287.0	3287.0	-1874.9	-2115.9	-2263.9	-2360.9	-2567.9	241.0	148.0	97.0											
7-14-54-18W5	984.0	2886	3097.0	3266.0	3287.0	3287.0	3287.0	-1902.0	-2113.0	-2284.0	-2303.0	-2568.0	211.0	171.0	19.0											
10-12-54-18W5	969.0	2932	3142.0	3355.0	3657.0	3704	3704	-1963.0	-2173.0	-2397.0	-2397.0	-2668.0	210.0	214.0	201.0	147.0										
5-21-52-17W5	946.6	3057	3260.0	3478.0	3690.0	3690.0	3690.0	-2110.4	-2313.4	-2531.4	-2531.4	-2743.4	203.0	218.0	212.0	128.0										
10-28-52-16W5	944.0	2967	3065.0	3261.0	3520.0	3622	3622	-1923.0	-2121.0	-2317.0	-2317.0	-2576.0	188.0	195.0	259.0	102.0										
11-5-53-15W5	907.1	2709	2914.0	3123.0	3405.0	3484	3484	-1801.9	-2006.9	-2215.9	-2215.9	-2497.9	205.0	209.0	282.0	79.0										
Location	KB (m)	T _{web} (md)	T _{sub} (md)	T _{iso} (md)	T _{div} (md)	T _{lid} (md)	T _{shk} (md)	T _{ent} (md)	T _g (md)	T _{web} (ss)	T _{sub} (ss)	T _{iso} (ss)	T _{div} (ss)	T _{lid} (ss)	T _{shk} (ss)	T _{ent} (ss)	T _g (ss)	T _{web} (iso)	T _{sub} (iso)	T _{iso} (iso)	T _{div} (iso)	T _{lid} (iso)	T _{shk} (iso)	T _{ent} (iso)	T _g (iso)	

APPENDIX V

Stable Isotope Data

UWI	SAMPLE #	Description/remarks	$^{13}\text{C}/^{12}\text{C}$	$^{18}\text{O}/^{16}\text{O}$	Data source
			(‰ PDB)	(‰ PDB)	
10-20-57-25W5	# 105	vein calcite	-10.708	-11.396	this study
01-32-57-25W5	# 087 (I)	fracture cc/late stage calcite	-10.971	-11.92	this study
09-22-58-24W5	# 75	cc-cements	-19.021	-7.749	this study
11-30-51-25W5	# 36A	cc-cement	-8.94	-13.443	this study
06-16-55-18W5	# 125A	Late calcite	-4.575	-11.597	this study
01-16-55-27W5	#MC7	cc-vug	-9.248	-8.46	this study
14-36-52-27W5	#15b	cc-vein	-3.658	-8.974	this study
10-15-56-27W5	#MC2	vein calcite	-2.496	-13.658	this study
09-20-59-22W5	#9-20/009	cc x-tal in pore	-24.69	-11.405	this study
05-13-58-24W5	#145	cc-cements	2.583	-6.546	this study
06-29-60-22W5	#56	fracture infills/cc	-5.907	-7.694	this study
01-18-56-16W5	#116A	vein calcite	-12.668	-8.112	this study
15-19-56-23W5	#136	Matrix dolostone	3.515	-8.088	this study
06-29-60-22W5	#52	Dolostone	0.466	-4.94	this study
09-22-58-24W5	#73	Host rock	1.508	-6.553	this study
01-32-57-25W5	#87 (II)	Host dolostone	1.953	-5.023	this study
06-16-55-18W5	#125B	Matrix dolostone	0.887	-5.41	this study
15-18-58-24W5	225	vein calcite	-14.595	-7.559	this study
07-18-52-24W5	252	vein calcite	-6.697	-11.291	this study
16-32-58-24W5	229	calcite	-12.396	-7.263	this study
11-29-59-16W5	208	calcite	-12.396	-7.263	this study
05-25-51-22W5	270	calcite	-2.994	-11.999	this study
07-07-53-26W5	14B	matrix dolomite	1.781	-7.168	this study
11-30-50-25W5	37A	saddle dolomite	-0.037	-9.882	this study
10-13-52-22W5	275C	matrix dolomite	2.914	-6.513	this study
09-05-57-17W5	290B	dolomite	0.929	-8.543	this study
16-22-58-19W5	305D	matrix dolomite	3.124	-6.274	this study
09-05-57-17W5	290 A	calcite	-0.356	-11.429	this study
04-26-58-20W5	194 B	calcite	-9.649	-10.654	this study
11-09-61-22W5	172 A	cc-cement	-12.05	-8.937	this study
16-16-52-21W5	4118.8 m	late calcite	-2.21	-10.05	this study
07-15-52-22W5	4188.3m	Late calcite	-2.78	-7.91	Manzano, unpubl.
	4190.7m	fracture late calcite	-15.33	-8.37	Manzano, unpubl.
	4191.3m	Late calcite	-13.88	-8.86	Manzano, unpubl.
02-22-52-22W5	4224.6m	Late calcite	-13.43	-9.28	Manzano, unpubl.
	4257.6m	Late calcite	-12.04	-9.62	Manzano, unpubl.

07-18-52-24W5	4835.4	Late calcite	-15.33	-7.86	Manzano, unpubl.
10-27-52-24W5	4686.5m	fracture cc/late stage calcite	-0.51	-8.46	Manzano, unpubl.
16-16-52-21W5	4104.6m	Saddle dolomite	1.27	-5.26	Patey, 1995
15-23-53-21W5	4046.5m	Saddle dolomite	-0.75	-6.71	Patey, 1995
02-36-54-23W5	4087.7m	Saddle dolomite	2.25	-3.98	Patey, 1995
01-11-59-18W5	n/a	Saddle dolomite	-6.3	-2.28	Green, 1999
10-27-58-18W5	n/a	Saddle dolomite	-6.6	-7.37	Green, 1999
01-02-59-18W5	n/a	Saddle dolomite	-7.9	-3.45	Green, 1999

APPENDIX VI

Strontium isotope data of solids

SAMPLE #	Description/remarks	Isotope #	⁸⁷Sr/⁸⁶Sr
# 9-20 005	75% loss while prep.	MB1-1	0.72371 +/- 2
# 089	(I) clean saddle dolomite	MB1-2	0.70921 +/- 2
# 087	(I) late stage cc-cement	MB1-3	0.73045 +/- 2
# 105	vein calcite	MB1-4	0.73069 +/- 2
# 075	fracture cc	MB1-5	0.70907 +/- 2
# 145	cc-cements	MB1-6	0.70837 +/- 2
# 9-20 009	cc x-tal in pore space	MB 2-1	0.72413 +/- 2
# 9-20 012	vein calcite	MB 2-2	0.72281 +/- 2
# 056	fracture fillings	MB 2-3	0.71380 +/- 2
# 089	big cc vug filling	MB 2-4	0.72613 +/- 2
# 094	(I) "funny (slow) reaction	MB 2-5	0.71282 +/- 2
# 087	(III) saddle dolomite	MB 2-6	0.72060 +/- 2
# 106	saddle dolomite	MB 3-1	0.71799 +/- 2
# 9-20 006	(I) vein filling/ calcite	MB 3-2	0.72252 +/- 2
# 148	cc-vein filling (how clean is samples?)	MB 3-3	0.70810 +/- 2
# 9-20 002	(I) vein	MB 3-4	0.72206 +/- 2
# 9-20 003	vein cc/ ssulfur smell	MB 3-5	0.72336 +/- 2
# 9-20 006	host rock/ dolostone	MB 3-6	0.71026 +/- 2
# 052	bulk host rock/matrix dolomite	MB 4-1	0.70844 +/- 2
# 073	(II) host rock/dolostone	MB 4-2	0.70854 +/- 2
# 094	(II) host rock/dolostone	MB 4-3	0.70840 +/- 2
# 078	(II) bulk rock/dolostone (mixture?)	MB 4-4	0.71509 +/- 2
# 136	whole rock samples	MB 4-5	0.70839 +/- 2
# 087	host rock/ whole dolostone	MB 4-6	0.70887 +/- 2
# PC 2	Cambrian red shale 10-31-54-12W5	MB 5-1	0.71618 +/- 2
# PC 3	grey cambr shale 10-31-54-12W5	MB 5-2	0.72498 +/- 2
# PC 4	Elk Pt. PF carb. 15-29-55-17W5	MB 5-3	0.71848 +/- 2
# PC 5	Elk Pt. Sst 15-29-55-17W5	MB 5-4	0.71877 +/- 2
# 10A	cc vein/ coarse xtal	MB 5-5	0.70989 +/- 2
# 124A	vein cc	MB 5-6	0.71782 +/- 2
#158A	vein calcite	MB 6-1	0.71942 +/- 2

# 009 A	calcite	MB 6-2	0.70970 +/- 2
# 125 A	vein cc	MB 6-3	0.71785 +/- 2
# 36A	cc-cement	MB 6-4	0.72117 +/- 2
# 114A	late cc-cement	MB 6-5	0.71895 +/- 2
# 158 A	vein calcite	MB 6-6	0.71943
# 15B	cc-vein + anhydr?	MB 7-1	0.71026 +/- 2
# 32 A	sulfur/cement mixture	MB 7-2	0.71025 +/- 2
# 37A	saddle dolomite	MB 7-3	0.71985 +/- 2
# 25 A	cc-cement	MB 7-4	0.72280 +/- 2
# 116 A	vein calcite	MB 7-5	0.71895 +/- 2
# 14B	matrix dolomite	MB 7-6	0.71051 +/- 2
MC 2 10-15-56-27W5	vein calcite (15272')	MB 8-1	0.73076 +/- 2
MC 3 10-15-56-27W5	vein calcite (15274')	MB 8-2	0.72829 +/- 2
MC 4 01-16-55-27W5	calcite xtal (16693')	MB 8-3	0.73233 +/- 2
MC 5 01-16-55-27W5	calcite vugs/vein (16700')	MB 8-4	0.72403 +/- 2
MC 6 01-16-55-27W5	vug calcite (16 708')	MB 8-5	0.72415 +/- 2
MC 7 01-16-55-27W5	cc-vug (16703')	MB 8-6	0.72348 +/- 2
# 225	I -vein calcite	MB 9-1	0.71995 +/- 2
# 252	I vein calcite	MB 9-2	0.72038 +/- 2
# 229	calcite	MB 9-3	0.72102 +/- 2
# 322	calcite	MB 9-4	0.71805 +/- 2
# 208	calcite	MB 9-5	0.71392 +/- 2
# 270	PI-calcite	MB 9-6	0.72055 +/- 2
# 214	Mudstone (Calmar/Blueridge)	MB 10-1	0.71721 +/- 2
# 236	calcite	MB 10-2	0.72102 +/- 2
# 251	calcite	Mb 10-3	0.72428 +/- 2
# 169A	cc-cement	MB 10-4	0.70887 +/- 2
# 194 B	cc-powder?	MB 10-5	0.71632 +/- 2
# 294	P1 calcite	MB 10-6	0.71125 +/- 2
# 302	vein calcite	MB11-1	0.71926 +/- 2
# 275A	vein calcite	MB11-2	0.71079 +/- 2
# 264	P1 vein calcite	MB11-3	0.72298 +/- 2

# 298	vein calcite	MB11-4	0.70869 +/- 2
# 244	vein calcite	MB11-5	0.70835 +/- 2
# 240 A	vug filling cc-xtals (mixture?)	MB11-6	0.71464 +/- 2
# 227A	cc xtals in vug (ccII /CcIII?)	MB 12-1	0.71187 +/- 2
# 290A	late vein cc	MB 12-2	0.71789 +/- 2
# 290 B	dolomite cement	MB 12-3	0.71415 +/- 2
# 326	matrix/cem mixture	MB 12-4	0.71342 +/- 2
# 334	calcite III	MB 12-5	0.71753 +/- 2
# 125 B	matrix	MB 13-1	0.71141 +/- 2
# 014A	Sulfate	MB 13-2	0.70890 +/- 2
# 181 A	Sulfate	MB 13-3	0.70918 +/- 2
# 275 C	Matrix	MB 13-4	0.70976 +/- 2
# 161A	Anhydrite	MB 13-5	0.70865 +/- 2
# 305	Matrix	MB 13-6	0.70884 +/- 2
# 127 A	Anhydrite	MB 14-1	0.71000 +/- 2
# 36 B	Matrix	MB 14-2	0.70959 +/- 2
# 276	Anhydrite	MB 14-3	0.70947 +/- 2
# 215	Saddle Dolomite	MB 14-4	0.71064 +/- 2
# 320	Matr + cement mixture	MB 14-5	0.71053 +/- 2
# 168	Matrix	MB 14-6	0.70873 +/- 2
XXX	Mt. Brussilof Magnesite	MB 15-1	0.71050 +/- 2

APPENDIX VII

Fluid Inclusion Data

Appendix VII A: Measured data

Appendix VII B: Pressure corrected data

Sample #	Host	Th	Tm(ice)	Tm(ice)corr	Salinity	Th
MB264-1-1	Calcite	160	-17.8	-18.2	21.1	160
MB264-1-2	Calcite	173	-17.5	-17.9	20.9	173
MB264-1-3	Calcite	157	-17.8	-18.2	21.1	157
MB264-1-4	Calcite	178	-17.8	-18.2	21.1	178
MB264-1-5	Calcite	150	-18.3	-18.7	21.5	150
MB264-1-6	Calcite	165	-19.0	-19.4	22.0	165
MB264-1-7	Calcite	159	-17.8	-18.2	21.1	159
MB264-1-8	Calcite	159	-19.1	-19.5	22.0	159
MB264-1-9	Calcite	158	-18.9	-19.3	21.9	158
MB264-1-10	Calcite	157	-18.6	-19.0	21.7	157
MB264-2-1	Calcite	145	-19.9	-20.3	22.6	145
MB264-2-2	Calcite	142	-21.4	-21.8	23.6	142
MB264-2-3	Calcite	139	-21.4	-21.8	23.6	139
MB264-2-4	Calcite	138	-20.4	-20.8	22.9	138
MB264-2-5	Calcite	145	-20.4	-20.8	22.9	145
MB264-2-6	Calcite	136	-21.4	-21.8	23.6	136
MB264-2-7	Calcite	136	-20.4	-20.8	22.9	136
MB264-2-8	Calcite	153	-16.4	-16.8	20.1	153
MB264-2-9	Calcite		-16.5			
MB264-2-10	Calcite	136	-19.9	-20.3	22.6	136
MB264-2-11	Calcite	137	-21.5	-21.9	23.6	137
MB264-2-12	Calcite	146	-19.9	-20.3	22.6	146
MB264-2-13	Calcite	151	-19.6	-20.0	22.4	151
MB264-2-14	Calcite	140	-19.9	-20.3	22.6	140
MB264-2-15	Calcite	137	-19.4	-19.8	22.2	137
MB264-2-16	Calcite		-19.9	-20.3	22.6	
MB15-1-1	Calcite	157	-12.6	-13.0	16.9	157
MB15-1-2	Calcite	162				162
MB15-1-3	Calcite	160	-13.7	-14.1	17.9	160
MB15-1-4	Calcite		-13.9	-14.3	18.0	
MB15-1-5	Calcite	153	-13.5	-13.9	17.7	153
MB15-1-6	Calcite	148				148
MB15-1-7	Calcite	143	-13.3	-13.7	17.5	143
MB15-1-8	Calcite	158	-13.4	-13.8	17.6	158
MB15-1-9	Calcite		-12.9	-13.3	17.2	
MB15-1-10	Calcite	153	-12.9	-13.3	17.2	153
MB15-1-11	Calcite	159	-13.6	-14.0	17.8	159
MB15-1-12	Calcite	150	-13.6	-14.0	17.8	150
MB15-2-1	Calcite	132	-13.4	-13.8	17.6	132
MB15-2-2	Calcite	132	-13.3	-13.7	17.5	132
MB15-2-3	Calcite					
MB15-2-4	Calcite	156	-12.5	-12.9	16.8	156
MB15-2-5	Calcite	164	-13.4	-13.8	17.6	164
MB15-2-6	Calcite	164	-13.7	-14.1	17.9	164
MB15-2-7	Calcite	163	-13.3	-13.7	17.5	163
MB201-1-1	Dolomite	133	-17.9	-18.3	21.2	133
MB201-1-2	Dolomite	140	-18.0	-18.4	21.3	140
MB201-1-3	Dolomite	135	-18.0	-18.4	21.3	135
MB201-1-4	Dolomite	145				145
MB201-1-5	Dolomite		-17.8	-18.2	21.1	
MB201-1-6	Dolomite	123	-18.0	-18.4	21.3	123
MB312-1-1	Calcite	104	-14.7	-15.1	18.7	104
MB312-1-2	Calcite	106	-14.7	-15.1	18.7	106

Sample #	Host	Th	Tm(ice)	Tm(ice)corr	Salinity	Th
MB312-1-3	Calcite	105				105
MB312-1-4	Calcite	117	-16.8	-17.2	20.4	117
MB312-1-5	Calcite	125	-16.6	-17.0	20.2	125
MB312-1-6	Calcite	127				127
MB312-1-7	Calcite	117	-17.4	-17.8	20.8	117
MB312-1-8	Calcite	116	-17.4	-17.8	20.8	116
MB312-1-9	Calcite	104	-17.2	-17.6	20.7	104
MB312-1-10	Calcite	122	-17.4	-17.8	20.8	122
MB312-1-11	Calcite	128	-16.6	-17.0	20.2	128
MB312-1-12	Calcite	137	-17.2	-17.6	20.7	137
MB312-1-13	Calcite	107	-16.9	-17.3	20.4	107
MB312-1-14	Calcite	108	-16.1	-16.5	19.8	108
MB312-1-15	Calcite	114	-16.6	-17.0	20.2	114
MB312-1-16	Calcite	122	-16.6	-17.0	20.2	122
MB312-1-17	Calcite	106	-16.3	-16.7	20.0	106
MB312-1-18	Calcite	117	-16.6	-17.0	20.2	117
MB312-2-1	Calcite	104	-16.3	-16.7	20.0	104
MB312-2-2	Calcite	114	-16.3	-16.7	20.0	114
MB312-2-3	Calcite	94	-16.3	-16.7	20.0	94
MB312-2-4	Calcite	105	-16.3	-16.7	20.0	105
MB312-2-5	Calcite	101	-16.3	-16.7	20.0	101
MB312-2-6	Calcite	92	-16.3	-16.7	20.0	92
MB312-2-7	Calcite	108	-16.3	-16.7	20.0	108
MB312-2-8	Calcite	98	-16.3	-16.7	20.0	98
MB312-2-9	Calcite	100	-16.3	-16.7	20.0	100
MB312-2-10	Calcite	112	-16.3	-16.7	20.0	112
MB312-2-11	Calcite	87	-16.3	-16.7	20.0	87
MB312-2-12	Calcite	89	-16.3	-16.7	20.0	89
MB312-2-13	Calcite	92	-16.3	-16.7	20.0	92
MB322-1-1	Calcite	118	-15.9	-16.3	19.7	118
MB322-1-2	Calcite	116	-15.9	-16.3	19.7	116
MB322-1-3	Calcite	116	-15.8	-16.2	19.6	116
MB322-1-4	Calcite	112	-15.9	-16.3	19.7	112
MB322-1-5	Calcite	112	-15.9	-16.3	19.7	112
MB322-1-6	Calcite	103	-15.9	-16.3	19.7	103
MB322-1-7	Calcite	112	-15.9	-16.3	19.7	112
MB322-1-8	Calcite	110	-15.9	-16.3	19.7	110
MB322-1-9	Calcite	113	-15.9	-16.3	19.7	113
MB322-1-10	Calcite	113	-15.9	-16.3	19.7	113
MB322-1-11	Calcite		-15.9	-16.3	19.7	
MB322-1-12	Calcite	126	-15.9	-16.3	19.7	126
MB322-1-13	Calcite	103	-16.1	-16.5	19.8	103
MB322-1-14	Calcite	112	-15.9	-16.3	19.7	112
MB322-1-15	Calcite	93	-15.9	-16.3	19.7	93
MB251-1-1	Calcite	126	-20.4	-20.8	22.9	126
MB251-1-2	Calcite	131	-20.4	-20.8	22.9	131
MB251-1-3	Calcite	141	-20.4	-20.8	22.9	141
MB251-1-4	Calcite		-20.3	-20.7	22.8	
MB251-1-5	Calcite	130	-20.4	-20.8	22.9	130
MB251-1-6	Calcite	132	-20.4	-20.8	22.9	132
MB251-1-7	Calcite	131	-20.4	-20.8	22.9	131
MB251-1-8	Calcite	148	-20.4	-20.8	22.9	148
MB251-1-9	Calcite	137	-20.4	-20.8	22.9	137

Sample #	Host	Th	Tm(ice)	Tm(ice)corr	Salinity	Th
MB251-1-10	Calcite	129	-20.2	-20.6	22.8	129
MB251-1-11	Calcite		-20.4	-20.8	22.9	
MB251-1-12	Calcite		-20.4	-20.8	22.9	
MB251-1-13	Calcite	130	-20.4	-20.8	22.9	130
MB251-1-14	Calcite	132	-18.2	-18.6	21.4	132
MB251-1-15	Calcite	127	-18.2	-18.6	21.4	127
MB251-1-16	Calcite	146	-18.5	-18.9	21.6	146
MB251-2-1	Calcite	115	-19.2	-19.6	22.1	115
MB251-2-2	Calcite	140	-20.4	-20.8	22.9	140
MB251-2-3	Calcite	115	-17.9	-18.3	21.2	115
MB251-2-4	Calcite	138	-20.2	-20.6	22.8	138
MB251-2-5	Calcite		-20.2	-20.6	22.8	
MB251-2-6	Calcite	130				130
MB251-2-7	Calcite		-20.2	-20.6	22.8	
MB251-2-8	Calcite	148	-20.2	-20.6	22.8	148
MB251-2-9	Calcite	144	-20.7	-21.1	23.1	144
MB251-2-10	Calcite	127	-20.0	-20.4	22.6	127
MB251-2-11	Calcite		-21.6	-22.0	23.7	
MB256-1-1	Calcite					
MB256-1-2	Calcite					
MB256-1-3	Calcite					
MB256-1-4	Calcite					
MB256-1-5	Calcite	132	-20.0	-20.4	22.6	132
MB256-1-6	Calcite	132	-19.8	-20.2	22.5	132
MB256-1-7	Calcite	134	-20.1	-20.5	22.7	134
MB256-1-8	Calcite	134	-20.1	-20.5	22.7	134
MB256-1-9	Calcite	121	-19.8	-20.2	22.5	121
MB256-1-10	Calcite	131	-19.6	-20.0	22.4	131
MB256-1-11	Calcite	128	-18.6	-19.0	21.7	128
MB256-1-12	Calcite	131	-19.8	-20.2	22.5	131
MB256-1-13	Calcite		-18.9	-19.3	21.9	
MB256-1-14	Calcite	124	-19.6	-20.0	22.4	124
MB256-1-15	Calcite	125				125
MB270-1-1	Calcite	135				135
MB270-1-2	Calcite	135	-17.2	-17.2	20.4	135
MB270-1-3	Calcite					
MB270-1-4	Calcite	140	-16.7	-16.7	20.0	140
MB270-1-5	Calcite	135	-16.5	-16.5	19.8	135
MB270-1-6	Calcite		-16.6	-16.6	19.9	
MB87-1-1	Calcite	133	-15.7	-15.7	19.2	133
MB87-1-2	Calcite	130	-21.2	-21.2	23.2	130
MB87-1-3	Calcite	129	-21.2	-21.2	23.2	129
MB87-1-4	Calcite	131	-21.9	-21.9	23.6	131
MB87-1-5	Calcite		-21.5	-21.5	23.4	
MB87-1-6	Calcite	133	-21.5	-21.5	23.4	133
MB87-1-7	Calcite	138	-21.5	-21.5	23.4	138
MB87-1-8	Calcite	135	-21.5	-21.5	23.4	135
MB87-1-9	Calcite	130	-21.5	-21.5	23.4	130
MB87-1-10	Calcite	134	-21.3	-21.3	23.2	134
MB87-1-11	Calcite	122	-18.0	-18.0	21.0	122
MB87-2-1	Calcite	135	-16.0	-16.0	19.4	135
MB87-2-2	Calcite	132	-16.0	-16.0	19.4	132
MB87-2-3	Calcite	132	-15.9	-15.9	19.4	132

Sample #	Host	Th	Tm(ice)	Tm(ice)corr	Salinity	Th
MB87-2-4	Calcite	132	-15.9	-15.9	19.4	132
MB87-2-5	Calcite	134	-16.0	-16.0	19.4	134
MB87-2-6	Calcite	134	-16.0	-16.0	19.4	134
MB87-2-7	Calcite	136	-15.9	-15.9	19.4	136
MB87-2-8	Calcite	120	-16.3	-16.3	19.7	120
MB87-2-9	Calcite	132	-16.0	-16.0	19.4	132
MB87-2-10	Calcite	140	-16.2	-16.2	19.6	140
MB87-2-11	Calcite	132	-16.1	-16.1	19.5	132
MB87-2-12	Calcite	139	-15.8	-15.8	19.3	139
MB87-2-13	Calcite	119	-16.3	-16.3	19.7	119
MB87-2-14	Calcite	122	-16.1	-16.1	19.5	122
MB87-2-15	Calcite	138	-15.9	-15.9	19.4	138
MB87-2-16	Calcite	137	-16.1	-16.1	19.5	137
MB87-2-17	Calcite	137	-16.0	-16.0	19.4	137
MB87-2-18	Calcite	137	-16.0	-16.0	19.4	137
MB87-2-19	Calcite	139	-16.0	-16.0	19.4	139
MB87-2-20	Calcite	139	-16.0	-16.0	19.4	139
MB87-2-21	Calcite	137	-15.9	-15.9	19.4	137
MB87-2-22	Calcite	137	-15.9	-15.9	19.4	137
MB87-2-23	Calcite	135	-15.8	-15.8	19.3	135
MB87-2-24	Calcite	135	-16.0	-16.0	19.4	135
MB87-2-25	Calcite	136	-16.0	-16.0	19.4	136
MB87-2-26	Calcite	137	-16.0	-16.0	19.4	137
MB87-2-27	Calcite	137	-16.0	-16.0	19.4	137
MB87-2-28	Calcite	139	-16.1	-16.1	19.5	139
MB87-2-29	Calcite	137	-15.8	-15.8	19.3	137

Sample #	Host	Depth (m)	Depth (m) corr	Th (°C)	Formation Pressure (kPa)	Hydrostat. Pressure (kPa)	Paleo Pressure (kPa)	Ttmin (°C)	Ttmax (°C)
MB264-1-1	Calcite	5091	7091	160		49942.71	69562.71	215	237
MB264-1-2	Calcite	5091	7091	173		49942.71	69562.71	228	250
MB264-1-3	Calcite	5091	7091	157		49942.71	69562.71	212	234
MB264-1-4	Calcite	5091	7091	178		49942.71	69562.71	233	255
MB264-1-5	Calcite	5091	7091	150		49942.71	69562.71	205	227
MB264-1-6	Calcite	5091	7091	165		49942.71	69562.71	220	242
MB264-1-7	Calcite	5091	7091	159		49942.71	69562.71	214	236
MB264-1-8	Calcite	5091	7091	159		49942.71	69562.71	214	236
MB264-1-9	Calcite	5091	7091	158		49942.71	69562.71	213	235
MB264-1-10	Calcite	5091	7091	157		49942.71	69562.71	212	234
MB264-2-1	Calcite	5091	7091	145		49942.71	69562.71	200	222
MB264-2-2	Calcite	5091	7091	142		49942.71	69562.71	197	219
MB264-2-3	Calcite	5091	7091	139		49942.71	69562.71	194	216
MB264-2-4	Calcite	5091	7091	138		49942.71	69562.71	193	215
MB264-2-5	Calcite	5091	7091	145		49942.71	69562.71	200	222
MB264-2-6	Calcite	5091	7091	136		49942.71	69562.71	191	213
MB264-2-7	Calcite	5091	7091	136		49942.71	69562.71	191	213
MB264-2-8	Calcite	5091	7091	153		49942.71	69562.71	208	230
MB264-2-9	Calcite	5091	7091			49942.71	69562.71	55	77
MB264-2-10	Calcite	5091	7091	136		49942.71	69562.71	191	213
MB264-2-11	Calcite	5091	7091	137		49942.71	69562.71	192	214
MB264-2-12	Calcite	5091	7091	146		49942.71	69562.71	201	223
MB264-2-13	Calcite	5091	7091	151		49942.71	69562.71	206	228
MB264-2-14	Calcite	5091	7091	140		49942.71	69562.71	195	217
MB264-2-15	Calcite	5091	7091	137		49942.71	69562.71	192	214
MB264-2-16	Calcite	5091	7091			49942.71	69562.71	55	77
MB15-1-1	Calcite	5220.8	7220.8	157		51216.048	70836.048	213	235
MB15-1-2	Calcite	5220.8	7220.8	162		51216.048	70836.048	218	240
MB15-1-3	Calcite	5220.8	7220.8	160		51216.048	70836.048	216	238
MB15-1-4	Calcite	5220.8	7220.8			51216.048	70836.048	56	78
MB15-1-5	Calcite	5220.8	7220.8	153		51216.048	70836.048	209	231
MB15-1-6	Calcite	5220.8	7220.8	148		51216.048	70836.048	204	226
MB15-1-7	Calcite	5220.8	7220.8	143		51216.048	70836.048	199	221
MB15-1-8	Calcite	5220.8	7220.8	158		51216.048	70836.048	214	236
MB15-1-9	Calcite	5220.8	7220.8			51216.048	70836.048	56	78
MB15-1-10	Calcite	5220.8	7220.8	153		51216.048	70836.048	209	231
MB15-1-11	Calcite	5220.8	7220.8	159		51216.048	70836.048	215	237
MB15-1-12	Calcite	5220.8	7220.8	150		51216.048	70836.048	206	228
MB15-2-1	Calcite	5220.8	7220.8	132		51216.048	70836.048	188	210
MB15-2-2	Calcite	5220.8	7220.8	132		51216.048	70836.048	188	210
MB15-2-3	Calcite	5220.8	7220.8			51216.048	70836.048	56	78
MB15-2-4	Calcite	5220.8	7220.8	156		51216.048	70836.048	212	234
MB15-2-5	Calcite	5220.8	7220.8	164		51216.048	70836.048	220	242
MB15-2-6	Calcite	5220.8	7220.8	164		51216.048	70836.048	220	242
MB15-2-7	Calcite	5220.8	7220.8	163		51216.048	70836.048	219	241
MB201-1-1	Dolomite	4075.6	6075.6	133	38400	39981.636	59601.636	177	199
MB201-1-2	Dolomite	4075.6	6075.6	140	38400	39981.636	59601.636	184	206
MB201-1-3	Dolomite	4075.6	6075.6	135	38400	39981.636	59601.636	179	201
MB201-1-4	Dolomite	4075.6	6075.6	145	38400	39981.636	59601.636	189	211

Sample #	Host	Depth (m)	Depth (m) corr	Th (°C)	Formation Pressure (kPa)	Hydrostat. Pressure (kPa)	Paleo Pressure (kPa)	Ttmin (°C)	Ttmax (°C)
MB201-1-5	Dolomite	4075.6	6075.6		38400	39981.636	59601.636	44	66
MB201-1-6	Dolomite	4075.6	6075.6	123	38400	39981.636	59601.636	167	189
MB312-1-1	Calcite	3560.4	5560.4	104	34400	34927.524	54547.524	142	164
MB312-1-2	Calcite	3560.4	5560.4	106	34400	34927.524	54547.524	144	166
MB312-1-3	Calcite	3560.4	5560.4	105	34400	34927.524	54547.524	143	165
MB312-1-4	Calcite	3560.4	5560.4	117	34400	34927.524	54547.524	155	177
MB312-1-5	Calcite	3560.4	5560.4	125	34400	34927.524	54547.524	163	185
MB312-1-6	Calcite	3560.4	5560.4	127	34400	34927.524	54547.524	165	187
MB312-1-7	Calcite	3560.4	5560.4	117	34400	34927.524	54547.524	155	177
MB312-1-8	Calcite	3560.4	5560.4	116	34400	34927.524	54547.524	154	176
MB312-1-9	Calcite	3560.4	5560.4	104	34400	34927.524	54547.524	142	164
MB312-1-10	Calcite	3560.4	5560.4	122	34400	34927.524	54547.524	160	182
MB312-1-11	Calcite	3560.4	5560.4	128	34400	34927.524	54547.524	166	188
MB312-1-12	Calcite	3560.4	5560.4	137	34400	34927.524	54547.524	175	197
MB312-1-13	Calcite	3560.4	5560.4	107	34400	34927.524	54547.524	145	167
MB312-1-14	Calcite	3560.4	5560.4	108	34400	34927.524	54547.524	146	168
MB312-1-15	Calcite	3560.4	5560.4	114	34400	34927.524	54547.524	152	174
MB312-1-16	Calcite	3560.4	5560.4	122	34400	34927.524	54547.524	160	182
MB312-1-17	Calcite	3560.4	5560.4	106	34400	34927.524	54547.524	144	166
MB312-1-18	Calcite	3560.4	5560.4	117	34400	34927.524	54547.524	155	177
MB312-2-1	Calcite	3560.4	5560.4	104	34400	34927.524	54547.524	142	164
MB312-2-2	Calcite	3560.4	5560.4	114	34400	34927.524	54547.524	152	174
MB312-2-3	Calcite	3560.4	5560.4	94	34400	34927.524	54547.524	132	154
MB312-2-4	Calcite	3560.4	5560.4	105	34400	34927.524	54547.524	143	165
MB312-2-5	Calcite	3560.4	5560.4	101	34400	34927.524	54547.524	139	161
MB312-2-6	Calcite	3560.4	5560.4	92	34400	34927.524	54547.524	130	152
MB312-2-7	Calcite	3560.4	5560.4	108	34400	34927.524	54547.524	146	168
MB312-2-8	Calcite	3560.4	5560.4	98	34400	34927.524	54547.524	136	158
MB312-2-9	Calcite	3560.4	5560.4	100	34400	34927.524	54547.524	138	160
MB312-2-10	Calcite	3560.4	5560.4	112	34400	34927.524	54547.524	150	172
MB312-2-11	Calcite	3560.4	5560.4	87	34400	34927.524	54547.524	125	147
MB312-2-12	Calcite	3560.4	5560.4	89	34400	34927.524	54547.524	127	149
MB312-2-13	Calcite	3560.4	5560.4	92	34400	34927.524	54547.524	130	152
MB322-1-1	Calcite	3030	5030	118	27500	29724.3	49344.3	151	172
MB322-1-2	Calcite	3030	5030	116	27500	29724.3	49344.3	149	170
MB322-1-3	Calcite	3030	5030	116	27500	29724.3	49344.3	149	170
MB322-1-4	Calcite	3030	5030	112	27500	29724.3	49344.3	145	166
MB322-1-5	Calcite	3030	5030	112	27500	29724.3	49344.3	145	166
MB322-1-6	Calcite	3030	5030	103	27500	29724.3	49344.3	136	157
MB322-1-7	Calcite	3030	5030	112	27500	29724.3	49344.3	145	166
MB322-1-8	Calcite	3030	5030	110	27500	29724.3	49344.3	143	164
MB322-1-9	Calcite	3030	5030	113	27500	29724.3	49344.3	146	167
MB322-1-10	Calcite	3030	5030	113	27500	29724.3	49344.3	146	167
MB322-1-11	Calcite	3030	5030		27500	29724.3	49344.3	33	54
MB322-1-12	Calcite	3030	5030	126	27500	29724.3	49344.3	159	180
MB322-1-13	Calcite	3030	5030	103	27500	29724.3	49344.3	136	157
MB322-1-14	Calcite	3030	5030	112	27500	29724.3	49344.3	145	166
MB322-1-15	Calcite	3030	5030	93	27500	29724.3	49344.3	126	147
MB251-1-1	Calcite	4040	6040	126	37000	39632.4	59252.4	170	191

Sample #	Host	Depth (m)	Depth (m) corr	Th (°C)	Formation Pressure (kPa)	Hydrostat. Pressure (kPa)	Paleo Pressure (kPa)	Ttmin (°C)	Ttmax (°C)
MB251-1-2	Calcite	4040	6040	131	37000	39632.4	59252.4	175	196
MB251-1-3	Calcite	4040	6040	141	37000	39632.4	59252.4	185	206
MB251-1-4	Calcite	4040	6040		37000	39632.4	59252.4	44	65
MB251-1-5	Calcite	4040	6040	130	37000	39632.4	59252.4	174	195
MB251-1-6	Calcite	4040	6040	132	37000	39632.4	59252.4	176	197
MB251-1-7	Calcite	4040	6040	131	37000	39632.4	59252.4	175	196
MB251-1-8	Calcite	4040	6040	148	37000	39632.4	59252.4	192	213
MB251-1-9	Calcite	4040	6040	137	37000	39632.4	59252.4	181	202
MB251-1-10	Calcite	4040	6040	129	37000	39632.4	59252.4	173	194
MB251-1-11	Calcite	4040	6040		37000	39632.4	59252.4	44	65
MB251-1-12	Calcite	4040	6040		37000	39632.4	59252.4	44	65
MB251-1-13	Calcite	4040	6040	130	37000	39632.4	59252.4	174	195
MB251-1-14	Calcite	4040	6040	132	37000	39632.4	59252.4	176	197
MB251-1-15	Calcite	4040	6040	127	37000	39632.4	59252.4	171	192
MB251-1-16	Calcite	4040	6040	146	37000	39632.4	59252.4	190	211
MB251-2-1	Calcite	4040	6040	115	37000	39632.4	59252.4	159	180
MB251-2-2	Calcite	4040	6040	140	37000	39632.4	59252.4	184	205
MB251-2-3	Calcite	4040	6040	115	37000	39632.4	59252.4	159	180
MB251-2-4	Calcite	4040	6040	138	37000	39632.4	59252.4	182	203
MB251-2-5	Calcite	4040	6040		37000	39632.4	59252.4	44	65
MB251-2-6	Calcite	4040	6040	130	37000	39632.4	59252.4	174	195
MB251-2-7	Calcite	4040	6040		37000	39632.4	59252.4	44	65
MB251-2-8	Calcite	4040	6040	148	37000	39632.4	59252.4	192	213
MB251-2-9	Calcite	4040	6040	144	37000	39632.4	59252.4	188	209
MB251-2-10	Calcite	4040	6040	127	37000	39632.4	59252.4	171	192
MB251-2-11	Calcite	4040	6040		37000	39632.4	59252.4	44	65
MB256-1-1	Calcite	4829.1	6829.1			47373.471	66993.471	52	74
MB256-1-2	Calcite	4829.1	6829.1			47373.471	66993.471	52	74
MB256-1-3	Calcite	4829.1	6829.1			47373.471	66993.471	52	74
MB256-1-4	Calcite	4829.1	6829.1			47373.471	66993.471	52	74
MB256-1-5	Calcite	4829.1	6829.1	132		47373.471	66993.471	184	206
MB256-1-6	Calcite	4829.1	6829.1	132		47373.471	66993.471	184	206
MB256-1-7	Calcite	4829.1	6829.1	134		47373.471	66993.471	186	208
MB256-1-8	Calcite	4829.1	6829.1	134		47373.471	66993.471	186	208
MB256-1-9	Calcite	4829.1	6829.1	121		47373.471	66993.471	173	195
MB256-1-10	Calcite	4829.1	6829.1	131		47373.471	66993.471	183	205
MB256-1-11	Calcite	4829.1	6829.1	128		47373.471	66993.471	180	202
MB256-1-12	Calcite	4829.1	6829.1	131		47373.471	66993.471	183	205
MB256-1-13	Calcite	4829.1	6829.1			47373.471	66993.471	52	74
MB256-1-14	Calcite	4829.1	6829.1	124		47373.471	66993.471	176	198
MB256-1-15	Calcite	4829.1	6829.1	125		47373.471	66993.471	177	199
MB270-1-1	Calcite	4468	6468	135	38800	43831.08	63451.08	183	205
MB270-1-2	Calcite	4468	6468	135	38800	43831.08	63451.08	183	205
MB270-1-3	Calcite	4468	6468		38800	43831.08	63451.08	48	70
MB270-1-4	Calcite	4468	6468	140	38800	43831.08	63451.08	188	210
MB270-1-5	Calcite	4468	6468	135	38800	43831.08	63451.08	183	205
MB270-1-6	Calcite	4468	6468		38800	43831.08	63451.08	48	70
MB87-1-1	Calcite	4257.7	6257.7	133	38200	41768.037	61388.037	179	201
MB87-1-2	Calcite	4257.7	6257.7	130	38200	41768.037	61388.037	176	198

Sample #	Host	Depth (m)	Depth (m) corr	Th (°C)	Formation Pressure (kPa)	Hydrostat. Pressure (kPa)	Paleo Pressure (kPa)	T _{min} (°C)	T _{max} (°C)
MB87-1-3	Calcite	4257.7	6257.7	129	38200	41768.037	61388.037	175	197
MB87-1-4	Calcite	4257.7	6257.7	131	38200	41768.037	61388.037	177	199
MB87-1-5	Calcite	4257.7	6257.7		38200	41768.037	61388.037	46	68
MB87-1-6	Calcite	4257.7	6257.7	133	38200	41768.037	61388.037	179	201
MB87-1-7	Calcite	4257.7	6257.7	138	38200	41768.037	61388.037	184	206
MB87-1-8	Calcite	4257.7	6257.7	135	38200	41768.037	61388.037	181	203
MB87-1-9	Calcite	4257.7	6257.7	130	38200	41768.037	61388.037	176	198
MB87-1-10	Calcite	4257.7	6257.7	134	38200	41768.037	61388.037	180	202
MB87-1-11	Calcite	4257.7	6257.7	122	38200	41768.037	61388.037	168	190
MB87-2-1	Calcite	4257.7	6257.7	135	38200	41768.037	61388.037	181	203
MB87-2-2	Calcite	4257.7	6257.7	132	38200	41768.037	61388.037	178	200
MB87-2-3	Calcite	4257.7	6257.7	132	38200	41768.037	61388.037	178	200
MB87-2-4	Calcite	4257.7	6257.7	132	38200	41768.037	61388.037	178	200
MB87-2-5	Calcite	4257.7	6257.7	134	38200	41768.037	61388.037	180	202
MB87-2-6	Calcite	4257.7	6257.7	134	38200	41768.037	61388.037	180	202
MB87-2-7	Calcite	4257.7	6257.7	136	38200	41768.037	61388.037	182	204
MB87-2-8	Calcite	4257.7	6257.7	120	38200	41768.037	61388.037	166	188
MB87-2-9	Calcite	4257.7	6257.7	132	38200	41768.037	61388.037	178	200
MB87-2-10	Calcite	4257.7	6257.7	140	38200	41768.037	61388.037	186	208
MB87-2-11	Calcite	4257.7	6257.7	132	38200	41768.037	61388.037	178	200
MB87-2-12	Calcite	4257.7	6257.7	139	38200	41768.037	61388.037	185	207
MB87-2-13	Calcite	4257.7	6257.7	119	38200	41768.037	61388.037	165	187
MB87-2-14	Calcite	4257.7	6257.7	122	38200	41768.037	61388.037	168	190
MB87-2-15	Calcite	4257.7	6257.7	138	38200	41768.037	61388.037	184	206
MB87-2-16	Calcite	4257.7	6257.7	137	38200	41768.037	61388.037	183	205
MB87-2-17	Calcite	4257.7	6257.7	137	38200	41768.037	61388.037	183	205
MB87-2-18	Calcite	4257.7	6257.7	137	38200	41768.037	61388.037	183	205
MB87-2-19	Calcite	4257.7	6257.7	139	38200	41768.037	61388.037	185	207
MB87-2-20	Calcite	4257.7	6257.7	139	38200	41768.037	61388.037	185	207
MB87-2-21	Calcite	4257.7	6257.7	137	38200	41768.037	61388.037	183	205
MB87-2-22	Calcite	4257.7	6257.7	137	38200	41768.037	61388.037	183	205
MB87-2-23	Calcite	4257.7	6257.7	135	38200	41768.037	61388.037	181	203
MB87-2-24	Calcite	4257.7	6257.7	135	38200	41768.037	61388.037	181	203
MB87-2-25	Calcite	4257.7	6257.7	136	38200	41768.037	61388.037	182	204
MB87-2-26	Calcite	4257.7	6257.7	137	38200	41768.037	61388.037	183	205
MB87-2-27	Calcite	4257.7	6257.7	137	38200	41768.037	61388.037	183	205
MB87-2-28	Calcite	4257.7	6257.7	139	38200	41768.037	61388.037	185	207
MB87-2-29	Calcite	4257.7	6257.7	137	38200	41768.037	61388.037	183	205

APPENDIX VIII

REFEREED PUBLICATIONS

Buschkuehle, B.E. & Machel, H.G. (2002): Diagenesis and paleofluid flow in the Devonian Southesk-Cairn carbonate complex in Alberta, Canada. *Marine and Petroleum Geology*, 19 (2002), p. 219-227.

Machel, H.G., Buschkuehle, B.E. and Michael, K., 2001, Squeegee flow in Devonian carbonate aquifers in Alberta, Canada. In: Cidu, R. (ed.), *Water-Rock Interaction*, Vol. 1. Proceedings of the Tenth International Symposium on Water-Rock-Interaction WRI-10, Villasimius, Italy, p. 631- 634.

Buschkuehle, B.E. Machel, H.G. (2000): Diagenese und Paleoporenwasserfluss in tiefen devonischen Gasfeldern von Alberta. *Zbl. Geol. Palaeont. Teil I, Heft ½*, p. 15-32, Stuttgart.

ABSTRACTS

Buschkuehle, B.E. & Machel, H.G. (2000): Geochemical evolution of diagenetic fluids in a deep Devonian Carbonate Complex, west central Alberta, Canada. *GeoCanada 2000*, Calgary, May 29-June 2, 2000

Buschkuehle, B.E. & Machel, H.G. (2000): Diagenesis in the Southesk-Cairn carbonate complex with implications for paleo fluid flow - Upper Devonian, Western Canada Sedimentary Basin. *AAPG Annual Convention*, New Orleans, April 16-19, 2000

Buschkuehle, B.E., Cavell, P.A., Machel, H.G., and Skilliter, C.C. (1999): Indications for tectonically induced fluid flow into the Rocky Mountain foreland basin - with implications for petroleum exploration. *CSPG Sedimentology Division*, February 1999, *CSPG Reservoir*, vol. 26-2, p. 14 to 15; February 1999.

Buschkuehle, B.E., Machel, H.G. and Cavell, P.A. (1998) Paleoporenwasserfluß in devonischen Karbonaten des Southesk-Cairn Karbonatkomplexes, Rocky Mountain Vorlandbecken, Alberta, Canada. *Terra Nostra*, *Schriften der Alfred Wegener Stiftung*, 98/3, p. V51.

Machel, H.G., Cavell, P.A., and Buschkuehle, B.E. (1998) Hinweise auf tektonisch induzierten Fluß von Formationswässern in das Rocky Mountain Vorlandbecken aufgrund der Gehalte an stabilen und Sr-isotopen. *Terra Nostra*, *Schriften der Alfred Wegener Stiftung*, 98/3, p. V215-V216.

Buschkuehle, B.E., Machel, H.G. and Cavell, P.A. (1998) Paleofluid flow within the Middle and Upper Devonian Southesk-Cairn carbonate complex, Rocky Mountain foreland basin, as determined from carbonate cements. *CSPG/CSEG/CWLS Joint Annual Convention*, *Geo-Triad '98*, abstracts p. 121-122.

REPORTS

Buschkuehle, B.E. (1997): Determination of timing and directions of paleofluid flow within the Middle and Upper Devonian Southesk-Cairn carbonate complex in the Rocky Mountain Foreland Basin, west-central Alberta, Canada; origins and compositions of diagenetic hydrothermal fluids, thesis update report for Chevron Canada resources and Amoco Canada Petroleum Company Ltd., 11pp.